TESE DE DOUTORAMENTO

MULTI-PARTICLE PRODUCTION IN THE COLOR GLASS CONDENSATE

Pedro Augusto Agostini Infante

ESCOLA DE DOUTORAMENTO INTERNACIONAL DA UNIVERSIDADE DE SANTIAGO DE COMPOSTELA

PROGRAMA DE DOUTORAMENTO EN FÍSICA NUCLEAR E DE PARTÍCULAS

SANTIAGO DE COMPOSTELA

2021

USC
UNIVERSIDADE
DE SANTIAGO
DE COMPOSTELA

DECLARACIÓN DO AUTOR/A DA TESE

D./Dna. **Pedro Augusto Agostini Infante**

Título da tese: **Multi-particle production in the Color Glass Condenste**

Presento a miña tese, seguindo o procedemento axeitado ao Regulamento, e declaro que:

1) A tese abarca os resultados da elaboración do meu traballo.
2) De ser o caso, na tese faise referencia ás colaboracións que tivo este traballo.
3) Confirmo que a tese non incorre en ningún tipo de plaxio doutros autores nin de traballos presentados por min para a obtención doutros títulos.
4) A tese é a versión definitiva presentada para a súa defensa e coincide a versión impresa coa presentada en formato electrónico

E comprométome a presentar o Compromiso Documental de Supervisión no caso de que o orixinal non estea na Escola.

En **Santiago de Compostela**, **11 de Setembro de 2021**.

Sinatura electrónica

USC
UNIVERSIDADE
DE SANTIAGO
DE COMPOSTELA

AUTORIZACIÓN DO DIRECTOR/TITOR DA TESE

D./Dna. **Néstor Armesto Pérez**

En condición de: **Titor/a e director/a**

Título da tese: **Multi-particle production in the Color Glass Condensate**

INFORMA:

Que a presente tese, correspóndese co traballo realizado por D/Dna Pedro Augusto Agostini Infante, baixo a miña dirección/titorización, e autorizo a súa presentación, considerando que reúne os requisitos esixidos no Regulamento de Estudos de Doutoramento da USC, e que como director/titor desta non incorre nas causas de abstención establecidas na Lei 40/2015.

En **Santiago de Compostela**, **14 de Setembro de 2021**

Sinatura electrónica

USC
UNIVERSIDADE
DE SANTIAGO
DE COMPOSTELA

AUTORIZACIÓN DO DIRECTOR / TITOR DA TESE

Multi-particle production in the Color Glass Condensate

D. Néstor Armesto Pérez
D. Tolga Altinoluk

INFORMAN:

Que a presente tese, correspóndese co traballo realizado por D. Pedro Augusto Agostini Infante, baixo a miña dirección/titorización, e autorizo a súa presentación, considerando que reúne os requisitos esixidos no Regulamento de Estudos de Doutoramento da USC, e que como director desta non incorre nas causas de abstención establecidas na Lei 40/2015.

De acordo co indicado no Regulamento de Estudos de Doutoramento, declara tamén que a presente tese de doutoramento é idónea para ser defendida en base á modalidade de Monográfica con reproducción de publicaciones, nos que a participación do/a doutorando/a foi decisiva para a súa elaboración e as publicacións se axustan ao Plan de Investigación.

En Santiago de Compostela, 14 de Setembro de 2021

USC
UNIVERSIDADE
DE SANTIAGO
DE COMPOSTELA

Para Regina, Charles e Lu.

USC
UNIVERSIDADE
DE SANTIAGO
DE COMPOSTELA

Acknowledgments

First, I want to show my deepest and most sincere gratitude to my directors Néstor and Tolga. To Néstor for being, since I met him in my first years as a student, an extremely attentive, friendly (although sometimes angry), hardworking and, above all, intelligent person. Throughout my years as his student, he has never failed to help me with my problems and, for this reason, I have always felt very lucky to have had him as an advisor. On the other hand, I met Tolga when I started my PhD studies, and he was a one of the most wonderful people I have ever met. Tolga was always very considerate, welcoming, and helped me with everything he could. He always gave me encouragement and, without a doubt, having him as my director was of immense help throughout these last four years.

I would also like to thank all the staff from the "Instituto Galego de Física de Altas Enerxías" (IGFAE) for the great welcome during my predoctoral stage. The IGFAE, apart from being a center of quality at a professional level, was a very pleasant working environment. I would like to thank Carlos for helping me with everything I needed and for making, together with others, a QCD group of worldwide reference. To Marcos for wasting hours solving our ignorance in computer issues. To Ana and Elvira for solving the bureaucratic hieroglyphics. To Ricardo for wasting time on the phone getting us favors. To Elena for putting us in touch with the real world. In general, I wanted to thank the rest of my colleagues for creating an unbeatable working environment.

Também quero agradecer à minha família por ter feito todo o possível para me ajudar a atingir meus objetivos. Aos meus pais, Charles e Regina, por terem feito muitos sacrifícios por mim e por meu irmão. Sem eles, nenhum dos meus sucessos acadêmicos seria possível e, portanto, esta tese se deve a seus esforços. Há poucas palavras para expressar minha gratidão aos meus pais por todo o apoio, amor e ajuda que eles me deram ao longo dos meus anos de estudo. Gostaria também de agradecer ao meu irmão, Lu, por todo o carinho e apoio que ele sempre me deu e que foi de vital importância durante toda a minha vida.

Finalmente, y no menos importante, quiero agradecer a mis amigos por ser parte fundamental de mi vida y por ayudarme a mantener la cordura a lo largo de estos años. A los amigos que estuvieron día y noche a lo largo de estos últimos cuatro años y que pasaron a ser familia: Adolfo, Alejandro, Pablo y Parga. A mis amigas que, gracias a sus consejos y sabiduría, me ayudaron a tomar las mejores decisiones: Manuela y Mariña. A los amigos que Santiago me dio el placer de conocer: Ana, Javi, Marta y Alberto. A los amigos de la juventud, por estar siempre ahí y ayudar en todo lo posible: Lolo, Ago, Fer, Ivi, Manolo, Marco, Gil, Eiriz, Pela, Zalabeite, Matito, Moli, Nico, Ruchi, Santalla y Albertito. Quiero hacer un agradecimiento especial a Manuel Eiriz cuya ayuda y enseñanza, con sus conocimientos magistrales en matemáticas, fue fundamental en mis éxitos académicos. Por último, quiero dar mi profundo y más sincero agradecimiento a

todos los amigos que estuvieron a lo largo de mi etapa académica y no aparecen en este apartado.

Esta tese estivo financiada pola Xunta de Galicia no programa "Axudas de apoio a etapa predoutoral".

Resumo

A Cromodinámica Cuántica, QCD polas súas siglas en inglés, é a teoría da interacción forte no modelo estándar da física de partículas e describe os bloques máis fundamentais que conforman os *hadróns* e os *núcleos atómicos* así como as forzas que actúan entre eles [1–3]. Este bloques fundamentais son partículas con espín-$\frac{1}{2}$ coñecidas como *quarks* [4, 5]. Os quarks aparecen na natureza en distintos *sabores* que os distinguen pola súa carga eléctrica fraccional e pola súa masa. Polo tanto podemos separalos entre quarks leves (u, d e s), con masas menores que 1 GeV/c^2, e quarks pesados (c, b e s), con masas maiores que 1 GeV/c^2 [6].

Como a función de onda dos hadróns é simétrica ante intercambio de quarks, o principio de Pauli impón que os quarks deben ter un novo número cuántico, coñecido como *cor* [7]. A nomenclatura cor é debido a que este número cuántico é un vector tridimensional e polo tanto débese á analoxía coas cores básicas (r,g,b). Polo tanto, ao introducir este novo grado de liberdade que transforma ante o grupo especial unitario tridimensional SU(3)$_c$, a función de onda do hadrón vólvese antisimétrica e satisfai o principio de Pauli. Ademais a función de onda hadrónica transforma como un singlete baixo SU(3)$_c$ o que implica que os hadróns non teñen cor.

Análogo á carga electromagnética, este novo número cuántico que aparece nos quarks é interpretado como unha *carga de cor* que permite que eles interaccionen entre eles e que estean nun estado ligado dentro dos hadrón ou núcleos. Inspirado pola Electrodinámica Cuántica (QED), onde as partículas cargadas interaccionan polo intercambio dun bosón sen masa que é introducido impoñendo que a teoría sexa simétrica ante o grupo U(1), un novo bosón gauge chamado *gluón* é introducido para explicar as interaccións debidas á carga de cor. Polo tanto, para incluír os gluóns dende un punto de vista máis teórico, unha teoría cuántica de campos foi proposta onde os gluón son tratados como un campo gauge, acoplado ós quarks por unha *constante de acoplo* g, que é introducido impoñendo que a teoría sexa invariante ante o grupo SU(3). Esta teoría, chamada Cromodinámica Cuántica, é, en contraste con QED, descrita por unha teoría gauge de Yang-Mills non-Abeliana [8]. Os gluóns transforman ante a representación adxunta de SU(3) e, polo tanto, existen oito deles. Ademais, por causa da natureza anti-conmutativa da teoría, os gluóns están acoplados a si mesmos. Esta é unha diferencia enorme con respecto ós fotóns en QED e por causa disto a QCD contén un comportamento moito máis complexo e exótico que QED.

Unha das diferenzas entre QCD e QED é que a interacción forte prohibe a existencia de estados asintóticos con cor o que implica que os partóns, unha forma de referirse ós quarks e gluóns, non poden ser observados como partículas illadas. Esta propiedade de QCD é coñecida como *confinamento de cor* [9] e segue sendo un dos problemas teóricos abertos da teoría. Outra propiedade importante de QCD é a *liberdade asintótica* [3, 10], que é a

diminución da constante de acoplo ao aumentar a enerxía da interacción ou, equivalente, diminuir a distancia das partículas. Grazas a esta propiedade, podemos resolver QCD en certos réximes cinemáticos, é dicir a altas enerxías ou baixas distancias, usando teoría de perturbación en termos da constante de acoplo. Polo tanto, no contexto de teoría de perturbación a QCD foi resolta e deu lugar a unha boa cantidade de predicións. Foi capaz de describir os datos experimentais de procesos como "Deep Inelastic Scattering" (dispersións inelásticas e profundas) [11,12], DIS, que son colisións entre leptóns e hadróns a moi altas enerxías, produción de jets [13] e aniquilacións de Drell-Yan con gran precisión. Por outra parte, procesos que ocorren a baixas enerxías ou largas distancias non poden ser descritos por teoría de perturbacións e polo tanto temos que usar outras técnicas como "lattice QCD" (QCD en redes). O problemas destas técnicas é que dependen do poder de computación dispoñible, o que fai que a súa capacidade de predición sexa, en moitos casos, limitada. A escala de enerxía que separa o réxime perturbativo do non-perturbativo chámase Λ_{QCD} e vale $\sim$200 MeV segundo os experimentos.

Debido a que as interaccións no interior dos hadróns ocorren a distancias que son da orde de $\Lambda_{\text{QCD}}^{-1}$, as dinámicas neste entorno son non-perturbativas. Sen embargo, aínda que non podamos calcular de forma perturbativa a estrutura partónica dos hadróns, podemos utilizar a teoría de perturbación para obter a súa evolución coa escala de enerxía característica do sistema. O conxunto de ecuacións diferenciais que definen esta dependencia chámanse *ecuacións de evolución* e son obtidas no contexto da teoría do grupo de renormalización. Así, esta evolución pode ser posta a proba en experimentos de DIS onde un leptón de alta enerxía interacciona cun hadrón, ou núcleo, a través de (tipicamente) un intercambio de fotón. Neste proceso, a enerxía intercambiada na colisión serve como unha escala de resolución que proba o hadrón a estas distancias. Polo tanto os experimentos de DIS serven tanto para dar unha condición inicial para as ecuación de evolución así como unha forma de comprobalas. Existen dous conxuntos de ecuacións de evolución, baseadas en radiación de gluóns, con especial importancia: As ecuacións DGLAP [14–17] e BFKL [18, 19]. Estas ecuacións foron utilizadas para obter unha gran cantidade de predicións e son unha das pezas máis importantes na fenomenoloxía de QCD. Sen embargo, elas predín un crecemento das distribucións partónicas que viola a propiedade cuántica de unitariedade rompendo o límite de Froissart [20]. Isto é debido a que elas non teñen en conta o fenómeno de recombinación de gluóns, que pasa a ser importante a altas enerxías, onde o sistema partónico volvese moi denso. Polo tanto, as ecuacións de DGLAP e BFKL teñen que ser corrixidas incluíndo termos non lineares que fan que o crecemento gluónico diminúa a altas enerxías.

A introdución de termos non lineares nas ecuacións de evolución das distribución partónicas separa o sistema hadrónico en dous réximes: o *réxime de saturación* onde os efectos non lineares son importantes e o *réxime diluído*, onde o sistema non é denso e podemos desprezar o proceso de recombinación de gluóns. Polo tanto introdúcese a chamada *escala de saturación*, Q_s, que separa ambos casos. Esta escala depende tanto da enerxía como do tamaño do sistema. A día de hoxe existen dous aceleradores de partículas que poden ser capaces que acadar o réxime de saturación: o Colisor Relativista de Ións Pesados (RHIC) en BNL e o Gran Colisor de Hadróns (LHC) no CERN. Estes colisores foron capaces de producir unha gran cantidade de datos experimentais en colisións de núcleo-núcleo (AA), protón-núcleo (pA) e protón-protón (pp). No comezo deste século, experimentos realizados en RHIC a través de colisións AA viron que un fluído case ideal era

xerado [21]. Esta foi a primeira evidencia dun estado da materia onde os quarks e os gluóns actúan como se estiveran libres, o Plasma de Quarks e Gluóns (QGP). As propiedades deste medio son estudadas a través de dous fenómenos: "jet quenching" [22] e correlacións por fluxo. Por un lado, "jet quenching" é o fenómeno no cal a partículas con un momento transverso alto están suprimidas con respecto ao que esperarías se só tiveramos en conta os nucleóns participantes na colisión. Estas partículas, ou jets, teñen unha perda de enerxía debido a súa interacción co plasma de quarks e gluóns. Polo tanto, estudar o fenómeno de "jet quenching" é de gran importancia para entender as propiedades do QGP xa que nos dan unha información directa de como o QGP comportase cando un partón o atravesa. Por outro lado, as correlacións de fluxo son correlacións en momento que son xeradas polo comportamento colectivo do fluído partónico. É dicir, a dinámica imposta pola teoría de hidrodinámica viscosa que describe o QGP implica que as anisotropías do sistema darán lugar a un incremento do gradiente de velocidade en certas rexións que farán que o medio se expanda máis rápido. Polo tanto a evolución hidrodinámica converte a anisotropías espaciais en anisotropías de momento. As correlación de fluxo son, en xeral, representadas a través do espectro de partículas con respecto a diferenza de pseudorapidez, $\Delta\eta$, e ángulo acimutal, $\Delta\phi$, das partículas producidas. As medidas realizadas en RHIC indicaron que hai correlación nun gran rango de $\Delta\eta$ e que a correlación é máis grande cando $\Delta\phi = 0, \pi$ [23]. Por causa da forma da función de correlación, este fenómeno é coñecido como o "*ridge*" (cresta).

O comportamento colectivo no sistema xerado nas colisións AA explícase a través de que o sistema contén un gran número de participantes e que o camiño libre medio das partículas no medio é moito máis pequeno que o tamaño do sistema. Polo tanto este medio pode ser descrito polas súas propiedades macroscópicas e a teoría hidrodinámica é o marco teórico ideal para describilo. Por esta razón, críase que o plasma de quarks e gluóns non era xerado en colisión pA e pp, xa que nin o número de participantes nin o tamaño do sistema son grandes. Sen embargo, no 2010 a colaboración CMS examinou eventos con alta multiplicidade en colisións pp e viron que se xeraban correlacións como a do "ridge" [24]. Logo, en 2012, a mesma colaboración tamén viu o mesmo fenómeno en colisións pA [25] indicando que tamén había indicios de comportamento colectivo en sistemas máis pequenos. Estes resultados abriron un gran debate na comunidade de física de altas enerxías en función se a orixe do "ridge" en sistemas pequenos é debido a formación de plasma de quarks e gluóns ou se é debido a efectos dos momentos iniciais da colisión, é dicir, que veñen da función de onda hadrónica ou nuclear.

Dado que o sistema xerado no estado inicial dunha colisión a altas enerxías é descrito por escalas de enerxía moito máis grandes que Λ_{QCD}, podemos estudar a súa dinámica a través da teoría de perturbación. Ademais como o sistema é denso, a física predominante é clásica. Isto fai posible describir os gluóns como campos clásicos que son xerados por cargas de cor distribuídas de forma aleatoria. Esta suposición coñécese como modelo de McLerran-Venugopalan (MV) [26,27]. O modelo MV, que é explicado ó longo da tese, nos da un marco teórico simple no cal os partóns de máis enerxía da función de onda nuclear ou hadrónica son modelados por unha fonte aleatoria mentras que a parte dinámica do sistema ven dada polo campo gluónico que, aínda que non é perturbativo, pódese ser calculado utilizando técnicas de constante de acoplo pequena. As correccións cuánticas deste modelo veñen dadas polas ecuacións de evolución non-lineares de JIMWLK [28–32]. A teoría efectiva que engloba o modelo MV e as súas correccións cuánticas chámase o

"*Color Glass Condensate*" (CGC) [33–37].

Dende fai unhas décadas, o CGC foi utilizado para describir unha gran cantidade de datos experimentais do LHC ou RHIC con moito éxito. Como se verá ó longo desta tese, o CGC ofrece un marco perfecto para calcular o espectro de partículas xerado con moita ou mediana pseudorapidez e para explicar o fenómeno do "ridge" en sistemas pequenos. Ademais o CGC ofrece unha ferramenta analítica para describir os primeiros momentos da colisión e polo tanto serve como unha condición inicial para a evolución hidrodinámica.

O obxectivo xeral da tese é presentar unha extensión ós mecanismos de produción de moitas partículas no réxime non-lineal da Cromodinámica Cuántica. Para isto utilizaremos a teoría efectiva do CGC para modelar as colisións de partículas a altas enerxías. A tese vai estar composta de seis capítulos que poden ser resumidos da seguinte forma:

1. No capítulo 1 expoñeremos os conceptos básicos do límite de alta enerxía da Cromodinámica Cuántica que será de fundamental importancia ó longo da tese. Na sección 1.1 presentaremos o Lagranxiano da QCD que é a peza máis importante para calcular as ecuacións que utilizaremos. Na sección 1.2 introduciremos o fenómeno de liberdade asintótica. Nas seccións 1.3, 1.4 e 1.5 resumiremos os puntos importantes das ecuacións DGLAP e BFKL. Finalmente nas seccións 1.6 e 1.7 introduciremos a teoría do "Color Glass Condensate" que será o marco teórico utilizado ó longo desta tese.

2. No capítulo 2 introduciremos os aspectos técnicos do CGC para calcular o espectro de partículas en colisións de alta enerxía. Na sección 2.1 repasaremos os aspectos básicos de teorías cuánticas de campos en presencia dun campo forte. Na sección 2.2 resolveremos as ecuacións de Yang-Mills linearizadas para obter o espectro non eikonal de partículas producidas en colisión protón-núcleo. Na sección 2.3 introduciremos a aproximación eikonal e calcularemos o espectro eikonal de un gluón producido en colisións pA. Na sección 2.4 veremos a función de Wigner que será importante no noso análise de correlacións entre varias partículas. Finalmente na sección 2.5 faremos o limite diluído do espectro de un só gluón e obteremos a chamada aproximación da "Glasma Graph".

3. No capítulo 3 veremos o fenómeno de correlacións de fluxo en sistemas pequenos e introduciremos posibles explicacións baseadas en modelos do estado inicial. Na sección 3.1 introduciremos os estados dunha colisión entre ións pesados e a estrutura do "ridge" que se ve en correlacións entre dúas partículas. Na sección 3.2 calcularemos o espectro de dúas partículas na aproximación da "Glasma Graph" para ver como este procedemento explica o fenómeno do "ridge". Logo, na sección 3.3 analizaremos o modelo dos dominios cromo-eléctricos que propón que o branco está formado por dominios cromo-eléctricos de tal forma que as correlacións entre partículas xorden de partículas que coliden no mesmo dominio. Finalmente na sección 3.4 faremos un breve resumo do método de cumulantes que tenta eliminar as correlacións que non son de fluxo da función de correlación.

4. No capítulo 4, que está baseado en [38], presentaremos o noso marco para calcular a produción de moitas partículas no limite denso-diluído de CGC e calcularemos o cumulante de dúas e catro partículas. Na sección 4.1 introduciremos o formalismo. Na sección 4.2 presentaremos as técnicas para calcular a media nas configuracións

dos brancos das liñas de Wilson no modelo MV e presentaremos o que chamamos o modelo AE para calcular multipolos. Na sección 4.3 calcularemos o espectro de dous gluóns no modelo AE e na sección 4.4 xeneralizaremos o noso resultado para o caso de moitos gluóns. Logo na sección 4.5 calcularemos de forma numérica o espectro de dous, tres e catro gluóns así como os seus respectivos cumulantes.

Veremos que a través do noso método, que consiste en asumir unha forma Gaussiana para o produto entre dous vértices de Lipatov, seremos capaces de obter unha expresión analítica para os coeficientes acimutais de dúas partículas. Esta suposición para os vértices de Lipatov implica que estaremos imitando o método das funcións de Wigner pero incluíndo correlacións na función de onda de proxectil. Por outro lado, vemos que o cumulante de catro partículas, $c_2\{4\}$, é negativo o que implica unha consistencia cos datos experimentais. Notamos que o resultado cando non temos en conta a correlación na función de ondas do proxectil é moito máis pequeno o que significa que ter en conta estas correlacións é de fundamental importancia no cálculo. Debido a que os nosos cálculos foron realizados asumindo formas Gaussianas, eles só poden ser considerados fiables cando o momento transverso das partículas é máis pequeno ou da orde que o momento de saturación. Ademais somos conscientes de que para facer un cálculo máis completo teríamos que ter en contra outros ingredientes como unha contribución de quarks, un modelo para o proxectil ou branco máis realista, ter en conta as función de fragmentación, etc. Todos estes aspectos deben estar presentes para facer un modelo fenomenolóxico fiable.

5. No Capítulo 5 calcularemos as correccións non eikonales para producción de partículas no CGC e para elo relaxaremos a chamada aproximación da onda de choque ("shock-wave approximation"), que asume que o branco ten anchura nula. Este tipo de correccións están normalmente incluídas en cálculos de "jet quenching" e foron expandidas de forma sistemática en [39]. Na sección 5.1 derivaremos unha expresión do vértice de Lipatov que inclúe correccións non eikonais ao ter en conta unha certa anchura para o branco. Logo, na sección 5.2, aplicaremos as correccións non eikonais no espectro dun só gluón na aproximación da "Glasma Graph". Veremos que estas correccións virán parametrizadas pola función $\mathcal{G}_1^{\mathrm{NE}}(k^-, \lambda^+)$ que é definida na ecuación (5.31), onde k^- é a enerxía do cono de luz do gluón producido. Por outro lado vemos que no límite $k^- \to 0$ recuperamos o resultado calculado en [39]. No noso análise numérico vemos que nalgúns rangos cinemáticos as correccións non eikonais poden chegar a ser do 15% con respecto o cálculo eikonal. Isto implica que dependendo da rexión cinemática que se estea estudando os efectos non eikonais deben ser tidos en conta.

   Na sección 5.3 faremos o mesmo cálculo pero para o caso de dous gluóns. Como un resultado novidoso veremos que a inclusión de correccións non eikonais no espectro de dous gluóns rompe a chamada simetría accidental, é dicir, que o espectro é simétrico con respecto ó ángulo acimutal, e polo tanto é capaz de xerar coeficientes de Fourier que son impares. Ademais, nesta sección analizaremos cada un dos termos xerados e veremos que poden ser identificados como correlacións debido á estatística cuántica. Os nosos resultados coinciden, sen ter en conta as correccións non eikonais, cos de [40] a parte da contaxe en potencias de N_c. Esta diferencia na contaxe é debido a que o cálculo feito en [40–42] non foi baseado na aproximación da "Glasma

Graph". Na sección 5.4 calculamos os coeficientes de Fourier impares e estudamos o seu comportamento con respecto a varias variables que están resumidos nas figuras 5.8, 5.9 e 5.10. Vemos que os coeficientes impares xerados a través das correccións non eikonais son visibles ata enerxías do centro de masa da orde de 100 GeV e polo tanto incluír estes efectos pode ser importantes para análises fenomenolóxicos en colisións pp. Tamén vemos que os efectos son importantes ata diferenzas entre pseudorapideces da orde de 2.

Finalmente na sección 5.5 vemos os efectos non eikonais na produción de tres gluóns. Logo comparamos os nosos resultados cos de [40] e vemos que, outra vez, o noso resultado é análogo pero ten unha distinta contaxe nas potencias de N_c.

6. No capítulo 6 xeralizaremos os resultados do capítulo 5 no caso de que un dos participantes na colisión é denso, é dicir, estudamos os efectos non-eikonais no espectro de moitos gluóns en colisións pA. Na sección 6.1 faremos unha breve introdución ao marco teórico, inspirado nos cálculos de "jet quenching", que utilizaremos ó longo do capítulo. Na sección 6.2 xeralizaremos os resultados da sección 4.2 para o caso non eikonal no cal as liñas de Wilson deben ser intercambiadas polo propagador escalar. Veremos que as medias na configuración do branco poden ser realizadas de forma analítica se utilizamos a aproximación de GBW, é dicir, asumimos que a forma do dipolo eikonal é Gaussiana. Esta aproximación está xustificada sempre e cando o tamaño de dipolo é moito menor que a inversa da escala perturbativa.

   Na sección 6.3 calcularemos o espectro dun só gluon no caso non-eikonal e analizaremos este efectos na sección 6.3.1. Os nosos resultados están resumidos nas figuras 6.2, 6.3 e 6.4 onde vemos que os efectos non-eikonais son visibles para enerxías no centro de masas menores que 100 GeV e para pseudorapideces menores que 1. Polo tanto concluímos que incluír as correccións non-eikonais para fenomenoloxía do RHIC, ás súas enerxías máis altas, ou do LHC, non é necesaria. Na sección 6.3.2 comparamos o noso resultado cos de [43, 44] e fumos capaces de conseguir unha parametrización, baseada na aproximación Gaussiana, dos chamados dipolos con cor.

   Na sección 6.4 introducimos o formalismo xeral para calcular o espectro de moitos gluóns en colisións protón-núcleo mais alá da aproximación eikonal. O procedemento está baseado no modelo AE que supoñemos que segue sendo válido no caso dun branco con anchura non nula. Logo, na sección 6.4.1 resolvemos de forma numérica o caso de dous gluóns. Vemos un resultado completamente análogo ó do capítulo 5 onde fixemos o cálculo non eikonal para colisión protón-protón, é dicir, vemos que o espectro de dous gluóns é asimétrico con respecto ó ángulo acimutal. Ademais, facemos un estudo do coeficiente de Fourier v_3 e vemos que o seu valor non é depreciable para valores da enerxía do centro de masas de 100 GeV. Polo tanto concluímos que os efectos non eikonais son maiores no caso de dous gluóns que no caso de só un. Notamos sen embargo que o noso análise numérico foi pobre e é mellorable en moitos aspectos. Somos conscientes disto e un análise máis completo será realizado nun futuro.

Contents

Abstract

In this thesis, we review the framework of multi-particle production in high energy collisions within the Color Glass Condensate effective theory. The main goal of this work is to provide a systematic basis for performing analysis on particle correlation both in proton-proton, pp, and in proton-nucleus, pA, scatterings such as those studied at the LHC or RHIC.

We provide the basic aspects of the high energy, or small-x, limit of Quantum Chromodynamics (QCD) and we introduce the Color Glass Condensate (CGC). We provide the technical approach for studying particle production in high energy collisions at leading order in the QCD coupling constant. We review the phenomenon of particle correlation that has been seen in pp and pA collisions and we explain it from first principles within the CGC framework.

On the other hand, based on [38], we generalize the usual approach for analyzing particle production at leading order within the CGC framework to the case in which an arbitrary number of particles are produced. We introduce and study the so-called Area Enhancement model which offers a simple alternative for evaluating high order Wilson lines correlators. We mimic the Gaussian ansatz of the Wigner distribution approach for studying multi-particle correlations but we break the usual factorization assumption. We compute the 4-particle cumulant, $c_2\{4\}$, and we obtain a negative value which agrees qualitatively with data.

Finally, based on [45, 46], we introduce sub-eikonal corrections to the dilute-dilute, or Glasma Graph, limit of the CGC by including finite width effects. We study the effects of non-eikonal corrections in single, double and triple gluon production. We see that the sub-eikonal effects introduces an asymmetry in the azimuthal distribution of gluons and therefore is able to explain the appearance of odd azimuthal harmonics in data. We perform a numerical study of the non-eikonal effects and see that they are negligible at relatively high energies. We generalize our approach to the dilute-dense limit, which is more suitable for pA collisions, by introducing the dense medium propagator, analogously to the jet quenching framework. We introduce a systematic approach for computing multi-gluon production in proton-nucleus collisions beyond the eikonal accuracy. We study the odd azimuthal harmonics generated in this approach.

USC
UNIVERSIDADE
DE SANTIAGO
DE COMPOSTELA

Introduction

Quantum Chromodynamics (QCD), the fundamental theory of the strong interactions within the Standard Model of particle physics, describes the building blocks of strongly interacting particles – *hadrons* and atomic *nuclei* – and the forces acting between them [1–3]. The building blocks of these particles are spin-$\frac{1}{2}$ fermions known as *quarks* [4, 5]. Quarks appear in nature in different *flavors* that distinguish them by their fractional electric charge and their masses. Thus we can separate them into light quarks (u, d and s), with masses smaller than 1 GeV/c^2, and heavy quarks (c, b and t), with masses larger than 1 GeV/c^2 [6].

Because the hadronic wave function is symmetric under the exchanges of quarks, the Pauli principle imposes that quarks must have a new quantum number, known as *color* [7]. The name comes from the fact that the quark's color is defined by a 3-dimensional vector and is an analogy with the basic colors (r, g, b). Thus, introducing this new degree of freedom that transforms under the 3-dimensional special unitary group SU(3)$_c$ the hadronic wave function becomes antisymmetric and the Pauli principle is satisfied. Moreover, the hadronic wave function transforms as a singlet under SU(3)$_c$ which implies that hadrons are colorless.

Analogous to the electromagnetic charge, the new quantum number defining the quarks is interpreted as a 3-dimensional *color charge* that allows them to interact between themselves and to be in a bound state within the hadrons. Inspired by Quantum Electrodynamics (QED), where charged particles interact electromagnetically by exchanging a massless boson which is introduced by imposing a symmetry under the U(1) group, a new gauge boson named *gluon* is introduced to explain the interactions due to the color charge. Therefore, in order to include gluons into a theoretical framework, a Quantum Field Theory was proposed where gluons are treated as bosonic *gauge fields*, coupled to the quark fields through a *coupling constant* g, which are introduced by imposing that the theory has to be invariant under the SU(3) group. This theory, named Quantum Chromodynamics, is, in contrast with QED, described by a non-Abelian Yang-Mills gauge theory [8]. Gluons transform under the adjoint representation of SU(3) and therefore there are eight of them. Moreover, because of the non commuting nature of the theory, gluons are coupled to themselves. This is a huge difference with respect to photons in QED and because of that QCD encodes a much richer and exotic behavior than QED.

One of the difference of QCD with respect to QED is that the strong interactions are assumed to forbid the existence of asymptotic colored states which implies that the *partons*, i.e. quarks and gluons, cannot be observed as isolated particles. This feature of QCD is known as *color confinement* [9] and is one of the big opened question in the theory. Another important property of QCD is *asymptotic freedom* [3, 10] which is a decrease of the QCD coupling constant with interactions that occur at higher energy or, equivalently,

smaller distances. Thanks to this feature QCD can be solved in some kinematic ranges, i.e. in small distance or high energy interactions, by using perturbative techniques in terms of the coupling constant. Thus, in the framework of perturbation theory, QCD has given a wealthy amount of predictions. It has been able to describe experimental data from processes such as Deep Inelastic scattering (DIS) [11,12], i.e. lepton-hadron collisions at high energy, jet production [13] and Drell-Yan annihilations with great precision. On the other hand, processes that occur at low energy or large distances cannot be described by perturbation theory and other techniques, such as lattice QCD, have to be applied. The main problem of these techniques is that they depend on the computation power available and therefore their predictability is limited. The energy scale that separates the perturbative from the non-perturbative regime is called Λ_{QCD} and is fixed to ~ 200 MeV by measurements.

Because the interactions in the interior of an hadron occur at distances that are of order $\Lambda_{\text{QCD}}^{-1}$, the dynamics of such an ensemble is non-perturbative. However, although we cannot compute the partonic structure of hadrons perturbatively, we can exploit perturbation theory to obtain its evolution with the energy scale of the problem. The set of differential equations that gives this trend are known as *evolution equations* and are obtained in the context of renormalization theory. This situation can be probed experimentally through the DIS process where a high energy lepton interacts with an hadron or nucleus through a, typically, photon exchange. In this process, the energy exchange in the collision serves as a resolution scale that probes the partonic structure at this distance. Thus DIS experiments provide the initial condition for the evolution equations as well as an experimental check for them. In this context there are two set of evolution equations, based on partonic radiations, that are of great importance: the DGLAP [14–17] and BFKL [18, 19] equations. These equations have provided a large amount of predictions and are one of the key ingredients in QCD phenomenology. However, they predict a growth with energy of the partonic distributions that violates unitarity by exceeding the Froissart bound [20]. The reason of that is because they do not include the phenomenon of gluon recombination that is important at high energy, where the hadronic ensemble becomes highly dense. Thus, the DGLAP and BFKL equations are corrected by including non-linear terms that tame the gluon growth at high energy.

The introduction of non-linear terms into the evolution equations of the parton distributions separate the hadronic system into two regimes: the *saturation regime* where non-linear effects are important and the *dilute regime* where the system is not dense and we can neglect the process of gluon recombination. The so-called *saturation scale*, Q_s, is introduced to separate both scenarios. This scale depends on the size and energy of the partonic system. At the moment there are two particle accelerators that are able to achieve the kinematics needed to obtain a saturated hadronic system: the Relativistic Heavy Ion Collider (RHIC) at BNL and the Large Hadron Collider (LHC) at CERN. These colliders have achieved a wealth amount of data obtained in nucleus-nucleus (AA), proton-nucleus (pA) and proton-proton (pp) collisions. A couple of decades ago, experiments performed at RHIC in AA collisions revealed that a quasi-ideal fluid is generated [21]. This was the first evidence of the existence of a state of matter in which quarks and gluons are deconfined – the Quark Gluon Plasma (QGP). The properties of this system are studied through two phenomena: *jet quenching* [22] and *flow correlations*. Jet quenching is the suppression of high transverse momentum particles or jet production relative to the mul-

tiplicity expected from the number of participants in the collision. These particles (or jets) have they energy loss due to its interaction with the Quark Gluon Plasma. Thus, studies around the jet quenching phenomenon reveal direct evidence on how the QGP responds when a high quark or gluon jet traverses it. On the other hand, flow correlations are the momentum correlations that are generated due to the collective behavior of the partonic fluid. The dynamics imposed by the viscous hydrodynamical description of the QGP implies that any anisotropy in the system would lead to a faster expansion in these directions with higher gradients. Therefore the hydrodynamics evolution converts spatial anisotropies into momentum anisotropy. Flow correlations are usually described by representing the double particle spectrum in a $(\Delta\eta, \Delta\phi)$ plane, where $\Delta\eta$ and $\Delta\phi$ are the difference in pseudorapidity and azimuthal angle of the produced particles respectively. Measurements performed at RHIC [23] indicates a long range correlation in $\Delta\eta$ and an enhancement of production in the $\Delta\phi = 0, \pi$ region of the plane. Because of the shape of this result it is usually referred to as the *ridge*.

The explanation of collective behavior in the system generated is AA collisions is justified through the large amount of participants in the collision and because the mean free path of the colliding particles is much smaller than the size of the ensemble. Thus the system can be described by its macroscopic properties and hydrodynamics offers a natural framework for explaining it. For this reason it has been believed that the Quark Gluon Plasma is not generated in collisions with a smaller number of participants such as in pp or pA scatterings. Until 2010, when the CMS collaboration examined high multiplicity events in pp collisions at the LHC and found that particles had long-range correlations in the $\Delta\phi = 0$ region of the plane [24]. Then in 2012, measurements in pPb collisions at the LHC [25] also revealed signatures for collective behavior in pA scatterings. These results opened a debate in the high energy physics community on whether the emergence of the ridge structure in small systems comes from the creation of a quasi-ideal partonic fluid, which in principle should not occur by the arguments given above, or if it comes from the initial state of the collision.

Since the system generated in the initial stage of these high energy collisions is described by energy scales much larger than Λ_{QCD}, we can study its dynamics from first principles by using weak coupling techniques. Moreover, because the ensemble is composed by a dense medium of gluons, the dominant physics is classical. Thus the gluon can be described by classical fields that are generated by randomly distributed color charges. This model is known as the Mclerran-Venugopalan (MV) model [26, 27]. The MV model, to be detailed later, provides a simple framework in which the high energy partons of the hadronic or nuclear wave function are described by random sources while the dynamics of the system is given by the gluon field which, although it is non-perturbative, can be computed by using weak coupling techniques. The quantum corrections to this approach are introduced by the JIMWLK non-linear evolution equations [28–32]. The overall framework is known as the *Color Glass Condensate* (CGC) effective theory [33–37].

Since the beginning of the century, the CGC framework have been used to describe a wealth amount of data from the LHC and RHIC. As we shall see along this thesis, this effective theory offers a picture for computing the particle spectrum of particles generated at forward or central rapidities and also to explain the ridge-like measurements obtained in small systems. Moreover, the CGC provides analytical tools to describe the early time dynamics of the collision that are quantified through the correlators of the gluon

field configurations. Thus it serves as an initial condition to the hydrodynamic evolution performed in AA collisions. In the rest of this thesis we will review this theory.

Objectives and methodology

In a broad sense, the main goal of this thesis is to provide new developments of the mechanism of multi-particle production in the non-linear regime of Quantum Chromodynamics (QCD). In order to do so the methodology applied in this thesis is the usual in the high energy limit of QCD. We use the Color Glass Condensate effective theory to model the low-x or high energy limit of the hadron or nucleus wave functions and we solve the equations of motion by linearizing the Yang-Mills equation or by expanding it in terms of the interaction Hamiltonian in the light-cone perturbation theory formalism. Then, we average the physical observables computed in this approach over all configurations of the hadron or nucleus. The details of this methodology will be explained along this thesis where we divide it into six chapters that are summarized as follows.

In Chapter 1 we provide the basis of Quantum Chromodynamics at high energy whose concepts will be applied along the thesis. The chapter is composed by a brief introduction to the QCD Lagrangian, in Section 1.1, which is the key piece for obtaining the equations of motion used through the thesis. In Section 1.2 we introduce the phenomenon of asymptotic freedom. In Sections 1.3 to 1.5 we summarize the key points in order to obtain the DGLAP and BFKL evolution equations. Then in Sections 1.6 and 1.7 we introduce the Color Glass Condensate effective theory which is the theoretical framework used through this thesis.

In Chapter 2 we introduce the technical aspects of the CGC in order the describe particle production in high energy collisions. In Section 2.1 we review the basic aspects of quantum field theories coupled to strong fields. In Section 2.2 we solve the linearized Yang-Mills equation in order to obtain the non-eikonal gluon spectrum in pA collisions. In Section 2.3 we review the eikonal approximation and we compute the eikonal single inclusive gluon production in proton-nucleus collisions. In Section 2.4 we introduce the Wigner function distributions that will be important in the numerical analysis of multi-particle correlations performed in Section 4.2. Then in Section 2.5 we perform the dilute limit of the eikonal gluon spectra leading to the so-called Glasma Graph approximation.

In Chapter 3 we review the effect of flow correlations and we introduce possible explanations for such a phenomenon in small systems. In Section 3.1 we introduce the stages of a heavy ion collisions as well as the ridge-like structure seen in double particle correlations. In Section 3.2 we compute the double gluon spectrum within the Glasma Graph approximation in order to see that this approach is able to explain many features of the ridge. In Section 3.3 we introduce the chromo-electric domain model which proposes that the target ensemble is composed by chromo-electric domains and that particle correlations arise from projectile partons that scatter at the same domain. Finally, in Section 3.4 we briefly review the cumulant method which aims to extract the "non-flow" components of the azimuthal harmonics and is extensively used in experimental analysis.

In Chapter 4 we present the framework of multi-particle production in the CGC in the dilute-dense situation (suitable for pA collisions), and the computation of the two and four particle cumulants. In Section 4.1 we introduce the formalism of multi-gluon production in the dilute-dense limit of the CGC. In Section 4.2 we present the techniques for computing target averages in the MV model and in what we call the *Area Enhancement* (AE) model. In Section 4.3 we compute the double gluon spectrum in the AE model and then in Section 4.4 we generalize our result to multi-gluon production. In Section 4.5 we present the numerical solutions of our approach for 2-, 3- and 4-gluon production as well as the corresponding cumulants for each case. Finally in Section 4.6 we give a summary of our results and the conclusions.

In Chapter 5 we compute non-eikonal corrections to particle production in the CGC that stem from relaxing the shock-wave approximation for the target, which becomes of finite length. These are the corrections included in jet quenching calculations and systematically expanded up to next-to-next-to-leading order in [43, 44]. In Section 5.1 we derive an expression for the Lipatov vertex that takes into account the finite longitudinal extent of the target field. Then, in Section 5.2 we apply our corrections to single gluon production in the dilute-dilute (Glasma graph) limit. In Section 5.3 we perform the non-eikonal corrections to the double gluon spectra computed in Section 3.2 within the Glasma Graph approximation. As a novel result we see that the inclusion of non-eikonal corrections break the accidental symmetry $\mathbf{k}_2 \to -\mathbf{k}_2$ and therefore, in this setup, we are able to compute odd azimuthal harmonics. In Section 5.4 we perform a numerical analysis of the non-eikonal 2-gluon spectra in order to study how important is the azimuthal asymmetry generated by the non-eikonal corrections. In Section 5.5 we compute the 3-gluon spectra beyond the eikonal approximation and we discuss about the quantum nature of each term. Finally, in Section 5.6 we discuss our results.

In Chapter 6 we generalize the results of Chapter 5 to the case in which one of the participants is dense, i.e. we study the finite width effects in multi-gluon production in the dilute-dense limit of the Color Glass Condensate framework which is suitable for pA collisions. In Section 6.1 we make a short introduction of the framework, which is similar to that used in jet quenching. In Section 6.2 we generalize the the results of Section 4.2 to the non-eikonal case in which the Wilson line has to be substituted by the scalar gluon propagator. In Section 6.3 we compute the single gluon spectrum beyond the eikonal accuracy and we analyze the effects of the non-eikonal corrections in Section 6.3.1. In Section 6.3.2 we compare our results with the next-to-next-to-eikonal expansion performed in [43, 44] and we obtain a parameterization, within the Gaussian approximation, for the so-called colored dipole functions. In Section 6.4 we introduce the general framework for computing the multi-gluon spectrum for a generic number of gluons and in Section 6.4.1 we solve the case in which two gluons are produced and we study the dependence of the double gluon spectrum with non-eikonal effects included. Finally, in Section 6.5 we conclude our results.

Chapter 1

Quantum Chromodynamics at high energy

Quantum Chromodynamics (QCD) [2] is the firmly established theory of the strong interactions between quarks and gluons whose status was acquired after many successful descriptions and predictions of different phenomena. Although this theory is written in terms of a relatively simple Lagrangian, there are few cases in which it can be solved exactly. A large amount of techniques were developed in the last decades in order to study the physical observables related with the QCD dynamics, being perturbation theory in powers of the QCD coupling the most successful of them. The use of perturbation theory in QCD is justified thanks to the asymptotic freedom phenomenon which states that at high energies the QCD coupling becomes weak. Thus, the studies at the high energy limit of QCD have taken special importance, first because of the applicability of weak coupling techniques to solve the theory, and second, due to the wealth of experimental data that have been collected, first at the Hadron-Electron Ring Accelerator at DESY, then by the Relativistic Heavy Ion Collider at BNL and finally by the Large Hadron Collider at CERN.

The goal of this chapter is to provide the basis of the subject of Quantum Chromodynamics at high energy whose concepts will be of fundamental importance along this thesis. We should note, however, that this chapter shall not be seen as an exhaustive review of high energy QCD. Instead, this chapter will be composed by a brief introduction to the QCD Lagrangian, in Section 1.1, which is the key piece for obtaining the equations used through this thesis. In Section 1.2 we will introduce the phenomenon of asymptotic freedom. In Sections 1.3 to 1.5 we will summarize the key points in order to obtain the DGLAP and BFKL evolution equations. Finally, in Sections 1.6 and 1.7 we will introduce the Color Glass Condensate effective theory which will be the theoretical framework used through all this thesis. For an exhaustive analysis on QCD at high energy we refer to [47].

1.1 The QCD Lagrangian

Quantum Chromodynamics is a quantum field theory (QFT) that is described, unlike Quantum Electrodynamics, by a non-Abelian Yang-Mills gauge theory, where the charges are denoted as *color*. In this formalism, quarks interact with each other through intermediate agents called *gluons*. Like photons, gluons are massless, spin-1 particles with two physical polarization states and they are represented by a 4-component vector potential $A^\mu(x)$. In order to select the physical degrees of freedom one has to impose *gauge conditions* over the field $A^\mu(x)$, for this reason we will also refer to it as the *gauge field*.

The QCD Lagrangian can be derived by imposing gauge invariance under the special unitary group, $\mathrm{SU}(N_c)$, where N_c is the number of color charges. It is well known since the beginning of QCD that $N_c = 3$, however we will keep this number generic for later convenience. In order to derive the QCD Lagrangian we start with the free quark Lagrangian. Assuming that quarks are described by Dirac fields, the kinetic quark Lagrangian is given by

$$\mathcal{L}_q = \overline{\psi}(x)(i\gamma_\mu\partial^\mu - m)\psi(x), \tag{1.1}$$

where $\psi(x)$ is the quark field and $\overline{\psi} = \psi^\dagger\gamma^0$ is the anti-quark field. Although we are not writing the indices explicitly, these fields are defined by a N_c-dimensional vector in the color space, i.e. they transform under the fundamental representation of $\mathrm{SU}(N_c)$, a 4-dimensional spinor and, for the sake of simplicity, we are just considering one quark's flavor. γ^μ are the Dirac matrices and m is the quark mass. It is easy to check that this Lagrangian is invariant under the global $\mathrm{SU}(N_c)$ transformations

$$\psi(x) \to U\psi(x), \qquad \overline{\psi}(x) \to \overline{\psi}(x)U^\dagger, \tag{1.2}$$

where the transformation matrix U is defined by the following relations

$$U^\dagger = U^{-1} \quad \text{and} \quad \det U = 1. \tag{1.3}$$

The elements $U \in \mathrm{SU}(N_c)$ can be related with the algebra of the special unitary group, $\mathfrak{su}(N_c)$, by writing

$$U(\vec{\theta}) = \exp\left\{i\theta^a t^a\right\}, \tag{1.4}$$

where θ^a, with $a = 1, \ldots, N_c^2 - 1$, are the parameters of the gauge transformation and t^a are the generators of the group in the fundamental representation which can be represented by $N_c \times N_c$ traceless matrices. The generators of $\mathrm{SU}(N_c)$ are defined through the structure constants, f^{abc}, satisfying the commutation relation

$$[t^a, t^b] = -if^{abc}t^c, \tag{1.5}$$

with the normalization $\mathrm{Tr}\left[t^a t^b\right] = \delta^{ab}$.

We can generalize the invariance under Eq. (1.2) to local $\mathrm{SU}(N_c)$ transformations, i.e. x-dependent ones, by introducing the gluon fields, $A_\mu(x) \equiv A_{\mu a}(x)t^a$, that transform as

$$A_\mu(x) \to U(x)A_\mu(x)U^\dagger(x) - \frac{i}{g}\left(\partial_\mu U(x)\right)U^\dagger(x), \tag{1.6}$$

where g is the QCD coupling constant, and changing the partial derivative in Eq. (1.1) by the covariant derivative

$$D_\mu = \partial_\mu - igA_\mu(x). \tag{1.7}$$

The covariant derivative has to transform under a gauge transformation as $D_\mu \to UD_\mu U^\dagger$ in order to preserve gauge invariance. The fields $A^\mu_a(x)$ define the *gluons* and are colored vector fields.

After introducing the covariant derivative the quark Lagrangian is written as

$$\mathcal{L}_q + \mathcal{L}_{qg} = \overline{\psi}_\beta(x)(i\gamma_\mu D^\mu - m)_{\beta\alpha}\psi_\alpha(x) = \mathcal{L}_q - g\overline{\psi}_\beta(x)\gamma_\mu A^\mu_a(x)t^a_{\beta\alpha}\psi_\alpha(x), \tag{1.8}$$

where we have introduced the color indices for convenience. Therefore, quarks interact with gluons in a way similar to electrons interacting with photons. A new feature is that the quark can change its color from α to β by emitting or absorbing a gluon of color a, coupling through the generator $t^a_{\alpha\beta}$ as shown in Fig. 1.1.

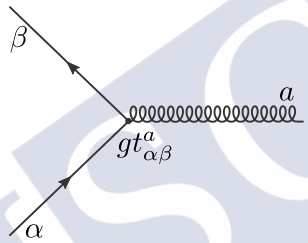

Figure 1.1.
The color of a quark can change from α to β by a gluon of color a, coupled through the SU(N_c) generator $t^a_{\alpha\beta}$.

On the other hand, gluons are physical degrees of freedom and therefore must carry energy and momentum themselves. In an analogous way to photons the gluon kinetic Lagrangian is given by

$$\mathcal{L}_g = -\frac{1}{4}F_{\mu\nu a}F^{\mu\nu a}, \tag{1.9}$$

where $F_{\mu\nu}$ is the non-Abelian strength tensor. In order to preserve gauge invariance the strength tensor has to transform under a gauge transformation as $F_{\mu\nu} \to UF_{\mu\nu}U^\dagger$. This condition is achieved by the following definition

$$F_{\mu\nu} = \frac{i}{g}[D_\mu, D_\nu] = \partial_\mu A_\nu(x) - \partial_\nu A_\mu(x) - ig[A_\mu(x), A_\nu(x)]. \tag{1.10}$$

Apart from the last term of this equation, the strength tensor takes the same form as in QED. The last term introduces a non-linearity to the QCD equations of motions and is the reason that it is much more complicated to solve than QED. Moreover, these terms introduces the possibility to the gluons to interact with themselves, a phenomenon that is not present for photons. This self interaction is achieved by the three- and four-gluon vertices that are depicted schematically in Fig. 1.2.

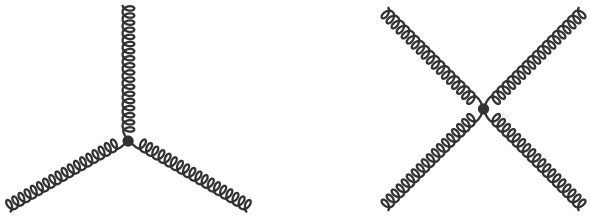

Figure 1.2.
Self-interactions of gluons which are responsible for many important properties of QCD, such as asymptotic freedom, color confinement and chiral symmetry breaking.

The full QCD Lagrangian is the sum of the quark and gluon terms and is given by

$$\mathcal{L}_{\text{QCD}} = \mathcal{L}_q + \mathcal{L}_{qg} + \mathcal{L}_g. \tag{1.11}$$

Because gluons carry color charges, their self-interactions are a source of remarkable differences between QCD and QED. In fact, these interactions are responsible for many unique properties of QCD, such as asymptotic freedom, chiral symmetry breaking, and color confinement.

Although we will not discuss about this topic here, we should note that Eq. (1.11) is not the complete QCD Lagrangian but only the "classical" part of it. This Lagrangian includes an infinite set of fields that are related to each other through all possible gauge transformations leading to a divergent value for the QCD partition function and making it impossible to quantize. In order to have a proper quantization of the theory one has to remove the physically equivalent configurations from the classical Lagrangian. This process is called *gauge fixing*. For a detailed procedure we refer to [48]. Since in this thesis we are only interested in the classical aspects of QCD we will not cover the quantization of the theory. In the remainder of this chapter we will briefly discuss some of the important properties of the color dynamics.

1.2 Asymptotic freedom

Besides the quark masses, which will be neglected along all the work presented in this thesis, the only parameter of QCD is the coupling constant g. However, even though it is not clear that the parameters appearing in the QCD Lagrangian are physically observable quantities, any physical observable can be calculated as a function of them (at least in perturbation theory) and their values can be extracted from measurements of physical observable.

Although it is out of the scope of this thesis, results that result directly from the utilization of renormalization techniques will appear constantly over this chapter. For this reason it is worthy of a short comment. When we perform higher order calculations in perturbation theory to compute some observable we shall encounter loop corrections with respect to the leading order (LO) calculation. These loop corrections introduce a scale, μ_R, that regulates the divergences appearing in the calculation. μ_R is known as *renormalization scale*. Since μ_R is an arbitrary scale, introduced by hand, the physics

should not depend on it. The way of making physical observable quantities independent of this artificial scale is by imposing a dependence of the coupling constant to $g(\mu_R)$. The set of differential equations that describe how the whole theory has to vary with the renormalization scale in order to keep physical quantities invariant are known as *renormalization group equations* (RGE).

One of the most important results achieved from RGEs and a remarkable property of QCD is *asymptotic freedom* [49, 50]. This property states that the interaction strength $\alpha_s = g^2/4\pi$ between quarks and gluons becomes smaller as the distance between them gets shorter or, equivalently, the momenta become larger. If we neglect higher order corrections, the solution of the renormalization group equation can be written as

$$\alpha_s(Q^2) = \frac{\alpha_s(\mu_R^2)}{1 + \alpha_s(\mu_R^2)\beta_0 \ln(Q^2/\mu_R^2)}, \tag{1.12}$$

where Q is an arbitrary momentum scale and

$$\beta_0 = \frac{11N_c - 2N_f}{12\pi}, \tag{1.13}$$

with $N_f = 6$ which implies that $\beta_0 > 0$ for $N_c = 3$.

Therefore it is obvious that

$$\lim_{Q^2 \to \infty} \alpha_s(Q^2) = 0. \tag{1.14}$$

Since Q can be interpreted as the inverse of the distance of the interaction the strength of the interaction becomes weaker at shorter distances. Thus quark and gluons interact weaker and weaker at smaller distances behaving as asymptotically free particles. This behavior has been verified by high energy experiments to a very high precision as shown in Fig. 1.3 with the data taken from the Particle Data Group collaboration [51]. In this figure Q stands for the running scale.

In QED, $\beta_0 < 0$, and thus the QED coupling constant becomes stronger at short distances in contrast to QCD. The reason of this difference is the self interacting nature of a non-Abelian theory. In QCD the gluon propagator not only receives corrections from quark loops (as in QED) but also from gluon loops. Equation (1.12) can be rewritten as

$$\alpha_s(Q^2) = \frac{1}{\beta_0 \ln(Q^2/\Lambda_{\mathrm{QCD}}^2)}, \tag{1.15}$$

where $\Lambda_{\mathrm{QCD}} \sim 200$ MeV is the perturbative scale of QCD. This parameter introduces a natural scale such that when $Q^2 < \Lambda_{\mathrm{QCD}}^2$ the coupling constant is not weak and one cannot apply weak-coupling techniques. However, when $Q^2 > \Lambda_{\mathrm{QCD}}^2$ we have $\alpha_s(Q^2) \ll 1$ and we can apply weak-coupling techniques. Thus, because of asymptotic freedom, the strong interaction physics can now be calculated in perturbation theory. In particular, the lowest order becomes a good approximation when $Q^2 \gg \Lambda_{\mathrm{QCD}}^2$. At present, the most accomplished result of QCD research is in the perturbative region, where many experimental data have been explained well by perturbative QCD (pQCD).

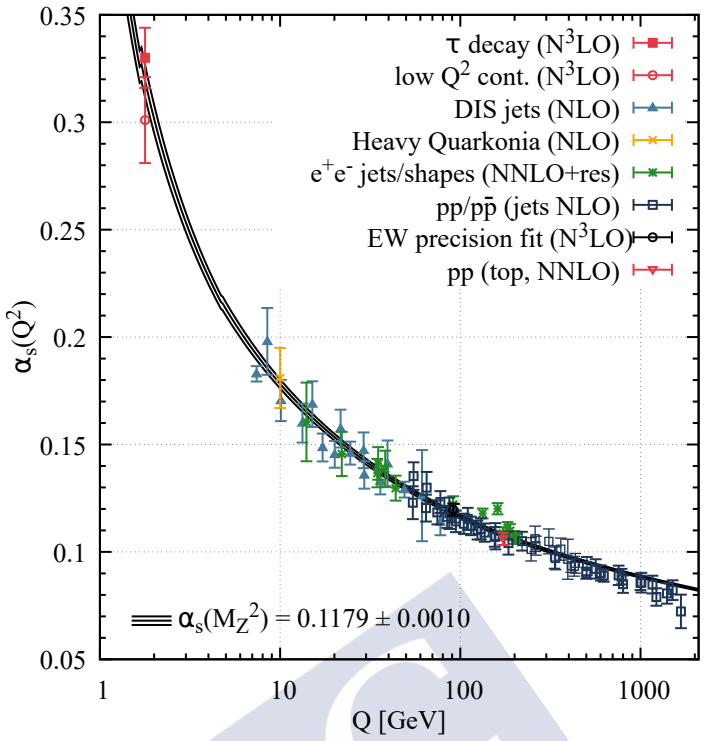

Figure 1.3.
The running of the QCD coupling constant as a function of momentum transfer. The figure has been taken from the Particle Data Group collaboration [51] with the authors' permission.

1.3 Deep Inelastic Scattering

One of the main challenges of QCD is to understand the inner structure of hadrons or nuclei. Nowadays, the nucleon is seen as a system of confined quarks and gluons. Therefore, only non-perturbative methods can describe its properties. In the non-perturbative regime of QCD, predictions of physical observable quantities related to the structure of the hadrons cannot be formulated from first principles but only within the framework of effective theories or phenomenological models. Non-perturbative methods have shown to be notoriously difficult in any quantum field theory and often provide only partial descriptions of the structure of hadrons.

Some of the more realistic non-perturbative predictions on the low-energy regime of hadronic systems are provided by lattice QCD calculations. However, despite of the success achieved in some subjects and the recent improvements [52], lattice QCD computations are still heavily limited by the available computational power.

Thus, experimental results are required to constrain models and to provide reliable information about the hadron inner structure. In particular, the study of deep inelastic electron-nucleon scattering is of great historical importance because it led to the first clear evidence for scattering from individual point-like constituents confined within the nucleon.

Deep Inelastic Scattering (DIS) is one of the simplest scattering processes that occur

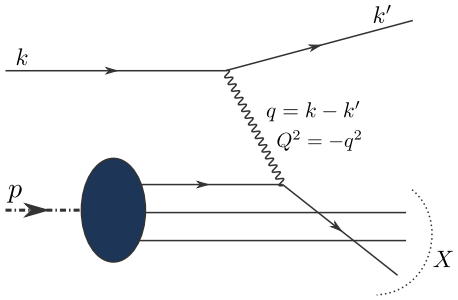

Figure 1.4.
Diagrammatic representation of a Deep Inelastic Scattering process where a high energetic lepton scatters in a hadron/nuclei by exchanging a boson.

at high energy. This process is given by the following reaction:

$$l + h \to l' + X, \tag{1.16}$$

where an incoming lepton l with 4-momentum k^μ interacts with the hadron h with 4-momentum p^μ by exchanging a virtual photon (we neglect the $W^\pm$ and Z^0 boson channels of the interaction) with 4-momentum $q^\mu = k^\mu - k'^\mu$. The final result is a lepton l' with 4-momentum k'^μ and a production of several hadrons labeled by X. This process is illustrated in Fig. 1.4. As the energy of the scattering is increased, much of the process is inelastic.

The kinematics of DIS can be characterized by the following Lorentz invariant quantities:

$$Q^2 \equiv -q^2, \tag{1.17}$$

$$x_{B_j} \equiv \frac{Q^2}{2p^\mu q_\mu}, \tag{1.18}$$

$$y \equiv \frac{p^\mu q_\mu}{p^\mu k_\mu}, \tag{1.19}$$

where Q^2 is usually referred as the virtuality of the photon and x_{B_j} is the Bjorken-x variable. The quantity Q^2 is always positive and represents a measure of the spacial resolution that can be resolved by a virtual photon with wavelength $1/|q|$. When $Q^2 > 1$ GeV^2 the virtual photon has enough resolution to probe the internal structure of the nucleon. Moreover, since the energies of the incident and scattered leptons are much larger than the lepton mass, the latter can be neglected in the definition of all kinematic variables introduced in this section.

In the inclusive measurements, the energy and scattering angle of the lepton are detected and the corresponding physical observables can be expressed only in terms of two independent variables such as x_{B_j} and Q^2. The DIS cross section can be written as the contraction of a leptonic tensor with a hadronic tensor,

$$\frac{d\sigma_{\text{DIS}}}{d^3k'} = \frac{\alpha^2}{2\hat{s}Q^4} L^{\mu\nu}(k,q) W_{\mu\nu}(p,q), \tag{1.20}$$

where α is the QED coupling constant, the leptonic tensor, $L^{\mu\nu}$, can be computed using perturbation theory and the hadronic tensor, at relatively low-Q^2 and in the single photon exchange approximation, can be parameterized in terms of two structure functions $F_{1,2}(x_{B_j}, Q^2)$

$$W_{\mu\nu} = -\left(g_{\mu\nu} - \frac{q_\mu q_\nu}{q^2}\right) F_1(x_{B_j}, Q^2) + \frac{(p_\mu + x_{B_j} q_\mu)(p_\nu + x_{B_j} q_\nu)}{m_p \nu} F_2(x_{B_j}, Q^2), \tag{1.21}$$

where $\nu = p \cdot q / m_p$ and m_p is the proton's mass. At leading order in perturbation theory a straightforward calculation leads to the following expression for the DIS cross section

$$\frac{d^2\sigma^{e^- p \to e^- X}}{dx_{B_j} dQ^2} = \frac{4\pi\alpha^2}{Q^4}\left[F_1(x_{B_j}, Q^2)[1 + (1-y)^2] + \left(F_2(x_{B_j}, Q^2) - 2x_{B_j} F_1(x_{B_j}, Q^2)\right)\frac{1-y}{x_{B_j}}\right]. \tag{1.22}$$

Through an analysis of current algebra, Bjorken predicted that the structure functions would become scale invariant at asymptotically large energies [53]:

$$\lim_{Q^2 \to \infty} F_{1,2}(x_{B_j}, Q^2) = F_{1,2}(x_{B_j}). \tag{1.23}$$

This property of $F_{1,2}$ is referred to as Bjorken scaling. A Q^2-independence of the structure functions would imply that the incoming lepton interacts with the same proton structure no matter how big the spatial resolution is. The observed scaling behavior could be successfully accounted for by considering scattering from point-like constituents within the proton, rather than from the proton as a whole. This was historically the first evidence of the quarks.

With the increased accuracy of DIS experiments and the broadening of kinematic regions explored, a noticeable Q^2 dependence of the structure functions appeared. This violation of the Bjorken scaling was a evidence of the dynamical structure of the proton as quarks can radiate gluons and was one of the earliest triumphs of QCD.

Moreover, Richard Feynman realized that the DIS measurements could be explained by assuming that the leptons were actually undergoing elastic scattering off of constituent objects inside the proton, which he called *partons*, that behaved as approximately free particles. This model is called *the quark parton model* (QPM) [54].

The QPM is conveniently formulated in a reference frame where the hadron moves with very high momentum, the so-called *infinite momentum frame*, such that the transverse momentum components and the rest mass of the constituents of the hadron can be neglected. In this frame the scattering can be seen as the absorption of a virtual photon by one of the collinearly moving partons inside the hadron. The struck parton, which carries a fraction $p_p = xp$ of the total momentum of the hadron, recoils with its original momentum reversed. If one assumes that the struck parton is on the mass-shell a straightforward calculation leads to $x = x_{B_j}$. Thus in the QPM the Bjorken x variable can be interpreted as the fractional momentum of the hadron carried by the struck quark. The model also requires the interaction between the individual partons to be weak on short distances. This situation is satisfied if the scattering occurs on sufficiently short time scales, i.e. much shorter than the typical time scales of the interactions between partons.

Moreover, in the QPM the hadron is described in terms of the *parton distribution functions* (PDFs) $f_i(x, Q^2)$, which represent the probability density to find in the nucleon a quark of flavour i and fraction momentum x at a given resolution Q^2. Therefore, the quantity $f_i(x, Q^2)dx$ represents the number of quarks with flavor i and fractional momentum in between x and $x + dx$. Thus, in the QPM the DIS cross section can be written as

$$\frac{d^2\sigma^{e^-p\to e^-X}}{dxdQ^2} = \int_0^1 dx f_i(x, Q^2)\hat{\sigma}_i(x, Q^2), \tag{1.24}$$

where $\hat{\sigma}_i(x, Q^2)$ is the cross section for the $\gamma^* q_i$ scattering process and can be computed using perturbation theory. Performing a leading order calculation in perturbation theory assuming that the partons are fermions with flavor i and electrical charge e_i leads to

$$\hat{\sigma}_i = \frac{4\pi\alpha^2}{Q^4}\frac{e_i^2}{2}[1 + (1 - y)^2]\delta(x_{B_j} - x). \tag{1.25}$$

A quick comparison between Eqs. (1.22) and (1.24) leads to the following relation between the structure functions

$$F_2(x, Q^2) = \sum_i e_i^2 x f_i(x, Q^2) = 2xF_1(x, Q^2). \tag{1.26}$$

This result is known as the Callan-Gross relation [55]. Experimental measurements were in agreement with the Callan-Gross relation and were the first evidence that partons are fermions.

Furthermore, if one adopts the quark interpretation of the partons, the PDFs would obey sum rules that momentum was conserved, the proton charge was exactly one, the isospin was equal to 1/2 and the net strangeness was 0. A careful analysis found that the momentum sum rule could only be satisfied by assuming that the strange and antistrange partons carried most of the proton's energy, or that there were partons that did not interact with the photons. This turned to be the first theoretical evidence for the existence of gluons in the interior of hadrons.

1.4 The improved parton model

As measurements in DIS processes became more accurate, the scaling of the structure functions, predicted by the quark parton model, turned out to be only approximately valid. Experimental results show that the structure function $F_2(x, Q^2)$ significantly increases at small x and slowly decreases at large x as a function of Q^2. This behavior cannot be explained in the framework of the QPM. However, this observation can be explained without abandoning the QPM, provided interaction among the partons, which were not accounted for in the early version of the model, are introduced. These interactions are provided by the framework of QCD and give rise to higher order corrections to the QPM. Next-to-leading order (NLO) calculations in perturbation theory of QCD introduces the possibility of gluon emission or absorption as well as virtual contributions. All these higher order corrections are taken into account in the so-called QCD improved Quark

Parton Model. According to this extended version of the QPM, quarks in the nucleons are dressed with a cloud of gluons and virtual quark-antiquark pairs, the so-called sea quarks.

The interaction among the partons together with the running coupling constant $\alpha_s(Q^2)$ could explain successfully the violation of the Bjorken scaling observed in the structure functions. The intuitive explanation of why these corrections become important as we go to *Regge limit* (small values of x at fixed Q^2) or the *Bjorken limit* (high values of Q^2 at fixed x) relays on the space-time interpretation of the kinematic variables x and Q^2. The variable x can be roughly interpreted as the time resolution of the virtual photon thus, in the Regge limit, the photon is able to probe shorter lived parton emissions that did not contribute at higher values of x. Analogously, in the Bjorken limit the space resolution of the virtual photon is higher and therefore it is able to resolve a larger number of quarks and gluons, all sharing the total hadronic momentum. For a detailed discussion on the space-time kinematics of DIS we refer to [47].

As discussed in Section 1.2 the calculation of virtual corrections to a physical observable introduces an artificial scale that has to be washed out through the renormalization group equations. Although the parton distribution functions are non-perturbative objects and therefore cannot be calculated analytically, the RGEs associated with these functions impose how the PDFs has to depend on the photon virtuality Q^2 through the Q^2-evolution equations. These equations were first proposed by Dokshitzer-Gribov-Lipatov-Altarelli-Parisi and are called DGLAP equations [14–17]. Here we will not perform a proper derivation of these equations since it is well introduced in the literature (see for example [47]). The DGLAP evolution equations for the sea quark and gluon PDFs can be written as

$$\frac{\partial}{\partial \ln Q^2}\begin{pmatrix}\Sigma(x,Q^2)\\ G(x,Q^2)\end{pmatrix} = \frac{\alpha_s(Q^2)}{2\pi}\int_x^1 \frac{dz}{z}\begin{pmatrix}P_{qq}(z) & P_{qg}(z)\\ P_{gq}(z) & P_{gg}(z)\end{pmatrix} \times \begin{pmatrix}\Sigma(x/z,Q^2)\\ G(x/z,Q^2)\end{pmatrix}, \tag{1.27}$$

where $\Sigma(x,Q^2) = f_q(x,Q^2) + f_{\bar{q}}(x,Q^2)$ is the sea quarks PDF and $G(x,Q^2)$ is the gluon PDF. $P_{ij}(z)$ are the so called (LO) splitting functions and give the probability of a parton i emitting another parton j carrying a fraction z of the longitudinal momentum of the parent parton. Despite of this result, Eq. (1.27) is only valid when $Q^2 > \Lambda^2_{\text{QCD}}$, where perturbation theory is a valid approach, and in order to be solved one needs to determine the PDFs at some initial virtuality Q_0^2. But once they are determined, they are universal and so pQCD can be predictive.

The procedure for determining PDFs in principle relies on using existing experimental data to fit PDFs, and use the PDFs afterwards as input for predictive calculations. The process of determining them is called *global QCD analysis*. In Fig. 1.5 we show the solution in NNLO NNPDF3.0 global analysis [56] evolved up to $Q^2 = 10$ GeV^2. Note that the gluon PDF is scaled down by a factor of 0.1. We can see clearly that the gluon and distribution dominate at small x.

The results of Fig. 1.5 can be anticipated analytically by realizing that as one moves to smaller values of x the integrand of Eq. (1.27) is enhanced by the $P_{qg} \sim 1/z$ and $P_{gq} \sim 1/z$ behavior while the other splitting functions are not. This behavior implies that, at small-x, the evolution of $G(x,Q^2)$ is enhanced with respect to $\Sigma(x,Q^2)$. Since we can assume that in this region the gluon PDF is much larger than the sea quarks PDF the splitting function P_{gq} can also be neglected. Thus, at low vales of x only the gluon

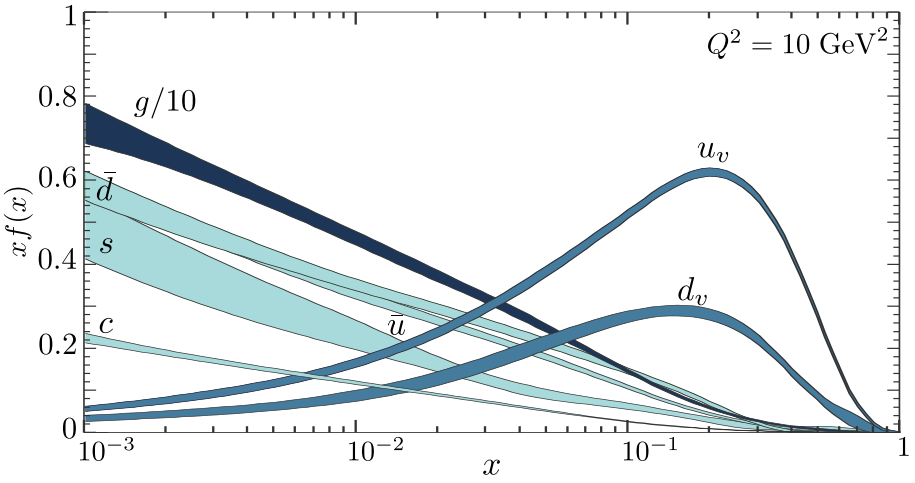

Figure 1.5.
The bands are x times the parton distribution functions obtained in NNLO NNPDF3.0 global analysis [56] at $Q^2 = 10$ GeV^2. In this plot c, s, $\bar{u}$ and $\bar{d}$ represent the sea quark PDFs (separately), g is the gluon PDF and u_v and d_v are the valence quarks PDFs. It is clear, since it is divided by 10, that the gluon PDF dominate at low-x. This figure has been taken from the Particle Data Group collaboration [51] with the authors' permission.

distribution functions play an important role and one can say that the hadronic dynamics is dominated by gluons. Since the region where x is small is equivalent to the high energy limit of the virtual photon-hadron collision we can also say that at high energy the degrees of freedom are populated by gluons.

We can move forward analytically by noting that the probability of a gluon emitting another gluon with transverse momentum $\mathbf{k}$ and with a small-x fraction of longitudinal momentum, i.e. in the soft ($x \ll 1$) and collinear ($|\mathbf{k}| \ll 1$) limits, is

$$P = \frac{\alpha_s N_c}{\pi} \frac{dx}{x} \frac{d^2\mathbf{k}}{\mathbf{k}^2}. \tag{1.28}$$

Thus, in the low-x and high-Q^2 regime the probability of gluon emission is not only enhanced by the logarithm of Q^2 but also by the logarithm of $1/x$. For this reason we usually refer to this regime as the double logarithm approximation (DLA). In the DLA DGLAP regime, the evolution of the gluon distribution function is governed by subsequent real gluon emissions. One can then construct the solution of the DLA DGLAP equation by summing diagrams that iterate the gluon-gluon splitting function [47]. Diagrams iterating the gluon emissions have a ladder structure as shown in Fig. 1.6. In this diagram the transverse momenta of the gluons in the rungs of the ladder are ordered as:

$$Q^2 \gg \mathbf{k}_n^2 \gg \mathbf{k}_{n-1}^2 \gg \cdots \gg \mathbf{k}_1^2 \gg Q_0^2 \gg \Lambda_{\text{QCD}}^2. \tag{1.29}$$

Moreover, since we are interested in the small-x limit of DGLAP, the longitudinal momenta of the gluons in Fig. 1.6 are also ordered as:

$$P^+ \gg k_1^+ \gg k_2^+ \gg \cdots k_{n-1}^+ \gg k_n^+ \gg k^+, \tag{1.30}$$

in order to generate logarithms of $1/x$. Here we have introduced the light-cone coordinates, explained in Appendix A, that will be used along the rest of this thesis. Therefore the probability of a gluon emitting n gluons that are ordered both in transverse and longitudinal momenta is given by

$$\begin{aligned} P_n &= \int_{Q_0^2}^{Q^2} \frac{\bar{\alpha}_s d^2\mathbf{k}_1}{\mathbf{k}_1^2} \int_{\mathbf{k}_1}^{Q^2} \frac{\bar{\alpha}_s d^2\mathbf{k}_2}{\mathbf{k}_2^2} \cdots \int_{\mathbf{k}_{n-1}}^{Q^2} \frac{\bar{\alpha}_s d^2\mathbf{k}_n}{\mathbf{k}_n^2} \int_{k^+}^{P^+} \frac{dk_1^+}{k_1^+} \int_{k^+}^{k_1^+} \frac{dk_2^+}{k_2^+} \cdots \int_{k^+}^{k_{n-1}^+} \frac{dk_n^+}{k_n^+} \\ &= \frac{1}{n!^2} \left[\bar{\alpha}_s \ln \frac{Q^2}{Q_0^2} \ln \frac{1}{x} \right]^n , \end{aligned} \tag{1.31}$$

where we have introduced $\bar{\alpha}_s \equiv \alpha_s N_c/\pi$ and we have neglected the running of the coupling constant.

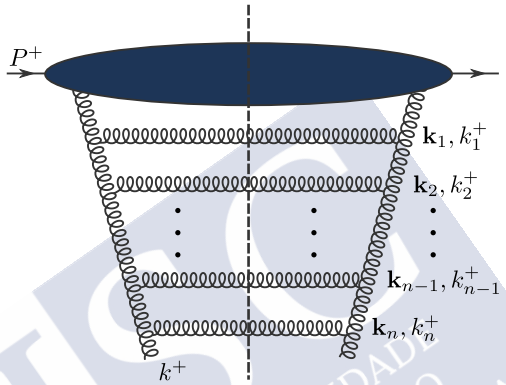

Figure 1.6.
Example of the ladder diagram that is used in the DLA DGLAP evolution equation. In this diagram both the transverse and longitudinal momenta are ordered.

The gluon distribution function can be estimated by summing the probability of subsequent gluon emission and the result is

$$G(x,Q^2) \sim \sum_{n=0}^{\infty} P_n = I_0\left(\sqrt{4\bar{\alpha}_s \ln\frac{Q^2}{Q_0^2}\ln\frac{1}{x}}\right) \approx \frac{\exp\left\{\sqrt{4\bar{\alpha}_s \ln\frac{Q^2}{Q_0^2}\ln\frac{1}{x}}\right\}}{\left(16\pi^2\bar{\alpha}_s \ln\frac{Q^2}{Q_0^2}\ln\frac{1}{x}\right)^{1/4}}, \tag{1.32}$$

where in the last equality we have used the fact that $x \ll 1$ and used the large argument expansion of the Bessel function. We can infer from Eq. (1.32) that the DLA DGLAP solution predicts a rise in the gluon distribution at low-x that is faster than any power of $\ln\frac{1}{x}$ but slower than $\frac{1}{x}$. This rise in concordance of what we have seen in Fig. 1.5. The prediction that the gluon PDF grows faster than any power of $\ln\frac{1}{x}$, as we will see later, implies a unitarity violation and is the indication that we are missing some information in the small-x calculation of the gluon distribution function.

1.5 The saturation regime

So far, the DGLAP equations offer a framework to study the dynamics of the hadrons in a region where we keep x fixed and we increase Q^2 or, in the case of the DLA DGLAP equation, we keep x small. However, if one is interested in studying the Regge limit of QCD, i.e. small values of x at a fixed value of Q^2, we have to go beyond the DGLAP approach. In the Regge limit we aim to resum powers of $\ln\frac{1}{x}$ rather than powers of $\ln Q^2$. Resummation of the leading logarithms of $1/x$ instead of those of Q^2 is the essential paradigm shift needed in studying the small-x asymptotics of QCD. The equation resumming leading logarithms of $1/x$ will be, unlike the DGLAP equation, an evolution equation in x and not in Q^2.

Because of the arguments presented when we discussed about the DLA DGLAP equation, in the Regge limit of QCD the relevant degrees of freedom are gluons and the leading mechanism for evolution is gluon radiation. This suggests that the gluon content of hadrons evolve at small-x via cascades such as those displayed in Fig. 1.6. The main difference with respect to the DLA DGLAP is that, since now we are only interested in resumming powers of $\ln\frac{1}{x}$ rather than $\ln Q^2$, we only have to impose ordering in the longitudinal momenta of the emitted gluons. We are thus abandoning the strong ordering in transverse momenta characteristic of the DGLAP radiative cascade, considering instead a random walk in the $\mathbf{k}$-space. As long as these cascades do not interact, the evolution can be described by a linear equation for the gluon distribution: the Balitsky-Fadin-Kuraev-Lipatov (BFKL) equation [18, 19], that provides the x-dependence of the *non-integrated gluon distribution*. The BFKL equation can be written as

$$\frac{\partial\phi(x,\mathbf{k}^2)}{\partial\ln\frac{1}{x}} = \frac{\alpha_s N_c}{\pi^2}\int\frac{d^2\mathbf{q}}{(\mathbf{k}-\mathbf{q})^2}\left[\phi(x,\mathbf{q}^2) - \frac{\mathbf{k}^2}{2\mathbf{q}^2}\phi(x,\mathbf{k}^2)\right], \tag{1.33}$$

where $\phi(x,\mathbf{k}^2)$ is the unintegrated gluon distribution (UGD). The UGD is related to the GPD as

$$xG(x,Q^2) = \int_0^{Q^2} d^2\mathbf{k}\phi(x,\mathbf{k}^2). \tag{1.34}$$

Thus $\phi(x,\mathbf{k}^2)$ counts the number of gluons in the interior of a hadron with a transverse momentum $\mathbf{k}$ and Bjorken-x while $xG(x,Q^2)$ counts the number of partons with momentum $\mathbf{k}^2 \leq Q^2$.

In the case of DIS, the BFKL equation succesfully predicted the rapid growth of the cross section with increasing energies, which was subsequently observed experimentally. However, the solution of the BFKL equation yields a gluon distribution that shows an even more singular behavior in the small-x limit than the DGLAP solution of Eq. (1.32). The solution of Eq. (1.33) behaves at small-x as

$$\phi(x,\mathbf{k}^2) \sim x^{-\frac{4N_c\ln 2}{\pi}\alpha_s}, \tag{1.35}$$

which also violates unitarity constraints as we will see below. The origin of this malfunction is the linear nature of Eq. (1.33).

We haven seen that the solution of the gluon distribution function has a growth with $1/x$ that is larger than any power of $\ln\frac{1}{x}$ both for the DLA DGLAP solution in Eq. (1.32)

and the BFKL solution in Eq. (1.35). Such asymptotic behavior leads to the violation of unitary, which is a fundamental requirement of any quantum theory. It is well known in particle physics that the requirement of unitarity introduces the following bound for hadron-hadron cross sections

$$\sigma_{tot}(s) \leq \frac{1}{m_\pi^2} \ln^2 s, \tag{1.36}$$

where m_π is the pion mass and s is center of mass energy of the collision. This is known as the Froissart bound [57]. This bound was derived by using the fact that there is a mass gap between the vacuum and the lowest energy state of QCD. However, it can also be derived by using the optical theorem and the black disk limit [47]. If one uses the BFKL solution for the GPD, the small-x cross section behaves as $\sigma(s) \sim s^{\frac{4N_c \ln 2}{\pi}\alpha_s}$ which clearly violates the Froissart bound. Since both the DGLAP and the BFKL equations are computed in the framework of perturbative QCD it makes sense to assume that whatever is the mechanism that is being missed in order to recover unitarity it has to happen in the perturbative regime.

For a better understanding of the small-x evolution of the hadron let us make a qualitative study of the space-time structure of the BFKL cascade in this regime. In the infinite momentum frame, the BFKL cascade can be seen as a cascade in the hadron's wave function. The fast hadron will decay into a system of partons long before the interaction with the virtual photon, that is at rest. The time ordering of emissions of the gluon cascade, with each gluon as a roughly fixed transverse momenta, is given by

$$x_1^+ \gg x_2^+ \gg \cdots \gg x_n^+, \tag{1.37}$$

where we have used the fact that $x_i^+ \propto 1/k^- \sim k_i^+/\mathbf{k}_i^2$. During the long time of the gluon-cascade evolution a large numbers of "wee" partons are created in the hadron's wave function. Thus, the QCD evolution of both DGLAP and BFKL leads to an increase in the number of "wee" partons with energy.

Since the transverse momenta of the radiated gluons are not ordered in the BFKL cascade, the transverse size of each gluon is roughly the same. As we decrease x the gluon density grows. When the gluons become densely packed in the hadron's wavefunction, the interaction between gluons from different cascades cannot be neglected anymore. These mergings of gluons from different cascades slow down the increase of the gluon distribution function at small-x. This effect is known as *saturation*.

In order to deal with the BFKL unitarity problem Gribov, Levin and Ryskin (GLR) [13] considered the gluon distribution function of a saturated hadron or nucleus. In this regime they considered the possibility of recombination of BFKL cascades. The resulting equation is the non-linear GLR evolution equation which reads

$$\frac{\partial \phi(x, \mathbf{k}^2)}{\partial \ln \frac{1}{x}} = \frac{\alpha_s N_c}{\pi} \int d^2\mathbf{q} K_{\text{BFKL}}(\mathbf{k}, \mathbf{q}) \phi(x, \mathbf{k}^2) - \frac{\alpha_s^2 N_c \pi}{2 C_F S_\perp} \left[\phi(x, \mathbf{k}^2)\right]^2, \tag{1.38}$$

where $K_{\text{BFKL}}(\mathbf{k}, \mathbf{q})$ is the BFKL kernel, $S_\perp = \pi r_h^2$ and r_h is the hadron radius. The first term of Eq. (1.38) is just the BFKL equation and the second term, responsible for ladder mergers, introduces damping and thus slows down the growth of the gluon distributions with energy. We note that the non-linear term comes with an extra power of α_s since the merging of two gluon cascades requires two extra powers of the strong coupling.

An analogous equation derived by Mueller and Qiu [58] by considering the merging of two DLA DGLAP cascades is the following

$$\frac{\partial^2 xG(x,Q^2)}{\partial \ln \frac{1}{x} \partial \ln Q^2/\Lambda^2} = \frac{\alpha_s N_c}{\pi} xG(x,Q^2) - \frac{\alpha_s^2 N_c \pi}{2C_F S_\perp} \left[xG(x,Q^2)\right]^2 . \tag{1.39}$$

This equation is known as the GLR-MQ equation and give us a evolution in both Q^2 and x.

We can define a critical value for the photon's virtuality Q, Q_s, at which saturation effects become important when $Q < Q_s$, i.e. the gluon recombination process starts to happen in the small-x hadron's evolution. This scale is known as *saturation momentum*. It can be estimated by equating the right hand side of Eq. (1.39) to zero leading to

$$Q_s^2 = \frac{\alpha_s \pi^2}{2S_\perp C_F} xG(x,Q_s^2). \tag{1.40}$$

Since the gluon distribution function behaves as $xG \sim x^{-\lambda}$, with $\lambda > 0$, near the saturation region and for a nucleus consisting of A nucleons we have to multiply the GPD by the factor A we can write the saturation momentum as

$$Q_s^2 \sim \frac{Ax^{-\lambda}}{S_\perp} \sim A^{1/3} x^{-\lambda}, \tag{1.41}$$

where we have used the fact that $S_\perp \sim A^{2/3}$. Therefore the saturation momentum not only grows with decreasing x but also it is larger for large nuclei. Thus saturation effects are more important for DIS on a nucleus than on a hadron. Phenomenological studies performed by using data from HERA [59, 60] suggests that $\lambda \sim 0.3$. We expect, for example, the numerical value of the saturation momentum to be $Q_s \approx 1.2$ GeV at RHIC (gold collisions at $x \sim 10^{-2}$) or $Q_s \approx 2$ GeV at LHC (lead collisions at $x \sim 10^{-4}$).

Since the saturation regime is achieved through the inequality $Q \leq Q_s$ and Q_s is defined as a function of x via Eq. (1.41) we can divide the (x,Q^2) plane into two domains: the saturation region where the non-linear effects are important and the dilute region where the BFKL and DGLAP evolution equations still hold. In Fig. 1.7 we illustrate these regimes.

Moreover, we should note that the relevant density in this system is the number of gluons per unit transverse area. Indeed, the boost in the longitudinal direction turns the nucleon into a thin pancake due to Lorentz contraction. The longitudinal resolution of the probe becomes larger than the thickness of the Lorentz contracted hadron, and the probe therefore cannot resolve the gluon distribution in the longitudinal direction. It only sees the total number of gluons integrated over the longitudinal direction. This surface density is roughly

$$\rho_g(x,Q^2) = \frac{xG(x,Q^2)}{S_\perp}. \tag{1.42}$$

Therefore we can write

$$\frac{\rho_g(x,Q_s^2)}{Q_s^2} \sim \frac{1}{\alpha_s}, \tag{1.43}$$

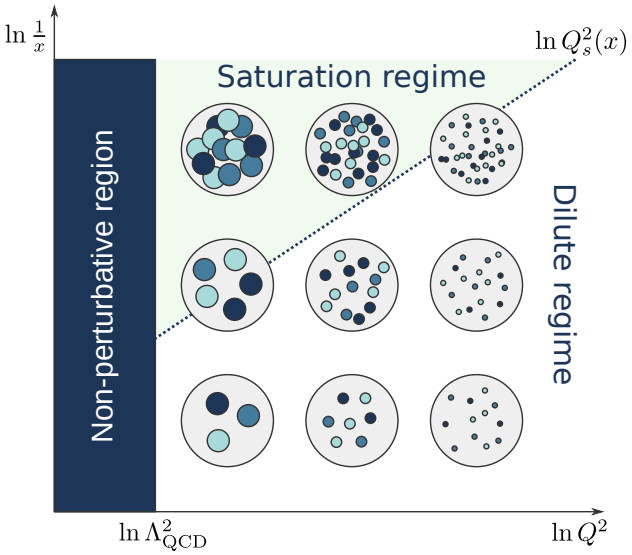

Figure 1.7.
The saturation regime is the region in the (x, Q^2) plane where non-linear effects become to be important and the DGLAP and BFKL equations are no longer valid.

i.e. the number of gluons per unit transverse area multiplied by the gluon transverse size has to be of order $1/\alpha_s$ in order to the non linear effects to become important. Noting that the gluon PDF is derived formally from the expected value of the gluon field square, $xG(x, Q^2) \sim \langle A^\mu A_\mu \rangle$, we can infer that in the critical limit where $Q = Q_s$ we have that

$$A_\mu \sim \frac{1}{g}. \tag{1.44}$$

Thus the gluon field in the small-x and $g \ll 1$ limit of the hadron's wave function is parametrically very strong.

1.6 The McLerran-Venugopalan model

In the previous section, we have described the phenomenon of gluon saturation at a qualitative level. Now we will move one step forward and provide a more theoretical description of the hadronic and nuclear systems in the saturation or low-x regime. The inclusion of gluon recombination processes in evolution introduced a dimensional scale at which they become relevant, the saturation momentum Q_s. As we have seen in Eq. (1.41), at small-x the saturation momentum becomes large. If $Q_s^2 \gg \Lambda^2_{\mathrm{QCD}}$, as experimental data suggest, then the coupling constant is weak since $\alpha_s(Q_s) \ll 1$. Field theories with small coupling are usually dominated by classical fields, with the quantum corrections suppressed by extra powers of the small coupling constant α_s. On the other hand, the large-x region of the hadronic wave function, mostly composed by the valence quarks as Fig. 1.5 suggests, is governed by a strong coupling and therefore we cannot use weak coupling techniques to describe this regime. Thus it is necessary to introduce some simplification in order to address the valence region of the hadron or nucleus.

In the infinite momentum frame (IMF), where the parton model is described, the hadron or nucleus moves by convenience in the positive x^3 direction with a very large light-cone momentum $P^+ \gg \Lambda_{\rm QCD}$. The IMF introduces a separation between *fast* and *soft* modes where partons that carry a large-x fraction of the hadron or nucleus momentum have a larger lifetime, with a mean life $\Delta x^+ \sim xP^+$, and are more sharply localized around the light cone, within a distance $\Delta x^- \sim 1/xP^+$, than the small-x partons. Thus the fast modes of the hadron/nucleus wave function are quasi-static over the time scales relevant in an interaction process. On the other hand, the small-x partons of the hadronic wave function, composed mostly by gluons, are not well localized in the longitudinal direction and its spread can be even larger than the size of the hadron or nucleus. However, the small-x gluons can be localized in the transverse direction on the scale $x_\perp \sim 1/k_\perp$, where $k_\perp \sim Q_s$ is the typical transverse momentum of the gluons in the hadron/nucleus wave function. If $k_\perp \gg \Lambda_{\rm QCD}$, which is the case in the high energy limit, the transverse extent of the gluons is much smaller than the size of the hadron. Because of that, the gluons only interact with part of the hadron in the transverse direction, as illustrated in Fig. 1.8. As a result the gluons interact with the net effective color charge of the large-x partons that are "seen" by them over the longitudinal direction.

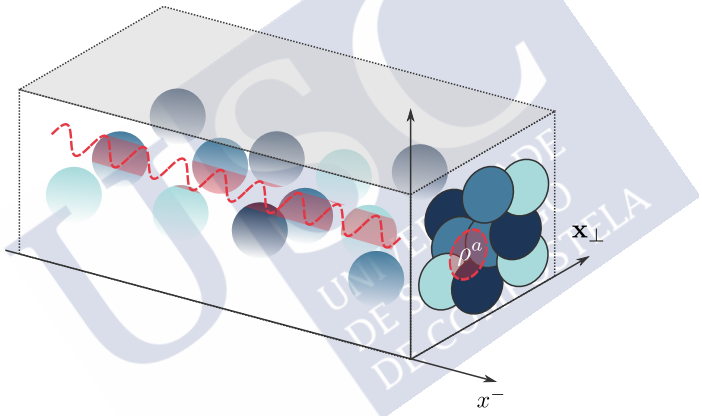

Figure 1.8.
A small-x gluon interacts with the whole hadron/nucleus coherently in the longitudinal direction but, since it is localized in the transverse direction, it only "sees" an effective color charge density ρ^a in the transverse plane.

The idea behind the McLerran-Venugopalan (MV) model [26,27] is to replace the fast modes of the hadron or nucleus wave function by simpler degrees of freedom that retain only the fundamental aspects that are needed to compute gluon radiation while continuing to treat the slow gluons as gauge fields. Because of the arguments presented above, in order to specify the fast partons degrees of freedom it is enough to know the color charge density related to these partons.

Therefore, the MV model introduces "by hand" a cutoff Λ^+ in the longitudinal momentum k^+ of the partons in order to separate the fast and slow modes. The fast partons will be defined by having $k^+ > \Lambda^+$ and will be replaced by some color source $\rho^a(x^-, \mathbf{x})$ defining the following color current:

$$J^{\mu,a}(x^-, \mathbf{x}) = g\delta^{\mu+}\rho^a(x^-, \mathbf{x}). \tag{1.45}$$

The + component of the current is the only important one because the source is traveling close to the speed of the light. The source $\rho^a(x^-, \mathbf{x})$ is a c-number color charge density which is a random variable on the transverse plane. The lack of dependence on the x^+ component expresses the fact that the fast partons have a very large lifetime and therefore can be assumed to be "frozen" in time.

The slow gluons are defined by having longitudinal momenta $k^+ < \Lambda^+$ and are still described by the usual gauge fields $A^{\mu,a}$ and their action is the standard Yang-Mills action. Because of the high occupancy number of the gluons in the small-x regime, the gauge field defining them can be assumed to be classical. The dynamics that governs the gluon fields can be summarized into the following action:

$$\mathcal{S} = \int d^4x \left(-\frac{1}{2} F^a_{\mu\nu} F^{\mu\nu,a} + J^a_\mu A^{\mu,a} \right), \tag{1.46}$$

where the first part is the classical Yang-Mills action and the interaction term $J^a_\mu A^{\mu,a}$ is the standard coupling between the sources and fields. We can obtain the equations of motions of the gluon field by minimizing this action obtaining

$$[D_\mu, F^{\mu\nu}] = J^\nu. \tag{1.47}$$

The last step for defining the theory is to specify a model for the color charge density ρ^a. ρ^a describes the distribution of charges of the fast moving partons with $k^+ > \Lambda^+$. Although the large-x partons have a large lifetime, much larger than the interaction time, their distribution will change from collision to collision. This phenomenon reminds the typical dynamics of a glass where the constituents of the glass appear to be frozen (acting as a solid) in a typical human lifetime but its structure changes at a very large times ($\sim$ 100 years). Thus, the color charge density ρ^a has to be treated as a stochastic variable and we should complement the MV model with a statistical distribution $W[\rho]$ for the sources.

The form of the functional $W[\rho]$ can be modeled if we assume a large nucleus[1]. The MV model assumes that the color charge density is not correlated in the transverse plane. Moreover, at some fixed transverse point $\mathbf{x}$, the source $\rho^a(x^-, \mathbf{x})$ is defined by a coherent sum of color charges of the nucleons in the longitudinal direction as illustrated in Fig. 1.8. These charges are also random and uncorrelated. Thus the Central Limit Theorem implies that the statistical distribution of the sources is a Gaussian distribution. Under these assumptions the distribution $W[\rho]$ reads

$$W[\rho] = \exp\left\{ -\int dx^- \int d^2\mathbf{x} \frac{\rho^a(x^-, \mathbf{x}) \rho^a(x^-, \mathbf{x})}{2\mu^2(x^-)} \right\}, \tag{1.48}$$

where $\mu^2(x^-)$ is a parameter proportional to the color source number density that acts as the spread of the Gaussian weight.

Given the distribution in Eq. (1.48) for the functional weight $W[\rho]$, the calculation of the expectation value of an observable $\mathcal{O}$ is performed in the MV model as follows. First, we compute the observable at some arbitrary configuration ρ^a of the color sources, obtaining $\mathcal{O}[\rho]$. At leading order it is enough to solve the classical Yang-Mills equation in

[1] The argument can be sometimes extended to hadrons by assuming that on such scales we perceive locally uncorrelated quarks whose charges add together in a random walk in color space.

Eq. (1.47). Then, we perform an average of the observable over all possible configurations for the color charge density

$$\langle \mathcal{O} \rangle = \frac{1}{\mathcal{N}} \int \mathcal{D}\rho W[\rho] \mathcal{O}[\rho], \tag{1.49}$$

where $\mathcal{N} = \int \mathcal{D}\rho W[\rho]$ is a normalization constant.

The main implications of the Gaussian ansatz is given by the following correlators

$$\langle \rho^a(x^-, \mathbf{x}) \rangle_{\text{MV}} = 0, \tag{1.50}$$

$$\langle \rho^a(x^-, \mathbf{x}) \rho^b(y^-, \mathbf{y}) \rangle_{\text{MV}} = \mu^2(x^-) \delta^{ab} \delta(x^- - y^-) \delta^{(2)}(\mathbf{x} - \mathbf{y}). \tag{1.51}$$

The MV model was able to achieve successful results in explaining many phenomenological observables. For example it was able to describe the DIS structure functions [61]. However, the assumption that the color charge density is local both in color and space can be sometimes unrealistic. For this reason many alternatives for the MV or Gaussian weight presented in this section were proposed recently to go beyond the quadratic form of Eq. (1.48), for example, by including cubic and quadruple terms [62] or by relaxing the eikonal approximation [63]. Moreover, the MV model is a semi-classical theory and therefore all the observable quantities are computed only at the tree level which may be not sufficient in some cases. In the next section we will discuss how to include quantum corrections to this model.

1.7 The Color Glass Condensate

Although the definition of the soft and fast moves of the nuclear wave function depend on the parameter Λ^+, the MV model does not have an explicit dependence on Λ^+. However we should note that this model is only valid when the small-x gluons have a fraction of momentum $x \lesssim \Lambda^+/P^+$. As we probe smaller values of x, the gluons are more likely to be generated from other soft modes than from the fast ones. The interaction between the soft modes are accounted by including quantum corrections to the classical field that will generate logarithms of Λ^+ [64]. As usual in any loop calculation, the inclusion of the quantum corrections will introduce a dependence on the artificial scale Λ^+ that will have to be "washed out" by the renormalization group equation. The RGE for the MV model was derived by Jalilian-Marian, Iancu, McLerran, Weigert, Leonidov and Kovner (JIMWLK) over a series of papers [28–32]. In order to do so, one has to absorb the logarithms of Λ^+ into a redefinition of the color sources $\rho^a(x^-, \mathbf{x})$ by adding "layers" of new sources at lower x. In this case the weight function obtain a dependence on Λ^+ through

$$W[\rho] \to W_{\Lambda^+}[\rho], \tag{1.52}$$

and it obeys an equation of the form

$$\frac{\partial W_{\Lambda^+}[\rho]}{\partial \ln \Lambda^+} = \mathcal{H}_{\text{JIMWLK}} W_{\Lambda^+}[\rho], \tag{1.53}$$

where $\mathcal{H}_{\text{JIMWLK}}$ is an operator that contains first and second order functional derivatives with respect ρ^a. Eq. (1.53) is the RGE of the MV model and is known as the JIMWLK equation where the MV weight of Eq. (1.48) serves as an initial condition for this equation.

Although Eq. (1.53) looks simple it is extremely difficult to be solved. Eq. (1.53) can also be written as an hierarchy of evolution equations for the correlator of the product of n Wilson lines[2] [65, 66], also known as n-point function or multipole. These equations are however nested since the evolution equation for the n-point function will depend on some m-point function with $m > n$. In particular the first equation of the hierarchy that evolves the 2-point function (dipole) will depend on the 4-point function (quadrupole). It has been proved [67, 68] that in the large-N_c limit and for a large nucleus, the quadrupole can be written as a product of two dipoles. In this case the JIMWLK equation for the dipole reduces to a closed and non-linear function known as the Balitsky-Kovchegov (BK) equation. Since the BK equation is much simpler than the JIMWLK equation, the first is mostly used in phenomenological analysis.

The effective theory that encodes the MV model, where we separate the soft and fast modes in the hadron/nucleus wave function through the scale Λ^+, and the JIMWLK evolution equation, where we make the physically observable quantities independent of the scale Λ^+, is known as the *Color Glass Condensate* (CGC). The name follows from the fact that the small-x limit of the hadronic wave function is populated by gluons which have *color* degrees of freedom. The *glass* nature follows because the fast partons are Lorentz dilated in time and evolve slowly compared to the interaction time. Moreover, the gluon fields produced by the sources are disordered in time a property that is also typical of glasses. Finally, the gluons are densely packed in the hadron/nucleus and we expect that the high density limit of such a system to be a Bose *condensate*. For an extensive review of the CGC we refer to [33–37].

[2] In the next chapter we will provide a proper definition of the Wilson lines.

Chapter 2

Particle production in the Color Glass Condensate

In the previous chapter we have introduced the Color Glass Condensate (CGC), an effective theory of high energy (or small-x) QCD where the hadronic or nuclear wave function is separated into fast modes, defined by a random color source $\rho^a(x^-, \mathbf{x})$, and slow modes, defined by a strong classical gluon field $A^\mu(x^-, \mathbf{x}) \sim 1/g$. The next goal is to introduce the process of particle production in high energy collisions which has been successful described within the CGC framework. In particular, we are interested in those scatterings where the participants are either a hadron or a nucleus, i.e. proton-proton (pp), proton-nucleus (pA) and heavy ion collisions (HICs).

The Bjorken-x of the collision's participants can be estimated by analyzing the kinematics of the scattering. High energy scatterings are performed in particle accelerators at some center-of-mass energy $\sqrt{s}$. If the energy of the collision is high, the scattering produces a very high number of particles (mostly hadrons) per unity of rapidity[1] in the final state. Moreover, mostly of the produced particles have a small transverse momentum compared to $\sqrt{s}$ and its value is similar to Q_s which suggests that the particle production mechanism is governed by saturation effects. In particular, a heavy ion collision can be understood as many partonic collisions and because of the high energy nature of the scattering mostly of these partons are gluons. Let us assume that an ultra-relativistic *projectile*'s gluon moves in the light-cone + direction with momentum $p_p^\mu = (p_p^+, 0, \mathbf{0})$ and collides with a *target*'s gluon moving in the − direction with momentum $p_T^\mu = (0, p_T^-, \mathbf{0})$. The simplest assumption is that a single particle is produced in this collision with momentum $P^\mu = (p_p^+, p_T^-, \mathbf{0})$. The fraction of the nucleus momentum carried by each gluon is given by $x_p = \sqrt{2}p_p^+/\sqrt{s}$ for the projectile and $x_T = \sqrt{2}p_T^+/\sqrt{s}$ for the target. By defining the transverse mass of the final state as $M_\perp = \sqrt{P^\mu P_\mu}$, the Bjorken-$x$ of each gluon can be defined in terms of the pseudorapidity η of the produced particle by using Eq. (2.1) as

$$x_p = \frac{M_\perp}{\sqrt{s}} e^{\eta}, \qquad x_T = \frac{M_\perp}{\sqrt{s}} e^{-\eta}. \tag{2.2}$$

[1] The rapidity y is a measure of the relativistic velocity of a particle. It is related with the Lorentz factor of some boost by $\gamma = \cosh y$. At high energy, the rapidity is equivalent to the pseudorapidity η which is a measure of the angle of the particle relative to the beam axis and can be defined as

$$y = \eta = \frac{1}{2} \ln \frac{p^+}{p^-} = \ln \frac{p^+}{\sqrt{2}|\mathbf{p}|}, \tag{2.1}$$

where $p^\mu = (p^+, p^-, \mathbf{p})$ is the 4-momentum of the particle in light-cone coordinates and, in the case where the particle is on-shell, $p^- = \mathbf{p}^2/2p^+$ is its light-cone energy.

Taking into account that $M_\perp \sim 1$ GeV at both the LHC ($\sqrt{s} \sim 10^3$ GeV) and RHIC ($\sqrt{s} \sim 10^2$ GeV), we can separate the origin of a single particle production into two regions. If the rapidity of the produced particle is not so large ($\eta \lesssim 4$ at LHC or $\eta \lesssim 1$ at RHIC), a region known as *mid-rapidity*, the fraction of momentum carried by the colliding particles are $x_T \ll x_p \ll 1$ and therefore both the projectile and the target are governed by the saturation physics and the CGC is a good framework for describing both of them. On the other hand, if the rapidity of the produced particle is large, a region known as *forward rapidity*, the fraction of momentum carried by the gluons are $x_T \ll x_p \lesssim 1$ and therefore the target is dominated by the saturation physics while the projectile is dilute. In this case the CGC is a good framework for describing the target while the projectile is described by the usual collinear approach, the overall formalism to describe this kind of collisions is known as the *hybrid formalism*.

Since the CGC offers a good framework for describing high energy collisions at both mid- and forward rapidities, the aim of this chapter is to introduce the technical aspects of the CGC in order the explain the particle production in such collisions. This chapter is organized as follows. In Section 2.1 we review the basic aspects of quantum field theories coupled to strong fields. In Section 2.2 we solve the linearized Yang-Mills equation in order to obtain the non-eikonal gluon spectrum in pA collisions. In Section 2.3 we review the eikonal approximation and we compute the eikonal single inclusive gluon production in pA collisions. In Section 2.4 we introduce the Wigner function approach that will be important in the numerical analysis of multi-particle correlations performed in Section 4.2. Finally, in Section 2.5 we perform the dilute limit of the eikonal gluon spectra leading to the so-called Glasma Graph approximation.

2.1 Basic aspects of field theories coupled to strong sources

As we have seen in Section 1.6, the Color Glass Condensate is described by a gluon field ruled by the classical Yang-Mills action coupled to a strong current, Eq. (1.46). This current is written in terms of a random color source $J \propto g\rho^a(x^-, \mathbf{x}) \sim 1/g$. The strength of the source implies that, although the coupling constant is weak, the theory is non-perturbative. Thus, in order to compute any observable in the saturation region of QCD one has to resum powers of $g^2\rho$. As we shall see in this chapter, in some cases it is possible to perform this resummation into a closed form in terms of the classical Yang-Mills equation's solution.

The action introduced in Eq. (1.46) is composed by a free term, the triple and quadruple self interaction vertices and the coupling of the gluon field with the source. The Feynman rules associated with this Lagrangian will be given by the triple gluon vertex that is of order g, the quadruple gluon vertex of order g^2 and the source vertex of order $\rho \sim 1/g^2$. Thus for a *connected* diagram, its order in the coupling constant will be given by [69]

$$\frac{1}{g^2} g^{n_g} g^{2n_L} (g^2\rho)^{n_S}, \tag{2.3}$$

where n_g is the number of produced gluons (external lines), n_L the number of loops and n_S the number of sources in the diagram. Since in the saturation region $g^2\rho \sim 1$, the order of all the connected diagrams in this regimes will be independent of the number of sources. Moreover, a counting in the powers of $\hbar$ of a given diagram will lead to $\hbar^{n_g+n_L-1}$. Thus in the case where $n_L = 0$ and $n_g = 1$ the diagram will be purely classical. Thus single gluon production at leading order in g will be ruled by the classical equations of motion.

The relation given in Eq. (2.3) introduces a double expansion of any observable calculated within the CGC framework. On one hand we have an expansion in powers of the coupling constant through the number of loops of a given diagram and on the other hand we have an expansion in the number of sources that, in the *dense limit* $g^2\rho \sim 1$, has to be resummed at all orders. For example, the amplitude for a single gluon production with momentum $(k^+, \mathbf{k})$ can be written schematically as

$$\mathcal{M}(k^+, \mathbf{k}) = \frac{1}{g} \left[a_0 + a_1 g^2 + a_2 g^4 + \cdots \right], \tag{2.4}$$

where each of the coefficients a_i have an expansion in powers of $g^2\rho$. In this thesis we will only be concerned in evaluating the multi-gluon spectrum at leading order and therefore we will only be interested in the first coefficient of this expansion, a_0, where the diagrams are computed at the tree level. Thus, depending on the parametric behavior of the source, we will distinguish between two cases: The *dilute limit* where $\rho \sim 1$ and therefore we can compute a_0 at leading order in $g^2\rho$ and the *dense limit* where $\rho \sim 1/g^2$ and therefore we cannot compute a_0 perturbatively.

On the other hand we should note that, although we are neglecting these corrections in this thesis, the loop corrections for the multi-gluon spectrum are important for many reasons. They contain logarithm divergences similar to those found in the JIMWLK equation and being able to factorize them is an important check for the consistency of

the CGC framework. Moreover, the gluon field calculated in nucleus-nucleus collisions by solving the classical Yang-Mills equation in presence of two nuclear sources has been found to be unstable; small changes in the initial condition lead to a exponential difference in the solutions [70–73]. Therefore, although loop corrections are subleading in the coupling constant, the coefficients that are attaching them may be large. A proper derivation of the first quantum corrections to multiple gluon production in heavy ion collisions can be found in [74–76].

To finalize this section we make the important point that in any quantum field theory coupled to a strong source the leading order n-particle inclusive spectrum can be written just as the product of n single particle spectra [69]. Thus, in the dense limit of the CGC framework, the multiple gluon spectrum at leading order can be written as

$$\left.\frac{d^n N[\rho]}{\prod_{i=1}^{n} dk_i^+ d^2\mathbf{k}_i}\right|_{\text{LO}} = \prod_{i=1}^{n} \left.\frac{dN[\rho]}{dk_i^+ d^2\mathbf{k}_i}\right|_{\text{LO}}, \tag{2.5}$$

where we have written the dependence of the source ρ explicitly to make emphasis that the source's configuration is fixed. This relation does not hold in the dilute limit where terms of order $g^n\rho^m$ with $m < n$ are not parametrically subleading and therefore have to be taken into account. However, as we shall see in Chapters 3 and 4, in the analysis of multi-particle azimuthal correlations, which is the main goal of this thesis, the main contribution comes from the factorization form of Eq. (2.5) where the corrections of order $g^n\rho^m$ are expected to give "non-flow" correlations. For this reason, unless indicated, we will assume that the factorization in Eq. (2.5) still holds in the dilute limit.

2.2 Gluon production in proton-nucleus collisions

Studies on particle production in proton-nucleus (pA) collisions became more relevant in the last decades because of the experiments performed in the Relativistic Heavy Ion Collider (RHIC) at BNL, where deuterium-gold collisions are performed at a center of mass energy per nucleon of $\sqrt{s} = 200$ GeV, and in the Large Hadron Collider (LHC) at CERN, where proton-lead collisions are performed at $\sqrt{s} = 8$ TeV. In particular, the LHC measurements revealed surprising properties of the system generated in pA collisions that will be discussed in Chapter 3, where we will review the phenomenon of particle correlation. For this reason it is important to have a good understanding of the dynamics of such collisions. Since these scatterings are performed at high energies, the CGC effective theory offers a reasonable theoretical framework for describing them.

In this section we will provide a description of high energy proton-nucleus collisions within the CGC framework. Both the target (nucleus) and the projectile (proton) will be then described by some random color source. However, since the partonic density in the nucleus is enhanced by a factor $A^{1/3}$, the nucleus will achieve the saturation region sooner than the proton, where the particle density is much smaller. Thus pA collisions provide an interesting physical environment where the proton projectile can be seen as a dilute parton gas with a color charge density $\rho_p \sim 1$ while the target nucleus is in the saturation regime with $\rho_T \sim g^{-2}$. Therefore, in this system we will have to resum all the powers of the target source $g^2\rho_T$ while it is still a good approximation to be at leading order in the projectile source $g^2\rho_p$.

The leading contribution to particle production is achieved by solving the classical Yang-Mills equation Eq. (1.47). The main difference with respect to the approach discussed in Section 1.6 is that now our system is composed by two color densities instead of just one. If we assume that the projectile, described by a source $\rho_p(x^-, \mathbf{x})$, moves in the + direction of the light cone and the target, described by $\rho_T(x^+, \mathbf{x})$ moves in the - direction, the color current coupled to the gluon field will be, at leading order in the sources ρ_p and ρ_T,

$$J^{\mu,a} = \delta^{\mu+} g\rho_p^a(x^-, \mathbf{x}) + \delta^{\mu-} g\rho_T^a(x^+, \mathbf{x}), \tag{2.6}$$

In general, the current $J^{\mu,a}$ receives higher order corrections in ρ_p and ρ_T because it must be conserved through

$$[D_\mu, J^\mu] = 0. \tag{2.7}$$

In order to evaluate any physical observable $\mathcal{O}$ we will have to average over all possible configurations of both the projectile's and target's source. Defining $W_p[\rho_p]$ and $W_T[\rho_T]$ as the projectile and target MV weight respectively, one has

$$\langle \mathcal{O} \rangle_{p,T} = \int [\mathcal{D}\rho_p]\, [\mathcal{D}\rho_T]\, W_p[\rho_p] W_T[\rho_T] \mathcal{O}[\rho_p, \rho_T], \tag{2.8}$$

where we have omitted the dependence on Λ^+ for simplicity[2]. However, both the target and the projectile weight functionals are subject to quantum corrections and follow the JIMWLK evolution equation.

The CGC also provides the appropriate framework for computing the gauge fields generated by the projectile and the target before the collision. Before the collision, the colliding particles are causally disconnected and therefore each field will be described independently through the Yang-Mills equation for a single source. Thus, we can separate the space-time intro 4 regions that are illustrated in Fig. 2.1. The region I, where $x^-, x^+ < 0$, is causally unreachable for both the projectile and the target and, because of the gauge freedom, we can assume that the gluon field is zero in this region. The case where the target and the projectile are causally disconnected is achieved in the region II and III. Thus the gauge field will only depend on ρ_T in the region II ($x^+ > 0$ and $x^- < 0$) and it will only depend on ρ_p in the region III ($x^+ < 0$ and $x^- > 0$). Finally, the non trivial dynamics of the collision is achieved in the region IV of space-time, where $x^-, x^+ > 0$. In this case the Yang-Mills equation will depend on both sources and solving it is extremely challenging. In the case of nucleus-nucleus collisions it has only been solved numerically [77–81]. However, as we shall see below, in the case of proton-nucleus collisions it is possible to find a closed-form solution for the gauge field in the region IV [82–87].

Our strategy in this section will be the following. First, we will solve the gauge field in the region II, obtaining an expression for the dense gluon field of the target. Second, since the projectile is dilute and its gauge field is much weaker than the target one, we will assume that the gluon field in the region IV is the sum of the target field plus a small perturbation. Second, we will linearize the Yang-Mills equation around the field

[2]In fact, in this case we should have two scales separating the soft and fast modes of both the projectile and target wave functions.

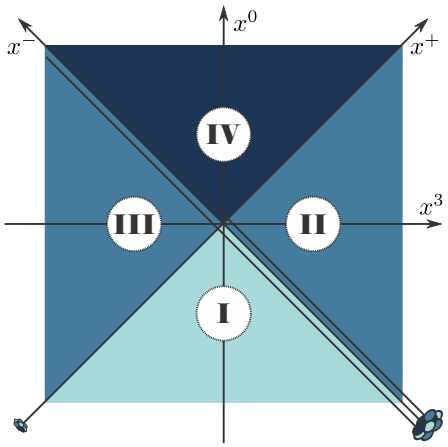

Figure 2.1.
Space-time diagram of a proton-nucleus ultra-relativistic collision. The proton moves in + direction of the light-cone while the nucleus moves in the - direction. The diagram is separated into 4 regions depending on the nature of the total gauge field. In the region I the gluon field is trivial and can be taken to be zero. In the regions II and III, the gluon field only depends on a single source and therefore is easy to be found. In the region IV the gauge field depend on both sources and is extremely non-trivial.

perturbation in order to find an expression for the total gauge field. Finally, we will use the reduction formulas to compute the single gluon spectra as a function of the gauge field.

Since in the region II of Fig. 2.1 the gauge field is completely described by the target color source ρ_T, the current in this region will be

$$J_T^{\mu,a} = \delta^{\mu-} g\rho_T^a(x^+, \mathbf{x}). \tag{2.9}$$

In the light-cone gauge $A^+ = 0$, which will be used over all this section, the equation of current conservation is automatically satisfied

$$[D_\mu, J_T^\mu] = \partial^+ J_T^- + [D^-, J_T^+] - [D^i, J_T^i] = g\frac{\partial \rho_T(x^+, \mathbf{x})}{\partial x^-} = 0, \tag{2.10}$$

where we have dropped for simplicity the color index. On the other hand, the classical Yang-Mills equations in the light-cone gauge simplifies to

$$[D_\mu, F^{\mu\nu}] = \partial^+ F^{-\nu} + [D^-, F^{+\nu}] - [D^i, F^{i\nu}] = J^\nu. \tag{2.11}$$

Thus we have a set of three differential equations defining the gauge field's dynamics

$$-\partial^+(\partial_\mu A^\mu) - ig[A^i, \partial^+ A^i] = J^+, \tag{2.12}$$

$$[D^-, \partial^+ A^-] - [D^i, F^{i-}] = J^-, \tag{2.13}$$

$$\partial^+ F^{-i} + [D^-, \partial^+ A^i] - [D^j, F^{ji}] = J^i. \tag{2.14}$$

The first equation does not contain any time derivative, ∂^-, and therefore can be seen as a constraint to the component of the field at equal times. In the region II of space-time,

we have to substitute $J^\mu \to J_T^\mu$ and $A^\mu \to A_T^\mu$, where we define A_T^μ as the target gauge field before the interaction with the projectile. One can easily check that the following is a solution of Eqs. (2.12) to (2.14)

$$A_T^i = A_T^+ = 0, \tag{2.15}$$

$$A_T^- = -\frac{1}{\nabla^2} J_T^- = -g\frac{1}{\nabla^2}\rho_T(x^+, \mathbf{x}). \tag{2.16}$$

We should note that Eq. (2.16) is also valid in the covariant gauge ($\partial_\mu A^\mu = 0$) [85] and it is a general result that is valid at all orders in $g\rho_T$. The operator $1/\nabla^2$ in Eq. (2.16) is an abuse of notation and should be understood as the convolution of the Green's function for the 2-dimensional Laplace operator with the source ρ_T. Finally, although it is not important for the discussion on this section, the projectile's gauge field of region III can be computed in the same fashion leading to an analogous result.

Now let us turn the analysis to the region IV of Fig. 2.1, where the dynamics is governed by both the projectile's and target's source. As we have pointed above, since the projectile is dilute and its field is much weaker than the target one, we will assume that the gauge field during the collision is the target field in absence of interaction A_T^μ plus a perturbation A_p^μ due to the interaction with the projectile. Thus, the gauge field can be written as

$$A^\mu = A_T^\mu + A_p^\mu, \tag{2.17}$$

where $A_T^\mu \sim g^{-1}$ and $A_p^\mu \sim g$. Moreover, the current presented in Eq. (2.6) will get higher order corrections in ρ_T due to the interaction. Therefore we will also assume that the total current after the collision is given by the target current before the interaction $J_T^\mu \sim g^{-1}$ plus the projectile one that will be assumed to be of order g:

$$J^\mu = \delta^{\mu-} J_T^- + \delta^{\mu+} J_p^+, \tag{2.18}$$

where we have supposed that the projectile does not recoil in the interaction with the target. This assumption relies on the *eikonal approximation* that will be reviewed in the next section.

The next step is to obtain an expression for the perturbation field A_p^μ. In order to do so we have to linearize the Yang-Mills equation in Eqs. (2.12) to (2.14) around it. Selecting only the terms that are $\mathcal{O}(g)$ we get the following set of equations:

$$-\partial^+(\partial_\mu A_p^\mu) = J_p^+, \tag{2.19}$$

$$\Box A_p^i - 2ig[A_T^-, \partial^+ A_p^i] = \partial^i(\partial_\mu A_p^\mu), \tag{2.20}$$

$$\Box A_p^- - 2ig[A_T^-, \partial^+ A_p^-] = J_p^- + 2ig[\partial^i A_T^-, A_p^i] + \partial^-(\partial_\mu A_p^\mu) - ig[A_T^-, \partial_\mu A_p^\mu]. \tag{2.21}$$

On the other hand, a linearization of the current conservation equation reads

$$D^- J_p^+ = (\partial^- - igA_T^-)J_p^+ = 0. \tag{2.22}$$

The initial condition to this equation can be taken by evaluating the projectile current in the region III of Fig. 2.1. The result is $J_p^+(x^+ = -\infty) = g\rho_p(x^-, \mathbf{x})$. Thus the solution of Eq. (2.22) is

$$J_p^{+,a}(x) = U^{ab}(x^+, -\infty, \mathbf{x}) g\rho_p^b(x^-, \mathbf{x}), \tag{2.23}$$

where we have recovered the color indices to express the fact that the matrix U, which accounts for the interaction of the projectile with the target, rotates the color of the projectile source while maintains the transverse coordinate $\mathbf{x}$ invariant. This matrix can be written as

$$U(x^+, y^+, \mathbf{x}) \equiv \mathcal{P}^+ \exp\left\{ ig \int_{y^+}^{x^+} dz^+ A_T^{-,a}(z^+, \mathbf{x}) T^a \right\} \tag{2.24}$$

and is known as the *Wilson line*. It is a color object that belongs to the adjoint representation of $\mathrm{SU}(N_c)$ and is the matrix scattering of a gluon[3] interacting with a strong field A_T^-. In Eq. (2.24) the operator $\mathcal{P}^+$ denotes the time ordering over x^+.

In order to simplify the analysis further, we will use the fact that the projectile is ultra-relativistic and therefore it is Lorentz contracted around $x^- = 0$. Thus we make the substitution $\rho_p(x^-, \mathbf{x}) \to \delta(x^-)\rho_p(\mathbf{x})$. In this case Eq. (2.19) can be written as[4] $\partial_\mu A_p^\mu = -\Theta(x^-)\tilde{J}_p^+(x^+, \mathbf{x})$. Substituting this result into Eq. (2.20) we obtain the following equation for the transverse component of the field perturbation

$$\Box A_p^i - 2ig[A_T^-, \partial^+ A_p^i] = -\Theta(x^-)\partial^i \left[U(x^+, -\infty, \mathbf{x}) g\rho_p(\mathbf{x}) \right]. \tag{2.25}$$

By performing a straightforward manipulation of this equation we can write its solution as a Green's equation

$$A_p^i(x) = -\int d^4y G(x, y)\Theta(y^-)\partial^i \left[U(y^+, -\infty, \mathbf{y}) g\rho_p(\mathbf{y}) \right], \tag{2.26}$$

where the Green's function $G(x, y)$ obeys the following equation of motion:

$$\left[\Box_x - 2igA_T^- \cdot T\partial_x^+ \right] G(x, y) = \delta^{(4)}(x - y), \tag{2.27}$$

where $A \cdot T = A^a T^a$.

Since the target field $A_T^-(x^+, \mathbf{x})$ defined in Eq. (2.16) is x^--independent, we can simplify the Green's equation by defining

$$G(x, y) = \int \frac{dk^+}{(2\pi)} e^{-ik^+(x^- - y^-)} \frac{i}{2k^+} \mathcal{G}_{k^+}(x^+\mathbf{x}; y^+, \mathbf{y}). \tag{2.28}$$

Thus Eq. (2.27) can be rewritten as

$$\left[i\partial_x^- + \frac{\nabla_x^2}{2k^+} + gA_T^- \cdot T \right] \mathcal{G}_{k^+}(x^+, \mathbf{x}; y^+, \mathbf{y}) = i\delta(x^+ - y^+)\delta^{(2)}(\mathbf{x} - \mathbf{y}). \tag{2.29}$$

Eq. (2.29) is the Green's equation of a 2-dimensional Schrodinger equation for a a particle with "mass" k^+ in a time-dependent matrix potential $-gA_T^-(x^+, \mathbf{x}) \cdot T$. The solution of this equation is well known in literature and is given by the Feynman path integral [88]

$$\mathcal{G}_{k^+}(x^+, \mathbf{x}; y^+, \mathbf{y}) = \int_{\mathbf{z}(y^+)=\mathbf{y}}^{\mathbf{z}(x^+)=\mathbf{x}} [\mathcal{D}\mathbf{z}(z^+)] \exp\left\{ \frac{ik^+}{2} \int_{y^+}^{x^+} dz^+ \dot{\mathbf{z}}^2(z^+) \right\} U(x^+, y^+; \mathbf{z}(z^+)). \tag{2.30}$$

[3] In the case of quarks, the Wilson line belongs to the fundamental representation of $\mathrm{SU}(N_c)$. The expression is the same as Eq. (2.24) but by changing $T^a \to t^a$.

[4] We have defined $\tilde{J}_p^+(x^+, \mathbf{x}) = U(x^+, -\infty, \mathbf{x}) g\rho_p(\mathbf{x})$.

This path integral describes the Brownian motion of a particle, that is interpreted as the produced gluon, in the transverse plane. We also note that in absence of the gauge field A_T^-, i.e. in the case where the particle is free, the solution of Eq. (2.29) can be simply written as [43]

$$\mathcal{G}^0_{k^+}(x^+,\mathbf{x};y^+,\mathbf{y}) = \frac{-ik^+}{2\pi}\frac{\Theta(x^+-y^+)}{x^+-y^+}\exp\left\{\frac{ik^+}{2(x^+-y^+)}(\mathbf{x}-\mathbf{y})^2\right\}, \tag{2.31}$$

where this solution can be identified as the *free scalar propagator* of a gluon in the transverse plane.

With Eqs. (2.26), (2.28) and (2.30) we have fully determined the transverse component of the field perturbation A_p^i. Before moving forward, let us touch some important points on the calculation. So far, we have not mentioned the minus component of the perturbation field, which is also necessary for obtaining a complete expression for the gauge field in the region IV. This component can be evaluated by performing an analogous calculation. However, as we shall see soon, we only need the transverse component of the perturbation field in order to compute the single gluon spectrum. This makes sense since only the transverse polarizations of the gluon are physical.

Moreover, we have assumed that the projectile is infinitely boosted in the + direction by supposing that it does not recoil in the interaction with the target and that it is Lorentz contracted to $\rho_p(x^-,\mathbf{x}) \propto \delta(x^-)$. As we will see in the next section, this assumption is known as the eikonal approximation and we say that the projectile is eikonal. However, Eq. (2.30) is completely general and in the case of both the produced gluon (defined through the transverse perturbation field) and the colliding target we have not used the eikonal approximation. Thus, the physical picture of the calculation performed above is the following. An infinitely boosted, i.e. eikonal, projectile interacts with the target which is characterized by a dense medium defined by $A_T^-(x^+,\mathbf{x})$. As a result of this interaction, a non-eikonal gluon is produced and measured in the final state.

Having an expression for A_p^i, the next step is to compute the single gluon spectrum. At leading order in g, i.e. at the classical level, a reduction formula leads to the following expression for the single gluon spectrum [69]

$$(2\pi)^3(2k^+)\frac{dN}{dk^+d^2\mathbf{k}} = \left\langle \mathcal{M}^a_\lambda(k^+,\mathbf{k})\mathcal{M}^{\dagger a}_\lambda(k^+,\mathbf{k})\right\rangle_{p,T}, \tag{2.32}$$

where $\mathcal{M}^a_\lambda(k^+,\mathbf{k})$ is the amplitude for production of an on-shell gluon with longitudinal momentum k^+, transverse momentum $\mathbf{k}$, polarization λ and color a. Its expression is given by

$$\mathcal{M}^a_\lambda(k^+,\mathbf{k}) = \int d^4x e^{ik\cdot x}\Box_x \epsilon^{\mu *}_\lambda(k) A^a_\mu(x), \tag{2.33}$$

where $\epsilon^{\mu *}_\lambda(k)$ is the gluon polarization vector and A^a_μ is the total gauge field defined in Eq. (2.17).

For physical gluons and in the light-cone gauge, the polarization vector is

$$\epsilon^\mu_\lambda(k) = \left(0, \frac{2\epsilon^{\lambda i}_\perp \mathbf{k}^i}{k^+}, \epsilon^\lambda_\perp\right), \qquad \epsilon^\lambda_\perp = -\frac{1}{\sqrt{2}}(\lambda, i), \tag{2.34}$$

where $\lambda = \pm 1$. Thus, in the light-cone gauge, $\epsilon^{\mu *}_{\lambda}(k) A^{a}_{\mu}(x) = -\epsilon^{\lambda i *}_{\perp} A^{i,a} = -\epsilon^{\lambda i *}_{\perp} A^{i,a}_{p}$, where we have used the fact that $A^{i}_{T} = 0$. As we have pointed above, the matrix amplitude will only depend on A^{i}_{p} and can be written as

$$\mathcal{M}^{a}_{\lambda}(k^{+}, \mathbf{k}) = -\epsilon^{\lambda i *}_{\perp} \int d^{4}x e^{ik\cdot x} \Box_{x} A^{i,a}_{p}(x). \tag{2.35}$$

Let us now assume that the target has a finite length L^{+} in such a way that it is defined by a dense medium restricted to $z^{+} \in [0, L^{+}]$. With this assumption the target field can be written schematically as $A^{-}_{T}(z^{+}, \mathbf{z}) = A^{-}_{T} \Theta(L^{+} - z^{+}) \Theta(z^{+})$. In this picture, the gluon will be emitted by the projectile due to the interaction with the medium at some time y^{+}, it will propagate through the medium with a Brownian motion defined by Eq. (2.30) and then it will be measured[5] at $x^{+} \gg L^{+}$. Then the gluon can be emitted before ($y^{+} < 0$), inside ($L^{+} < y^{+} < 0$) and after ($y^{+} > L^{+}$) the interaction of the projectile with the medium. Depending on the situation, the trajectory followed by the gluon will be very different. In the cases where the gluon propagates outside the medium, the propagation will be defined by Eq. (2.31).

In order to evaluate Eq. (2.33) we will have to substitute Eqs. (2.26) and (2.28). By using the convolution relation of the Green's function and doing some exhaustive algebra the result can be written as [43]

$$\begin{aligned}\mathcal{M}^{a}_{\lambda}(k^{+}, \mathbf{k}) = \epsilon^{\lambda i *}_{\perp} e^{ik^{-}L^{+}} \frac{g}{\pi} \int_{\mathbf{y},\mathbf{z}} e^{-i\mathbf{k}\cdot\mathbf{z}} \frac{(\mathbf{z}-\mathbf{y})^{i}}{(\mathbf{z}-\mathbf{y})^{2}} \Bigg\{ \int_{\mathbf{z}'} e^{i\mathbf{k}\cdot(\mathbf{z}-\mathbf{z}')} \mathcal{G}_{k^{+}}(L^{+}, \mathbf{z}'; 0, \mathbf{z}) - U(L^{+}, 0, \mathbf{y}) \\ + \int_{\mathbf{z}', y^{+}} e^{i\mathbf{k}\cdot(\mathbf{z}-\mathbf{z}')} \frac{1}{2ik^{+}} \nabla^{2}_{\mathbf{z}} \Big[\mathcal{G}_{k^{+}}(L^{+}, \mathbf{z}'; y^{+}, \mathbf{z}) \Big] U(y^{+}, 0, \mathbf{y}) \Bigg\}^{ab} \rho^{b}_{p}(\mathbf{y}),\end{aligned} \tag{2.36}$$

where $\int_{\mathbf{x}} \equiv \int d^{2}\mathbf{x}$ and $\int_{x^{+}} \equiv \int dx^{+}$. The first term inside the brackets of this expression can be recognized as the case where the gluon is emitted before the interaction of the projectile with the target and thus follows a Brownian trajectory in the transverse plane. The second term corresponds to the case where the gluon is emitted after the collision and therefore the scattering is only accounted by the color rotation of the projectile's source through the Wilson line. The last and third term corresponds to the case where the gluon is emitted inside the target at a point y^{+}. The diagrams representing these possibilities are illustrated in Fig. 2.2.

Alternatively, we can write the matrix amplitude, $\mathcal{M}^{a}_{\lambda}(k^{+}, \mathbf{k})$, in a factorized form in momentum space as

$$\mathcal{M}^{a}_{\lambda}(k^{+}, \mathbf{k}) = g \int \frac{d^{2}\mathbf{q}}{(2\pi)^{2}} \overline{\mathcal{M}}^{ab}_{\lambda}(k^{+}, \mathbf{k}, \mathbf{q}) \rho^{b}_{p}(\mathbf{q}), \tag{2.37}$$

where $\rho^{b}_{p}(\mathbf{q})$ is the Fourier transform of the projectile's source[6] and $\overline{\mathcal{M}}^{ab}_{\lambda}$ is the reduced

[5] The word measured here is an abuse of language. Because of confinement, gluons and quarks cannot be measured. Instead, they propagate over time and at some moment after the collision, when the partonic density is small, they undergo a process called *hadronization*. Hadronization is a non-perturbative, and therefore highly non-trivial, process where hadrons are created out of quarks and gluons.

[6] We are using the same definition for both functions although they have different expressions.

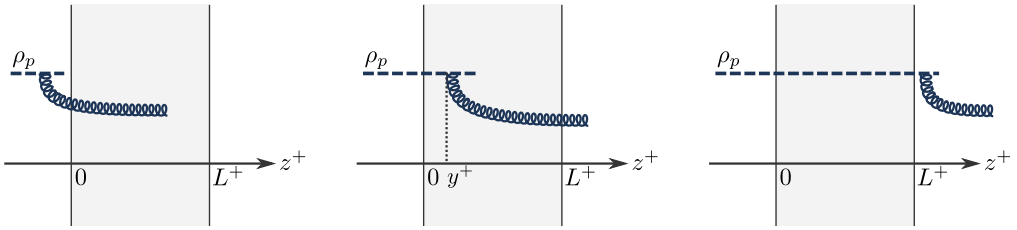

Figure 2.2.
The three diagrams contributing to gluon production in proton-nucleus collision. In the first diagram the gluon is emitted before the interaction of the projectile with the target, in the second the gluon is emitted inside the target and in the third the gluon is emitted after the interaction.

matrix amplitude which reads [43]

$$\overline{\mathcal{M}}^{ab}_{\lambda}(k^+,\mathbf{k},\mathbf{q}) = \epsilon^{\lambda i *}_{\perp} i e^{ik^- L^+}\left\{2\frac{\mathbf{k}^i}{\mathbf{k}^2}\int_{\mathbf{y}} e^{-i(\mathbf{k}-\mathbf{q})\cdot\mathbf{y}} U^{ab}(L^+,0,\mathbf{y}) - 2\frac{\mathbf{q}^i}{\mathbf{q}^2}\int_{\mathbf{y},\mathbf{x}} e^{i\mathbf{q}\cdot\mathbf{y}-i\mathbf{k}\cdot\mathbf{x}}\mathcal{G}^{ab}_{k^+}(L^+,\mathbf{x};0,\mathbf{y})\right.$$
$$\left. + \int_{\mathbf{x},\mathbf{y}} e^{i\mathbf{q}\cdot\mathbf{y}-i\mathbf{k}\cdot\mathbf{x}}\frac{1}{k^+}\int_0^{L^+} dy^+ [\partial_{\mathbf{y}^i}\mathcal{G}^{ac}_{k^+}(L^+,\mathbf{x};y^+,\mathbf{y})] U^{cb}(y^+,0,\mathbf{y})\right\}. \tag{2.38}$$

With Eqs. (2.32), (2.37) and (2.38) we have finalized our discussion on gluon production in proton-nucleus collisions at leading order in the coupling constant. We note that, because of Eq. (2.5), the expression for n-gluon production at leading order and neglecting corrections of order $g^{2n}\rho_p^{2m}$ $(m<n)$ will be given by

$$2^n(2\pi)^{3n}\frac{d^nN}{\prod_{i=1}^n dk_i^+/k_i^+ d^2\mathbf{k}_i} = g^{2n}\int_{\mathbf{q}_1,\ldots,\mathbf{q}_{2n}}\left\langle \rho_p^{b_1}(\mathbf{q}_1)\rho_p^{*b_2}(\mathbf{q}_2)\cdots\rho_p^{*b_{2n}}(\mathbf{q}_{2n})\right\rangle_p$$
$$\times\left\langle \overline{\mathcal{M}}^{a_1b_1}_{\lambda_1}(\underline{k}_1,\mathbf{q}_1)\overline{\mathcal{M}}^{\dagger b_2a_1}_{\lambda_1}(\underline{k}_1,\mathbf{q}_2)\cdots\overline{\mathcal{M}}^{a_nb_{2n-1}}_{\lambda_n}(\underline{k}_n,\mathbf{q}_{2n-1})\overline{\mathcal{M}}^{\dagger b_{2n}a_n}_{\lambda_n}(\underline{k}_n,\mathbf{q}_{2n})\right\rangle_T, \tag{2.39}$$

where we have used Eq. (2.37) and defined the shorthand notation $\underline{k}\equiv(k^+,\mathbf{k})$. In Chapter 6 we will revise this result and perform a numerical analysis on single and double inclusive gluon production in proton-nucleus collisions in order to study the flow correlations encoded in this expression.

To conclude this section, we note that in the case that both the target and the emitted gluon are assumed to be infinitely boosted, i.e. we use the eikonal approximation, Eq. (2.38) simplifies enormously. In this case the longitudinal momentum of the emitted gluon is very high and we can assume that $k^+\to\infty$. On the other hand, the nucleus is Lorentz contracted and therefore $L^+\to 0^+$. Thus, the gluon propagator through the medium in Eq. (2.30) simplifies to

$$\mathcal{G}_{\text{eik}}(x^+,\mathbf{x},y^+,\mathbf{y}) = U(x^+,y^+,\mathbf{x})\delta^{(2)}(\mathbf{x}-\mathbf{y}), \tag{2.40}$$

that is, the gluon propagation through the target is diagonal in the transverse space and is accounted by a color rotation through the Wilson line as we should expect on an eikonal scattering. Substituting this propagator into Eq. (2.38) we obtain the eikonal expression

for the reduced matrix amplitude

$$\overline{\mathcal{M}}_{\lambda}^{ab}(\mathbf{k},\mathbf{q}) = 2i\epsilon_{\lambda}^{i*}\left(\frac{\mathbf{k}^i}{\mathbf{k}^2} - \frac{\mathbf{q}^i}{\mathbf{q}^2}\right)\int_{\mathbf{y}} e^{-i(\mathbf{k}-\mathbf{q})\cdot\mathbf{y}}U^{ab}(\mathbf{y}), \tag{2.41}$$

where we have made the substitution $U(0^+,0,\mathbf{y}) \to U(\mathbf{y})$.

2.3 Particle production in the eikonal approximation

In Section 2.2 we have computed the single gluon spectrum in the case of a fast-moving projectile interacting with a non-eikonal target. Now, we will perform the same calculation but in the case of a very high energy produced gluon. This type of scattering relays on the eikonal approximation, that will be reviewed in a more formal way than in Section 2.2. The calculation of this section will be performed in the light-cone wave function (LCWF) formalism and, as we shall see, the result will be equal to Eq. (2.41). Thus, although it may look redundant, the result will give us a new picture of proton-nucleus scattering and will serve us as a double check of the theory's consistency.

Let us begin by reviewing the eikonal approximation in proton-nucleus scattering. The derivation performed here will be based on [89, 90]. Any physical system undergoing a scattering process is described by the S-matrix or *scattering matrix* which relates the initial and final state of such a system

$$S_{\beta\alpha} \equiv \langle\beta_{\text{out}}|\alpha_0\rangle = \langle\beta_0|\hat{U}(+\infty,-\infty)|\alpha_0\rangle\,, \tag{2.42}$$

where $\hat{U}$ is the time-evolution operator evolving a state in the interaction picture from an initial time $x^+ = -\infty$ towards $x^+ = +\infty$. It is defined as

$$\hat{U}(x_f^+,x_i^+) \equiv \mathcal{P}^+\exp\left\{i\int_{x_i^+}^{x_f^+}dx^+\int dx^- d^2\mathbf{x}\mathcal{L}_{\text{int}}\left[\hat{A}^\mu, A_T^\mu\right]\right\}, \tag{2.43}$$

where $\mathcal{L}_{\text{int}}$ is the interaction Lagrangian that contains the self interactions of the fields and their interactions with the external field. In the analysis performed in this section, the projectile consists of a not so large number of partons which are defined by the field operator $\hat{A}^\mu(x)$ and scatter on a large target. The target defines the classical external field A_T^μ that will be coupled to $\hat{A}^\mu(x)$. In Eq. (2.42), $|\alpha_0\rangle$ is a free initial state which, in our case, is described by the projectile quark valence states and is an eigenstate of the QCD Yang-Mills Hamiltonian. Moreover, $|\beta_0\rangle$ is also a free state but, because of the interaction of the projectile with the target, it is different than the initial state $|\alpha_0\rangle$.

As we have seen in the last section, in the light-cone gauge $A^+ = 0$, the dynamical degrees of freedom are completely determined by the transverse component of the gauge field. From a second-quantization point of view, we can write $\hat{A}^i$ in terms of the gluon creation and annihilation operators as

$$\hat{A}_i^a(x) = \int\frac{d^4p}{(2\pi)^4\sqrt{2p^+}}\left(e^{ip\cdot x}\hat{a}_i^a(p) + e^{-ip\cdot x}\hat{a}_i^{a\dagger}(p)\right), \tag{2.44}$$

where a_i and $a_i^\dagger$ are defined by their commutation relation that will be written down later and we have omitted the polarization vector for simplicity.

In the eikonal approximation, we assume that the projectile has a very high energy and therefore it is highly boosted in the longitudinal direction. The Lorentz transformation of a general scalar operator $\hat{\mathcal{O}}(x)$ in the longitudinal direction is achieved by multiplying it by the longitudinal Lorentz boost generator K_3 as

$$e^{\omega K_3}\hat{\mathcal{O}}(x)e^{-\omega K_3} = \hat{\mathcal{O}}(e^{-\omega}x^+, e^{\omega}x^-, \mathbf{x}), \tag{2.45}$$

where ω is the rapidity of the boost. On the other hand, if $\hat{\mathcal{O}}$ is in the momentum space, the boost is written as

$$e^{\omega K_3}\hat{\mathcal{O}}(p)e^{-\omega K_3} = \hat{\mathcal{O}}(e^{\omega}p^+, e^{-\omega}p^-, \mathbf{x}). \tag{2.46}$$

Thus in the high energy limit, $\omega \to \infty$, the projectile gauge field can be written as

$$\hat{A}_i^a(x^-, \mathbf{x}) = \int \frac{dp^+ d^2\mathbf{p}}{(2\pi)^3\sqrt{2p^+}} \left(e^{i(p^+x^- - \mathbf{p}\cdot\mathbf{x})}\hat{a}_i^a(p^+, \mathbf{p}) + e^{-i(p^+x^- - \mathbf{p}\cdot\mathbf{x})}\hat{a}_i^{a\dagger}(p^+, \mathbf{p})\right), \tag{2.47}$$

where we got rid of the x^+ dependence of the field, which is $\delta(x^+)$, and therefore the gluon field operator is only non-zero at $x^+ = 0$. We have also made the change $e^w x^- \to x^-$ and $e^\omega p^+ \to p^+$. The creation and annihilation operator will be defined by the following commutation relations

$$\left[\hat{a}_i^a(p^+, \mathbf{p}), \hat{a}_j^{b\dagger}(q^+, \mathbf{q})\right] = \delta^{ab}\delta_{ij}(2\pi)^3\delta(p^+ - q^+)\delta^{(2)}(\mathbf{p} - \mathbf{q}), \tag{2.48}$$

$$\left[\hat{a}_i^a(p^+, \mathbf{p}), \hat{a}_j^b(q^+, \mathbf{q})\right] = \left[\hat{a}_i^{a\dagger}(p^+, \mathbf{p}), \hat{a}_j^{b\dagger}(q^+, \mathbf{q})\right] = 0. \tag{2.49}$$

As we know, the coupling of the target with the dynamical field is of the form $A_T^\mu \hat{J}_\mu$, where $\hat{J}^\mu[\hat{A}^\mu]$ is a Noether vector current built from the dynamical fields. In order to simplify the discussion, we also assume that the external field A_T^μ is non-zero only in a finite range in x^+, $x^+ \in [0, L^+]$ (as we did in the last section). Therefore, the time-evolution operator can be split into three factors

$$\hat{U}(+\infty, -\infty) = \hat{U}_0(+\infty, L^+)\hat{U}(L^+, 0)\hat{U}_0(0, -\infty), \tag{2.50}$$

where $\hat{U}_0$ has the same definition as $\hat{U}$ in Eq. (2.43) but with $A_T^\mu = 0$. Since the self-interaction terms of $\mathcal{L}_{\text{int}}$ are Lorentz invariant, they will not be modified by the boost. On the other hand, the vector current is proportional to first order space-time derivatives and will change under the longitudinal boost as $\hat{J}^\mu \to (e^\omega \hat{J}^+, e^{-\omega}\hat{J}^-, \hat{\mathbf{J}})$. The target is not boosted and thus the components of A_T^μ are also not modified by the boost. However, because of the transformation $x^+ \to e^{-\omega}x^+$ under the boost, the time spent by the incoming particles in the region where the external field is acting goes to zero, i.e. $L^+ \to 0$ when $\omega \to \infty$. This approximation is usually referred to as the *shock-wave approximation*. Therefore we can write, in the high energy limit,

$$\lim_{\omega\to\infty} e^{\omega K_3}\hat{U}_0(+\infty, x^+)e^{-\omega K_3} = \hat{U}_0(+\infty, 0), \tag{2.51}$$

$$\lim_{\omega\to\infty} e^{\omega K_3}\hat{U}(x^+, y^+)e^{-\omega K_3} = \mathcal{P}^+\text{exp}\left\{ig\int d^4x \hat{J}^+(x^-, \mathbf{x})A_T^-(x^+, \mathbf{x})\right\}, \tag{2.52}$$

where we have used the fact that K_3 does not modify the ordering in x^+ and that, under the change of variables $e^{\mp\omega}x^\pm \to x^\pm$, $A_T^\mu(x) \to A_T^\mu(e^\omega x^+, 0, \mathbf{x}) \equiv A_T^\mu(x^+, \mathbf{x})$. Moreover, only the minus component of the external field matters, because this is the component that couples to the longitudinal current $\hat{J}^+$ which is enhanced by the boost.

Therefore, after we have performed the high energy limit, the S-matrix can be written as

$$S_{\beta\alpha} = \langle\beta|\mathcal{P}^+\exp\left\{ig\int d^2\mathbf{x}\hat{\rho}^a(\mathbf{x})\chi^a(\mathbf{x})\right\}|\alpha\rangle\,, \tag{2.53}$$

where $\hat{\rho}^a(\mathbf{x}) \equiv \int dx^- \hat{J}^{+,a}(x^-, \mathbf{x})$, $\chi^a(\mathbf{x}) \equiv \int dx^+ A_T^{-,a}(x^+, \mathbf{x})$ and $|\alpha\rangle = \hat{U}_0(0, -\infty)|\alpha_0\rangle$. For $|\beta\rangle$ we have used the same definition and the fact that $\hat{U}_0(+\infty, 0) = \hat{U}_0^\dagger(0, -\infty)$. The states $|\alpha\rangle$ and $|\beta\rangle$ are eigenstates of the QCD Hamiltonian with no external field. We say that these states are *dressed* since they can be seen as the eigenstate of the free QCD Hamiltonian, i.e. *bare* states, surrounded by interacting quarks and gluons defined by the time-evolution operator. Eq. (2.53) is a closed expression for the high energy limit of the scattering matrix and defines the *eikonal scattering*. It is important to keep in mind that this result is valid at all orders in the coupling constant.

The dressed states have to be computed perturbatively by performing a Fock expansion of the initial state

$$|\alpha\rangle = \sum_{\delta_0} |\delta_0\rangle\langle\delta_0|\hat{U}_0(0, -\infty)|\alpha_0\rangle. \tag{2.54}$$

This Fock expansion reflects the fact that the initial state $|\alpha_0\rangle$ may fluctuate to other states $|\delta_0\rangle$ before interacting with the target. Moreover, the final state may fluctuate to other states after the interaction with the target. In practice, the time-evolution operator has to be expanded in powers of g. In high energy collisions, this expansion is called light-cone perturbation theory (LCPT) where the QCD Hamiltonian is written in light-cone coordinates. The main difference of the LCPT and the usual perturbation theory is that the time evolution of the bare states goes from $-\infty$ to 0 instead of over all the real axis. In momentum space, this implies that the minus component of the momentum, known as the light-cone energy, is not conserved at the vertices and we will have energy denominators instead of dirac deltas. However, the analysis using LCPT is out of the scope of this thesis and we will only touch some of the basic points. For a detailed review on this topic we refer to [91].

Therefore, in order to proceed further with the analysis of the scattering matrix, we will have to evaluate the following matrix element

$$\left\langle\gamma_0\middle|\mathcal{P}^+\exp\left\{ig\int d^2\mathbf{x}\hat{\rho}^a(\mathbf{x})\chi^a(\mathbf{x})\right\}\middle|\delta_0\right\rangle \equiv \langle\gamma_0|\hat{\mathcal{S}}|\delta_0\rangle. \tag{2.55}$$

This matrix element can be computed by writing the operator $\hat{\rho}^a(\mathbf{x})$ in terms of the creation and annihilation operators of the bare states of the QCD Hamiltonian. By solving the conserved current of the light-cone Hamiltonian one finds that

$$\hat{\rho}^a(\mathbf{x}) = \int \frac{dp^+}{(2\pi)}\frac{d^2\mathbf{p}}{(2\pi)^2}\frac{d^2\mathbf{q}}{(2\pi)^2}\Bigg\{e^{i(\mathbf{p}-\mathbf{q})\cdot\mathbf{x}}\hat{b}_\alpha^\dagger(p^+, \mathbf{p})t^a_{\alpha\beta}\hat{b}_\beta(p^+, \mathbf{q})$$

$$- e^{-i(\mathbf{p}-\mathbf{q})\cdot\mathbf{x}}\hat{d}^\dagger_\alpha(p^+,\mathbf{p})t^a_{\alpha\beta}\hat{d}_\beta(p^+,\mathbf{q}) + e^{i(\mathbf{p}-\mathbf{q})\cdot\mathbf{x}}\hat{a}^\dagger_b(p^+,\mathbf{p})T^a_{bc}\hat{a}_c(p^+,\mathbf{q})\Bigg\}, \quad (2.56)$$

where $\hat{b}^\dagger_\alpha(p^+,\mathbf{p})$ is the creation operator for a bare quark with color α, longitudinal momentum p^+ and transverse momentum $\mathbf{p}$ and $\hat{b}_\beta(p^+,\mathbf{q})$ the annihilation operator. Analogously, $\hat{d}^\dagger$ and $\hat{d}$ are the creation and annihilation operators of antiquarks. We have omitted in this equation the helicity and polarization components of quarks (antiquarks) and gluons, respectively, as well as the Lorentz components. It is clear from this expression that the operator $\hat{\rho}^a(\mathbf{x})$ is diagonal in the number and type of particles and therefore its matrix element has to be diagonal, i.e. the eigenstates $|\gamma_0\rangle$ and $|\delta_0\rangle$ have to be conformed by the same particles. Moreover, a straightforward calculation leads to that the + momentum of the particles in both states have also to be identical. The only difference between the states will be the color and the transverse momentum of the bare particles. It is convenient to write these states in a *mixed representation* where we perform a Fourier transform only in the transverse momenta of the creation and annihilation operators. Thus we write

$$\hat{a}^\dagger_a(k^+,\mathbf{x}) = \int \frac{d^2\mathbf{k}}{(2\pi)^2} e^{-i\mathbf{k}\cdot\mathbf{x}}\hat{a}^\dagger_a(k^+,\mathbf{k}), \quad (2.57)$$

$$[\hat{a}_a(k^+,\mathbf{x}),\hat{a}^\dagger_b(p^+,\mathbf{y})] = \delta_{ab}(2\pi)\delta(k^+-p^+)\delta^{(2)}(\mathbf{x}-\mathbf{y}), \quad (2.58)$$

and analogous expressions for the the creation and annihilation operators of the other particles. In this representation the operator $\hat{\rho}^a$ can be written as

$$\hat{\rho}^a(\mathbf{x}) = \int_{p^+}\Bigg\{\hat{b}^\dagger_\alpha(p^+,\mathbf{x})t^a_{\alpha\beta}\hat{b}_\beta(p^+,\mathbf{x}) - \hat{d}^\dagger_\alpha(p^+,\mathbf{x})t^a_{\alpha\beta}\hat{d}_\beta(p^+,\mathbf{x}) + \hat{a}^\dagger_b(p^+,\mathbf{x})T^a_{bc}\hat{a}_c(p^+,\mathbf{x})\Bigg\}, \quad (2.59)$$

where we have introduced the shorthand notation $\int_{p^+} = \int dp^+/(2\pi)$. Therefore, it is easy to check that the operator $\hat{\mathcal{S}}$, defined in Eq. (2.55), has the property $\hat{\mathcal{S}}\hat{O}^\dagger_a[R](k^+,\mathbf{y})\hat{\mathcal{S}}^{-1} = \mathcal{P}^+ e^{ig\chi^c(\mathbf{y})(T[R])^c_{ab}}\hat{O}^\dagger_b[R](k^+,\mathbf{y})$, where $\hat{O}^\dagger_b[R]$ is a generic creation operator (it can be $\hat{b}^\dagger$, $\hat{d}^\dagger$ or $\hat{a}^\dagger$) in the representation R (fundamental for quarks and antiquarks or adjoint for gluons) and $T[R]$ is the SU(N_c) generator in the representation R. Thus the operator $\hat{\mathcal{S}}$ is also diagonal in transverse positions and we can write

$$\hat{\mathcal{S}}|\delta_0\rangle = \mathcal{P}^+\exp\left\{ig\int d^2\mathbf{x}\hat{\rho}^a(\mathbf{x})\chi^a(\mathbf{x})\right\}|\delta_0\rangle = \prod_{i\in\delta}\int_{\mathbf{x}_i} e^{i\mathbf{k}_i\cdot\mathbf{x}_i}U^{b_ia_i}_{R_i}(\mathbf{x}_i)|\{k^+_i,\mathbf{x}_i,b_i\}\rangle, \quad (2.60)$$

where we have used the fact that $\hat{\mathcal{S}}|0\rangle = |0\rangle$ and $\{k^+_i,\mathbf{x}_i,b_i\}$ is the set of bare particles in the state $|\delta_0\rangle$ with longitudinal momentum k^+_i, transverse position $\mathbf{x}_i$ and color b_i. The matrix $U^{a_ib_i}_R(\mathbf{x}_i)$ can be written as

$$U^{ab}_R(\mathbf{x}) = \mathcal{P}^+\exp\left\{ig\int dx^+ A^{-,c}_T(x^+,\mathbf{x})T^{ab}_c[R]\right\}, \quad (2.61)$$

and is the eikonal Wilson line in the representation R of SU(N_c). Finally, defining the *light-cone wavefunction* as

$$\Psi_{\delta\alpha}(\{k^+_i,\mathbf{x}_i,b_i\}) \equiv \prod_{i\in\delta}\int\frac{d^2\mathbf{k}_i}{(2\pi)^2}e^{-i\mathbf{k}_i\cdot\mathbf{x}_i}\langle\tilde{\delta}_0|\hat{U}_0(0,-\infty)|\alpha_0\rangle, \quad (2.62)$$

where $|\tilde{\delta}_0\rangle$ is the state $|\delta_0\rangle$ in the mixed representation, the S-matrix reads

$$S_{\beta\alpha} = \sum_{\delta} \prod_{i\in\delta} \int_{\mathbf{x}_i} \int_{k_i^+} \Psi^\dagger_{\delta\beta}(\{k_i^+, \mathbf{x}_i, b_i\}) U^{b_i a_i}_{R_i}(\mathbf{x}_i) \Psi_{\delta\alpha}(\{k_i^+, \mathbf{x}_i, a_i\}). \tag{2.63}$$

The physics behind Eq. (2.63) is clear and is illustrated in Fig. 2.3. The projectile, defined by a bare valence state $|\alpha_0\rangle$, comes from $x^+ = -\infty$ and, because of the interacting nature of QCD, evolves to another bare state $|\delta_0\rangle$ composed by a different number of particles. The amplitude for this process is given by the light-cone wave function $\Psi_{\delta\alpha}$. Then, at $x^+ = 0$, the particles in the state $|\delta_0\rangle$ interact with the external field A^μ_T during an infinitesimal short time (shock-wave approximation). The effect of this interaction is a color rotation of each parton but keeping their transverse momentum invariant, and the object defining this eikonal interaction is the Wilson line $U^{ab}(\mathbf{x})$ which accounts for the multiple scatterings of each parton in the target. After the interaction, the state δ_0, which now has its color changed, evolves to a new state $|\beta_0\rangle$ at $x^+ = \infty$.

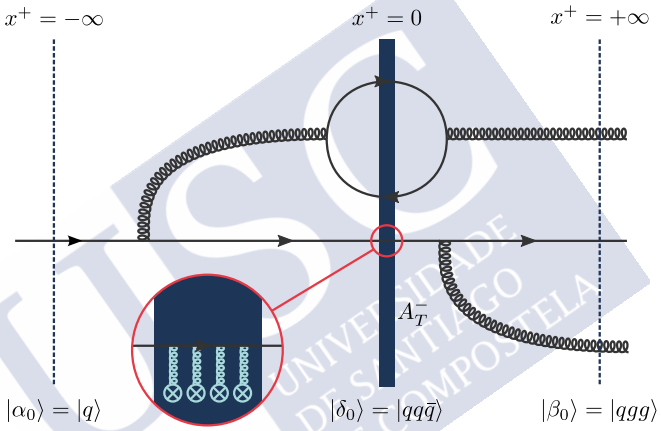

Figure 2.3.
The physical picture of Eq. (2.63). An initial bare quark state at $x^+ = -\infty$ evolves to a $|qq\bar{q}\rangle$ bare state at $x^+ = 0$. Then it interacts with a Lorentz contracted target and its color is rotated through the Wilson line. The Wilson line accounts for the multiple interactions of each parton with the target and is illustrated in the red circle of this figure. After the interaction, the system evolves to a $|qgg\rangle$ state.

In this formalism, computing particle production is straightforward. As we have seen, we start with a perturbative initial state $|\alpha_0\rangle$ and we end up, after an eikonal interaction of the particles with the target, with a bare state $|\beta_0\rangle$. The S-matrix for such a process is given in Eq. (2.63) and can be computed perturbatively in the LCPT formalism. The number of produced particles of type o (o can be quarks, antiquarks or gluons) with momentum $(k^+, \mathbf{k})$ in the final state will be given by the expectation value of the number operator $\hat{\mathcal{N}}_o(k^+, \mathbf{k}) = \hat{O}^\dagger_a(k^+, \mathbf{k})\hat{O}_a(k^+, \mathbf{k})$ in this state, being $\hat{O}^\dagger$ and $\hat{O}$ the creation and annihilation operators of the particles of type o. Thus, the single particle spectrum of particles o will be given by

$$(2\pi)^3 \frac{dN^{\alpha+A\to o+X}}{dk^+ d^2\mathbf{k}} = \langle\alpha_0| S^\dagger_{\alpha\beta} \hat{\mathcal{N}}_o(k^+, \mathbf{k}) S_{\beta\alpha} |\alpha_0\rangle \,. \tag{2.64}$$

In practice, the initial state is usually taken to be a single particle state, i.e. a single gluon or quark. If the produced particle has a forward rapidity, the dynamics of the initial parton will be described by the linear evolution equations. In this case the projectile large-x degrees of freedom are represented by the usual PDFs of collinear factorization and we have to perform a convolution of the spectrum at the partonic level with the PDF in question. Moreover, since the partonic final state goes through the non-perturbative process of hadronization, in order to perform a phenomenological analysis we also have to convolute the final state partons with the so-called *fragmentation functions*. The fragmentation functions $D_{h/p}$ can be roughly interpreted as the probability that a parton p hadronizes to an observed hadronic final state h. Thus, we can write schematically

$$\frac{dN^{p+A\to h+X}}{dk^+d^2\mathbf{k}} = f_{q(g)/p} \otimes \frac{dN^{q(g)+A\to o+X}}{dk_o^+d^2\mathbf{k}_o} \otimes D_{h/o}. \tag{2.65}$$

This approach is known as the *hybrid formalism* and was first proposed in [92]. However, the hybrid formalism is out of the scope of this thesis since we are interested in particles generated at mid rapidity.

Now let us turn our discussion to the case where the particle is produced at mid rapidity, i.e. ,$k^+/P^+ \ll 1$, where P^+ is the longitudinal momentum of the projectile. To simplify our discussion further, we will assume that the only degrees of freedom are gluons – however, the following arguments will be completely general. In this case, the operator $\hat{\rho}^a$ can be written just as

$$\hat{\rho}^a(\mathbf{x}) = \int_{p^+} \hat{a}_b^\dagger(p^+,\mathbf{x}) T^a_{bc} \hat{a}_c(p^+,\mathbf{x}). \tag{2.66}$$

Although we have not pointed it before, this operator can be simply identified as the color charge density operator. However, this is not the Color Glass Condensate charge density discussed in the last sections since the integral in p^+ is running over all the positive real axis, and therefore we are including both the soft and fast modes in this operator, in contrast with the CGC density which only includes the fast modes. In order to make a connection of the light-cone wave function formalism with the Color Glass Condensate effective theory we will have to make a distinction between the soft and fast modes.

The strategy for evaluating the gluon spectrum in the CGC framework is the following. We will assume that the initial state is a high energy projectile given by some wave function $|\alpha_0\rangle = |P\rangle_{\text{in}}$. This state is supposed to be dilute, i.e. the number of particles in this ensemble is not very large $n \ll g^{-2}$, so that we can use perturbation theory. Moreover, it will only be composed by valence partons with longitudinal momentum $k_i^+ > \Lambda^+$. We can write this state in the Fock space as

$$|P\rangle_{\text{in}} = |0\rangle_{\text{soft}} \otimes \sum_i \psi(\{k_i^+,\mathbf{x}_i,\alpha_i\})|\{k_i^+ > \Lambda^+,\mathbf{x}_i,\alpha_i\}\rangle \equiv |0\rangle_{\text{soft}} \otimes |v\rangle, \tag{2.67}$$

where we have separated the Hilbert space into two subspaces: the soft space, where only these creation operators with $k^+ < \Lambda^+$ give a non-zero value under multiplication, and the valence space, where only the creation operators with $k^+ > \Lambda^+$ operate. Thus, the projectile in the initial state is composed of a bunch of valence gluons and quarks (antiquarks) and does not have any soft gluon. We are not interested in the specific content of the valence state $|v\rangle$ and we will keep it general.

This initial state projectile will be evolved from $x^+ = -\infty$ to $x^+ = 0$ by the time-evolution operator and thus will be dressed. At leading order in g, the time-evolution operator in the interaction picture will be given by

$$\begin{aligned}\hat{U}(0,-\infty) &= \mathcal{P}^+\exp\left\{-i\int_{-\infty}^{0} dx^+ \hat{H}_I(x^+)\right\} = 1 - i\int_{-\infty}^{0} dx^+ \hat{H}_I(x) + \mathcal{O}(g^2) \\ &= 1 - i\int_{-\infty}^{0} dx^+ e^{-i\hat{H}_0 x^+}\hat{H}_{\text{int}} e^{i\hat{H}_0 x^+} + \mathcal{O}(g^2),\end{aligned} \tag{2.68}$$

where $\hat{H}_I$ is the interaction light-cone Hamiltonian in the Schrodinger picture, $\hat{H}_{\text{int}}$ the interaction light-cone Hamiltonian in the interaction picture and $\hat{H}_0$ is the free light-cone Hamiltonian. Thus, any bare state $|i\rangle$ will be dressed by the time-evolution operator as

$$\hat{U}(0,-\infty)|i\rangle = |i\rangle - \sum_f |f\rangle \frac{\langle f|\hat{H}_{\text{int}}|i\rangle}{\omega_f - \omega_i} + \mathcal{O}(g^2), \tag{2.69}$$

where $\omega_f = \sum_{j\in f} k_j^-$ is the sum of the light-cone energy of the particles in the state $|f\rangle$ and $k^- = \mathbf{k}^2/(2k^+)$ is the light-cone energy. The next step is to separate the slow and valence degrees of freedom in the interaction Hamiltonian and to compute the dressed projectile state. Because of the dispersion relation $k^- = \mathbf{k}^2/(2k^+)$, the valence modes will have much smaller light-cone energy (frequency) than the soft gluons. Thus, they will vary much slower in time than the slow modes and therefore we can assume that the valence states are frozen while the soft states will be our dynamical degrees of freedom. This, of course, is the idea behind the Color Glass Condensate.

Since the soft space of the initial projectile wave function is empty, we would like to dress it with soft gluons. The part of the light-cone interaction Hamiltonian which accounts for gluon emission is given by [93]

$$\begin{aligned}\hat{H}_{g\to gg} = \int_{k^+,q^+>0}\int_{\mathbf{k},\mathbf{q}} \frac{-gT^a_{bc}}{2\sqrt{2k^+q^+(q^+-k^+)}}\left((2\mathbf{q}-\mathbf{k})^i - \frac{2q^+-k^+}{k^+}\mathbf{k}^i\right) \\ \times\left[\hat{a}_i^{a\dagger}(k^+,\mathbf{k})\hat{a}_j^{b\dagger}(q^+-k^+,\mathbf{q}-\mathbf{k})\hat{a}_j^c(q^+,\mathbf{q}) + \textbf{h.c.}\right],\end{aligned} \tag{2.70}$$

where we have only written the part of the Hamiltonian that is relevant for our analysis. This Hamiltonian describes an initial gluon with momentum $(q^+,\mathbf{q})$ and color b emitting a gluon with momentum $(k^+,\mathbf{k})$ and color a.

Since we are assuming that the soft modes are generated by the valence partons, the original gluon has to be in a valence state where $q^+ > \Lambda^+$ while the emitted gluon is soft with $k^+ < \Lambda^+$. Taking the soft limit ($k^+ \ll q^+$) of this expression we can rewrite it as

$$\hat{H}_{\rho\to\rho g} = g\int_{\mathbf{x},\mathbf{y}} \hat{\rho}_p^a(\mathbf{x})\int_{\mathbf{k},k^+<\Lambda^+}\frac{1}{\sqrt{2k^+}}\frac{\mathbf{k}^i}{k^+}e^{-i\mathbf{k}\cdot(\mathbf{x}-\mathbf{y})}\hat{a}_i^{a\dagger}(k^+,\mathbf{y}) + \textbf{h.c.}, \tag{2.71}$$

where we have defined the projectile's valence color charge density operator as

$$\hat{\rho}_p^a(\mathbf{x}) = \int_{q^+>\Lambda^+}\hat{a}_b^\dagger(q^+,\mathbf{x})T^a_{bc}\hat{a}_c(q^+,\mathbf{x}). \tag{2.72}$$

Because the valence partons are frozen in the collision, we will forget about the self-interaction of the $q^+ > \Lambda^+$ modes of the Hamiltonian, that is, we consider that the valence partons are free collinear particles moving in the + direction. On the other hand, we are keeping the self interaction of the soft modes as it is. Moreover, although the operator $\hat{\rho}_p^a(\mathbf{x})$ operates on the valence Hilbert space, as far as the soft fields is concerned, it is a c-number function and since we are only interested in the dynamics of the soft gluons we will drop the hat from $\hat{\rho}_p^a(\mathbf{x})$ from now on. Furthermore, since the projectile is dilute, $\rho_p \sim \mathcal{O}(1)$, we can use perturbation theory.

Let us now see how this interaction Hamiltonian dresses the vacuum soft state in the projectile wave function. By using Eq. (2.68) at leading order in g we can write

$$\begin{aligned}\hat{U}(0,-\infty)|0\rangle &= |0\rangle - \int_{\mathbf{k},k^+<\Lambda^+} |g^a(k^+,\mathbf{k})\rangle \frac{\langle g^a(k^+,\mathbf{k})|\hat{H}_{\rho\to\rho g}|0\rangle}{\mathbf{k}^2/2k^+} + \mathcal{O}(g^2) \\ &= |0\rangle - i\int_{\mathbf{z}}\int_{k^+<\Lambda^+} b_i^a(\mathbf{z})\frac{1}{\sqrt{2k^+}}\hat{a}_i^{a\dagger}(k^+,\mathbf{z})|0\rangle + \mathcal{O}(g^2) \\ &\approx \exp\left\{-i\int_{\mathbf{z}}\int_{k^+<\Lambda^+} b_i^a(\mathbf{z})\frac{1}{\sqrt{2k^+}}\hat{a}_i^{a\dagger}(k^+,\mathbf{z}) + \mathbf{h.c.}\right\}|0\rangle \equiv \hat{\Omega}|0\rangle, \end{aligned} \tag{2.73}$$

where we have removed the sub-index "soft" from the soft vacuum state since, from now on, all the creation and annihilation operators are supposed to be soft and the valence state will be static. In order to obtain the second equality of this equation we have used that

$$\int \frac{d^2\mathbf{k}}{(2\pi)^2}\frac{\mathbf{k}^i}{\mathbf{k}^2}e^{-i\mathbf{k}\cdot x} = \frac{-i}{(2\pi)}\frac{\mathbf{x}^i}{\mathbf{x}^2}, \tag{2.74}$$

and defined the following functions

$$b_i^a(\mathbf{x}) = \frac{g}{\pi}\int_{\mathbf{y}} f_i(\mathbf{x}-\mathbf{y})\rho_p^a(\mathbf{y}), \qquad f_i(\mathbf{x}-\mathbf{y}) = \frac{(\mathbf{x}-\mathbf{y})^i}{(\mathbf{x}-\mathbf{y})^2}. \tag{2.75}$$

We call the operator $\hat{\Omega}$, defined in Eq. (2.73), the *gluon cloud operator* [94]. $\hat{\Omega}$ is a coherent unitary operator that generates soft gluons around the soft vacuum of the dilute projectile wave function. In this evolution operator, the soft gluon fields are coupled to the valence color charge density through the Weizsaker-Williams field $b_i(\mathbf{x})$. The Weizsaker-Williams (WW) field [95, 96], which was firstly proposed in the context of QED, is the resulting transverse electric field generated by infinitely boosting a Coulomb field created by a static charge in the longitudinal direction. In a quantum field theory, the generation of new transverse modes would imply an increase in the number of bosons with transverse polarization. Thus, $b_i^a(\mathbf{x})$ can be identified as the non-Abelian Weizsaker-Williams field of the valence charge density ρ^a [26].

Knowing how the initial projectile state $|P\rangle_{\text{in}}$ evolves with time, let us compute the single gluon production spectrum using Eq. (2.64)

$$(2\pi)^3\frac{dN}{dk^+d^2\mathbf{k}} = {}_{\text{in}}\langle P|\hat{\Omega}^\dagger\hat{\mathcal{S}}^\dagger\hat{\Omega}\hat{a}_i^{a\dagger}(k^+,\mathbf{k})\hat{a}_i^a(k^+,\mathbf{k})\hat{\Omega}^\dagger\hat{\mathcal{S}}\hat{\Omega}|P\rangle_{\text{in}} = \left|\hat{a}_i^a(k^+,\mathbf{k})\hat{\Omega}^\dagger\hat{\mathcal{S}}\hat{\Omega}|P\rangle_{\text{in}}\right|^2, \tag{2.76}$$

where since $\hat{Omega}$ is the time evolution operator, this is the amplitude squared of evolving the initial projectile state via $\hat{\Omega}$, having into account the interaction through the operator $\hat{\mathcal{S}}$, evolving the resulting state to $x^+ = +\infty$ using $\hat{\Omega}^\dagger$ and counting the number of produced gluons using $\hat{a}$.

In order to perform this calculation we note that

$$\hat{\Omega}\hat{a}_i^a(k^+,\mathbf{k})\hat{\Omega}^\dagger = \int_{\mathbf{z}} e^{-i\mathbf{k}\cdot\mathbf{z}}\left(\hat{a}_i^a(k^+,\mathbf{z}) + \frac{i}{\sqrt{2k^+}}b_i^a(\mathbf{z})\right). \tag{2.77}$$

Therefore

$$\begin{aligned}\hat{\Omega}^\dagger\hat{\Omega}\hat{a}_i^a(k^+,\mathbf{k})\hat{\Omega}^\dagger\hat{\mathcal{S}} &= \int_{\mathbf{z}} e^{-i\mathbf{k}\cdot\mathbf{z}}\hat{\Omega}^\dagger\hat{\mathcal{S}}\hat{\mathcal{S}}^\dagger\left(\hat{a}_i^a(k^+,\mathbf{z}) + \frac{i}{\sqrt{2k^+}}b_i^a(\mathbf{z})\right)\hat{\mathcal{S}} \\ &= \hat{\Omega}^\dagger\hat{\mathcal{S}}\int_{\mathbf{z}} e^{-i\mathbf{k}\cdot\mathbf{z}}\left(U^{ba}(\mathbf{z})\hat{a}_i^b(k^+,\mathbf{z}) + \frac{i}{\sqrt{2k^+}}\frac{g}{\pi}\int_{\mathbf{y}} f_i(\mathbf{z}-\mathbf{y})U^{ba}(\mathbf{y})\rho_p^b(\mathbf{y})\right),\end{aligned} \tag{2.78}$$

and finally, we act with this operator on $\hat{\Omega}|0\rangle$ in order to get

$$\hat{a}_i^a(k^+,\mathbf{k})\hat{\Omega}^\dagger\hat{\mathcal{S}}\hat{\Omega}|0\rangle = \hat{\Omega}^\dagger\hat{\mathcal{S}}\int_{\mathbf{z}} e^{-i\mathbf{k}\cdot\mathbf{z}}\frac{ig}{\pi\sqrt{2k^+}}\int_{\mathbf{x}} f_i(\mathbf{z}-\mathbf{x})\rho_p^b(\mathbf{x})\left[U^{ba}(\mathbf{x}) - U^{ba}(\mathbf{z})\right]|0\rangle. \tag{2.79}$$

Since the operator $\hat{\Omega}^\dagger\hat{\mathcal{S}}$ in front of this expression will not be relevant when we square this quantity, we can conclude that the matrix amplitude for generating a single gluon with momentum $(k^+,\mathbf{k})$, color a and polarization i from an initial projectile with no soft modes interacting with a strong external field A_T^- is

$$\mathcal{M}_i^a(k^+,\mathbf{k}) = \int_{\mathbf{z}} e^{-i\mathbf{k}\cdot\mathbf{z}}\frac{ig}{\pi\sqrt{2k^+}}\int_{\mathbf{x}} f_i(\mathbf{z}-\mathbf{x})\rho_p^b(\mathbf{x})\left[U(\mathbf{x}) - U(\mathbf{z})\right]^{ba}. \tag{2.80}$$

Usually, it is convenient to write this expression in momentum space. By performing an easy manipulation we can write

$$\mathcal{M}_i^a(k^+,\mathbf{k}) = \frac{2g}{\sqrt{2k^+}}\int_{\mathbf{q}} L^i(\mathbf{k},\mathbf{q})\rho_p^b(\mathbf{q})U^{ba}(\mathbf{k}-\mathbf{q}), \tag{2.81}$$

where $\rho_p(\mathbf{q})$ and $U(\mathbf{k}-\mathbf{q})$ are the Fourier transform of the projectile's valence charge density and the Wilson line, and we have defined the *Lipatov vertex*

$$L^i(\mathbf{k},\mathbf{q}) = \frac{\mathbf{k}^i}{\mathbf{k}^2} - \frac{\mathbf{q}^i}{\mathbf{q}^2}. \tag{2.82}$$

The Lipatov vertex [18] is an effective vertex which accounts for the possibility of the soft gluon being emitted before the interaction of the valence states with the target shock-wave or being emitted after the interaction with the target.

All in all, the leading order single inclusive gluon spectrum can be computed by squaring Eq. (2.81) and performing the projectile and target average. The result is

$$2(2\pi)^3\frac{dN}{d\eta d^2\mathbf{k}} = 4g^2\int_{\mathbf{q}_1\mathbf{q}_2} L^i(\mathbf{k},\mathbf{q}_1)L^i(\mathbf{k},\mathbf{q}_2)\left\langle\rho_p^{b_1}(\mathbf{q}_1)\rho_p^{*b_2}(\mathbf{q}_2)\right\rangle_p$$

$$\times \left\langle \left[U(\mathbf{k}-\mathbf{q}_1)U^\dagger(\mathbf{k}-\mathbf{q}_2)\right]^{b_1 b_2} \right\rangle_T, \tag{2.83}$$

where we have written $d\eta = dk^+/k^+$, by using the definition of the pseudorapidity in Equation (2.1). On the one hand the average over the target color charge density is performed by writing A_T^- in terms of ρ_T by using the relation given in Eq. (2.16). On the other hand, since ρ_p is in reality the expectation value $\langle v|\hat{\rho}_p|v\rangle$, we will assume that it is a stochastic variable that also follows the MV distribution. This equation is exactly the same as the one obtained in the last section by using the eikonal approximation in Eq. (2.41). Thus, it serves as a double check that the CGC framework gives the same result by solving the linearized Yang-Mills equation or by using the light-cone perturbation theory.

2.4 Wigner function distributions

To finalize our discussion on particle production in proton-nucleus collisions we will summarize another framework, that will be useful in Chapter 4, which we will refer to as the *Wigner function* approach. The Wigner distribution is a function that encodes the correlation between the momentum and space coordinates of a given quantum system. These distributions have been used for various purposes in very diverse areas such as heavy-ion collisions, quantum information, quantum molecular dynamics, etc. In high energy QCD they are important for given a description of both the spatial and momentum distribution of quarks and gluons within the hadron or nucleus wave function. Thanks to this distribution, it is possible to obtain the so-called transverse momentum dependent distributions (TMDs), the PDFs or the impact parameter distributions, which are of great importance in order to understand the inner structure of the proton. An analysis of these functions in high energy QCD is out of the scope of this thesis and thus we will restrict ourselves to give the basic aspects of it that are important to analyze particle correlations. For a review of the Wigner distribution applied to the proton structure we refer, for example, to [97].

The Wigner distribution is defined through the density matrix[7] $\hat{\omega}$ of a given quantum system. Let us denote the dressed projectile's wave function by $|P\rangle$, thus its density matrix is given by

$$\hat{\omega} = |P\rangle\langle P|\,. \tag{2.84}$$

In the case of CGC, this operator have acquired importance in the last years due to the interest in computing the entropy entanglement of the soft modes in the high energy projectile wave function [98–101]. In our case, we are interested in the reduced n-gluon density matrix $\hat{\omega}_n$ defined as

$$\hat{\omega}_n = |\{g^{a_i}(k_i^+,\mathbf{x}_i)\}\rangle\langle\{g^{a_i}(k_i^+,\mathbf{x}_i)\}|\,\hat{\omega}\,|\{g^{b_i}(q_i^+,\mathbf{y}_i)\}\rangle\langle\{g^{b_i}(q_i^+,\mathbf{y}_i)\}|\,, \tag{2.85}$$

where $|\{g^{a_i}(k_i^+,\mathbf{x}_i)\}\rangle$ is the state of n gluons with longitudinal momentum k_i^+, transverse position $\mathbf{x}_i$ and color a_i. We also define for convenience the matrix element of the n-gluon

[7] Here we use the notation ω for the density matrix instead of usual notation ρ in order to do not overlap with the definition of the color charge density.

reduced matrix as

$$\omega_n\left[\{g^{a_i}(k_i^+,\mathbf{x}_i)\},\{g^{b_i}(q_i^+,\mathbf{y}_i)\}\right]\equiv\langle\{g^{a_i}(k_i^+,\mathbf{x}_i)\}|\,\hat{\omega}\,|\{g^{b_i}(q_i^+,\mathbf{y}_i)\}\rangle\,. \tag{2.86}$$

Now, let us study the case of single inclusive gluon production. By using Eq. (2.64) with $|\alpha_0\rangle=|P\rangle$ we have that

$$(2\pi)^3\frac{dN}{dk^+d^2\mathbf{k}}=\int_{\mathbf{z},\bar{\mathbf{z}}}e^{-i\mathbf{k}\cdot(\mathbf{z}-\bar{\mathbf{z}})}\langle P|\hat{U}^\dagger\hat{\mathcal{S}}^\dagger\hat{U}\hat{a}^{\dagger c}(k^+,\mathbf{z})\hat{a}^c(k^+,\bar{\mathbf{z}})\hat{U}^\dagger\hat{\mathcal{S}}\hat{U}|P\rangle. \tag{2.87}$$

Assuming that the gluon is emitted before the interaction of the projectile with the shock-wave, i.e. that $\hat{U}|P\rangle=|g\rangle\otimes|P\rangle$, it is a matter of easy algebra to find that

$$(2\pi)^3\frac{dN}{dk^+d^2\mathbf{k}}=\int_{\mathbf{z},\bar{\mathbf{z}}}e^{-i\mathbf{k}\cdot(\mathbf{z}-\bar{\mathbf{z}})}\,\omega_1\left[g^a(k^+,\mathbf{z}),g^b(k^+,\bar{\mathbf{z}})\right]\left[U^\dagger(\bar{\mathbf{z}})U(\mathbf{z})\right]^{ba}. \tag{2.88}$$

On the other hand, we define the n-particle Wigner distribution as[8]

$$W_n^{\{a_ib_i\}}(\{\mathbf{b}_i,\mathbf{k}_i\})=\int_{\mathbf{q}_1,\ldots,\mathbf{q}_n}e^{-i\mathbf{q}_1\cdot\mathbf{b}_1\cdots-i\mathbf{q}_n\cdot\mathbf{b}_n}\,\langle\{g^{a_i}(\mathbf{k}_i+\mathbf{q}_i/2)\}|\,\hat{\omega}_n\,|\{g^{b_i}(\mathbf{k}_i-\mathbf{q}_i/2)\}\rangle\,, \tag{2.89}$$

where we have dropped the k^+ dependence of the quantum states since, at leading order, the eikonal multi-gluon spectrum is boost invariant. Therefore the single gluon Wigner function will be given by

$$\begin{aligned}W_1^{ab}(\mathbf{b},\mathbf{k})&=\int_{\mathbf{q}}e^{-i\mathbf{q}\cdot\mathbf{b}}\,\langle g^a(\mathbf{k}+\mathbf{q}/2)|\,\hat{\omega}_1\,|g^b(\mathbf{k}-\mathbf{q}/2)\rangle\\&=\int_{\mathbf{z},\bar{\mathbf{z}}}e^{-i\mathbf{k}\cdot(\mathbf{z}-\bar{\mathbf{z}})}\omega_1\left[g^a(k^+,\mathbf{z}),g^b(k^+,\bar{\mathbf{z}})\right]\delta^{(2)}\left(\mathbf{b}-\frac{\mathbf{z}+\bar{\mathbf{z}}}{2}\right),\end{aligned} \tag{2.90}$$

and thus Eq. (2.88) can be rewritten as

$$\frac{dN}{d^2\mathbf{k}}=\int_{\mathbf{b},\mathbf{r}}\int_{\mathbf{q}}e^{-i(\mathbf{k}-\mathbf{q})\cdot\mathbf{r}}W_1^{ab}(\mathbf{b},\mathbf{q})\left[U^\dagger\left(\mathbf{b}-\frac{\mathbf{r}}{2}\right)U\left(\mathbf{b}+\frac{\mathbf{r}}{2}\right)\right]^{ba}, \tag{2.91}$$

where we have introduced the factor $1/(2\pi)^3$ in the definition of the Wigner function. The idea behind Eq. (2.91) is very similar to the PDF approach used in the hybrid formalism, in fact, the PDFs and the Wigner distributions are related by an integral. The single gluon Wigner function is a non-perturbative object that gives the probability of finding a gluon with transverse momentum $\mathbf{q}$ and at a position $\mathbf{x}$, then this gluon scatters in the dense medium with the eikonal matrix amplitude given by the Wilson line. When the gluon is generated at mid rapidity, i.e., we probe the low-x regime of the projectile wave function, the Wigner function can be computed analytically [85, 100].

The factorization given in Eq. (2.91) has been used recently in order to perform studies in multi-particle correlation [102–106]. Since the Wigner function is a non-perturbative

[8] This definition differs from the one that appears in literature by the color dependence of the Wigner function. The reason that we are including this color dependence is because, in order to account for the color correlation between the partons within the projectile wave function, we should have a color structure in the Wigner function.

object, one has to assume some parameterization to this object. It has been proposed in [103] to use the following Gaussian form

$$W_1^{ab}(\mathbf{b},\mathbf{q}) = \frac{\delta^{ab}}{N_c^2-1}\frac{1}{\pi^2}e^{-\mathbf{b}^2/B_p}e^{-\mathbf{q}^2 B_p}, \tag{2.92}$$

where B_p is the gluonic transverse area of the projectile. Although this form is not realistic, it is simple enough and therefore very useful for performing qualitative studies in multi-particle correlation.

The expression for the multi-gluon inclusive spectrum can be generalized from Eq. (2.91) and reads

$$\frac{d^n N}{d^2\mathbf{k}_1\cdots d^2\mathbf{k}_n} = \prod_{i=1}^{n}\int_{\mathbf{b}_i,\mathbf{r}_i}\int_{\mathbf{q}_i} W_n^{a_1b_1\cdots a_nb_n}(\mathbf{b}_1,\mathbf{q}_1,\ldots,\mathbf{b}_n,\mathbf{q}_n) \times e^{-i(\mathbf{k}_i-\mathbf{q}_i)\cdot\mathbf{r}_i}\left[U^\dagger\left(\mathbf{b}_i-\frac{\mathbf{r}_i}{2}\right)U\left(\mathbf{b}_i+\frac{\mathbf{r}_i}{2}\right)\right]^{b_ia_i}. \tag{2.93}$$

In order to perform studies on particle correlations, it is usually assumed the following factorization for the n-gluon Wigner function [103, 105]

$$W_n^{a_1b_1\cdots a_nb_n}(\mathbf{b}_1,\mathbf{q}_1,\ldots,\mathbf{b}_n,\mathbf{q}_n) = \prod_{i=1}^{n} W_1^{a_ib_i}(\mathbf{b}_i,\mathbf{q}_i), \tag{2.94}$$

with the single gluon Wigner distribution given by Eq. (2.92). This factorization assumption is inconvenient since it neglects any kind of correlation coming from the gluons in the projectile wave function and therefore, as we will see in Chapter 3, it neglects the Bose Enhancement terms that are one of the leading sources of flow correlations. For this reason, in Chapter 4, we will mimic the Gaussian ansatz of the Wigner distribution but without assuming the factorization condition of Eq. (2.94). The strategy for doing that is to compare Eqs. (2.83) and (2.91) and to realize that, after making the change of variables $\mathbf{q}_{1(2)} = \mathbf{q} \pm \mathbf{p}/2$ in the second equation, we can identify the single gluon Wigner distribution as [38]

$$W^{ab}(\mathbf{b},\mathbf{q}) = \int_{\mathbf{p}} e^{-i\mathbf{p}\cdot\mathbf{b}} L^i(\mathbf{k},\mathbf{q}+\mathbf{p}/2)L^i(\mathbf{k},\mathbf{q}-\mathbf{p}/2)\left\langle \rho_p^a(\mathbf{q}+\mathbf{p}/2)\rho_p^{*b}(\mathbf{q}-\mathbf{p}/2)\right\rangle_p. \tag{2.95}$$

This equation depends on $\mathbf{k}$ through the product of the Lipatov vertices and therefore is not a proper definition of the Wigner distribution. Thus, we look for a parameterization of the product of the Lipatov vertices that is $\mathbf{k}$ independent and keep the Gaussian form given in Eq. (2.92). This approach is unrealistic and should not be considered reliable for phenomenological analysis. However, it keeps the simplicity of the Gaussian ansatz by miming it and allows us to write, as we shall see in Chapter 4, the n-gluon Wigner function as

$$W_n^{a_1b_1\cdots a_nb_n}(\mathbf{b}_1,\mathbf{q}_1,\ldots,\mathbf{b}_n,\mathbf{q}_n) = \left(\prod_{\lambda=1}^{n}\int_{\mathbf{p}_\lambda} e^{-i\mathbf{p}_\lambda\cdot\mathbf{b}_\lambda} L^{i_\lambda}(\mathbf{k}_\lambda,\mathbf{q}_\lambda+\mathbf{p}_\lambda/2)L^{i_\lambda}(\mathbf{k}_\lambda,\mathbf{q}_\lambda-\mathbf{p}_\lambda/2)\right) \times\left\langle\prod_{\lambda=1}^{n}\rho_p^{a_\lambda}(\mathbf{q}_\lambda+\mathbf{p}_\lambda/2)\rho_p^{*b_\lambda}(\mathbf{q}_\lambda-\mathbf{p}_\lambda/2)\right\rangle_p, \tag{2.96}$$

and we will break the factorization ansatz given in Eq. (2.94) through the Wick's expansion of the projectile's average. Therefore we expect that this approach, although unrealistic, may give a good framework for studying, at least qualitatively, the properties of multi-particle correlations while maintaining the simplicity of the Gaussian ansatz.

2.5 Particle production in proton-proton collisions

In the last sections we have discussed the case of particle production in proton-nucleus collisions, where a dilute projectile ($\rho_p \sim \mathcal{O}(1)$) scatters in a dense target ($\rho_p \sim \mathcal{O}(g^{-2})$). Our final result for the eikonal single inclusive gluon spectrum at leading order in g was given in Eq. (2.83). This equation involves the target average of two Wilson lines and, because of the non-linear dependence of the Wilson lines with ρ_T, it is difficult to be solved analytically[9]. Nevertheless, if one takes the dilute limit of the target, solving Eq. (2.83) is not so difficult as we shall see. The approximation where we take the dilute limit of ρ_T is known in the literature as *Glasma Graph Approximation* [107, 108].

Before starting our discussion, let us note that the single gluon amplitude in Eq. (2.81) can be expanded in powers of ρ_T as

$$\mathcal{M}_i^a(k^+, \mathbf{k}) = \frac{2g}{\sqrt{2k^+}} \int_{\mathbf{q}} L^i(\mathbf{k}, \mathbf{q}) \rho_p^b(\mathbf{q}) \left[ig^2 T_{ab}^c \frac{\rho_T^c(\mathbf{k}-\mathbf{q})}{(\mathbf{k}-\mathbf{q})^2} + \mathcal{O}\left(\frac{g^4 \rho_T^2(\mathbf{k}-\mathbf{q})}{(\mathbf{k}-\mathbf{q})^4} \right) \right], \tag{2.97}$$

where we have expanded the Wilson line in powers of $A_T^-(x^+, \mathbf{x}) = -g\delta(x^+)\rho_T(\mathbf{x})/\nabla^2$ and performed the Fourier transform. In the dilute limit, the projectile probes gluons with momentum $(\mathbf{k}-\mathbf{q})^2 \gg Q_s^2$ while the density of these gluonic modes is parametrically small $\rho_T(\mathbf{k}-\mathbf{q}) \sim 1$. For this reason we can assume that, in the dilute limit, $\rho_T(\mathbf{k}-\mathbf{q})/(\mathbf{k}-\mathbf{q})^2 \ll 1$ and Eq. (2.97) reduces to

$$\mathcal{M}_i^a(k^+, \mathbf{k}) = \frac{2ig^3}{\sqrt{2k^+}} T_{bc}^a \int_{\mathbf{q}} L^i(\mathbf{k}, \mathbf{q}) \frac{\rho_p^b(\mathbf{q}) \rho_T^c(\mathbf{k}-\mathbf{q})}{(\mathbf{k}-\mathbf{q})^2}. \tag{2.98}$$

Therefore, the amplitude is completely symmetric by interchanging the projectile and the target. Since the high momentum modes of the projectile are also probed by the target, the transverse momentum of the emitted gluon has to be large, $\mathbf{k}^2 \gg Q_s^2$.

Thus, the Glasma Graph Approximation gives us a framework for studying high momenta gluon production where the amplitude depends linearly on the sources ρ_p and ρ_T. Because of both the projectile and the target are dilute, this approximation is more suitable for proton-proton collisions – or not very energetic small nuclei.

Moreover, the 2-point correlator can be computed in the MV model using Eq. (1.51):

$$\langle \rho_{p(T)}^a(\mathbf{k}) \rho_{p(T)}^{*b}(\mathbf{q}) \rangle_{p(T)} = \mu^2 \delta^{ab} (2\pi)^2 \delta^{(2)}(\mathbf{k}-\mathbf{q}). \tag{2.99}$$

Therefore, in the Glasma Graph approximation, the single gluon spectrum can be written just as

$$\frac{dN}{d\eta d^2\mathbf{k}} = \frac{\mu^4 g^6 S_\perp N_c (N_c^2-1)}{4\pi^3} \frac{1}{\mathbf{k}^2} \int_{\mathbf{q}} \frac{1}{\mathbf{q}^2 (\mathbf{k}-\mathbf{q})^2}, \tag{2.100}$$

[9] We shall see on Section 4.2 that the target n-point function can be solved exactly in the MV model.

where we have defined $S_\perp = (2\pi)^2\delta^{(2)}(\mathbf{q}-\mathbf{q})$, used the fact that $\mathrm{Tr}\,[T^aT^a] = N_c(N_c^2-1)$ and performed the product of the Lipatov vertices. This result was derived in [109, 110]. The remaining integral has to be regularized by introducing a finite color neutralization sale Λ^2, and can be written as $\ln(\mathbf{k}^2/\Lambda^2)/\mathbf{k}^2$. Because of its simplicity, the Glasma Graph approximation is an optimal framework for performing qualitative studies in high energy collisions. Moreover, it has been able to explain successfully a wealth amount of data in *pp* collisions [111–114]. In the next chapter we will use the double gluon spectrum in this approximation for studying particle correlations.

USC
UNIVERSIDADE
DE SANTIAGO
DE COMPOSTELA

Chapter 3

Particle correlations from the initial state

We have seen in the last chapter that the Color Glass Condensate offers a good framework for studying particle production in high energy collisions for nucleus-nucleus, proton-nucleus or proton-proton scatterings. We will now explore some of the consequences of the results obtained in Chapter 2, in particular, the phenomenon of multi-particle correlations generated in high energy collisions. The studies on particle correlations in high energy QCD has acquired special importance in the last years due to the discovery by the CMS collaboration [24, 25] that there are traces of collective behavior in proton-proton o proton-nucleus collisions. Until then, collective behavior was though to only be a property of large systems generated in heavy ion collision due to hydrodynamic flow. This phenomenon introduced a division in the heavy-ion community between initial state models, mostly based on the CGC framework, and final state models, mostly based in viscous hydrodynamics, to explain the collective behavior in small systems.

The goal of this chapter will be to review the effect of flow correlations as well as to introduce possible explanations for such a phenomenon in small systems. The chapter is organized as follows. In Section 3.1 we will introduce the stages of a heavy ion collisions as well as the ridge-like structure seen in two particle correlations. In Section 3.2 we will compute the two gluon spectrum within the Glasma Graph approximation in order to see that this approach is able to explain many features of the ridge. In Section 3.3 we introduce the chromo-electric domain model which proposes that the target ensemble is composed by chromo-electric domains and that particle correlations arise from projectile partons that interact on the same domain. Finally, in Section 3.4 we will briefly review the cumulant method which aims to extract the "non-flow" components of the azimuthal harmonics and is extensively used in experimental analysis.

3.1 Flow correlations

To begin the discussion about correlations in high energy collisions, let us first recapitulate what are the stages of a typical nucleus-nucleus collision performed at the LHC or RHIC. The collision of large nuclei constitutes an example of a many-body problem in QCD and, because of the non-perturbative behavior of this theory, involves many complex dynamics over the time evolution of the collision. In the last decades, huge theoretical efforts were made in order to describe the evolution of such a dense system over time. The result was a high interdisciplinary framework where the evolution of a high energy collision is separated into different stages, each of them described by the most prominent physical features that they encode. Thus, the picture of the dense system evolution is completely analogous to the cosmological evolution after the Big Bang, where we use many theoretical frameworks to describe the different stages of the expansion of the dense matter generated at the beginning of the universe.

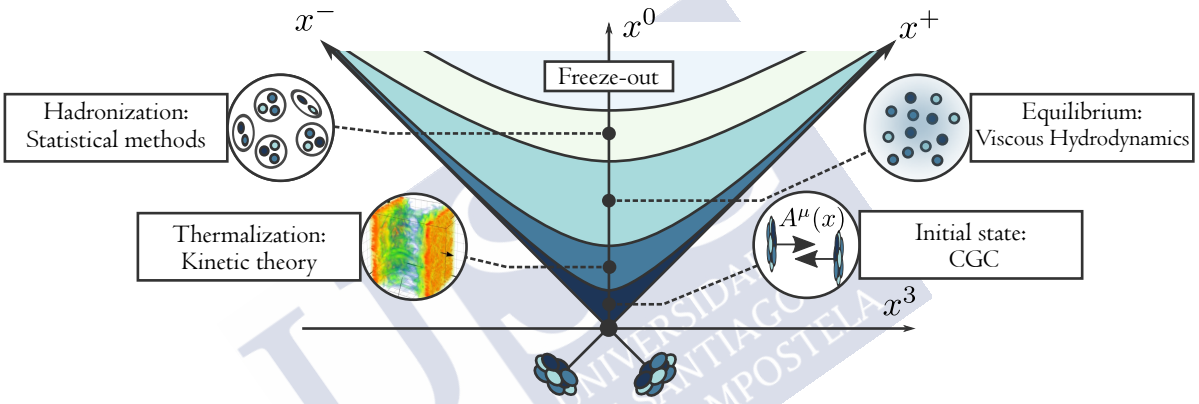

Figure 3.1.
The evolution dynamics of a high energy nucleus-nucleus collision. The expanding system formed in the collision moves from an initial state, usually described by the CGC EFT, towards a quasi-ideal partonic fluid after undergoing a complex process known as thermalization. After some time, the fluid cools down and hadronizes. Then, the hadronic system freeze-out and moves toward the detectors.

The picture that we have for a high energy nucleus-nucleus collision is illustrated in Fig. 3.1. In what follows we will summarize the dynamics of the expanding system but we should note that each topic discussed below have their own extensive literature as well as big opened questions. First, at an infinitesimal proper time $\tau = 0^+$ after the collision, we have a dense classical system constituted by the interaction of the small-x gluons that were in the nucleus wave functions. As we have seen in the last chapters, such a system is well described by the Color Glass Condensate effective theory. We will refer to this stage as the *initial state* and having a good knowledge of this stage is essential since it serves as the initial condition for the system evolution. The state of matter generated in this stage is sometimes referred to as *Glasma* [115].

After the Glasma is created, the system expands to an *out of equilibrium* state that is driven by a large number of interactions between quarks and gluons. Because of the expansion, the system becomes dilute and the CGC is unable to explain its dynamics.

By using the Heisenberg uncertainty principle, one can infer that the CGC is only able to describe the system up to a proper time $\tau \sim Q_s^{-1}$ (~ 0.2 fm/c for RHIC or 0.1 fm/c for LHC). After this time, the system rapidly evolves to a thermal equilibrium state where the non-trivial process towards this equilibrium is known as *thermalization*. The thermalization is then a weak-coupling process[1] where the system changes from a over-occupied far from equilibrium state to a thermal state. This stage is supposed to be described by an effective kinetic theory [116].

Once the system achieves thermal equilibrium, the size of the expanding system is much larger than the mean free path of the interacting particles and, therefore, the medium can be described by its thermodynamical variables. In such a system, the evolution of the expanding *fireball* medium is well described by the quasi-ideal *relativistic hydrodynamics* framework [117]. According to the hydrodynamics theory, the approach to ideal hydrodynamics should be described by *viscous hydrodynamics*, which gives predictions that depend on the shear viscosity η of the matter as well as other coefficients such as bulk viscosity, relaxation times, etc. The state of matter generated at this stage is known as the *quark gluon plasma* (QGP).

As the dense matter expands and cools down, the typical energies of the collisions become lower and the system makes a transition to a confined phase. Therefore, the medium will be described by a hadronic system and the process of going from a quasi-ideal fluid of quarks and gluons to a hadronic system is known as *hadronization*. Hadronization processes are highly non-trivial and it is challenging to describe them from first principles of QCD. In practice, statistical methods based on conservation laws are used to describe such a transition. Once hadronization is completed, the system can still be described by hydrodynamics as a hadronic fluid.

Finally, the hadron gas keeps expanding and cooling down until it quickly becomes dilute and the interaction between its constituents become negligible. This will lead to a chemical and kinetic *freeze-out*. After this point, only resonance decays or annihilations will modify the number of produced particles. The resulting hadrons will propagate freely toward the detectors.

As a consequence of this evolution, there are two final state phenomena that will be important in the discussion of this section: *jet quenching* and *flow correlations*. Jet quenching [118] is the suppression of high transverse momentum particle or jet production relative to the multiplicity expected from the number of participant nucleons in the collision. These particles (or jets) have they energy loss due to its interaction with the quark gluon plasma. Studies around the jet quenching phenomenon are very important because they give us direct evidence of how the QGP responds when a quark or gluon jet traverses it because the energy loss depends on the characteristics of the medium. This phenomenon was discovered at RHIC in Au-Au collisions [21] and was the first evidence of the QGP's formation in a high energy nucleus-nucleus (AA) collision.

Other strong signal of the presence of QGP in AA collisions are those that come from its collective behavior in the fast expansion of the medium, typically referred as *flow*. The dynamics imposed by the viscous hydrodynamical description of the QGP implies that any space anisotropy in the system would lead to a faster expansion in these directions with higher density gradients. Therefore the hydrodynamics evolution converts

[1] At the moment there is still a open debate on whether thermalization is ruled by a strong or weak coupling.

spatial anisotropies into momentum anisotropy. For a perfect circular system this would imply that the momentum distribution of the particles would be isotropic. However, for anisotropic systems, as those generated in non-central AA collisions, we will have high anisotropies in the particle spectrum. These anisotropies are usually quantified in terms of a Fourier expansion of the particle spectra. For example, in the case of single particle spectrum we can write

$$\frac{dN}{p_\perp dp_\perp d\phi} \propto 1 + \sum_n 2v_n(p_\perp)\cos[n(\phi - \Psi_n)], \tag{3.1}$$

where $p_\perp$ and ϕ are the transverse momentum and azimuthal angle of each particle and Ψ_n is the reaction plane angle. The Fourier coefficients v_n are known as *flow coefficients*. Collective flow effects were also measured at RHIC and hydrodynamic calculations using the CGC as initial condition are able to describe the measured flow coefficients [119] being other indicator of the QGP existence in AA collisions.

By measuring two or more particle correlations we can extract crucial information about the collective behavior of the QGP. These correlations are often parameterized in terms of the particles azimuthal angle $\Delta\phi$ in the transverse plane and their relative longitudinal pseudorapidity $\Delta\eta$. In Fig. 3.2 (left) we show the 2-particle correlation function $C(\Delta\phi, \Delta\eta)$ measured at the LHC for Pb+Pb collisions [120]. It can be seen that long-range correlations in pseudorapidity dominate around the *near-side* $\Delta\phi = 0$ and the *away-side* $\Delta\phi = \pi$. Because of the shape of this correlation function, it is often referred to as the *ridge*. Although this function can give us information about the collective behavior of the QGP we have to be careful when analyzing it since not all the correlations come from collective flow. Some correlations, known as *non-flow*, are given from sources that have nothing to do with the flowing medium. For example, hadronic resonances, such as $\Delta^{++} \to p + \pi^+$, lead to particle correlations. Another example is the so-called jet contributions where two partons are emitted from the same source and therefore they are back-to-back in azimuth ($\Delta\phi = \pi$) and have opposite rapidities because of momentum conservation. Thus the jets produced by these partons will populate the full acceptance in $\Delta\eta$ at $\Delta\phi = \pi$. These kind of correlations must be accounted for in order to isolate the contribution from the flow behavior. Finally, the dominant peak around $\Delta\phi = 0$ and $\Delta\eta = 0$ comes from jet fragmentation particles, resonance decays, etc. and also have to be washed out in order to study flow correlations. In Section 3.4 we will introduce the so-called *cumulant method* which is a technique for only selecting the flow contribution to multi-particle correlations.

So far, we have only discussed the evolution and properties the system generated in a high energy AA collision, we now turn our discussion to smaller systems generated in pp and pA collisions [122–125]. The time-evolution picture described for large nuclei is still valid for smaller systems with the big difference that, at the moment, is still unclear whether a small expanding partonic system can achieve thermal equilibrium before hadronizing. For this reason, pp and pA collisions were usually used only as control measurements, for example, in constraining nuclear modified parton distribution functions in the analysis of jet quenching in AA collisions. This was so until 2010, when the CMS collaboration examined high multiplicity events in pp collisions at the LHC and found that particles had long-range correlations in the near-side [24]. Then in 2012, measurements in pPb collisions at the LHC [25] also revealed signatures for collective flow in pA scatterings.

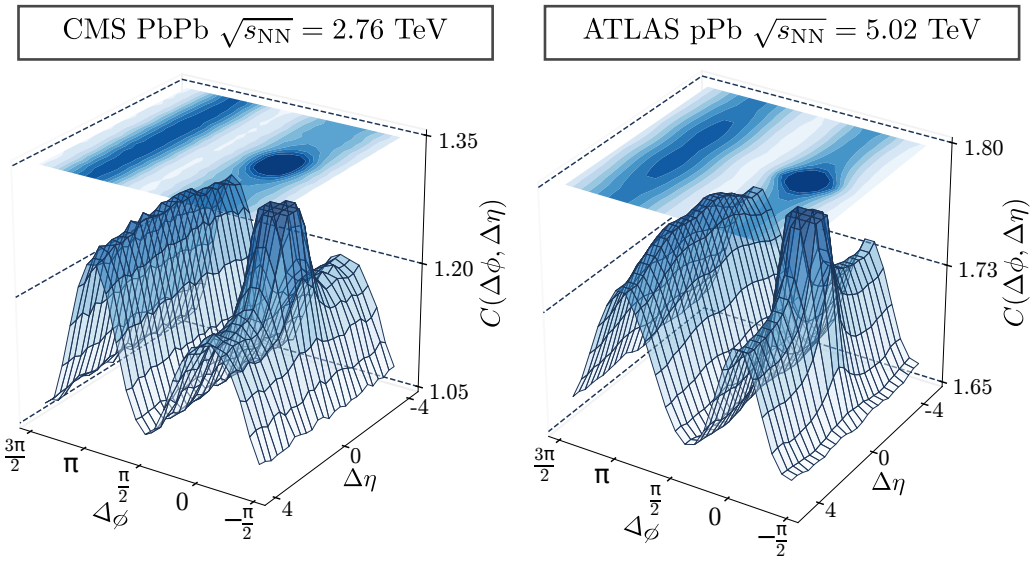

Figure 3.2.
Angular and rapidity correlations in AA collisions (left) and high multiplicity pA collisions (right). Left: data from the CMS collaboration for Pb+Pb collisions where 2-dimensional per-trigger-particle associated yield of charged hadrons for $3 < p_T^{\rm trig} < 3.5$ Gev/c in PbPb collisions at $\sqrt{s_{\rm NN}} = 2.76$ TeV and centrality 60-70% [120] are plotted. Right: Data from the ATLAS collaboration for p+Pb collisions at $\sqrt{s_{\rm NN}} = 5.02$ TeV where the correlation from particles with $1 < p_T < 3$ GeV and multiplicity $N > 220$ are selected [121].

The most surprising fact was that the correlation strength in pA collisions was almost as large as in AA collisions. In Fig. 3.2 (right) we show the ridge structure in pA systems with data extracted from the ATLAS collaboration for pPb collisions [121]. Thus an intense debate, still unsolved at the moment, started: is the source of the ridge in small systems the same as in AA collisions or does it comes from different phenomena?

Another question that we should make is if the collective behavior is only true for 2-particle correlations or if this correlation still persists among more produced particles. Motivated by the flow studies in AA collisions, correlation analysis in pp and pA collisions are also analyzed in terms of the flow coefficients v_n, i.e. the Fourier decomposition of the particle spectra. However, in the multi-particle case, results are sometimes presented in terms of the n-particle cumulant $c_m\{n\}$, to be defined in Section 3.4. Measurements of the 4-particle cumulant have been performed by CMS [126–128], ALICE [129] and ATLAS [130–133] collaborations. The results presented in these papers also revealed collective behavior in small systems and, for example, it has been seen that the 4-particle cumulant changes of sign from low to high multiplicities.

Viscous hydrodynamics have successfully described correlation in small systems for 2-particle production [134–139] and a not so well description in multi-particle correlations [140]. Moreover, the similarity of data observed in high multiplicity pp or pA collisions with those seen in AA collisions may suggest that correlations from collective behavior are also generated in small systems. Thus it is sometimes argued that small droplets of QGP are generated in small system collisions. As we shall see in the next sections, some of the correlation data are also well described by initial state calculations, in particular

within the CGC framework. Therefore, the community has been divided between initial state models, usually described by the CGC, or final-state models, usually described by viscous hydrodynamics, depending whether we assume that the momentum anisotropy was generated at the beginning of the collision or during the strong final state interactions.

Despite of the good description of hydrodynamics on particle correlations in small systems, the applicability of this theory in such systems has to be questioned by the following reasons. A well established condition to the applicability of hydrodynamics in a system is that the number of particles has to be large, the collision mean free path in the system has to much smaller than its dimensions and the system has to be in a statistical equilibrium. This condition can be parameterized by the dimensionless Knudsen number $K_N = l_{\text{fmp}}/R$, where R is the size of the system and l_{fmp} is the collision mean free path of the particles. If $K_N \ll 1$ the system can be described by hydrodynamics and if $K_N > 1$ it cannot. Recent simulations revealed that the Knudsen number is larger than one in sizable regions of the space-time in pA collisions [141], implying that higher order corrections to hydrodynamics may be important.

Another key condition for the applicability of hydrodynamics in small systems is the dominance of hydrodynamics modes over non-hydrodynamics modes. Hydrodynamic modes are long wavelength modes whose dispersion relation satisfies $\lim_{|\mathbf{k}|\to 0} \omega(\mathbf{k}) = 0$ while non-hydrodynamics modes have a finite value of $\omega(\mathbf{k})$ as $\mathbf{k}$ approaches zero [117]. Studies on the non-hydrodynamics modes in a weak coupling quasi-particle system indicates that they are non-negligible in small systems [142]. Finally, hydrodynamics calculations are very sensitive to the initial condition and the predictions can vary drastically depending on the model that we use for the initial geometry of the system. Thus, the lack of knowledge that we have about these initial conditions can lead to incorrect conclusions.

The arguments presented above, although none of them is completely conclusive and a lot of research has still to be done, motivates the search for new explanations for (multi) particle correlations in small system collisions. The most favorite alternative is that these correlations are generated in the initial stage of the collision. This, however, introduces the assumption that the momentum anisotropy generated at the beginning of the collision is not washed out by the process of hadronization or strong final state interactions. Nevertheless, there is a type of correlation that has to be generated at the initial stage of the collision that is independently of the thermalization or hadronization processes; it is the correlation between pairs of particles well separated in rapidity.

In Fig. 3.3 we illustrate the space time trajectory of two particles A and B measured with rapidities y_A and y_B, respectively. As we have pointed above, there is a time τ_{fo} where the produced particles freeze-out and move almost freely toward the detectors. Thus any event that had an influence in those particles have to occur in the particles backward light-cone defined when it crosses the freeze-out surface. Any interaction between the particles A and B has to occur in the overlap of their backward light-cones. A straightforward geometric calculation leads that the maximum time where the interaction between the particles could occur is

$$\tau = \tau_{\text{fo}} e^{-|y_A - y_B|/2}. \tag{3.2}$$

Estimates for the freeze out time at RHIC energy give $\tau_{\text{fo}} \sim 10$ fm/c and the maximum time for applicability of CGC is $\tau \sim Q_s^{-1} \sim 0.2$ fm/c at RHIC. Thus, these correlations with $|y_A - y_B| > 7.8$ will be well described by the Color Glass Condensate framework.

We can see that, because of causality, any correlation that is long-range in rapidity has to come from the initial stage of the collision. In the next sections we will explore more CGC-based models in order to explain angular correlations at smaller values of the rapidity difference.

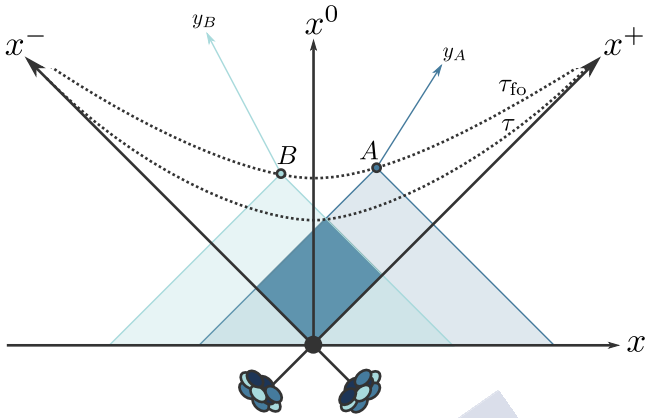

Figure 3.3.
Two correlated particles, well separated in rapidity, have received their correlation from some previous time imposed by causality.

3.2 Double gluon production in the Glasma Graphs

As we have seen in Section 2.5, we can easily solve the gluon spectra within the CGC framework by using the Glasma Graph approximation. This approach is well justified when the transverse momenta of the produced particles are high, i.e., $\mathbf{k}_i^2 > Q_s^2$, and is equivalent to taking the dilute limit of the target color charge density. Thus, although this approach is more suitable for describing pp collisions, it may reveal many qualitative aspects of 2-particle correlations in small systems.

By using Eq. (2.98), and neglecting the contributions of order $g^4\rho_p\rho_T$ in the amplitude as discussed in Section 2.1, we can write the double inclusive gluon spectrum, for gluons with pseudorapidity η_i and transverse momentum $\mathbf{k}_i$, in the Glasma Graph approximation as

$$\begin{aligned} 2^2(2\pi)^6\frac{d^2N}{d\eta_1 d^2\mathbf{k}_1 d\eta_2 d^2\mathbf{k}_2} &= (2g^3)^4 T^a_{b_1c_1}T^a_{c_2b_2}T^b_{b_3c_3}T^b_{c_4b_4}\int_{\mathbf{q}_1,\ldots,\mathbf{q}_4} L^i(\mathbf{k}_1,\mathbf{q}_1)L^i(\mathbf{k}_1,\mathbf{q}_2) \\ &\times L^j(\mathbf{k}_2,\mathbf{q}_3)L^j(\mathbf{k}_2,\mathbf{q}_4)\left\langle \rho_p^{b_1}(\mathbf{q}_1)\rho_p^{*b_2}(\mathbf{q}_2)\rho_p^{b_3}(\mathbf{q}_3)\rho_p^{*b_4}(\mathbf{q}_4)\right\rangle_p \\ &\times \left\langle \rho_T^{c_1}(\mathbf{k}_1-\mathbf{q}_1)\rho_T^{*c_2}(\mathbf{k}_1-\mathbf{q}_2)\rho_T^{c_3}(\mathbf{k}_2-\mathbf{q}_3)\rho_T^{*c_4}(\mathbf{k}_2-\mathbf{q}_4)\right\rangle_T . \end{aligned} \tag{3.3}$$

Since we assume that both the projectile and the target color charge densities are described by the MV model, i.e. they follow a Gaussian distribution, we can use Wick's theorem and write

$$\left\langle \rho_p^{b_1}(\mathbf{q}_1)\rho_p^{*b_2}(\mathbf{q}_2)\rho_p^{b_3}(\mathbf{q}_3)\rho_p^{*b_4}(\mathbf{q}_4)\right\rangle_p = \left\langle \rho_p^{b_1}(\mathbf{q}_1)\rho_p^{*b_2}(\mathbf{q}_2)\right\rangle_p \left\langle \rho_p^{b_3}(\mathbf{q}_3)\rho_p^{*b_4}(\mathbf{q}_4)\right\rangle_p$$

$$+\left\langle \rho_p^{b_1}(\mathbf{q}_1)\rho_p^{*b_4}(\mathbf{q}_4)\right\rangle_p \left\langle \rho_p^{b_3}(\mathbf{q}_3)\rho_p^{*b_2}(\mathbf{q}_2)\right\rangle_p$$
$$+\left\langle \rho_p^{b_1}(\mathbf{q}_1)\rho_p^{b_3}(\mathbf{q}_3)\right\rangle_p \left\langle \rho_p^{*b_2}(\mathbf{q}_2)\rho_p^{*b_4}(\mathbf{q}_4)\right\rangle_p, \tag{3.4}$$

and analogously for the target average. The 2-point functions will be described by Eq. (2.99). Thus the Wick's expansion introduces a sum of 9 terms where each of them will describe an unique dependence on the azimuthal angle, $\Delta\phi$, of the two produced gluons. On the other hand, Eq. (3.5) is clearly pseudorapidity independent and will lead to correlations at all values of $\Delta\eta = \eta_2 - \eta_1$. This, of course, will not be true once we include quantum corrections through the small-x evolution of the projectile's and target's average. Studying the effects of including quantum corrections in particle correlations is out of the scope of this thesis. We should note, however, that these studies where performed in [74–76, 143] and a numerical analysis on the dependence of the 2-gluon spectrum with $\Delta\eta$ was performed in [144]. The analysis performed here will be valid when the pseudorapidity difference between the produced particles is not very large, $\Delta\eta \ll 1/\alpha_s$, and we can neglect quantum corrections.

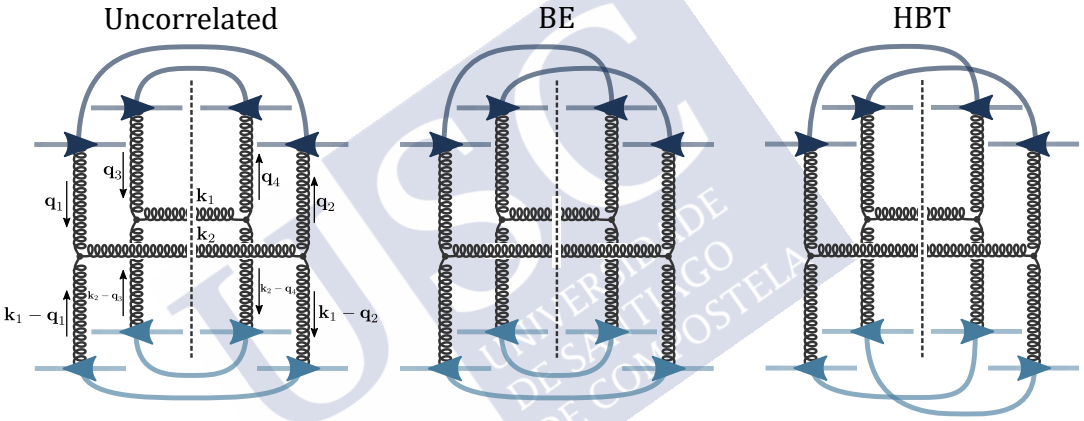

Figure 3.4.
Three examples of the diagrams contributing to Eq. (3.5). The first diagram corresponds to the full uncorrelated piece, the second to one of the 6 diagrams that gives a Bose Enhancement contribution and the third one is an example of a HBT contribution.

Depending on how we contract the terms of the Wick's expansion of the target's or projectile's average we will obtain a different diagram accounting for different source of correlations. As we have pointed above, the number of diagrams in the 2-gluon production case are 9 and we plot three of them in Fig. 3.4. By performing a straightforward color algebra we can rewrite Eq. (3.3), after the Wick's expansion, as [107]

$$\frac{d^2N}{d\eta_1 d^2\mathbf{k}_1 d\eta_2 d^2\mathbf{k}_2} = 2^8\alpha_s^6 S_\perp^2 N_c^2(N_c^2-1)^2\mu^8 \int_{\mathbf{q}_1,\mathbf{q}_2}\Bigg[I_{\text{uncorr.}}(\mathbf{k}_i,\mathbf{q}_i)$$
$$+\frac{1}{S_\perp(N_c^2-1)}\Big(I_{\text{BE}}(\mathbf{k}_i,\mathbf{q}_i)+I_{\text{HBT}}(\mathbf{k}_i,\mathbf{q}_i)\Big)\Bigg], \tag{3.5}$$

where

$$I_{\text{uncorr.}}(\mathbf{k}_i,\mathbf{q}_i) = L^i(\mathbf{k}_1,\mathbf{q}_1)L^i(\mathbf{k}_1,\mathbf{q}_1)L^j(\mathbf{k}_2,\mathbf{q}_2)L^j(\mathbf{k}_2,\mathbf{q}_2), \tag{3.6}$$

$$I_{\rm BE}(\mathbf{k}_i,\mathbf{q}_i) = L^i(\mathbf{k}_1,\mathbf{q}_1)L^i(\mathbf{k}_1,\mathbf{q}_1)L^j(\mathbf{k}_2,\mathbf{q}_2)L^j(\mathbf{k}_2,\mathbf{q}_2)\delta^{(2)}[(\mathbf{k}_1-\mathbf{q}_1)-(\mathbf{k}_2-\mathbf{q}_2)] + L^i(\mathbf{k}_1,\mathbf{q}_1)L^i(\mathbf{k}_1,\mathbf{q}_2)L^j(\mathbf{k}_2,\mathbf{q}_1)L^j(\mathbf{k}_2,\mathbf{q}_2) \times \left[\delta^{(2)}[\mathbf{q}_1-\mathbf{q}_2]+\frac{1}{2}\delta^{(2)}[(\mathbf{k}_1-\mathbf{q}_1)+(\mathbf{k}_2-\mathbf{q}_2)]\right] + \mathbf{k}_2 \to -\mathbf{k}_2, \quad (3.7)$$

$$I_{\rm HBT}(\mathbf{k}_i,\mathbf{q}_i) = L^i(\mathbf{k}_1,\mathbf{q}_1)L^i(\mathbf{k}_1,\mathbf{q}_2)L^j(\mathbf{k}_2,\mathbf{q}_1)L^j(\mathbf{k}_2,\mathbf{q}_2)\delta^{(2)}(\mathbf{k_1}-\mathbf{k}_2) + \mathbf{k}_2 \to -\mathbf{k}_2. \quad (3.8)$$

The first term given in Eq. (3.5), $I_{\rm uncorr.}$, does not include correlations and is the single inclusive gluon spectrum, Eq. (2.100), squared. This term gives the leading contribution in powers of $1/(N_c^2-1)$ and in the collision's area $S_\perp$. The other 8 terms encoded in $I_{\rm BE}$ and $I_{\rm HBT}$ include azimuthal correlations but, as we shall see below, the source of these correlations is different.

Let us being with the correlations encoded in $I_{\rm BE}$. In these term, we have 6 contributions that are proportional to $\delta^{(2)}[\mathbf{q}_1 \pm \mathbf{q}_2]$ or $\delta^{(2)}[(\mathbf{k}_1-\mathbf{q}_1)\pm(\mathbf{k}_2-\mathbf{q}_2)]$, where $\mathbf{k}_i-\mathbf{q}_i$ is the momentum transfer from the target's source i and $\mathbf{q}_i$ is the momentum transfer from the projectile's source i. The correlations coming from these terms can be seen qualitatively by noting that the transverse momentum flowing from the projectile or target has to be of the order of their wave function's intrinsic momentum[2] μ. Therefore, by imposing $|\mathbf{k}_1-\mathbf{q}_1| = |\mathbf{k}_2-\mathbf{q}_2| \sim \mu_T$ or $|\mathbf{q}_1| = |\mathbf{q}_2| \sim \mu_p$, the produced gluons are constrained to have similar transverse momentum $|\mathbf{k}_1| \sim |\mathbf{k}_2|$ and to be (anti) parallel $\Delta\phi = \phi_2 - \phi_1 = 0, \pi$. This feature have to be contrasted by a detailed analytical or numerical evaluation of Eq. (3.5). Moreover, since this term accounts for correlations coming from the case in where the transverse momentum of the two gluons coming from the projectile's or target's wave function is the same, we can identify it as a *Bose Enhancement* correlation.

In order to illustrate the phenomenon of Bose Enhancement let us follow [145] and consider a quantum state with fixed occupation number of N gluons at different transverse momenta $\mathbf{k}_i$, for simplicity we will omit the color or polarization dependence,

$$|\phi\rangle = \frac{1}{\mathcal{N}}\prod_{\mathbf{k}_i}\left[\hat{a}^\dagger(\mathbf{k}_i)\right]^{n(\mathbf{k}_i)}|0\rangle\,, \quad (3.9)$$

where $\mathcal{N}$ is some normalization factor and $n(\mathbf{k}_i)$ is the density of gluons with momentum $\mathbf{k}_i$. Thus, the mean particle density of this system will be given by

$$n \equiv \langle\phi|\,\hat{a}^\dagger(\mathbf{x})\hat{a}(\mathbf{x})\,|\phi\rangle = \int \frac{d^2\mathbf{k}}{(2\pi)^2}n(\mathbf{k}) \quad (3.10)$$

and the two particle correlator in position space by

$$D(\mathbf{x},\mathbf{y}) \equiv \int_{\mathbf{q}_1,\ldots,\mathbf{q}_4} e^{-i(\mathbf{q}_1-\mathbf{q}_3)\cdot\mathbf{x}-i(\mathbf{q}_2-\mathbf{q}_4)\cdot\mathbf{y}}\,\langle\phi|\,\hat{a}^\dagger(\mathbf{q}_1)\hat{a}^\dagger(\mathbf{q}_2)\hat{a}(\mathbf{q}_3)\hat{a}(\mathbf{q}_4)\,|\phi\rangle\,. \quad (3.11)$$

The particle correlator in this equation can be written as [145]

$$\langle\phi|\,\hat{a}^\dagger(\mathbf{q}_1)\hat{a}^\dagger(\mathbf{q}_2)\hat{a}(\mathbf{q}_3)\hat{a}(\mathbf{q}_4)\,|\phi\rangle \approx (2\pi)^6\left[\delta^{(2)}(\mathbf{q}_1-\mathbf{q}_3)\delta^{(2)}(\mathbf{q}_2-\mathbf{q}_4)+\delta^{(2)}(\mathbf{q}_1-\mathbf{q}_4)\delta^{(2)}(\mathbf{q}_2-\mathbf{q}_3)\right]n(\mathbf{q}_1)n(\mathbf{q}_2), \quad (3.12)$$

[2]If we assume that the projectile or target are saturated, the intrinsic momentum would be their respective saturation scale.

where we have omitted the terms that are subleading in the phase space volume. Therefore the correlation function of the gluons in this system will be

$$D(\mathbf{x},\mathbf{y}) = n^2 + \int_{\mathbf{q}_1} e^{-i\mathbf{q}_1\cdot(\mathbf{x}-\mathbf{y})} n(\mathbf{q}_1) \int_{\mathbf{q}_2} e^{i\mathbf{q}_2\cdot(\mathbf{x}-\mathbf{y})} n(\mathbf{q}_2), \tag{3.13}$$

or equivalent, in momentum space,

$$D(\mathbf{k},\mathbf{q}) = \sum_i n_i(\mathbf{k}) \sum_j n_j(\mathbf{q}) + (2\pi)^2 \delta^{(2)}(\mathbf{k}-\mathbf{q}) \int_{\mathbf{q}_2} \sum_i n_i(\mathbf{q}_2-\mathbf{k}) n_i(\mathbf{q}_2), \tag{3.14}$$

where we have written for convenience the summation in i which means a summation over all quantum numbers. Thus we see that in a system of bosons, it is more likely to find two bosons with same momenta than anything else. This enhancement will be suppressed by the number of boson types and by the size of the system since in the second term there is one less summation with respect to the first one. The type of correlation encoded in the second term of this expression is what is known as Bose Enhancement (BE) correlation. Thus we can easily see that the term I_{BE} in Eq. (3.5) is a Bose Enhancement term, since it is suppressed by $S_\perp(N_c^2-1)$ with respect to the uncorrelated piece and is enhanced when the momenta of the gluons in the projectile's or target's wave function are identical.

On the other hand, the term I_{HBT} in Eq. (3.5) is proportional to $\delta^{(2)}(\mathbf{k}_1 \pm \mathbf{k}_2)$ and therefore is enhanced when the two produced particles have the same transverse momenta and are (anti) parallel. The physical effect that it encodes is the Hanbury-Brown-Twiss (HBT) correlation between the produced gluons. The existence of HBT correlations in the CGC was pointed in [146] and we refer to [147] for a detailed review.

We should note that the delta functions appearing both in the HBT and the BE terms will be broadened by hadronization and by the use of a more realistic model for the averages than the MV model. For this reason the delta functions are usually replaced by Gaussian functions where this replacement can be seen as a rupture of translational invariance in the MV average. Moreover, it has been shown in [147] that the spread of the Gaussian should be R^{-1} in the HBT correlations, where R is the radius of the gluon cloud inside the proton, while the spread of the BE correlations should be $\sim Q_s^{-1}$.

To finalize this section we have to point that, in the dilute-dilute limit, there is another mechanism that competes with the Glasma Graphs in the double inclusive gluon spectrum: the so-called *Jet Graphs*. The Jet Graph is illustrated in Fig. 3.5 and is of order $\rho_p \rho_T g^4$ while the Glasma Graphs, which account for double gluon exchange, are of order $\rho_p^2 \rho_T^2 g^6$. Thus, although in the dense-dense case they are $\mathcal{O}(g^0)$ and therefore subleading with respect to the Glasma Graphs, that are $\mathcal{O}(g^{-2})$, in the dilute-dilute limit they are $\mathcal{O}(g^4)$ and dominate over the Glasma Graphs. These graphs account for generations of back-to-back jets and therefore populate the $\Delta\phi = \pi$ region of the ridge. Since the jet graph gives a non-flow contribution we will not study it in this thesis and for a review on this topic we refer to [148].

In order to perform phenomenological studies in pp collisions, which is described by the dilute-dilute limit of the CGC framework, one has therefore to compute the double gluon spectrum by using both the Glasma and Jet Graphs and convolute it with a gluon-to-hadron fragmentation function. By performing this procedure it has been achieved a successful description of the azimuthal correlation in pp collisions [149,150]. Although the Glasma Graph approach is able to explain the shape of the ridge at a relatively long range

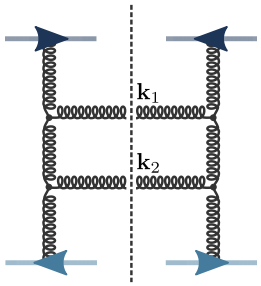

Figure 3.5.
An example of a jet graph diagram that contributes to the double inclusive gluon spectrum in the dilute-dilute limit.

rapidities it is still unable to reproduce some of the data. It has been seen the presence of a large and positive value of the odd azimuthal coefficient v_3 in pA collisions but, since Eq. (3.5) is symmetric under the change $\mathbf{k}_2 \to -\mathbf{k}_2$, the Glasma Graph approximation give zero value for any odd harmonic and the Jet Graphs give a negative value for v_3. On the other hand, as we have pointed out in the introduction, the CMS collaboration has measured a negative value for the 4-particle cumulant at high multiplicity in pp or pA collisions. The Glasma and Jet graphs predict a positive value for $c_2\{4\}$. However, in Section 4.5.3 we will see that by relaxing the dilute approximation in the target we will be able to obtain a negative value for $c_2\{4\}$.

3.3 The chromo-electric domain model

The ridge structure seen in small systems can also be explained by the structure of the chromo-electric fields inside the target as well as the boost invariance of the projectile's wave function. Following the work from Kovner and Lublinsky [151–153] the argument for explaining the long range and azimuthal correlations in high energy collisions is the following. As we have seen in the last chapters, the projectile's or target's wave function is approximately boost invariant and is populated by gluons at high energy. Because of the gluons are vector particles, they will be homogeneously distributed in rapidity in a Lorentz invariant ensemble. Thus, the rapidity independence of the ridge structure could be a reflection of the high energy nature of QCD.

To illustrate this effect, let us consider a high energy projectile scattering in a target at rest in the laboratory frame. Two gluons from the projectile's wave function with rapidities y_1 and y_2 will scatter in the target and be measured in the final state. Since the projectile's wave function is approximately boost invariant, the distribution function of both gluons would be the same. Thus, for some fixed target configuration ρ_T, the probability of gluon's production at some given transverse position and with rapidity y_1 will be the same to produce another gluon with rapidity y_2 at the same position. Therefore the long range correlations appear naturally whenever the energy is high enough so that the projectile's wave function is Lorentz invariant.

On the other hand, the azimuthal structure of the ridge can be explained by the saturation effects within the target ensemble. In order to do so it is convenient to take

a look at the chromo-electric field configurations in the target. The saturated target's wave function is characterized by its saturation momentum Q_s. It is well known that the field modes with $\mathbf{q}^2 < Q_s^2$ are suppressed in the wave function and enhanced when $|\mathbf{q}| \sim Q_s$ [154]. Thus the chromo-electric fields in the target will have a typical correlation length of Q_s^{-1} and can be though as having a domain structure as illustrated in Fig. 3.6. On the other hand, a saturated target will have a field $A_T^- \sim 1/g$ thus, by using dimensional arguments, we can inspect that the strength of the chromo-electric field is $g|\vec{E}| \sim Q_s$. Now let us consider a parton coming from projectile's wave function that scatters into one of the chromo-electric domains of the target with strength E^i. After traversing the target field, the parton with charge q will acquire the following transverse momentum

$$\delta\mathbf{k}^i = gq \int dx^+ F^{-i} = qgE^i \sim \hat{a}^i q Q_s, \tag{3.15}$$

where $\hat{a}^i$ is the direction of the field. Thus a parton with different rapidity but with the same charge will pick up the same momentum if it scatters from the same domain. This will lead to long-range azimuthal correlations in the near-side. The long range correlations in the away-side can be explained by noting that, since gluons belong to a real representation of $\mathrm{SU}(N_c)$, the number of gluons with charge q in the projectile is the same as the gluons with charge $-q$ at any rapidity. Because the momentum transfer by the target is proportional to q, an equal number of gluons will be kicked by the target in the same and in the opposite directions. This therefore explain the approximate symmetry between the near- and away-side of the ridge. For quarks, in the fundamental representation, this would not be the case and the azimuthal symmetry of the ridge would be broken.

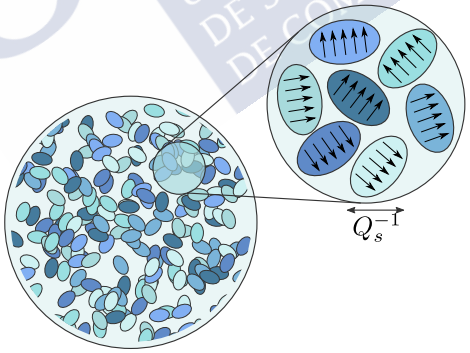

Figure 3.6.
Domain structure of the chromo-electric fields in a given configuration of the target ensemble.

Let us now discuss the domain model in a more quantitative way. As we will see in the next chapter, when we study correlations in pA collisions, the scattering amplitude of a parton colliding in a target is given by the dipole operator $\mathcal{D}(\mathbf{r}) = \mathrm{Tr}\left[U^\dagger(0)U(\mathbf{r})\right]/D_R$, where $U(\mathbf{x})$ is the Wilson line in the parton's representation and D_R is the dimension of the representation. For simplicity, let us assume that we have a quark scattering into the target so that $D_R = N_c$. In the MV model the dipole function can be written as $D(\mathbf{r}) = \langle\mathcal{D}(\mathbf{r})\rangle_T = e^{C_F\gamma(|\mathbf{r}|)}$, where $\gamma(|\mathbf{r}|)$ is the 2-point correlator of the target field.

Moreover, using the fact that the chromo-electric field in the target is $E^i(\mathbf{x}) = \partial^i A_T^-(\mathbf{x})$ we can expand the dipole function at small distances as

$$D(\mathbf{x},\mathbf{y}) - 1 \approx \frac{(ig)^2}{2N_c}\mathbf{r}^i\mathbf{r}^j\langle E_a^i(\mathbf{b})E_a^j(\mathbf{b})\rangle_T \approx -\frac{Q_s^2}{4}\mathbf{r}^2, \tag{3.16}$$

where $\mathbf{r} = \mathbf{x} - \mathbf{y}$ is the dipole's size and $\mathbf{b} = (\mathbf{x}+\mathbf{y})/2$. We have also written $C_F\gamma(|\mathbf{r}|) = -\frac{Q_s^2}{4}\mathbf{r}^2$ which is known as the GBW model, to be introduced in Section 4.2. This substitution was performed in order to make the discussion simpler but the following will be independent of the model chosen for $\gamma(|\mathbf{r}|)$. It is easy to realize that this short distance expansion is equivalent to the Glasma Graph approximation and because of that, the chromo-electric fields also follow a Gaussian distribution where the 2-point correlator, in this model, is given by

$$g^2\langle E_a^i(\mathbf{b}_1)E_b^j(\mathbf{b}_2)\rangle_T = \frac{\delta^{ab}}{C_F}\frac{Q_s^2}{4}\delta^{ij}, \tag{3.17}$$

with $C_F = (N_c^2-1)/2N_c$.

Eq. (3.17) describes an isotropic scattering which is caused by performing the average over all field configurations. The idea behind the domain model is that, in order to explain anisotropies in the target wave function, the rotational symmetry in the target has to be broken from event to event. In order to account for this assumption we have to rewrite Eq. (3.17) as [155–157]

$$g^2\langle E_a^i(\mathbf{b}_1)E_b^j(\mathbf{b}_2)\rangle_{\hat{a}} = \frac{\delta^{ab}}{C_F}\frac{Q_s^2}{4}\Delta(\mathbf{b}_1-\mathbf{b}_2)\left[\delta^{ij} - \mathcal{A}\delta^{ij} + 2\mathcal{A}\hat{a}^i\hat{a}^j\right], \tag{3.18}$$

where $\hat{a}$ is the direction of the chromo-electric field in the domain, $\mathcal{A}$ gives the degree of polarization of the target field and $\Delta(\mathbf{b}_1 - \mathbf{b_2})$ is a 2-point correlator function that accounts for the domain structure of the target and, without loss of generality, it can be written just as a Gaussian

$$\Delta(\mathbf{b}_1 - \mathbf{b_2}) = \exp\left\{-\frac{(\mathbf{b}_1-\mathbf{b_2})^2}{Q_s^2}\right\}. \tag{3.19}$$

Therefore, the spirit of this model is that we first compute any observable at a fixed direction for the chromo-electric field $\hat{a}$ by using Eq. (3.18) and then, since this direction from even to event is random, we perform an average over all directions $\hat{a}$. The rotational invariance is then restored by averaging over the whole target ensemble rather than configuration by configuration.

This model was able to explain qualitatively azimuthal correlations in single particle production as well as a new mechanism for generating odd azimuthal harmonics [155]. Both of these features are not described by the Glasma Graph approximation. Moreover, an analysis at large-N_c of 4-particle production lead to the following result for the 4-particle cumulant [156], see Section 3.4 for the definition,

$$c_2\{4\} = \frac{-1}{n_D^3}\left[\mathcal{A}^4 - \frac{1}{4(N_c^2-1)^3}\right], \tag{3.20}$$

where $n_D = S_\perp Q_s^2/2\pi$ is the number of chromo-electric domains in the collision area. Thus the domain model is able to explain the negativity of the 4-particle cumulant if $\mathcal{A}$ is large enough.

Although the domain model is simple, the physics behind it is still unclear. The domain model assumes that the target valence partons generate an electric field in some direction $\hat{a}$ and that the projectile's partons are collimated in this direction. On the other hand, an average over the target electric field is performed at fixed $\hat{a}$. This, somehow, introduces a difference in time-scale between the field direction life time, which appears to be frozen during the time scale of the average, and the color charge density configuration life time. Moreover, as discussed in [103], since only the 2-point correlator of the field is usually used in the calculations, one may think that Eq. (3.18) describes a Gaussian distribution for the fields. However, by inspecting the 4-point function described by the domain model we can see that it cannot be written in terms of products of 2-point functions [103] (Wick's theorem) and therefore the domain model is a non Gaussian model of the target field correlators.

3.4 Multi-particle cumulants

To finalize this chapter we introduce the so-called cumulant method [158–160], a technique introduced for extracting "non-flow" contributions to the overall particle correlation functions measured in high energy accelerators. Although historically this method was introduced for studying the azimuthal harmonics of the particle correlations generated by the anisotropic hydrodynamic flow in heavy ion collisions, it is extensively used in small systems collisions where it is still unknown if the source of correlation is due to collective behavior. For this reason, even that we use along this thesis the terminology "flow coefficients" or "flow correlations", it should be clear that the analysis performed here is based on the initial state of the collision and, therefore, has nothing to do with collective behavior induced by final state interactions.

In order to introduce the cumulant method we will assume a heavy ion collision although, as stated above, the technique can still be used in absence of hydrodynamic flow. In high energy heavy ion collisions, the anisotropic flow is a response of the system generated in the collision due to anisotropies in the initial geometry. As pointed out in Section 3.1, anisotropic flow is quantified through the Fourier azimuthal coefficients of the single particle spectra relative to the reaction plane:

$$f_1(\mathbf{k}) \equiv \frac{dN}{d\eta d^2\mathbf{k}} = \frac{1}{2\pi}\frac{dN}{p_\perp dp_\perp d\eta}\left(1 + \sum_{n=1}^{\infty} 2v_n(p_\perp)\cos\left[n(\phi - \Psi_R)\right]\right), \tag{3.21}$$

where $p_\perp = |\mathbf{k}|$ is the particle's transverse momentum, ϕ the azimuthal angle and Ψ_R is the reaction plane angle. In Fig. 3.7 we illustrate the transverse plane of this collision. The coefficients $v_n(p_\perp)$ are the *differential flow coefficients* or *differential azimuthal harmonics*. In Eq. (3.21) we have denoted the single inclusive particle spectra as $f_1(\mathbf{k})$ where, from now on, we will omit the pseudorapidity dependence of the particle yield.

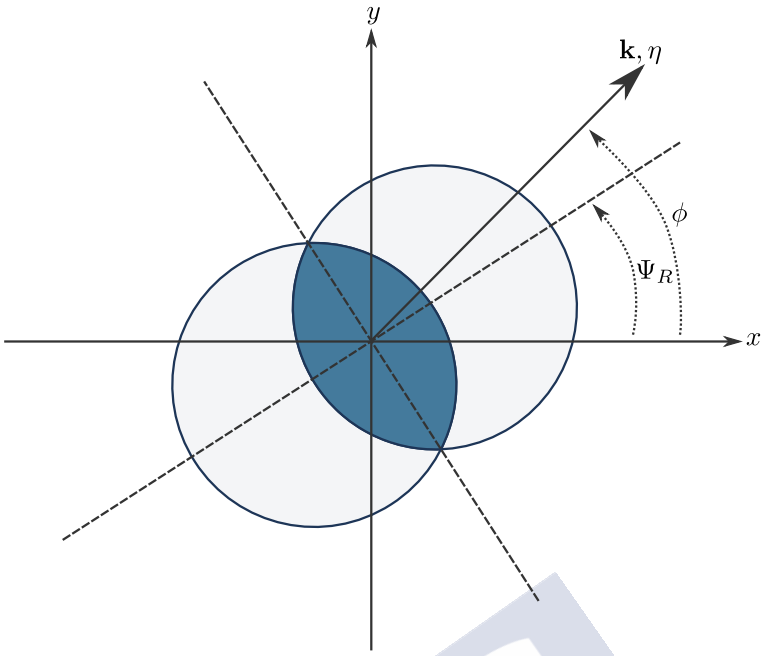

Figure 3.7.
The transverse projection of a heavy ion collision. The angle Ψ_R defines the reaction plane in where the generated system is symmetric.

The (integrated) azimuthal harmonics v_n are defined as

$$v_n(\Psi_R) = \langle e^{in(\phi-\Psi_R)} \rangle = \frac{\int_{\mathbf{k}} e^{in(\phi-\Psi_R)} f_1(\mathbf{k})}{\int_{\mathbf{k}} f_1(\mathbf{k})}, \tag{3.22}$$

where we have written explicitly that the azimuthal harmonics depend on the reaction plane angle. Since the reaction plane angle is not accessible experimentally one has to relay on the azimuthal angle relative to other particles in order to obtain the azimuthal harmonics. Moreover, we note that because of the particle source is symmetric with respect to the reaction plane, the azimuthal harmonics have to be real.

Let us start our discussion with the case of 2-particle correlations, where we denote the double particle spectrum as $f_2(\mathbf{k}_1, \mathbf{k}_2)$. This spectrum can be written as

$$f_2(\mathbf{k}_1, \mathbf{k}_2) = f_1(\mathbf{k}_1) f_1(\mathbf{k}_2) + \tilde{f}_2(\mathbf{k}_1, \mathbf{k}_2), \tag{3.23}$$

where $\tilde{f}_2$ is the part of f_2 that encodes the genuine 2-particle correlations. Thus, the 2-particle azimuthal correlation

$$\left\langle e^{in(\phi_1-\phi_2)} \right\rangle \equiv \frac{\int_{\mathbf{k}_1,\mathbf{k}_2} e^{in(\phi_1-\phi_2)} f_2(\mathbf{k}_1, \mathbf{k}_2)}{\int_{\mathbf{k}_1,\mathbf{k}_2} f_2(\mathbf{k}_1, \mathbf{k}_2)} \tag{3.24}$$

can be written as

$$\left\langle e^{in(\phi_1-\phi_2)} \right\rangle = \left\langle e^{in\phi_1} \right\rangle \left\langle e^{-in\phi_2} \right\rangle + \left\langle e^{in(\phi_1-\phi_2)} \right\rangle_{\text{corr}} = v_n\{2\}^2 + \left\langle e^{in(\phi_1-\phi_2)} \right\rangle_{\text{corr}}, \tag{3.25}$$

where we have introduced the notation $v_n\{m\}$ to make emphasis that we are evaluating the azimuthal harmonics from m-particle correlations and $\langle\cdots\rangle_{\text{corr}}$ denotes the correlation function from genuine correlations. On the other hand, the correlated function $\tilde{f}_2$ is suppressed by $1/N$ [158], where N is the multiplicity of the event. Then the azimuthal harmonics can be extracted in high-multiplicity events as

$$v_n\{2\}^2 = \left\langle e^{in(\phi_1-\phi_2)}\right\rangle + \mathcal{O}\left(\frac{1}{N}\right). \tag{3.26}$$

We now move our discussion for multi-particle correlations, where we define the m-particle spectrum as $f_m(\mathbf{k}_1,\ldots,\mathbf{k}_m)$. The arguments are analogous to the 2-particle case, that is, we can break this yield as a genuine correlated term $\tilde{f}_n$ plus the summation of all possible partitions of the function f_m. However, it is convenient to compute the correlation function in the case where the m-particle spectrum is isotropic in such away that v_n vanishes as well as any correlation function of the form $\left\langle e^{in(\phi_1+\cdots+\phi_k-\phi_{k+1}\cdots-\phi_{k+l})}\right\rangle$ with $k \neq l$. In this case we can write, for example, the 4-particle correlation function as

$$\begin{aligned}\left\langle e^{in(\phi_1+\phi_2-\phi_3-\phi_4)}\right\rangle = \left\langle e^{in(\phi_1-\phi_3)}\right\rangle\left\langle e^{in(\phi_2-\phi_4)}\right\rangle + \left\langle e^{in(\phi_1-\phi_4)}\right\rangle\left\langle e^{in(\phi_2-\phi_3)}\right\rangle \\ + \left\langle e^{in(\phi_1+\phi_2-\phi_3-\phi_4)}\right\rangle_{\text{corr}}.\end{aligned} \tag{3.27}$$

Defining the m^{th} order or m-particle cumulant $c_n\{m\}$ as the genuine correlation function in the case of an isotropic distribution, we can write the 4-particle cumulant, by inverting Eq. (3.27), as

$$c_n\{4\} = \left\langle e^{in(\phi_1+\phi_2-\phi_3-\phi_4)}\right\rangle - 2\left\langle e^{in(\phi_1-\phi_3)}\right\rangle^2. \tag{3.28}$$

Going back to the general case where the 4-particle spectrum is not isotropic, we can manipulate the factorization expansion of the 4-particle correlation function and noting that the genuine spectrum of order k, $\tilde{f}_k$, is of order N^{1-k}, we can write [158]

$$v_n\{4\}^4 = -c_n\{4\} + \mathcal{O}\left(\frac{1}{N^2}\right). \tag{3.29}$$

Therefore the azimuthal harmonics can be extracted, up to a sign, from the 4-particle cumulant with better accuracy than from the 2-particle correlation function in Eq. (3.26). This is the original idea behind the cumulant method, that by going to higher orders of the cumulants one can extract the azimuthal harmonics with better accuracy. Although this method was originally proposed for studying the azimuthal coefficients generated in heavy ion collisions, it has given a set of observables, i.e., the m-particle cumulants, to study many properties of multi-particle correlations in the collisions performed at the LHC or RHIC. Since the multi-particle cumulants can be computed both from the hydrodynamic or the CGC frameworks, it also offers a good working basis for studying the origin of particle correlations at high energy collisions.

The process for computing the azimuthal harmonics from the cumulants presented above can be generalized to higher orders cumulants and the approach is given in [159]. Here we show the first three of them

$$c_n\{2\} = \langle\langle 2\rangle\rangle, \tag{3.30}$$

$$c_n\{4\} = \langle\langle 4 \rangle\rangle - 2\langle\langle 2 \rangle\rangle^2, \tag{3.31}$$

$$c_n\{6\} = \langle\langle 6 \rangle\rangle - 9\langle\langle 4 \rangle\rangle\langle\langle 2 \rangle\rangle + 12\langle\langle 2 \rangle\rangle^3, \tag{3.32}$$

where we have defined

$$\langle\langle 2m \rangle\rangle = \left\langle e^{in(\phi_1+\cdots+\phi_m-\phi_{m+1}-\cdots-\phi_{2m})} \right\rangle \equiv \frac{\kappa_n\{2m\}}{\kappa_0\{2m\}}, \tag{3.33}$$

and we refer to

$$\kappa_n\{2m\} = \int \left(\prod_{i=1}^{2m} \frac{d^2\mathbf{k}_i}{(2\pi)^2} \right) \frac{d^{2m}N}{\prod_{i=1}^{2m} d^2\mathbf{k}_i} e^{in(\phi_1+\cdots+\phi_m-\phi_{m+1}-\cdots-\phi_{2m})} \tag{3.34}$$

as the κ-function of order $2m$.

The azimuthal harmonics are given by

$$v_n\{2\} = \sqrt{c_n\{2\}}, \quad v_n\{4\} = (-c_n\{4\})^{\frac{1}{4}}, \quad v_n\{4\} = \left(\frac{1}{4} c_n\{6\} \right)^{\frac{1}{6}}. \tag{3.35}$$

To finalize this section we note that the differential azimuthal harmonics can be computed in a similar where the first two m^{th} *order differential cumulants*, $d_n\{m\}$, are defined as [161]

$$d_n\{2\}(p_\perp) = \langle\langle 2' \rangle\rangle, \tag{3.36}$$

$$d_n\{4\}(p_\perp) = \langle\langle 4' \rangle\rangle - 2\langle\langle 2' \rangle\rangle\langle\langle 2 \rangle\rangle, \tag{3.37}$$

where we have defined

$$\langle\langle 2m' \rangle\rangle \equiv \frac{\tilde{\kappa}_n\{2m\}(p_\perp)}{\tilde{\kappa}_0\{2m\}(p_\perp)}, \tag{3.38}$$

and we refer to

$$\tilde{\kappa}_n\{2m\}(p_\perp) \equiv \frac{d\kappa_n\{2m\}}{p_\perp dp_\perp} = \int_0^{2\pi} d\phi_1 \int \left(\prod_{i=2}^{2m} \frac{d^2\mathbf{k}_i}{(2\pi)^2} \right) \frac{d^{2m}N}{\prod_{i=1}^{2m} d^2\mathbf{k}_i} \Bigg|_{\mathbf{k}_1=\mathbf{p}_\perp} \times e^{in(\phi_1+\cdots+\phi_m-\phi_{m+1}-\cdots-\phi_{2m})} \tag{3.39}$$

as the differential κ-function of order $2m$.

With this prescription, the differential azimuthal harmonics are given by[3]

$$v_n\{2\}(p_\perp) = [d_n\{2\}(p_\perp)]^{1/2}, \qquad v_n\{4\}(p_\perp) = [-d_n\{4\}(p_\perp)]^{1/4}. \tag{3.40}$$

[3]In experimental analysis, e.g. [162], these harmonics are usually normalized as

$$v_n\{2\}(p_\perp) = \frac{d_n\{2\}(p_\perp)}{(c_n\{2\})^{1/2}},$$

$$v_n\{4\}(p_\perp) = \frac{-d_n\{4\}(p_\perp)}{(-c_n\{4\})^{3/4}}.$$

USC
UNIVERSIDADE
DE SANTIAGO
DE COMPOSTELA

Chapter 4

Multi-particle correlation in proton-nucleus collisions

In Chapter 3 we have seen that small collision systems, proton-proton (pp) and proton-nucleus (pA), studied at the Large Hadron Collider (LHC) show many of the characteristics that in heavy ion collisions are considered as signatures of the formation of hot deconfined partonic matter, the Quark Gluon Plasma. The most prominent example is the existence of azimuthal correlations in the two-particle inclusive distributions that are extended in pseudorapidity and show maxima when the particle transverse momenta are either parallel or antiparallel, i.e. the ridge.

The success of the application of hydrodynamics for describing azimuthal asymmetries in small systems, pp and pPb, while requiring careful choices of the initial conditions, pushes this description to small collision areas and low particle densities where non-hydrodynamic modes play a very important role. Therefore, it seems sensible to explore other alternatives where the Color Glass Condensate offers a framework where azimuthal asymmetries can be calculated from first principles, as seen in Sections 3.2 and 3.3. Correlations in the final state reflect those found in the wave function of the projectile and target hadrons or nuclei, assuming that final state effects, including hadronization, do not wash them out.

The initial versus final state origin of azimuthal correlations in small systems has been subject to intense scrutiny in recent years. At present, no CGC-based model is able to fully describe the existing experimental data. Still, the search for observables that may discriminate initial from final effect continues, e.g., the correlation of v_2 with the mean transverse momentum of the particles produced in the collisions [163–166] that has also been analyzed in the CGC [167]. Also many particle cumulants are expected to be crucial. For example, four particle cumulants $c_2\{4\}$, with $v_2\{4\} = [-c_2\{4\}]^{1/4}$, change sign from positive to negative with increasing particle multiplicity in the event, with a smooth behavior from small to large systems and from smaller to larger energies.

This change of sign is associated with the onset of true collective flow of final state origin because higher order cumulants are less sensitive to non-flow contributions than those computed from two-particle correlations. In the CGC numerical implementation in [104, 105] the change of sign of $c_2\{4\}$ was interpreted as the transition from a dilute-dilute situation, described by the Glasma Graph approach where azimuthal correlations correspond to the Bose enhancement of the gluons in the wave function of the colliding hadrons and to the Hanbury-Brown-Twiss (HBT) effect for the final gluons, to a dilute-dense situation where multiple scattering dominates.

The goal of this chapter is to present the framework of multi-particle production in

the CGC in the dilute-dense situation (suitable for pA collisions), and the computation of the two and four particle cumulants. Note that up to four gluon production was previously computed in the Glasma Graph approach [168], and arguments in [156] suggested that in such approximation $c_2\{4\} > 0$ – a result also found in [105] where only quark scattering is considered and partons in the projectile wave function are uncorrelated. In this chapter we use the argument in [169, 170] that captures those contributions of the ensembles of Wilson lines to multi-particle production that are leading in the overlap area of the collision (i.e., in the number of colour domains or correlated particle sources), while keeping contributions to all orders in the number of colors. Thus the chapter is organized as follows. In Section 4.1 we introduce the formalism of multi-gluon production in the dilute-dense limit of the CGC that will be used along this chapter, and we motivate the importance of computing the target averages of Wilson lines. In Section 4.2 we presented the techniques for computing target averages in the MV model and in what we call the *Area Enhancement* (AE) model. In Section 4.3 we compute the double gluon spectrum in the AE model and then in Section 4.4 we generalize our result to multi-gluon production. In Section 4.5 we present the numerical solutions of our approach for 2-, 3- and 4-gluon production as well as the corresponding cumulants for each case. Finally in Section 4.6 we give a summary of our results and the conclusions.

This chapter is based on the following paper:

Multi-particle production in proton–nucleus collisions in the color glass condensate, *Eur. Phys. J. C* **81** (2021) 760

Authors

Pedro Agostini,[ab] Tolga Altinoluk,[c] Néstor Armesto,[ab]

[a] Departamento de Física de Partículas, Universidade de Santiago de Compostela, E-15782 Santiago de Compostela, Spain

[b] Instituto Galego de Física de Altas Enerxías (IGFAE), Universidade de Santiago de Compostela, E-15782 Santiago de Compostela, Spain

[c] National Centre for Nuclear Research, 00-681 Warsaw, Poland

Journal and Article Information

Journal name: The European Physical Journal C

Publisher: Springer

ISSN: 1434-6052 (print)

Year of publication: 2021

DOI: https://doi.org/10.1140/epjc/s10052-021-09475-0

4.1 Introduction

We have introduced in Section 2.2 the formalism of eikonal particle production in the dilute-dense limit of the CGC, i.e. for proton-nucleus collisions. Then in Section 3.2 we reviewed the dilute-dilute limit, also known as the Glasma Graph approximation, for computing the double inclusive gluon spectrum. Although the Glasma Graph approximation was able to explain many quantitative and qualitative aspects of the collective behavior seen in small systems it has some limitations. On one hand, it is unable to explain the appearance of a large azimuthal harmonic v_3 in pA collisions and, on the other hand, it predicts a positive 4-particle cumulant $c_2\{4\}$ while experimental data show that $c_2\{4\} < 0$ at high multiplicity. For this reason it is important to go beyond the Glasma Graph Approximation in order to look for a better description of experimental data, especially in the case of proton-nucleus collisions. In what follows we will see that by going to the dense limit of the target, although only including disconnected diagrams where each gluon is emitted by just one source, we will be able to reproduce qualitatively the negativity of the 4$^{\text{th}}$ order cumulant and therefore to improve the description given by the Glasma Graphs.

In order to compute the multi-gluon spectrum in pA collisions we will use the result of Eq. (2.81) and write the following formula that will be used along this chapter:

$$2^n(2\pi)^{3n}\frac{d^nN}{d^2\mathbf{k}_1\cdots d^2\mathbf{k}_n} = \left\langle \left| \mathcal{M}_{i_1}^{a_1}(\mathbf{k}_1)\cdots\mathcal{M}_{i_n}^{a_n}(\mathbf{k}_n)\right|^2\right\rangle_{p,T}, \tag{4.1}$$

where

$$\mathcal{M}_i^a(\mathbf{k}) = 2g\int_{\mathbf{q}} L^i(\mathbf{k},\mathbf{q})\rho_p^b(\mathbf{q})U^{ba}(\mathbf{k}-\mathbf{q}). \tag{4.2}$$

Note that we have dropped the dependence over the gluon's pseudorapidity η_i since this equation is boost invariant as long as the pseudorapidity difference between the produced particles is not large, i.e. $|\eta_i - \eta_j| \ll 1/\alpha_s$. In the case where $|\eta_i - \eta_j| > 1/\alpha_s$ we have to include quantum evolution corrections to Eq. (4.1). Moreover, Eq. (4.1) is not complete since it is missing terms that are subleading in powers of ρ_p and therefore are non negligible in the dilute limit of the projectile.

In order to illustrate the main properties and problems of Eq. (4.1) let us study the simple case of double inclusive gluon production. In this case Eq. (4.2) can be written as

$$\begin{aligned}\frac{d^2N}{d^2\mathbf{k}_1 d^2\mathbf{k}_2} = \frac{g^4}{(2\pi)^6}\int_{\mathbf{q}_1,\mathbf{q}_2,\mathbf{q}_3,\mathbf{q}_4} & L^i(\mathbf{k}_1,\mathbf{q}_1)L^i(\mathbf{k}_1,\mathbf{q}_2)L^j(\mathbf{k}_2,\mathbf{q}_3)L^j(\mathbf{k}_2,\mathbf{q}_4)\\ &\times\left\langle \rho_p^{b_1}(\mathbf{q}_1)\rho_p^{*b_2}(\mathbf{q}_2)\rho_p^{b_3}(\mathbf{q}_3)\rho_p^{*b_4}(\mathbf{q}_4)\right\rangle_p\\ &\times\left\langle U^{a_1b_1}(\mathbf{k}_1-\mathbf{q}_1)U^{\dagger b_2a_1}(\mathbf{k}_1-\mathbf{q}_2)U^{a_2b_3}(\mathbf{k}_2-\mathbf{q}_3)U^{\dagger b_4a_2}(\mathbf{k}_2-\mathbf{q}_4)\right\rangle_T.\end{aligned} \tag{4.3}$$

Analogous to the Glasma Graph approximation, since both the Wilson lines and the sources are in the adjoint representation and therefore are real, this equation in symmetric under the change $\mathbf{k}_2 \to -\mathbf{k}_2$. Therefore the formalism described in this section via Eq. (4.1) will not be able to explain the odd azimuthal harmonics seen in experiments.

However, the $\mathbf{k}_2 \to -\mathbf{k}_2$ invariance of the spectrum is not a symmetry of the theory but is an *accidental symmetry* generated by neglecting higher order corrections in the coupling constant [171]. In the third diagram of Fig. 4.1 we illustrate one of the diagrams that we are neglecting which has been shown that breaks this accidental symmetry and generate odd harmonics [172].

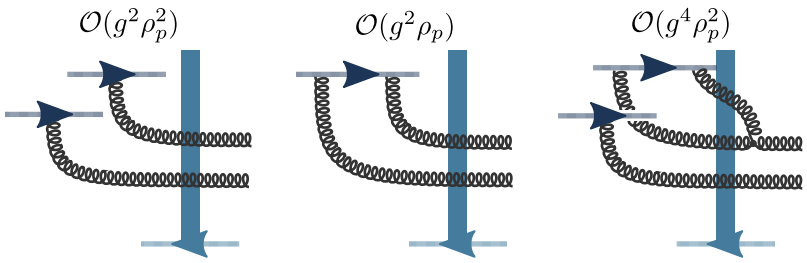

Figure 4.1.
Different diagrams contributing to the double gluon spectrum. The first diagram, starting from the left, is $\mathcal{O}(g^2\rho_p^2)$ and is the one that we are having into account in Eq. (4.3). The second diagram is $\mathcal{O}(g^2\rho_p)$ and although it is subleading in the dense limit of the projectile it is, parametrically, equally important in the dilute limit $\rho_p \sim 1$. The last diagram is subleading in the coupling constant with respect to the other two but breaks the symmetry $\mathbf{k}_2 \to -\mathbf{k}_2$ and thus generates odd azimuthal harmonics.

The contributions where more than one gluon are emitted by the same source or the gluon is emitted by another gluon are parametrically, in the case of double gluon production, of order $g^2\rho_p$. Therefore, in the dilute limit of the projectile $\rho_p \sim 1$ these contributions are not subleading. An example of a diagram from this case is illustrated in the second diagram of Fig. 4.1. The diagrams that are not disconnected have been computed in [173, 174]. However, we expect that these contributions will give "non-flow" like correlations and therefore will be subleading in the cumulant analysis performed in this chapter. For this reason we will neglect them and assume that the dominant part to azimuthal correlations in the multi-particle spectrum is given by Eq. (4.1). Nevertheless, for a complete study of multi-particle correlations we should have them into account.

Before moving forward with our analysis, let us simplify Eq. (4.3) by using a generalized version of the MV model. The MV model describes a nucleus that is infinitely large in the transverse direction and color neutral. However, in order to perform more realistic phenomenological studies, it is convenient to drop the locality in the transverse plane encoded in the MV model by making the change $\mu^2 \to \mu^2(\mathbf{x})$ in Eq. (1.48) [175, 176]. Thus, the MV 2-point function is modified as

$$\left\langle \rho^a(\mathbf{x})\rho^b(\mathbf{y})\right\rangle = \delta^{ab}\mu^2(\mathbf{x})\delta^{(2)}(\mathbf{x}-\mathbf{y}), \tag{4.4}$$

where the function $\mu^2(\mathbf{x})$ has to be peaked around $|\mathbf{x}| = 0$. Without loss of generality, we can assume that $\mu^2(\mathbf{x})$ is a Gaussian function and therefore, in the case of the projectile's source correlator, we will have that

$$\left\langle \rho_p^a(\mathbf{x})\rho_p^{*b}(\mathbf{y})\right\rangle_p = \delta^{ab}\mu_p^2(\mathbf{x})\delta^{(2)}(\mathbf{x}-\mathbf{y}), \qquad \mu_p^2(\mathbf{x}) = \tilde{\mu}^2 \exp\left\{-\frac{\mathbf{x}^2}{B_p}\right\}, \tag{4.5}$$

or in momentum space

$$\left\langle \rho_p^a(\mathbf{k})\rho_p^{*b}(\mathbf{q})\right\rangle_p = \delta^{ab}\mu_p^2(\mathbf{k},\mathbf{q}), \qquad \mu_p^2(\mathbf{k},\mathbf{q}) = \pi\tilde{\mu}^2 B_p \exp\left\{-\frac{(\mathbf{k}+\mathbf{q})^2}{4B_p^{-1}}\right\}, \tag{4.6}$$

where $\tilde{\mu}$ is a constant with dimensions of momentum that will be irrelevant in the studies of azimuthal correlations and B_p^{-1} is the transverse area of the gluon cloud in the projectile's wave function. By using this generalization of the MV model and using the Wick's theorem we can write Eq. (4.3) as [40]

$$\begin{aligned}\frac{d^2N}{d^2\mathbf{k}_1 d^2\mathbf{k}_2} \propto \int_{\mathbf{q}_1,\mathbf{q}_2,\mathbf{q}_3,\mathbf{q}_4} & L^i(\mathbf{k}_1,\mathbf{q}_1)L^i(\mathbf{k}_1,\mathbf{q}_2)L^j(\mathbf{k}_2,\mathbf{q}_3)L^j(\mathbf{k}_2,\mathbf{q}_4) \\ & \times \Big[\mu_p^2(\mathbf{q}_1,-\mathbf{q}_2)\mu_p^2(\mathbf{q}_3,-\mathbf{q}_4)\Big\langle \mathcal{D}(\mathbf{k}_1-\mathbf{q}_1,\mathbf{k}_1-\mathbf{q}_2)\mathcal{D}(\mathbf{k}_2-\mathbf{q}_3,\mathbf{k}_2-\mathbf{q}_4)\Big\rangle_T \\ & + \mu_p^2(\mathbf{q}_1,-\mathbf{q}_4)\mu_p^2(\mathbf{q}_3,-\mathbf{q}_2)\Big\langle \mathcal{Q}(\mathbf{k}_1-\mathbf{q}_1,\mathbf{k}_2-\mathbf{q}_4,\mathbf{k}_2-\mathbf{q}_3,\mathbf{k}_1-\mathbf{q}_2)\Big\rangle_T \\ & + \mu_p^2(\mathbf{q}_1,\mathbf{q}_3)\mu_p^2(\mathbf{q}_2,\mathbf{q}_4)\Big\langle \mathcal{Q}(\mathbf{k}_1-\mathbf{q}_1,-(\mathbf{k}_2-\mathbf{q}_3),\mathbf{k}_1-\mathbf{q}_2,-(\mathbf{k}_2-\mathbf{q}_4))\Big\rangle_T\Big],\end{aligned} \tag{4.7}$$

where

$$\mathcal{D}(\mathbf{k}_1,\mathbf{k}_2) = \int_{\mathbf{x}_1,\mathbf{x}_2} e^{-i\mathbf{k}_1\cdot\mathbf{x}_1+i\mathbf{k}_2\cdot\mathbf{x}_2}\frac{1}{N_c^2-1}\mathrm{Tr}\left[U(\mathbf{x}_1)U^\dagger(\mathbf{x}_2)\right] \tag{4.8}$$

is the Fourier transform of the *dipole operator* and

$$\begin{aligned}\mathcal{Q}(\mathbf{k}_1,\mathbf{k}_2,\mathbf{k}_3,\mathbf{k}_4) = \int_{\mathbf{x}_1,\mathbf{x}_2,\mathbf{x}_3,\mathbf{x}_4} & e^{-i\mathbf{k}_1\cdot\mathbf{x}_1+i\mathbf{k}_2\cdot\mathbf{x}_2-i\mathbf{k}_3\cdot\mathbf{x}_3+i\mathbf{k}_4\cdot\mathbf{x}_4} \\ & \times \frac{1}{N_c^2-1}\mathrm{Tr}\left[U(\mathbf{x}_1)U^\dagger(\mathbf{x}_2)U(\mathbf{x}_3)U^\dagger(\mathbf{x}_4)\right]\end{aligned} \tag{4.9}$$

is the Fourier transform of the *quadrupole operator*. Thus, in order to solve the double gluon spectrum, or, more generally, the multi-gluon spectrum, we will have to deal with the average over the target configurations of traces of Wilson lines. These averages can be solved analytically in some cases that will be explored in the next section.

4.2 Target averaging

In Sections 2.5 and 3.2 we have seen that the target average can be easily solved if we take the dilute limit of the target and use the Wick's theorem. However, in the dense limit the Wilson line is a non linear function of the target's source and therefore computing the target average of a product of Wilson lines is not so straightforward. As we shall see below, in the MV model it is possible to evaluate them by expanding the Wilson lines in terms of the target field and using the Wick's theorem to rearrange the terms and then resum it.

In the strict MV model, the field correlator can be evaluated by inverting Eq. (2.16)

$$A_T^-(z^+,\mathbf{x}) = g\int_{\mathbf{z}} G(\mathbf{x}-\mathbf{z})\rho_c(z^+,\mathbf{z}), \qquad G(\mathbf{x}) = \int_{\mathbf{k}} \frac{e^{i\mathbf{k}\cdot\mathbf{x}}}{\mathbf{k}^2}. \tag{4.10}$$

Thus the 2-point field correlator can be written as

$$g^2\left\langle A_T^{-,a}(x^+,\mathbf{x})A_T^{-,b}(y^+,\mathbf{y})\right\rangle_T = \delta^{ab}\delta(x^+-y^+)\mu^2(x^+)L_{\mathbf{xy}}, \tag{4.11}$$

where

$$L_{\mathbf{xy}} \equiv g^4\int_{\mathbf{z}} G(\mathbf{x}-\mathbf{z})G(\mathbf{y}-\mathbf{z}). \tag{4.12}$$

The simplest average that one can compute in the MV model is the average of a single Wilson line $\langle U(\mathbf{x})\rangle$. In this section we will keep the representation of the Wilson line general and assume that it can be in the fundamental or adjoint representation. By expanding the Wilson line and using the Wick's theorem it is easy to check that [177]

$$\langle U^{ab}(\mathbf{x})\rangle_T = \delta^{ab}\exp\left\{-\frac{C_R\mu^2}{2}L_{\mathbf{xx}}\right\}, \tag{4.13}$$

where $\mu^2 \equiv \int_{x^+}\mu^2(x^+)$ and C_R is the Casimir in the representation of the Wilson line, i.e. $C_F = (N_c^2-1)/(2N_c)$ for the fundamental and $C_A = N_c$ for the adjoint representation. As explained in [177], this resummation can be expressed in a diagrammatic way and is the result of summing *tadpole* contributions. The tadpole contributions are those where we have two field insertions in the same longitudinal and transverse point and, because of Eq. (4.11), gives rise to a factor $-C_R\mu^2 L_{\mathbf{xx}}$.

The second object that we will analyze is the average of the trace of two Wilson lines. This object is known in the literature as the *dipole function* because it represents the amplitude of a color dipole scattering in a dense medium. The average of two Wilson lines can be computed by performing the expansion of both Wilson lines and realizing that the tadpole contributions can be factorized. The result is

$$\frac{1}{D_R}\left\langle \mathrm{Tr}\left[U(\mathbf{x})U^\dagger(\mathbf{y})\right]\right\rangle_T = \exp\left\{-\frac{C_R\mu^2}{2}\left[L_{\mathbf{xx}}+L_{\mathbf{yy}}-2L_{\mathbf{xy}}\right]\right\}, \tag{4.14}$$

where D_R is the dimension of the representation of the Wilson line. We note that the same result can be obtained by using other method which consists in discretizing the longitudinal axis in such a way that we can break the Wilson lines into a path ordered product of Wilson lines where each of them are evaluated between the discretization points. Then we perform an expansion of the Wilson lines to leading order in the discretization length and we exploit the longitudinal locality of the MV model. By using this approach it is possible to re-exponentiate the result and to obtain Eq. (4.14) [178].

The argument of the exponential in Eq. (4.14) can be simplified by using Eq. (4.12),

$$F_{\mathbf{xy}} \equiv L_{\mathbf{xx}}+L_{\mathbf{yy}}-2L_{\mathbf{xy}} = g^4\int_{\mathbf{z}}\left[G(\mathbf{x}-\mathbf{z})-G(\mathbf{y}-\mathbf{z})\right]^2 = \frac{g^4}{\pi}\int_{k>\Lambda_{\mathrm{QCD}}}\frac{dk}{k^3}\left[1-J_0(kr)\right], \tag{4.15}$$

where $J_0(x)$ is the Bessel function of first kind, $k = |\mathbf{k}|$, $r = |\mathbf{x} - \mathbf{y}|$ and we have introduced Λ_{QCD} as an infrared regulator. This integral can be solved by assuming that the dipole's size is small $r \ll \Lambda_{\text{QCD}}^{-1}$ and expanding the Bessel function at leading order $J_0(x) \approx 1 - x^2/4$. Then we can write the dipole function as

$$\frac{1}{D_R}\Big\langle \text{Tr}\left[U(\mathbf{x})U^\dagger(\mathbf{y})\right]\Big\rangle_T = \exp\left\{-\frac{Q_s^2}{4}\mathbf{r}^2 \ln\left(\frac{1}{\mathbf{r}^2\Lambda_{\text{QCD}}^2} + e\right)\right\}, \tag{4.16}$$

where we have introduced a regulator e to avoid a wrong behavior of the dipole function when $r \sim \Lambda_{\text{QCD}}$ and we have defined the saturation momentum as

$$Q_s^2 = \frac{g^4 C_R \mu^2}{4\pi}. \tag{4.17}$$

This definition of the saturation momentum is arbitrary and depends on the representation of the target partons that interact with the projectile. However it is convenient since it makes the dipole function independent of the Casimir's value.

There is another approximation to Eq. (4.16) that is extensively used in literature which is known as the *Golec-Biernat-Wusthoff* (GBW) model [179]. This approximation uses the fact that when $r \lesssim Q_s^{-1} \ll \Lambda_{\text{QCD}}^{-1}$ the dipole function depends very slowly in the logarithm and therefore it drops the dependence on $\ln \frac{1}{\mathbf{r}^2\Lambda_{\text{QCD}}^2}$ leading to the following parameterization of the dipole function:

$$\frac{1}{D_R}\Big\langle \text{Tr}\left[U(\mathbf{x})U^\dagger(\mathbf{y})\right]\Big\rangle_T = \exp\left\{-\frac{Q_s^2}{4}\mathbf{r}^2\right\}. \tag{4.18}$$

In Fig. 4.2 we plot the difference between all the parameterizations of the dipole function which we call the Bessel dipole Eq. (4.15), the MV dipole Eq. (4.16) or the GBW dipole Eq. (4.18).

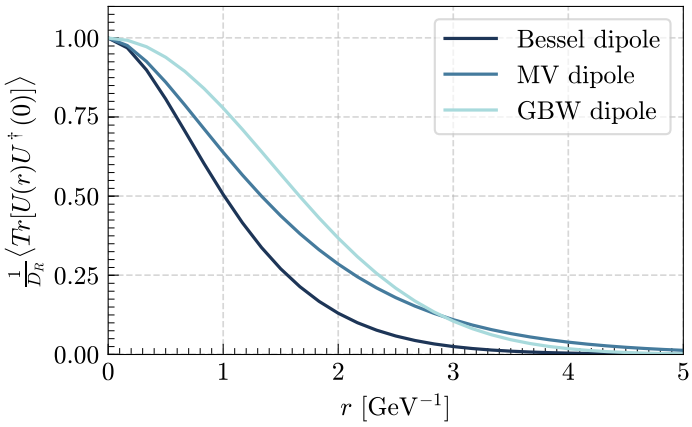

Figure 4.2.
Value of the dipole function using the parameterizations of Eq. (4.15), Eq. (4.16) and Eq. (4.18). For this plot we have used $Q_s = 1$ GeV, $\Lambda_{\text{QCD}} = 200$ MeV and $e = 1$.

We now turn our discussion to the average of 4 Wilson lines. In this case there are 2 objects of interest: the trace of 4 Wilson lines, known in the literature as the

quadrupole function, and the average of two dipoles that we will refer a the double dipole function. The technique for computing these objects is the same as for computing the dipole function but the color algebra is more complicated because we have to deal with the product of many generators. In the case of Wilson lines in the fundamental representation it is possible to exploit the Fierz identity to generate an iterative method for computing the average [180, 181]. The result for the double dipole function in the fundamental representation using this approach is

$$\frac{1}{N_c^2}\Big\langle \mathrm{Tr}\left[V(\mathbf{x})V^\dagger(\mathbf{y})\right]\mathrm{Tr}\left[V(\mathbf{u})V^\dagger(\mathbf{v})\right]\Big\rangle_T = e^{-\frac{C_F\mu^2}{2}(F_{\mathbf{xy}}+F_{\mathbf{uv}})-\frac{N_c}{4}\mu^2 K_{\mathbf{xuyv}}+\frac{1}{2N_c}\mu^2 K_{\mathbf{xyuv}}}$$
$$\times\left[\left(\frac{K_{\mathbf{xuyv}}+\sqrt{\Delta}}{2\sqrt{\Delta}}-\frac{K_{\mathbf{xyuv}}}{N_c^2\sqrt{\Delta}}\right)e^{\frac{N_c}{4}\mu^2\sqrt{\Delta}}-\left(\frac{K_{\mathbf{xuyv}}-\sqrt{\Delta}}{2\sqrt{\Delta}}-\frac{K_{\mathbf{xyuv}}}{N_c^2\sqrt{\Delta}}\right)e^{-\frac{N_c}{4}\mu^2\sqrt{\Delta}}\right], \quad (4.19)$$

where we have made the change $U \to V$ to emphasize that $V(\mathbf{x})$ is the Wilson line in the fundamental representation and defined the following functions

$$K_{\mathbf{xyuv}} = F_{\mathbf{xu}} + F_{\mathbf{yv}} - F_{\mathbf{xv}} - F_{\mathbf{yu}}, \quad (4.20)$$

$$\Delta = K_{\mathbf{xuyv}}^2 + \frac{4}{N_c^2}K_{\mathbf{xyuv}}K_{\mathbf{xvuy}}. \quad (4.21)$$

For the quadrupole function we obtain a similar expression [182]

$$\frac{1}{N_c}\Big\langle \mathrm{Tr}\left[V(\mathbf{x})V^\dagger(\mathbf{y})V(\mathbf{u})V^\dagger(\mathbf{v})\right]\Big\rangle_T = e^{-\frac{C_F\mu^2}{2}(F_{\mathbf{xy}}+F_{\mathbf{uv}})-\frac{N_c}{4}\mu^2 K_{\mathbf{xuyv}}+\frac{1}{2N_c}\mu^2 K_{\mathbf{xyuv}}}$$
$$\times\left[\left(\frac{K_{\mathbf{xuyv}}+\sqrt{\Delta}}{2\sqrt{\Delta}}-\frac{K_{\mathbf{xyuv}}}{\sqrt{\Delta}}\right)e^{\frac{N_c}{4}\mu^2\sqrt{\Delta}}-\left(\frac{K_{\mathbf{xuyv}}-\sqrt{\Delta}}{2\sqrt{\Delta}}-\frac{K_{\mathbf{xyuv}}}{\sqrt{\Delta}}\right)e^{-\frac{N_c}{4}\mu^2\sqrt{\Delta}}\right]. \quad (4.22)$$

We should note that these equations simplify enormously if we use the GBW approximation

$$C_F\mu^2 F_{\mathbf{xy}} = \frac{Q_s^2}{2}(\mathbf{x}-\mathbf{y})^2, \qquad \mu^2 K_{\mathbf{xyuv}} = \frac{Q_s^2}{2C_F}(\mathbf{x}-\mathbf{y})\cdot(\mathbf{u}-\mathbf{v}). \quad (4.23)$$

Moreover, in the case of the double dipole and quadrupole function in the adjoint representation it is more convenient to use the technique presented in [178]. We will not show the expression here but we refer to this paper for them

In order to compute higher order averages of the Wilson lines we should use the same methodology. The sextupole function is presented in [183] and a general expression for the multi-pole function is given in [184]. The problem of this methodology is that as we move to higher orders of the multi-pole functions the expressions become messier and less useful for analytical or even numerical analysis. For this reason it is useful to look for reliable alternatives to this approach.

4.2.1 The Area Enhancement model

Looking for arguments of quantum correlations in dilute-dense systems, it has been proposed in [169, 170] a simple model for computing target averages of Wilson lines that

we will refer to as the *Area Enhancement* (AE) model. This approximation is based on the chromo-electric domain model presented in Section 3.3. Since the target ensemble in the transverse plane is composed by domains of chromo-electric fields with a typical correlation length Q_s^{-1}, any Wilson line sitting at some transverse point $\mathbf{x}$ will be uncorrelated with another Wilson line sitting at a point $\mathbf{y}$ as long as $|\mathbf{x}-\mathbf{y}| \gg Q_s^{-1}$. Thus the multi-pole function can be broken into smaller multi-poles where the transverse points of the Wilson lines are sitting in the same domain. Noting that those configurations where a single Wilson line is sitting at some domain is suppressed by $\exp\left\{-Q_s^2/\Lambda^2_{\mathrm{QCD}}\right\} \ll 1$ (Eq. (4.13)), the smallest multi-pole possible in such a factorization is the dipole function, i.e. the Wilson lines have at least to be grouped pairwise in a domain. This assumption can be written schematically as

$$\Big\langle U(\mathbf{x}_1)\cdots U(\mathbf{x}_n)\Big\rangle_T \approx \prod_{\text{domains}} \Big\langle \prod_{\text{i}\in\text{domain}} U(\mathbf{x}_i)\Big\rangle_T, \tag{4.24}$$

where the coordinates $\mathbf{x}_i$ are fixed and the first product is over all domains while the second is over all coordinates sitting at a given domain.

The second argument of the AE model is that, since the multi-pole function always appear integrated over as a Fourier transform in the particle spectra, those configurations where more than two Wilson lines are sitting in the same domain are subleading in the inverse of the phase space area. This is because that, assuming that the multi-pole functions are smooth functions over the phase space integral, those configurations that maximize the integral are those where the Wilson lines transverse points are as far away as possible and this condition is fulfilled if only two Wilson lines sit at the same domain and the remaining pairs of them are as far away as possible. This is equivalent as saying that the multi-pole's configuration that maximizes the integral is that where the multi-pole is broken into dipole functions. In order to illustrate how this approach works let us compute the quadrupole function in the adjoint representation:

$$Q(\mathbf{y}_1,\mathbf{y}_2,\mathbf{y}_3,\mathbf{y}_4) = \frac{1}{N_c^2-1}\Big\langle \mathrm{Tr}\left[U(\mathbf{y}_1)U^\dagger(\mathbf{y}_2)U(\mathbf{y}_3)U^\dagger(\mathbf{y}_4)\right]\Big\rangle_T. \tag{4.25}$$

By using the first argument, illustrated in Eq. (4.24), the quadrupole function can be written as

$$\begin{aligned} Q(\mathbf{y}_1,\mathbf{y}_2,\mathbf{y}_3,\mathbf{y}_4) \approx & \lim_{\substack{|\mathbf{y}_1-\mathbf{y}_2|\lesssim Q_s^{-1}\\ |\mathbf{y}_3-\mathbf{y}_4|\lesssim Q_s^{-1}\\ |\mathbf{y}_1-\mathbf{y}_3|\lesssim Q_s^{-1}}} Q(\mathbf{y}_1,\mathbf{y}_2,\mathbf{y}_3,\mathbf{y}_4) + \lim_{\substack{|\mathbf{y}_1-\mathbf{y}_2|\lesssim Q_s^{-1}\\ |\mathbf{y}_3-\mathbf{y}_4|\lesssim Q_s^{-1}\\ |\mathbf{y}_1-\mathbf{y}_3|\gg Q_s^{-1}}} Q(\mathbf{y}_1,\mathbf{y}_2,\mathbf{y}_3,\mathbf{y}_4) \\ + & \lim_{\substack{|\mathbf{y}_1-\mathbf{y}_3|\lesssim Q_s^{-1}\\ |\mathbf{y}_2-\mathbf{y}_4|\lesssim Q_s^{-1}\\ |\mathbf{y}_1-\mathbf{y}_2|\gg Q_s^{-1}}} Q(\mathbf{y}_1,\mathbf{y}_2,\mathbf{y}_3,\mathbf{y}_4) + \lim_{\substack{|\mathbf{y}_1-\mathbf{y}_4|\lesssim Q_s^{-1}\\ |\mathbf{y}_2-\mathbf{y}_3|\lesssim Q_s^{-1}\\ |\mathbf{y}_1-\mathbf{y}_2|\gg Q_s^{-1}}} Q(\mathbf{y}_1,\mathbf{y}_2,\mathbf{y}_3,\mathbf{y}_4), \end{aligned} \tag{4.26}$$

where the first term of this equation is the contribution where the 4 points are sitting in the same domain and, therefore, is constrained to a smaller region of phase space than the other 3 terms. This will imply that, after performing the Fourier transform, it will be suppressed by the phase space area with respect to the other ones. On the other hand, the other three terms can be just written as a product of dipole functions. For example,

the second term can be written as

$$\lim_{\substack{|\mathbf{y}_1-\mathbf{y}_2|\lesssim Q_s^{-1}\\ |\mathbf{y}_3-\mathbf{y}_4|\lesssim Q_s^{-1}\\ |\mathbf{y}_1-\mathbf{y}_3|\gg Q_s^{-1}}} \left\langle U(\mathbf{y}_1)^{a_1b_1}U^\dagger(\mathbf{y}_2)^{b_1a_2}U(\mathbf{y}_3)^{a_2b_2}U^\dagger(\mathbf{y}_4)^{b_2a_1}\right\rangle_T \approx \left\langle U(\mathbf{y}_1)^{a_1b_1}U^\dagger(\mathbf{y}_2)^{b_1a_2}\right\rangle_T \left\langle U(\mathbf{y}_3)^{a_2b_2}U^\dagger(\mathbf{y}_4)^{b_2a_1}\right\rangle_T, \tag{4.27}$$

where we have dropped the factor $1/(N_c^2-1)$ for simplicity. Thus, by neglecting the first term in Eq. (4.26), we can write the quadrupole function as a sum of products of 2-point functions,

$$\begin{aligned}\left\langle U(\mathbf{y}_1)^{a_1b_1}U^\dagger(\mathbf{y}_2)^{b_1a_2}U(\mathbf{y}_3)^{a_2b_2}U^\dagger(\mathbf{y}_4)^{b_2a_1}\right\rangle_T &\approx \left\langle U(\mathbf{y}_1)^{a_1b_1}U^\dagger(\mathbf{y}_2)^{b_1a_2}\right\rangle_T \left\langle U(\mathbf{y}_3)^{a_2b_2}U^\dagger(\mathbf{y}_4)^{b_2a_1}\right\rangle_T \\ &+ \left\langle U(\mathbf{y}_1)^{a_1b_1}U(\mathbf{y}_3)^{a_2b_2}\right\rangle_T \left\langle U^\dagger(\mathbf{y}_2)^{b_1a_2}U^\dagger(\mathbf{y}_4)^{b_2a_1}\right\rangle_T \\ &+ \left\langle U(\mathbf{y}_1)^{a_1b_1}U^\dagger(\mathbf{y}_4)^{b_2a_1}\right\rangle_T \left\langle U^\dagger(\mathbf{y}_2)^{b_1a_2}U(\mathbf{y}_3)^{a_2b_2}\right\rangle_T,\end{aligned} \tag{4.28}$$

where we should keep in mind that this approximation is only good after performing the phase space integral since otherwise the first term in Eq. (4.26) is not subleading in the collision area.

This result can be generalized to the case of any number or configuration of the Wilson lines by noting that the contribution of the multi-pole that is enhanced by the phase space area, i.e., that is leading in $1/B_pQ_s^{-2}$ with B_p the gluonic area of the projectile (taken as the overlap area of the collision), is always a sum over all possible combinations of 2-point functions. This is analogous to assume that the Wilson lines follow a Gaussian distribution and thus we are able to apply Wick's theorem to them:

$$\left\langle U(\mathbf{y}_1)^{a_1b_1}U(\mathbf{y}_2)^{a_2b_2}\cdots U(\mathbf{y}_{2n})^{a_{2n}b_{2n}}\right\rangle_T = \sum_{\sigma\in\Pi(\chi)}\prod_{\{\alpha,\beta\}\in\sigma}\left\langle U(\mathbf{y}_\alpha)^{a_\alpha b_\alpha}U(\mathbf{y}_\beta)^{a_\beta b_\beta}\right\rangle_T, \tag{4.29}$$

being $\chi=\{1,2,\ldots,2n\}$ and $\Pi(\chi)$ the set of partitions of χ with disjoint pairs. Eq. (4.29) simplifies enormously the evaluation of multi-poles and shares its simplicity with the Glasma Graph approximation through the Wick's theorem. The main difference between them is that the first does not rely on the dilute limit and thus is applicable to dilute-dense scattering. This approach has been used recently [40, 167] in order to evaluate the phase space integral of 4- and 6-point functions.

In order to simplify further the 2-point functions that appear in Eq. (4.29) we should use the fact that the target ensemble is color neutral from domain to domain and therefore the average of any object in such a ensemble has to be in a color singlet state. Thus, we can write the 2-point function of the Wilson lines as a dipole function:

$$\left\langle U(\mathbf{x})^{ab}U^\dagger(\mathbf{y})^{dc}\right\rangle_T = \frac{\delta^{ac}\delta^{bd}}{(N_c^2-1)^2}\left\langle \mathrm{Tr}\left[U(\mathbf{x})U^\dagger(\mathbf{y})\right]\right\rangle_T \equiv \frac{\delta^{ac}\delta^{bd}}{N_c^2-1}D(\mathbf{x},\mathbf{y}), \tag{4.30}$$

where we have written the dipole function as $D(\mathbf{x},\mathbf{y})$.

In order to compare the Area Enhancement model with the MV approach presented above let us study the quadrupole and double dipole functions in both approaches. For the sake of simplicity we will work in the fundamental representation of the Wilson lines instead of the adjoint representation. By using the equivalent expression of Eq. (4.28) in the fundamental representation and Eq. (4.30) we can write the double dipole function in the AE model as

$$\langle \mathcal{D}^{(F)}(\mathbf{x},\mathbf{y})\mathcal{D}^{(F)}(\mathbf{u},\mathbf{v})\rangle_T^{\mathrm{AE}} = D^{(F)}(\mathbf{x},\mathbf{y})D^{(F)}(\mathbf{u},\mathbf{v}) + \frac{1}{N_c^2}D^{(F)}(\mathbf{x},\mathbf{v})D^{(F)}(\mathbf{u},\mathbf{y}), \tag{4.31}$$

where we have introduced the dipole operator $\mathcal{D}^{(F)}(\mathbf{x},\mathbf{y}) = \frac{1}{N_c}\mathrm{Tr}[V(\mathbf{x})V^\dagger(\mathbf{y})]$ and the dipole function $D^{(F)}(\mathbf{x},\mathbf{y})$ in the fundamental representation. Moreover, we have used the fact that $\langle V(\mathbf{x})V(\mathbf{y})\rangle_T = 0$ in the fundamental representation.

The double dipole function in the AE model can be compared analytically to the one computed in Eq. (4.19) within the MV model by doing the large-N_c limit of the later. Using the GBW approximation defined in Eq. (4.23) and doing $N_c \to \infty$ in Eq. (4.19) we obtain that

$$\begin{aligned}\langle \mathcal{D}^{(F)}(\mathbf{x},\mathbf{y})\mathcal{D}^{(F)}(\mathbf{u},\mathbf{v})\rangle_T^{\mathrm{MV}} &= D^{(F)}(\mathbf{x},\mathbf{y})D^{(F)}(\mathbf{u},\mathbf{v}) \\ + \frac{1}{N_c^2}\frac{K^2_{\mathbf{xyuv}}}{K^2_{\mathbf{xuyv}}}&\left[D^{(F)}(\mathbf{x},\mathbf{v})D^{(F)}(\mathbf{u},\mathbf{y}) + D^{(F)}(\mathbf{x},\mathbf{y})D^{(F)}(\mathbf{u},\mathbf{v})\left(\frac{Q_s^2}{2}(\mathbf{u}-\mathbf{x})\cdot(\mathbf{v}-\mathbf{y}) - 1\right)\right].\end{aligned} \tag{4.32}$$

Thus, in the large-N_c limit, the ratio between the integral of the double dipole computed in the MV and AE models is

$$\begin{aligned}\frac{\int_{\mathbf{x},\mathbf{y},\mathbf{u},\mathbf{v}}\langle \mathcal{D}\mathcal{D}\rangle^{\mathrm{MV}}}{\int_{\mathbf{x},\mathbf{y},\mathbf{u},\mathbf{v}}\langle \mathcal{D}\mathcal{D}\rangle^{\mathrm{AE}}} &= 1 + \frac{1}{N_c^2}\int_{\mathbf{x},\mathbf{y},\mathbf{u},\mathbf{v}}\left[\left(\frac{K^2_{\mathbf{xyuv}}}{K^2_{\mathbf{xuyv}}} - 1\right)D(\mathbf{x},\mathbf{v})D(\mathbf{u},\mathbf{y})\right. \\ &\left. + \frac{K^2_{\mathbf{xyuv}}}{K_{\mathbf{xuyv}}}\left(\frac{Q_s^2}{2}(\mathbf{u}-\mathbf{x})\cdot(\mathbf{v}-\mathbf{y}) - 1\right)D(\mathbf{x},\mathbf{y})D(\mathbf{u},\mathbf{v})\right] \Big/ \int_{\mathbf{x},\mathbf{y},\mathbf{u},\mathbf{v}} D(\mathbf{x},\mathbf{y})D(\mathbf{u},\mathbf{v}),\end{aligned} \tag{4.33}$$

where we have dropped the super-index (F) from the dipole functions for simplicity. The dipole functions will be given by the GBW model of Eq. (4.18) and therefore are Gaussian functions with a spread of order Q_s^{-1}. Therefore, using the saddle point approximation, and noting that $K_{\mathbf{xyuv}} \to 0$ when $\mathbf{x} \to \mathbf{y}$ or $\mathbf{u} \to \mathbf{v}$, it is straightforward to see that the MV and the AE model lead to the same result. For such approximation to hold we must consider the Gaussian functions, with width $\propto 1/Q_s$, to behave δ-like with respect to the integration area. Therefore, corrections must be order $1/Q_s^2$ that, by dimensional reasons, has to be multiplied by an inverse area, with the size of the proton B_p, being the only parameter with such dimensions. Thus we conclude that, at least in the large-N_c limit, the Area Enhancement model gives the leading contribution in powers of $1/B_pQ_s^2$ to the MV model.

So far the argument discussed above relies on the large-N_c limit and only depends on the target's dynamics and for this reason B_p does not appear in the expressions. In order to take into account all orders in N_c and to introduce a dependence on the area of the collision B_p we will perform the integral numerically through the following phase space

measure

$$d\Omega = d^2\mathbf{x}d^2\mathbf{y}d^2\mathbf{u}d^2\mathbf{v}\Theta\left(\sqrt{2B_p} - |\mathbf{x}|\right)\Theta\left(\sqrt{2B_p} - |\mathbf{y}|\right)\Theta\left(\sqrt{2B_p} - |\mathbf{u}|\right)\Theta\left(\sqrt{2B_p} - |\mathbf{v}|\right), \tag{4.34}$$

that is, we integrate over a 4-sphere of radius $\sqrt{2B_p}$ in such a way that the integral over the phase space leads to the expected result

$$\int d\Omega = (2\pi B_p)^4 = S_\perp^4. \tag{4.35}$$

In order to compare the MV and AE models, we perform a Fourier transform over this phase space measure defined as

$$\langle \mathcal{D}(\mathbf{q}_1, \mathbf{q}_2)\mathcal{D}(\mathbf{q}_3, \mathbf{q}_4)\rangle_T = \int d\Omega e^{i\mathbf{q}_1\cdot\mathbf{x} - i\mathbf{q}_2\cdot\mathbf{y} + i\mathbf{q}_3\cdot\mathbf{u} - i\mathbf{q}_4\cdot\mathbf{v}}\langle \mathcal{D}(\mathbf{x}, \mathbf{y})\mathcal{D}(\mathbf{u}, \mathbf{v})\rangle_T. \tag{4.36}$$

In Fig. 4.3 we show the result for the ratio of the Fourier transforms of Eq. (4.19) and Eq. (4.31) for different values of B_p, taking $Q_s^2 = 1$ GeV^2. The result was generated by using four sets of random momenta with moduli between 0.5 and 1.5 GeV. We see that, as expected, as we increase the value of $B_pQ_s^2$ the results in the AE model tends to those in the MV model, being the difference between both approaches of order a few % at relatively high B_p.

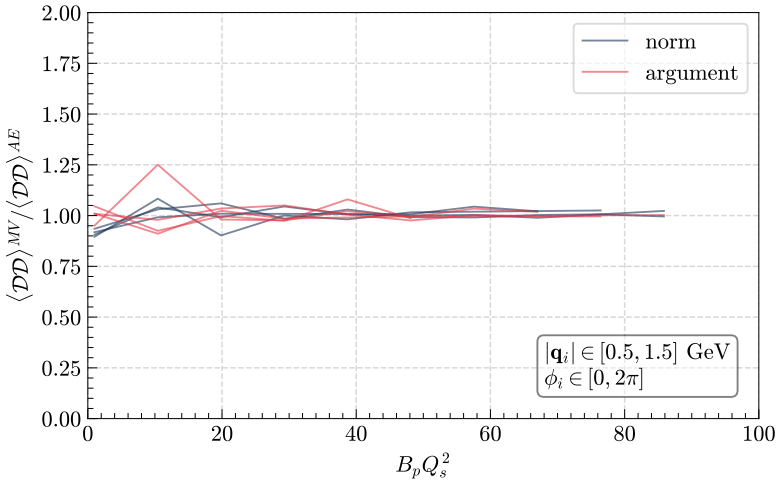

Figure 4.3.
Ratio of the Fourier transforms of Eq. (4.19) and Eq. (4.31) at different values of B_p. The values of the ratio were computed using four sets of random momenta with moduli between 0.5 GeV and 1.5 GeV. We present both the norm (blue lines) and the argument (red lines). We have suppressed the values where the estimated error in the Monte Carlo integration becomes larger than 10 %.

Now we turn our discussion to the quadrupole function. In the AE model it can be written as

$$\langle \mathcal{Q}(\mathbf{x}, \mathbf{y}, \mathbf{u}, \mathbf{v})\rangle_T^{\text{AE}} = D(\mathbf{x}, \mathbf{y})D(\mathbf{u}, \mathbf{v}) + D(\mathbf{x}, \mathbf{v})D(\mathbf{u}, \mathbf{y}), \tag{4.37}$$

where $\mathcal{Q}(\mathbf{x},\mathbf{y},\mathbf{u},\mathbf{v}) = \frac{1}{N_c}\mathrm{Tr}[V(\mathbf{x})V^\dagger(\mathbf{y})V(\mathbf{u})V^\dagger(\mathbf{v})]$ is the quadrupole operator. On the other hand, the large-N_c limit of the MV quadrupole function Eq. (4.22) in the GBW approximation is given by

$$\langle \mathcal{Q}(\mathbf{x},\mathbf{y},\mathbf{u},\mathbf{v})\rangle_T^{\mathrm{MV}} = D(\mathbf{x},\mathbf{y})D(\mathbf{u},\mathbf{v}) - \frac{K_{\mathbf{xyuv}}}{K_{\mathbf{xuyv}}}\Big[D(\mathbf{x},\mathbf{y})D(\mathbf{u},\mathbf{v}) - D(\mathbf{x},\mathbf{v})D(\mathbf{u},\mathbf{y})\Big]. \tag{4.38}$$

It is easy to see, again, that by using the saddle point approximation and the same arguments given above that the quadrupole function is the same in both models at leading order in $1/B_pQ_s^2$. However, in the case of the quadrupole the difference between Eqs. (4.37) and (4.38) is not suppressed by any power of $1/N_c^2$ and, therefore, we expect a larger discrepancy between both models.

In Fig. 4.4 we plot the ratio between the Fourier transform, defined analogous to Eq. (4.36), of Eqs. (4.22) and (4.37) for three sets of random momenta with moduli between 0.5 and 1.5 GeV for different values of B_p, taking again $Q_s^2 = 1$ GeV^2. In this case the difference between both models is of order 30% at relatively high B_p, being larger than in Fig. 4.3 due to the $1/N_c^2$ suppression present for the double dipole and absent for the quadrupole. It also looks that at high B_p the AE model tends to the MV model but the integrals become very time consuming which prevents reaching larger values of $B_pQ_s^2$. Therefore, the tendency is not as clear as in Fig. 4.3.

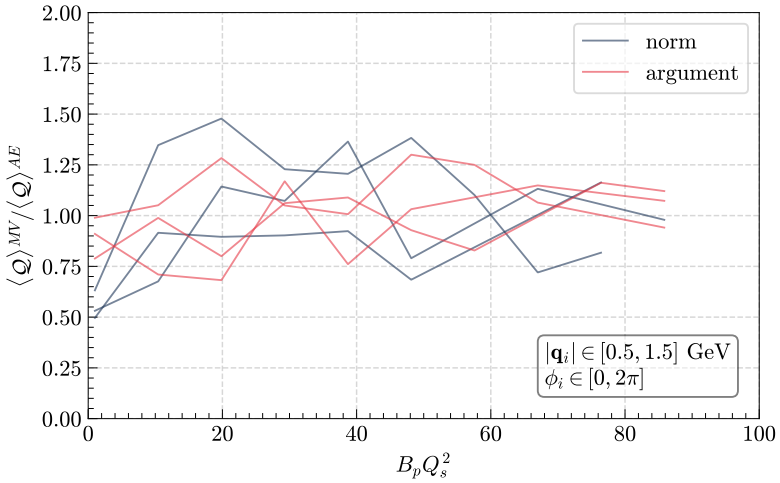

Figure 4.4.
Ratio of the Fourier transform of Eqs. (4.22) and (4.37) at different values of B_p. The values of the ratio were computed using three sets of random momenta with moduli between 0.5 GeV and 1.5 GeV. We present both the norm (blue lines) and the argument (red lines). We have suppressed the values where the estimated error in the Monte Carlo integration becomes larger than 10 %.

We then conclude that the Area Enhancement model provides a similar description of the target averages of Wilson lines compared to the MV model. The main problem of this approximation is that it assumes that $B_pQ_s^2 \gg 1$ while in practice this value is not so large. On the other hand, it neglects these contributions where more than two particles

scatter in the same domain. These contributions may be dominant when studying multi-particle correlations and therefore for a complete description of such a problem we should have them into account. However, because of practical reasons we will use the AE model in the rest of this chapter.

4.3 Double gluon production in the AE model

We now go back to the double gluon spectrum presented in Eq. (4.7) where we will analyze it by using the Area Enhancement model. In order to make the notation lighter let us make the change of variables $\mathbf{q}_i \to \mathbf{k}_i - \mathbf{q}_i$ in such a way that now the momentum transfer by the projectile is $\mathbf{k}_i - \mathbf{q}_i$ and the momentum transfer by the target is $\mathbf{q}_i$. We also redefine the Lipatov vertex as

$$L^i(\mathbf{k},\mathbf{q}) = \frac{\mathbf{k}^i}{\mathbf{k}^2} - \frac{(\mathbf{k}-\mathbf{q})^i}{(\mathbf{k}-\mathbf{q})^2}. \tag{4.39}$$

Then Eq. (4.7) is rewritten as

$$\begin{aligned}\frac{d^2N}{d^2\mathbf{k}_1 d^2\mathbf{k}_2} \propto \int_{\mathbf{q}_1,\mathbf{q}_2,\mathbf{q}_3,\mathbf{q}_4} & L^i(\mathbf{k}_1,\mathbf{q}_1)L^i(\mathbf{k}_1,\mathbf{q}_2)L^j(\mathbf{k}_2,\mathbf{q}_3)L^j(\mathbf{k}_2,\mathbf{q}_4) \\ \times \Big[& \mu_p^2(\mathbf{k}_1-\mathbf{q}_1,-\mathbf{k}_1+\mathbf{q}_2)\mu_p^2(\mathbf{k}_2-\mathbf{q}_3,-\mathbf{k}_2+\mathbf{q}_4)\Big\langle \mathcal{D}(\mathbf{q}_1,\mathbf{q}_2)\mathcal{D}(\mathbf{q}_3,\mathbf{q}_4)\Big\rangle_T \\ & + \mu_p^2(\mathbf{k}_1-\mathbf{q}_1,-\mathbf{k}_2+\mathbf{q}_4)\mu_p^2(\mathbf{k}_2-\mathbf{q}_3,-\mathbf{k}_1+\mathbf{q}_2)\Big\langle \mathcal{Q}(\mathbf{q}_1,\mathbf{q}_4,\mathbf{q}_3,\mathbf{q}_2)\Big\rangle_T \\ & + \mu_p^2(\mathbf{k}_1-\mathbf{q}_1,\mathbf{k}_2-\mathbf{q}_3)\mu_p^2(\mathbf{k}_1-\mathbf{q}_2,\mathbf{k}_2-\mathbf{q}_4)\Big\langle \mathcal{Q}(\mathbf{q}_1,-\mathbf{q}_3,\mathbf{q}_2,-\mathbf{q}_4)\Big\rangle_T \Big]. \end{aligned} \tag{4.40}$$

In the rest of this chapter we will use the GBW approximation for the dipole functions. In this case the Fourier transform of the dipole can be written as

$$D(\mathbf{k},\mathbf{q}) = \int_{\mathbf{x},\mathbf{y}} e^{i\mathbf{k}\cdot\mathbf{x}-i\mathbf{q}\cdot\mathbf{y}} D(|\mathbf{x}-\mathbf{y}|) = (2\pi)^2\delta^{(2)}(\mathbf{k}-\mathbf{q})d(\mathbf{k}), \tag{4.41}$$

where

$$d(\mathbf{k}) = \frac{4\pi}{Q_s^2}\exp\left\{-\frac{\mathbf{k}^2}{Q_s^2}\right\}, \tag{4.42}$$

and we have used Eq. (4.18).

Thus, by using the Area Enhancement model in Eq. (4.29) and the color neutralization condition in Eq. (4.30), the Fourier transform of the double dipole can be written as

$$\begin{aligned}\Big\langle \mathcal{D}(\mathbf{q}_1,\mathbf{q}_2)\mathcal{D}(\mathbf{q}_3,\mathbf{q}_4)\Big\rangle_T = & (2\pi)^4\delta^{(2)}(\mathbf{q}_1-\mathbf{q}_2)\delta^{(2)}(\mathbf{q}_3-\mathbf{q}_4)d(\mathbf{q}_1)d(\mathbf{q}_3) \\ & + \frac{1}{N_c^2-1}\Big[(2\pi)^4\delta^{(2)}(\mathbf{q}_1-\mathbf{q}_4)\delta^{(2)}(\mathbf{q}_3-\mathbf{q}_2)d(\mathbf{q}_1)d(\mathbf{q}_3)\end{aligned}$$

$$+ (2\pi)^4\delta^{(2)}(\mathbf{q}_1+\mathbf{q}_3)\delta^{(2)}(\mathbf{q}_2+\mathbf{q}_4)d(\mathbf{q}_1)d(\mathbf{q}_2)\Big], \quad (4.43)$$

and the quadrupole's Fourier transform as

$$\begin{aligned}\Big\langle \mathcal{Q}(\mathbf{q}_1,\mathbf{q}_2,\mathbf{q}_3,\mathbf{q}_4)\Big\rangle_T &= (2\pi)^4\delta^{(2)}(\mathbf{q}_1-\mathbf{q}_2)\delta^{(2)}(\mathbf{q}_3-\mathbf{q}_4)d(\mathbf{q}_1)d(\mathbf{q}_3)\\ &\quad + (2\pi)^4\delta^{(2)}(\mathbf{q}_1-\mathbf{q}_4)\delta^{(2)}(\mathbf{q}_3-\mathbf{q}_2)d(\mathbf{q}_1)d(\mathbf{q}_3)\\ &\quad + \frac{1}{N_c^2-1}(2\pi)^4\delta^{(2)}(\mathbf{q}_1+\mathbf{q}_3)\delta^{(2)}(\mathbf{q}_2+\mathbf{q}_4)d(\mathbf{q}_1)d(\mathbf{q}_2). \quad (4.44)\end{aligned}$$

By substituting these equations into Eq. (4.40) we will obtain a sum of 9 terms analogous when we discussed the double gluon spectrum in the Glasma Graph approximation in Section 3.2. We will not write the full expression here and we refer to [40] for the result. The important conclusion of this result is that, because of the δ-like behavior of the functions $\mu_p^2(\mathbf{k},\mathbf{q})$, we will obtain contributions where the momentum transfer of both projectile or target sources are the same, i.e. Bose Enhancement correlations, or the momenta of the produced gluons are the same, i.e. HBT correlations. Therefore, quantum statistics effects are not a property only of the dilute limit but are also included in the target's dense limit. Moreover, since the next order correction to the Area Enhancement model, that may give correlations from other kind, is parametrically of order $1/(B_pQ_s^2)$ which we assume that is small, we conclude that the main source of correlations in double particle production at mid-rapidity is the Bose Enhancement and HBT correlations. The goal of the next section will be to generalize this result to multi-gluon production.

4.4 Multi-gluon production in the AE model

We now turn our discussion to multi-gluon production within the Area Enhancement approximation presented in the last section. By making the change $\mathbf{q}_i \to \mathbf{k}_i - \mathbf{q}_i$, Eq. (4.1) is rewritten as

$$\begin{aligned}&2^n(2\pi)^{3n}\frac{d^nN}{d^2\mathbf{k_1}d^2\mathbf{k}_3\cdots d^2\mathbf{k}_{2n-1}}\\ &\quad= 2^{2n}g^{2n}\int_{\mathbf{q}_1,\ldots,\mathbf{q}_{2n}} L^{i_1}(\mathbf{k}_1,\mathbf{q}_1)L^{i_1}(\mathbf{k}_1,\mathbf{q}_2)\cdots L^{i_{2n-1}}(\mathbf{k}_{2n-1},\mathbf{q}_{2n-1})L^{i_{2n-1}}(\mathbf{k}_{2n-1},\mathbf{q}_{2n})\\ &\qquad\times\Big\langle U^{b_1a_1}(\mathbf{q}_1)\cdots U^{b_{2n-1}a_{2n-1}}(\mathbf{q}_{2n-1})U^{\dagger a_{2n-1}b_{2n}}(\mathbf{q}_{2n})\cdots U^{\dagger a_1b_2}(\mathbf{q}_2)\Big\rangle_T\\ &\qquad\times\Big\langle \rho_p^{b_1}(\mathbf{k}_1-\mathbf{q}_1)\rho_p^{*b_2}(\mathbf{k}_1-\mathbf{q}_2)\cdots\rho_p^{b_{2n-1}}(\mathbf{k}_{2n-1}-\mathbf{q}_{2n-1})\rho_p^{*b_{2n}}(\mathbf{k}_{2n-1}-\mathbf{q}_{2n})\Big\rangle_p, \quad (4.45)\end{aligned}$$

where we have made the change of labeling $\mathbf{k}_i \to \mathbf{k}_{2i-1}$, i.e. we are labeling the transverse momenta of the produced gluons by odd indices for later convenience. In order to make the notation lighter it is convenient to introduce the following object:

$$\Lambda_j \equiv 2L^{i_j}U^{b_ja_j}(\mathbf{q}_j), \quad (4.46)$$

where $j = 1,\ldots,2n$. In this notation, when j is even the Wilson line is hermitian (i.e., to the right of the cut) and when j is odd it is not (i.e., to the left of the cut). Furthermore,

since the produced gluon has the same momentum, polarization and color both in the real and conjugate spaces we have to apply the following constraints:

$$\mathbf{k}_{2m} = \mathbf{k}_{2m-1} \ , \tag{4.47}$$

$$i_{2m} = i_{2m-1} \ , \tag{4.48}$$

$$a_{2m} = a_{2m-1} \ , \tag{4.49}$$

with $m = 1, \ldots, n$. With this convention we can write the $2n$-point function of the Wilson lines and the Lipatov vertices as

$$\begin{aligned} &2^{2n} L^{i_1}(\mathbf{k}_1, \mathbf{q}_1) L^{i_1}(\mathbf{k}_1, \mathbf{q}_2) \cdots L^{i_{2n-1}}(\mathbf{k}_{2n-1}, \mathbf{q}_{2n-1}) L^{i_{2n-1}}(\mathbf{k}_{2n-1}, \mathbf{q}_{2n}) \\ &\times \left\langle U^{b_1 a_1}(\mathbf{q}_1) \cdots U^{b_{2n-1} a_{2n-1}}(\mathbf{q}_{2n-1}) U^{\dagger a_{2n-1} b_{2n}}(\mathbf{q}_{2n}) \cdots U^{\dagger a_1 b_2}(\mathbf{q}_2) \right\rangle_T \\ &\qquad = \left\langle \Lambda_1 \Lambda_2 \cdots \Lambda_{2n-1} \Lambda_{2n} \right\rangle_T . \end{aligned} \tag{4.50}$$

In order to compute the target average we use the Area Enhancement model defined in Eq. (4.29). Thus Eq. (4.50) can be written as

$$\left\langle \Lambda_1 \Lambda_2 \cdots \Lambda_{2n-1} \Lambda_{2n} \right\rangle_T = \sum_{\sigma \in \Pi(\chi)} \prod_{\{\alpha,\beta\} \in \sigma} \left\langle \Lambda_\alpha \Lambda_\beta \right\rangle_T , \tag{4.51}$$

with $\chi = \{1, 2, \ldots, 2n\}$ and $\Pi(\chi)$ the set of partitions of χ with disjoint pairs.

The two point function can be computed in the same way as we did for the double gluon production in Eq. (4.41), i.e., we use the GBW model and the condition of color neutralization of the target, the result reads

$$\left\langle \Lambda_\alpha \Lambda_\beta \right\rangle_T = 4 \frac{\delta^{a_\alpha a_\beta} \delta^{b_\alpha b_\beta}}{N_c^2 - 1} (2\pi)^2 \delta^{(2)}[\mathbf{q}_\alpha + (-1)^{\alpha+\beta} \mathbf{q}_\beta] L^{i_\alpha}(\mathbf{k}_\alpha, \mathbf{q}_\alpha) L^{i_\beta}(\mathbf{k}_\beta, \mathbf{q}_\beta) d(\mathbf{q}_\alpha), \tag{4.52}$$

where $d(\mathbf{q})$ is defined in Eq. (4.42) and the factor $(-1)^{\alpha+\beta}$ in the Dirac's delta is introduced in order to have into account the change of sign in the momenta when both of them are evaluated in the same side of the cut.

The next step is to evaluate the projectile average. Here we will also follow the generalized version of the MV model defined in Eq. (4.6). Analogous to the target average, we define the following object to make the notation shorter

$$g \rho^{b_i}(\mathbf{k}_i - \mathbf{q}_i) \equiv \Omega_i \ , \tag{4.53}$$

thus we can write the $2n$-point function as

$$\begin{aligned} &g^{2n} \left\langle \rho^{b_1}(\mathbf{k}_1 - \mathbf{q}_1) \rho^{b_2 \dagger}(\mathbf{k}_1 - \mathbf{q}_2) \cdots \rho^{b_{2n-1}}(\mathbf{k}_n - \mathbf{q}_{2n-1}) \rho^{b_{2n} \dagger}(\mathbf{k}_n - \mathbf{q}_{2n}) \right\rangle_p \\ &\qquad = \left\langle \Omega_1 \Omega_2 \cdots \Omega_{2n-1} \Omega_{2n} \right\rangle_p . \end{aligned} \tag{4.54}$$

Here, as in Eq. (4.50), even indices correspond to complex conjugates.

By using the the Wick's theorem we can write again

$$\left\langle \Omega_1 \Omega_2 \cdots \Omega_{2n-1} \Omega_{2n} \right\rangle_p = \sum_{\omega \in \Pi(\chi)} \prod_{\{i,j\} \in \omega} \left\langle \Omega_i \Omega_j \right\rangle_p , \tag{4.55}$$

where the projectile 2-point function is given by

$$\left\langle \Omega_i \Omega_j \right\rangle_p = \frac{\delta^{b_i b_j}}{N_c^2 - 1} \mu_p^2 \left[\mathbf{k}_i - \mathbf{q}_i, (-1)^{i+j} (\mathbf{k}_j - \mathbf{q}_j) \right] . \tag{4.56}$$

We note that we have included a factor $1/(N_c^2 - 1)$ in order to normalize the single inclusive spectrum to one, however, this factor will not be relevant in our analysis since all correlation functions have to be normalized and the addition of any constant factor should not alter them.

Therefore, using the area enhancement argument for computing the target correlator and the MV model for computing the projectile one, we arrive at the following general result for the n-gluon spectrum:

$$2^n (2\pi)^{3n} \frac{d^n N}{\prod_{i=1}^n d^2\mathbf{k}_i} = \int \left(\prod_{i=1}^{2n} \frac{d^2\mathbf{q}_i}{(2\pi)^2} \right) \left(\sum_{\sigma \in \Pi(\chi)} \prod_{\{i,j\} \in \sigma} \left\langle \Omega_i \Omega_j \right\rangle_p \right) \left(\sum_{\omega \in \Pi(\chi)} \prod_{\{\alpha,\beta\} \in \omega} \left\langle \Lambda_\alpha \Lambda_\beta \right\rangle_T \right) , \tag{4.57}$$

that, together with Eqs. (4.52) and (4.56), provides the full expression that will be used along this chapter.

4.4.1 Wick diagrams

Since the expression of Eq. (4.57) involves the product of two Wick expansions, it includes the sum of $(2n-1)!!^2$ products of $2n$ 2-point functions. Thus, when $n > 2$ we will have to deal with a large number of terms and, for this reason, it is convenient to introduce a shorthand notation for each of these objects involved in the sum. For this reason, we introduce in this section a diagrammatic notation for each term inside the sum of Eq. (4.57) analogous to the diagrams introduced in [185] within the Glasma Graph approximation. In our case, the diagrams consist of two parts that are separated by a vertical dashed line. In both parts we draw 2 rows and n columns of dots where the dots of the upper row are labeled by odd numbers and the ones of the lower row are labeled by even numbers, and the labels are the same in both sides:

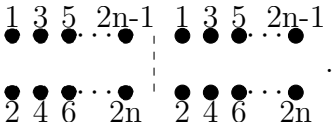

. (4.58)

Each column of both parts of the diagram corresponds to a produced gluon. The columns defined by (1,2) corresponds to gluon 1, the ones defined by (3,4) to gluon 2 and so on. The upper row (odd indices) will represent the real space and the lower row (even indices) will represent the conjugate space. As we have said, each term of the sum of Eq. (4.57) will have a product of n 2-point functions coming from the projectile average and n 2-point functions coming from the target average that are labeled by 2 indices that goes from 1 to $2n$. We will draw these 2-point functions as lines that connect the dots in the diagram. We choose the left part of the diagram to represent the 2-point correlators of the projectile and the right part to represent the 2-point correlators of the target and

schematically what we will draw is the following[1]:

$$\Big\langle \Omega_i \Omega_j \Big\rangle_p \Big\langle \Lambda_\alpha \Lambda_\beta \Big\rangle_T = \quad . \tag{4.59}$$

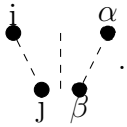

As an illustrative example let us select one of the $5!!^2 = 225$ terms that appear in Eq. (4.57) when $n = 3$:

$$\int \left(\prod_{i=1}^{6} \frac{d^2\mathbf{q}_i}{(2\pi)^2} \right) \Big\langle \Omega_1 \Omega_6 \Big\rangle_p \Big\langle \Omega_3 \Omega_4 \Big\rangle_p \Big\langle \Omega_2 \Omega_5 \Big\rangle_p \Big\langle \Lambda_1 \Lambda_5 \Big\rangle_T \Big\langle \Lambda_3 \Lambda_4 \Big\rangle_T \Big\langle \Lambda_2 \Lambda_6 \Big\rangle_T . \tag{4.60}$$

This term will be represented by the following diagram:

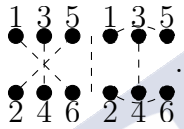

(4.61)

Note that the integration over the $\mathbf{q}'s$ is implicit.

If we want to write the diagram in an equation form we just have to use Eqs. (4.52) and (4.56). For example, the diagram in Eq. (4.61) reads (remember that we are labeling $\mathbf{k}_i$ with odd indices, and Eqs. (4.47) to (4.49))

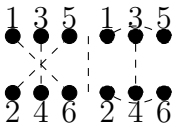

$$\begin{aligned}
&= \int \left(\prod_{i=1}^{6} \frac{d^2\mathbf{q}_i}{(2\pi)^2} \right) \frac{1}{(N_c^2-1)^6} \delta^{b_1 b_6} \delta^{b_2 b_5} \delta^{b_3 b_4} \mu_p^2[\mathbf{k}_1 - \mathbf{q}_1, -(\mathbf{k}_5 - \mathbf{q}_6)] \mu_p^2[\mathbf{k}_1 - \mathbf{q}_2, -(\mathbf{k}_5 - \mathbf{q}_5)] \\
&\times \mu_p^2[\mathbf{k}_3 - \mathbf{q}_3, -(\mathbf{k}_3 - \mathbf{q}_4)] \delta^{a_1 a_5} \delta^{b_1 b_5} \delta^{a_1 a_5} \delta^{b_2 b_6} \delta^{a_3 a_3} \delta^{b_3 b_4} 4^3 L^{i_1}(\mathbf{k}_1, \mathbf{q}_1) L^{i_1}(\mathbf{k}_1, \mathbf{q}_2) L^{i_5}(\mathbf{k}_5, \mathbf{q}_6) \\
&\times L^{i_5}(\mathbf{k}_5, \mathbf{q}_5) L^{i_3}(\mathbf{k}_3, \mathbf{q}_3) L^{i_3}(\mathbf{k}_3, \mathbf{q}_4) (2\pi)^6 \delta^{(2)}[\mathbf{q}_1 + \mathbf{q}_5] \delta^{(2)}[\mathbf{q}_2 + \mathbf{q}_6] \delta^{(2)}[\mathbf{q}_3 - \mathbf{q}_4] d(\mathbf{q}_1) d(\mathbf{q}_2) d(\mathbf{q}_3) \\
&= 4^3 \frac{1}{(N_c^2-1)^2} \int_{\mathbf{q}_1, \mathbf{q}_2, \mathbf{q}_3} d(\mathbf{q}_1) d(\mathbf{q}_2) d(\mathbf{q}_3) L^i(\mathbf{k}_1, \mathbf{q}_1) L^i(\mathbf{k}_1, \mathbf{q}_2) L^j(\mathbf{k}_3, \mathbf{q}_3) L^j(\mathbf{k}_3, \mathbf{q}_3) L^k(\mathbf{k}_5, -\mathbf{q}_1) \\
&\times L^k(\mathbf{k}_5, -\mathbf{q}_2) \mu_p^2[\mathbf{k}_1 - \mathbf{q}_1, -(\mathbf{k}_5 + \mathbf{q}_2)] \mu_p^2[\mathbf{k}_1 - \mathbf{q}_2, -(\mathbf{k}_5 + \mathbf{q}_1)] \mu_p^2[\mathbf{k}_3 - \mathbf{q}_3, -(\mathbf{k}_3 - \mathbf{q}_3)].
\end{aligned} \tag{4.62}$$

Besides making the notation more compact we can also exploit the structure of the diagrams in order to find symmetries between them, the associated power in $(N_c^2 - 1)$ for each diagram and which kind of quantum correlations (Bose enhancement or HBT) it includes, by making use of the following properties:

i) *Interchanging two dots within a column, $2m \leftrightarrow 2m-1$, of a given diagram is equivalent to make the change of variables $\boldsymbol{k}_{2m-1} \to -\boldsymbol{k}_{2m-1}$.*

[1] This diagrammatic approach is also very similar to the notation used in [170] where they wrote the terms of the Wick expansion of the target as $[i_1, i_2][i_3, i_4] \cdots [i_{2n-1}, i_{2n}]$, being the indices inside the brackets the ones that define the 2-point functions in the expansion. For the projectile they used the same notation changing the brackets by curly brackets.

For example,

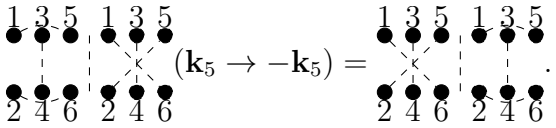

(4.63)

In order to prove this property it is enough to evaluate

$$\Big\langle \Omega_{2m}\Omega_i \Big\rangle_p \Big\langle \Omega_{2m-1}\Omega_j \Big\rangle_p \Big\langle \Lambda_{2m}\Lambda_\gamma \Big\rangle_T \Big\langle \Lambda_{2m-1}\Lambda_\beta \Big\rangle_T, \tag{4.64}$$

being i, j, γ and β arbitrary indices, since it is the only piece of Eq. (4.57) that depends on the dots $2m$ and $2m-1$. This expression can be computed using Eqs. (4.52) and (4.56). Then, if one makes the change of variables with unit Jacobian $\mathbf{q}_{2m} \to -\mathbf{q}_{2m-1}$ and $\mathbf{q}_{2m-1} \to -\mathbf{q}_{2m}$ and uses the fact that $L^\lambda(\mathbf{k}, -\mathbf{q}) = -L^\lambda(-\mathbf{k}, \mathbf{q})$ and $\mu^2(-\mathbf{k}, -\mathbf{q}) = \mu^2(\mathbf{k}, \mathbf{q})$, we see that

$$\begin{aligned}
&\Big\langle \Omega_{2m}\Omega_i \Big\rangle_p \Big\langle \Omega_{2m-1}\Omega_j \Big\rangle_p \Big\langle \Lambda_{2m}\Lambda_\gamma \Big\rangle_T \Big\langle \Lambda_{2m-1}\Lambda_\beta \Big\rangle_T \\
=&\Big\langle \Omega_{2m-1}\Omega_i \Big\rangle_p \Big\langle \Omega_{2m}\Omega_j \Big\rangle_p \Big\langle \Lambda_{2m-1}\Lambda_\gamma \Big\rangle_T \Big\langle \Lambda_{2m}\Lambda_\beta \Big\rangle_T (\mathbf{k}_{2m-1} \to -\mathbf{k}_{2m-1}).
\end{aligned} \tag{4.65}$$

ii) *Interchanging two columns* $(2m, 2m-1)$ *and* $(2k, 2k-1)$ *of a given diagram is equivalent to make the change of variables* $\boldsymbol{k}_{2m-1} \leftrightarrow \boldsymbol{k}_{2k-1}$.

For example,

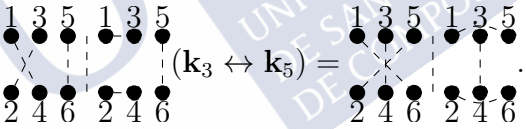

(4.66)

The proof of this property is trivial since, by definition, each column of dots corresponds to a momentum $\mathbf{k}_i$ and, therefore, interchanging two columns in both sides is equivalent to interchange the label of two momenta.

iii) We can extract the powers of $(N_c^2 - 1)$ by looking at the structure of each side of the diagram. Before making a statement of the property we will start by using Eq. (4.61) as an illustrative example. Using Eqs. (4.52) and (4.56) we can extract the counting in powers of $(N_c^2-1)^{-1}$ of this diagram by writing the Kronecker deltas

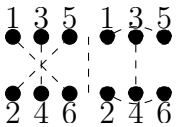

$$\propto \frac{1}{(N_c^2-1)^6} \delta^{a_1 a_5}\delta^{a_3 a_4}\delta^{a_2 a_6} \times \delta^{a_1 a_2}\delta^{a_3 a_4}\delta^{a_5 a_6} \times \delta^{b_1 b_5}\delta^{b_3 b_4}\delta^{b_2 b_6} \times \delta^{b_1 b_6}\delta^{b_2 b_5}\delta^{b_3 b_4}, \tag{4.67}$$

where the second group of deltas of the first line is introduced to preserve Eq. (4.49), that is, that the color of the produced gluons is the same in the real and the conjugate spaces. The first group of deltas of both lines accounts to the target configuration (right side of the diagram) and the last group of deltas accounts to the projectile

configuration. If we organize this equation in such a way that all the indices in the deltas are closed we have that

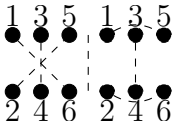

$$\propto \frac{1}{(N_c^2-1)^6}\left(\delta^{a_5a_1}\delta^{a_1a_2}\delta^{a_2a_6}\delta^{a_6a_5}\right)\times\left(\delta^{a_4a_3}\delta^{a_3a_4}\right)$$
$$\times\left(\delta^{b_5b_1}\delta^{b_1b_6}\delta^{b_6b_2}\delta^{b_2b_5}\right)\times\left(\delta^{b_4b_3}\delta^{b_3b_4}\right)$$
$$=\frac{(N_c^2-1)^2(N_c^2-1)^2}{(N_c^2-1)^6}=(N_c^2-1)^{-2}, \tag{4.68}$$

where we have written the deltas that come from the target side of the diagram in a different color by convenience. We can do the same procedure that we did in the last equation in a diagrammatic and faster way by just drawing the target (right) side of the diagram on top of the left side and counting the number of closed lines that we obtain (which is equivalent to the second line of Eq. (4.68)) and drawing vertical lines in the right side of the diagram and counting the number of closed lines that we obtain (which is equivalent to the first line of Eq. (4.68)),

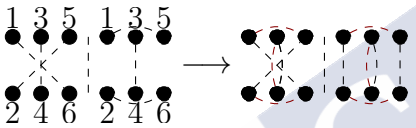

$$\longrightarrow \frac{(N_c^2-1)^2(N_c^2-1)^2}{(N_c^2-1)^6}=(N_c^2-1)^{-2}, \tag{4.69}$$

where we can identify the red lines in the second diagram as the red Kronecker deltas of Eq. (4.68). In general, *if we call n_p the number of closed lines that we obtain by projecting the right side of the diagram on top of the left side and n_T the number of closed lines that we obtain by projecting vertical lines on top of the right side of the diagrams the counting in powers of (N_c^2-1) of a given diagram for general n is*

$$\frac{(N_c^2-1)^{n_p}(N_c^2-1)^{n_T}}{(N_c^2-1)^{2n}}=(N_c^2-1)^{n_p+n_T-2n}. \tag{4.70}$$

As we will see through this work, this property is useful for organising the terms of Eq. (4.57) in powers of $(N_c^2-1)^{-1}$ in a systematic way, especially when n is large.

iv) The types of quantum correlation that we have in a given diagram can be obtained as follows. *If the same two dots are linked in both sides of the diagram we have two possibilities: if the dots belong to the same column labelled by $(2k, 2k-1)$ it means that the gluon k is uncorrelated (disconnected piece) and if the dots belong to different columns it means that the gluons that define these columns have an HBT correlation. By exclusion, all the gluons involved in other kind of links have a Bose enhancement correlation either in the projectile or in the target wave function.*

For example,

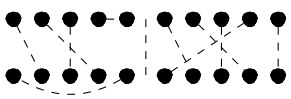

(4.71)

in this diagram the 3^{rd} produced gluon is uncorrelated, gluons 1-2 and 2-4 have an HBT correlation and gluons 1-4-5 have a Bose enhancement correlation.

In order to check this property it is enough to evaluate the terms in Eq. (4.57) that contain the same links in both the projectile and target sides. That is, we are interested in terms that contain

$$\left\langle \Omega_a \Omega_b \right\rangle_p \left\langle \Lambda_a \Lambda_b \right\rangle_T, \tag{4.72}$$

where $a, b = 1, ..., 2n$ are generic dots. The objects of Eq. (4.52) and Eq. (4.56) that contain the information of the quantum interference correlations are the Dirac deltas and the functions $\mu_p^2(\mathbf{k}, \mathbf{q})$ respectively (the Lipatov vertices and the dipole functions give a different kind of correlation). Thus, we can write

$$\begin{aligned}\left\langle \Omega_a \Omega_b \right\rangle_p \left\langle \Lambda_a \Lambda_b \right\rangle_T &\propto \mu_p^2 \left[\mathbf{k}_a - \mathbf{q}_a, (-1)^{a+b}(\mathbf{k}_b - \mathbf{q}_b)\right] \delta^{(2)} \left[\mathbf{q}_a + (-1)^{a+b}\mathbf{q}_b\right] \\ &= \mu_p^2 \left[\mathbf{k}_a - \mathbf{q}_a, (-1)^{a+b}\mathbf{k}_b + \mathbf{q}_a\right] \delta^{(2)} \left[\mathbf{q}_a + (-1)^{a+b}\mathbf{q}_b\right]. \end{aligned} \tag{4.73}$$

Since $\mu_p^2(\mathbf{k}, \mathbf{q})$ is peaked around $\mathbf{k} = -\mathbf{q}$ this implies that we have a peak around $\mathbf{k}_a = -(-1)^{a+b}\mathbf{k}_b$ which is an HBT correlation. In the case in which a and b belong to the same column, that is, $a = 2k - 1$ and $b = 2k$ (or vice-versa), it is clear that we loose the correlation in function μ_p^2 – in fact we loose any kind of correlation since in this case the Lipatov vertices and the dipole function can be factorized.

4.5 Numerical Analysis

In this section we present the calculation of Eq. (4.57) for $n = 2$, 3 and 4. Larger values of n can be also considered in the same fashion, contingent upon sufficient computation power. In order to compute Eq. (4.57) we will use Eqs. (4.52) and (4.56) and for the functions $\mu_p^2(\mathbf{k}, \mathbf{q})$ and $d(\mathbf{q})$ we will use Eq. (4.6) and Eq. (4.42) respectively. In the case of $\mu_p^2(\mathbf{k}, \mathbf{q})$ we will not have into account the factor $\tilde{\mu}^2 \pi B_p$ in order to normalize the integrated single gluon spectrum to one, however, as stated above, this will not change the analysis on the multi-particle cumulants.

On the other hand, we should account for the infrared divergences of the Lipatov vertices. The product of two Lipatov vertices is

$$L^i(\mathbf{k}, \mathbf{q}_1) L^i(\mathbf{k}, \mathbf{q}_2) = \left[\frac{\mathbf{k}^i}{\mathbf{k}^2} - \frac{(\mathbf{k} - \mathbf{q}_1)^i}{(\mathbf{k} - \mathbf{q}_1)^2}\right] \left[\frac{\mathbf{k}^i}{\mathbf{k}^2} - \frac{(\mathbf{k} - \mathbf{q}_2)^i}{(\mathbf{k} - \mathbf{q}_2)^2}\right]. \tag{4.74}$$

Usually these divergences are regulated by introducing an infrared cutoff in the momenta integrations. However, in order to mimic the Wigner function parameterization introduced in Section 2.4 through Eq. (2.92), in this work we use the following parameterization for the product of two Lipatov vertices:

$$L^i(\mathbf{k}, \mathbf{q}_1) L^i(\mathbf{k}, \mathbf{q}_2) = \frac{(2\pi)^2}{\xi^2} \exp\left\{-\frac{[\mathbf{k} - (\mathbf{q}_1 + \mathbf{q}_2)/2]^2}{\xi^2}\right\}, \tag{4.75}$$

where ξ^2 is a parameter with dimensions of momentum squared. This choice, although it does not maintain some important properties of the Lipatov vertices and should not be reliable for phenomenological studies, is much simpler to deal with and is equivalent to

using the Wigner function approach but including quantum correlations in the projectile wave function as discussed in Section 2.4. We will therefore assume that this ansatz is good enough for performing qualitative analysis on multi-particle correlations although we are aware that for a more realistic approach we have to take into account Eq. (4.74) instead of Eq. (4.75).

Thus, taking the Gaussian ansatz of Eq. (4.75) is equivalent in the case of 2-particle correlations, for example, to use the following Wigner distribution

$$\begin{aligned} W^{b_1b_2b_3b_4}(\mathbf{b}_1,\mathbf{p}_1,\mathbf{b}_2,\mathbf{p}_2) = \frac{1}{(N_c^2-1)^2}\frac{1}{\pi^4\xi^4 B_p^2} e^{-(\mathbf{p}_1^2+\mathbf{p}_2^2)/\xi^2} e^{-(\mathbf{b}_1^2+\mathbf{b}_2^2)/B_p} \Big[\delta^{b_1b_2}\delta^{b_3b_4} \\ + \delta^{b_1b_3}\delta^{b_2b_4} 2\pi B_p \delta^{(2)}(\mathbf{b}_1-\mathbf{b}_2) e^{-(\mathbf{p}_1+\mathbf{p}_2)^2/(2B_p^{-1})} \\ + \delta^{b_1b_4}\delta^{b_2b_3} 2\pi B_p \delta^{(2)}(\mathbf{b}_1-\mathbf{b}_2) e^{-(\mathbf{p}_1-\mathbf{p}_2)^2/(2B_p^{-1})}\Big], \end{aligned} \tag{4.76}$$

which obviously breaks the factorization assumption Eq. (2.94) used in literature.

We note that the main problem of Eq. (4.75) is that it only depends on the momentum of the parent parton, $\mathbf{k}_i - \mathbf{q}_i$, and not on the final momentum, $\mathbf{k}_i$. Therefore, Eq. (4.75) only includes the contribution in which the gluon is emitted from the source and then interacts with the target, thus missing part of the physics. The final momentum is acquired by the interaction with the target which is suitable for the projectile collinear limit. In principle, in this limit the hybrid factorization is employed and it corresponds to forward production of partons near the proton fragmentation region [92]. The approach that we adopt in this section is suitable for central production even though the approximation used for the Lipatov vertices in Eq. (4.75) is more appropriate for considering the forward limit. Therefore, admittedly the validity of our approach is reduced to the forward region but not yet near the proton fragmentation one. In this region, the projectile partons are defined in terms of Wigner functions (see [102–106]). However, we would like to emphasize that the Wigner functions adopted in these references are factorized for two partons and do not include quantum correlations in the projectile. The two parton joint Wigner function (given in Eq. (4.76)) that we use in our approach indeed encodes the correlations in the projectile which is one of the novelties of the present thesis[2]. Moreover, adopting Eq. (4.75) for the Lipatov vertices and Eq. (4.76) for the joint Wigner function to describe the projectile partons, allows us to perform the computation analytically until the very end, even though they restrict the validity region of our results. In our approach, one can generalize the computation to the production of any number of particles and can perform the study analytically within its limits of the validity. Other approaches that are strictly valid for central production, such as the study performed in [167] or the one in [105], rely on final numerical integrations which would be extremely difficult in the case of four particle correlations, or the computation is performed numerically from the very beginning making it difficult to control, respectively. Finally, due to the assumed Gaussian forms, our final expressions cannot be considered reliable for transverse momenta sizable larger than the saturation scale.

[2]Quantum correlations in the projectile have been taken into account in [169, 170] but not for more than two partons.

4.5.1 Double inclusive gluon production

The case $n = 2$ of Eq. (4.57), that is, the spectrum for double inclusive gluon production is the most studied case. It has been described using the exact solution for the dipole correlators in the MV model [103, 106], in the Glasma Graph approximation [107] and using the Area Enhancement model [40, 186]. The result that we present in this section is the same obtained in [40] and that we have seen at the beginning of this chapter but now, with the help of Eq. (4.75), we are able to obtain a closed-form solution for both the multiplicity and the azimuthal harmonics.

In this case, the expansion of Eq. (4.57) in terms of the Wick diagrams is

$$\frac{d^2N}{d^2\mathbf{k}_1 d^2\mathbf{k}_3} =$$

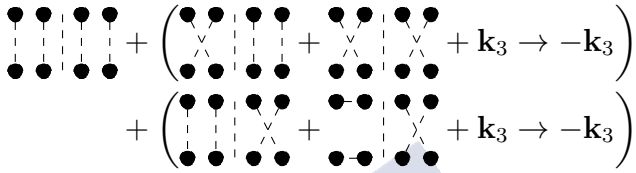

$$+ \mathbf{k}_3 \to -\mathbf{k}_3 \Big) + \Big($$

$$+ \mathbf{k}_3 \to -\mathbf{k}_3 \Big), \tag{4.77}$$

where we have grouped the 9 diagrams by their powers in $(N_c^2 - 1)^{-1}$.

The Wick diagrams of Eq. (4.77) can be computed using Eqs. (4.6), (4.42), (4.52), (4.56) and (4.75) in a straightforward way since all the arguments of the $\mathbf{q}_i$ integrals are Gaussian functions and, therefore, they can be trivially solved. The result is

$$= \frac{1}{\pi^2(\xi^2 + Q_s^2)^2} \exp\left\{-\frac{\mathbf{k}_1^2 + \mathbf{k}_3^2}{\xi^2 + Q_s^2}\right\}, \tag{4.78}$$

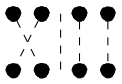

$$= \frac{1}{(N_c^2 - 1)} \frac{1}{\pi^2(\xi^2 + Q_s^2)[Q_s^2 + \xi^2(1 + B_p Q_s^2)]} \times \exp\left\{-\frac{2\xi^2 B_p(\mathbf{k}_1 + \mathbf{k}_3)^2 + [Q_s^2 + \xi^2(1 + B_p Q_s^2)](\mathbf{k}_1^2 + \mathbf{k}_3^2)}{(\xi^2 + Q_s^2)[Q_s^2 + \xi^2(1 + B_p Q_s^2)]}\right\}, \tag{4.79}$$

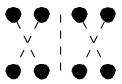

$$= \frac{1}{(N_c^2 - 1)} \frac{1}{\pi^2\xi^2(\xi^2 + Q_s^2)} \times \exp\left\{-\frac{2\xi^2(\mathbf{k}_1^2 + \mathbf{k}_3^2) + (B_p Q_s^2 \xi^2 + B_p \xi^4 + Q_s^2)(\mathbf{k}_1 + \mathbf{k}_3)^2}{2\xi^2(\xi^2 + Q_s^2)}\right\}, \tag{4.80}$$

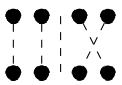

$$= \frac{1}{(N_c^2 - 1)^2} \frac{1}{\xi^2\pi^2(\xi^2 + Q_s^2)(1 + B_p Q_s^2)} \times \exp\left\{-\frac{2\xi^2(\mathbf{k}_1^2 + \mathbf{k}_3^2) + Q_s^2(\mathbf{k}_1 + \mathbf{k}_3)^2}{2\xi^2(\xi^2 + Q_s^2)}\right\}, \tag{4.81}$$

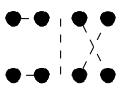

$$= \frac{1}{(N_c^2 - 1)^2} \frac{1}{\pi^2\xi^2[Q_s^2 + \xi^2(1 + B_p Q_s^2)]} \times \exp\left\{-\frac{B_p\xi^4(\mathbf{k}_1 - \mathbf{k}_3)^2 + (Q_s^2 + B_p Q_s^2\xi^2)(\mathbf{k}_1 + \mathbf{k}_3)^2 + 2\xi^2(\mathbf{k}_1^2 + \mathbf{k}_3^2)}{2\xi^2[Q_s^2 + \xi^2(1 + B_p Q_s^2)]}\right\}. \tag{4.82}$$

With these 5 equations we have determined the differential multiplicity in Eq. (4.77). In order to obtain the value of the integrated spectrum we just have to perform again Gaussian integrations over $\mathbf{k}_i$ obtaining

$$N = \kappa_0\{2\} = 1 + \frac{2}{N_c^2 - 1}\left[\frac{2}{1 + B_p\xi^2}\right] + \frac{2}{(N_c^2 - 1)^2}\left[\frac{1}{1 + B_p Q_s^2} + \frac{1}{1 + B_p\xi^2}\right]. \tag{4.83}$$

We can see from this equation that, apart from the suppression in powers of $(N_c^2-1)^{-1}$, the correlated terms contain suppression factors $(1+B_pQ_s^2)^{-1}$ and $(1+B_p\xi^2)^{-1}$. Following the domain picture that we have discussed in Section 3.3, $B_pQ_s^2 \equiv n_D$ is the number of chromo-electric domains in the overlap area of the projectile with the target in the transverse plane. We should expect decorrelation of the produced gluons in the limit of $n_D \to \infty$ since the probability of two gluons scattering off the same domain vanishes in this limit. Therefore, to fix ξ^2 it makes sense to choose a value that is proportional to Q_s^2 in order to preserve decorrelation in the limit $n_D \to \infty$. For this reason we will choose $\xi^2 = \alpha Q_s^2$, being α a real number, in the rest of this work[3].

The 2-particle azimuthal harmonics, defined in Eq. (3.30), can be obtained by performing the integration over $\mathbf{k}_i$ with the help of Eq. (B.12). The result for the second order κ-function is

$$\begin{aligned}
\kappa_{2n}\{2\} =& \frac{8\Gamma(n+1)^2}{\Gamma(2n+1)}\Bigg\{\frac{\alpha(1+\alpha)}{N_c^2-1}\Bigg[\frac{(1+\alpha+\alpha n_D)}{\alpha^4 n_D^2}\left(\frac{\alpha^2 n_D}{2+\alpha^2 n_D+2\alpha(1+n_D)}\right)^{2(n+1)} \\
&\times {}_2F_1\left(n+1,n+1;2n+1;\left(\frac{\alpha^2 n_D}{2+\alpha^2 n_D+2\alpha(1+n_D)}\right)^2\right) \\
&+\frac{1}{(1+\alpha^2 n_D+\alpha(2+n_D))^2}\left(\frac{1+\alpha n_D+\alpha^2 n_D}{1+\alpha^2 n_D+\alpha(2+n_D)}\right)^{2n} \\
&\times {}_2F_1\left(n+1,n+1;2n+1;\left(\frac{1+\alpha n_D+\alpha^2 n_D}{1+\alpha^2 n_D+\alpha(2+n_D)}\right)^2\right)\Bigg] \\
&+\frac{1}{(N_c^2-1)^2}\Bigg[\frac{\alpha(1+\alpha+\alpha n_D)}{(1+\alpha^2 n_D+\alpha(2+n_D))^2}\left(\frac{1+\alpha n_D-\alpha^2 n_D}{1+\alpha^2 n_D+\alpha(2+n_D)}\right)^{2n} \\
&\times {}_2F_1\left(n+1,n+1;2n+1;\left(\frac{1+\alpha n_D-\alpha^2 n_D}{1+\alpha^2 n_D+\alpha(2+n_D)}\right)^2\right) \\
&\times +\frac{\alpha(1+\alpha)}{1+n_D}(1+2\alpha)^{-2(n+1)}\,{}_2F_1\left(n+1,n+1;2n+1;\frac{1}{(1+2\alpha)^2}\right)\Bigg]\Bigg\}, \quad (4.84)
\end{aligned}$$

where we have defined $\alpha = \xi^2/Q_s^2$, we have taken $n > 0$ and due to the symmetry $\mathbf{k}_3 \to -\mathbf{k}_3$ of Eq. (4.77) all odd harmonics vanish. Using Eqs. (4.83) and (4.84) we can evaluate the 2-particle azimuthal harmonics as

$$v_{2n}\{2\} = \sqrt{\frac{\kappa_{2n}\{2\}}{\kappa_0\{2\}}}. \quad (4.85)$$

In Fig. 4.5 we plot the dependence of $v_{2n}\{2\}$ with respect to n_D and α by fixing $N_c = 3$. The value of the even azimuthal harmonics grows rapidly as both n_D and α approach zero and it decreases slowly when these parameters are large. This decrease with n_D is

[3]Since ξ^2 is a momentum scale of the projectile wave function it should be related with B_p^{-1} and not with Q_s^2 which is a momentum scale of the target wave function. However, the choice $\xi^2 = Q_s^2$ is the one that has given more consistent phenomenological results and for this reason we use it through all this work. In [102, 103] and [106] the choices $\xi^2 = B_p^{-1}$ and $\xi = Q_s/4$ have been made, respectively, and the sensitivity of the results to variations of these choices has been examined.

what we should expect in the color domain picture of particle correlation since as n_D gets larger the probability of two gluons scattering in the same domain is smaller and thus the overall correlation. On the other hand, the decrease with α must be taken with care because α gives the ratio between the momentum transfers from projectile and target. The dilute-dense approximation that we are using makes sense only for α sizable smaller than 1.

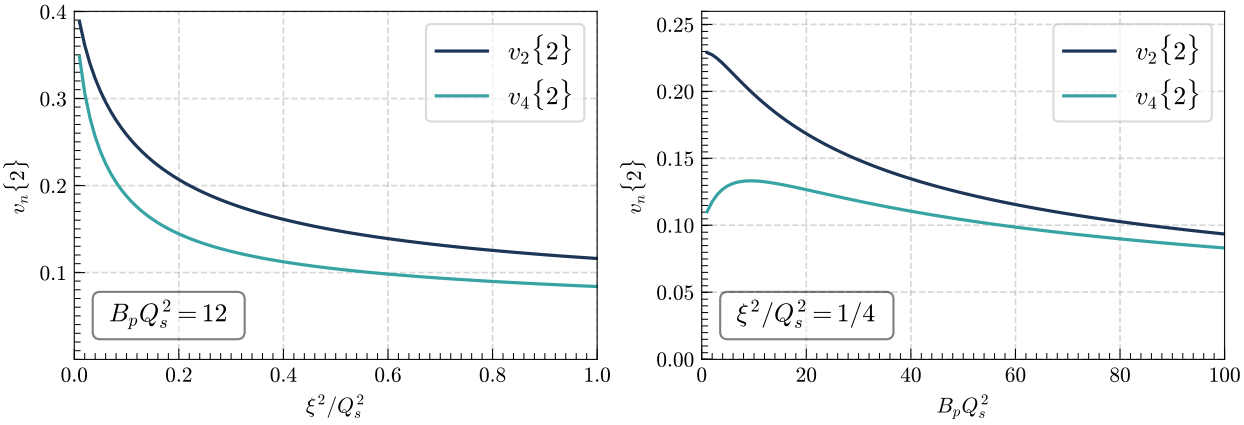

Figure 4.5.
Dependence of the even 2-particle azimuthal harmonics, $v_{2n}\{2\}$, on $\alpha \equiv \xi^2/Q_s^2$ (left, for $B_pQ_s^2 = 12$) and $n_D \equiv B_pQ_s^2$ (right, for $\xi^2/Q_s^2 = 1/4$).

As we have seen in Section 3.4, we can also compute the azimuthal harmonics as a function of transverse momentum by using the differential κ-function defined in Eq. (3.39). The $\mathbf{k}_i$ integral can be solved with the help of Eq. (B.11) and the result is

$$\tilde{\kappa}_0\{2\}(p_\perp) = \frac{e^{-\frac{p_\perp^2}{\alpha Q_s^2}}}{Q_s^2}\left\{\frac{2e^{\frac{p_\perp^2}{\alpha(1+\alpha)Q_s^2}}}{1+\alpha} + \frac{8}{N_c^2-1}\left[\frac{e^{\frac{(1+\alpha n_D-\alpha^2 n_D)p_\perp^2}{\alpha[1+\alpha^2 n_D+\alpha(2+n_D)]Q_s^2}}}{1+\alpha^2 n_D+\alpha(2+n_D)} + \frac{e^{\frac{(2+2\alpha n_D-\alpha^2 n_D)p_\perp^2}{\alpha[2+\alpha^2 n_D+2\alpha(1+n_D)]Q_s^2}}}{2+\alpha^2 n_D+2\alpha(1+n_D)}\right]\right.$$
$$\left. + \frac{8}{(N_c^2-1)^2}\left[\frac{e^{\frac{p_\perp^2}{\alpha(1+2\alpha)Q_s^2}}}{(1+2\alpha)(1+n_D)} + \frac{e^{\frac{(1+\alpha n_D-\alpha^2 n_D)p_\perp^2}{\alpha[1+\alpha^2 n_D+\alpha(2+n_D)]Q_s^2}}}{1+\alpha^2 n_D+\alpha(2+n_D)}\right]\right\}, \tag{4.86}$$

and

$$\tilde{\kappa}_{2n}\{2\}(p_\perp) = \frac{8\Gamma(1+n)}{Q_s^2\Gamma(1+2n)}\left(\frac{p_\perp^2}{2Q_s^2}\right)^n e^{-\frac{p_\perp^2}{\alpha Q_s^2}}$$
$$\times\left\{\frac{1}{N_c^2-1}\left[\frac{e^{-\frac{(-1+\alpha n_D+\alpha^2 n_D)p_\perp^2}{2\alpha(1+\alpha)Q_s^2}}}{1+\alpha^2 n_D+\alpha(2+n_D)}\left(\frac{(1+\alpha n_D+\alpha^2 n_D)^2}{\alpha(1+\alpha)(1+\alpha^2 n_D+\alpha(2+n_D))}\right)^n\right.\right.$$
$$\left.\times\ {}_1F_1\left(n+1;2n+1;\frac{(1+\alpha n_D+\alpha^2 n_D)^2 p_\perp^2}{2\alpha(1+\alpha)[1+\alpha^2 n_D+\alpha(2+n_D)]Q_s^2}\right)\right.$$
$$\left.+\frac{e^{-\frac{[-2+\alpha^3 n_D-2\alpha(1+n_D)]p_\perp^2}{2\alpha(1+\alpha)(1+\alpha+\alpha n_D)Q_s^2}}}{2+\alpha^2 n_D+2\alpha(1+n_D)}\left(\frac{\alpha^4 n_D^2}{(1+\alpha)(1+\alpha+\alpha n_D)[2+\alpha^2 n_D+2\alpha(1+n_D)]}\right)^n\right.$$

$$\times\ {}_1F_1\left(n+1;2n+1;\frac{\alpha^4 n_D^2 p_\perp^2}{2(1+\alpha)(1+\alpha+\alpha n_D)[2+\alpha^2 n_D+2\alpha(1+n_D)]Q_s^2}\right)\Bigg]$$
$$+\frac{1}{(N_c^2-1)^2}\Bigg[\frac{e^{-\frac{(-1-\alpha n_D+\alpha^2 n_D)p_\perp^2}{2\alpha(1+\alpha+\alpha n_D)Q_s^2}}}{1+\alpha^2 n_D+\alpha(2+n_D)}\left(\frac{(1+\alpha n_D-\alpha^2 n_D)^2}{\alpha(1+\alpha+\alpha n_D)(1+\alpha^2 n_D+\alpha(2+n_D))}\right)^n$$
$$\times\ {}_1F_1\left(n+1;2n+1;\frac{(1+\alpha n_D-\alpha^2 n_D)^2 p_\perp^2}{2\alpha(1+\alpha+\alpha n_D)(1+\alpha^2 n_D+\alpha(2+n_D))Q_s^2}\right)$$
$$+\frac{e^{-\frac{p_\perp^2}{2\alpha(1+\alpha)Q_s^2}}}{(1+2\alpha)(1+n_D)}\left(\frac{1}{\alpha(1+\alpha)(1+2\alpha)}\right)^n {}_1F_1\left(n+1;2n+1;\frac{p_\perp^2}{2\alpha(1+\alpha)(1+2\alpha)Q_s^2}\right)\Bigg]\Bigg\}, \tag{4.87}$$

where $n>0$. The fact that $\tilde{\kappa}_{2n}(p_\perp)$ is proportional to $(p_\perp^2/Q_s^2)^n$ was also obtained in [106] although there a different model for the target average was employed. The differential 2-particle even azimuthal harmonics can be obtained by evaluating

$$v_{2n}\{2\}(p_\perp)=\sqrt{\frac{\tilde{\kappa}_{2n}\{2\}(p_\perp)}{\tilde{\kappa}_0\{2\}(p_\perp)}} \tag{4.88}$$

and the result is plotted in Fig. 4.6 for $n=1,2,3$ and $B_p=6$ GeV^{-2}, $\xi=Q_s/2$, $Q_s^2=2$ GeV^2 and $N_c=3$. Although we do not aim for a comparison with experimental data, the obtained values are in the ballpark of them. Note that due to the Gaussian forms that we employ, our results cannot be considered reliable for $p_\perp$ sizable larger than Q_s.

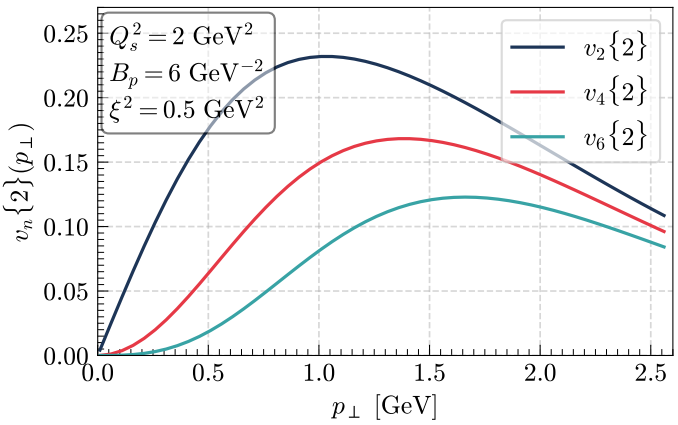

Figure 4.6.
Dependence of the differential 2-particle even azimuthal harmonics, $v_{2n}\{2\}$, on transverse momentum $p_\perp$. In this graph we have used $B_p=6$ GeV^{-2}, $\xi=Q_s/2$, $Q_s^2=2$ GeV^2 and $N_c=3$.

4.5.2 Triple inclusive gluon production

In this section we show the result for Eq. (4.57) when $n=3$, that is, the triple inclusive gluon spectrum. Since in this work we are mainly interested in computing azimuthal harmonics we will just show the expansion of the spectrum in terms of the Wick diagrams.

However, it has be shown recently [167] that this result is useful for studying the correlation between the 2-particle azimuthal harmonics and multiplicity and average transverse momentum.

As we did for $n = 2$, we can group the Wick diagrams in the expression for the $n = 3$ gluon spectrum in powers of $(N_c^2 - 1)^{-1}$ as

$$8(2\pi)^9 \frac{d^3N}{d^2\mathbf{k}_1 d^2\mathbf{k}_3 d^2\mathbf{k}_5} = N_3^{(0)} + N_3^{(1)} + N_3^{(2)} + N_3^{(3)} + N_3^{(4)}. \tag{4.89}$$

In order to obtain each one of these terms we have to use the property iii) of Section 4.4.1. In this case the suppression of each diagram is given by $(N_c^2 - 1)^{n_p+n_T-6}$ and we can have three kind of configurations on each side of the diagram

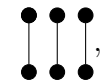
, (4.90)

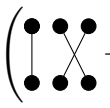
$+ \mathbf{k}_5 \to -\mathbf{k}_5 \Big) + \mathbf{k}_1 \leftrightarrow \mathbf{k}_3 + \mathbf{k}_1 \leftrightarrow \mathbf{k}_5,$ (4.91)

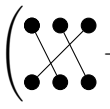
$+ \mathbf{k}_1 \to -\mathbf{k}_1 + \mathbf{k}_3 \to -\mathbf{k}_3 + \mathbf{k}_5 \to -\mathbf{k}_5 \Big) + \mathbf{k}_1 \leftrightarrow \mathbf{k}_5.$ (4.92)

It is easy to see that the only way of obtaining $n_T = 3$,2 and 1 is having the first, second and third configuration on the right side of the diagram, Eqs. (4.90) to (4.92) respectively. On the other hand, the only way of obtaining $n_p = 3$, 2 and 1 is having the same configuration on the left side of the diagram as the one on the right side, a configuration on the left side that has one link equal to the configuration on the right side and the other 2 links different, and a configuration on the left side that has all the links different than the configuration on the right side, respectively. One can also check that for a given configuration on the right side of the diagram the number of possibilities for $n_p = 3$ is 1, for $n_p = 2$ is 6 and for $n_p = 1$ is 8.

With this taken into account, let us show as an example how to find all the Wick diagrams suppressed by $(N_c^2-1)^{-2}$. In this case $n_p+n_T = 4$. There are three possibilities:

i) $n_p = 1$ and $n_T = 3$.

This implies that we have to have the configuration of Eq. (4.90) on the right side and configurations on the left side that has all the links different than the one on the right side. As we have said, there are 8 possibilities for this case:

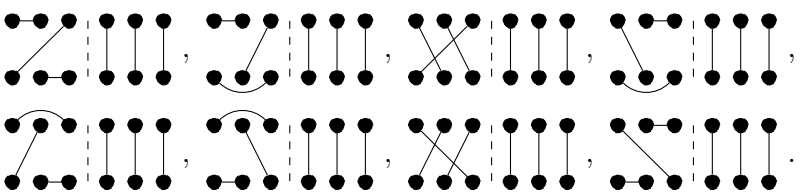

ii) $n_p = 2$ and $n_T = 2$.

This implies that we have to have the configuration of Eq. (4.91) on the right side of the diagram and configurations on the left side that have one link in common with

the right side and the other ones different. There are 6×6 possibilities in this case:

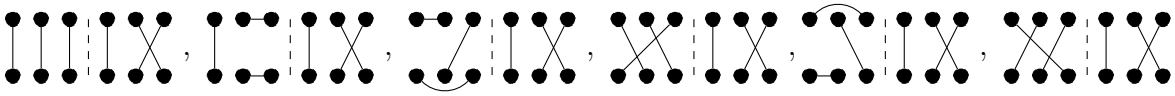

and the 5 permutations of Eq. (4.91) for each diagram.

iii) $n_p = 3$ and $n_T = 1$.

This implies that we have to have the configuration of Eq. (4.92) on the right side of the diagram and configurations on the left side that have all the links in common with the right side. There are 1×8 possibilities in this case:

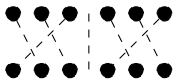

and the 7 permutations of Eq. (4.92).

All in all, we can write all the 52 Wick diagrams that have a suppression of $(N_c^2-1)^{-2}$ as

$$N_3^{(2)} =$$

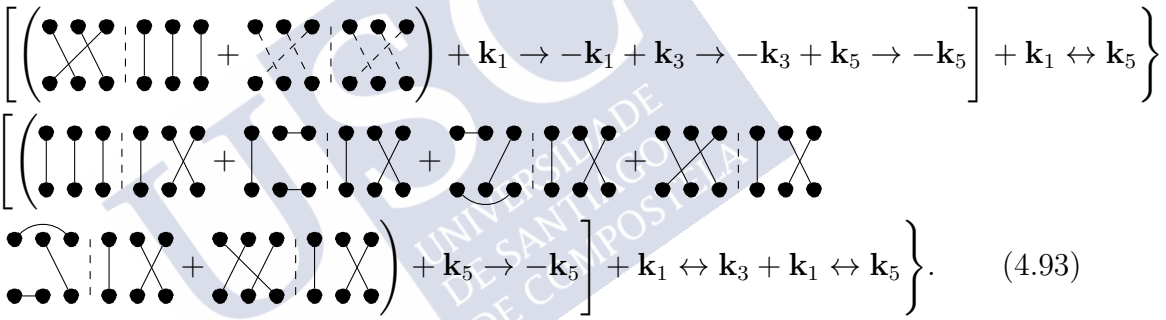

$$+ \mathbf{k}_1 \to -\mathbf{k}_1 + \mathbf{k}_3 \to -\mathbf{k}_3 + \mathbf{k}_5 \to -\mathbf{k}_5 \Big] + \mathbf{k}_1 \leftrightarrow \mathbf{k}_5 \Big\}$$

$$+ \Big\{ \Big[\Big($$

$$+ \mathbf{k}_5 \to -\mathbf{k}_5 \Big] + \mathbf{k}_1 \leftrightarrow \mathbf{k}_3 + \mathbf{k}_1 \leftrightarrow \mathbf{k}_5 \Big\}. \tag{4.93}$$

This procedure, although tedious, is straightforward to implement on a computer. Repeating it we find that there is 1 diagram suppressed by $(N_c^2-1)^0$:

$$N_3^{(0)} =$$

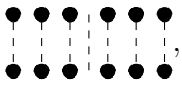

, (4.94)

12 diagrams suppressed by $(N_c^2-1)^{-1}$:

$$N_3^{(1)} =$$

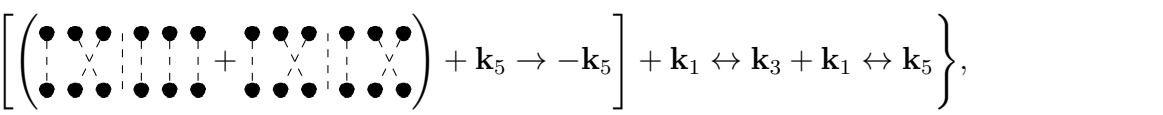

(4.95)

96 diagrams suppressed by $(N_c^2-1)^{-3}$:

$$N_3^{(3)} =$$

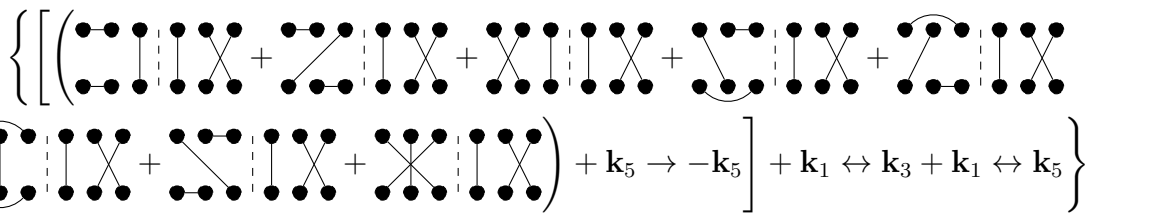

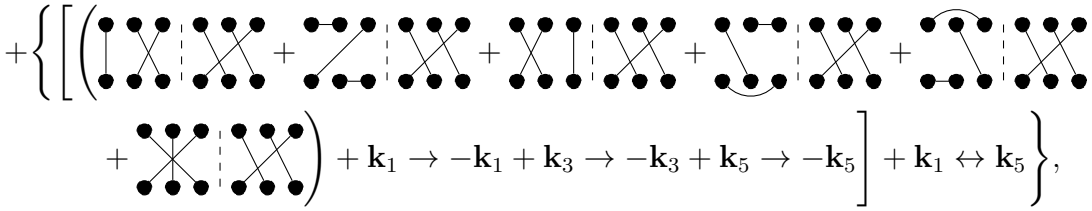

(4.96)

and 64 diagrams suppressed by $(N_c^2-1)^{-4}$:

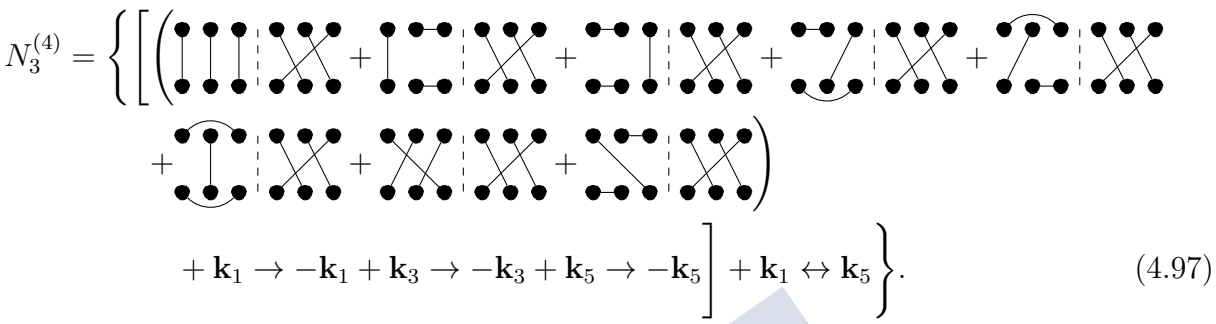

(4.97)

All in all, we get the $225 = (5!!)^2$ diagrams. Eqs. (4.93) to (4.97) give the full Wick expansion of the triple inclusive gluon spectrum to all orders in $(N_c^2-1)^{-1}$. These equations were computed in [40] up to order $(N_c^2-1)^{-2}$. In order to write Eq. (4.89) just as a function of $\mathbf{k}_i$ one just has to employ Eqs. (4.6), (4.42), (4.52), (4.56) and (4.75) and then perform the $\mathbf{q}_i$ integrals. These integrals are easy to be performed if the arguments of them are Gaussian functions, as we have assumed before.

4.5.3 Four gluon inclusive production

In this section we evaluate Eq. (4.57) for $n = 4$, that is, the four gluon inclusive spectrum. Since in this case the number of diagrams involved is very large ($[7!!]^2 = 11025$) and thus their writing is not viable, we will start by discussing the simpler case in which the partons in the wave function of the projectile are initially not correlated. Then we will consider to the more general case that is explained in detail in Appendix C.

The case in which the partons in the projectile wave function are initially uncorrelated was discussed for scattering quarks [105], and for gluons [168] within the glasma graph approach. In our case, this implies writing Eq. (4.57) as

$$2^n(2\pi)^{3n}\frac{d^nN}{\prod_{i=1}^n d^2\mathbf{k}_i} = \int\left(\prod_{i=1}^{2n}\frac{d^2\mathbf{q}_i}{(2\pi)^2}\right)\prod_{i=1}^{n}\left\langle\Omega_{2i-1}\Omega_{2i}\right\rangle_p\left(\sum_{\sigma\in\Pi(\chi)}\prod_{\{\alpha,\beta\}\in\sigma}\left\langle\Lambda_\alpha\Lambda_\beta\right\rangle_T\right), \tag{4.98}$$

and, instead of having $[(2n-1)!!]^2$ terms in the sum, we just have $(2n-1)!!$. Using Eq. (4.98) we can write the 4-gluon inclusive production as the sum of 105 diagrams (also known as rainbow diagrams [185]) in the following form:

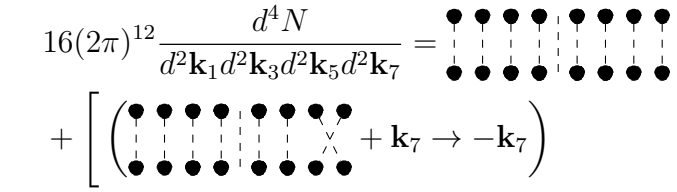

$$+ \mathbf{k}_1 \leftrightarrow \mathbf{k}_5 + \mathbf{k}_1 \leftrightarrow \mathbf{k}_7 + \mathbf{k}_3 \leftrightarrow \mathbf{k}_5 + \mathbf{k}_3 \leftrightarrow \mathbf{k}_7 + (\mathbf{k}_3 \leftrightarrow \mathbf{k}_5)(\mathbf{k}_1 \leftrightarrow \mathbf{k}_7)\Bigg]$$

$$+ \Bigg\{\Bigg[\Bigg(+ \mathbf{k}_3 \to -\mathbf{k}_3 + \mathbf{k}_5 \to -\mathbf{k}_5 + \mathbf{k}_7 \to -\mathbf{k}_7\Bigg)$$

$$+ \mathbf{k}_3 \leftrightarrow \mathbf{k}_7\Bigg] + \mathbf{k}_1 \leftrightarrow \mathbf{k}_3 + \mathbf{k}_1 \leftrightarrow \mathbf{k}_5 + \mathbf{k}_1 \leftrightarrow \mathbf{k}_7\Bigg\}$$

$$+ \Bigg[\Bigg(+ \mathbf{k}_1 \to -\mathbf{k}_1 + \mathbf{k}_5 \to -\mathbf{k}_5 + (\mathbf{k}_1 \to -\mathbf{k}_1)(\mathbf{k}_5 \to -\mathbf{k}_5)\Bigg)$$

$$+ \mathbf{k}_3 \leftrightarrow \mathbf{k}_5 + \mathbf{k}_3 \leftrightarrow \mathbf{k}_7\Bigg]$$

$$+ \Bigg\{\Bigg[+ \mathbf{k}_1 \to -\mathbf{k}_1 + \mathbf{k}_3 \to -\mathbf{k}_3 + \mathbf{k}_5 \to -\mathbf{k}_5 + \mathbf{k}_7 \to -\mathbf{k}_7$$

$$+ \frac{1}{2}\Bigg((\mathbf{k}_1 \to -\mathbf{k}_1)(\mathbf{k}_3 \to -\mathbf{k}_3) + (\mathbf{k}_1 \to -\mathbf{k}_1)(\mathbf{k}_5 \to -\mathbf{k}_5) + (\mathbf{k}_1 \to -\mathbf{k}_1)(\mathbf{k}_7 \to -\mathbf{k}_7)$$

$$+ (\mathbf{k}_3 \to -\mathbf{k}_3)(\mathbf{k}_5 \to -\mathbf{k}_5) + (\mathbf{k}_3 \to -\mathbf{k}_3)(\mathbf{k}_7 \to -\mathbf{k}_7) + (\mathbf{k}_5 \to -\mathbf{k}_5)(\mathbf{k}_7 \to -\mathbf{k}_7)\Bigg)\Bigg]$$

$$+ \mathbf{k}_1 \leftrightarrow \mathbf{k}_3 + \mathbf{k}_1 \leftrightarrow \mathbf{k}_7 + \mathbf{k}_3 \leftrightarrow \mathbf{k}_5 + \mathbf{k}_3 \leftrightarrow \mathbf{k}_7 + \mathbf{k}_5 \leftrightarrow \mathbf{k}_7\Bigg\}. \tag{4.99}$$

In this expression, the term in the first line corresponds to the case in which all the generated gluons are uncorrelated . The 12 terms in the second line correspond to the case in which 2 gluons are uncorrelated and 2 gluons are correlated. The 32 terms in the third line correspond to the case in which 1 gluon is uncorrelated and the remaining 3 ones are correlated. The 12 terms of the fourth line correspond to the case in which two pair of gluons are correlated independently, i.e., factorisable connected diagrams. Finally, the 48 terms of the last lines (the factor 1/2 avoids double counting of the diagrams) correspond to the case in which all the gluons are correlated between them, i.e., fully connected diagrams. Note that the first, second, third and fourth, and fifth terms in the sum on the right hand side correspond to terms with increasing powers in $(N_c^2 - 1)^{-2}$.

The Wick diagrams of Eq. (4.99) can be computed in the same fashion as in Section 4.5.1. However, since we are only interested in computing the 4-particle cumulant, Eq. (3.31), we will exploit the $\mathbf{k}_i \leftrightarrow \mathbf{k}_j$ and $\mathbf{k}_i \to -\mathbf{k}_i$ symmetries in order to simplify the calculation. When evaluating the 4-particle κ-function in Eq. (3.34) all the terms that contain at least one disconnected piece, i.e., two vertical lines in both sides of the diagram, will vanish trivially due to rotational invariance. For this reason the diagrams of the first three lines of Eq. (4.99) will not contribute to the 4-particle κ-function when $n > 0$ and therefore we can write

$$\kappa_{2n}\{4\} = \int d^2\mathbf{k}_1 d^2\mathbf{k}_3 d^2\mathbf{k}_5 d^2\mathbf{k}_7 e^{i2n(\phi_1+\phi_3-\phi_5-\phi_7)}\Bigg[\Bigg(+ \text{perm}_4\Bigg)$$

$$+ \left(\text{ 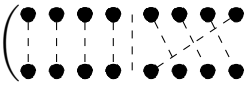 } + \text{perm}_5 \right) \Bigg], \quad (4.100)$$

where we have written schematically perm_4, which encodes all the factorizable connected diagrams, and perm_5, which includes all the fully connected diagrams, as all the permutations of the fourth and fifth diagrams of Eq. (4.99) respectively. Note that we have also dropped the factors 2 and 2π as they cancel in the definition of the cumulant.

On the other hand, we can read from the permutations for the fully connected diagrams perm_5, that all the diagrams that are related by a change of variables $\mathbf{k}_i \to -\mathbf{k}_i$ will give the same result for the integral in Eq. (4.100) since this transformation is equivalent to making $\phi_i \to \phi_i + \pi$ in the argument of the exponential and, thus, leaves the integral invariant. Furthermore, it is easy to check that all the diagrams of the last three lines of Eq. (4.99) that are related by the change of variables $\mathbf{k}_1 \leftrightarrow \mathbf{k}_3$, $\mathbf{k}_5 \leftrightarrow \mathbf{k}_7$ and $\mathbf{k}_3 \leftrightarrow \mathbf{k}_7$ also give the same value for the integral. By inspection of the symmetries, which is detailed in Appendix C, we can write the 48 integrals defined by the permutations of the last three lines of Eq. (4.99) as

$$\begin{aligned} &\int d^2\mathbf{k}_1 d^2\mathbf{k}_3 d^2\mathbf{k}_5 d^2\mathbf{k}_7 e^{i2n(\phi_1+\phi_3-\phi_5-\phi_7)} \left(\text{ 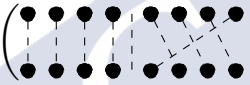 } + \text{perm}_5 \right) \\ &= \int d^2\mathbf{k}_1 d^2\mathbf{k}_3 d^2\mathbf{k}_5 d^2\mathbf{k}_7 e^{i2n(\phi_1+\phi_3-\phi_5-\phi_7)} \left(32 \text{ 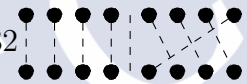 } + 16 \text{ 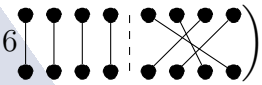 } \right), \end{aligned} \quad (4.101)$$

where the last diagram can be seen as the first one with the change of variables $\mathbf{k}_1 \leftrightarrow \mathbf{k}_7$.

Furthermore, 4 out of the 12 diagrams of the fourth term of Eq. (4.99)

$$\text{ 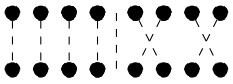 } + \mathbf{k}_1 \to -\mathbf{k}_1 + \mathbf{k}_3 \to -\mathbf{k}_3 + (\mathbf{k}_1 \to -\mathbf{k}_1)(\mathbf{k}_3 \to -\mathbf{k}_3) \quad (4.102)$$

only depend on $\phi_1 - \phi_3$ and $\phi_5 - \phi_7$ and therefore vanish due to rotational invariance. Having this into account we can write Eq. (4.100) as

$$\begin{aligned} \kappa_{2n}\{4\} = &\int d^2\mathbf{k}_1 d^2\mathbf{k}_3 d^2\mathbf{k}_5 d^2\mathbf{k}_7 e^{i2n(\phi_1+\phi_3-\phi_5-\phi_7)} \\ &\times \left(8 \text{ 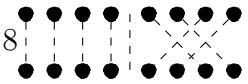 } + 32 \text{ 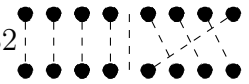 } + 16 \text{ 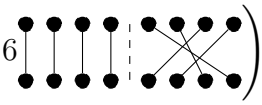 } \right). \end{aligned} \quad (4.103)$$

On the other hand, the 2-particle κ-function in the case in which the partons are initially uncorrelated in the projectile wave function is

$$\begin{aligned} 2\kappa_{2n}\{2\}^2 &= 2 \left(2 \int d^2\mathbf{k}_1 d^2\mathbf{k}_3 e^{i2n(\phi_1-\phi_3)} \text{  } \right)^2 \\ &= 8 \int d^2\mathbf{k}_1 d^2\mathbf{k}_3 d^2\mathbf{k}_5 d^2\mathbf{k}_7 e^{i2n(\phi_1+\phi_3-\phi_5-\phi_7)} \text{ 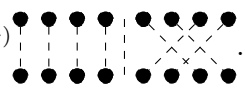 }. \end{aligned} \quad (4.104)$$

Therefore we can write Eq. (4.103) as

$$\kappa_{2n}\{4\} = \int d^2\mathbf{k}_1 d^2\mathbf{k}_3 d^2\mathbf{k}_5 d^2\mathbf{k}_7 e^{i2n(\phi_1+\phi_3-\phi_5-\phi_7)}$$

$$\times \left(32 \; + 16 \; \right) + 2\kappa_n\{2\}^2. \tag{4.105}$$

In order to compute $\kappa_0\{4\}$ we have to have into account all the diagrams of Eq. (4.99). However, since all the permutations are related by the change of variables $\mathbf{k}_i \to -\mathbf{k}_i$ or $\mathbf{k}_i \leftrightarrow \mathbf{k}_j$ $(i \neq j)$ that leave the integral invariant we can write

$$\kappa_0\{4\} = \int d^2\mathbf{k}_1 d^2\mathbf{k}_3 d^2\mathbf{k}_5 d^2\mathbf{k}_7 \left(\; + 12 \; \right.$$
$$\left. + 32 \; + 12 \; + 48 \; \right). \tag{4.106}$$

This integral can be easily performed since all the terms are just Gaussian functions.

All in all, the 4-particle cumulant can be computed by using Eq. (3.31) and Eqs. (4.105) and (4.106)

$$c_{2n}\{4\} = \frac{1}{\kappa_0\{4\}} \int_{\mathbf{k}_1,\mathbf{k}_3,\mathbf{k}_5,\mathbf{k}_7} e^{i2n(\phi_1+\phi_3-\phi_5-\phi_7)} \left(32 \; + 16 \; \right)$$
$$+ 2\kappa_{2n}\{2\}^2 \left(\frac{1}{\kappa_0\{4\}} - \frac{1}{\kappa_0\{2\}^2} \right) \tag{4.107}$$

and the four particle even azimuthal harmonics is obtained as

$$v_{2n}\{4\} = (-c_{2n}\{4\})^{1/4}. \tag{4.108}$$

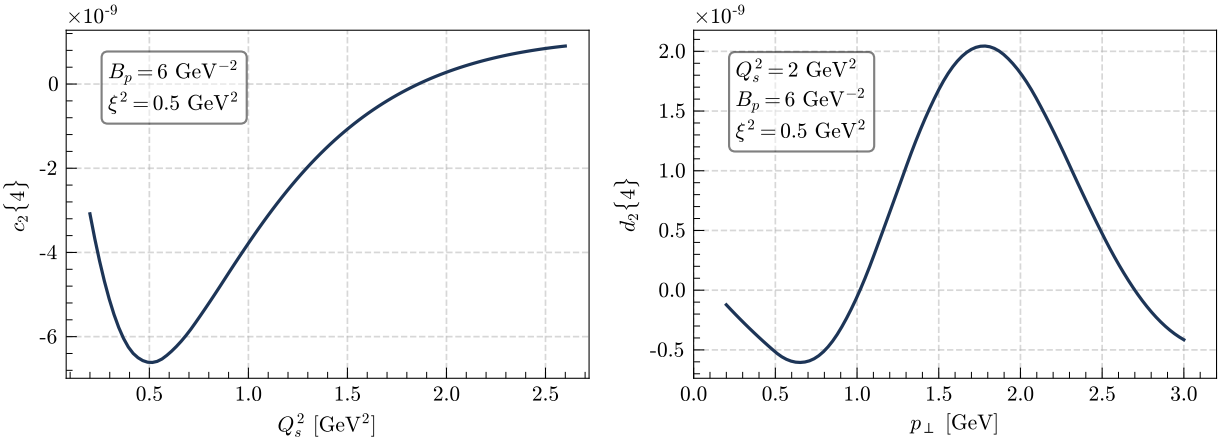

Figure 4.7.
Dependence of the 4-particle integrated cumulants on Q_s^2 (left) and of the differential cumulants on $p_\perp$ (right) in the case in which the partons in the projectile wave function are uncorrelated. In these graphs we have used $N_c = 3$ and the values of the remaining parameters are indicated on the plots.

In the left part of Fig. 4.7 we have plotted our results for Eq. (4.107) as a function of Q_s^2. The absolute values of the cumulant are very small and it becomes positive with

increasing Q_s^2. The reason why it is so comes from the fact that we are not having into account all the contributions that come from the correlation of the partons in the projectile ensemble. Below, see Fig. 4.8, these contributions are taken into account and the values are reasonable and in the ballpark of the ones in experimental data.

The differential 4-particle cumulant in Eq. (3.37) can be computed in the same fashion but since we are fixing one of the momenta we have to be more careful with the symmetries discussed in the last paragraphs. In Appendix C we show that we can write (again dropping factors 2 and 2π)

$$\int_0^{2\pi} d\phi_1 \int d^2\mathbf{k}_3 d^2\mathbf{k}_5 d^2\mathbf{k}_7 e^{i2n(\phi_1+\phi_3-\phi_5-\phi_7)} \left(+ \text{perm}_5 \right) \Big|_{|\mathbf{k}_1|=p_\perp}$$

$$= \int_0^{2\pi} d\phi_1 \int d^2\mathbf{k}_3 d^2\mathbf{k}_5 d^2\mathbf{k}_7 e^{i2n(\phi_1+\phi_3-\phi_5-\phi_7)}$$

$$\times \left(32 + 16 \right) \Big|_{|\mathbf{k}_1|=p_\perp} \tag{4.109}$$

and, therefore,

$$\tilde{\kappa}_{2n}\{4\}(p_\perp) = \int_0^{2\pi} d\phi_1 \int d^2\mathbf{k}_3 d^2\mathbf{k}_5 d^2\mathbf{k}_7 e^{i2n(\phi_1+\phi_3-\phi_5-\phi_7)}$$

$$\times \left(32 + 16 \right) \Big|_{|\mathbf{k}_1|=p_\perp} + 2\tilde{\kappa}_n\{2\}(p_\perp)\kappa_n\{2\}. \tag{4.110}$$

In order to compute $\tilde{\kappa}_0\{4\}(p_\perp)$ we cannot use the same symmetries that we have employed for computing $\kappa_0\{4\}$ because now one of the momenta is fixed. All the Wick diagrams of Eq. (4.99) that are related by a change of variables $\mathbf{k}_i \to -\mathbf{k}_i$ still leave the integral invariant but now, since we are fixing $|\mathbf{k}_1| = p_\perp$, all the diagrams that are related by a change of variable $\mathbf{k}_1 \leftrightarrow \mathbf{k}_j$ will give a different value for the integral but the ones that are related by $\mathbf{k}_i \leftrightarrow \mathbf{k}_j$, with $i, j \neq 1$, still leave the integral invariant. Performing a simple counting of the permutations of Eq. (4.99) we can write

$$\tilde{\kappa}_0\{4\}(p_\perp) = \int_0^{2\pi} d\phi_1 \int d^2\mathbf{k}_3 d^2\mathbf{k}_5 d^2\mathbf{k}_7 \Bigg[\Big|_{|\mathbf{k}_1|=p_\perp}$$

$$+ \left(6 + 6(\mathbf{k}_1 \leftrightarrow \mathbf{k}_5) \right) \Big|_{|\mathbf{k}_1|=p_\perp} + \left(8 + 24(\mathbf{k}_1 \leftrightarrow \mathbf{k}_3) \right) \Big|_{|\mathbf{k}_1|=p_\perp}$$

$$+ 12 \Big|_{|\mathbf{k}_1|=p_\perp} + \left(32 + 16(\mathbf{k}_1 \leftrightarrow \mathbf{k}_3) \right) \Big|_{|\mathbf{k}_1|=p_\perp} \Bigg]. \tag{4.111}$$

Thus, using Eqs. (4.110) and (4.111) the differential 4-particle cumulant can be written in a similar form as Eq. (4.107):

$$d_{2n}\{4\}(p_\perp) = \frac{1}{\tilde{\kappa}_0\{4\}(p_\perp)} \int_0^{2\pi} d\phi_1 \int d^2\mathbf{k}_3 d^2\mathbf{k}_5 d^2\mathbf{k}_7 e^{i2n(\phi_1+\phi_3-\phi_5-\phi_7)}$$

$$\times \left(32 \; + 16 \; \right)\Bigg|_{|\mathbf{k}_1|=p_\perp}$$

$$+ 2\tilde{\kappa}_{2n}\{2\}(p_\perp)\kappa_{2n}\{2\}\left(\frac{1}{\tilde{\kappa}_0\{4\}(p_\perp)} - \frac{1}{\tilde{\kappa}_0\{2\}(p_\perp)\kappa_0\{2\}}\right), \tag{4.112}$$

and the differential 4-particle azimuthal harmonics is defined as

$$v_n\{4\}(p_\perp) = (-d_{2n}\{4\}(p_\perp))^{1/4}. \tag{4.113}$$

In Fig. 4.7 right we have plotted our result for Eq. (4.112). Again, the values are very small and they even become positive with increasing $p_\perp$ because we are not including the diagrams that take into account the correlation of the partons inside the projectile.

With the results of Fig. 4.7 we have finished our discussion of 4-gluon production in the case in which the partons are not correlated in the projectile wave function. So far, let us recapitulate what we did in this section. First, we wrote the 4-gluon spectrum in terms of the Wick diagrams by classifying them in different topologies and, thus, with a different suppression in powers of $(N_c^2-1)^{-1}$. Then we wrote the diagrams with the same topology as just one plus a bunch of permutations, as in Eq. (4.99). Then we exploited the symmetries of these permutations in order to reduce the number of integrals to be performed in the 4-particle cumulant functions Eqs. (4.107) and (4.112). We also noticed that the contribution of the non vanishing factorizable connected diagrams to $\kappa_n\{4\}$ can be written as $2\kappa_n\{2\}^2$. Finally, we solved numerically these integrals for given values of Q_s^2 and B_p.

Now let us jump to the case in which we take into account all the terms of the Wick expansion of the projectile correlator. In this case we have to deal with $(7!!)^2 = 11025$ terms instead of $7!! = 105$. While the calculation becomes more cumbersome, the approach is exactly the same. First, we group all the Wick diagrams in the 4-gluon spectrum by their topology that defines the power in $(N_c^2-1)^{-1}$, by using the property iii) of Section 4.4.1. Then, we relate the diagrams with the same topology by permutations. Then, in order to compute the 4-particle cumulant we exploit the symmetries of these permutations and reduce as much as possible the number of integrals to be performed. Finally, we solve numerically each one of these integrals and obtain a result for the azimuthal harmonics. The detailed discussion of this procedure can be found in Appendix C.

In Figs. 4.8 and 4.9 we show our results for the four gluon cumulants as a function of Q_s^2, the differential cumulants as a function of $p_\perp$ and the corresponding azimuthal harmonics for $n = 2$ and 4. We use the same parameters that we have employed in the two gluon case. Now, in contrast with the case seen above, the values obtained are negative (for the cumulants, thus real for the Fourier coefficients), larger in absolute value and in the ballpark of experimental data. Monte Carlo integration is used, yielding negligible errors except for the smallest $p_\perp$ for $d_4\{4\}$. On the other hand, it is known that when the multiplicity gets low the 4-particle cumulant turns positive [187,188]. The naive assumption that the multiplicity is proportional to the saturation momentum suggests a change of sign in the cumulant as $Q_s^2 \to 0$. Indeed, in the Glasma Graph approach, suitable for dilute-dilute collisions and therefore for lower multiplicities, arguments [156] suggested that $c_2\{4\} > 0$ – a result also found in [105] where a transition from positive to negative is found when multiple scattering (that goes beyond glasma graphs) is introduced. This

is not seen in Fig. 4.8. A more detailed calculation should be done in this regime of low multiplicities where the transition for the Glasma Graph approach is expected.

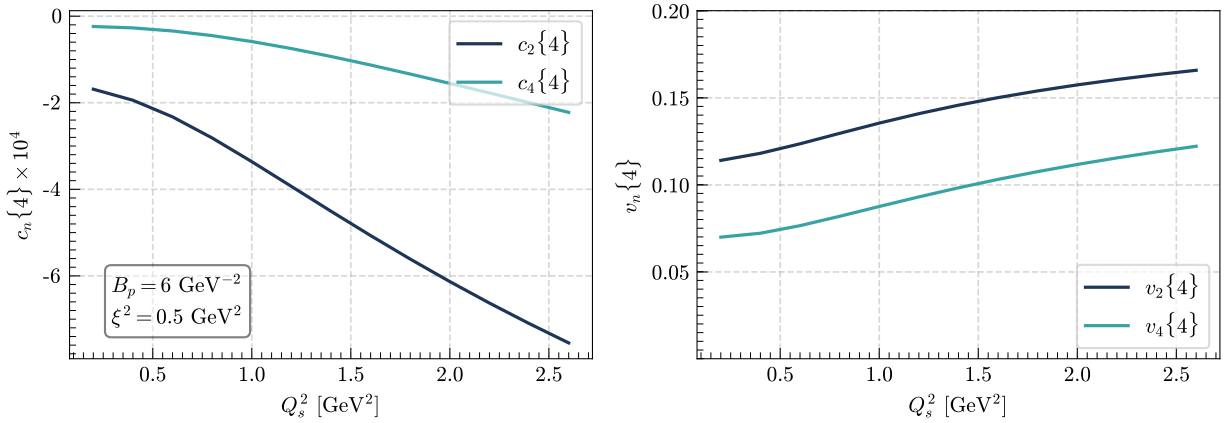

Figure 4.8.
Dependence of the 4-particle cumulant (left) and azimuthal harmonic (right) of second and fourth order with Q_s^2. In these graphs we have used $N_c = 3$ and the values of the remaining parameters are indicated on the plots.

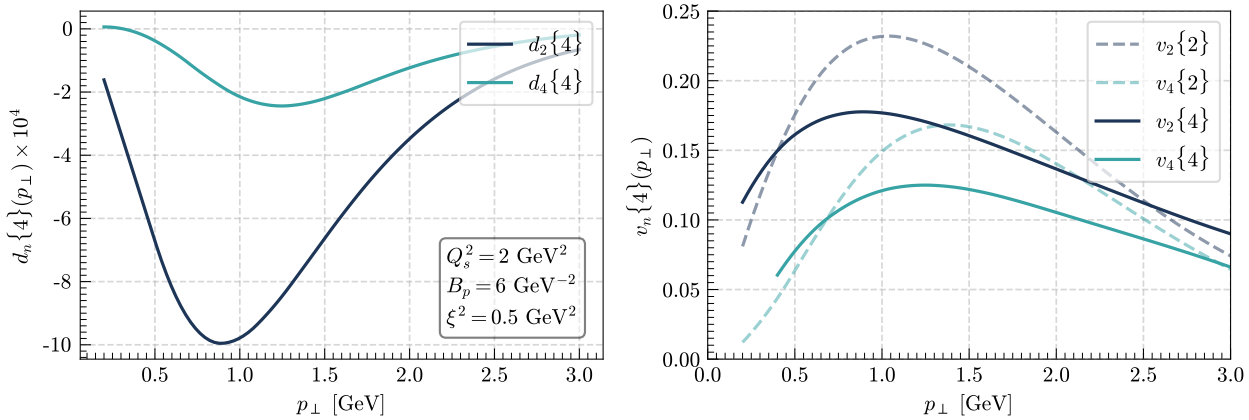

Figure 4.9.
Dependence of the differential 4-particle cumulant (left) and azimuthal harmonic (right) of second and fourth order with $p_\perp$. For the latter we also show the results obtained from 2-particle correlations. In these graphs we have used $N_c = 3$ and the values of the remaining parameters are indicated on the plots.

With the results for the azimuthal harmonics in the case of 4-gluon inclusive production we finish our discussion on multi-gluon production. We point out that the procedure that we have developed can be generalized for larger values of n. It implies dealing with a large number of diagrams ($[(2n-1)!!]^2$). There is not conceptual problem for doing it since, as we have shown, we can always use the property iii) of Section 4.4.1 to group all the diagrams in a systematic way and then exploit the symmetries to reduce the number

of integrals to be performed. The remaining issue is dealing with a large number of $2n$-dimensional integrals that must be solved numerically.

We should also note that, although the results shown in this section are consistent with experimental data, no attempt is done to compare with them. We have used the area enhancement argument that should only be valid in the case when the overlap area is large. We also have assumed the Gaussian form for the product of Lipatov vertices in Eq. (4.75) which should not give realistic results in many kinematic regimes. Furthermore, we have only taken into account the scattering of gluons. For more realistic results, we should at least compute the differential multiplicities for scattering quarks, consider more involved projectile and target averages (e.g. fluctuations) and convolute the results with fragmentation functions.

4.6 Conclusions and Outlook

In this chapter we have reviewed the work of [38] where we have computed multi-gluon production in the CGC in dilute-dense (pA) collisions, extending the work in [40] to four gluons. Our calculation includes the contributions that are leading in the overlap area of the collision [40, 169, 170, 186], while keeping all orders in the expansion in the number of colors. We develop a diagrammatic technique to write the numerous color contractions and exploit the symmetries to group the diagrams and simplify the expressions. This technique reduces dramatically the number of integrals needed to compute the multiplicity distributions and integrated and differential cumulants, which results essential for the large number of diagrams, more than 10000, that appears for four gluon production. We use the GBW model [189, 190] for the dipoles that result from the target averages, and the generalized MV model [26, 27] for projectile averages. In order to proceed analytically as far as possible and simplify the final calculations, we use the Wigner function approach [103, 105, 106] that we extend to include quantum correlations in the projectile wave function. The Wigner function approach supposes that the final momenta of gluons is mainly acquired through interaction with the dense target and is thus suitable for a collinear projectile approximation.

Apart from the techniques developed and the discussions on the validity of the area enhancement argument and the Wigner function approach, our main results can be summarized in Figs. 4.5, 4.6, 4.8 and 4.9. For two gluon correlations, we provide analytic expressions for integrated and differential cumulants which show smooth dependences on the parameters defining the projectile and target Wigner function and dipole, respectively. For four gluon correlations we find that the second order four particle cumulant $c_2\{4\} < 0$ – thus providing a sensible second order Fourier coefficient $v_2\{4\}$, a result found in [105] (where only quark scattering is considered and partons in the projectile wave function are uncorrelated) and attributed to multiple scattering. We note that the approximation in which gluons in the projectile are uncorrelated gives results for the cumulants that are much smaller in absolute value than when correlations are included, and becoming positive for some values of Q_s and $p_\perp$. This emphasizes the importance of including the full correlations in the projectile.

Our numerical results, due to the Gaussian forms that we employ for the Wigner function and dipole, cannot be considered reliable for $p_\perp$ sizable larger than Q_s. They lie

in the ballpark of experimental data, for values of parameters that look reasonable. But we are aware that further analytic understanding is still required, and several pieces are still missing in our formalism: the contribution from quarks, more involved projectile and target averages, fragmentation functions,.... All these aspects should be explored before we can establish a model ready for phenomenology.

USC
UNIVERSIDADE
DE SANTIAGO
DE COMPOSTELA

Chapter 5

Non-eikonal corrections in proton-proton collisions

Particle production at high energies in the soft and semihard regimes is usually computed resourcing to high energy approximations [47], namely the eikonal approximation. This is the case in the Color Glass Condensate, as we have seen in Chapter 2. In this framework, the process of propagation of an energetic parton from the projectile through the target, considered as a background field, is computed in the light cone gauge neglecting its transverse components and considering it as infinitely time dilated and Lorentz contracted, i.e. as a shock-wave. Also terms subleading in energy (among them, spin flip ones) are neglected. On the other hand, in the calculation of elastic and radiative energy loss of energetic partons traversing a medium composed of colored scattering centers – jet quenching – the shockwave approximation is relaxed and the target is considered to have a finite length, see e.g. the reviews [191, 192]. In this context, a systematic expansion of the gluon propagator in non-eikonal terms was done in [43, 44] and applied to particle production in the CGC in [39]. Non-eikonal corrections at high energies have also been treated recently in the context of Transverse Momentum Distributions and spin physics [193–199], and soft gluon exponentiation [200–205].

As discussed in Chapters 2 and 3, in the CGC particle production and correlations have been computed within several approximation schemes, providing an alternative explanation to final state interactions for the ridge phenomenon observed in small systems, proton-proton and proton-nucleus at the LHC and RHIC. The Glasma Graph approximation, suitable for collisions between two dilute objects like proton-proton and containing both Bose enhancement and Hanbury-Brown-Twiss effects, has been used to describe experimental data, and to compute three and four gluon correlations. It was later extended to dilute-dense (proton-nucleus) collisions both numerically [103] and analytically [40, 186, 206], and used to calculate three gluon correlations [40].

Beyond the analytical extension to dense-dense collisions, the remaining key theoretical problem for the description of azimuthal structure in small systems in the CGC lies in odd harmonics that are absent in usual calculations. For this, density corrections in the projectile [171, 172, 207], quark correlations [104, 106, 157, 208] and a more involved description of the target [153, 156] than the one provided by the MV model, have been proposed.

In this chapter, based on [45, 46], we deal with non-eikonal corrections to particle production in the CGC that stem from relaxing the shock-wave approximation for the target, which becomes of finite length. These are the corrections included in jet quenching calculations and systematically expanded up to next-to-next-to-leading order in [43, 44].

In Section 5.1 we derive an expression for the Lipatov vertex that takes into account the finite longitudinal extent of the target field. While by itself this result is not new and similar calculations and expressions can be found in the literature, see e.g. Refs. [209,210], its identification for use to include non-eikonal corrections in CGC calculations is done in [46] for the first time. Then, in Section 5.2 we apply our corrections to single gluon production in the dilute-dilute (Glasma graph) limit. In Section 5.3 we perform the non-eikonal corrections to the double gluon spectra computed in Section 3.2 within the Glasma Graph approximation. As a result we see that the inclusion of non-eikonal corrections break the accidental symmetry $\mathbf{k}_2 \to -\mathbf{k}_2$ and therefore, in this setup, we are able to compute odd azimuthal harmonics. In Section 5.4 we perform a numerical analysis of the non-eikonal 2-gluon spectra in order to study how important is the azimuthal asymmetry generated by the non-eikonal corrections. In Section 5.5 we compute the 3-gluon spectra beyond the eikonal approximation and we discuss about the quantum nature of each term. Finally, in Section 5.6 we discuss our results.

This chapter is based on:

Non-eikonal corrections to multi-particle production in the Color Glass Condensate, *Eur. Phys. J. C* **79** (2019) 600

Authors

Pedro Agostini,[ab] Tolga Altinoluk,[c] Néstor Armesto,[ab]

[a] Departamento de Física de Partículas, Universidade de Santiago de Compostela, E-15782 Santiago de Compostela, Spain

[b] Instituto Galego de Física de Altas Enerxías (IGFAE), Universidade de Santiago de Compostela, E-15782 Santiago de Compostela, Spain

[c] National Centre for Nuclear Research, 00-681 Warsaw, Poland

Journal and Article Information

Journal name: The European Physical Journal C

Publisher: Springer

ISSN: 1434-6052 (print)

Year of publication: 2019

DOI: https://doi.org/10.1140/epjc/s10052-019-7097-5

Effect of non-eikonal corrections on azimuthal asymmetries in the Color Glass Condensate, *Eur. Phys. J. C* **79** (2019) 790

Authors

Pedro Agostini,[ab] Tolga Altinoluk,[c] Néstor Armesto,[ab]

[a] Departamento de Física de Partículas, Universidade de Santiago de Compostela, E-15782 Santiago de Compostela, Spain

[b] Instituto Galego de Física de Altas Enerxías (IGFAE), Universidade de Santiago de Compostela, E-15782 Santiago de Compostela, Spain

[c] National Centre for Nuclear Research, 00-681 Warsaw, Poland

Journal and Article Information

Journal name: The European Physical Journal C

Publisher: Springer

ISSN: 1434-6052 (print)

Year of publication: 2019

DOI: https://doi.org/10.1140/epjc/s10052-019-7315-1

5.1 Derivation of the non-eikonal Lipatov vertex

As we have seen in Chapter 2, pA collisions are described by a right moving dilute projectile which interacts with a left moving dense target described by a random and intense ($\mathcal{O}(1/g)$) classical gluon field $A^\mu_T(x)$. Then in Section 2.5 we have seen that pp collisions are well described by taking the dilute limit of the target, i.e., in the Glasma Graph approximation. In this section we will see that it is possible to introduce non-eikonal corrections to the Glasma Graph approximation by introducing the *non-eikonal Lipatov vertex*. The simplest setup for deriving the non-eikonal Lipatov vertex is to consider the emission of a gluon from a projectile massless quark in the process of a single scattering with the target where we relax the shock-wave approximation[1]. As we have seen in Section 2.2, in the light cone gauge and using the shock-wave approximation the target field can be written as

$$A^\mu_T(x) \approx \delta^{\mu-}\delta(x^+)A^-_T(\mathbf{x}). \tag{5.1}$$

However, in some applications these suppressed terms may be sizable. For this reason, in this chapter we will relax the infinite boost approximation, in order to calculate the corresponding non-eikonal corrections to the usual Lipatov vertex computed at $\mathcal{O}(g^2)$.

To proceed, we analyze gluon production in pp collisions in the quark initiated channel and we compute the Lipatov vertex. In contrast with the calculation performed in the last chapters we will compute it by using the usual Feynman rules. For doing that one needs to sum the amplitudes where the gluon is emitted before, during and after the interaction with the field as shown in Fig. 5.1.

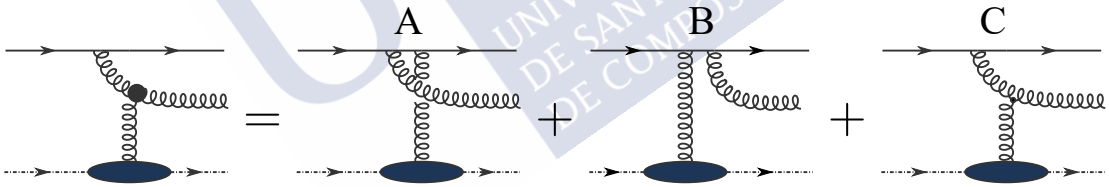

Figure 5.1.
Diagrams that contribute to the computation of the Lipatov vertex. The black dot represents the Lipatov vertex which is the sum of all real diagrams for gluon production shown on the right hand side of the equation.

Our setup is such that the right moving quark with 4-momentum $p+k-q$ is generated by the source $J(p+k-q) = J(p^+ + k^+ - q^+)$ at $x_0^+ = -\infty$ and $(x_0^-, \mathbf{x}_0 = 0$, and then interacts with the classical gluon field $A^\mu_T(x)$ generated by one scattering source located at x_1, picking up a 4-momentum q. However, since we are interested in non-eikonal corrections, we consider the field $A^\mu_T(x)$ with a x^+ dependence which has a finite support instead of treating it as a shock-wave at $x^+ = 0$, on the other hand, we still assume that there is no dependence on x^-. Thus Eq. (5.1) is rewritten as

$$A^\mu(x) \approx \delta^{\mu-}A^\mu(x^+, \mathbf{x}), \tag{5.2}$$

[1] An analogous calculation leading to the same conclusions on the non-eikonal corrections holds for a projectile gluon.

or, in momentum space,

$$A^\mu(q) \approx \delta^{\mu-}\, 2\pi\delta(q^+)A^-(q^-,\mathbf{q}), \tag{5.3}$$

where we have dropped the subscript T from the field A^μ for convenience. Furthermore, we assume that the outgoing quark has a large momentum p^+ compared to all other momenta in the process. The general strategy in this case is to keep the leading terms in +-momenta in the numerator algebra, while taking the full phase corrections coming from the integration of the denominators, see below, as done in the Furry approximation and its non-Abelian generalization [211].

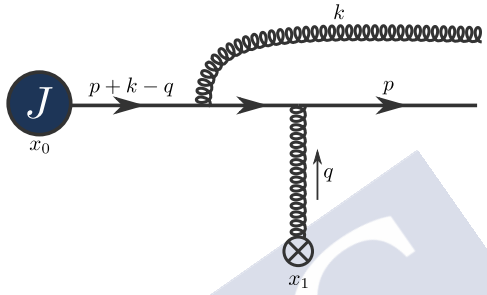

Figure 5.2.
Diagram A where the gluon is emitted before the interaction of the quark with the target field.

We start by computing the diagram A in Fig. 5.1 where the gluon is emitted with 4-momentum k before the quark interaction with the target field as shown in Fig. 5.2. Using the Feynman rules, we find that the amplitude for fixed gluon and final quark momenta is

$$i\mathcal{M}_A = \bar{u}(p)(-ig\gamma^\mu t^a)\int \frac{d^4q}{(2\pi)^4} A^a_\mu(q) e^{iq\cdot x_1} \frac{i(\not{p}-\not{q})}{(p-q)^2+i\epsilon}(-ig\gamma^\nu t^b)\epsilon^{b*}_\nu(k) \\ \times \frac{i(\not{p}+\not{k}-\not{q})}{(p+k-q)^2+i\epsilon} e^{i(p+k-q)\cdot x_0} J(p+k-q), \tag{5.4}$$

with t^a the SU(N_c) generator in the fundamental representation.

By taking the $p^+ \to \infty$ limit, we approximate $\not{p}-\not{q} \approx \not{p}$ and $\not{p}+\not{k}-\not{q} \approx \not{p}$ and we write

$$i\mathcal{M}_A \approx \bar{u}(p) e^{i(p+k)\cdot x_0} g^2 t^a t^b \int \frac{d^4q}{(2\pi)^4} \frac{\not{A}^a(q)\not{p}\not{\epsilon}^{b*}(k)\not{p}}{[(p-q)^2+i\epsilon][(p+k-q)^2+i\epsilon]} e^{iq\cdot(x_1-x_0)} \\ \times J(p^+ + k^+ - q^+). \tag{5.5}$$

Using again the eikonal approximation in the projectile's quark, $p^+ \to \infty$, we can approximate $(p-q)^2 \approx -2p^+q^-$ and $(p+k-q)^2 \approx 2p^+(k^- - q^-)$. Employing $\not{a}\not{b} = 2a\cdot b - \not{b}\not{a}$ and the massless Dirac equation $\bar{u}(p)\not{p} = 0$, we get $\bar{u}(p)\not{A}^a(q)\not{p}\not{\epsilon}^{b*}(k)\not{p} = \bar{u}(p) 4(p\cdot A^a(q))(p\cdot \epsilon^{b*}(k))$. Therefore, the amplitude for the diagram A can be written as

$i\mathcal{M}_A$

$$\approx -\bar{u}(p)e^{i(p+k)\cdot x_0}g^2t^at^b\int\frac{d^4q}{(2\pi)^4}\frac{(p\cdot A^a(q))(p\cdot\epsilon^{b*}(k))}{[p^+q^- - i\epsilon][p^+(k^- - q^-)+i\epsilon]}e^{iq\cdot(x_1-x_0)}J(p^+ + k^+ - q^+)$$
$$= -\bar{u}(p)e^{i(p+k)^-x_0^+}g^2t^at^b\int\frac{d^2\mathbf{q}}{(2\pi)^2}e^{-i\mathbf{q}\cdot\mathbf{x}_1}(p\cdot\epsilon^{b*}(k))\int\frac{dq^+}{2\pi}e^{iq^+x_1^-}J(p^+ + k^+ - q^+)$$
$$\times(2\pi)\delta(q^+)\int\frac{dq^-}{2\pi}\frac{e^{iq^-(x_1^+ - x_0^+)}p^+A^{-a}(q^-,\mathbf{q})}{(p^+)^2[q^- - i\epsilon][k^- - q^- + i\epsilon]}, \quad (5.6)$$

where in the last line we have used Eq. (5.3) and we have set $\mathbf{x}_0 = x_0^- = 0$. Performing the q^+ and q^- integrals we obtain

$$i\mathcal{M}_A \approx -\bar{u}(p)e^{ip\cdot x_0}J(p^+ + k^+)g^2t^at^b\int\frac{d^2\mathbf{q}}{(2\pi)^2}e^{-i\mathbf{q}\cdot\mathbf{x}_1}p\cdot\epsilon^{b*}(k)$$
$$\times\times\frac{i\left[e^{ik^-x_0^+}A^{-a}(0,\mathbf{q}) - e^{ik^-x_1^+}A^{-a}(k^-,\mathbf{q})\right]}{p^+k^-}\,\Theta(x_1^+ - x_0^+). \quad (5.7)$$

Since the outgoing gluon is on-shell, we have that $k^- = \mathbf{k}^2/2k^+$ and, furthermore, in the light cone gauge we have $\epsilon^{*-}(k) = \mathbf{k}^i\epsilon^i/k^+$. Therefore, making use of $p^\mu\epsilon^*_\mu \approx p^+\epsilon^{*-}$, we obtain

$$i\mathcal{M}_A \approx 2i\bar{u}(p)e^{ip\cdot x_0}J(p^+ + k^+)g^2t^at^b\Theta(x_1^+ - x_0^+)\frac{\mathbf{k}^i\epsilon^{bi}}{\mathbf{k}^2}$$
$$\times\int\frac{d^2\mathbf{q}}{(2\pi)^2}e^{-i\mathbf{q}\cdot\mathbf{x}_1}\left(e^{ik^-x_1^+}A^{-a}(k^-,\mathbf{q}) - e^{ik^-x_0^+}A^{-a}(0,\mathbf{q})\right). \quad (5.8)$$

Now, sending $x_0^+ \to -\infty$, we can finally write

$$i\mathcal{M}_A \approx 2i\bar{u}(p)e^{ip\cdot x_0}J(p^+ + k^+)g^2t^at^be^{ik^-x_1^+}\frac{\mathbf{k}^i\epsilon^{bi}}{\mathbf{k}^2}\int\frac{d^2\mathbf{q}}{(2\pi)^2}e^{-i\mathbf{q}\cdot\mathbf{x}_1}A^{-a}(k^-,\mathbf{q}). \quad (5.9)$$

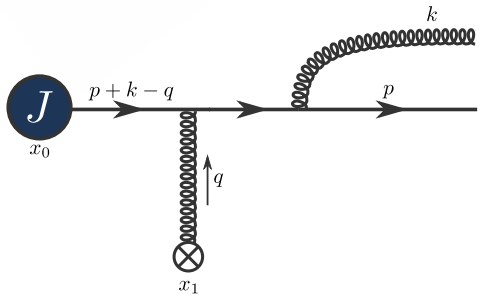

Figure 5.3.
Diagram B where the gluon is emitted after the interaction of the quark with the target field.

Now we proceed to calculate diagram B where the gluon is emitted with momentum k after the interaction of the quark with the target field, as shown in Fig. 5.3. Following the previous procedure we find that

$$i\mathcal{M}_B \approx -2i\bar{u}(p)e^{ip\cdot x_0}J(p^+ + k^+)g^2t^bt^ae^{ik^-x_1^+}\frac{\mathbf{k}^i\epsilon^{bi}}{\mathbf{k}^2}\int\frac{d^2\mathbf{q}}{(2\pi)^2}e^{-i\mathbf{q}\cdot\mathbf{x}_1}A^{-a}(k^-,\mathbf{q}). \quad (5.10)$$

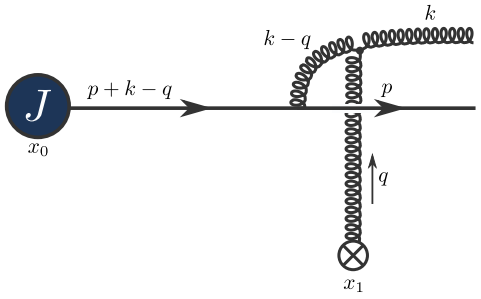

Figure 5.4.
Diagram C where the emitted gluon interacts with the target field.

The diagram C, shown in Fig. 5.4, where the emitted gluon interacts with the target field, requires dealing with the three-gluon vertex. Applying the Feynman rules we have that

$$i\mathcal{M}_C = \bar{u}(p)(-ig\gamma^\mu t^a)\int \frac{d^4q}{(2\pi)^4}\frac{i(\not{p}+\not{k}-\not{q})}{(p+k-q)^2+i\epsilon}e^{i(p+k-q)\cdot x_0}J(p+k-q) \\ \times \frac{-id_{\mu\alpha}(k-q)}{(k-q)^2+i\epsilon}V^{\alpha\nu\beta}_{abc}A^c_\beta(q)\epsilon^{b*}_\nu(k)e^{iq\cdot x_1}, \qquad (5.11)$$

where $V^{\alpha\nu\beta}_{abc} = gf^{abc}\left[g^{\alpha\nu}(q-2k)^\beta + g^{\nu\beta}(k+q)^\alpha + g^{\beta\alpha}(k-2q)^\nu\right]$ is the three-gluon vertex, $d_{\mu\alpha}(k) = g_{\mu\alpha} - \frac{\mathbf{k}_\mu n_\alpha + \mathbf{k}_\alpha n_\mu}{k\cdot n}$ the gluon propagator in the light cone gauge and $n^\mu = \delta^{\mu-}$.

Considering Eq. (5.3), we only need the $V^{\alpha\nu+}_{abc}$ component of the vertex. Furthermore, using the Dirac equation and the gamma matrices anti-commutation relation we have that $\bar{u}(p)\gamma^\mu\not{p} = \bar{u}(p)2p^\mu$. Thus,

$$i\mathcal{M}_C = -2i\bar{u}(p)e^{i(p+k)\cdot x_0}g^2t^a\int\frac{d^4q}{(2\pi)^4}\frac{p^\mu d_{\mu\alpha}(k-q)V^{\alpha\nu+}_{abc}\epsilon^{b*}_\nu(k)}{[(p+k-q)^2+i\epsilon][(k-q)^2+i\epsilon]} \\ \times A^{-c}(q)e^{iq\cdot(x_1-x_0)}J(p^+ + k^+ - q^+). \qquad (5.12)$$

After some algebra we find, in the eikonal approximation,

$$p^\mu d_{\mu\alpha}(k-q)V^{\alpha\nu+}_{abc}\epsilon^{b*}_\nu(k) \approx -2gf^{abc}p^+(\mathbf{k}-\mathbf{q})^i\cdot\epsilon^{bi}, \qquad (5.13)$$

and

$$(k-q)^2 = -2k^+\left(q^- - \frac{\mathbf{k}^2-(\mathbf{k}-\mathbf{q})^2}{2k^+}\right) + 2q^+q^- - 2k^-q^+ \\ \approx -2k^+\left(q^- - \frac{\mathbf{k}^2-(\mathbf{k}-\mathbf{q})^2}{2k^+}\right). \qquad (5.14)$$

Thus, defining $\tilde{k} = \frac{\mathbf{k}^2-(\mathbf{k}-\mathbf{q})^2}{2k^+}$, we get

$$i\mathcal{M}_C \approx -i\bar{u}(p)g^2t^af^{abc}e^{i(p+k)\cdot x_0}\int\frac{d^4q}{(2\pi)^4}(\mathbf{k}-\mathbf{q})^i\epsilon^{bi}\frac{e^{iq\cdot(x_1-x_0)}}{k^+[k^- - q^- + i\epsilon][q^- - \tilde{k} - i\epsilon]} \\ \times A^{-c}(q)J(p^+ + k^+ - q^+). \qquad (5.15)$$

Using Eq. (5.3) and performing the q^+ and q^- integrals we obtain

$$\begin{aligned} i\mathcal{M}_C \approx & 2\bar{u}(p)J(p^+ + k^+)e^{ip\cdot x_0}g^2 t^a f^{abc}\int \frac{d^2\mathbf{q}}{(2\pi)^2}\frac{(\mathbf{k}-\mathbf{q})^i}{(\mathbf{k}-\mathbf{q})^2}\epsilon^{bi}e^{-i\mathbf{q}\cdot\mathbf{x}_1} \\ & \times e^{i\tilde{k}x_1^+}\left(e^{i(k^- - \tilde{k})x_0^+}A^{-c}(\tilde{k},\mathbf{q}) - e^{i(k^- - \tilde{k})x_1^+}A^{-c}(k^-,\mathbf{q})\right)\Theta(x_1^+ - x_0^+). \end{aligned} \tag{5.16}$$

Finally, making use of $it^a f^{abc} = [t^b, t^c]$ and tanking the limit $x_0^+ \to -\infty$, we obtain

$$i\mathcal{M}_C \approx -2i\bar{u}(p)J(p^+ + k^+)e^{ip\cdot x_0}g^2[t^a,t^b]\int \frac{d^2\mathbf{q}}{(2\pi)^2}\frac{(\mathbf{k}-\mathbf{q})^i}{(\mathbf{k}-\mathbf{q})^2}\epsilon^{bi}e^{ik^- x_1^+}A^{-a}(k^-,\mathbf{q})e^{-i\mathbf{q}\cdot\mathbf{x}_1}. \tag{5.17}$$

Summing up the three diagrams we get

$$\begin{aligned} & i(\mathcal{M}_A + \mathcal{M}_B + \mathcal{M}_C) \\ & \approx -2i\bar{u}(p)J(p^+ + k^+)e^{ip\cdot x_0}g^2[t^a,t^b]\int \frac{d^2\mathbf{q}}{(2\pi)^2}L^i(\mathbf{k},\mathbf{q})\epsilon^{bi}e^{ik^- x_1^+}A^{-a}(k^-,\mathbf{q})e^{-i\mathbf{q}\cdot\mathbf{x}_1}, \end{aligned} \tag{5.18}$$

where

$$L^i(\mathbf{k},\mathbf{q}) = \frac{(\mathbf{k}-\mathbf{q})^i}{(\mathbf{k}-\mathbf{q})^2} - \frac{\mathbf{k}^i}{\mathbf{k}^2} \tag{5.19}$$

is the eikonal Lipatov vertex that has been introduced in Eq. (2.82), although with another convention for the momenta. We see that in our calculation, as announced, the non-eikonal corrections result in the sum of the amplitudes simply picking up a phase (important for $k^- x_1^+ \sim 1$ and negligible for $\mathbf{k}^2 x_1^+/k^+ \ll 1$ where we recover the eikonal result) that can be absorbed in a redefinition of the Lipatov vertex. Therefore, we define the non-eikonal Lipatov vertex as

$$L^i_{\mathrm{NE}}(\underline{k},\mathbf{q};x_1^+) = \left[\frac{(\mathbf{k}-\mathbf{q})^i}{(\mathbf{k}-\mathbf{q})^2} - \frac{\mathbf{k}^i}{\mathbf{k}^2}\right]e^{i\frac{\mathbf{k}^2}{2k^+}x_1^+}, \tag{5.20}$$

with $\underline{k} \equiv (k^-, \mathbf{k})$.

As stated in the introduction of this chapter, this result is not new by itself and similar calculations and expressions can be found in the literature, e.g. in Refs. [209,210]. But the identification of this building block for its use to include non-eikonal corrections in CGC calculations was done by us in [45,46] for the first time. Note that using the non-eikonal expression of the gluon propagator from [43,44], the two first terms of the expansion of the exponential were obtained in [39] and the exponential form guessed. Furthermore an analogous result could be obtained by taking the dilute limit of Eq. (2.38) that, as we shall see in the next chapter, will be the master formula for generalizing this result for dilute-dense collisions.

5.2 Single inclusive gluon production

In the previous section we have presented the derivation of the non-eikonal Lipatov vertex. Now, we would like to use this expression in order to calculate multi-gluon production

cross section at mid rapidity within the Glasma Graph approximation, introduced in Section 2.5, in order to study the effects of finite target width corrections to those observables.

The double and triple inclusive gluon production cross sections in pA collisions have been recently studied in [168, 212] in the Glasma graph approximation, and in [40] going beyond it, i.e. taking into account multiple scattering effects of the dense target by using the Area Enhancement model, introduced in Section 4.2.1. For each observable, the contributions to Bose enhancement of the projectile gluons and HBT contributions of the final state gluons are identified. However, the studies in [40, 168, 212] are performed within the eikonal approximation without taking into account the corrections due to the finite longitudinal width of the target.

In the rest of this section, we take this extra step. Namely, we first expand the single, double and triple inclusive gluon production cross section in powers of the background field of the target, analogous as in Sections 2.5 and 3.2. Then, we introduce the non-eikonal Lipatov vertex Eq. (5.20) in the expanded cross sections and get the explicit expressions of the Bose enhancement and HBT contributions beyond the strict eikonal limit for the double and triple inclusive gluon production.

Within the CGC framework, the single spectrum of a gluon with transverse momenta k and rapidity η can be written as, Eq. (2.80),

$$\frac{dN}{d^2\mathbf{k}d\eta} = \frac{g^2}{\pi(2\pi)^4}\int_{\mathbf{z},\bar{\mathbf{z}}} e^{i\mathbf{k}\cdot(\mathbf{z}-\bar{\mathbf{z}})}\int_{\mathbf{x},\mathbf{y}} f^i(\mathbf{x}-\mathbf{z})f^i(\bar{\mathbf{z}}-\mathbf{y})\Big\langle \rho^a_{\mathbf{x}}\rho^b_{\mathbf{y}}\Big\rangle_p \times \Big\langle \big[U_{\mathbf{z}}-U_{\mathbf{x}}\big]^{ac}\big[U^\dagger_{\bar{\mathbf{z}}}-U^\dagger_{\mathbf{y}}\big]^{cb}\Big\rangle_T, \tag{5.21}$$

where we have introduced the shorthand notation $\rho^a_{\mathbf{x}} \equiv \rho^a_p(\mathbf{x})$ and $U_{\mathbf{x}} \equiv U(\mathbf{x})$, $\langle\cdots\rangle_{p(T)}$ denote the average over the projectile (target) configurations and $f^i(\mathbf{x})$ is the Weizsaker-Williams field defined in Eq. (2.75). In the Glasma graph approximation we assume that the target field is dilute and, therefore, we expand the Wilson line to first order in the color field of the target:

$$U_{ab}(\mathbf{x}) \approx 1 + igT^c_{ab}\int dx^+ A^-_c(x^+,\mathbf{x}) = 1 + igT^c_{ab}\int dx^+\int_{\mathbf{q}} e^{i\mathbf{q}\cdot\mathbf{x}}\, A^-_c(x^+,\mathbf{q})\,. \tag{5.22}$$

Using Eq. (5.22) we can write the single inclusive gluon spectrum in the dilute limit as

$$\begin{aligned}\frac{dN}{d^2\mathbf{k}d\eta}\bigg|_{\text{dilute}} &= \frac{g^2}{\pi(2\pi)^4}\int_{\mathbf{z}\bar{\mathbf{z}}} e^{i\mathbf{k}\cdot(\mathbf{z}-\bar{\mathbf{z}})}\int_{\mathbf{xy}} f^i(\mathbf{x}-\mathbf{z})f^i(\bar{\mathbf{z}}-\mathbf{y})\Big\langle \rho^a_{\mathbf{x}}\rho^b_{\mathbf{y}}\Big\rangle_p \\ &\times g^2\int dx_1^+\,dx_2^+\int_{\mathbf{q}_1,\mathbf{q}_2}\Big\langle A^-_c(x_1^+,\mathbf{q}_1)A^-_{\bar{c}}(x_2^+,\mathbf{q}_2)\Big\rangle_T (T^cT^{\bar{c}})_{ab} \\ &\times\Big[e^{-i\mathbf{q}_1\cdot\mathbf{z}}-e^{-i\mathbf{q}_1\cdot\mathbf{x}}\Big]\Big[e^{i\mathbf{q}_2\cdot\bar{\mathbf{z}}}-e^{i\mathbf{q}_2\cdot\mathbf{y}}\Big]\,.\end{aligned} \tag{5.23}$$

We can now perform the color averaging over the projectile color charge densities. For the correlator of two projectile color charge densities, we use the generalized MV model defined in Eq. (4.5)

$$\Big\langle \rho^a_{\mathbf{x}}\rho^b_{\mathbf{y}}\Big\rangle_p = \delta^{ab}\,\mu^2(\mathbf{x},\mathbf{y}), \tag{5.24}$$

where we have dropped the superscript p of the function $\mu^2(\mathbf{x},\mathbf{y})$. Inserting Eq. (5.24) into the expression for the dilute limit of the single inclusive production cross section given in Eq. (5.23) and integrating over the transverse coordinates, we can simply write the dilute limit of the single inclusive production cross section as

$$\left.\frac{dN}{d^2\mathbf{k}d\eta}\right|_{\text{dilute}} = \delta^{c\bar{c}}\frac{g^4}{\pi(2\pi)^2}C_A\int dx_1^+\,dx_2^+\int_{\mathbf{q}_1,\mathbf{q}_2} L^i(\mathbf{k},\mathbf{q}_1)L^i(\mathbf{k},\mathbf{q}_2) \times\ \mu^2\big[\mathbf{k}-\mathbf{q}_1,\mathbf{q}_2-\mathbf{k}\big]\Big\langle A_c^-(x_1^+,\mathbf{q}_1)A_{\bar{c}}^-(x_2^+,\mathbf{q}_2)\Big\rangle_T, \tag{5.25}$$

where $L^i(\mathbf{k},\mathbf{q})$ is the strict eikonal Lipatov vertex Eq. (5.19). Note that Eq. (5.25) is equivalent to perform the square of Eq. (2.98).

At this point, the effects of finite longitudinal width of the target can be implemented in the single inclusive gluon production cross section. Effectively, the implementation of these effects corresponds to two modifications in the cross section given in Eq. (5.25). The first modification is to replace the eikonal Lipatov vertices by the non-eikonal ones derived in Section 5.1:

$$L^i(\mathbf{k},\mathbf{q}) \to L^i_{\text{NE}}(\underline{k},\mathbf{q};x^+). \tag{5.26}$$

The non-eikonal Lipatov vertex given in Eq. (5.20) takes into account the finite longitudinal width of the target to all orders as discussed in Section 5.1. The second modification that is needed to account for the finite longitudinal width of the target is adopting a modified expression for the correlator of two target fields. Since the target has finite longitudinal width, the target fields can be located at two different longitudinal positions. Therefore, for the correlator of two target fields, we consider a generalization of the MV model in which the two color fields are located at different longitudinal coordinates and are connected via gauge links along the longitudinal axis [39]. In that case, the color field correlator of two fields can be written as

$$\Big\langle A_c^-(x_1^+,\mathbf{q}_1)A_{\bar{c}}^-(x_2^+,\mathbf{q}_2)\Big\rangle_T = g^2\delta^{c\bar{c}}\,n(x_1^+)\,\frac{1}{2\lambda^+}\Theta\Big(\lambda^+-|x_1^+-x_2^+|\Big) \times(2\pi)^2\delta^{(2)}(\mathbf{q}_1-\mathbf{q}_2)\,|a(\mathbf{q}_1)|^2, \tag{5.27}$$

where λ^+ is the color correlation length in the target and much smaller than the total longitudinal width of the target L^+. Moreover, the function $n(x^+)$ defines the one dimensional target density along the longitudinal axis. For simplicity, we assume that this function is constant with a finite support, $n(x^+)=n_0$ for $0\le x^+\le L^+$ and 0 elsewhere. Finally, the function $a(\mathbf{q})$ that appears in the definition of the two field correlator is the functional form of the potential in momentum space which is usually taken to be a Yukawa type potential in jet quenching calculations [191, 192, 209, 210]:

$$|a(\mathbf{q})|^2 = \frac{m^2}{\left(\mathbf{q}^2+m^2\right)^2}, \tag{5.28}$$

with m the Debye screening mass or the inverse color correlation length. We would like to emphasize that in the limit of vanishing correlation length λ^+ together with a constant longitudinal target density $n(x_1^+)$, the two target field correlator defined in Eq. (5.27) reduces to the standard MV model correlator seen in Eq. (4.11).

By implementing these two modifications in the single inclusive gluon production cross section and using the expression of the non-eikonal Lipatov vertex given in Eq. (5.20) together with the two field correlator introduced in Eq. (5.27), we can write the non-eikonal generalization of the dilute limit of the single inclusive gluon cross section, which accounts for the finite longitudinal width of the target, as

$$\left.\frac{dN}{d^2\mathbf{k}d\eta}\right|^{\rm NE}_{\rm dilute} = \frac{g^6}{\pi(2\pi)^2} C_A\left(N_c^2-1\right)\int_{\mathbf{q}} \mu^2\big[\mathbf{k}-\mathbf{q},\mathbf{q}-\mathbf{k}\big]\, L^i(\mathbf{k},\mathbf{q})L^i(\mathbf{k},\mathbf{q})\left|a(\mathbf{q})\right|^2 \times\, n_0\frac{1}{2\lambda^+}\int_0^{L^+} dx_1^+\int_{x_1^+-\lambda^+}^{x_1^++\lambda^+} dx_2^+\, e^{i\frac{\mathbf{k}^2}{2k^+}(x_1^+-x_2^+)}. \quad (5.29)$$

In this expression the non-eikonal Lipatov vertex is incorporated via the phase that appears under the longitudinal coordinate integral, the Θ-function provides the limits of the integral in x_2^+ and the one dimensional target density along the longitudinal axis is taken to be constant, n_0 for $0 \leq x_1^+ \leq L^+$. The integrations over the longitudinal coordinates x_1^+ and x_2^+ can be performed in a straight forward manner and the final result for the dilute limit of the non-eikonal single inclusive gluon production cross section reads

$$\left.\frac{dN}{d^2\mathbf{k}d\eta}\right|^{\rm NE}_{\rm dilute} = \frac{g^6}{\pi(2\pi)^2} C_A\left(N_c^2-1\right)\left(n_o L^+\right)\mathcal{G}_1^{\rm NE}(k^-;\lambda^+) \times\int_{\mathbf{q}} \mu^2\big[\mathbf{k}-\mathbf{q},\mathbf{q}-\mathbf{k}\big]\, L^i(\mathbf{k},\mathbf{q})L^i(\mathbf{k},\mathbf{q})\left|a(\mathbf{q})\right|^2, \quad (5.30)$$

where we have used the fact that $\lambda^+ \ll L^+$ for the integration over the longitudinal coordinates. Here, $\mathcal{G}_1^{\rm NE}(k^-,\lambda^+)$ is the function that encodes all the non-eikonal information of the single inclusive gluon production and reads

$$\mathcal{G}_1^{\rm NE}(k^-;\lambda^+) = \frac{1}{k^-\lambda^+}\sin(k^-\lambda^+), \quad (5.31)$$

with $k^- = \frac{\mathbf{k}^2}{2k^+}$. We would like to emphasize that the factor $(n_0 L^+)$ in Eq. (5.30) stands for the the number of scattering centers inside the finite longitudinal extend L^+ of the target. In the dilute target limit, we only take account one single scattering both in the amplitude and in the complex conjugate amplitude. Therefore, in this limit this factor will be set to one hereafter and we get

$$\left.\frac{dN}{d^2\mathbf{k}d\eta}\right|^{\rm NE}_{\rm dilute} = \frac{g^6}{4\pi^3} C_A\left(N_c^2-1\right)\mathcal{G}_1^{\rm NE}(k^-;\lambda^+) \times\int_{\mathbf{q}} \mu^2\big[\mathbf{k}-\mathbf{q},\mathbf{q}-\mathbf{k}\big]\, L^i(\mathbf{k},\mathbf{q})L^i(\mathbf{k},\mathbf{q})\left|a(\mathbf{q})\right|^2, \quad (5.32)$$

where by noting that $\mu^2(\mathbf{k},-\mathbf{k}) = S_\perp$ can be easily identified, apart from the non-eikonal factor, with Eq. (2.100). Eq. (5.32) is the final result for the dilute target limit of the non-eikonal single inclusive gluon spectrum. Note that in the limit of vanishing correlation length λ^+ one can expand the non-eikonal single inclusive production cross section to second order in $(k^-\lambda^+)$ which corresponds to the single inclusive gluon production cross section at next-to-next-to-eikonal accuracy and the result coincides with the expression derived in [39].

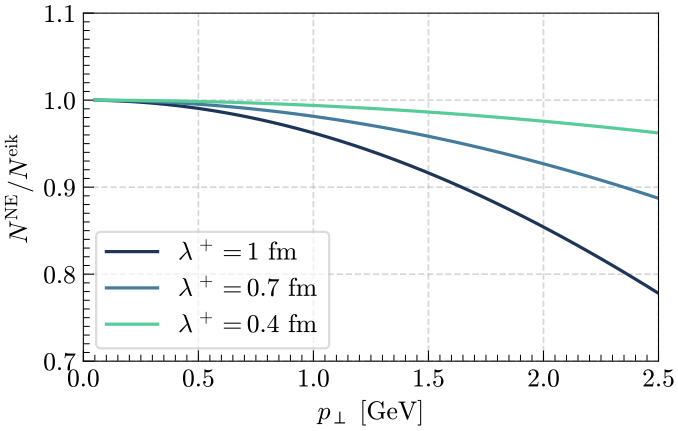

Figure 5.5.
The ratio of non-eikonal to eikonal single inclusive gluon spectra, Eq. (5.31), as a function of the transverse momenta of the produced gluon for different values of the correlation length λ^+, at fixed pseudorapidity $\eta = 2$.

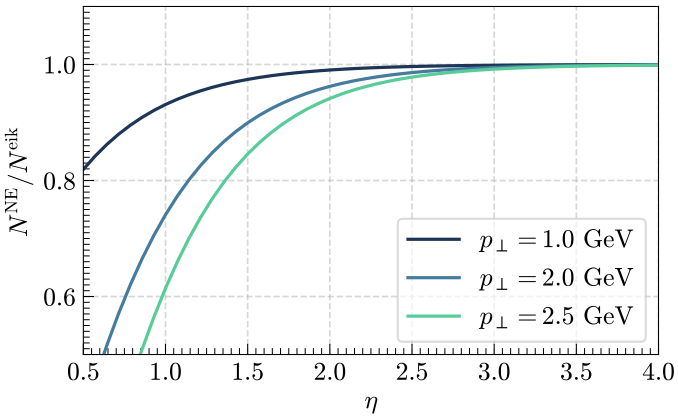

Figure 5.6.
The ratio of non-eikonal to eikonal single inclusive gluon spectra, Eq. (5.31), as a function of the pseudorapidity of the produced gluon for different values of its transverse momenta at a fixed correlation length $\lambda^+ = 0.5$ fm.

Before concluding this section, let us comment on the relative importance of the non-eikonal corrections, that are accounted for in Eq. (5.32) via the function $\mathcal{G}_1^{\mathrm{NE}}(k^-;\lambda^+)$ that encodes the non-eikonal effects, with respect to the eikonal limit of the single inclusive gluon production cross section in the dilute target limit. First of all, in the limit of vanishing $(k^-\lambda^+)$, we have

$$\lim_{k^-\lambda^+\to 0} \mathcal{G}_1^{\mathrm{NE}}(k^-;\lambda^+) = 1 \tag{5.33}$$

and we recover the well known eikonal limit of the single inclusive gluon production in the limit of the dilute target. In Fig. 5.5, we have plotted the ratio of the non-eikonal to eikonal single inclusive gluon spectra, i.e. Eq. (5.31), as a function of the transverse

momenta of the produced gluon at fixed pseudorapidity $\eta = 2$ for different values of the color correlation length λ^+. In the limit of vanishing transverse momenta of the produced gluon, the non-eikonal and eikonal cross sections coincide and the ratio becomes one as expected. The ratio shows up to 20% relative weight of the non-eikonal corrections for $\lambda^+ = 1$ fm, for smaller values of λ^+ the results show a suppression from a few to up to 10%.

In Fig. 5.6, we have plotted the ratio of the non-eikonal to eikonal single inclusive gluon spectra as a function of pseudorapidity for different values of the transverse momenta of the produced gluon at a fixed correlation length $\lambda^+ = 0.5$ fm. The ratio of the non-eikonal to eikonal cross sections goes to one with increasing pseudorapidity as expected, since the relative importance of the non-eikonal corrections should vanish for large values of η. The results show that up to pseudorapidity $\eta = 2.5$, depending on the value of the transverse momenta of the produced gluon, the relative weight of the non-eikonal corrections can vary roughly between 15% and 2%. These results confirm our analytical predictions for the importance of the non-eikonal corrections in certain kinematic regions.

5.3 Double inclusive gluon production

In this section we consider the case of double inclusive gluon production in the Glasma Graph approximation beyond the eikonal approximation. Our strategy for this section is the same as the calculation performed for single inclusive gluon production in the previous section. Namely, we start with the double inclusive gluon production cross section that takes into account multiple scatterings in the target in [40]. Then, we consider the dilute target limit of this expression which effectively corresponds to the Glasma Graph approximation by expanding the dipole and quadrupole operators in powers of the background field of the target. Finally, we introduce the finite longitudinal width of the target effects via the non-eikonal Lipatov vertex Eq. (5.20) and the generalized MV model for the two field correlator Eq. (5.27) in the expanded expression of the double inclusive gluon production cross section.

The general expression for the production of two gluons with pseudorapidities η_1 and η_2, and with transverse momenta $\mathbf{k}_1$ and $\mathbf{k}_2$ reads

$$\begin{aligned}\frac{d^2N}{d^2\mathbf{k}_1 d\eta_1 d^2\mathbf{k}_2 d\eta_2} = \frac{g^4}{\pi^2(2\pi)^8}\int_{\mathbf{z}_1\bar{\mathbf{z}}_1\mathbf{z}_2\bar{\mathbf{z}}_2} e^{i\mathbf{k}_1\cdot(\mathbf{z}_1-\bar{\mathbf{z}}_1)+i\mathbf{k}_2\cdot(\bar{\mathbf{z}}_2-\mathbf{y}_2)}\int_{\mathbf{x}_1\mathbf{x}_2\mathbf{y}_1\mathbf{y}_2}\left\langle\rho^{a_1}_{\mathbf{x}_1}\rho^{a_2}_{\mathbf{x}_2}\rho^{b_1}_{\mathbf{y}_1}\rho^{b_2}_{\mathbf{y}_2}\right\rangle_p \\ \times\ f^i(\mathbf{x}_1-\mathbf{z}_1)f^i(\bar{\mathbf{z}}_1-\mathbf{y}_1)f^j(\mathbf{x}_2-\mathbf{z}_2)f^j(\bar{\mathbf{z}}_2-\mathbf{y}_2) \\ \times\ \left\langle\left[U_{\mathbf{z}_1}-U_{\mathbf{x}_1}\right]^{a_1c}\left[U^\dagger_{\bar{\mathbf{z}}_1}-U^\dagger_{\mathbf{y}_1}\right]^{cb_1}\left[U_{\mathbf{z}_2}-U_{\mathbf{x}_2}\right]^{a_2d}\left[U^\dagger_{\bar{\mathbf{z}}_2}-U^\dagger_{\mathbf{y}_2}\right]^{db_2}\right\rangle_T. \quad (5.34)\end{aligned}$$

In the dilute limit of the target, or equivalently in the Glasma graph approximation, the Wilson lines are expanded in powers of the background field of the target as in Eq. (5.22). Therefore, the double inclusive gluon spectrum can be written as

$$\begin{aligned}\left.\frac{d^2N}{d^2\mathbf{k}_1 d\eta_1 d^2\mathbf{k}_2 d\eta_2}\right|_{\text{dilute}} = \frac{g^8}{\pi^2(2\pi)^8}\int_{\mathbf{z}_1\bar{\mathbf{z}}_1\mathbf{z}_2\bar{\mathbf{z}}_2} e^{i\mathbf{k}_1\cdot(\mathbf{z}_1-\bar{\mathbf{z}}_1)+i\mathbf{k}_2\cdot(\bar{\mathbf{z}}_2-\mathbf{y}_2)}\int_{\mathbf{x}_1\mathbf{x}_2\mathbf{y}_1\mathbf{y}_2}\left\langle\rho^{a_1}_{\mathbf{x}_1}\rho^{a_2}_{\mathbf{x}_2}\rho^{b_1}_{\mathbf{y}_1}\rho^{b_2}_{\mathbf{y}_2}\right\rangle_p \\ \times\ f^i(\mathbf{x}_1-\mathbf{z}_1)f^i(\bar{\mathbf{z}}_1-\mathbf{y}_1)f^j(\mathbf{x}_2-\mathbf{z}_2)f^j(\bar{\mathbf{z}}_2-\mathbf{y}_2)\end{aligned}$$

$$\times \int_{x_1^+,\ldots,x_4^+} \int_{\mathbf{q}_1,\ldots,\mathbf{q}_4} \left\langle A_a^-(x_1^+,\mathbf{q}_1) A_b^-(x_2^+,\mathbf{q}_2) A_c^-(x_3^+,\mathbf{q}_3) A_d^-(x_4,\mathbf{q}_4) \right\rangle_T (T^a T^b)_{a_1 b_1} (T^c T^d)_{a_2 b_2}$$
$$\times \left[e^{-i\mathbf{q}_1\cdot\mathbf{z}_1} - e^{-i\mathbf{q}_1\cdot\mathbf{x}_1}\right]\left[e^{i\mathbf{q}_2\cdot\bar{\mathbf{z}}_1} - e^{i\mathbf{q}_2\cdot\mathbf{y}_1}\right]\left[e^{-i\mathbf{q}_3\cdot\mathbf{z}_2} - e^{-i\mathbf{q}_3\cdot\mathbf{x}_2}\right]\left[e^{i\mathbf{q}_4\cdot\bar{\mathbf{z}}_2} - e^{i\mathbf{q}_4\cdot\mathbf{y}_2}\right]. \quad (5.35)$$

Let us now perform the averaging of the double inclusive production cross section with respect to the color charge densities of the projectile. Since we are using a generalized MV model, the average of any product of the color charge densities factorize into products of all possible Wick contractions:

$$\left\langle \rho^{a_1}_{\mathbf{x}_1} \rho^{a_2}_{\mathbf{x}_2} \rho^{b_1}_{\mathbf{y}_1} \rho^{b_2}_{\mathbf{y}_2} \right\rangle_p$$
$$= \left\langle \rho^{a_1}_{\mathbf{x}_1} \rho^{a_2}_{\mathbf{x}_2} \right\rangle_p \left\langle \rho^{b_1}_{\mathbf{y}_1} \rho^{b_2}_{\mathbf{y}_2} \right\rangle_p + \left\langle \rho^{a_1}_{\mathbf{x}_1} \rho^{b_1}_{\mathbf{y}_1} \right\rangle_p \left\langle \rho^{a_2}_{\mathbf{x}_2} \rho^{b_2}_{\mathbf{y}_2} \right\rangle_p + \left\langle \rho^{a_1}_{\mathbf{x}_1} \rho^{b_2}_{\mathbf{y}_2} \right\rangle_p \left\langle \rho^{a_2}_{\mathbf{x}_2} \rho^{b_1}_{\mathbf{y}_1} \right\rangle_p. \quad (5.36)$$

For the correlator of two color charge densities, we use the generalized MV model introduced in Eq. (5.24). After implementing Eq. (5.36), the double inclusive gluon spectra can be written as a sum of three contributions:

$$\left.\frac{d^2N}{d^2\mathbf{k}_1 d\eta_1 d^2\mathbf{k}_2 d\eta_2}\right|_{\text{dilute}} = \frac{g^8}{\pi^2(2\pi)^8} \int_{\mathbf{z}_1\bar{\mathbf{z}}_1\mathbf{z}_2\bar{\mathbf{z}}_2} e^{i\mathbf{k}_1\cdot(\mathbf{z}_1-\bar{\mathbf{z}}_1)+i\mathbf{k}_2\cdot(\bar{\mathbf{z}}_2-y_2)}$$
$$\times \int_{\mathbf{x}_1\mathbf{x}_2\mathbf{y}_1\mathbf{y}_2} f^i(\mathbf{x}_1-\mathbf{z}_1) f^i(\bar{\mathbf{z}}_1-\mathbf{y}_1) f^j(\mathbf{x}_2-\mathbf{z}_2) f^j(\bar{\mathbf{z}}_2-\mathbf{y}_2) \left\{ \mathrm{Tr}\left[T^a T^b T^d T^c\right] \mu^2(\mathbf{x}_1,\mathbf{x}_2)\mu^2(\mathbf{y}_1,\mathbf{y}_2) \right.$$
$$\left. + \mathrm{Tr}\left[T^a T^b\right]\mathrm{Tr}\left[T^c T^d\right]\mu^2(\mathbf{x}_1,\mathbf{y}_1)\mu^2(\mathbf{x}_2,\mathbf{y}_2) + \mathrm{Tr}\left[T^a T^b T^c T^d\right]\mu^2(\mathbf{x}_1,\mathbf{y}_2)\mu^2(\mathbf{x}_2,\mathbf{y}_1) \right\}$$
$$\times \int_{x_1^+,\ldots,x_4^+} \int_{\mathbf{q}_1,\ldots,\mathbf{q}_4} \left\langle A_a^-(x_1^+,\mathbf{q}_1) A_b^-(x_2^+,\mathbf{q}_2) A_c^-(x_3^+,\mathbf{q}_3) A_d^-(x_4,\mathbf{q}_4) \right\rangle_T$$
$$\times \left[e^{-i\mathbf{q}_1\cdot\mathbf{z}_1} - e^{-i\mathbf{q}_1\cdot\mathbf{x}_1}\right]\left[e^{i\mathbf{q}_2\cdot\bar{\mathbf{z}}_1} - e^{i\mathbf{q}_2\cdot\mathbf{y}_1}\right]\left[e^{-i\mathbf{q}_3\cdot\mathbf{z}_2} - e^{-i\mathbf{q}_3\cdot\mathbf{x}_2}\right]\left[e^{i\mathbf{q}_4\cdot\bar{\mathbf{z}}_2} - e^{i\mathbf{q}_4\cdot\mathbf{y}_2}\right]. \quad (5.37)$$

In order to preserve the consistency of the notations introduced for different contributions in [40], here after we refer to the first contribution as Type A, the second one as Type B and the last one as Type C, in Eq. (5.37).

Let us focus on Type A contributions to the dilute limit of the double inclusive gluon production cross section and adopt the same procedure applied in single inclusive gluon production in order to incorporate the non-eikonal effects due to the finite longitudinal thickness of the target. The same procedure and arguments hold for the calculation of Type B and Type C contributions. After integrating over the transverse coordinates, the Type A contribution can be written as

$$\left.\frac{d^2N^{\text{Type A}}}{d^2\mathbf{k}_1 d\eta_1 d^2\mathbf{k}_2 d\eta_2}\right|_{\text{dilute}} = \frac{g^8}{\pi^2(2\pi)^4}\mathrm{Tr}\left[T^a T^b T^d T^c\right] \int_{x_1^+,\ldots,x_4^+} \int_{\mathbf{q}_1,\ldots,\mathbf{q}_4}$$
$$\times \left\langle A_a^-(x_1^+,\mathbf{q}_1) A_b^-(x_2^+,\mathbf{q}_2) A_c^-(x_3^+,\mathbf{q}_3) A_d^-(x_4,\mathbf{q}_4) \right\rangle_T$$
$$\times \mu^2\left[\mathbf{k}_1-\mathbf{q}_1,\mathbf{k}_2+\mathbf{q}_4\right] \mu^2\left[\mathbf{q}_2-\mathbf{k}_1,-\mathbf{k}_2-\mathbf{q}_3\right]$$
$$\times L^i(\mathbf{k}_1,\mathbf{q}_1) L^i(\mathbf{k}_1,\mathbf{q}_2)\, L^j(\mathbf{k}_2,-\mathbf{q}_3) L^j(\mathbf{k}_2,-\mathbf{q}_4). \quad (5.38)$$

Moreover, we can factorize the average of the color fields of the target into all possible Wick contractions and write it in the following factorized way:

$$\left\langle A_a^-(x_1^+,\mathbf{q}_1) A_b^-(x_2^+,\mathbf{q}_2) A_c^-(x_3^+,\mathbf{q}_3) A_d^-(x_4,\mathbf{q}_4) \right\rangle_T$$

$$
\begin{aligned}
&= \Big\langle A_a^-(x_1^+,\mathbf{q}_1)A_b^-(x_2^+,\mathbf{q}_2)\Big\rangle_T \Big\langle A_c^-(x_3^+,\mathbf{q}_3)A_d^-(x_4,\mathbf{q}_4)\Big\rangle_T \\
&+ \Big\langle A_a^-(x_1^+,\mathbf{q}_1)A_d^-(x_4,\mathbf{q}_4)\Big\rangle_T \Big\langle A_c^-(x_3^+,\mathbf{q}_3)A_b^-(x_2^+,\mathbf{q}_2)\Big\rangle_T \\
&+ \Big\langle A_a^-(x_1^+,\mathbf{q}_1)A_c^-(x_3^+,\mathbf{q}_3)\Big\rangle_T \Big\langle A_b^-(x_2^+,\mathbf{q}_2)A_d^-(x_4,\mathbf{q}_4)\Big\rangle_T . \quad (5.39)
\end{aligned}
$$

We can now incorporate the non-eikonal effects due to the finite width of the target. This is achieved by replacing the Lipatov vertices by the non-eikonal ones and using the generalized MV model for the correlator of two target fields as defined in Eq. (5.27). After implementing these two modifications, the Type A contribution to the dilute limit of the non-eikonal double inclusive gluon production cross section reads

$$
\begin{aligned}
\frac{d^2N^{\text{Type A}}}{d^2\mathbf{k}_1 d\eta_1\, d^2\mathbf{k}_2\eta_2}\bigg|^{\text{NE}}_{\text{dilute}} &= \frac{g^{12}}{\pi^2(2\pi)^4} C_A^2\,(N_c^2-1)\int_{\mathbf{q}_1,\mathbf{q}_2} \big|a(\mathbf{q}_1)\big|^2\,\big|a(\mathbf{q}_2)\big|^2 \int_{x_1^+,\ldots,x_4^+} e^{ik_1^-(x_1^+-x_2^+)+ik_2^-(x_4^+-x_3^+)} \\
\times\ \Big\{ &\mu^2\big[\mathbf{k}_1-\mathbf{q}_1,\mathbf{k}_2-\mathbf{q}_2\big]\,\mu^2\big[\mathbf{q}_1-\mathbf{k}_1,\mathbf{q}_2-\mathbf{k}_2\big]\,L^i(\mathbf{k}_1,\mathbf{q}_1)L^i(\mathbf{k}_1,\mathbf{q}_1)\,L^j(\mathbf{k}_2,\mathbf{q}_2)L^j(\mathbf{k}_2,\mathbf{q}_2) \\
&\qquad\times \frac{1}{2\lambda^+} n(x_1^+)\Theta\Big(\lambda^+-|x_1^+-x_2^+|\Big)\,\frac{1}{2\lambda^+} n(x_3^+)\Theta\Big(\lambda^+-|x_3^+-x_4^+|\Big) \\
+\ &\mu^2\big[\mathbf{k}_1-\mathbf{q}_1,\mathbf{k}_2+\mathbf{q}_1\big]\,\mu^2\big[\mathbf{q}_2-\mathbf{k}_1,-\mathbf{k}_2-\mathbf{q}_2\big]\,L^i(\mathbf{k}_1,\mathbf{q}_1)L^i(\mathbf{k}_1,\mathbf{q}_2)\,L^j(\mathbf{k}_2,-\mathbf{q}_2)L^j(\mathbf{k}_2,-\mathbf{q}_1) \\
&\qquad\times \frac{1}{2\lambda^+} n(x_1^+)\Theta\Big(\lambda^+-|x_1^+-x_4^+|\Big)\,\frac{1}{2\lambda^+} n(x_2^+)\Theta\Big(\lambda^+-|x_2^+-x_3^+|\Big) \\
+\ &\frac{1}{2}\mu^2\big[\mathbf{k}_1-\mathbf{q}_1,\mathbf{k}_2-\mathbf{q}_2\big]\,\mu^2\big[\mathbf{q}_2-\mathbf{k}_1,\mathbf{q}_1-\mathbf{k}_2\big]\,L^i(\mathbf{k}_1,\mathbf{q}_1)L^i(\mathbf{k}_1,\mathbf{q}_2)\,L^j(\mathbf{k}_2,\mathbf{q}_1)L^j(\mathbf{k}_2,\mathbf{q}_2) \\
&\qquad\times \frac{1}{2\lambda^+} n(x_1^+)\Theta\Big(\lambda^+-|x_1^+-x_3^+|\Big)\,\frac{1}{2\lambda^+} n(x_2^+)\Theta\Big(\lambda^+-|x_2^+-x_4^+|\Big)\Big\}, \quad (5.40)
\end{aligned}
$$

where we have used the following color algebra identities

$$
\mathrm{Tr}\big[T^aT^aT^bT^b\big] = C_A^2\,(N_c^2-1), \quad (5.41)
$$

$$
\mathrm{Tr}\big[T^aT^bT^aT^b\big] = \frac{1}{2}\,C_A^2\,(N_c^2-1), \quad (5.42)
$$

with $C_A = N_c$ the quadratic Casimir in the adjoint representation. Now, the integral over the longitudinal coordinates can be performed in the same way as in the single inclusive gluon production. After using the Θ-functions to determine the limits of the integrals, a straightforward integration gives

$$
\begin{aligned}
\frac{d^2N^{\text{Type A}}}{d^2\mathbf{k}_1 d\eta_1\, d^2\mathbf{k}_2\eta_2}\bigg|^{\text{NE}}_{\text{dilute}} &= \frac{g^{12}N_c^2\,(N_c^2-1)}{\pi^2(2\pi)^4}\int_{\mathbf{q}_1,\mathbf{q}_2} \big|a(\mathbf{q}_1)\big|^2\,\big|a(\mathbf{q}_2)\big|^2 \mathcal{G}_1^{\text{NE}}(k_1^-;\lambda^+)\,\mathcal{G}_1^{\text{NE}}(k_2^-;\lambda^+) \\
\times\ \Big\{ &\mu^2\big[\mathbf{k}_1-\mathbf{q}_1,\mathbf{k}_2-\mathbf{q}_2\big]\,\mu^2\big[\mathbf{q}_1-\mathbf{k}_1,\mathbf{q}_2-\mathbf{k}_2\big]\,L^i(\mathbf{k}_1,\mathbf{q}_1)L^i(\mathbf{k}_1,\mathbf{q}_1)\,L^j(\mathbf{k}_2,\mathbf{q}_2)L^j(\mathbf{k}_2,\mathbf{q}_2) \\
+\ &\mu^2\big[\mathbf{k}_1-\mathbf{q}_1,\mathbf{k}_2+\mathbf{q}_1\big]\,\mu^2\big[\mathbf{q}_2-\mathbf{k}_1,-\mathbf{k}_2-\mathbf{q}_2\big]\,L^i(\mathbf{k}_1.\mathbf{q}_1)L^i(\mathbf{k}_1,\mathbf{q}_2)\,L^j(\mathbf{k}_2,-\mathbf{q}_2)L^j(\mathbf{k}_2,-\mathbf{q}_1) \\
&\qquad\qquad\times \mathcal{G}_2^{\text{NE}}(k_1^-,-k_2^-;L^+) \\
+\ &\mu^2\big[\mathbf{k}_1-\mathbf{q}_1,\mathbf{k}_2-\mathbf{q}_2\big]\,\mu^2\big[\mathbf{q}_2-\mathbf{k}_1,\mathbf{q}_1-\mathbf{k}_2\big]\,L^i(\mathbf{k}_1,\mathbf{q}_1)L^i(\mathbf{k}_2,\mathbf{q}_2)\,L^j(\mathbf{k}_2,\mathbf{q}_1)L^j(\mathbf{k}_2,\mathbf{q}_2) \\
&\qquad\qquad\times \frac{1}{2}\mathcal{G}_2^{\text{NE}}(k_1^-,k_2^-;L^+)\Big\} \quad (5.43)
\end{aligned}
$$

where, on top of the function $\mathcal{G}_1^{\mathrm{NE}}(k^-;\lambda^+)$ that takes into account the non-eikonal effects defined in Eq. (5.31), we have introduced a new function $\mathcal{G}_2^{\mathrm{NE}}(k_1^-,k_2^-;L^+)$ that also accounts for the non-eikonal effects in the dilute target limit of the double inclusive gluon production cross section and reads

$$\mathcal{G}_2^{\mathrm{NE}}(k_1^-,k_2^-;L^+)=\left\{\frac{2}{\left(k_1^--k_2^-\right)L^+}\sin\left[\frac{\left(k_1^--k_2^-\right)}{2}L^+\right]\right\}^2. \tag{5.44}$$

Again, this function goes to 1 when we consider the shockwave (eikonal) limit $L^+\to 0$.

The same procedure can be adopted to calculate the Type B and Type C contributions to the dilute target limit of the non-eikonal double inclusive gluon production cross section. The results read

$$\begin{aligned}\left.\frac{d^2N^{\mathrm{Type\,B}}}{d^2\mathbf{k}_1d\eta_1\,d^2\mathbf{k}_2\eta_2}\right|^{\mathrm{NE}}_{\mathrm{dilute}}&=\frac{g^{12}N_c^2\left(N_c^2-1\right)}{\pi^2(2\pi)^4}\int_{\mathbf{q}_1,\mathbf{q}_2}\left|a(\mathbf{q}_1)\right|^2\left|a(\mathbf{q}_2)\right|^2\mathcal{G}_1^{\mathrm{NE}}(k_1^-;\lambda^+)\,\mathcal{G}_1^{\mathrm{NE}}(k_2^-;\lambda^+)\\
&\times\Big\{\left(N_c^2-1\right)\mu^2\left[\mathbf{k}_1-\mathbf{q}_1,\mathbf{q}_1-\mathbf{k}_1\right]\mu^2\left[\mathbf{k}_2-\mathbf{q}_2,\mathbf{q}_2-\mathbf{k}_2\right]L^i(\mathbf{k}_1,\mathbf{q}_1)L^i(\mathbf{k}_1,\mathbf{q}_1)\,L^j(\mathbf{k}_2,\mathbf{q}_2)L^j(\mathbf{k}_2,\mathbf{q}_2)\\
&+\mu^2\left[\mathbf{k}_1-\mathbf{q}_1,\mathbf{q}_2-\mathbf{k}_1\right]\mu^2\left[\mathbf{k}_2-\mathbf{q}_2,\mathbf{q}_1-\mathbf{k}_2\right]L^i(\mathbf{k}_1,\mathbf{q}_1)L^i(\mathbf{k}_1,\mathbf{q}_2)\,L^j(\mathbf{k}_2,\mathbf{q}_2)L^j(\mathbf{k}_2,\mathbf{q}_1)\\
&\qquad\times\mathcal{G}_2^{\mathrm{NE}}(k_1^-,k_2^-;L^+)\\
&+\mu^2\left[\mathbf{k}_1-\mathbf{q}_1,\mathbf{q}_2-\mathbf{k}_1\right]\mu^2\left[\mathbf{k}_2+\mathbf{q}_1,-\mathbf{k}_2-\mathbf{q}_2\right]L^i(\mathbf{k}_1,\mathbf{q}_1)L^i(\mathbf{k}_1,\mathbf{q}_2)\,L^j(\mathbf{k}_2,-\mathbf{q}_1)L^j(\mathbf{k}_2,-\mathbf{q}_2)\\
&\qquad\times\mathcal{G}_2^{\mathrm{NE}}(k_1^-,-k_2^-;L^+)\Big\},\end{aligned} \tag{5.45}$$

and

$$\begin{aligned}\left.\frac{d^2N^{\mathrm{Type\,C}}}{d^2\mathbf{k}_1d\eta_1d^2\mathbf{k}_2d\eta_2}\right|^{\mathrm{NE}}_{\mathrm{dilute}}&=\frac{g^{12}N_c^2\left(N_c^2-1\right)}{\pi^2(2\pi)^4}\int_{\mathbf{q}_1,\mathbf{q}_2}\left|a(\mathbf{q}_1)\right|^2\left|a(\mathbf{q}_2)\right|^2\mathcal{G}_1^{\mathrm{NE}}(k_1^-;\lambda^+)\,\mathcal{G}_1^{\mathrm{NE}}(k_2^-;\lambda^+)\\
&\times\Big\{\mu^2\left[\mathbf{k}_1-\mathbf{q}_1,\mathbf{q}_2-\mathbf{k}_1\right]\mu^2\left[\mathbf{k}_2-\mathbf{q}_2,\mathbf{q}_1-\mathbf{k}_2\right]L^i(\mathbf{k}_1,\mathbf{q}_1)L^i(\mathbf{k}_1,\mathbf{q}_1)\,L^j(\mathbf{k}_2,\mathbf{q}_2)L^j(\mathbf{k}_2,\mathbf{q}_2)\\
&+\mu^2\left[\mathbf{k}_1-\mathbf{q}_1,\mathbf{q}_1-\mathbf{k}_2\right]\mu^2\left[\mathbf{k}_2-\mathbf{q}_2,\mathbf{q}_2-\mathbf{k}_1\right]L^i(\mathbf{k}_1,\mathbf{q}_1)L^i(\mathbf{k}_1,\mathbf{q}_2)\,L^j(\mathbf{k}_2,\mathbf{q}_1)L^j(\mathbf{k}_2,\mathbf{q}_2)\\
&\qquad\times\mathcal{G}_2^{\mathrm{NE}}(k_1^-,k_2^-;L^+)\\
&+\mu^2\left[\mathbf{k}_1-\mathbf{q}_1,-\mathbf{k}_2-\mathbf{q}_2\right]\mu^2\left[\mathbf{k}_2+\mathbf{q}_1,\mathbf{q}_2-\mathbf{k}_1\right]L^i(\mathbf{k}_1,\mathbf{q}_1)L^i(\mathbf{k}_1,\mathbf{q}_2)\,L^j(\mathbf{k}_2,-\mathbf{q}_1)L^j(\mathbf{k}_2,-\mathbf{q}_2)\\
&\qquad\times\frac{1}{2}\mathcal{G}_2^{\mathrm{NE}}(k_1^-,-k_2^-;L^+)\Big\}.\end{aligned} \tag{5.46}$$

Finally, we can add the three contributions Eqs. (5.43), (5.45) and (5.46) and organize the full result of the dilute limit of the non-eikonal double inclusive gluon production cross section as

$$\begin{aligned}\left.\frac{d^2N}{d^2\mathbf{k}_1d\eta_1d^2\mathbf{k}_2d\eta_2}\right|^{\mathrm{NE}}_{\mathrm{dilute}}=&\frac{g^{12}N_c^2\left(N_c^2-1\right)}{\pi^2(2\pi)^4}\int_{\mathbf{q}_1,\mathbf{q}_2}\left|a(\mathbf{q}_1)\right|^2\left|a(\mathbf{q}_2)\right|^2\mathcal{G}_1^{\mathrm{NE}}(k_1^-;\lambda^+)\\
&\times\mathcal{G}_1^{\mathrm{NE}}(k_2^-;\lambda^+)\left\{I_{2\mathrm{tr}}^{(0)}+\frac{1}{N_c^2-1}\left[I_{2\mathrm{tr}}^{(1)}+I_{1\mathrm{tr}}^{(1)}\right]\right\},\end{aligned} \tag{5.47}$$

where the subscripts denote the single trace terms ($I^{(i)}_{1\text{tr}}$) or the double trace term ($I^{(i)}_{2\text{tr}}$) in the double inclusive gluon production cross section given in Eq. (5.37). The explicit expressions for these terms read

$$I^{(0)}_{2\text{tr}} = \mu^2\big[\mathbf{k}_1-\mathbf{q}_1,\mathbf{q}_1-\mathbf{k}_1\big]\,\mu^2\big[\mathbf{k}_2-\mathbf{q}_2,\mathbf{q}_2-\mathbf{k}_2\big] \times L^i(\mathbf{k}_1,\mathbf{q}_1)L^i(\mathbf{k}_1,\mathbf{q}_1)\,L^j(\mathbf{k}_2,\mathbf{q}_2)L^j(\mathbf{k}_2,\mathbf{q}_2), \quad (5.48)$$

$$I^{(1)}_{2\text{tr}} = \Big\{\mathcal{G}_2^{\text{NE}}(k_1^-,k_2^-;L^+)\mu^2\big[\mathbf{k}_1-\mathbf{q}_1,\mathbf{q}_2-\mathbf{k}_1\big]\,\mu^2\big[\mathbf{k}_2-\mathbf{q}_2,\mathbf{q}_1-\mathbf{k}_2\big] \times\; L^i(\mathbf{k}_1,\mathbf{q}_1)L^i(\mathbf{k}_1,\mathbf{q}_2)\,L^j(\mathbf{k}_2,\mathbf{q}_2)L^j(\mathbf{k}_2,\mathbf{q}_1)\Big\} + (\underline{k}_2\to-\underline{k}_2) \quad (5.49)$$

and, finally,

$$\begin{aligned} I^{(1)}_{1\text{t}} = \Big\{&\mu^2\big[\mathbf{k}_1-\mathbf{q}_1,\mathbf{q}_2-\mathbf{k}_2\big]\,\mu^2\big[\mathbf{k}_2-\mathbf{q}_2,\mathbf{q}_1-\mathbf{k}_1\big]\,L^i(\mathbf{k}_1,\mathbf{q}_1)L^i(\mathbf{k}_1,\mathbf{q}_1)\,L^j(\mathbf{k}_2,\mathbf{q}_2)L^j(\mathbf{k}_2,\mathbf{q}_2)\\ &+\;\mathcal{G}_2^{\text{NE}}(k_1^-,k_2^-;L^+)\Big(\mu^2\big[\mathbf{k}_1-\mathbf{q}_1,\mathbf{q}_1-\mathbf{k}_2\big]\,\mu^2\big[\mathbf{k}_2-\mathbf{q}_2,\mathbf{q}_2-\mathbf{k}_1\big]\\ &\qquad+\frac{1}{2}\mu^2\big[\mathbf{k}_1-\mathbf{q}_1,\mathbf{k}_2-\mathbf{q}_2\big]\,\mu^2\big[\mathbf{q}_2-\mathbf{k}_1,\mathbf{q}_1-\mathbf{k}_2\big]\Big)\\ &\times\; L^i(\mathbf{k}_1,\mathbf{q}_1)L^i(\mathbf{k}_1,\mathbf{q}_2)\,L^j(\mathbf{k}_2,\mathbf{q}_1)L^j(\mathbf{k}_2,\mathbf{q}_2)\Big\} + (\underline{k}_2\to-\underline{k}_2). \end{aligned} \quad (5.50)$$

Let us now identify the terms that appear in the dilute target limit of the non-eikonal double inclusive gluon production cross section. For this analysis, we follow the procedure introduced in [40]. The function $\mu^2(\mathbf{k},\mathbf{p})$ can be considered as function of the total transverse momenta and a function of the average transverse momenta:

$$\mu^2(\mathbf{k},\mathbf{p}) = T\left(\frac{|\mathbf{k}-\mathbf{p}|}{2}\right)F\big[|\mathbf{k}+\mathbf{p}|R\big], \quad (5.51)$$

where function T can be identified with a transverse momentum dependent distribution of the color charge densities, and function F is a soft form factor which is peaked when the argument of the function F vanishes and rapidly decreases when $|\mathbf{k}+\mathbf{p}|R>1$, with R the radius of the projectile. In our set up, the transverse momenta $\mathbf{k}_1-\mathbf{q}_1$ and $\mathbf{k}_2-\mathbf{q}_2$ are the momenta of the two gluons in the projectile, $\mathbf{k}_1$ and $\mathbf{k}_2$ are the momenta of the two gluons in the final state and the momenta $\mathbf{q}_1$ and $\mathbf{q}_2$ are the transverse momenta that are transferred from the target to the projectile during their interaction. In such a set up, the (forward/backward) Bose enhancement of the gluons in the projectile is identified by the form factor that is peaked around $(\mathbf{k}_1-\mathbf{q}_1)\mp(\mathbf{k}_2-\mathbf{q}_2)$, the (forward/backward) HBT correlations of the final state gluons are identified by the form factor that is peaked around $\mathbf{k}_1\mp\mathbf{k}_2$ and finally the (forward/backward) Bose enhancement of the gluons in the target is identified by the form factor that is peaked around $\mathbf{q}_1\mp\mathbf{q}_2$. We proceed to analyze them all:

- First of all, it is straightforward to realize that the first term in Eq. (5.47), whose explicit expression is given in Eq. (5.48), is nothing but the square of the single inclusive gluon emission probability. Therefore, this term is completely factorized and does not give any contribution to the correlated production.

- The second contribution to the non-eikonal double inclusive gluon production cross section is given in Eq. (5.49). This term is proportional to

$$\mu^2\big[\mathbf{k}_1-\mathbf{q}_1,\mathbf{q}_2-\mathbf{k}_1\big]\,\mu^2\big[\mathbf{k}_2-\mathbf{q}_2,\mathbf{q}_1-\mathbf{k}_2\big] = T\left[\mathbf{k}_1-\frac{(\mathbf{q}_1+\mathbf{q}_2)}{2}\right]T\left[\mathbf{k}_2-\frac{(\mathbf{q}_1+\mathbf{q}_2)}{2}\right]F^2\Big(\big|\mathbf{q}_1-\mathbf{q}_2\big|R\Big). \quad (5.52)$$

  The form factor F in Eq. (5.52) is strongly peaked when the transverse momenta transferred from the target are very close to each other. Therefore, the term defined in Eq. (5.49) is the term responsible for the Bose enhancement in the target wave function.

- Let us now consider the third contribution to the double inclusive gluon production cross section which is defined in Eq. (5.50). This contribution consists of three different terms:

  (i) The first term in this contribution is proportional to

$$\mu^2\big[\mathbf{k}_1-\mathbf{q}_1,\mathbf{q}_2-\mathbf{k}_2\big]\,\mu^2\big[\mathbf{k}_2-\mathbf{q}_2,\mathbf{q}_1-\mathbf{k}_1\big] = T^2\left[\frac{(\mathbf{k}_1-\mathbf{q}_1)}{2}+\frac{(\mathbf{k}_2-\mathbf{q}_2)}{2}\right]F^2\Big[\big|(\mathbf{k}_1-\mathbf{q}_1)-(\mathbf{k}_2-\mathbf{q}_2)\big|R\Big]. \quad (5.53)$$

  Since the transverse momenta $\mathbf{k}_1-\mathbf{q}_1$ and $\mathbf{k}_2-\mathbf{q}_2$ are the momenta of the two gluons in the projectile wave function and the form factor F is peaked around when the momenta of the two gluons in the projectile wave function are close to each other in this term, it is the Bose enhancement contribution in the projectile wave function.

  (ii) The second term in Eq. (5.50) is proportional to

$$\mu^2\big[\mathbf{k}_1-\mathbf{q}_1,\mathbf{q}_1-\mathbf{k}_2\big]\,\mu^2\big[\mathbf{k}_2-\mathbf{q}_2,\mathbf{q}_2-\mathbf{k}_1\big] = T\left[\frac{(\mathbf{k}_1+\mathbf{k}_2)}{2}-\mathbf{q}_1\right]T\left[\frac{(\mathbf{k}_1+\mathbf{k}_2)}{2}-\mathbf{q}_2\right]F^2\Big[\big|\mathbf{k}_1-\mathbf{k}_2\big|R\Big]. \quad (5.54)$$

  Now the form factor F is peaked for the transverse momenta of the two gluons in the final state is close to each other, so this term corresponds to the HBT contribution.

  (iii) The last term in Eq. (5.50) is proportional to

$$\mu^2\big[\mathbf{k}_1-\mathbf{q}_1,\mathbf{k}_2-\mathbf{q}_2\big]\,\mu^2\big[\mathbf{q}_2-\mathbf{k}_1,\mathbf{q}_1-\mathbf{k}_2\big] = T\left[\frac{(\mathbf{k}_1-\mathbf{q}_1)}{2}-\frac{(\mathbf{k}_2-\mathbf{q}_2)}{2}\right]T\left[\frac{(\mathbf{k}_2+\mathbf{q}_2)}{2}-\frac{(\mathbf{k}_1+\mathbf{q}_1)}{2}\right] \times F^2\Big[\big|(\mathbf{k}_1-\mathbf{q}_1)+(\mathbf{k}_2-\mathbf{q}_2)\big|R\Big]. \quad (5.55)$$

  In this term, the form factor is peaked for the transverse momenta of the two gluons in the projectile wave function are close and opposite to each other. Therefore, this term is a contribution to the backward peak of Bose enhancement of gluons in the projectile wave function.

Apart from the non-eikonal effects that are encoded in the functions $\mathcal{G}_1^{\rm NE}(k^-;\lambda^+)$ and $\mathcal{G}_2^{\rm NE}(k_1^-,k_2^-;L^+)$, the main difference between the dilute target limit of the double inclusive gluon production cross section calculated in this section and the double inclusive gluon production cross section derived in [40] is the N_c counting of some of the contributions. Our main result, Eq. (5.47), shows that apart from the uncorrelated contribution that is identified as the square of the single inclusive gluon production cross section, all terms that contribute to the correlated production come with the same N_c power. However, in [40], the Bose enhancement contribution of the gluons in the target and part of the Bose enhancement contribution of the gluons in the projectile have shown to be N_c-suppressed with respect to the rest of the terms. This is a well known consequence of the fact that some aspects of N_c counting are different in the dilute and dense limits [41, 42].

Let us comment on the function $\mathcal{G}_2^{\rm NE}(k_1^-,k_2^-;L^+)$, Eq. (5.44), which is one of the functions that encode the non-eikonal effects in the double inclusive gluon production in the dilute target limit. As it can be seen clearly from the final expression, Eq. (5.47) together with Eqs. (5.48) to (5.50), the mirror image of the terms that contribute to the correlated production of two gluons which is given by $(\underline{k}_2 \to -\underline{k}_2)$, is accompanied by $\mathcal{G}_2^{\rm NE}(k_1^-,-k_2^-;L^+)$. However, in certain kinematic regimes the behavior of $\mathcal{G}_2^{\rm NE}(k_1^-,k_2^-;L^+)$ differs completely from $\mathcal{G}_2^{\rm NE}(k_1^-,-k_2^-;L^+)$. Namely, in the kinematic region where $k_1^- \sim k_2^-$ we get

$$\mathcal{G}_2^{\rm NE}(k_1^-,k_2^-;L^+) \gg \mathcal{G}_2^{\rm NE}(k_1^-,-k_2^-;L^+) \tag{5.56}$$

which creates an asymmetry between the terms with $(\underline{k}_1,\underline{k}_2)$ and their partners with $(\underline{k}_2 \to -\underline{k}_2)$. This asymmetry created by the non-eikonal effects immediately reminds the asymmetry between the forward and backward peaks of the ridge structure observed in two particle production.

In order to see the size of this asymmetry we compare Eq. (5.47) with the eikonal expression computed in Section 3.2. The result for the 2-gluon spectrum is given in Fig. 5.7 in the two approaches, where for performing the numerical analysis we have taken $N_c = 3$, $m = 0.4$ GeV in Eq. (5.28), $\mu^2(\mathbf{k},\mathbf{q})$ is given by Eq. (4.6) where we have used $B_p = 6$ GeV^{-2} and we have regulated the infrared divergences in the Lipatov vertices by substituting the corresponding squared transverse momenta in the denominator by $\mathbf{q}^2 \to \mathbf{q}^2 + m_g^2$, where we have used the numerical value $m_g = 0.2$ GeV.

In Fig. 5.7 we plot the non-eikonal and eikonal double inclusive gluon spectra in arbitrary units as a function of the azimuthal angle between the two produced gluons $\Delta\phi$. We have taken $L^+ \sim 20A^{1/3}/\sqrt{s_{\rm NN}}$ (see the next section) with $A^{1/3} = 6$, i.e. a Lead nucleus, and $\sqrt{s_{\rm NN}} = 60$ GeV. On the other hand we have fixed the produced gluons to have pseudorapidities $\eta_1 = \eta_2 = 0.2$ and transverse momenta $|\mathbf{k}_1| = 1$ GeV and $|\mathbf{k}_2| = 1.1$ GeV. The goal of this plot is to illustrate the asymmetry generated by the non-eikonal corrections. Because of the asymmetry between the near- and away-side we expect existence of odd azimuthal harmonics in the non-eikonal 2-gluon spectra. For this reason in the next section we will study the azimuthal harmonics encoded in Eq. (5.47).

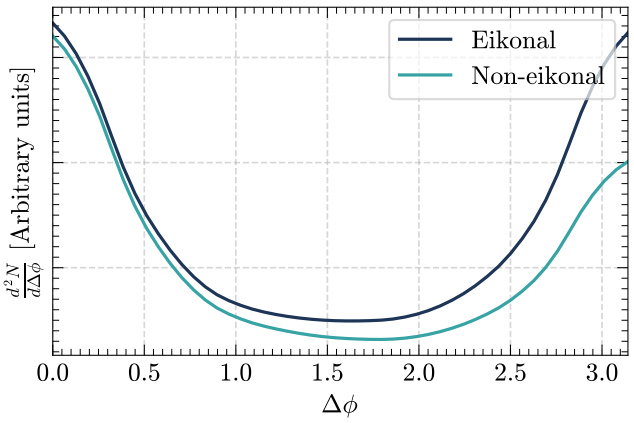

Figure 5.7.
The non-eikonal and eikonal double inclusive gluon spectra as a function of azimuthal angle between the two produced gluons $\Delta\phi$. We see that by including non-eikonal correction we break the symmetry between the near- and away-sides.

5.4 Odd azimuthal harmonics due to non-eikonal corrections

In the last section we have seen that by including the non-eikonal correction through the Lipatov vertices we break the accidental asymmetry $\mathbf{k}_2 \to -\mathbf{k}_2$ as seen in Fig. 5.7. The rupture of this symmetry implies that by including the non-eikonal correction we are able to generate odd azimuthal harmonics in contrast with the eikonal calculation performed in Chapter 4. For this reason in this section we will perform a numerical analysis around the azimuthal harmonics in order to see the strength of the odd azimuthal harmonics, in particular, of v_3.

The non-eikonal corrections to the 2-gluon spectra are described by the function given in Eq. (5.44). By noting that $k^- = \frac{1}{\sqrt{2}}|\mathbf{k}|e^{-\eta}$, we can rewrite Eq. (5.44) as

$$\mathcal{G}_2^{\mathrm{NE}}(k_1^-, k_2^-; L^+) = \left\{ \frac{\sqrt{2}\, e^{\eta_1}}{\left(k_1 - k_2\, e^{-\Delta\eta}\right) L^+} \sin\left[\frac{\left(k_1 - k_2\, e^{-\Delta\eta}\right)}{\sqrt{2}} e^{-\eta_1} L^+ \right] \right\}^2 , \tag{5.57}$$

where $\Delta\eta = \eta_2 - \eta_1$ and $k_i \equiv |\mathbf{k}_i|$. Thus the non-eikonal corrections will depend on three parameters: the transverse momenta, k_i, and the pseudorapidity, η_i, of the produced particles, and the Lorentz contracted longitudinal length of the target, L^+. On the other hand the longitudinal length of the target is related to center-of-mass energy of the collision per nucleon, $\sqrt{s\mathrm{NN}}$, and the mass number of the target, A, by $L^+ = \frac{L}{\gamma\sqrt{2}} \approx 2A^{1/3}/\gamma$ fm $\approx 10A^{1/3}/\gamma$ GeV^{-1}, $L \sim 2\sqrt{2}A^{1/3}$ fm is the length of the target in its rest frame and $\gamma \simeq \sqrt{s_{\mathrm{NN}}}/(2m_N)$ is the Lorentz factor in the center of mass frame. Thus the non-eikonal corrections will be sensible to the values of η_i, k_i, $\sqrt{s_{\mathrm{NN}}}$ and A. For simplicity we will fix $A^{1/3} = 6$, i.e. a Lead nucleus, in order to enhance as much as possible the effects of the non-eikonal corrections although, since our formalism is suitable for pp collisions, a more realistic value would be $A \sim 1$.

On the other hand, our result will also depend on the values of the Debye mass m, Eq. (5.28), on the infrared regulator, μ, of the Lipatov vertices and on the projectile's

area, B_p, as we are using Eq. (4.6) to define $\mu^2(\mathbf{k},\mathbf{q})$. Thus, in all the results presented in this section we will fix $m = 0.4$ GeV, $\mu = 0.2$ GeV and $B_p = 6$ GeV^{-2}. We have checked in [45] that our results are almost insensible to the variation of the regulators as long as $m \sim \mu \sim \Lambda_{\rm QCD}$.

We start by the dependence of the non-eikonal differential azimuthal harmonics, defined by 2-gluon spectrum in Eq. (5.47), with respect to the transverse momentum $p_\perp \equiv k_1$. The result is plotted in Fig. 5.8, where the differential harmonics was computed by using Eq. (3.40), and we have set $\eta_1 = 0.2$ and $\eta_2 = 0.4$. We see that at relatively small center-of-mass energy, i.e. at $\sqrt{s_{\rm NN}} = 50$ GeV, the odd azimuthal harmonics generated by the non-eikonal corrections is sizable while as we go to higher energies it takes lower values, being almost negligible at high energies. However, we should be careful since the x-value probed in the collision is $x \sim \frac{1\ \text{GeV}}{\sqrt{s_{\rm NN}}}$, thus $x \sim 2 \cdot 10^{-2}$ at $\sqrt{s_{\rm NN}} = 50$ GeV which is near the limit of applicability of the CGC.

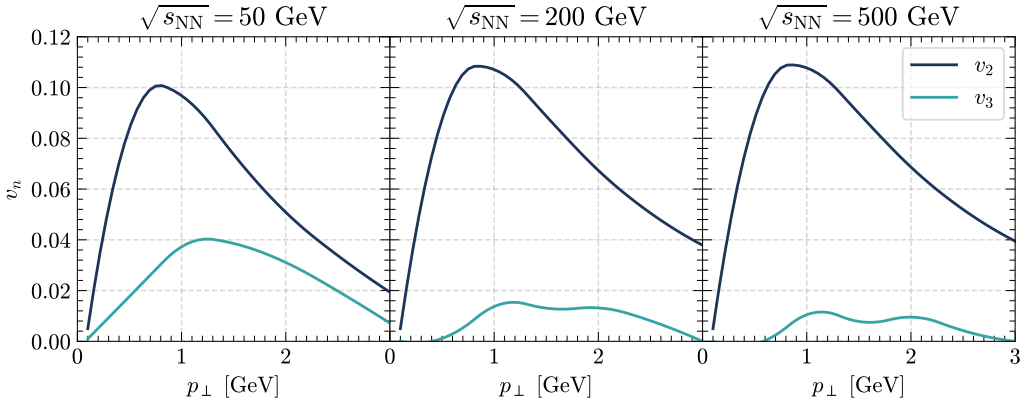

Figure 5.8.
Non-eikonal azimuthal harmonics in proton-proton collisions. For this plot we have take that pseudorapidities of the generated particles as $\eta_1 = 0.2$ and $\eta_2 = 0.4$.

In Fig. 5.9 (left) we have plotted the azimuthal harmonics against the center-of-mass at a fixed value of $p_\perp = 1$ GeV, $\eta_1 = 0.2$ and $\eta_2 = 0.4$. We see that the even azimuthal harmonics vary much slower with the center-of-mass energy compared with the v_3. Moreover, the size of v_3 generated by non-eikonal corrections is non-negligible even at relatively high values of $\sqrt{s_{\rm NN}}$. On the other hand, in the right side of Fig. 5.9 we plot the azimuthal harmonics against $\Delta\eta = \eta_2 - \eta_1$ at a fixed value of $\sqrt{s_{\rm NN}} = 50$ GeV, $p_\perp = 1$ GeV and $\eta_1 = 0$. We see, again, that v_2 does not change too much with $\Delta\eta$ while v_3 decrease the half of its initial value in 2 units of pseudorapidity.

Finally, in Fig. 5.10 we plot the 2-gluon spectrum given in Eq. (5.47) against $\Delta\eta$ and $\Delta\phi$ by fixing $\eta_1 = 0$, $k_1 = 1$ GeV, $k_2 = 1.2$ GeV and $\sqrt{s_{\rm NN}} = 50$ GeV. We see that the differences between the forward and backward peaks are visible up to 2 pseudorapidity units as we should expect from Fig. 5.9 (right).

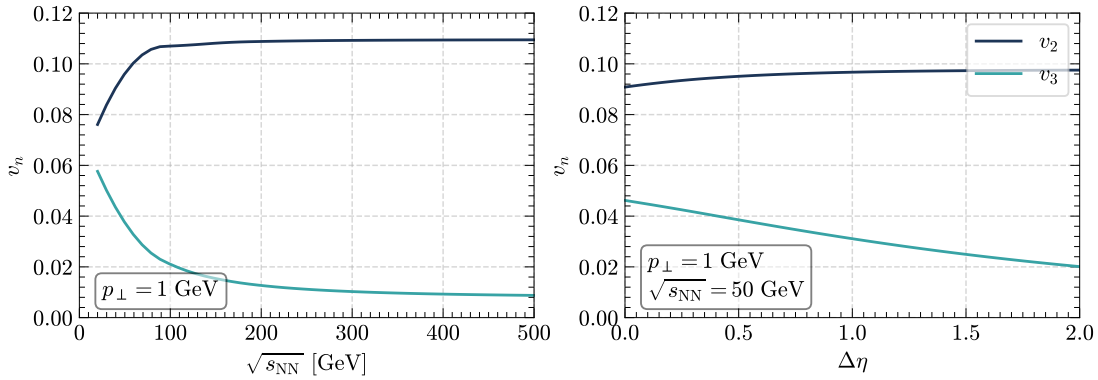

Figure 5.9.
Dependence of the azimuthal harmonics with both the center-of-mass energy of the collision (left) and the pseudorapidity (right). For the figure of the left we have fixed $p_\perp = 1$ GeV, $\eta_1 = 0.2$ and $\eta_2 = 0.4$, and for the one to the right we have fixed $\sqrt{s_{\rm NN}} = 50$ GeV, $p_\perp = 1$ GeV.

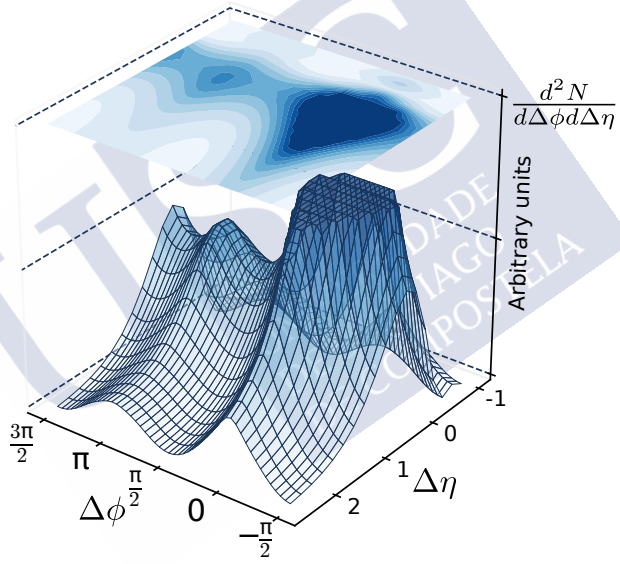

Figure 5.10.
Dependence of the 2-gluon spectrum, defined in Eq. (5.47), with respect to the azimuthal angle and the rapidity difference. In order to make the non-eikonal effects more visible, we have cut the near-side peak.

5.5 Triple inclusive gluon production

Let us now proceed with the triple inclusive gluon production cross section. The general expression for the production of three gluons, with transverse momenta $\mathbf{k}_1$, $\mathbf{k}_2$ and $\mathbf{k}_3$ and with pseudorapidities η_1, η_2 and η_3 in the dilute-dense set up reads [40]

$$\frac{d^3N}{d^2\mathbf{k}_1 d\eta_1 d^2\mathbf{k}_2 d\eta_2 d^2\mathbf{k}_3 d\eta_3} = \frac{g^{12}}{\pi^3(2\pi)^{12}} \int_{\mathbf{z}_1\mathbf{z}_2\mathbf{z}_3\bar{\mathbf{z}}_1\bar{\mathbf{z}}_2\bar{\mathbf{z}}_3} e^{i\mathbf{k}_1\cdot(\mathbf{z}_1-\bar{\mathbf{z}}_1)+i\mathbf{k}_2\cdot(\mathbf{z}_2-\bar{\mathbf{z}}_2)+i\mathbf{k}_3\cdot(\mathbf{z}_3-\bar{\mathbf{z}}_3)}$$

$$\times \int_{\mathbf{x}_1\mathbf{x}_2\mathbf{x}_3\mathbf{y}_1\mathbf{y}_2\mathbf{y}_3} f^i(\mathbf{x}_1-\mathbf{z}_1)f^i(\bar{\mathbf{z}}_1-\mathbf{y}_1)f^j(\mathbf{x}_2-\mathbf{z}_2)f^j(\bar{\mathbf{z}}_2-\mathbf{y}_2)f^k(\mathbf{x}_3-\mathbf{z}_3)f^k(\bar{\mathbf{z}}_3-\mathbf{y}_3)$$
$$\times \left\langle \left\{ \left[U_{\mathbf{z}_1}-U_{\mathbf{x}_1}\right]\left[U^\dagger_{\bar{\mathbf{z}}_1}-U^\dagger_{\mathbf{y}_1}\right]\right\}^{a_1b_1} \left\{ \left[U_{\mathbf{z}_2}-U_{\mathbf{x}_2}\right]\left[U^\dagger_{\bar{\mathbf{z}}_2}-U^\dagger_{\mathbf{y}_2}\right]\right\}^{a_2b_2} \right.$$
$$\left. \times \left\{ \left[U_{\mathbf{z}_3}-U_{\mathbf{x}_3}\right]\left[U^\dagger_{\bar{\mathbf{z}}_3}-U^\dagger_{\mathbf{y}_3}\right]\right\}^{a_3b_3} \right\rangle_T \left\langle \rho^{a_1}_{\mathbf{x}_1}\rho^{a_2}_{\mathbf{x}_2}\rho^{a_3}_{\mathbf{x}_3}\rho^{b_1}_{\mathbf{y}_1}\rho^{b_2}_{\mathbf{y}_2}\rho^{b_3}_{\mathbf{y}_3}\right\rangle_p . \tag{5.58}$$

After the manipulations described in Appendix D.1, we can organize the dilute target limit of the non-eikonal triple inclusive gluon production cross section according to the powers in the number of colors and the result reads

$$\left.\frac{d^3N}{d^2\mathbf{k}_1 d\eta_1 d^2\mathbf{k}_2 d\eta_2 d^2\mathbf{k}_3 d\eta_3}\right|^{\rm NE}_{\rm dilute} = \frac{g^{18}N_c^3\,(N_c^2-1)^3}{\pi^3(2\pi)^6}\int_{\mathbf{q}_1,\mathbf{q}_2,\mathbf{q}_3} \left|a(\mathbf{q}_1)\right|^2\left|a(\mathbf{q}_2)\right|^2\left|a(\mathbf{q}_3)\right|^2$$
$$\times \mathcal{G}_1(k_1^-;\lambda^+)\,\mathcal{G}_1(k_2^-;\lambda^+)\mathcal{G}_1(k_3^-;\lambda^+)\left\{ I^{(0)}_{\rm 3tr} + \frac{1}{(N_c^2-1)}\left[I^{(1)}_{\rm 3tr}+I^{(1)}_{\rm 2tr,1}+I^{(1)}_{\rm 2tr,2}\right]\right.$$
$$\left. + \frac{1}{(N_c^2-1)^2}\left[\left(I^{(2)}_{\rm 3tr,1}+I^{(2)}_{\rm 3tr,2}\right)+\left(I^{(2)}_{\rm 2tr,1}+I^{(2)}_{\rm 2tr,2}+I^{(2)}_{\rm 2tr,3}\right)+\left(I^{(2)}_{\rm 1tr,1}+I^{(2)}_{\rm 1tr,2}+I^{(2)}_{\rm 1tr,3}+I^{(2)}_{\rm 1tr,4}\right)\right]\right\}, \tag{5.59}$$

where the functions $I^{(k)}_{i\text{tr},j}$ can be found in Eqs. (D.14) to (D.20), Eqs. (D.22) to (D.31) and Eqs. (D.33) to (D.40). This is our final result for the dilute target limit of the non-eikonal triple inclusive gluon production cross section. Apart from the fact that this result accounts for the finite longitudinal width target effects through non-eikonal Lipatov vertices which leave their imprints in the functions $\mathcal{G}_i^{\rm NE}$ upon integration over the longitudinal coordinates, it is valid to all orders in the number of colors. It differs from the dilute target limit of the result calculated in [40]. The study performed in [40], while it is valid for the dense target limit, is truncated at $\mathcal{O}\big(1/(N_c^2-1)^3\big)$. This obviously affects the total number of terms in the final result. As we discuss in Appendix D.2, some of the N_c-suppressed terms that were discarded in [40], have been identified in our study and shown to establish some interference effects that were absent there.

5.6 Discussion and outlook

To conclude, we have derived the non-eikonal Lipatov vertex that takes into account the finite longitudinal width of the target to all orders. This result was conjectured in [39] after considering the first two corrections to the eikonal limit of the Lipatov vertex coming from the non-eikonal expansion of the gluon propagator obtained in [43, 44]. However, here we have presented a different derivation from first principles. Then, we have used the non-eikonal Lipatov vertex to study the single, double and triple inclusive gluon spectra in pp collisions at mid pseudorapidity. Our results are valid for dilute-dilute collisions since we consider the dilute target limit which, for double and triple inclusive gluon production, corresponds to the original Glasma Graph calculation with the exception that we take into account the non-eikonal corrections due to the finite longitudinal thickness of the target.

In the single inclusive gluon spectrum, we have shown that the non-eikonal corrections are encoded in function $\mathcal{G}_1^{\mathrm{NE}}(k^-, \lambda^+)$ that is defined in Eq. (5.31) with k^- being the light cone energy of the produced gluon and λ^+ the color correlation length along the longitudinal direction in the target. On the one hand, in the limit of $(k^-\lambda^+) \to 0$, our result reproduces the well known eikonal expression which is often referred to as the k_t-factorized formula in the CGC. On the other hand, by expanding our result to second order in $(k^-\lambda^+)$, we recover the result calculated in [39]. Our numerical results show that in the kinematic region where the non-eikonal effects are expected to be sizable, the relative importance of the non-eikonal corrections can vary from 2 to 15% with respect to the eikonal result. This shows that, depending on the kinematic region that one is interested in, the non-eikonal effects might very well be sizable.

We have also used the non-eikonal Lipatov vertex to calculate the double inclusive gluon spectrum for dilute-dilute scatterings. Adopting the same strategy that was introduced in [40], we have identified the terms that contribute to uncorrelated production, those that are responsible for Bose enhancement of the gluons in the projectile and in the target wave functions, and the terms that contribute to HBT interference effects. Our results agree with the results in [40] up to the N_c counting of the target Bose enhancement and part of the projectile Bose enhancement terms. However, it is known that this difference is a consequence of the fact that some aspects of N_c counting are different in the dilute and dense limits [40–42].

Moreover, including the non-eikonal corrections in the 2-gluon spectra has a direct consequence. On top of the function $\mathcal{G}_1^{\mathrm{NE}}(k_1^-; \lambda^+)$ that also exists in the single inclusive case, a new function $\mathcal{G}_2^{\mathrm{NE}}(k_1^-, k_2^-; L^+)$, defined in Eq. (5.44), appears which also encodes non-eikonal effects. The partners of the terms that contain $\mathcal{G}_2^{\mathrm{NE}}(k_1^-, k_2^-; L^+)$, obtained via $(\underline{k}_2 \to -\underline{k}_2)$, also appear in the double inclusive gluon production cross section but they are accompanied by $\mathcal{G}_2^{\mathrm{NE}}(k_1^-, -k_2^-; L^+)$. However, in some specific kinematic regions, namely when $k_1^- \sim k_2^-$, $\mathcal{G}_2^{\mathrm{NE}}(k_1^-, k_2^-; L^+) \gg \mathcal{G}_2^{\mathrm{NE}}(k_1^-, -k_2^-; L^+)$ which creates a sizable azimuthal asymmetry. We would like to emphasize that this asymmetry is absent in the eikonal limit. One can immediately realize that this asymmetry created by the non-eikonal corrections in the double inclusive gluon production indeed mimics the asymmetry between the forward and backward peaks in the ridge observed in the two particle correlations as we have illustrated in Fig. 5.7.

Then in Section 5.4, we have performed a numerical study of azimuthal anisotropies generated by the non-eikonal corrections which are summarized in Figs. 5.8 to 5.10. We saw that the odd azimuthal harmonics generated due to this asymmetry are sizable when the center-of-mass energy of the collisions is around $\sqrt{s_{\mathrm{NN}}} \sim 100$ GeV and therefore, in this case, including the non-eikonal corrections may be important for phenomenological studies of correlations in pp collisions. We have also seen that this effect is also sizable up to 2 units in the pseudorapidity difference. However, since this result is only applicable to pp collisions in the next section we will generalize it to proton-nucleus collisions, i.e. we will assume that the target is dense.

Finally, we have also considered the non-eikonal triple inclusive gluon production cross section in the dilute target limit. We have identified all the terms that appear in the final result. Compared to the work performed in [40], the main difference – apart from non-eikonal corrections that we have included in our study – is that we have included all terms while only the leading N_c ones were considered in [40]. This difference is again due to the

fact that N_c counting is different in the dilute and dense regimes. In our study, we have identified the terms that correlate all three gluons which originate from three-trace or double-trace contributions, which were absent in [40] since they are suppressed in powers of N_c in the dense target limit and therefore discarded there. Moreover, the non-eikonal effects enter through two new functions $\mathcal{G}_3(k_1^-, k_2^-, k_3^-; L^+)$ and $\mathcal{G}_4(k_1^-, k_2^-, k_3^-; L^+)$ that are defined in Eqs. (D.8) and (D.9) respectively, on top of the functions $\mathcal{G}_1(k^-; \lambda^+)$ and $\mathcal{G}_2(k_1^-, k_2^-; L^+)$ that already appeared in the double inclusive case. Obviously, in the limit of the vanishing L^+ these functions become one and provide the eikonal limit of the triple inclusive gluon production cross section in the dilute target limit.

USC
UNIVERSIDADE
DE SANTIAGO
DE COMPOSTELA

Chapter 6

Non-eikonal corrections in proton-nucleus collisions

Particle production in proton-nucleus (pA) collisions is commonly studied in the case in which a high energy dilute probe scatters off a dense color field. These processes, as stated in Chapter 2, are well described by the Color Glass Condensate effective theory where the scattering projectile probes the small-x gluons inside the target. This framework relays on the eikonal approximation, introduced in Section 2.3, where the collision is described by infinitely boosted partons that traverse a medium with infinitesimal width – a situation referred to as the shock-wave approximation. Since the sub-eikonal effects scale with the inverse of the beam energy, the approximation is well justified at the kinematics of the Large Hadron Collider (LHC) at CERN where pA collisions are performed at center-of-mass energies per nucleon, $\sqrt{s_{\rm NN}}$, of order 10^3 GeV and it is approximately accurate, with the corrections being of order a few percent [45, 46] (see Section 5.4), at top energies in the Relativistic Heavy Ion Collider (RHIC) where particles collide at $\sqrt{s_{\rm NN}} = 200$ GeV. However, with the upcoming Electron-Ion Collider (EIC) [213] where electron-nucleus collisions will be performed at center-of-mass energies from $\sim$ 20 GeV to $\sim$ 100 GeV these sub-eikonal contributions will become relevant. For this reason studies of including non-eikonal corrections, such as finite width effects, have experimented an intense growth in the last years. Besides, as an attempt to describe the spin physics, which is absent in the eikonal approximation, sub-eikonal corrections are introduced to the quark propagator by assuming a target with finite width [43, 44, 199, 204, 205]. In order to compute quark and anti-quark helicity TMDs and PDFs, modifications to the JIMWLK evolution equations to include helicity-dependent effects are introduced through the so-called *polarized Wilson lines* [195, 196, 214–216] which has been solved numerically recently [197, 217]. Moreover, studies by including the effects of a x^--dependent, i.e. dynamical, target field in the quark propagator are also being performed [203]. It has also been seen that by including finite width effects in double gluon production the so-called accidental symmetry, i.e. an artificial azimuthal symmetry that appears in the leading order multi-gluon spectrum within the CGC [171], is broken [45, 46]. Thus, finite width effects open a new window for explaining the away- and near-side asymmetry seen at small system collisions at RHIC, where non-eikonal corrections are still sizable, within the CGC framework.

Finite with effects appear naturally in the jet quenching framework, where in order to study the phenomenon of radiative energy loss one assumes that a high energy parton traverse a finite, dense and colored medium and loses its energy through gluon emissions [118]. The building blocks sensitive to the longitudinal extent of the target are the propagators of gluons and quarks in the background field, as reviewed in Section 2.2.

Thus, inspired by jet quenching calculations, the approach of this manuscript will be to include the non-eikonal effects to the multi-gluon spectrum through the scalar gluon propagator given in Eq. (2.30).

The main goal of this work is to generalize the results of [45, 46], where we have relaxed the shock-wave approximation and analyzed the effects of including non-eikonal corrections in multi-gluon production in proton-proton collisions, to the case in which one of the participants is dense, i.e. we study the finite width effects in multi-gluon production in the dilute-dense limit of the Color Glass Condensate framework which is suitable for pA collisions. This chapter is organized as follows. In Section 6.1 we present a short introduction of the framework, which is similar to jet quenching models, that will be used along this chapter. In Section 6.2 we generalize the results of Section 4.2, where we have computed the target averages of Wilson lines, to the non-eikonal case in which the Wilson line has to be substituted by the scalar gluon propagator. In Section 6.3 we compute the single gluon spectrum beyond the eikonal accuracy and we analyze the effects of the non-eikonal corrections in Section 6.3.1. In Section 6.3.2 we compare our results with the next-to-next-to-eikonal expansion performed in [43, 44] and we obtain a parameterization, within the Gaussian approximation, to the so-called colored dipole functions. In Section 6.4 we introduce the general framework for computing the multi-gluon spectrum for a generic number of gluons and in Section 6.4.1 we solve the case in which two gluons are produced and we study the dependence of the double gluon spectrum with the non-eikonal effects. Finally, in Section 6.5 we conclude our results.

6.1 Introduction

In Chapter 5 we have introduced the non-eikonal corrections by defining the non-eikonal Lipatov vertex in Eq. (5.20). However, the technique presented there consisted in using a generalization of the MV model field correlator that is non-local in the longitudinal direction and therefore it is only possible to be applied within the Glasma Graph approximation, i.e. an expansion of the Wilson lines in terms of the target field. For this reason, we will have to find another approach for including non-eikonal corrections in the dense limit of the target since, in this case, the Wilson lines cannot be expanded.

The formalism that will be used in this section was presented in Section 2.2. We assume that the projectile is described by a highly boosted source $\rho_p^a(\mathbf{x})$, i.e. eikonal, that interacts with the target that is described by a dense medium. This medium is defined through the target field $A_T^-(x^+,\mathbf{x})$ that has a finite support in the longitudinal direction in between 0 and L^+. As a result of the interaction of the projectile with the target a gluon is emitted before, after or inside the medium. The propagation of the produced gluon inside the medium is given by the scalar retarded propagator defined in Eq. (2.30) and reads

$$\mathcal{G}_{k^+}(x^+,\mathbf{x};y^+,\mathbf{y})=\int_{\mathbf{z}(y^+)=\mathbf{y}}^{\mathbf{z}(x^+)=\mathbf{x}}[\mathcal{D}\mathbf{z}(z^+)]\exp\left\{\frac{ik^+}{2}\int_{y^+}^{x^+}dz^+\dot{\mathbf{z}}^2(z^+)\right\}U(x^+,y^+;\mathbf{z}(z^+)). \tag{6.1}$$

This propagator describes a Brownian motion of the gluon in the transverse plane while it is inside the dense medium. On the other hand, the motion of the gluon outside the medium is described by the free scalar propagator defined in Eq. (2.31).

Therefore, the single gluon production amplitude is described by the sum of three terms depending if the gluon is emitted before, after or in between the interaction of the projectile source with the medium. The amplitude for producing a gluon with momentum $(k^+,\mathbf{k})$, color a and polarization λ was given in Eq. (2.37) and reads

$$\mathcal{M}_\lambda^a(k^+,\mathbf{k})=g\int\frac{d^2\mathbf{q}}{(2\pi)^2}\overline{\mathcal{M}}_\lambda^{ab}(k^+,\mathbf{k},\mathbf{q})\rho_p^b(\mathbf{q}), \tag{6.2}$$

with the so-called reduced matrix amplitude given by

$$\begin{aligned}\overline{\mathcal{M}}_\lambda^{ab}(k^+,\mathbf{k},\mathbf{q})=\epsilon_\perp^{\lambda i*}ie^{ik^-L^+}\Bigg\{&2\frac{\mathbf{k}^i}{\mathbf{k}^2}\int_{\mathbf{y}}e^{-i(\mathbf{k}-\mathbf{q})\cdot\mathbf{y}}U^{ab}(L^+,0,\mathbf{y})-2\frac{\mathbf{q}^i}{\mathbf{q}^2}\int_{\mathbf{y},\mathbf{x}}e^{i\mathbf{q}\cdot\mathbf{y}-i\mathbf{k}\cdot\mathbf{x}}\mathcal{G}_{k^+}^{ab}(L^+,\mathbf{x};0,\mathbf{y})\\&+\int_{\mathbf{x},\mathbf{y}}e^{i\mathbf{q}\cdot\mathbf{y}-i\mathbf{k}\cdot\mathbf{x}}\frac{1}{k^+}\int_0^{L^+}dy^+[\partial_{\mathbf{y}^i}\mathcal{G}_{k^+}^{ac}(L^+,\mathbf{x};y^+,\mathbf{y})]U^{cb}(y^+,0,\mathbf{y})\Bigg\}.\end{aligned} \tag{6.3}$$

The goal of this chapter is to generalize the results given in Section 2.2 in the case of the single gluon spectra to multi-gluon inclusive production. In order to do so, we will adopt the same assumption that we have used along this thesis and neglect the contributions where more than one gluon is emitted by the projectile source. In this setup the non-eikonal n-gluon spectrum can be written as

$$2^n(2\pi)^{3n}\frac{d^nN}{\prod_{i=1}^n dk_i^+/k_i^+d^2\mathbf{k}_i}=g^{2n}\int_{\mathbf{q}_1,\ldots,\mathbf{q}_{2n}}\left\langle\rho_p^{b_1}(\mathbf{q}_1)\rho_p^{*b_2}(\mathbf{q}_2)\cdots\rho_p^{*b_{2n}}(\mathbf{q}_{2n})\right\rangle_p$$

$$\times \left\langle \overline{\mathcal{M}}^{a_1 b_1}_{\lambda_1}(\underline{k}_1, \mathbf{q}_1)\overline{\mathcal{M}}^{\dagger b_2 a_1}_{\lambda_1}(\underline{k}_1, \mathbf{q}_2)\cdots\overline{\mathcal{M}}^{a_n b_{2n-1}}_{\lambda_n}(\underline{k}_n, \mathbf{q}_{2n-1})\overline{\mathcal{M}}^{\dagger b_{2n} a_n}_{\lambda_n}(\underline{k}_n, \mathbf{q}_{2n})\right\rangle_T, \tag{6.4}$$

where we have defined the shorthand notation $\underline{k} \equiv (k^+, \mathbf{k})$. This equation is analogous to the eikonal multi-gluon spectra presented in Eq. (4.1). The main difference is that, because of the finite longitudinal extent of the target field, the interaction of the gluon with the target is non diagonal in the transverse space, i.e. it is not described by Wilson lines. This makes the computation of multi-particle production in the non-eikonal case more difficult compared to the eikonal case since in order to compute the target averages we will have to deal with a more complex object, i.e., the scalar gluon propagator in Eq. (6.1). In the next section, we will discuss how to solve the target average of Eq. (6.4) in the non-eikonal case. The strategy that we will use is similar to the one presented in Section 4.2, that is, we will use the Area Enhancement model to write the non-eikonal (NE) multi-pole function in terms of NE dipole functions. Then we will compute the NE dipole functions by using a similar method as the one presented in [178] by discretizing the longitudinal axis and computing the averages locally at each slice of the discretized space.

6.2 Non-eikonal target averaging

In Section 4.2 we have reviewed how to perform the Wilson line's averages over all the target's configurations. We have observed that within the MV model it is relatively simple to obtain a closed-form expression for the 2-point functions, i.e. the dipole function. Then in Section 4.2.1 we introduced the Area Enhancement (AE) model, an ansatz that uses the fact that those configurations of the multi-pole function that maximizes the phase space integral, i.e. that are dominant in the collision area, are those in where the multi-pole is written in terms of dipole functions through a Wick's expansion. Thus the AE model assumes that, after the integration over the phase space, the Wilson lines can be approximately described by a Gaussian distribution being the correction of this approach of order the inverse of the phase space's area. In this section we will review the technique to generalize the approach of Section 4.2 to the non-eikonal case where the scattering of the gluon with the medium is described by the scalar propagator instead of the Wilson line.

We will start our discussion by analyzing the non-eikonal 2-point functions that appear in the single inclusive spectra defined by the $n = 1$ case of Eq. (6.3). In this case there are three objects that we will have to evaluate:

$$\frac{1}{N_c^2 - 1}\left\langle \mathrm{Tr}\left[U_{\mathbf{y}}(x^+, y^+)U^\dagger_{\bar{\mathbf{y}}}(x^+, y^+)\right]\right\rangle_T \equiv d^{(0)}(x^+, y^+|\mathbf{y}, \bar{\mathbf{y}}) \tag{6.5}$$

$$\frac{1}{N_c^2 - 1}\left\langle \mathrm{Tr}\left[\mathcal{G}_{k^+}(x^+, \mathbf{x}; y^+, \mathbf{y})U^\dagger_{\bar{\mathbf{y}}}(x^+, y^+)\right]\right\rangle_T \equiv d^{(1)}(x^+, y^+|\mathbf{x}, \mathbf{y}, k^+; \bar{\mathbf{y}}), \tag{6.6}$$

$$\frac{1}{N_c^2 - 1}\left\langle \mathrm{Tr}\left[\mathcal{G}_{k_1^+}(x^+, \mathbf{x}; y^+, \mathbf{y})\mathcal{G}^\dagger_{k_2^+}(x^+, \bar{\mathbf{x}}; y^+, \bar{\mathbf{y}})\right]\right\rangle_T \equiv d^{(2)}(x^+, y^+|\mathbf{x}, \mathbf{y}, k_1^+; \bar{\mathbf{x}}, \bar{\mathbf{y}}, k_2^+), \tag{6.7}$$

where we have defined $U_{\mathbf{x}}(x^+, y^+) \equiv U(x^+, y^+; \mathbf{x})$ for simplicity. We can identify Eq. (6.5) as the eikonal dipole function evaluated over a longitudinal section $z^+ \in [y^+, x^+]$ of the

target. The functions defined in Eqs. (6.6) and (6.7) are non-eikonal generalizations of the dipole function.

In order to make the analysis as simple as possible, we will assume that the eikonal dipole function is described by the GBW model which is valid as long as the dipole size is much smaller than $\Lambda_{\rm QCD}^{-1}$. In this case we can write

$$d^{(0)}(x^+,y^+|\mathbf{y},\bar{\mathbf{y}}) = \exp\left\{-\frac{q_s^2(x^+,y^+)}{4}(\mathbf{x}-\mathbf{y})^2\right\}, \tag{6.8}$$

where we define $q_s(x^+,y^+)$ as the effective saturation momentum in a longitudinal slice $[y^+,x^+]$ of the target. By using the definition of the saturation momentum given in Eq. (4.17) we can write

$$q_s^2(x^+,y^+) = \frac{g^4 N_c}{4\pi}\int_{y^+}^{x^+} dz^+ \tilde{\mu}^2(z^+). \tag{6.9}$$

Thus, if we assume that the color density $\tilde{\mu}^2(z^+)$ is constant along the target's longitudinal extent, i.e. $\tilde{\mu}^2(z^+) = \mu^2/L^+$, we can write

$$q_s^2(x^+,y^+) = \frac{x^+-y^+}{L^+}Q_s^2. \tag{6.10}$$

We now move our discussion to the calculation of the object given in Eq. (6.6) that we will refer to as the 1st *order NE dipole function*. This object involves averaging the scalar propagator defined in Eq. (6.1) and therefore implies solving a path integral. As usual in computing path integrals it is convenient to discretize the phase space in order to solve the integral. Thus, we discretize the longitudinal space into N slices where we name each point of the discretization z_i^+. In this case the scalar propagator can be written as [43, 44, 86, 86]

$$\begin{aligned}\mathcal{G}_{k^+}^{ab}(\underline{x},\underline{y}) = \lim_{N\to\infty}\Theta(x^+-y^+)\int\left(\prod_{n=1}^{N-1}d^2\mathbf{z}_n\right)\left(\frac{-ik^+N}{2(x^+-y^+)}\right)^N \\ \times\exp\left\{\frac{ik^+N}{2(x^+-y^+)}\sum_{n=1}^{N}(\mathbf{z}_{n+1}-\mathbf{z}_n)^2\right\}\prod_{n=1}^{N}U_{\mathbf{z}_n}^{ab}(z_{n-1}^+,z_n^+),\end{aligned} \tag{6.11}$$

where we have defined $\underline{x}\equiv(x^+,\mathbf{x})$. This equation describes the discrete random walk of the emitted gluon through the transverse points $\mathbf{z}_n(z_n^+)$ inside the target. The emitted gluon is propagated from $\mathbf{z}_0(z_0^+)=\mathbf{y}$ with $z_0^+=y^+$ to $\mathbf{z}_N(z_N^+)=\mathbf{x}$ with $z_N^+=x^+$. The only piece of Eq. (6.11) that depends on the target configuration are the discretized Wilson lines, $U_{\mathbf{z}_n}^{ab}(z_{n-1}^+,z_n^+)$, which account for an eikonal propagation from slice to slice. Therefore we can write Eq. (6.6) as

$$\begin{aligned}d^{(1)}(x^+,y^+|\mathbf{x},\mathbf{y},k^+;\bar{\mathbf{y}}) = \lim_{N\to\infty}\int\left(\prod_{n=1}^{N-1}d^2\mathbf{z}_n\right)\exp\left\{\frac{ik^+N}{2(x^+-y^+)}\sum_{n=1}^{N}(\mathbf{z}_{n+1}-\mathbf{z}_n)^2\right\} \\ \times\left(\frac{-ik^+N}{2(x^+-y^+)}\right)^N\left\langle\mathrm{Tr}\left[\left(\prod_{n=1}^{N}U_{\mathbf{z}_n}(z_{n-1}^+,z_n^+)\right)U_{\bar{\mathbf{y}}}^\dagger(x^+,y^+)\right]\right\rangle_T.\end{aligned} \tag{6.12}$$

This equation can be simplified further by noting that, due to the properties of path-ordered exponentials, the Wilson line evaluated over some longitudinal extent $[y^+, x^+]$ can be factorized into a product of independent contributions at each slice of the discretized axis:

$$U_{\mathbf{x}}(x^+, y^+) = \prod_{i=1}^{n} U_{\mathbf{x}}(x_{i-1}^+, x_i^+), \tag{6.13}$$

where $x_0^+ = y^+$ and $x_n^+ = x^+$. Moreover, the MV model is local in the longitudinal direction and therefore the average of Wilson lines evaluated at different points of the longitudinal axis factorizes into independent averages. For example

$$\left\langle U_{\mathbf{x}}(x^+, y^+) U_{\mathbf{y}}(y^+, z^+) \right\rangle_T = \left\langle U_{\mathbf{x}}(x^+, y^+) \right\rangle_T \left\langle U_{\mathbf{y}}(y^+, z^+) \right\rangle_T, \tag{6.14}$$

where $x^+ > y^+ > z^+$. Thus, assuming that the target averages are computed within the MV model which is local in the longitudinal direction, the average inside Eq. (6.12) simplifies to

$$\left\langle \mathrm{Tr}\left[\left(\prod_{n=1}^{N} U_{\mathbf{z}_n}(z_{n-1}^+, z_n^+) \right) U_{\bar{\mathbf{y}}}^\dagger(x^+, y^+) \right] \right\rangle_T = \prod_{n=1}^{N} \left\langle \mathrm{Tr}\left[U_{\mathbf{z}_n}(z_{n-1}^+, z_n^+) U_{\bar{\mathbf{y}}}^\dagger(z_{n-1}^+, z_n^+) \right] \right\rangle_T . \tag{6.15}$$

Furthermore, by using the local GBW model given in Eq. (6.8) and noting that $z_i^+ - z_{i-1}^+ = L^+/N$ we can write

$$\begin{aligned} d^{(1)}(x^+, y^+|\mathbf{x}, \mathbf{y}, k^+; \bar{\mathbf{y}}) = \lim_{N\to\infty} \int \left(\prod_{n=1}^{N-1} d^2\mathbf{z}_n \right) \left(\frac{-ik^+ N}{2(x^+ - y^+)} \right)^N \\ \times \exp\left\{ \frac{ik^+ N}{2(x^+ - y^+)} \sum_{n=1}^{N} (\mathbf{z}_{n+1} - \mathbf{z}_n)^2 - \frac{Q_s^2}{4N} \sum_{n=1}^{N} (\mathbf{z}_n - \bar{\mathbf{y}})^2 \right\}. \end{aligned} \tag{6.16}$$

Defining $\mathbf{r} = \mathbf{z} - \bar{\mathbf{y}}$ and taking the continuous limit, the path integral can be written as

$$d^{(1)}(x^+, y^+|\mathbf{x}, \mathbf{y}, k^+; \bar{\mathbf{y}}) = \int [\mathcal{D}\mathbf{r}] \exp\left\{ \int_{y^+}^{x^+} dz^+ \left[\frac{ik^+}{2} \dot{\mathbf{r}}^2 - \frac{Q_s^2}{4L^+} \mathbf{r}^2 \right] \right\}. \tag{6.17}$$

Note that we could have obtained this result in a straightforward way by using Eq. (6.1) and applying the GBW model directly, i.e. without discretizing the longitudinal space. However, in this way it is obvious that the approach that we are using depends on the locality of the target average. Moreover, in order to solve Eq. (6.17) we still have to discretize the longitudinal space (as we do in Appendix E). This equation is the well known path integral of the harmonic oscillator with "mass" $ik^+/2$ and imaginary "frequency" $\sqrt{-iQ_s^2/2L^+k^+}$ [118], where its solution is derived in Appendix E and given in Eq. (E.22). Thus, after performing the path integral, we can write Eq. (6.17) as

$$d^{(1)}(x^+, y^+|\mathbf{x}, \mathbf{y}, k_i^+; \bar{\mathbf{y}}) = \frac{-Q_s^2}{4\pi\epsilon_i \sin\frac{\epsilon_i \Delta^+}{L^+}} \exp\left\{ \frac{Q_s^2}{4\epsilon_i} \left[\frac{\mathbf{r}_0^2 + \mathbf{r}_N^2}{\tan\frac{\epsilon_i\Delta^+}{L^+}} - 2\frac{\mathbf{r}_0 \cdot \mathbf{r}_N}{\sin\frac{\epsilon_i\Delta^+}{L^+}} \right] \right\}, \tag{6.18}$$

where we have defined $\Delta^+ = x^+ - y^+$, $\mathbf{r}_0 = \mathbf{y} - \bar{\mathbf{y}}$, $\mathbf{r}_N = \mathbf{x} - \bar{\mathbf{y}}$ and

$$\epsilon_i^2 = \frac{Q_s^2 L^+}{2ik_i^+}. \tag{6.19}$$

Note that ϵ_i^2 is a dimensionless parameter that vanishes in the eikonal limit, $k_i^+ \to \infty$ and $L^+ \to 0$, and therefore we call it the *non-eikonal parameter* – its role is to weight the strength of the finite length effects..

The object defined in Eq. (6.7), that we will refer to as the 2$^{\text{nd}}$ *order NE dipole* function, can be computed in the same fashion. By using the GBW model and the locality of the MV model we can write it as

$$d^{(2)}(x^+, y^+|\mathbf{x}, \mathbf{y}, k_1^+; \bar{\mathbf{x}}, \bar{\mathbf{y}}, k_2^+) = \int [\mathcal{D}\mathbf{r}][\mathcal{D}\bar{\mathbf{r}}] \exp\left\{ \int_{y^+}^{x^+} dz^+ \left[\frac{ik_1^+}{2}\dot{\mathbf{r}}^2 - \frac{ik_2^+}{2}\dot{\bar{\mathbf{r}}}^2 - \frac{Q_s^2}{4L^+}(\mathbf{r} - \bar{\mathbf{r}})^2 \right] \right\}, \tag{6.20}$$

where $\mathbf{r}(y^+) = \mathbf{y}$, $\mathbf{r}(x^+) = \mathbf{x}$, $\bar{\mathbf{r}}(y^+) = \bar{\mathbf{y}}$ and $\bar{\mathbf{r}}(x^+) = \bar{\mathbf{x}}$. This equation can be identified as the path integral of two coupled harmonic oscillators whose solution is derived in Appendix E and given in Eq. (E.44). Thus we can write it as

$$d^{(2)}(x^+, y^+|\mathbf{x}, \mathbf{y}, k_1^+; \bar{\mathbf{x}}, \bar{\mathbf{y}}, k_2^+) = \frac{-Q_s^4}{(4\pi)^2} \frac{\epsilon_- L^+}{\Delta^+ \epsilon_1^2 \epsilon_2^2 \sin\frac{\Delta^+\epsilon_-}{L^+}} \exp\left\{ \frac{Q_s^2}{4\epsilon_-^2} \left(\frac{\epsilon_-(\mathbf{r}_0^2 + \mathbf{r}_N^2)}{\tan\frac{\Delta^+\epsilon_-}{L^+}} - 2\frac{\epsilon_- \mathbf{r}_0 \cdot \mathbf{r}_N}{\sin\frac{\Delta^+\epsilon_-}{L^+}} + \frac{L^+}{\Delta^+ \epsilon_1^2 \epsilon_2^2 \epsilon_+^4} \left[2\epsilon_1^2 \epsilon_2^2 (\mathbf{r}_N - \mathbf{r}_0) - \epsilon_+^2 \epsilon_-^2 (\mathbf{b}_N - \mathbf{b}_0) \right]^2 \right) \right\}, \tag{6.21}$$

where we have defined for simplicity $\epsilon_-^2 = \epsilon_1^2 - \epsilon_2^2$, $\epsilon_+^2 = \epsilon_1^2 + \epsilon_2^2$, $\mathbf{r}_0 = \mathbf{y} - \bar{\mathbf{y}}$, $\mathbf{r}_N = \mathbf{x} - \bar{\mathbf{x}}$, $\mathbf{b}_0 = (k_1^+\mathbf{y} + k_2^+\bar{\mathbf{y}})/(k_1^+ + k_2^+)$ and $\mathbf{b}_N = (k_1^+\mathbf{x} + k_2^+\bar{\mathbf{x}})/(k_1^+ + k_2^+)$.

We note that in the case where $k_2^+ = k_1^+$ this equation simplifies and leads to the known result [192, 218]

$$d^{(2)}(x^+, y^+|\mathbf{x}, \mathbf{y}, k_1^+; \bar{\mathbf{x}}, \bar{\mathbf{y}}, k_1^+) = -\left(\frac{L^+ Q_s^2}{4\pi\Delta^+\epsilon_1^2} \right)^2 \times \exp\left\{ -\frac{Q_s^2}{12\epsilon_1^2} \left[\epsilon_1^2 \frac{\Delta^+}{L^+}(\mathbf{r}_0^2 + \mathbf{r}_N^2 + \mathbf{r}_0 \cdot \mathbf{r}_N) - 6\frac{L^+}{\Delta^+}(\mathbf{r}_N - \mathbf{r}_0) \cdot (\mathbf{b}_N - \mathbf{b}_0) \right] \right\}. \tag{6.22}$$

With Eqs. (6.8), (6.18) and (6.21) we have determined the non-eikonal dipole function evaluated within a longitudinal extent Δ^+ of the target medium. We note that these functions are extensively used by the jet quenching community where the effects of the parton propagation within a dense medium, the Quark Gluon Plasma, is computed. In this case, the GBW model is usually referred to as the *harmonic oscillator approximation* and the effective saturation scale in Eq. (6.8) is written as $q_s^2(x^+, y^+) = \int_{y^+}^{x^+} \hat{q}(z^+)dz^+$, where $\hat{q}(z^+)$ is the medium transport coefficient. In the case in which $\hat{q}(z^+)$ is constant, i.e. the medium is static, we can write $\hat{q} = Q_s^2/L^+$.

We now move our discussion to higher order functions, i.e., multi-poles, in where we will have to evaluate the non-eikonal target average of multiple Wilson lines and scalar

propagators. As stated in the introduction of this chapter, in order to compute the NE multi-poles we use the Area Enhancement model introduced in Section 4.2.1. This model is based on the chromo-electric domain structure in the target transverse plane and leads to a similar result compared to the MV model. The advantage of this approach is that we can assume that, after integration over the transverse phase space, the Wilson lines follow approximately a Gaussian distribution – with the non-Gaussian corrections suppressed by the collision's area – and therefore we can use the Wick's theorem. However, in the case treated in this chapter we have to be more careful since the target has a finite width and thus the chromo-electric domains may decohere in the longitudinal direction.

Let us justify the application of the AE model in target ensembles with non-zero width, L^+, by examining the space-time kinematics of the interaction in the center-of-mass (CoM) frame. In the CoM frame, the Lorentz contracted target width is $L^+ \sim 20A^{1/3}/\sqrt{s_{\mathrm{NN}}}$. On the other hand, the chromo-electric fields are defined by the low-x gluons which have the following spread in the longitudinal direction: $\Delta x^+ \sim 1/q^- = A/(xQ_T^-)$, where $Q_T^- = A\sqrt{s_{\mathrm{NN}}}/\sqrt{2}$ and q^- are the longitudinal momentum, in the CoM frame, of the gluon and the target respectively. Thus, as long as $\Delta x^+ \gg L^+$ the domain structure of the target will not decohere within the extent of the target and the AE model is justified. Since $L^+/\Delta x^+ \sim xA^{1/3} \ll 1$, we conclude that the Area Enhancement model is still a good approximation in the non-eikonal case.

Thus, in the framework presented in this chapter, we use that the AE approximation and we write the non-eikonal multi-poles of the Wilson lines and the scalar propagators as their Wick expansions in terms of the 2-point functions given in Eqs. (6.8), (6.18) and (6.21) as we did in Section 4.2.1 in the case of the eikonal multi-pole functions.

6.3 Single inclusive gluon production

In order to warm up, let us compute the multi-gluon spectrum given in Eq. (6.4) in the case of single gluon production. In this case the particle yield can be written as

$$(2\pi)^3(2k^+)\frac{dN}{dk^+d^2\mathbf{k}} = g^2\int_{\mathbf{q}_1\mathbf{q}_2}\left\langle\rho^{b_1}(\mathbf{q}_1)\rho^{*b_2}(\mathbf{q}_2)\right\rangle_p\left\langle\overline{\mathcal{M}}_\lambda^{b_1a_1}(\underline{k},\mathbf{q}_1)\overline{\mathcal{M}}_\lambda^{\dagger a_1b_2}(\underline{k},\mathbf{q}_2)\right\rangle_T. \tag{6.23}$$

Analogous to the procedure of Chapter 4, we use the generalized MV model, given in Eq. (4.6), in order to compute the projectile's average:

$$\left\langle\rho^{b_1}(\mathbf{q}_1)\rho^{*b_2}(\mathbf{q}_2)\right\rangle_p = \frac{\delta^{b_1b_2}}{N_c^2-1}\mu^2(\mathbf{q}_1,-\mathbf{q}_2), \tag{6.24}$$

where the factor $1/(N_c^2-1)$ is introduced by convenience but will not be relevant in the analysis performed in this chapter.

Since this contribution is proportional to $\delta^{b_1b_2}$, it will close the trace of the reduced amplitudes in Eq. (6.23). By using Eq. (6.3), we can write the target average of the matrix amplitudes' trace as

$$\frac{1}{N_c^2-1}\left\langle\mathrm{Tr}\left[\overline{\mathcal{M}}_\lambda(\underline{k},\mathbf{q}_1)\overline{\mathcal{M}}_\lambda^\dagger(\underline{k},\mathbf{q}_2)\right]\right\rangle_T = \int_{\mathbf{y},\bar{\mathbf{y}}} e^{i\mathbf{q}_1\cdot\mathbf{y}-i\mathbf{q}_2\cdot\bar{\mathbf{y}}}\left\{\frac{2}{\mathbf{k}^2}e^{-i\mathbf{k}\cdot(\mathbf{y}-\bar{\mathbf{y}})}d^{(0)}(L^+,0|\mathbf{y};\bar{\mathbf{y}})\right.$$

$$
\begin{aligned}
&+2\frac{\mathbf{q}_1\cdot\mathbf{q}_2}{\mathbf{q}_1^2\mathbf{q}_2^2}\int_{\mathbf{x}\bar{\mathbf{x}}} e^{-i\mathbf{k}\cdot(\mathbf{x}-\bar{\mathbf{x}})}d^{(2)}(L^+,0|,\mathbf{x},\mathbf{y},k^+;\bar{\mathbf{x}},\bar{\mathbf{y}},k^+)\\
&-4\frac{\mathbf{k}\cdot\mathbf{q}_1}{\mathbf{k}^2\mathbf{q}_1^2}\int_{\mathbf{x}} e^{-i\mathbf{k}\cdot(\mathbf{x}-\bar{\mathbf{y}})}d^{(1)}(L^+,0|\mathbf{x},\mathbf{y},k^+;\bar{\mathbf{y}})\\
&+2\frac{\mathbf{k}^i}{\mathbf{k}^2}\frac{1}{k^+}\int_0^{L^+}dy^+\int_{\mathbf{x}} e^{-i\mathbf{k}\cdot(\mathbf{x}-\bar{\mathbf{y}})}d^{(0)}(y^+,0|\mathbf{y};\bar{\mathbf{y}})\left[\partial_{\mathbf{y}^i}d^{(1)}(L^+,0|\mathbf{x},\mathbf{y},k^+;\bar{\mathbf{y}})\right]\\
&-2\frac{\mathbf{q}_1^i}{\mathbf{q}_1^2}\frac{1}{k^+}\int_0^{L^+}dy^+\int_{\mathbf{x}\bar{\mathbf{x}}\mathbf{u}} e^{-i\mathbf{k}\cdot(\mathbf{x}-\bar{\mathbf{x}})}\left[\partial_{\bar{\mathbf{y}}^i}d^{(2)}(L^+,0|,\mathbf{x},\mathbf{y},k^+;\bar{\mathbf{x}},\bar{\mathbf{y}},k^+)\right]\\
&\qquad\times d^{(1)}(L^+,0|\mathbf{x},\mathbf{y},k^+;\bar{\mathbf{y}})\\
&+\frac{1}{(k^+)^2}\int_0^{L^+}dy^+\int_{y^+}^{L^+}d\bar{y}^+\int_{\mathbf{x}\bar{\mathbf{x}}\mathbf{u}} e^{-\mathbf{k}\cdot(\mathbf{x}-\bar{\mathbf{x}})}\left[\partial_{\bar{\mathbf{y}}^i}d^{(2)}(L^+,0|,\mathbf{x},\mathbf{y},k^+;\bar{\mathbf{x}},\bar{\mathbf{y}},k^+)\right]\\
&\qquad\times\left[\partial_{\mathbf{y}^i}d^{(1)}(L^+,0|\mathbf{x},\mathbf{y},k^+;\bar{\mathbf{y}})\right]d^{(0)}(y^+,0|\mathbf{y};\bar{\mathbf{y}})\Big\}+\mathbf{c.c.},
\end{aligned}
\tag{6.25}
$$

where, in order to break the target average of the scalar propagator into their local pieces, we have used the convolution property

$$
\mathcal{G}_{k^+}(x^+,\mathbf{x};y^+,\mathbf{y})=\int_{\mathbf{u}}\mathcal{G}_{k^+}(x^+,\mathbf{x};z^+,\mathbf{u})\mathcal{G}_{k^+}(z^+,\mathbf{u};y^+,\mathbf{y}),
\tag{6.26}
$$

with $y^+<z^+<x^+$. We note that this equation is, apart from some terms, the medium-induced radiation spectrum used in jet quenching calculations [219–221]. The difference is that Eq. (6.3) includes interference terms with the contribution where the gluon is emitted before the interaction of the source with the target and therefore are absent in the jet quenching framework [118].

We also note that since we are assuming the GBW model, i.e., a Gaussian form, for the non-eikonal dipole functions, all the integrals over the transverse positions or momenta appearing in Eq. (6.25), or in this chapter, will be of the form

$$
\int_{\mathbf{x}}(a+\mathbf{b}^i\mathbf{x}^i+\mathbf{c}^i\mathbf{d}^j\mathbf{x}^i\mathbf{x}^j)e^{-A\mathbf{x}^2+\mathbf{B}\cdot\mathbf{x}}=\frac{\pi}{A}e^{\frac{\mathbf{B}^2}{4A}}\left[a+\mathbf{b}^i\frac{\mathbf{B}^i}{2A}+\frac{\mathbf{c}^i\mathbf{d}^j}{2A}\left(\delta^{ij}+\frac{\mathbf{B}^i\mathbf{B}^j}{2A}\right)\right],
\tag{6.27}
$$

and therefore it will be straightforward, although tedious in some cases, to solve them. Moreover, the argument of the integrals over $\mathbf{y}$ and $\bar{\mathbf{y}}$ is translational invariant under these coordinates and thus the integral will be proportional to $\delta^{(2)}(\mathbf{q}_1-\mathbf{q}_2)$. We then write Eq. (6.23) as

$$
\frac{dN}{d\eta d^2\mathbf{k}}=\frac{g^2\pi B_p}{(2\pi)^3}\int_{\mathbf{q}}\mathrm{Re}\left\{\mathcal{I}_{\text{aft-aft}}+\mathcal{I}_{\text{bef-bef}}+\mathcal{I}_{\text{bef-aft}}+\mathcal{I}_{\text{aft-in}}+\mathcal{I}_{\text{bef-in}}+\mathcal{I}_{\text{in-in}}\right\},
\tag{6.28}
$$

where we have used the fact that $\mu^2(\mathbf{q},-\mathbf{q})=\pi B_p$ and written $dk^+/k^+=d\eta$. The terms in the argument of the integral are the result of squaring the contributions of Eq. (6.3) where the gluon is emitted before, after or inside the target medium and are summarized in Fig. 6.1.

The term $\mathcal{I}_{\text{aft-aft}}$ is the contribution where the gluon is emitted after the source interacts with the target at both sides of the cut and reads

$$
\mathcal{I}_{\text{aft-aft}}=\frac{2}{\mathbf{k}^2}\int_{\mathbf{r}}e^{-i(\mathbf{k}-\mathbf{q})\cdot\mathbf{r}}d^{(0)}\left(L^+,0\Big|\frac{\mathbf{r}}{2};-\frac{\mathbf{r}}{2}\right)=\frac{8\pi}{Q_s^2}\frac{1}{\mathbf{k}^2}\exp\left\{-\frac{(\mathbf{k}-\mathbf{q})^2}{Q_s^2}\right\}.
\tag{6.29}
$$

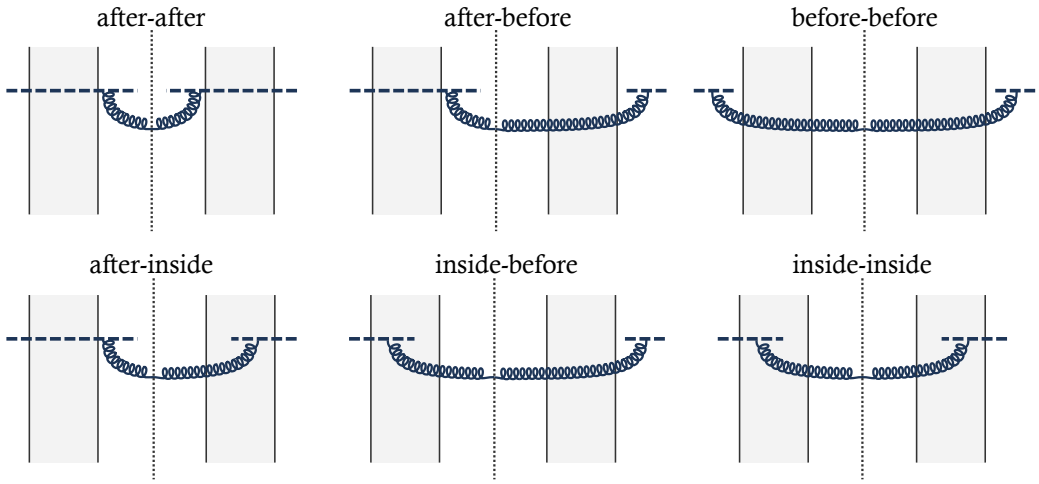

Figure 6.1.
All possible contributions to the single gluon spectrum given in Eq. (6.28) which are the result of squaring the amplitude of a gluon being emitted before, in between or after the interaction of the source with the medium.

Note that we have dropped the dependence on the impact parameter $\mathbf{b}$ because the eikonal dipole function is translational invariant.

The term $\mathcal{I}_{\text{bef-bef}}$ is the contribution where the gluon is emitted before the source's interaction with the target at both sides of the cut and is

$$\mathcal{I}_{\text{bef-bef}} = \frac{2}{\mathbf{q}^2}\int_{\mathbf{r}} e^{-i\mathbf{q}\cdot\mathbf{r}} \int_{\mathbf{x}\bar{\mathbf{x}}} e^{-i\mathbf{k}\cdot(\mathbf{x}-\bar{\mathbf{x}})} d^{(2)}\left(L^+, 0\middle|, \mathbf{x}, \mathbf{b}+\frac{\mathbf{r}}{2}, k^+; \bar{\mathbf{x}}, \mathbf{b}-\frac{\mathbf{r}}{2}, k^+\right). \tag{6.30}$$

Although in this equation we are keeping the dependence on the impact parameter $\mathbf{b}$ for consistency we should note that, after performing the Fourier transforms, the final result is independent of $\mathbf{b}$, i.e. it is translationally invariant. Moreover, the Fourier transform of the second order NE dipole function in the case where both longitudinal momenta are equal, Eq. (6.22), is simply:

$$\int_{\mathbf{x}\bar{\mathbf{x}}} e^{-i\mathbf{k}(\mathbf{x}-\bar{\mathbf{x}})} d^{(2)}(x^+, y^+|\mathbf{x}, \mathbf{y}, k^+; \bar{\mathbf{x}}, \bar{\mathbf{y}}, k^+) = \exp\left\{-\frac{\Delta^+ Q_s^2}{4L^+}(\mathbf{y}-\bar{\mathbf{y}})^2 - i\mathbf{k}\cdot(\mathbf{y}-\bar{\mathbf{y}})\right\}, \tag{6.31}$$

that is, in this case the 2nd order NE dipole function does not give any non-eikonal correction. As we shall see later, this is not the case when the longitudinal momenta are different. Thus, having into account this result we can write

$$\mathcal{I}_{\text{bef-bef}} = \frac{8\pi}{Q_s^2}\frac{1}{\mathbf{q}^2}\exp\left\{-\frac{(\mathbf{k}-\mathbf{q})^2}{Q_s^2}\right\}. \tag{6.32}$$

$\mathcal{I}_{\text{bef-aft}}$ gives the contribution where the gluon is emitted before the medium on one side of the cut and after on the other side. Note that it does not matter in which side of the cut the gluon is emitted before since we are taking the real part of the contribution and therefore accounting for the two possibilities. This term can be written as

$$\mathcal{I}_{\text{bef-aft}} = -4\frac{\mathbf{k}\cdot\mathbf{q}}{\mathbf{k}^2\mathbf{q}^2}\int_{\mathbf{r}} e^{-i\mathbf{q}\cdot\mathbf{r}} \int_{\mathbf{x}} e^{-i\mathbf{k}\cdot(\mathbf{x}-\mathbf{b}+\mathbf{r}/2)} d^{(1)}\left(L^+, 0\middle|\mathbf{x}, \mathbf{b}+\frac{\mathbf{r}}{2}, k^+; \mathbf{b}-\frac{\mathbf{r}}{2}\right). \tag{6.33}$$

Thus, noting that the Fourier transform over $\mathbf{x}$ of Eq. (6.18) is

$$\int_{\mathbf{x}} e^{-i\mathbf{k}\mathbf{x}} d^{(1)}_{k^+}(x^+, y^+|\mathbf{x}, \mathbf{y}; \bar{\mathbf{y}}) = \frac{1}{\sin\frac{\Delta^+\epsilon}{L^+}} e^{-i\mathbf{k}\cdot\bar{\mathbf{y}}} \exp\left\{\left(-\frac{Q_s^2}{4\epsilon}(\mathbf{y}-\bar{\mathbf{y}})^2 + \epsilon\frac{\mathbf{k}^2}{Q_s^2}\right)\tan\frac{\Delta^+\epsilon}{L^+} + i\frac{\mathbf{k}\cdot(\mathbf{y}-\bar{\mathbf{y}})}{\sin\frac{\Delta^+\epsilon}{L^+}}\right\}, \quad (6.34)$$

we can write

$$\mathcal{I}_{\text{bef-aft}} = -\frac{16\pi\epsilon}{Q_s^2\sin\epsilon}\frac{\mathbf{k}\cdot\mathbf{q}}{\mathbf{k}^2\mathbf{q}^2}\exp\left\{-\frac{\epsilon}{Q_s^2}\left[\frac{\mathbf{k}^2+\mathbf{q}^2}{\tan\epsilon} - 2\frac{\mathbf{k}\cdot\mathbf{q}}{\sin\epsilon}\right]\right\}. \quad (6.35)$$

It is easy to realize that by taking the eikonal limit $\epsilon \to 0$ we recover the Fourier transform of the GBW model.

$\mathcal{I}_{\text{aft-in}}$ gives the contribution where the gluon is emitted after the interaction of the source with the target on one side of the cut and inside the target on the other side of the cut. This contribution can be written as

$$\mathcal{I}_{\text{aft-in}} = \frac{\mathbf{k}^i}{\mathbf{k}^2}\frac{2}{k^+}\int_0^{L^+} dy^+ \int_{\mathbf{x},\mathbf{r}} e^{-i\mathbf{q}\cdot\mathbf{r}-i\mathbf{k}\cdot(\mathbf{x}-\bar{\mathbf{y}})} d^{(0)}(y^+, 0|\mathbf{y}; \bar{\mathbf{y}})\left[\partial_{\mathbf{y}^i} d^{(1)}(L^+, y^+|\mathbf{x}, \mathbf{y}, k^+; \bar{\mathbf{y}})\right], \quad (6.36)$$

where $\mathbf{y} = \mathbf{b} + \frac{\mathbf{r}}{2}$, $\bar{\mathbf{y}} = \mathbf{b} - \frac{\mathbf{r}}{2}$ and y^+ is the longitudinal point where the gluon is emitted inside the target. By using Eq. (6.34) and defining $\alpha = \frac{L^+ - y^+}{L^+}$ as the fraction of the medium where the gluon propagates we can write this contribution as

$$\mathcal{I}_{\text{aft-in}} = \frac{16\pi\epsilon^3}{Q_s^4}\int_0^1 d\alpha \frac{\sec^2(\alpha\epsilon)}{(\epsilon\tilde{\alpha} + \tan(\alpha\epsilon))^2}\frac{\mathbf{k}^2\tilde{\alpha}\epsilon + \mathbf{k}\cdot\mathbf{q}\sin(\alpha\epsilon)}{\mathbf{k}^2} \times \exp\left\{-\frac{\epsilon}{Q_s^2(\epsilon\tilde{\alpha} + \tan(\alpha\epsilon))}\left[\mathbf{k}^2\big(1 - \tilde{\alpha}\epsilon\tan(\alpha\epsilon)\big) + \mathbf{q}^2 - 2\mathbf{k}\cdot\mathbf{q}\sec(\alpha\epsilon)\right]\right\}, \quad (6.37)$$

where we have defined $\tilde{\alpha} = 1 - \alpha$, that is, it is the longitudinal fraction of the target's medium traveled by the source before emitting the gluon. It is not hard to realize that, by expanding the trigonometric functions at leading order in ϵ, this contribution is $\mathcal{O}(\epsilon^2)$ while the first three contributions are $\mathcal{O}(\epsilon^0)$. Therefore, this term is the first contribution that is purely non-eikonal. This should not be a surprise since it is the result of taking into account the situation where the gluon is emitted inside the target which is absent in the shock-wave approximation.

The interference term where the gluon is emitted inside the target on one side of the cut and before on the other side, $\mathcal{I}_{\text{bef-in}}$, can be written as

$$\mathcal{I}_{\text{bef-in}} = -\frac{\mathbf{q}^i}{\mathbf{q}^2}\frac{2}{k^+}\int_0^{L^+} dy^+ \int_{\mathbf{x},\bar{\mathbf{x}},\mathbf{u},\mathbf{r}} e^{-i\mathbf{q}\cdot\mathbf{r}-i\mathbf{k}\cdot(\mathbf{x}-\bar{\mathbf{x}})}\left[\partial_{\bar{\mathbf{y}}^i} d^{(2)}(L^+, y^+|\mathbf{x}, \mathbf{u}, k^+; \bar{\mathbf{x}}, \bar{\mathbf{y}}, k^+)\right] \times d^{(1)}(y^+, 0|\mathbf{u}, \mathbf{y}, k^+; \bar{\mathbf{y}}). \quad (6.38)$$

This integral can be solved analogously as above by using Eq. (6.31) and the same definition of α. The result reads

$$\mathcal{I}_{\text{bef-in}} = -\frac{16\pi\epsilon^3}{Q_s^4}\int_0^1 d\alpha \frac{\sec^2(\alpha\epsilon)}{(\epsilon\tilde{\alpha} + \tan(\alpha\epsilon))^2}\frac{\mathbf{q}^2\tilde{\alpha}\epsilon + \mathbf{k}\cdot\mathbf{q}\sin(\alpha\epsilon)}{\mathbf{q}^2}$$

$$\times \exp\left\{-\frac{\epsilon}{Q_s^2(\epsilon\tilde{\alpha}+\tan(\alpha\epsilon))}\left[\mathbf{k}^2+\mathbf{q}^2\left[1-\tilde{\alpha}\epsilon\tan(\alpha\epsilon)\right]-2\mathbf{k}\cdot\mathbf{q}\sec(\alpha\epsilon)\right]\right\}, \quad (6.39)$$

Finally, $\mathcal{I}_{\text{in-in}}$ is the last term in Eq. (6.28) and accounts for the case in which the gluon is emitted inside the target at both sides of the cut. This contribution can be written as

$$\mathcal{I}_{\text{in-in}} = \frac{1}{(k^+)^2}\int_0^{L^+} dy^+ \int_{y^+}^{L^+} d\bar{y}^+ \int_{\mathbf{x},\bar{\mathbf{x}},\mathbf{u},\mathbf{r}} e^{-i\mathbf{q}\cdot\mathbf{r}-\mathbf{k}\cdot(\mathbf{x}-\bar{\mathbf{x}})}\left[\partial_{\bar{\mathbf{y}}^i} d^{(2)}(L^+,\bar{y}^+|\mathbf{x},\mathbf{u},k^+;\bar{\mathbf{x}},\bar{\mathbf{y}},k^+)\right] \times\left[\partial_{\mathbf{y}^i} d^{(1)}(\bar{y}^+,y^+|\mathbf{u},\mathbf{y},k^+;\bar{\mathbf{y}})\right] d^{(0)}(y^+,0|\mathbf{y};\bar{\mathbf{y}}). \quad (6.40)$$

Here the gluon on the left side of the cut is emitted at a longitudinal point y^+ while the one on the right side of the cut is emitted at $\bar{y}^+ > y^+$. By defining $\xi = (\bar{y}^+ - y^+)/L^+$ as the fractional length traveled by the first gluon before the second is emitted, $\tilde{\alpha} = y^+/L^+$ and using Eqs. (6.8), (6.18) and (6.31), we can write

$$\begin{aligned}\mathcal{I}_{\text{in-in}} = &-\frac{16\pi\epsilon^5}{Q_s^6}\int_0^1 d\tilde{\alpha}\int_0^{1-\tilde{\alpha}} d\xi \frac{\csc^2(\xi\epsilon)}{\left[1-\epsilon^2\tilde{\alpha}\gamma+(1-\xi)\epsilon\cot(\xi\epsilon)\right]^3}\\ &\times\Bigg[\epsilon\tilde{\alpha}\gamma Q_s^2\left(1-\epsilon^2\tilde{\alpha}\gamma+(1-\xi)\epsilon\cot(\xi\epsilon)\right)+\epsilon\tilde{\alpha}\mathbf{k}^2\Big(1+\epsilon\tilde{\alpha}\cot(\xi\epsilon)\Big)\\ &+\epsilon\gamma\mathbf{q}^2\Big(1+\epsilon\gamma\cot(\xi\epsilon)\Big)+\frac{\epsilon^2\tilde{\alpha}\gamma+\sin^2(\xi\epsilon)\Big(1+\epsilon\tilde{\alpha}\cot(\xi\epsilon)\Big)\Big(1+\epsilon\gamma\cot(\xi\epsilon)\Big)}{\sin(\xi\epsilon)}\mathbf{k}\cdot\mathbf{q}\Bigg]\\ &\times\exp\left\{-\frac{\epsilon\Big(\epsilon\tilde{\alpha}-\cot(\xi\epsilon)\Big)\mathbf{k}^2+\Big(\epsilon\gamma-\cot(\xi\epsilon)\Big)\mathbf{q}^2+2\csc(\xi\epsilon)\mathbf{k}\cdot\mathbf{q}}{Q_s^2\left[1-\epsilon^2\tilde{\alpha}\gamma+(1-\xi)\epsilon\cot(\xi\epsilon)\right]}\right\}, \quad (6.41)\end{aligned}$$

where we have defined $\gamma = 1-\xi-\tilde{\alpha}$ which is the longitudinal fraction of the target in where the two gluons travel at the same time. By expanding the trigonometric functions at leading order in powers of ϵ, we can realize that this term is $\mathcal{O}(\epsilon^4)$ and therefore is subleading in the non-eikonal corrections with respect to the other contributions.

With Eqs. (6.29), (6.32), (6.35), (6.37), (6.39) and (6.41) we have determined the non-eikonal single inclusive gluon spectrum, Eq. (6.28), in proton-nucleus collisions. In the next section we will solve this equation and explore the finite width effects.

6.3.1 Numerical results

In this section we will solve Eq. (6.28) numerically in order to analyze the effects of the non-eikonal corrections in single gluon production in pA collisions. The finite width effects are encoded in this expression through the dimensionless parameter ϵ defined in Eq. (6.19) which depends on Q_s, k^+ and L^+. Performing analogous arguments as in Section 5.4, where we have discussed the NE correction in proton-proton collisions, we can write $k^+ = \frac{1}{\sqrt{2}}|\mathbf{k}|e^{\eta}$ and $L^+ = 20A^{1/3}/\sqrt{s_{\text{NN}}}$. Thus, the NE correction will depend on the values of A, η, $\sqrt{s_{\text{NN}}}$ and $p_\perp \equiv |\mathbf{k}|$, and for this reason we analyze the dependence of the single gluon spectrum with respect to these variables.

In order to regulate the infrared divergences we introduce a mass in the denominators that lead to these divergences, i.e., we make the change $1/\mathbf{q}^2 \to 1/(\mathbf{q}^2+\mu^2)$ in Eqs. (6.32),

(6.35) and (6.39), where we fix the regulator to $\mu = 0.6$ GeV. We have checked that the results change slightly by changing this regulator, being the non-eikonal corrections smaller when μ^2 is also smaller. Moreover, we fix the value of the saturation scale to $Q_s = \sqrt{2}$ GeV and the target mass number to $A = 197$ – a gold nucleus. However, since the non-eikonal parameter depend on the mass number as $A^{1/3}$ we should not expect a large dependence of our results with A.

In Fig. 6.2, we plot the ratio of the non-eikonal yield given in Eq. (6.28) to the full eikonal result (where $\epsilon = 0$) as a function of the transverse momentum, $p_\perp$, for three values of the center-of-mass energy per nucleon and with $\eta = 0$. We see that non-eikonal corrections decrease the spectra at low $p_\perp$ and enhance it at $p_\perp \gtrsim 1$ GeV. Moreover, the NE corrections are sizable when $\sqrt{s_{\rm NN}} = 50$ GeV, being of order 10 % when $p_\perp \sim 3$ GeV, but are almost negligible when $\sqrt{s_{\rm NN}} = 200$ GeV, which is the usual energy of pA collisions performed at the RHIC. Thus, the impact of the finite width effects for performing phenomenology studies in single gluon production at relatively high energies is negligible.

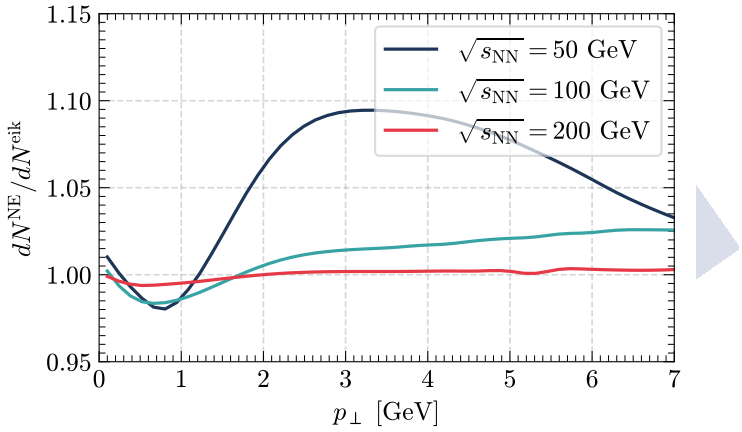

Figure 6.2.
Ratio of the non-eikonal single inclusive gluon spectrum, Eq. (6.28), to the full eikonal result when $\epsilon = 0$ as a function of the transverse momentum, $p_\perp$, for three values of the center-of-mass energy per nucleon and with $\eta = 0$.

In Fig. 6.3, we plot the ratio of the non-eikonal single gluon spectrum, given in Eq. (6.28), with respect to the eikonal one as a function of the center-of-mass energy per nucleon for three values of the pseudorapidity and with $p_\perp = 2$ GeV. We see that when $\eta = 0$ the finite width effects are sizable up to $\sqrt{s_{\rm NN}} \sim 100$ GeV, when $\eta = 0.5$ up to $\sqrt{s_{\rm NN}} \sim 50$ GeV and when $\eta = 1$ they are negligible. Moreover, although we are plotting the result starting from $\sqrt{s_{\rm NN}} = 20$ GeV we should note that since the Bjorken-x of the target's parton probed by the projectile is $x \sim \frac{1\text{ GeV}}{\sqrt{s_{\rm NN}}} e^{-\eta}$, when $\sqrt{s_{\rm NN}} = 20$ GeV we are by no means in the low-x regime and our approach should not be valid.

Finally, in Fig. 6.4 we plot the ratio of the non-eikonal single gluon spectrum, given in Eq. (6.28), with respect to the eikonal one as a function of the pseudorapidity of the produced gluon for three values of $\sqrt{s_{\rm NN}}$ and at $p_\perp = 2$ GeV. The conclusion is analogous to the other figures: the effect of the non-eikonal corrections is sizable when $\eta < 1$ and

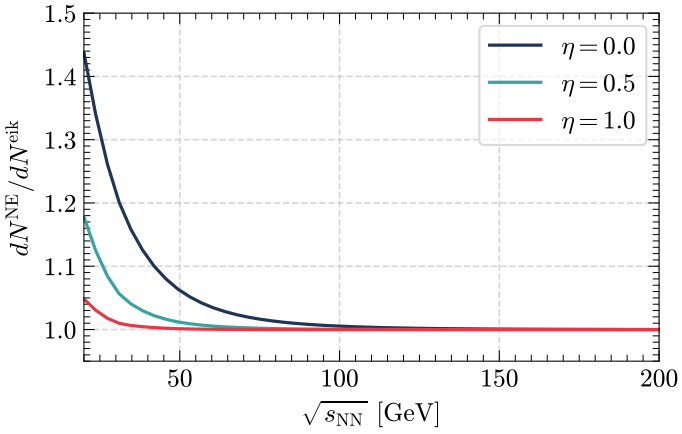

Figure 6.3.
Ratio of the non-eikonal single gluon spectrum, given in Eq. (6.28), with respect to the eikonal one as a function of the center-of-mass energy per nucleon for three values of the pseudorapidity and with $p_\perp = 2$ GeV.

when $\sqrt{s_{\mathrm{NN}}} = 50$ GeV but it is almost negligible to higher energies at all values of the pseudorapidity.

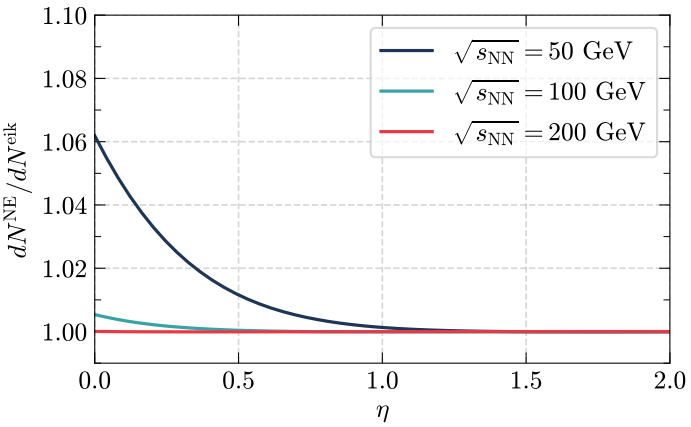

Figure 6.4.
Ratio of the non-eikonal single gluon spectrum, given in Eq. (6.28), with respect to the eikonal one as a function of the pseudorapidity of the produced gluon for three values of $\sqrt{s_{\mathrm{NN}}}$ and at $p_\perp = 2$ GeV.

6.3.2 Comparison with Altinoluk et al.

To finalize this section we compare our result with the next-to-next-to-eikonal calculation performed in [43,44]. It is proposed in [43,44] an approach to expand the scalar propagator given Eq. (6.1) around its classical solution, i.e. the one that minimizes the path integral and leads to a linear path instead of the Brownian motion. They also assume that the angle

of the straight path with respect to the longitudinal axis is small, since it is proportional to L^+/k^+, and that the target field is weak far away from the classical solution. The corresponding result is an expansion in powers of $\frac{L^+}{k^+} = \frac{2i\epsilon^2}{Q_s^2}$ and reads

$$\mathcal{R}_{\underline{k}}(L^+,0;\mathbf{y}) = U + \frac{2i\epsilon^2}{Q_s^2}\left[\mathbf{k}^i U^i_{[0,1]} + \frac{i}{2}U_{[1,0]}\right] + \left(\frac{2i\epsilon^2}{Q_s^2}\right)^2\left[\mathbf{k}^i\mathbf{k}^j U^{ij}_{[0,2]} + \frac{i}{2}\mathbf{k}^i U^i_{[1,1]} - \frac{1}{4}U_{[2,0]}\right] + \mathcal{O}\left(\epsilon^6\right), \tag{6.42}$$

where this function was defined as the *modified factor*, $\mathcal{R}_{\underline{k}}(L^+,0;\mathbf{y})$, and is, up to a phase, the Fourier transform of the scalar propagator

$$\int_{\mathbf{x}} e^{-i\mathbf{k}\mathbf{x}}\mathcal{G}_{k^+}(L^+,\mathbf{x};0,\mathbf{y}) = e^{-ik^-L^+}e^{-i\mathbf{k}\mathbf{y}}\mathcal{R}_{\underline{k}}(L^+,0;\mathbf{y}). \tag{6.43}$$

In Eq. (6.42), the color objects $U^{i\cdots j}_{[\alpha,\beta]}(L^+,0;\mathbf{y})$, where we have dropped the function argument to make the equation shorter, are referred to as the *decorated Wilson lines* and are non-eikonal corrections to the usual Wilson lines. For the definition of these objects we refer to [44].

Thus, the Fourier transform of the non-eikonal dipole function, Eqs. (6.6) and (6.7), can be written in terms of the modified factor as

$$\int_{\mathbf{x}} e^{-i\mathbf{k}\cdot\mathbf{x}} d^{(1)}(L^+,0|\mathbf{x},\mathbf{y},k^+;\bar{\mathbf{y}}) = \frac{e^{-ik^-L^+}e^{-i\mathbf{k}\cdot\mathbf{y}}}{(N_c^2-1)}\left\langle \mathrm{Tr}\left[\mathcal{R}_{\underline{k}}(L^+,0;\mathbf{y})U^\dagger_{\bar{\mathbf{y}}}(L^+,0)\right]\right\rangle_T, \tag{6.44}$$

$$\int_{\mathbf{x},\bar{\mathbf{x}}} e^{-i\mathbf{k}\cdot(\mathbf{x}-\bar{\mathbf{x}})} d^{(2)}(L^+,0|\mathbf{x},\mathbf{y},k^+;\bar{\mathbf{x}},\bar{\mathbf{y}},k^+) = \frac{e^{-i\mathbf{k}\cdot(\mathbf{y}-\bar{\mathbf{y}})}}{(N_c^2-1)}\left\langle \mathrm{Tr}\left[\mathcal{R}_{\underline{k}}(L^+,0;\mathbf{y})\mathcal{R}^\dagger_{\underline{k}}(L^+,0;\bar{\mathbf{y}})\right]\right\rangle_T. \tag{6.45}$$

Therefore, by using the non-eikonal expansion given in Eq. (6.42) we can write the Fourier transform of the 1st order NE dipole function as

$$e^{ik^-L^+ + i\mathbf{k}\cdot\mathbf{y}}\int_{\mathbf{x}} e^{-i\mathbf{k}\cdot\mathbf{x}} d^{(1)}(L^+,0|\mathbf{x},\mathbf{y},k^+;\bar{\mathbf{y}}) = \mathcal{O}(\mathbf{r}) + \frac{2i\epsilon^2}{Q_s^2}\left[\mathbf{k}^i\mathcal{O}^i_{[0,1]}(\mathbf{r}) + \frac{i}{2}\mathcal{O}_{[1,0]}(\mathbf{r})\right] + \left(\frac{2i\epsilon^2}{Q_s^2}\right)^2\left[\mathbf{k}^i\mathbf{k}^j\mathcal{O}^{ij}_{[0,2]}(\mathbf{r}) + \frac{i}{2}\mathbf{k}^i\mathcal{O}^i_{[1,1]}(\mathbf{r}) - \frac{1}{4}\mathcal{O}_{[2,0]}(\mathbf{r})\right] + \mathcal{O}\left(\epsilon^6\right), \tag{6.46}$$

where the tensors $\mathcal{O}^{i\cdots j;l\cdots m}_{[\alpha,\beta];[\gamma,\delta]}(\mathbf{r})$ are referred to as the *decorated dipoles* and are the leading eikonal corrections to the eikonal dipole function $\mathcal{O}(\mathbf{r}) = d^{(0)}(\mathbf{r})$. Furthermore, we note that in order to write Eq. (6.46) we have assumed translational invariance of the decorated dipoles and written $\mathbf{r} = \mathbf{y} - \bar{\mathbf{y}}$. The definition of these objects is

$$\mathcal{O}(\mathbf{r}) = \frac{1}{N_c^2-1}\left\langle \mathrm{Tr}\left[U_{\mathbf{y}}(L^+,0)U^\dagger_{\bar{\mathbf{y}}}(L^+,0)\right]\right\rangle_T, \tag{6.47}$$

$$\mathcal{O}^{i\cdots j}_{[\alpha,\beta]}(\mathbf{r}) = \frac{1}{N_c^2-1}\left\langle \mathrm{Tr}\left[U^{i\cdots j}_{[\alpha,\beta]}(L^+,0;\mathbf{y})U^\dagger_{\bar{\mathbf{y}}}(L^+,0)\right]\right\rangle_T, \tag{6.48}$$

$$\mathcal{O}^{i\cdots j;l\cdots m}_{[\alpha,\beta];[\gamma,\delta]}(\mathbf{r}) = \frac{1}{N_c^2-1}\left\langle \mathrm{Tr}\left[U^{i\cdots j}_{[\alpha,\beta]}(L^+,0;\mathbf{y})U^{l\cdots m\dagger}_{[\gamma,\delta]}(L^+,0;\bar{\mathbf{y}})\right]\right\rangle_T. \tag{6.49}$$

On the other hand, the Fourier transform of the 2nd order NE dipole function can be written in the same fashion and is

$$
\begin{aligned}
&e^{i\mathbf{k}\cdot(\mathbf{y}-\bar{\mathbf{y}})}\int_{\mathbf{x},\bar{\mathbf{x}}} e^{-i\mathbf{k}\cdot(\mathbf{x}-\bar{\mathbf{x}})}d^{(2)}(L^+,0|\mathbf{x},\mathbf{y},k^+;\bar{\mathbf{x}},\bar{\mathbf{y}},k^+)\\
&\quad=\mathcal{O}(\mathbf{r})+\frac{2i\epsilon^2}{Q_s^2}\left[\mathbf{k}^i\left(\mathcal{O}^i_{[0,1]}(\mathbf{r})+\mathcal{O}^i_{[0,1]}(-\mathbf{r})\right)+\frac{i}{2}\left(\mathcal{O}_{[1,0]}(\mathbf{r})-\mathcal{O}_{[1,0]}(-\mathbf{r})\right)\right]\\
&\quad+\left(\frac{2i\epsilon^2}{Q_s^2}\right)^2\left[\mathbf{k}^i\mathbf{k}^j\Big(\mathcal{O}^{ij}_{[0,2]}(\mathbf{r})+\mathcal{O}^{ij}_{[0,2]}(-\mathbf{r})+\mathcal{O}^{ij}_{[0,1];[0,1]}(\mathbf{r})\Big)\right.\\
&\qquad+\mathbf{k}^i\frac{i}{2}\Big(\mathcal{O}^i_{[1,1]}(\mathbf{r})-\mathcal{O}^i_{[1,1]}(-\mathbf{r})+\mathcal{O}^i_{[1,0];[0,1]}(\mathbf{r})-\mathcal{O}^i_{[1,0];[0,1]}(-\mathbf{r})\Big)\\
&\qquad\left.-\frac{1}{4}\Big(\mathcal{O}_{[2,0]}(\mathbf{r})-\mathcal{O}_{[2,0]}(-\mathbf{r})+\mathcal{O}_{[1,0];[1,0]}(\mathbf{r})\Big)\right]+\mathcal{O}\left(\epsilon^6\right). \qquad (6.50)
\end{aligned}
$$

Therefore we can make a one-to-one comparison between Eqs. (6.34) and (6.46), and Eqs. (6.31) and (6.50) in order to obtain a parameterization of the decorated dipoles within the GBW model, i.e., assuming a Gaussian form for them. From one side we have that the expansion of Eq. (6.34) in terms of ϵ^2 up to order ϵ^6 is

$$
\begin{aligned}
&e^{ik^-L^+ + i\mathbf{k}\cdot\mathbf{y}}\int_{\mathbf{x}} e^{-i\mathbf{k}\cdot\mathbf{x}}d^{(1)}(L^+,0|\mathbf{x},\mathbf{y},k^+;\bar{\mathbf{y}})\\
&=e^{-\frac{Q_s^2}{4}\mathbf{r}^2}\left\{1-\frac{2i\epsilon^2}{Q_s^2}\frac{Q_s^2}{4}\left[\mathbf{k}^i\mathbf{r}^i-i\left(\frac{Q_s^2}{6}\mathbf{r}^2-1\right)\right]+\left(\frac{2i\epsilon^2}{Q_s^2}\right)^2\left[\mathbf{k}^i\mathbf{k}^j\left(\frac{Q_s^4}{32}\mathbf{r}^i\mathbf{r}^j-\frac{Q_s^2}{12}\delta^{ij}\right)\right.\right.\\
&\quad\left.\left.-i\mathbf{k}^i\mathbf{r}^iQ_s^4\left(\frac{11}{96}+\frac{Q_s^2}{96}\mathbf{r}^2\right)+Q_s^4\left(-\frac{5}{96}+\frac{3}{160}Q_s^2\mathbf{r}^2-\frac{Q_s^4}{1152}\mathbf{r}^4\right)\right]\right\}+\mathcal{O}(\epsilon^6). \qquad (6.51)
\end{aligned}
$$

Performing a term by term comparison between Eqs. (6.46) and (6.51), we find the following parameterization for the decorated dipoles in the Gaussian ansatz:

$$\mathcal{O}(\mathbf{r})=e^{-\frac{Q_s^2}{4}\mathbf{r}^2}, \qquad (6.52)$$

$$\mathcal{O}^i_{[0,1]}(\mathbf{r})=-\frac{Q_s^2}{4}\mathbf{r}^ie^{-\frac{Q_s^2}{4}\mathbf{r}^2}, \qquad (6.53)$$

$$\mathcal{O}_{[1,0]}(\mathbf{r})=\frac{Q_s^2}{12}\left(-6+Q_s^2\mathbf{r}^2\right)e^{-\frac{Q_s^2}{4}\mathbf{r}^2}, \qquad (6.54)$$

$$\mathcal{O}^{ij}_{[0,2]}(\mathbf{r})=\frac{Q_s^2}{4}\left(-\frac{1}{3}\delta^{ij}+\frac{Q_s^2}{8}\mathbf{r}^i\mathbf{r}^j\right)e^{-\frac{Q_s^2}{4}\mathbf{r}^2}, \qquad (6.55)$$

$$\mathcal{O}^i_{[1,1]}(\mathbf{r})=-\frac{Q_s^4}{48}\mathbf{r}^i\left(11+Q_s^2\mathbf{r}^2\right)e^{-\frac{Q_s^2}{4}\mathbf{r}^2}, \qquad (6.56)$$

$$\mathcal{O}_{[2,0]}(\mathbf{r})=\frac{Q_s^4}{8}\left(\frac{5}{3}-\frac{3}{5}Q_s^2\mathbf{r}^2+\frac{1}{36}Q_s^4\mathbf{r}^4\right)e^{-\frac{Q_s^2}{4}\mathbf{r}^2}. \qquad (6.57)$$

On the other hand, using Eq. (6.31) we can write

$$e^{i\mathbf{k}\cdot(\mathbf{y}-\bar{\mathbf{y}})}\int_{\mathbf{x},\bar{\mathbf{x}}} e^{-i\mathbf{k}\cdot(\mathbf{x}-\bar{\mathbf{x}})}d^{(2)}(L^+,0|\mathbf{x},\mathbf{y},k^+;\bar{\mathbf{x}},\bar{\mathbf{y}},k^+)=e^{-\frac{1}{4}Q_s^2\mathbf{r}^2}. \qquad (6.58)$$

Since the the 2nd order NE dipole function does not encode any finite width effect in the case in where both longitudinal momenta are equal, it is $\mathcal{O}(\epsilon^0)$. Thus by comparing Eqs. (6.50) and (6.58) keeping in mind that the NE corrections in Eq. (6.50) have to be zero in the Gaussian approximation, we obtain the following constraints to the decorated dipoles:

$$\mathcal{O}^{ij}_{[0,1];[0,1]}(\mathbf{r}) = -2\mathcal{O}^{ij}_{[0,2]}(\mathbf{r}), \tag{6.59}$$

$$\mathcal{O}^{i}_{[1,0];[0,1]}(\mathbf{r}) - \mathcal{O}^{i}_{[1,0];[0,1]}(-\mathbf{r}) = -2\mathcal{O}^{i}_{[1,1]}(\mathbf{r}), \tag{6.60}$$

$$\mathcal{O}_{[1,0];[1,0]}(\mathbf{r}) = 2\mathcal{O}_{[2,0]}(\mathbf{r}). \tag{6.61}$$

Therefore we conclude that by comparing the non-eikonal expansion given in [43, 44], which is independent of the model, with our approach, which relays on the Gaussian form of the dipole functions, we are able to obtain a parameterization of the color dipoles in the Gaussian ansatz that should be valid for small size dipoles. This parameterization may be useful for performing phenomenological studies in calculations that include finite width effects.

6.4 Non-eikonal multi-gluon production

We now move to the general case given in Eq. (6.4) where n-gluons are produced. As stated in Section 6.2, in this chapter we will assume that the Area Enhancement approximation still holds in the non-eikonal case and therefore we write Eq. (6.4), analogous to Eq. (4.57), as

$$\frac{d^n N}{\prod_{i=1}^n d\eta_{2i-1} d^2\mathbf{k}_{2i-1}} = \frac{1}{2^n (2\pi)^{3n}} \int \left(\prod_{i=1}^{2n} \frac{d^2\mathbf{q}_i}{(2\pi)^2} \right) \left(\sum_{\sigma\in\Pi(\chi)} \prod_{\{i,j\}\in\sigma} \left\langle \Omega_i \Omega_j \right\rangle_p \right) \times \left(\sum_{\omega\in\Pi(\chi)} \prod_{\{\alpha,\beta\}\in\omega} \left\langle \Lambda_\alpha \Lambda_\beta \right\rangle_T \right), \tag{6.62}$$

where $\chi = \{1, 2, \ldots, 2n\}$ and $\Pi(\chi)$ the set of partitions of χ with disjoint pairs. The function Ω_i was defined in Eq. (4.53) and is proportional to the projectile source where when i is odd the source sits on the left side of the cut and when i is even it sits on the right side. The 2-point function of this object can be written as

$$\left\langle \Omega_i \Omega_j \right\rangle_p = \frac{\delta^{b_i b_j}}{N_c^2 - 1} \mu_p^2\big((-1)^{i+1}\mathbf{q}_i, (-1)^{j+1}\mathbf{q}_j\big), \quad \mu_p^2(\mathbf{k}, \mathbf{q}) = \pi B_p e^{-\frac{(\mathbf{k}+\mathbf{q})^2}{4} B_p}. \tag{6.63}$$

Note that this equation differs with respect to Eq. (4.53) since in Section 4.4 we did the change of variable $\mathbf{q} \to \mathbf{k} - \mathbf{q}$. The factor $(-1)^{i+1}$ is introduced in order to take into account the change of sign in the transverse momentum when the source is on the right side of the cut, i.e., with i even.

On the other hand, the object Λ_α is, in contrast with the one defined in Eq. (4.46), a non-eikonal function and is defined as

$$\Lambda_\alpha = \overline{\mathcal{M}}^{a_\alpha b_\alpha}_{\lambda_\alpha}(\underline{k}_\alpha, \mathbf{q}_\alpha), \tag{6.64}$$

where, again, when α is odd it belongs to the left side of the cut and when α is even it is on the right side, i.e., it is hermitian.

We note that, as in Eqs. (4.47) to (4.49), we have to impose the constraints

$$\underline{k}_{2n} = \underline{k}_{2n-1}, \tag{6.65}$$
$$a_{2n} = a_{2n-1}, \tag{6.66}$$
$$\lambda_{2n} = \lambda_{2n-1}, \tag{6.67}$$

namely that the color, polarization and momenta, both transverse and longitudinal, of the produced gluons have to be the same at both sides of the cut. We are also adopting the convenience that these variables are labeled by odd indices.

With the same arguments as in Section 6.2 when we discussed the justification of the Area Enhancement model, in the case where the target has a finite width, L^+, the fluctuation time of the target's field is much larger than its extent and we can assume that the chromo-electric domains do not decohere within the interaction of the produced gluon with the target. Thus we argue that each domain has to be color neutral and the target average has to be a singlet. Therefore we can write

$$\Big\langle \Lambda_\alpha \Lambda_\beta \Big\rangle_T = \frac{\delta^{a_\alpha a_\beta}\delta^{b_\alpha b_\beta}}{(N_c^2-1)^2} \Big\langle \mathrm{Tr}\left[\overline{\mathcal{M}}_{\lambda_\alpha}(\underline{k}_\alpha, \mathbf{q}_\alpha)\overline{\mathcal{M}}_{\lambda_\beta}(\underline{k}_\beta, \mathbf{q}_\beta)\right] \Big\rangle_T . \tag{6.68}$$

The target average given in this equation can be expanded by squaring Eq. (6.3) leading to

$$\begin{aligned}
\Big\langle \Lambda_\alpha \Lambda_\beta \Big\rangle_T = \frac{\delta^{a_\alpha a_\beta}\delta^{b_\alpha b_\beta}}{N_c^2-1} \int_{\mathbf{y}_\alpha,\mathbf{y}_\beta,\mathbf{x}_\alpha,\mathbf{x}_\beta} & e^{i(-1)^{\alpha+1}(\mathbf{q}_\alpha\cdot\mathbf{y}_\alpha - \mathbf{k}_\alpha\cdot\mathbf{x}_\alpha) + i(-1)^{\beta+1}(\mathbf{q}_\beta\cdot\mathbf{y}_\beta - \mathbf{k}_\beta\cdot\mathbf{x}_\beta)} \\
\times \Bigg\{ & 2\frac{\mathbf{k}_\alpha^{\lambda_\alpha}\mathbf{k}_\beta^{\lambda_\beta}}{\mathbf{k}_\alpha^2\mathbf{k}_\beta^2}\delta^{(2)}(\mathbf{x}_\alpha-\mathbf{y}_\alpha)\delta^{(2)}(\mathbf{x}_\beta-\mathbf{y}_\beta)d^{(0)}(L^+,0|\mathbf{y}_\alpha,\mathbf{y}_\beta) \\
& - 4\frac{\mathbf{k}_\alpha^{\lambda_\alpha}\mathbf{q}_\beta^{\lambda_\beta}}{\mathbf{k}_\alpha^2\mathbf{q}_\beta^2}\delta^{(2)}(\mathbf{x}_\alpha-\mathbf{y}_\alpha)d^{(1)}(L^+,0|\mathbf{y}_\alpha;\mathbf{x}_\beta,\mathbf{y}_\beta,(-1)^{\beta+1}k_\beta^+) \\
& + 2\frac{\mathbf{q}_\alpha^{\lambda_\alpha}\mathbf{q}_\beta^{\lambda_\beta}}{\mathbf{q}_\alpha^2\mathbf{q}_\beta^2}d^{(2)}(L^+,0|\mathbf{x}_\alpha,\mathbf{y}_\alpha,(-1)^{\alpha+1}k_\alpha^+;\mathbf{x}_\beta,\mathbf{y}_\beta,(-1)^{\beta}k_\beta^+) \\
& + 2\frac{L^+}{k_\beta^+}\frac{\mathbf{k}_\alpha^{\lambda_\alpha}}{\mathbf{k}_\alpha^2}\delta^{(2)}(\mathbf{x}_\alpha-\mathbf{y}_\alpha)\int_0^1 df_\beta \Big[\partial_{\mathbf{y}_\alpha^{\lambda_\alpha}} d^{(1)}(L^+,f_\beta L^+|\mathbf{y}_\alpha;\mathbf{x}_\beta,\mathbf{y}_\beta,(-1)^{\beta+1}k_\beta^+)\Big] \\
& \qquad \times d^{(0)}(f_\beta L^+,0|\mathbf{y}_\alpha,\mathbf{y}_\beta) \\
& - 2\frac{L^+}{k_\beta^+}\frac{\mathbf{q}_\alpha^{\lambda_\alpha}}{\mathbf{q}_\alpha^2}\int_0^1 df_\beta \int_{\mathbf{u}} \Big[\partial_{\mathbf{y}_\beta^{\lambda_\beta}} d^{(2)}(L^+,f_\beta L^+|\mathbf{x}_\alpha,\mathbf{u},(-1)^{\alpha+1}k_\alpha^+;\mathbf{x}_\beta,\mathbf{y}_\beta,(-1)^{\beta}k_\beta^+)\Big] \\
& \qquad \times d^{(1)}(f_\beta L^+,0|\mathbf{y}_\beta;\mathbf{u},\mathbf{y}_\alpha,(-1)^{\alpha+1}k_\alpha^+) \\
& + \frac{L^+}{k_\alpha^+}\frac{L^+}{k_\beta^+}\int_0^1 df_\beta \int_0^{f_\beta} df_\alpha \int_{\mathbf{u}} \Big[\partial_{\mathbf{y}_\beta^{\lambda_\beta}} d^{(2)}(L^+,f_\beta L^+|\mathbf{x}_\alpha,\mathbf{u},(-1)^{\alpha+1}k_\alpha^+;\mathbf{x}_\beta,\mathbf{y}_\beta,(-1)^{\beta}k_\beta^+)\Big] \\
& \qquad \times \Big[\partial_{\mathbf{y}_\alpha^{\lambda_\alpha}} d^{(1)}(f_\beta L^+,f_\alpha L^+|\mathbf{y}_\beta;\mathbf{u},\mathbf{y}_\alpha,(-1)^{\alpha+1}k_\alpha^+)\Big] d^{(0)}(f_\alpha L^+,0|\mathbf{y}_\alpha,\mathbf{y}_\beta) \\
& \qquad + (\alpha \leftrightarrow \beta) \Bigg\},
\end{aligned} \tag{6.69}$$

where we have defined $f_\alpha = y_\alpha^+/L^+$ and analogously with f_β. In this equation the factors like $(-1)^\alpha$ are introduced in order to account for which side of the cut is the object Λ_α. Note that in the case $\alpha = 1$ and $\beta = 2$ this equation reduces to, apart from the Kronecker deltas, Eq. (6.25).

The integrals over the transverse coordinates in Eq. (6.69) can be solved by using the definition of the non-eikonal dipole functions, Eqs. (6.8), (6.18) and (6.21), and the solution of the Gaussian-like integral, Eq. (6.27). In order to make the expressions shorter let us introduce the notation $\pm k_a \equiv (-1)^{a+1}k_a$, i.e. when the respective momentum, longitudinal or transverse, is on the left side of the cut it is multiplied by $+1$ and when it is on the right side, changing its sign due to the Fourier transform, by -1. Thus, by performing the integrals over the transverse space and introducing this notation we can write Eq. (6.69) as

$$
\begin{aligned}
\Big\langle \Lambda_\alpha \Lambda_\beta \Big\rangle_T &= \frac{\delta^{a_\alpha a_\beta}\delta^{b_\alpha b_\beta}}{N_c^2-1}(2\pi)^2\delta^{(2)}\big[\pm(\mathbf{k}_\alpha-\mathbf{q}_\alpha)+\pm(\mathbf{k}_\beta-\mathbf{q}_\beta)\big] \\
&\times\Bigg\{2\frac{\mathbf{k}_\alpha^{\lambda_\alpha}\mathbf{k}_\beta^{\lambda_\beta}}{\mathbf{k}_\alpha^2\mathbf{k}_\beta^2}I_{\text{aft}-\text{aft}}\big(\mathbf{k}_\beta,\mathbf{q}_\beta\big)-4\frac{\mathbf{k}_\alpha^{\lambda_\alpha}\mathbf{q}_\beta^{\lambda_\beta}}{\mathbf{k}_\alpha^2\mathbf{q}_\beta^2}I_{\text{aft}-\text{bef}}\Big(\mathbf{k}_\beta,\mathbf{q}_\beta,\pm k_\beta^+\Big) \\
&+2\frac{\mathbf{q}_\alpha^{\lambda_\alpha}\mathbf{q}_\beta^{\lambda_\beta}}{\mathbf{q}_\alpha^2\mathbf{q}_\beta^2}I_{\text{bef}-\text{bef}}\Big(\pm\mathbf{k}_\alpha,\pm\mathbf{q}_\alpha,\pm\mathbf{k}_\beta,\pm\mathbf{q}_\beta;\pm k_\alpha^+,\pm k_\beta^+\Big) \\
&+2\frac{L^+}{k_\beta^+}\frac{\mathbf{k}_\alpha^{\lambda_\alpha}}{\mathbf{k}_\alpha^2}\int_0^1 df_\beta I_{\text{aft}-\text{in}}^{\lambda_\beta}\Big(\pm\mathbf{k}_\beta,\pm\mathbf{q}_\beta,\pm k_\beta^+;f_\beta\Big) \\
&-2\frac{L^+}{k_\beta^+}\frac{\mathbf{q}_\alpha^{\lambda_\alpha}}{\mathbf{q}_\alpha^2}\int_0^1 df_\beta I_{\text{bef}-\text{in}}^{\lambda_\beta}\Big(\pm\mathbf{k}_\alpha,\pm\mathbf{q}_\alpha,\pm\mathbf{k}_\beta,\pm\mathbf{q}_\beta;\pm k_\alpha^+,\pm k_\beta^+;f_\beta\Big) \\
&+\frac{L^+}{k_\alpha^+}\frac{L^+}{k_\beta^+}\int_0^1 df_\beta\int_0^{f_\beta} df_\alpha I_{\text{in}-\text{in}}^{\lambda_\alpha\lambda_\beta}\Big(\pm\mathbf{k}_\alpha,\pm\mathbf{k}_\beta,\pm\mathbf{q}_\beta;\pm k_\alpha^+,\pm k_\beta^+;f_\alpha,f_\beta\Big) \\
&+(\alpha\leftrightarrow\beta)\Bigg\}.
\end{aligned}
\tag{6.70}
$$

Each term of this equation corresponds to the result of performing an integral like Eq. (6.27) on each term of Eq. (6.69).

The first contribution of Eq. (6.70) is the case where both gluons are emitted after the interaction of the source with the target and reads

$$
I_{\text{aft}-\text{aft}}\big(\mathbf{k}_\beta,\mathbf{q}_\beta\big)=\frac{4\pi}{Q_s^2}\exp\left\{-\frac{(\mathbf{k}_\beta-\mathbf{q}_\beta)^2}{Q_s^2}\right\}. \tag{6.71}
$$

Note that this term is independent of the sign of the transverse momenta and because of that its argument does not carry the $\pm$ notation in Eq. (6.70). Moreover, this term is invariant under the change $\alpha \leftrightarrow \beta$ because of the δ-function in Eq. (6.70).

The second contribution corresponds to the case where the gluon represented by the index α, which we call gluon α, is emitted after the interaction of the source with the target and the gluon β is emitted before. On the other hand, the inverse situation is given by the mirror term $\alpha \leftrightarrow \beta$. This contribution can be computed by solving the integrals

over the transverse coordinates and is written as

$$I_{\text{aft}-\text{bef}}\left(\mathbf{k}_\beta, \mathbf{q}_\beta, k_\beta^+\right) = \frac{4\pi}{Q_s^2}\frac{\epsilon_\beta}{\sin\epsilon_\beta}\exp\left\{-\frac{\epsilon_\beta}{Q_s^2\sin\epsilon_\beta}\left[(\mathbf{k}_\beta^2+\mathbf{q}_\beta^2)\cos\epsilon_\beta - 2\mathbf{k}_\beta\cdot\mathbf{q}_\beta\right]\right\}, \quad (6.72)$$

where the dependence on k^+ is given implicitly on ϵ, Eq. (6.19). This equation only depends on k_β^+ because only the gluon β traverses the target.

The third contribution in Eq. (6.70) correspond to the case in which both gluons are emitted before the target and can be written as

$$I_{\text{bef}-\text{bef}}\left(\mathbf{k}_\alpha, \mathbf{q}_\alpha, \mathbf{k}_\beta, \mathbf{q}_\beta; k_\alpha^+, k_\beta^+\right) = \frac{4\pi}{Q_s^2}\frac{\epsilon_+}{\sin\epsilon_+} \times \exp\left\{-\frac{1}{Q_s^2}\left[\frac{\epsilon_\alpha^2\epsilon_\beta^2}{\epsilon_+^2}(\mathbf{k}_\alpha+\mathbf{k}_\beta)^2 + \frac{\epsilon_+}{\tan\epsilon_+}(\mathbf{K}^2+\mathbf{Q}^2) - 2\frac{\epsilon_+}{\sin\epsilon_+}\mathbf{K}\cdot\mathbf{Q}\right]\right\}, \quad (6.73)$$

where we have defined $\epsilon_+^2 = \epsilon_\alpha^2 + \epsilon_\beta^2$ and

$$\mathbf{K} = \frac{k_\beta^+\mathbf{k}_\alpha - k_\alpha^+\mathbf{k}_\beta}{k_\alpha^+ + k_\beta^+}, \qquad \mathbf{Q} = \frac{k_\beta^+\mathbf{q}_\alpha - k_\alpha^+\mathbf{q}_\beta}{k_\alpha^+ + k_\beta^+}. \quad (6.74)$$

Note that in the case where the gluons have the same momenta and are sitting at different sides of the cut, which in our notation means that $\alpha = 2m-1$ and $\beta = 2m$ (or vice-versa) for some integer m, we will have that $k_\beta^+ = k_\alpha^+$ and $\mathbf{k}_\beta = \mathbf{k}_\alpha$ because of Eq. (6.65). However, since the momenta at the right side of the cut are evaluated with a different sign in Eq. (6.70), we would have $\epsilon_+ \to 0$, $\mathbf{K}\to\mathbf{k}_\alpha$ and[1] $\mathbf{Q}\to\mathbf{q}_\alpha$, and the non-eikonal corrections are washed out leading to the same result as in Eq. (6.32). Furthermore, Eq. (6.73) is symmetric under the change $\alpha\leftrightarrow\beta$ as we should expect.

The fourth contribution in Eq. (6.70) corresponds to the case where the gluon α is emitted after the interaction of the source with the target and the gluon β is emitted inside the target, the opposite situation is given by the mirror term $\alpha\leftrightarrow\beta$. The expression of this contribution reads

$$I_{\text{aft}-\text{in}}^{\lambda_\beta}\left(\mathbf{k}_\beta, \mathbf{q}_\beta, k_\beta^+; f_\beta\right) = -\frac{4\pi i}{Q_s^2\left[1+\epsilon_\beta f_\beta\cot(\tilde{f}_\beta\epsilon_\beta)\right]^2}\frac{\epsilon_\beta}{\sin(\tilde{f}_\beta\epsilon_\beta)}\left[\mathbf{q}_\beta^{\lambda_\beta} + \frac{f_\beta\epsilon_\beta}{\sin(\tilde{f}_\beta\epsilon_\beta)}\mathbf{k}_\beta^{\lambda_\beta}\right] \times \exp\left\{-\frac{\epsilon_\beta}{Q_s^2\left[1+f_\beta\epsilon_\beta\cot(\tilde{f}_\beta\epsilon_\beta)\right]}\left[\frac{\mathbf{k}_\beta^2+\mathbf{q}_\beta^2}{\tan(\tilde{f}_\beta\epsilon_\beta)} - 2\frac{\mathbf{k}_\beta\cdot\mathbf{q}_\beta}{\sin(\tilde{f}_\beta\epsilon_\beta)} - \epsilon_\beta f_\beta\mathbf{k}_\beta^2\right]\right\}, \quad (6.75)$$

where we have defined $\tilde{f}_\beta = 1-f_\beta = \frac{L^+-y_\beta^+}{L^+}$ which is the fraction of the medium traversed by gluon β. This result is identical to the one evaluated in the single production case, Eq. (6.37). The reason is that the main difference between the calculation performed in this section and the one in Section 6.3 is that we are assuming that the 2$^{\text{nd}}$ order NE dipole function is evaluated at different longitudinal momenta and therefore its expression is different than the one used in Section 6.3. However, since both Eqs. (6.71), (6.72)

[1]Because of the δ-function in Eq. (6.70) we have that $\mathbf{q}_\beta = \mathbf{q}_\alpha$ and it will be evaluated with different sign.

and (6.75) only contain a single longitudinal momenta, i.e., the 2$^{\text{nd}}$ order NE dipole is not present in them, their expressions will be, up to some factors, analogous to the ones derived in Section 6.3.

The fifth contribution in Eq. (6.70) corresponds to the case where the gluon α is emitted before the interaction of the source with the target and the gluon β is emitted inside the target, the opposite situation is given by its mirror term $\alpha \leftrightarrow \beta$. We can write this contribution as

$$
\begin{aligned}
I^{\lambda_\beta}_{\text{bef}-\text{in}}\Big(\mathbf{k}_\alpha,\mathbf{q}_\alpha,\mathbf{k}_\beta,\mathbf{q}_\beta;k^+_\alpha,k^+_\beta;f_\beta\Big) &= -\frac{4\pi i\epsilon_\alpha \csc(\tilde{f}_\beta\epsilon_+)\csc(f_\beta\epsilon_\alpha)}{\epsilon_+ Q_s^2\left[\epsilon_\alpha\cot(f_\beta\epsilon_\alpha)+\epsilon_+\cot(\tilde{f}_\beta\epsilon_+)\right]^2} \\
&\times\left[\left(\epsilon_+^2+\frac{\epsilon_\beta^2}{\cos(f_\beta\epsilon_\alpha)}+\frac{\epsilon_\alpha\epsilon_+\tan(f_\beta\epsilon_\alpha)}{\tan(\tilde{f}_\beta\epsilon_+)}\right)\epsilon_\alpha\Delta\mathbf{k}^{\lambda_\beta}-\frac{\epsilon_\alpha\epsilon_+^2}{\cos(f_\beta\epsilon_\alpha)}\mathbf{Q}^{\lambda_\beta}-\frac{\epsilon_+^3\tan(f_\beta\epsilon_\alpha)}{\sin(\tilde{f}_\beta\epsilon_+)}\mathbf{K}^{\lambda_\beta}\right] \\
&\times\exp\Bigg\{-\frac{\cot(\tilde{f}_\beta\epsilon_+)}{\epsilon_+ Q_s^2\left[\epsilon_\alpha\cot(f_\beta\epsilon_\alpha)+\epsilon_+\cot(\tilde{f}_\beta\epsilon_+)\right]}\left[\epsilon_+^2\left(\frac{\epsilon_\alpha}{\tan(f_\beta\epsilon_\alpha)}-\epsilon_+\tan(\tilde{f}_\beta\epsilon_+)\right)\mathbf{K}^2\right. \\
&-\epsilon_\alpha^2\epsilon_+^2\left(\frac{\cot(f_\beta\epsilon_\alpha)}{\epsilon_\alpha}-\frac{\tan(\tilde{f}_\beta\epsilon_+)}{\epsilon_+}\right)\mathbf{q}_\alpha^2+\frac{\epsilon_\alpha\epsilon_\beta^2}{\epsilon_+^2}\left(\left(\frac{\epsilon_\beta^2}{\tan(f_\beta\epsilon_\alpha)}+\epsilon_\alpha\epsilon_+^2\tilde{f}_\beta\right)+\frac{\epsilon_\alpha^2\epsilon_+\tilde{f}_\beta\tan(\tilde{f}_\beta\epsilon_+)}{\tan(f_\beta\epsilon_\alpha)}\right)\Delta\mathbf{k}^2 \\
&\left.+2\frac{\epsilon_\alpha\epsilon_\beta^2}{\sin(f_\beta\epsilon_\alpha)}\Delta\mathbf{k}\cdot\mathbf{q}_\alpha-2\frac{\epsilon_\alpha\epsilon_+^2\sec(\tilde{f}_\beta\epsilon_+)}{\sin(f_\beta\epsilon_\alpha)}\mathbf{K}\cdot\mathbf{q}_\alpha-2\frac{\epsilon_\alpha\epsilon_\beta^2\sec(\tilde{f}_\beta\epsilon_+)}{\tan(f_\beta\epsilon_\alpha)}\Delta\mathbf{k}\cdot\mathbf{K}\right]\Bigg\}, \quad (6.76)
\end{aligned}
$$

where we have introduced $\Delta\mathbf{k}=\mathbf{k}_\alpha+\mathbf{k}_\beta$. Because we are including the non-eikonal effects due to the difference between the longitudinal momenta, we have performed the derivative in $\mathbf{y}^{\lambda_\beta}$ and we have integrated over an extra transverse position, $\mathbf{u}$, in the fifth term of Eq. (6.69), this expression is very long and non-trivial in the non-eikonal parameters ϵ_α and ϵ_β. We note that in the case where both momenta are equal, i.e. when $\Delta\mathbf{k}\to 0$, $\epsilon_+\to 0$, $\mathbf{K}\to\mathbf{k}_\alpha$ and $\mathbf{Q}\to\mathbf{q}_\alpha$, this equation simplifies to, apart from the prefactors, Eq. (6.39).

Finally, the last contribution of Eq. (6.70), $I^{\lambda_\alpha\lambda_\beta}_{\text{in}-\text{in}}\Big(\mathbf{k}_\alpha,\mathbf{k}_\beta,\mathbf{q}_\beta;k^+_\alpha,k^+_\beta;f_\alpha,f_\beta\Big)$, accounts to the situation in which both gluons are emitted in the interior of the target. However, since this equation involves an extra derivative in $\mathbf{y}^{\lambda_\alpha}$ with respect to Eq. (6.76) it is even longer. For this reason we will not write it explicitly in this manuscript. We simply note that in order to obtain this contribution one has to introduce the NE dipole functions, Eqs. (6.8), (6.18) and (6.21), in the last term of Eq. (6.69), to perform the derivatives in $\mathbf{y}^{\lambda_\alpha}$ and $\mathbf{y}^{\lambda_\beta}$ and the result will be five integrals of the form of Eq. (6.27) which can be solved trivially, although giving a long expression.

With Eqs. (6.71) to (6.73), (6.75) and (6.76) we have finalized our analysis on multi-gluon production beyond eikonal accuracy. Let us recapitulate the results of this section. In order to compute the n-gluon spectra we have to evaluate the Wick expansions given in Eq. (6.62) which, since we are assuming the MV model for the projectile configurations, depends only on the 2-point correlator of the projectile given in Eq. (6.63) and, since we are using the Area Enhancement model in the target average, on the 2-point correlator of the reduced matrix amplitude given in Eq. (6.70). By expanding the $\left(\frac{(2n)!}{2^n n!}\right)^2$ terms of Eq. (6.62) and evaluating the 2-point correlators we are able to compute the n-gluon

spectra at any value of n neglecting, of course, contributions that are subleading in powers of ρ_p that may be important. Because in this approach the multi-gluon spectra contain a large number of terms in the sum it is convenient to use the diagrammatic approach presented in Section 4.4.1. However, since in this manuscript we will restrict ourselves to the case of 2-gluon production, which only contains 9 terms, we will not use the Wick diagrams. To finalize our discussion let us note that the single gluon spectrum can be computed in the approach presented in this section just by writing

$$\frac{dN}{d\eta d^2\mathbf{k}} = \frac{g^2}{2(2\pi)^3}\int_{\mathbf{q}_1,\mathbf{q}_2}\left\langle\Omega_1\Omega_2\right\rangle_p\left\langle\Lambda_1\Lambda_2\right\rangle_T, \tag{6.77}$$

where it is straightforward to see that, by using Eqs. (6.63) and (6.70), this equation reduces to Eq. (6.28). In the next section we will explore the case of double gluon production.

6.4.1 Double gluon production

In the case of double gluon production, i.e., $n = 2$, Eq. (6.62) can be written as

$$\begin{aligned}\frac{d^2N}{d\eta_1 d^2\mathbf{k}_1 d\eta_3 d^2\mathbf{k}_3} = \frac{g^4}{4(2\pi)^6}\int_{\mathbf{q}_1,\mathbf{q}_2,\mathbf{q}_3,\mathbf{q}_4} &\times\left(\left\langle\Omega_1\Omega_2\right\rangle_p\left\langle\Omega_3\Omega_4\right\rangle_p + \left\langle\Omega_1\Omega_3\right\rangle_p\left\langle\Omega_2\Omega_4\right\rangle_p + \left\langle\Omega_1\Omega_4\right\rangle_p\left\langle\Omega_2\Omega_3\right\rangle_p\right)\\ &\times\left(\left\langle\Lambda_1\Lambda_2\right\rangle_T\left\langle\Lambda_3\Lambda_4\right\rangle_T + \left\langle\Lambda_1\Lambda_3\right\rangle_T\left\langle\Lambda_2\Lambda_4\right\rangle_T + \left\langle\Lambda_1\Lambda_4\right\rangle_T\left\langle\Lambda_2\Lambda_3\right\rangle_T\right),\end{aligned} \tag{6.78}$$

where the 2-point functions are given in Eqs. (6.63) and (6.70). This equation contains the same features as the eikonal case presented in Section 4.3, that is, it has a fully uncorrelated piece which is dominant in powers of (N_c^2-1) and the collision's area $B_pQ_s^2$, $\left\langle\Omega_1\Omega_2\right\rangle_p\left\langle\Omega_3\Omega_4\right\rangle_p\left\langle\Lambda_1\Lambda_2\right\rangle_T\left\langle\Lambda_3\Lambda_4\right\rangle_T$, and it has Bose Enhancement and HBT-like correlations encoded in the subleading terms. The main difference between Eq. (6.78) and Eq. (4.7) is that the first, although invariant under the change[2] $\underline{k}_3 \to -\underline{k}_3$, is not symmetric under $\mathbf{k}_3 \to -\mathbf{k}_3$ and therefore introduces an asymmetry in the spectrum with respect to the azimuthal angle. This result is not a surprise since, as we have seen in Section 5.3, non-eikonal corrections break the accidental symmetry. For this reason the goal of this section will be to evaluate Eq. (6.78) numerically in order to see the impact of the finite width effects in the azimuthal asymmetries and, in particular, to study the odd azimuthal harmonic v_3 generated from these corrections.

In order to solve Eq. (6.78) we just have to expand the terms in between the parenthesis and to use Eqs. (6.63) and (6.70). Although this is an exhaustive work of doing by hand it is straightforward with the help of a computer. The infrared divergences that appear in the limit $\mathbf{q}_i \to 0$ in Eq. (6.70) are regulated by introducing and artificial mass μ^2 in the

[2]Making the change $\underline{k}_3 \to -\underline{k}_3$ is equivalent to interchanging the indices 3 and 4 in Eq. (6.78) which obviously leaves the spectrum invariant. This is the generalization, in the non-eikonal case, of the property Item i) given in Section 4.4.1.

denominators, i.e. we make the change $1/\mathbf{q}_i^2 \to 1/(\mathbf{q}_i^2+\mu^2)$, where its value is fixed to $\mu = 0.4$ GeV. We also fix in the numerical evaluation along this section $N_c = 3$, $A^{1/3} = 6$, $B_p = 6$ GeV^{-2} and $Q_s^2 = 2$ GeV^2.

In Fig. 6.5 we plot the solution of Eq. (6.78) and its respective eikonal limit as a function of the azimuthal angle $\Delta\phi = \arccos \frac{\mathbf{k}_1\cdot\mathbf{k}_3}{|\mathbf{k}_1||\mathbf{k}_3|}$. For this figure we have fixed $\sqrt{s_{\rm NN}} =$ 100 GeV, $\eta_1 = \eta_3 = 0.2$ and $|\mathbf{k}_1| = |\mathbf{k}_3| = 1$ GeV. We see, as we should expect, a clear asymmetry between the near- and away-side in the non-eikonal double gluon spectrum. Moreover, the finite width effects in these kinematics introduce a suppression with respect to the eikonal spectrum. This is in contrast with the results of Section 6.3.1 in which the non-eikonal corrections enhanced the single particle spectrum. We have checked that depending on the values of $\Delta\eta = \eta_3 - \eta_1$ and $\Delta k = |\mathbf{k}_3| - |\mathbf{k}_1|$ the non-eikonal corrections may enhance or suppress the eikonal result. However, due to the lack of numerical data, we cannot conclude a clear trend of the NE corrections with respect to $\Delta\eta$ or Δk. We also note that in this case the NE spectrum differs from the eikonal one by a factor 4% in the near-side and 8% in the away-side peak. This is a larger correction with respect to the single inclusive gluon spectrum discussed in Section 6.3.1.

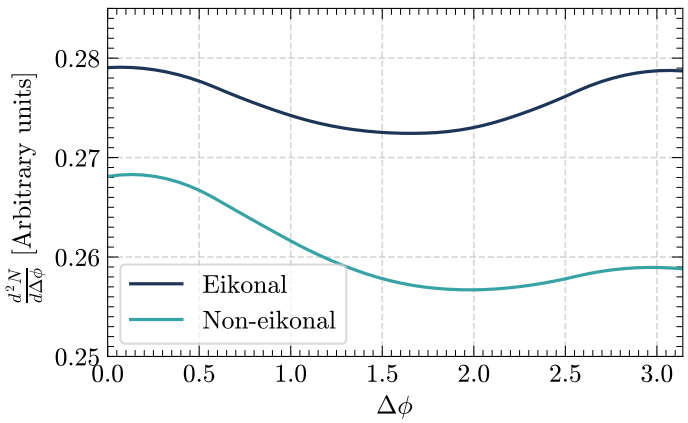

Figure 6.5.
The double inclusive gluon spectrum, Eq. (6.78), and its eikonal limit as a function of the azimuthal angle $\Delta\phi$. In this plot we have fixed $\sqrt{s_{\rm NN}} = 100$ GeV, $\eta_1 = \eta_3 = 0.2$ and $|\mathbf{k}_1| = |\mathbf{k}_3| = 1$ GeV.

In order to study the differential azimuthal harmonics of Eq. (6.78) we will use a different definition than Section 3.4 and we will write them as [126]

$$v_n(p_\perp) = \frac{V_n(p_\perp, p_\perp^{\rm ref})}{\sqrt{V_n(p_\perp^{\rm ref}, p_\perp^{\rm ref})}}, \tag{6.79}$$

where

$$V_n(|\mathbf{k}_1|, |\mathbf{k}_3|) = \frac{\int_0^{2\pi} d\Delta\phi \frac{d^2N}{d\eta_1 d^2\mathbf{k}_1 d\eta_3 d^2\mathbf{k}_3} e^{in\Delta\phi}}{\int_0^{2\pi} d\Delta\phi \frac{d^2N}{d\eta_1 d^2\mathbf{k}_1 d\eta_3 d^2\mathbf{k}_3}}. \tag{6.80}$$

Thus we use the definition given in Section 3.4 but, rather than integrating over $|\mathbf{k}_3|$, we fix $|\mathbf{k}_3| = p_\perp^{\rm ref}$. In practice, $p_\perp^{\rm ref}$ is taken to be a bin within a range of transverse momentum,

however we will take it as a fix value. The reason of this change of prescription is that, since the integrand of Eq. (6.78) is a highly oscillatory multi-dimensional function, the numerical integral over $|\mathbf{k}_3|$ gives a poor accuracy. One solution to this problem is to expand the integrand of Eq. (6.78) at next-to-next-to-eikonal accuracy, i.e. at order ϵ^4, in such a way that the function simplifies and the longitudinal integrals over y_i^+ can be performed in a closed-form. So far, in this section we define the differential azimuthal harmonics at fixed $|\mathbf{k}_3|$ and we leave a more detailed analysis for a future work.

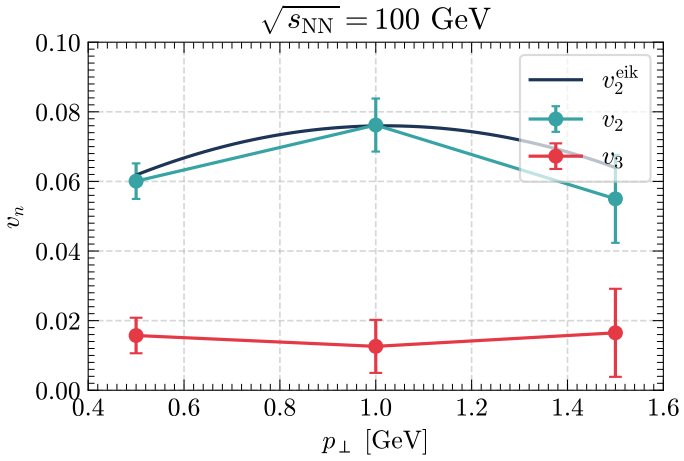

Figure 6.6.
The azimuthal harmonics of Eq. (6.78) and the elliptic harmonic in the eikonal case. For this plot we have taken $\sqrt{s_{\mathrm{NN}}} = 100$ GeV, $\eta_1 = \eta_2 = 0.2$ and $p_\perp^{\mathrm{ref}} \equiv |\mathbf{k}_3| = 1$ GeV.

In Fig. 6.6 we plot the 2-particle differential azimuthal harmonics $v_2(p_\perp)$ and $v_3(p_\perp)$ defined in Eq. (6.79) as a function of $p_\perp \equiv |\mathbf{k}_1|$. For this calculation we have fixed $\sqrt{s_{\mathrm{NN}}} = 100$ GeV, $\eta_1 = \eta_2 = 0.2$ and $p_\perp^{\mathrm{ref}} \equiv |\mathbf{k}_3| = 1$ GeV. Because of the highly oscillatory and complex nature of the integrand of Eq. (6.78) we only have been able to compute a small range of $p_\perp$ with a relatively high numerical error. However, this result is enough to conclude that we obtain a sizable value of v_3 when $\sqrt{s_{\mathrm{NN}}} = 100$ GeV and, as pointed out above, we leave a more detailed analysis for a future work.

6.5 Conclusions and Outlook

In this chapter we have obtained a generalization of the framework proposed in Chapter 4 to compute multi-gluon spectra in proton-nucleus collisions within the Area Enhancement model, i.e. contributions that are dominant in the area of the collision, by including non-eikonal corrections. The formalism of this chapter is inspired by the jet quenching framework [192] in which a non-zero longitudinal extent of the dense medium is necessary in order to study the effects of the Quark Gluon Plasma in parton propagation. Thus, although the framework presented here is not new per se, it is the first time that it has been used in order to study the finite width effects in particle production within the Color Glass Condensate.

We have seen that the non-eikonal corrections in the target 2-point average can be computed analytically if we restrict ourselves to the GBW approximation, that is, we assume that the eikonal dipole function has a Gaussian form. This approximation is justified as long as the dipole size is much smaller that $\Lambda_{\rm QCD}^{-1}$. The result for the non-eikonal dipole functions was given in Eqs. (6.8), (6.18) and (6.21), where the finite width effects are weighted by the dimensionless parameter $\epsilon^2 = \frac{Q_s^2 L^+}{2ik^+}$, and from them we were able to evaluate the single inclusive gluon spectrum beyond eikonal accuracy. Our results are summarized in Figs. 6.2 to 6.4 where we have seen that the effects of including non-eikonal corrections to the single gluon spectrum are sizable for center-of-mass energies per nucleon smaller than 100 GeV and for pseudorapidities of the produced particle smaller than 1. Thus we conclude that including the non-eikonal corrections to phenomenological studies in single gluon production is irrelevant at the energies of the LHC or the top energies of RHIC. In Section 6.3.2 we have compared the next-to-next-to-eikonal approximation of our result, i.e., an expansion up to order ϵ^4, with the one presented in [43, 44] and we have been able to find a parameterization of the so-called decorated dipoles within the Gaussian ansatz.

In Section 6.4 we have presented the formalism for computing the non-eikonal multi-gluon spectrum in pA collisions for an arbitrary number of produced gluons. The approach is based in the Area Enhancement model which we argue that it should be valid for a target with finite width since the coherence length of the chromo-electric domains are much larger than the longitudinal extent of the target. We have then solved the case in which two gluons are produced and, analogous to the analysis performed in Section 5.4 in the case of pp collisions, we have seen that the non-eikonal corrections induces an azimuthal asymmetry in the double gluon spectrum. In Section 6.4.1 we performed a numerical analysis of the azimuthal harmonics and we have found that the odd azimuthal harmonic v_3 due to non-eikonal corrections is sizable at relatively high energies, i.e., $\sqrt{s_{\rm NN}} = 100$ GeV. Thus we conclude that the effect of the non-eikonal correction is larger in the double gluon spectrum than in the single gluon spectrum. We note that, due to the lack of numerical data, the analysis performed in Section 6.4.1 can be improved by studying the dependence of v_3 with $\Delta\eta$, by using the proper definition of the azimuthal harmonics given in Section 3.4 or by analyzing more values of the collision center-of-mass energy. We therefore leave this analysis for a future work.

USC
UNIVERSIDADE
DE SANTIAGO
DE COMPOSTELA

Conclusions and outlook

In this thesis we address the problem of multi-particle production in the non-linear regime of Quantum Chromodynamics. We use the Color Glass Condensate (CGC) effective theory do describe the initial state of proton-proton (pp) or proton-nucleus (pA) collisions. Our original results are given in Chapter 4, based on [38], in Chapter 5, based on [45, 46] and in Chapter 6. They can be summarized as follows.

In Chapter 4 we compute the multi-gluon spectrum in dilute-dense, or proton-nucleus, collisions, extending the work in [40] to four gluons. We introduce the Area Enhancement model [40, 169, 170, 186] for computing the n-point target averages that includes the contributions that are leading in the overlap area of the collision, while keeping all orders in the expansion in the number of colors. We develop a diagrammatic technique to write the numerous color contractions and exploit the symmetries to group the diagrams and simplify the expressions. This technique reduces dramatically the number of integrals needed to compute the multiplicity distributions and integrated and differential cumulants, which results essential for the large number of diagrams, more than 10000, that appears for four gluon production. We use the GBW model for the dipoles that result from the target averages, and the generalized MV model for projectile averages. In order to proceed analytically as far as possible and simplify the final calculations, we use the Wigner function approach [103, 105, 106] that we extend to include quantum correlations in the projectile wave function. The Wigner function approach supposes that the final momenta of gluons is mainly acquired through interaction with the dense target and is thus suitable for a collinear projectile approximation.

Our main results in this chapter can be summarized in Figs. 4.5, 4.6, 4.8 and 4.9. For two gluon correlations, we provide analytic expressions for integrated and differential cumulants which show smooth dependences on the parameters defining the projectile and target Wigner function and dipole, respectively. For four gluon correlations we find that the second order four particle cumulant $c_2\{4\} < 0$ – thus providing a sensible second order Fourier coefficient $v_2\{4\}$, a result found in [105] (where only quark scattering is considered and partons in the projectile wave function are uncorrelated) and attributed to multiple scattering. We note that the approximation in which gluons in the projectile are uncorrelated gives results for the cumulants that are much smaller in absolute value than when correlations are included, and becoming positive for some values of Q_s and $p_\perp$. This emphasizes the importance of including the full correlations in the projectile. Our numerical results, due to the Gaussian forms that we employ for the Wigner function and dipole, cannot be considered reliable for $p_\perp$ sizable larger than Q_s. They lie in the ballpark of experimental data, for values of parameters that look reasonable. But we are aware that further analytic understanding is still required, and several pieces are still missing in our formalism: the contribution from quarks, more involved projectile and target averages,

fragmentation functions,.... All these aspects should be explored we studying multi-particle correlations before we can establish a model ready for phenomenology.

We derive in Chapter 5 the non-eikonal Lipatov vertex that takes into account the finite longitudinal width of the target to all orders. This result was conjectured in [39] after considering the first two corrections to the eikonal limit of the Lipatov vertex coming from the non-eikonal expansion of the gluon propagator obtained in [43, 44]. However, here we have presented a different derivation from first principles. Then, we have used the non-eikonal Lipatov vertex to study the single, double and triple inclusive gluon spectra in pp collisions at mid pseudorapidity. Our results are valid for dilute-dilute collisions since we consider the dilute target limit which, for double and triple inclusive gluon production, corresponds to the original Glasma Graph calculation with the exception that we take into account the non-eikonal corrections due to the finite longitudinal thickness of the target.

In the single inclusive gluon spectrum, we have shown that the non-eikonal corrections are encoded in function $\mathcal{G}_1^{\mathrm{NE}}(k^-, \lambda^+)$ that is defined in Eq. (5.31) with k^- being the light cone energy of the produced gluon and λ^+ the color correlation length along the longitudinal direction in the target. On the one hand, in the limit of $(k^-\lambda^+) \to 0$, our result reproduces the well known eikonal expression which is often referred to as the k_t-factorized formula in the CGC. On the other hand, by expanding our result to second order in $(k^-\lambda^+)$, we recover the result calculated in [39]. Our numerical results show that in the kinematic region where the non-eikonal effects are expected to be sizable, the relative importance of the non-eikonal corrections can vary from 2 to 15% with respect to the eikonal result. This shows that, depending on the kinematic region that one is interested in, the non-eikonal effects might very well be sizable.

We have also used the non-eikonal Lipatov vertex to calculate the double inclusive gluon spectrum for dilute-dilute scatterings. Adopting the same strategy that was introduced in [40], we have identified the terms that contribute to uncorrelated production, those that are responsible for Bose enhancement of the gluons in the projectile and in the target wave functions, and the terms that contribute to HBT interference effects. Our results agree with the results in [40] up to the N_c counting of the target Bose enhancement and part of the projectile Bose enhancement terms. However, it is known that this difference is a consequence of the fact that some aspects of N_c counting are different in the dilute and dense limits [40–42].

Moreover, including the non-eikonal corrections in the 2-gluon spectra has a direct consequence. On top of the function $\mathcal{G}_1^{\mathrm{NE}}(k_1^-; \lambda^+)$ that also exists in the single inclusive case, a new function $\mathcal{G}_2^{\mathrm{NE}}(k_1^-, k_2^-; L^+)$, defined in Eq. (5.44), appears which also encodes non-eikonal effects. The partners of the terms that contain $\mathcal{G}_2^{\mathrm{NE}}(k_1^-, k_2^-; L^+)$, obtained via $(\underline{k}_2 \to -\underline{k}_2)$, also appear in the double inclusive gluon production cross section but they are accompanied by $\mathcal{G}_2^{\mathrm{NE}}(k_1^-, -k_2^-; L^+)$. However, in some specific kinematic regions, namely when $k_1^- \sim k_2^-$, $\mathcal{G}_2^{\mathrm{NE}}(k_1^-, k_2^-; L^+) \gg \mathcal{G}_2^{\mathrm{NE}}(k_1^-, -k_2^-; L^+)$ which creates a sizable azimuthal asymmetry. We would like to emphasize that this asymmetry is absent in the eikonal limit. One can immediately realize that this asymmetry created by the non-eikonal corrections in the double inclusive gluon production indeed mimics the asymmetry between the forward and backward peaks in the ridge observed in the two particle correlations as we have illustrated in Fig. 5.7.

Then in Section 5.4, we have performed a numerical study of azimuthal anisotropies

generated by the non-eikonal corrections which are summarized in Figs. 5.8 to 5.10. We have seen that the odd azimuthal harmonics generated due to this asymmetry are sizable when the center-of-mass energy of the collisions is around $\sqrt{s_{\rm NN}} \sim 100$ GeV and therefore, in this case, including the non-eikonal corrections may be important for phenomenological studies of correlations in pp collisions. We have also seen that this effect is also sizable up to 2 units in the pseudorapidity difference.

Finally, we have also considered the non-eikonal triple inclusive gluon production cross section in the dilute target limit. We have identified all the terms that appear in the final result. Compared to the work performed in [40], the main difference – apart from non-eikonal corrections that we have included in our study – is that we have included all terms while only the leading N_c ones were considered in [40]. This difference is again due to the fact that N_c counting is different in the dilute and dense regimes. In our study, we have identified the terms that correlate all three gluons which originate from three-trace or double-trace contributions, which were absent in [40] since they are suppressed in powers of N_c in the dense target limit and therefore discarded there. Moreover, the non-eikonal effects enter through two new functions $\mathcal{G}_3(k_1^-, k_2^-, k_3^-; L^+)$ and $\mathcal{G}_4(k_1^-, k_2^-, k_3^-; L^+)$ that are defined in Eqs. (D.8) and (D.9) respectively, on top of the functions $\mathcal{G}_1(k^-; \lambda^+)$ and $\mathcal{G}_2(k_1^-, k_2^-; L^+)$ that already appeared in the double inclusive case. Obviously, in the limit of the vanishing L^+ these functions become one and provide the eikonal limit of the triple inclusive gluon production cross section in the dilute target limit.

In Chapter 6 we provide a generalization of the framework proposed in Chapter 4 to compute multi-gluon spectra in proton-nucleus collisions within the Area Enhancement model, i.e., contributions that are dominant in the area of the collision, by including non-eikonal corrections. The formalism of this chapter is inspired by the jet quenching framework [192] in which a non-zero longitudinal extent of the dense medium is necessary in order to study the effects of the Quark Gluon Plasma on parton propagation.

We have seen that the non-eikonal corrections in the target's 2-point average can be computed analytically if we restrict ourselves to the GBW approximation, that is, we assume that the eikonal dipole function has a Gaussian form. This approximation is justified as long as the dipole's size is much smaller that $\Lambda_{\rm QCD}^{-1}$. The result for the non-eikonal dipole functions was given in Eqs. (6.8), (6.18) and (6.21), where the finite width effects are weighted by the dimensionless parameter $\epsilon^2 = \frac{Q_s^2 L^+}{2ik^+}$, and from them we were able to evaluate the single inclusive gluon spectrum beyond eikonal accuracy. Our results are summarized in Figs. 6.2 to 6.4 where we have seen that the effects of including non-eikonal corrections to the single gluon spectrum are sizable for center-of-mass energies per nucleon smaller than 100 GeV and for pseudorapidities of the produced particle smaller than 1. Thus we conclude that including the non-eikonal corrections to phenomenological studies in single gluon production is irrelevant at the energies of the LHC or the top energies of RHIC. In Section 6.3.2 we have compared the next-to-next-to-eikonal approximation of our result, i.e. an expansion up to order ϵ^4, with the one presented in [43, 44] and we have been able to find a parameterization of the so-called decorated dipoles within the Gaussian ansatz.

In Section 6.4 we present the formalism for computing the non-eikonal multi-gluon spectrum in pA collisions for an arbitrary number of produced gluons. The approach is based in the Area Enhancement model which we argue that it should be valid for a target with finite width since the coherence length of the chromo-electric domains are much

larger than the longitudinal extent of the target. We have then solved the case in which two gluons are produced and, analogous to the analysis performed in Chapter 5 in the case of pp collisions, we have seen that the non-eikonal corrections induces an azimuthal asymmetry in the double gluon spectrum. In Section 6.4.1 we perform a numerical analysis of the azimuthal harmonics and we find that the odd azimuthal harmonic v_3 due to non-eikonal corrections is sizable at relatively high energies. Thus we conclude that the effect of the non-eikonal correction is larger in the double gluon spectrum than in the single gluon spectrum. We note that, due to the lack of numerical data, the analysis performed in Section 6.4.1 can be improved by studying the dependence of v_3 with $\Delta\eta$, by using the proper definition of the azimuthal harmonics given in Section 3.4 or by analyzing more values of the collision center-of-mass energy.

Appendices

USC
UNIVERSIDADE
DE SANTIAGO
DE COMPOSTELA

Appendix A

Light-Cone coordinates

The dynamical aspects of high energy collisions simplifies in the so-called *light-cone coordinates* introduced by Dirac. This frame is motivated by the almost invariance of the high energy systems under boosts in the longitudinal direction. For this reason, in this appendix we will define the light-cone coordinates that will be used over all this thesis.

Let $x^\mu = (x^0, x^1, x^2, x^3) \equiv (x^0, \mathbf{x}, x^3)$ be a generic 4-vector in the Cartesian representation of the Minkowski metric, $g_{\mu\nu} = \mathrm{diag}(1, -1, -1, -1)$. The light-cone coordinates are defined by the following change of variables:

$$x^+ = \frac{x^0 + x^3}{\sqrt{2}}, \quad x^- = \frac{x^0 - x^3}{\sqrt{2}}, \tag{A.1}$$

and the transverse components, $\mathbf{x} = (x^1, x^2)$, remain unchanged. This change is equivalent to performing a 45^{o} rotation of the Cartesian system in such a way that the x^0 and x^3 axis fall on top of the light-cone. The product of two 4-vectors x^μ and y^μ in the light-cone notation will be given by

$$x^\mu y_\mu = x^+ y^- + x^- y^+ - \mathbf{x} \cdot \mathbf{y}. \tag{A.2}$$

Thus the metric in this frame has non-zero components $g_{+-} = g_{-+} = 1$ and $g_{11} = g_{22} = -1$. This implies that

$$x_- = x^+, \quad x_+ = x^-. \tag{A.3}$$

An important property of the light-cone coordinates is that they do not mix under Lorentz boosts in the x^3 direction. In the Cartesian system a boost of rapidity η is given by the following transformation:

$$\tilde{x}^0 = x^0 \cosh\eta - x^3 \sinh\eta, \tag{A.4}$$
$$\tilde{x}^3 = x^3 \cosh\eta - x^0 \sinh\eta, \tag{A.5}$$

while in the light-cone coordinates it is simply given by a scaling transformation:

$$\tilde{x}^+ = e^{-\eta} x^+, \tag{A.6}$$
$$\tilde{x}^- = e^{\eta} x^-. \tag{A.7}$$

This feature of the light-cone coordinates introduce a huge simplification in the case of highly boosted systems where $\eta \to \infty$.

Finally, the derivatives in the light-cone frame are given by

$$\partial^- \equiv \frac{\partial}{\partial x^+} = \frac{1}{\sqrt{2}}\left(\frac{\partial}{\partial x^0} + \frac{\partial}{\partial x^3}\right), \tag{A.8}$$

$$\partial^+ \equiv \frac{\partial}{\partial x^-} = \frac{1}{\sqrt{2}}\left(\frac{\partial}{\partial x^0} - \frac{\partial}{\partial x^3}\right). \tag{A.9}$$

This implies that they transform under a boost as $\partial^\pm \to e^{\mp\eta}\partial^\pm$.

Appendix B

Table of integrals

In this section we present all the closed-form solutions of the integrals that have been used in this thesis, in particular in Chapter 4. First, let us introduce the well known definitions:

$$I_n(x) = \sum_{k=0}^{\infty} \left(\frac{x}{2}\right)^{2k+n} \frac{1}{k!\Gamma(k+n+1)}, \tag{B.1}$$

$${}_pF_q(a_1,\ldots,a_p;b_1,\ldots,b_q;z) = \sum_{n=0}^{\infty} \frac{(a_1)_n \cdots (a_p)_n}{(b_1)_n \cdots (b_q)_n} \frac{z^n}{n!}, \tag{B.2}$$

$$(a)_n = \frac{\Gamma(a+n)}{\Gamma(a)}, \tag{B.3}$$

$$\Gamma(k) = \int_0^{\infty} dx e^{-x} x^{k-1}, \tag{B.4}$$

where $I_n(x)$ is the modified Bessel function of the first kind, ${}_pF_q(a_1,\ldots,a_p;b_1,\ldots,b_q;z)$ is the generalized hyper-geometric function, $(a)_n$ is the rising factorial (or Pochhammer symbol) and $\Gamma(k)$ is the gamma function.

We will also introduce for convenience the Jacobi-Anger expansion

$$e^{x\cos\phi} = \sum_{n=-\infty}^{\infty} I_n(x) e^{-in\phi}. \tag{B.5}$$

The first integral and the one that will be the most used in this work is the well known Gaussian integral

$$\int d^2\mathbf{k} e^{-A\mathbf{k}^2 + \mathbf{B}\cdot\mathbf{k}} = \frac{\pi}{A} e^{\frac{\mathbf{B}^2}{4A}}. \tag{B.6}$$

When computing the 2-particle differential cumulant we will have to deal with the following integral

$$\begin{aligned}
&\int_0^{2\pi} d\phi_1 \int d^2\mathbf{k}_2 e^{i2n(\phi_1-\phi_2)} e^{-A_1\mathbf{k}_1^2 - A_2\mathbf{k}_2^2 + A_{12}\mathbf{k}_1\cdot\mathbf{k}_2}\Big|_{|\mathbf{k}_1|=p_\perp} \\
=&\int_0^{2\pi} d\phi_1 d\phi_2 e^{i2n(\phi_1-\phi_2)} \int_0^{\infty} dk_2 k_2 e^{-A_1 p_\perp^2 - A_2 k_2^2 + A_{12} p_\perp k_2 \cos(\phi_1-\phi_2)} \\
=&2\pi e^B \int_0^{\infty} dk_2 k_2 e^{-A_2 k_2^2} \int_0^{2\pi} d\phi e^{i2n\phi + Ck_2\cos\phi},
\end{aligned} \tag{B.7}$$

where we have defined $B = -A_1 p_\perp^2$ and $C = A_{12} p_\perp$. Taking into account the Jacobi-Anger expansion Eq. (B.5) and the fact that n is an integer we can write

$$\begin{aligned}
&2\pi e^B \int_0^\infty dk_2 k_2 e^{-A_2 k_2^2} \int_0^{2\pi} d\phi e^{i2n\phi + Ck_2 \cos\phi} \\
&= 2\pi e^B \sum_{m=-\infty}^{\infty} \int_0^\infty dk_2 k_2 e^{-A_2 k_2^2} I_m(Ck_2) \int_0^{2\pi} d\phi e^{i(2n-m)\phi} \\
&= (2\pi)^2 e^B \int_0^\infty dk_2 k_2 e^{-A_2 k_2^2} I_{2n}(Ck_2).
\end{aligned} \tag{B.8}$$

Using the definition of Eq. (B.1) and then making the change of variable $x = A_2 k_2^2$ we have that

$$\begin{aligned}
&(2\pi)^2 e^B \int_0^\infty dk_2 k_2 e^{-A_2 k_2^2} I_{2n}(Ck_2) \\
=&(2\pi)^2 e^B \sum_{k=0}^{\infty} \int_0^\infty dk_2 k_2 e^{-A_2 k_2^2} \left(\frac{Ck_2}{2}\right)^{2k+2n} \frac{1}{k!\Gamma(k+2n+1)} \\
=&(2\pi)^2 e^B \sum_{k=0}^{\infty} \frac{1}{k!\Gamma(k+2n+1)} \int_0^\infty \frac{dx}{2A_2} e^{-x} \left(\frac{C^2 x}{4A_2}\right)^{k+n} \\
=&\frac{(2\pi)^2}{2A_2} e^B \left(\frac{C^2}{4A_2}\right)^n \sum_{k=0}^{\infty} \left(\frac{C^2}{4A_2}\right)^k \frac{1}{k!\Gamma(k+2n+1)} \int_0^\infty e^{-x} x^{k+n} \\
=&\frac{(2\pi)^2}{2A_2} e^B \left(\frac{C^2}{4A_2}\right)^n \sum_{k=0}^{\infty} \left(\frac{C^2}{4A_2}\right)^k \frac{1}{k!\Gamma(k+2n+1)} \Gamma(k+n+1),
\end{aligned} \tag{B.9}$$

where in the last line we have used the definition of the Gamma function Eq. (B.4). Using the definition of the hypergeometric function Eq. (B.2) we can write the last sum as

$$\sum_{k=0}^{\infty} \left(\frac{C^2}{4A_2}\right)^k \frac{1}{k!\Gamma(k+2n+1)} \Gamma(k+n+1) = \frac{\Gamma(n+1)}{\Gamma(2n+1)} {}_1F_1\left(n+1; 2n+1; \frac{C^2}{4A_2}\right) \tag{B.10}$$

and, therefore, the result for the integral is

$$\begin{aligned}
&\int_0^{2\pi} d\phi_1 \int d^2\mathbf{k}_2 e^{i2n(\phi_1-\phi_2)} e^{-A_1\mathbf{k}_1^2 - A_2\mathbf{k}_2^2 + A_{12}\mathbf{k}_1\cdot\mathbf{k}_2}\Big|_{|\mathbf{k}_1|=p_\perp} \\
=&\frac{(2\pi)^2}{2A_2} e^{-A_1 p_\perp^2} \left(\frac{A_{12}^2 p_\perp^2}{4A_2}\right)^n \frac{\Gamma(n+1)}{\Gamma(2n+1)} {}_1F_1\left(n+1; 2n+1; \frac{A_{12}^2 p_\perp^2}{4A_2}\right).
\end{aligned} \tag{B.11}$$

The solution of the integrals that we will find when we evaluate the 2-particle cumulant can be obtained in the same fashion and the result is

$$\begin{aligned}
&\int d^2\mathbf{k}_1 d^2\mathbf{k}_2 e^{i2n(\phi_1-\phi_2)} e^{-A_1\mathbf{k}_1^2 - A_2\mathbf{k}_2^2 + A_{12}\mathbf{k}_1\cdot\mathbf{k}_2} \\
&= \frac{(2\pi)^2}{4A_1A_2} \left(\frac{A_{12}^2}{4A_1A_2}\right)^n \frac{\Gamma(n+1)^2}{\Gamma(2n+1)} {}_2F_1\left(n+1, n+1; 2n+1; \frac{A_{12}^2}{4A_1A_2}\right).
\end{aligned} \tag{B.12}$$

Appendix C

Calculation of four gluon inclusive production

In this section we analyze the four gluon inclusive spectrum by taking into account all the terms in Eq. (4.57). In order to do so we will follow the same arguments that we have used for writing down the triple gluon spectrum in Section 5.5. First we note that after performing the Wick expansion of either the target or projectile correlators we have 105 contributions on each side that can be written schematically as

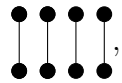 , (C.1)

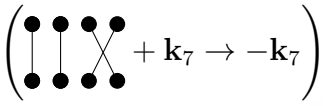

$$+\mathbf{k}_1 \leftrightarrow \mathbf{k}_5 + \mathbf{k}_1 \leftrightarrow \mathbf{k}_7 + \mathbf{k}_3 \leftrightarrow \mathbf{k}_5 + \mathbf{k}_3 \leftrightarrow \mathbf{k}_7 + (\mathbf{k}_3 \leftrightarrow \mathbf{k}_5)(\mathbf{k}_1 \leftrightarrow \mathbf{k}_7), \tag{C.2}$$

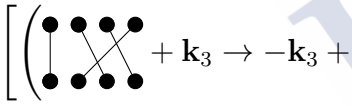

$$+\mathbf{k}_1 \leftrightarrow \mathbf{k}_3 + \mathbf{k}_1 \leftrightarrow \mathbf{k}_5 + \mathbf{k}_1 \leftrightarrow \mathbf{k}_7, \tag{C.3}$$

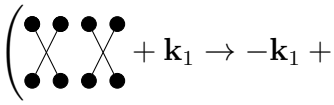

$$+\mathbf{k}_3 \leftrightarrow \mathbf{k}_5 + \mathbf{k}_3 \leftrightarrow \mathbf{k}_7, \tag{C.4}$$

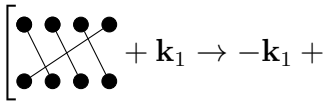

$$+\mathbf{k}_1 \leftrightarrow \mathbf{k}_3 + \mathbf{k}_1 \leftrightarrow \mathbf{k}_7 + \mathbf{k}_3 \leftrightarrow \mathbf{k}_5 + \mathbf{k}_3 \leftrightarrow \mathbf{k}_7 + \mathbf{k}_5 \leftrightarrow \mathbf{k}_7, \tag{C.5}$$

where the permutations $\mathbf{k}_i \to -\mathbf{k}_i$ and $\mathbf{k}_i \leftrightarrow \mathbf{k}_j$ are an abuse of notation since we have not contracted the diagrams and thus we cannot apply properties i) and ii) yet. In order to make the notation lighter we write these permutations as

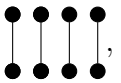 , (C.6)

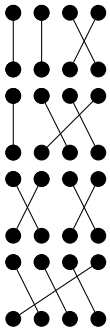
$+ \text{perm}_2,$ (C.7)

$+ \text{perm}_3,$ (C.8)

$+ \text{perm}_4,$ (C.9)

$+ \text{perm}_5.$ (C.10)

Now we generate the Wick diagrams in such a way that they are grouped by their powers of $(N_c^2-1)^{-1}$. In order to do so we exploit property iii) of Section 4.4.1. In this case the suppression of a given diagram is given by $(N_c^2-1)^{n_p+n_T-8}$, with the values of n_p and n_T fixing the topology of the diagram.

It is straightforward to realize that all the diagrams with $n_T = 4$ will have the configuration of Eq. (C.1) on the right side. All the diagrams with $n_T = 3$ will have one of the 12 configurations of Eq. (C.2) on the right side. All the diagrams with $n_T = 2$ will have one of the 32 configurations of Eq. (C.3) or one of the 12 configurations of Eq. (C.4) on the right side and all the diagrams with $n_T = 1$ will have one of the 48 configurations of Eq. (C.5) on the right side. Therefore the value of n_T is fixed by the configuration that we have on the right side of the diagram.

The value of n_p, on the other hand, will depend on the configuration that we have on both sides. It is determined by the number of disconnected pieces that we obtain after drawing the right configuration of the diagram on top of the left one. Thus, the only way of obtaining $n_p = 4$ is by having a configuration on the left that has the same links as the one on the right. The only way of obtaining $n_p = 3$ is by having a configuration on the left that has just two links that are equal to the ones on the right. The way of obtaining $n_p = 2$ is by having a configuration on the left that has only one link that is equal to the right configuration or by having all the links different but in such a way that, after the projection, we obtain two disconnected pieces. Finally, the only way of obtaining $n_p = 1$ is by having a configuration on the left side that has all the links different to the right configuration in such a way that, after the projection, we have a fully connected piece. The number of possibilities for $n_p = 4$ is 1, for $n_p = 3$ is 12, for $n_p = 2$ is 32 and 12, respectively, and for $n_p = 1$ is 48.

Having this into account we can find all the diagrams with a given suppression in powers of $(N_c^2-1)^{-1}$. As an example, let us see which are the diagrams with power suppression $(N_c^2-1)^{-3}$. In this case we have $n_p + n_T = 5$ and we will have 4 different topologies that are fixed by this constraint: $n_T = 4$ and $n_p = 1$; $n_T = 3$ and $n_p = 2$; $n_T = 2$ and $n_p = 3$; $n_T = 1$ and $n_p = 4$. Let us study this situation case by case:

i) $n_T = 4$ and $n_p = 1$. In this case we will have the configuration of Eq. (C.1) on the right side of the diagram and on the left side we will have all the diagrams that have zero links in common with the one on the right in such a way that after the projection we just have one connected piece. Thus we will have 1×48 possibilities that are

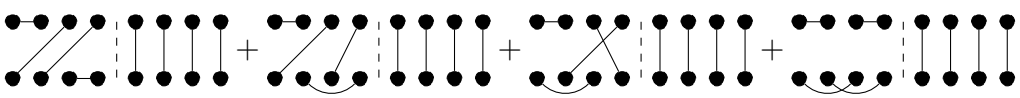

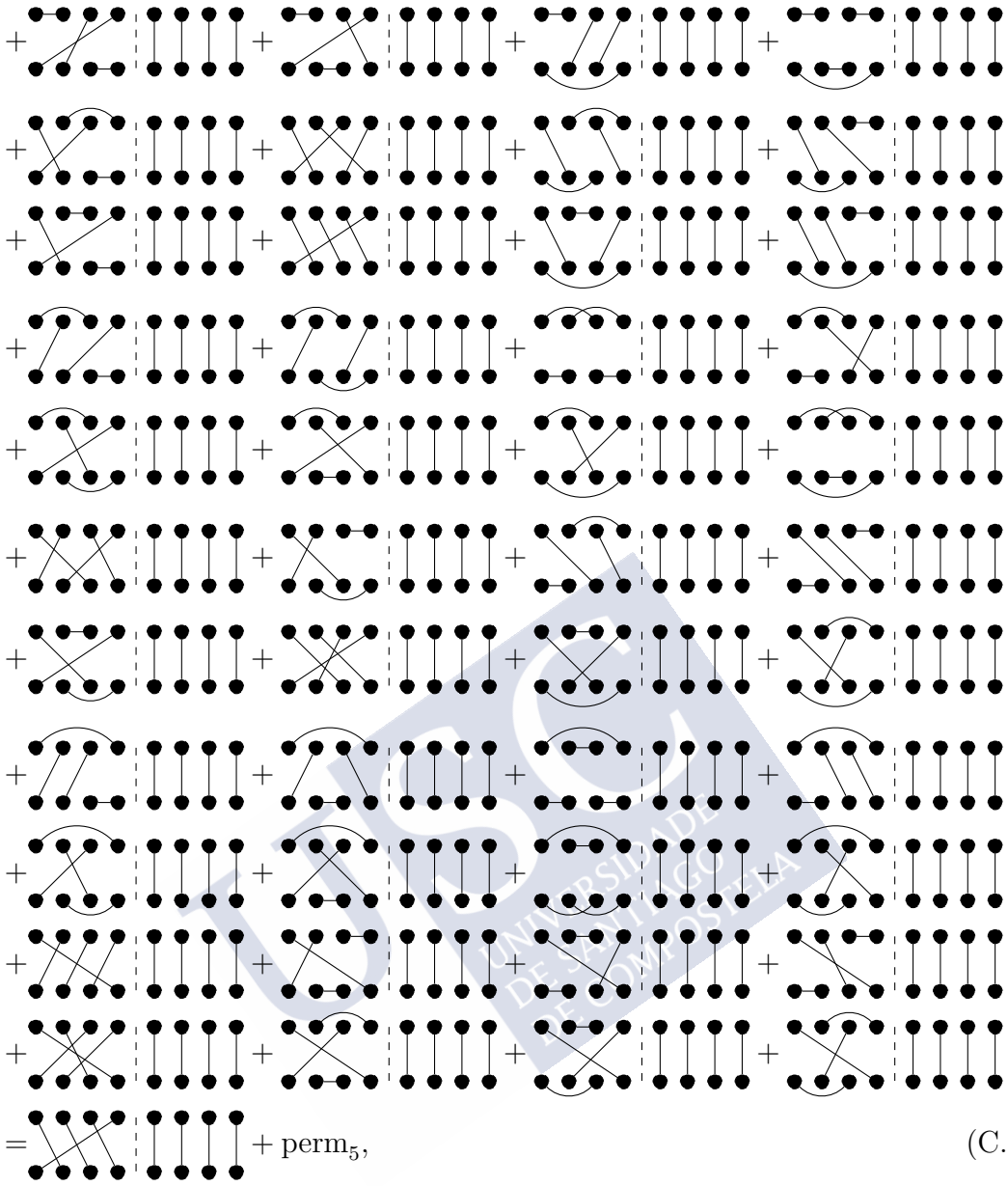

(C.11)

where in the last line we have used the fact that since on the right side of the diagram we have a fully disconnected piece we can write the sum of these 48 diagrams as just one plus perm_5.

ii) $n_T = 3$ and $n_p = 2$. In this case we will have the configurations of Eq. (C.2) on the right side of the diagram and on the left side we will have all the diagrams that have just one link in common with the right one. This gives a total of 12×32 possibilities

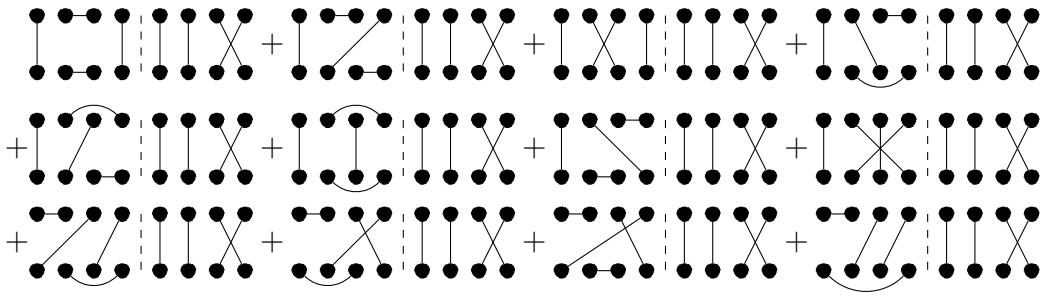

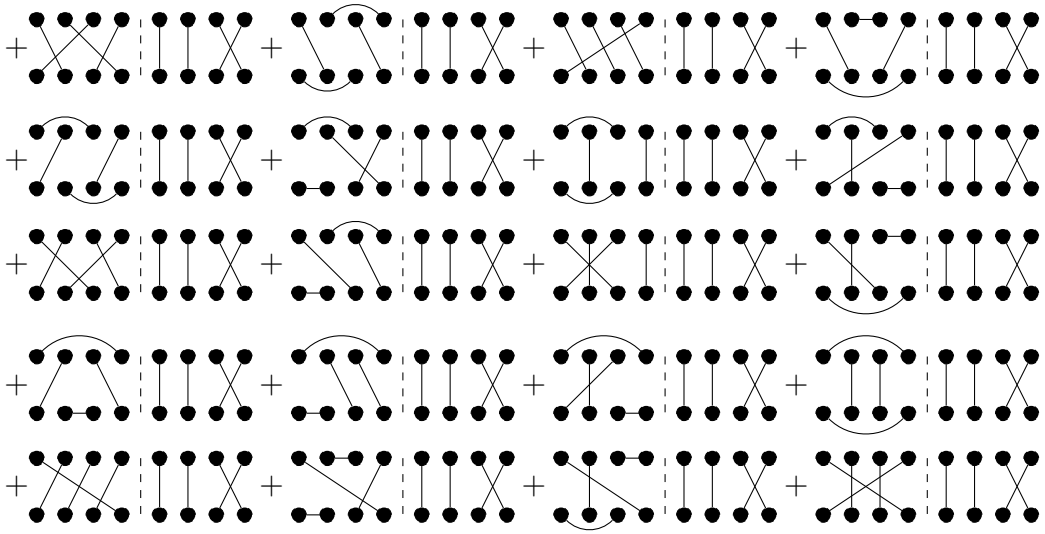

$+\text{perm}_2,$ (C.12)

or we can have on the left side the configurations that have no links in common with the one on the right in such a way that, after the projection, we have two connected pieces. This gives a total of 12×12 possibilities:

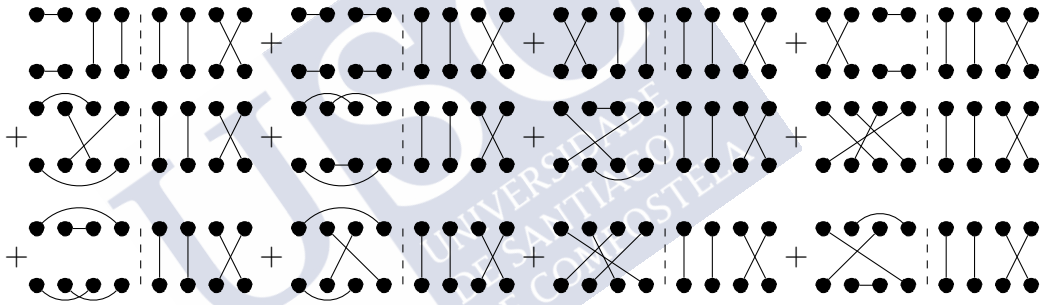

$+\text{perm}_2.$ (C.13)

iii) $n_T = 2$ and $n_p = 3$. This implies that we will have the configurations of Eq. (C.3) or Eq. (C.4) on the right side of the diagram and on the left side we will have the configurations that have two links equal to the one on the right. This gives a total of 32×12 possibilities for the first case,

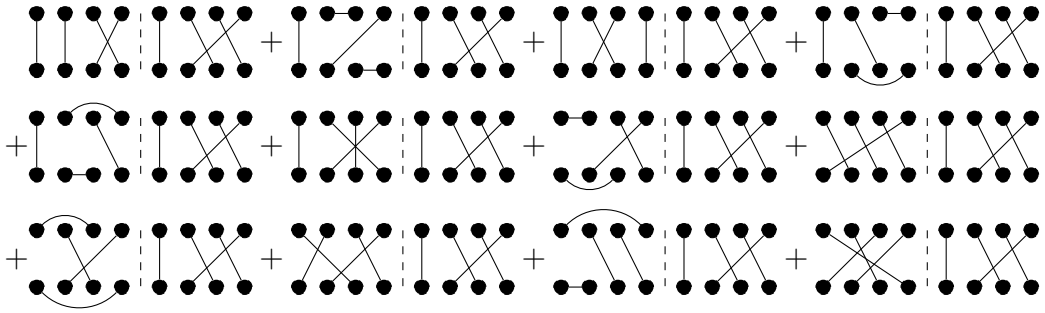

$+\text{perm}_3,$ (C.14)

and 12×12 possibilities for the second case,

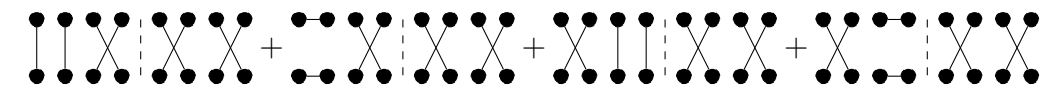

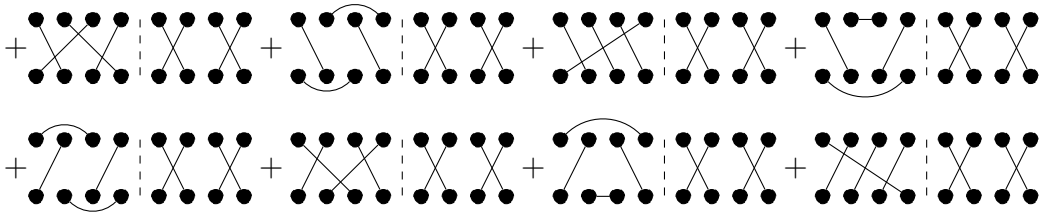

$+\text{perm}_4.$ (C.15)

iv) $n_T = 1$ and $n_p = 4$. This implies that we have the configurations of Eq. (C.5) on the right side of the diagram and on the left side we have the configuration that have the same links with respect to the right one. This gives a total of 48×1 possibilities:

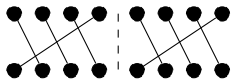

$+\text{perm}_5.$ (C.16)

With Eqs. (C.11) to (C.16) we have found all the 1152 diagrams with a suppression of $(N_c^2-1)^{-3}$ and written them as a bunch of diagrams plus permutations – which was our goal. We should also note that some of the diagrams that are drawn in these equations can also be related by symmetries $\mathbf{k}_i \to -\mathbf{k}_i$ or $\mathbf{k}_i \leftrightarrow \mathbf{k}_j$, which could lead to a better optimization of the calculation but we have not found any systematic way of finding these symmetries. Therefore, we have decided to not include them in the calculation since we see not advantage in doing this by hand.

We can find the other diagrams with a different suppression in the same fashion obtaining 1 diagram with a suppression of $(N_c^2-1)^0$, 24 diagrams with a suppression of $(N_c^2-1)^{-1}$, 232 diagrams with a suppression of $(N_c^2-1)^{-2}$, 3088 diagrams with a suppression of $(N_c^2-1)^{-4}$, 4224 diagrams with a suppression of $(N_c^2-1)^{-5}$ and 2304 diagrams with a suppression of $(N_c^2-1)^{-6}$.

The next step is to exploit the symmetries encoded within the permutations in order to evaluate the cumulants through Eq. (3.34). We will do as an example the calculation only for the terms that contribute, again, with a power $(N_c^2-1)^{-3}$. Let us introduce the shorthand notation $\hat{\mathcal{D}}_{n_p}$ as the sum of all the diagrams that satisfy the topology given by n_p with a given configuration on the right side. Then we can write the contribution of order $(N_c^2-1)^{-3}$ to the 4-gluon spectrum as

$$N^{(3)} = \Big(\text{perm}_5\Big) + \Big(\hat{\mathcal{D}}_2^{(1)} + \hat{\mathcal{D}}_2^{(2)} + \text{perm}_2\Big) + \Big(\hat{\mathcal{D}}_3 + \text{perm}_3\Big) + \Big(\hat{\mathcal{D}}_3 + \text{perm}_4\Big) + \Big(\text{perm}_5\Big), \tag{C.17}$$

with $\hat{\mathcal{D}}_2^{(1)}$ and $\hat{\mathcal{D}}_2^{(2)}$ referring to the first and second contributions to Item ii) discussed above, respectively.

In order to evaluate $\kappa_0\{4\}$ we can use the fact that all the permutations, perm_i, of Eqs. (C.1) to (C.2) will give the same result since we are integrating over all the momentum $\mathbf{k}_i$. Thus we can write

$$\kappa_0^{(3)}\{4\} = \int_{\mathbf{k}_1\mathbf{k}_3\mathbf{k}_5\mathbf{k}_7} \Big[48 + 12\hat{\mathcal{D}}_2^{(1)} + 12\hat{\mathcal{D}}_2^{(2)}$$

$$+ 32\hat{\mathcal{D}}_3$$ 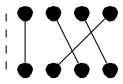 $$+ 12\hat{\mathcal{D}}_3$$ 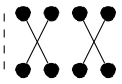 $$+ 48$$ 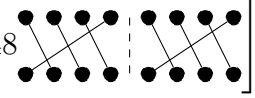 . (C.18)

When we evaluate $\kappa_n\{4\}$ with $n \neq 0$ we have to integrate the spectrum times $e^{in(\phi_1+\phi_3-\phi_5-\phi_7)}$ which will break some of the symmetries encoded in the permutations, perm_i. In order to check how we can simplify the integration let us start with the permutations of the $n_T = 3$ case with a generic n_p. In this case we can define the sum of the diagrams without the permutations as

$$\hat{\mathcal{D}}_{n_p}$$ 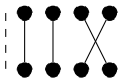 $$\equiv f_2(\mathbf{k}_1, \mathbf{k}_3, \mathbf{k}_5, \mathbf{k}_7).$$ (C.19)

By using the properties i) and ii) of Section 4.4.1 we can check that this sum has the following symmetry

$$f_2(\mathbf{k}_1, \mathbf{k}_3, \mathbf{k}_5, \mathbf{k}_7) = f_2(\mathbf{k}_1, \mathbf{k}_3, \mathbf{k}_7, \mathbf{k}_5). \tag{C.20}$$

Thus, the contribution of the $n_T = 3$ diagrams to the κ-function can be written as

$$\begin{aligned}
&\int_{\mathbf{k}_1\mathbf{k}_3\mathbf{k}_5\mathbf{k}_7} e^{in(\phi_1+\phi_3-\phi_5-\phi_7)} \Bigg[\hat{\mathcal{D}}_{n_p}$$ 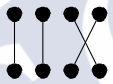 $$+ \text{perm}_2\Bigg] \\
&= 2\int_{\mathbf{k}_1\mathbf{k}_3\mathbf{k}_5\mathbf{k}_7} e^{in(\phi_1+\phi_3-\phi_5-\phi_7)} \Big[f_2(\mathbf{k}_1, \mathbf{k}_3, \mathbf{k}_5, \mathbf{k}_7) + f_2(\mathbf{k}_5, \mathbf{k}_3, \mathbf{k}_1, \mathbf{k}_7) + f_2(\mathbf{k}_7, \mathbf{k}_3, \mathbf{k}_5, \mathbf{k}_1) \\
&\qquad + f_2(\mathbf{k}_1, \mathbf{k}_5, \mathbf{k}_3, \mathbf{k}_7) + f_2(\mathbf{k}_1, \mathbf{k}_7, \mathbf{k}_5, \mathbf{k}_3) + f_2(\mathbf{k}_7, \mathbf{k}_5, \mathbf{k}_3, \mathbf{k}_1)\Big] \\
&= 2\int_{\mathbf{k}_1\mathbf{k}_3\mathbf{k}_5\mathbf{k}_7} e^{in(\phi_1+\phi_3-\phi_5-\phi_7)} \Big[2f_2(\mathbf{k}_1, \mathbf{k}_3, \mathbf{k}_5, \mathbf{k}_7) + 4f_2(\mathbf{k}_1, \mathbf{k}_5, \mathbf{k}_3, \mathbf{k}_7)\Big],
\end{aligned} \tag{C.21}$$

where the factor 2 comes from exploiting the symmetries $\mathbf{k}_i \to -\mathbf{k}_i$ that are in Eq. (C.2) and in the last equality we have used Eq. (C.20) and relabeled the variables. Therefore, we can write

$$\begin{aligned}
&\int_{\mathbf{k}_1\mathbf{k}_3\mathbf{k}_5\mathbf{k}_7} e^{in(\phi_1+\phi_3-\phi_5-\phi_7)} \Bigg[\hat{\mathcal{D}}_{n_p}$$ 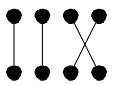 $$+ \text{perm}_2\Bigg] \\
&= \int_{\mathbf{k}_1\mathbf{k}_3\mathbf{k}_5\mathbf{k}_7} e^{in(\phi_1+\phi_3-\phi_5-\phi_7)} \Bigg[4\hat{\mathcal{D}}_{n_p}$$ 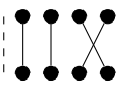 $$+ 8\hat{\mathcal{D}}_{n_p}$$ 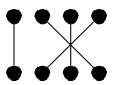 .
\end{aligned} \tag{C.22}$$

For the $n_T = 2$ diagrams that are defined by Eq. (C.3) we can follow the same arguments by defining

$$\hat{\mathcal{D}}_{n_p}$$ 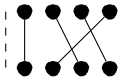 $$\equiv f_3(\mathbf{k}_1, \mathbf{k}_3, \mathbf{k}_5, \mathbf{k}_7).$$ (C.23)

We can check that this function has the following symmetries

$$\begin{aligned}
f_3(\mathbf{k}_1, \mathbf{k}_3, \mathbf{k}_5, \mathbf{k}_7) &= f_3(-\mathbf{k}_1, -\mathbf{k}_7, -\mathbf{k}_5, -\mathbf{k}_3) \\
&= f_3(-\mathbf{k}_1, -\mathbf{k}_3, -\mathbf{k}_7, -\mathbf{k}_5) = f_3(-\mathbf{k}_1, -\mathbf{k}_5, -\mathbf{k}_3, -\mathbf{k}_7).
\end{aligned} \tag{C.24}$$

Thus, exploiting this symmetries we can write the contribution of the diagrams that have the configuration of Eq. (C.3) on the right side with generic n_p to the cumulant as

$$\int_{\mathbf{k}_1\mathbf{k}_3\mathbf{k}_5\mathbf{k}_7} e^{in(\phi_1+\phi_3-\phi_5-\phi_7)}\left[\hat{\mathcal{D}}_{n_p}\right.$$
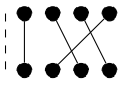
$$\left.+\,\mathrm{perm}_3\right]$$
$$= 32\int_{\mathbf{k}_1\mathbf{k}_3\mathbf{k}_5\mathbf{k}_7} e^{in(\phi_1+\phi_3-\phi_5-\phi_7)}\hat{\mathcal{D}}_{n_p}$$
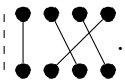
. (C.25)

For the $n_T = 2$ diagrams that are defined by Eq. (C.4) we define

$$\hat{\mathcal{D}}_{n_p}$$
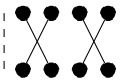
$$\equiv f_4(\mathbf{k}_1, \mathbf{k}_3, \mathbf{k}_5, \mathbf{k}_7), \tag{C.26}$$

which has the following symmetries

$$f_4(\mathbf{k}_1, \mathbf{k}_3, \mathbf{k}_5, \mathbf{k}_7) = f_4(\mathbf{k}_3, \mathbf{k}_1, \mathbf{k}_5, \mathbf{k}_7) = f_4(\mathbf{k}_1, \mathbf{k}_3, \mathbf{k}_7, \mathbf{k}_5). \tag{C.27}$$

Thus, the contribution of the diagrams that have the configuration of Eq. (C.4) on the right side with generic n_p to the cumulant is

$$\int_{\mathbf{k}_1\mathbf{k}_3\mathbf{k}_5\mathbf{k}_7} e^{in(\phi_1+\phi_3-\phi_5-\phi_7)}\left[\hat{\mathcal{D}}_{n_p}\right.$$
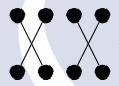
$$\left.+\,\mathrm{perm}_4\right]$$
$$= \int_{\mathbf{k}_1\mathbf{k}_3\mathbf{k}_5\mathbf{k}_7} e^{in(\phi_1+\phi_3-\phi_5-\phi_7)}\left[4\hat{\mathcal{D}}_{n_p}\right.$$
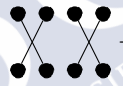
$$+\,8\hat{\mathcal{D}}_{n_p}$$
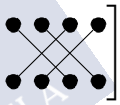
$$\left.\right]. \tag{C.28}$$

For the $n_T = 1$ diagrams that are defined by Eq. (C.5) we define

$$\hat{\mathcal{D}}_{n_p}$$
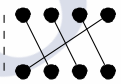
$$\equiv f_5(\mathbf{k}_1, \mathbf{k}_3, \mathbf{k}_5, \mathbf{k}_7). \tag{C.29}$$

This function has the following symmetries

$$\begin{aligned} f_5(\mathbf{k}_1, \mathbf{k}_3, \mathbf{k}_5, \mathbf{k}_7) &= f_5(-\mathbf{k}_5, -\mathbf{k}_3, -\mathbf{k}_1, -\mathbf{k}_7) \\ =& f_5(-\mathbf{k}_1, -\mathbf{k}_7, -\mathbf{k}_5, -\mathbf{k}_3) = f_5(-\mathbf{k}_3, -\mathbf{k}_1, -\mathbf{k}_7, -\mathbf{k}_5). \end{aligned} \tag{C.30}$$

Therefore, the contribution of the diagrams that have the configuration of Eq. (C.5) on the right side with generic n_p to the cumulant is

$$\int_{\mathbf{k}_1\mathbf{k}_3\mathbf{k}_5\mathbf{k}_7} e^{in(\phi_1+\phi_3-\phi_5-\phi_7)}\left[\hat{\mathcal{D}}_{n_p}\right.$$
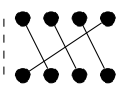
$$\left.+\,\mathrm{perm}_5\right]$$
$$= \int_{\mathbf{k}_1\mathbf{k}_3\mathbf{k}_5\mathbf{k}_7} e^{in(\phi_1+\phi_3-\phi_5-\phi_7)}\left[32\hat{\mathcal{D}}_{n_p}\right.$$
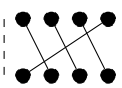
$$+\,16\hat{\mathcal{D}}_{n_p}$$
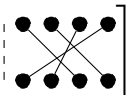
$$\left.\right]. \tag{C.31}$$

All in all, using Eq. (C.17) and the simplifications in Eqs. (C.22), (C.25), (C.28) and (C.31), we can reduce the number of integrals when computing $\kappa_n\{4\}$ at order $(N_c^2-1)^{-3}$ down to

$$\kappa_n^{(3)}\{4\} = \int_{\mathbf{k}_1\mathbf{k}_3\mathbf{k}_5\mathbf{k}_7} e^{in(\phi_1+\phi_3-\phi_5-\phi_7)}\left[32\right.$$
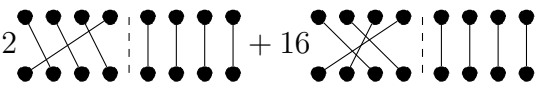

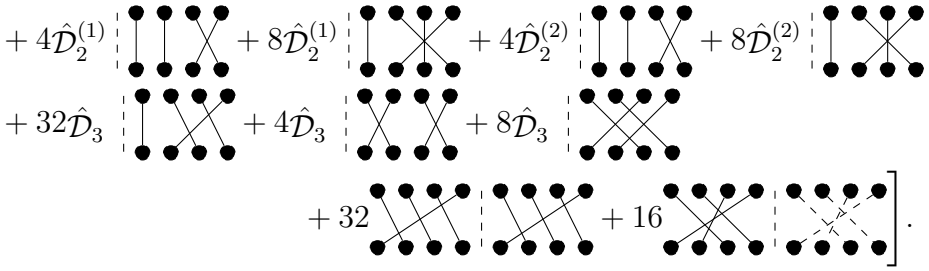

(C.32)

We compute the contribution at different orders of $(N_c^2-1)^{-1}$ in the same way. Finally, we just have to solve numerically Eqs. (C.18) and (C.32) and the equivalent ones at different orders. By doing that we are able to obtain Fig. 4.8.

Appendix D

Triple inclusive gluon production beyond the eikonal approximation

D.1 Details of the calculation

As in the case of single and double inclusive gluon production, we first take the dilute target limit which corresponds to the expansion of the Wilson lines in powers of the background field of the target, Eq. (5.22). Then the triple inclusive gluon production cross section reads

$$\begin{aligned}
\left.\frac{d\sigma}{d^2\mathbf{k}_1 d\eta_1\, d^2\mathbf{k}_2 d\eta_2\, d^2\mathbf{k}_3 d\eta_3}\right|_{\text{dilute}} &= \frac{g^{12}}{\pi^3(2\pi)^{12}} \int_{\mathbf{z}_1\bar{\mathbf{z}}_1\mathbf{z}_2\bar{\mathbf{z}}_2\mathbf{z}_3\bar{\mathbf{z}}_3} e^{i\mathbf{k}_1\cdot(\mathbf{z}_1-\bar{\mathbf{z}}_1)+i\mathbf{k}_2\cdot(\mathbf{z}_2-\bar{\mathbf{z}}_2)+i\mathbf{k}_3\cdot(\mathbf{z}_3-\bar{\mathbf{z}}_3)} \\
&\times \int_{\mathbf{x}_1\mathbf{x}_2\mathbf{x}_3\mathbf{y}_1\mathbf{y}_2\mathbf{y}_3} f^i(\mathbf{x}_1-\mathbf{z}_1) f^i(\bar{\mathbf{z}}_1-\mathbf{y}_1) f^j(\mathbf{x}_2-\mathbf{z}_2) f^j(\bar{\mathbf{z}}_2-\mathbf{y}_2) f^k(\mathbf{x}_3-\mathbf{z}_3) f^k(\bar{\mathbf{z}}_3-\mathbf{y}_3) \\
&\times \left\langle \rho^{a_1}_{\mathbf{x}_1}\rho^{a_2}_{\mathbf{x}_2}\rho^{a_3}_{\mathbf{x}_3}\rho^{b_1}_{\mathbf{y}_1}\rho^{b_2}_{\mathbf{y}_2}\rho^{b_3}_{\mathbf{y}_3}\right\rangle_p \int_{x_1^+,\ldots,x_6^+} \int_{\mathbf{q}_1,\ldots,\mathbf{q}_6} (T^{c_1}T^{c_2})_{a_1b_1} (T^{c_3}T^{c_4})_{a_2b_2} (T^{c_5}T^{c_6})_{a_3b_3} \\
&\times \left\langle A^-_{c_1}(x_1^+,\mathbf{q}_1) A^-_{c_2}(x_2^+,\mathbf{q}_2) A^-_{c_3}(x_3^+,\mathbf{q}_3) A^-_{c_4}(x_4^+,\mathbf{q}_4) A^-_{c_5}(x_6^+,\mathbf{q}_6)\right\rangle_T \left[e^{-i\mathbf{q}_1\cdot\mathbf{z}_1} - e^{-i\mathbf{q}_1\cdot\mathbf{x}_1}\right] \\
&\times \left[e^{i\mathbf{q}_2\cdot\bar{\mathbf{z}}_1} - e^{i\mathbf{q}_2\cdot\mathbf{y}_1}\right]\left[e^{-i\mathbf{q}_3\cdot\mathbf{z}_2} - e^{-i\mathbf{q}_3\cdot\mathbf{x}_2}\right]\left[e^{i\mathbf{q}_4\cdot\bar{\mathbf{z}}_2} - e^{i\mathbf{q}_4\cdot\mathbf{y}_2}\right]\left[e^{-i\mathbf{q}_5\cdot\mathbf{z}_3} - e^{-i\mathbf{q}_5\cdot\mathbf{x}_3}\right]\left[e^{i\mathbf{q}_6\cdot\bar{\mathbf{z}}_3} - e^{i\mathbf{q}_6\cdot\mathbf{y}_3}\right].
\end{aligned} \tag{D.1}$$

In the calculation of the single and double inclusive gluon spectrum in Section 5.2, we have performed the averaging over the color charge densities of the projectile first. However, it can also be left for further stages of the calculation for convenience since the expressions for the triple inclusive gluon production are longer. Therefore, we leave it for later and perform the integrals over the transverse coordinates which yields

$$\begin{aligned}
\left.\frac{d\sigma}{d^2\mathbf{k}_1 d\eta_1\, d^2\mathbf{k}_2 d\eta_2\, d^2\mathbf{k}_3 d\eta_3}\right|_{\text{dilute}} &= \frac{g^{12}}{\pi^3(2\pi)^6} \int_{x_1^+,\ldots,x_6^+} \int_{\mathbf{q}_1,\ldots,\mathbf{q}_6} (T^{c_1}T^{c_2})_{a_1b_1} (T^{c_3}T^{c_4})_{a_2b_2} (T^{c_5}T^{c_6})_{a_3b_3} \\
&\times \left\langle A^-_{c_1}(x_1^+,\mathbf{q}_1) A^-_{c_2}(x_2^+,\mathbf{q}_2) A^-_{c_3}(x_3^+,\mathbf{q}_3) A^-_{c_4}(x_4^+,\mathbf{q}_4) A^-_{c_5}(x_6^+,\mathbf{q}_6)\right\rangle_T \\
&\times \left\langle \rho^{a_1}_{\mathbf{k}_1-\mathbf{q}_1}\,\rho^{a_2}_{\mathbf{k}_2-\mathbf{q}_3}\,\rho^{a_3}_{\mathbf{k}_3-\mathbf{q}_5}\,\rho^{b_1}_{\mathbf{q}_2-\mathbf{k}_1}\,\rho^{b_2}_{\mathbf{q}_4-\mathbf{k}_2}\,\rho^{b_3}_{\mathbf{q}_6-\mathbf{k}_3}\right\rangle_p \\
&\times L^i(\mathbf{k}_1,\mathbf{q}_1) L^i(\mathbf{k}_1,\mathbf{q}_2)\, L^j(\mathbf{k}_2,\mathbf{q}_3) L^j(\mathbf{k}_2,\mathbf{q}_4)\, L^k(\mathbf{k}_3,\mathbf{q}_5) L^k(\mathbf{k}_3,\mathbf{q}_6),
\end{aligned} \tag{D.2}$$

where $L^i(k,q)$ is the eikonal Lipatov vertex defined in Eq. (5.19) and $\rho_{\mathbf{k}} \equiv \rho(\mathbf{k})$ is the Fourier transform of the projectile source. At this point, we can incorporate the non-

eikonal effects for the triple inclusive gluon production cross section. As discussed earlier, these effects are taken into account by exchanging each eikonal Lipatov vertex in Eq. (D.2) with the corresponding non-eikonal Lipatov vertex given in Eq. (5.20), and using Eq. (5.27) for the correlator of two target fields. After exchanging each eikonal Lipatov vertex with the corresponding non-eikonal one, the dilute target limit of the non-eikonal triple inclusive gluon production cross section reads

$$\begin{aligned}
&\frac{d\sigma}{d^2\mathbf{k}_1 d\eta_1\, d^2\mathbf{k}_2 d\eta_2\, d^2\mathbf{k}_3 d\eta_3}\bigg|^{\mathrm{NE}}_{\mathrm{dilute}} = \frac{g^{12}}{\pi^3(2\pi)^6}\int_{x_1^+,\ldots,x_6^+}\int_{\mathbf{q}_1,\ldots,\mathbf{q}_6} e^{ik_1^-(x_1^+-x_2^+)+ik_2^-(x_3^+-x_4^+)+i\mathbf{k}_3(x_5^+-x_6^+)} \\
&\times \Big\langle A^-_{c_1}(x_1^+,\mathbf{q}_1)A^-_{c_2}(x_2^+,\mathbf{q}_2)A^-_{c_3}(x_3^+,\mathbf{q}_3)A^-_{c_4}(x_4^+,\mathbf{q}_4)A^-_{c_5}(x_6^+,\mathbf{q}_6)\Big\rangle_T \\
&\times \Big\langle \rho^{a_1}_{\mathbf{k}_1-\mathbf{q}_1}\rho^{a_2}_{\mathbf{k}_2-\mathbf{q}_3}\rho^{a_3}_{\mathbf{k}_3-\mathbf{q}_5}\rho^{b_1}_{\mathbf{q}_2-\mathbf{k}_1}\rho^{b_2}_{\mathbf{q}_4-\mathbf{k}_2}\rho^{b_3}_{\mathbf{q}_6-\mathbf{k}_3}\Big\rangle_p \left(T^{c_1}T^{c_2}\right)_{a_1b_1}\left(T^{c_3}T^{c_4}\right)_{a_2b_2}\left(T^{c_5}T^{c_6}\right)_{a_3b_3} \\
&\times L^i(\mathbf{k}_1,\mathbf{q}_1)L^i(\mathbf{k}_1,\mathbf{q}_2)\,L^j(\mathbf{k}_2,\mathbf{q}_3)L^j(\mathbf{k}_2,\mathbf{q}_4)\,L^k(\mathbf{k}_3,\mathbf{q}_5)L^k(\mathbf{k}_3,\mathbf{q}_6). \qquad \text{(D.3)}
\end{aligned}$$

Let us now consider the averaging over the colour fields of the target. As in the case of the double inclusive gluon production, the average over six colour fields of the target can be factorized into all possible Wick contractions:

$$\begin{aligned}
&\big\langle A_1^- A_2^- A_3^- A_4^- A_5^- A_6^-\big\rangle_T \\
&= \big\langle A_1^- A_2^-\big\rangle_T\Big[\big\langle A_3^- A_4^-\big\rangle_T\big\langle A_5^- A_6^-\big\rangle_T + \big\langle A_3^- A_5^-\big\rangle_T\big\langle A_4^- A_6^-\big\rangle_T + \big\langle A_3^- A_6^-\big\rangle_T\big\langle A_4^- A_5^-\big\rangle_T\Big] \\
&+ \big\langle A_1^- A_3^-\big\rangle_T\Big[\big\langle A_2^- A_4^-\big\rangle_T\big\langle A_5^- A_6^-\big\rangle_T + \big\langle A_2^- A_5^-\big\rangle_T\big\langle A_4^- A_6^-\big\rangle_T + \big\langle A_2^- A_6^-\big\rangle_T\big\langle A_4^- A_5^-\big\rangle_T\Big] \\
&+ \big\langle A_1^- A_4^-\big\rangle_T\Big[\big\langle A_2^- A_3^-\big\rangle_T\big\langle A_5^- A_6^-\big\rangle_T + \big\langle A_2^- A_5^-\big\rangle_T\big\langle A_3^- A_6^-\big\rangle_T + \big\langle A_2^- A_6^-\big\rangle_T\big\langle A_3^- A_5^-\big\rangle_T\Big] \\
&+ \big\langle A_1^- A_5^-\big\rangle_T\Big[\big\langle A_2^- A_3^-\big\rangle_T\big\langle A_4^- A_6^-\big\rangle_T + \big\langle A_2^- A_4^-\big\rangle_T\big\langle A_3^- A_6^-\big\rangle_T + \big\langle A_2^- A_6^-\big\rangle_T\big\langle A_3^- A_4^-\big\rangle_T\Big] \\
&+ \big\langle A_1^- A_6^-\big\rangle_T\Big[\big\langle A_2^- A_3^-\big\rangle_T\big\langle A_4^- A_5^-\big\rangle_T + \big\langle A_2^- A_4^-\big\rangle_T\big\langle A_3^- A_5^-\big\rangle_T + \big\langle A_2^- A_5^-\big\rangle_T\big\langle A_3^- A_4^-\big\rangle_T\Big], \qquad \text{(D.4)}
\end{aligned}$$

where we have introduced a shorthand notation for the target fields $A_i^- \equiv A^-_{c_i}(x_i^+,\mathbf{q}_i)$ for convenience. The target fields are originating from the expansion of the Wilson line in the amplitude (complex conjugate amplitude) when the subscript i is odd (even). With this shorthand notation, the correlator of two target fields defined in Eq. (5.27), can be written in the most convenient way as

$$\big\langle A_i^- A_j^-\big\rangle_T = g^2 n(x_i^+)\frac{1}{2\lambda^+}\Theta\Big(\lambda^+ - \big|x_i^+ - x_j^+\big|\Big)\,\Delta^{ij}, \qquad \text{(D.5)}$$

where Δ^{ij} is defined as

$$\Delta^{ij} = \delta^{c_i c_j}(2\pi)^2\,\delta^{(2)}\Big[\mathbf{q}_i + (-1)^{i+j}\mathbf{q}_j\Big]\,\big|a(\mathbf{q}_i)\big|^2. \qquad \text{(D.6)}$$

Note that Eq. (D.3) can now be integrated over the longitudinal coordinates. After plugging the factorized expression for averaging of the colour fields of the target given in Eq. (D.4) into Eq. (D.3), the longitudinal coordinate dependent part of the dilute target limit of the non-eikonal triple inclusive gluon production cross section can be written as

$$\int_{x_1^+,\ldots,x_6^+} e^{ik_1^-(x_1^+-x_2^+)+ik_2^-(x_3^+-x_4^+)+i\mathbf{k}_3(x_5^+-x_6^+)}\,\big\langle A_1^- A_2^- A_3^- A_4^- A_5^- A_6^-\big\rangle_T$$

$$
\begin{aligned}
&= \mathcal{G}_1^{\rm NE}(k_1^-;\lambda^+)\,\mathcal{G}_1^{\rm NE}(k_2^-;\lambda^+)\,\mathcal{G}_1^{\rm NE}(k_3^-;\lambda^+)\Big\{\Delta^{12}\Delta^{34}\Delta^{56}\\
&+\ \Delta^{12}\Big[\mathcal{G}_2^{\rm NE}(k_2^-,-k_3^-;L^+)\Delta^{35}\Delta^{46}+\mathcal{G}_2^{\rm NE}(k_2^-,k_3^-;L^+)\Delta^{36}\Delta^{45}\Big]\\
&+\ \Delta^{34}\Big[\mathcal{G}_2^{\rm NE}(k_1^-,-k_3^-;L^+)\Delta^{15}\Delta^{26}+\mathcal{G}_2^{\rm NE}(k_1^-,k_3^-;L^+)\Delta^{16}\Delta^{25}\Big]\\
&+\ \Delta^{56}\Big[\mathcal{G}_2^{\rm NE}(k_1^-,-k_2^-;L^+)\Delta^{13}\Delta^{24}+\mathcal{G}_2^{\rm NE}(k_1^-,k_2^-;L^+)\Delta^{14}\Delta^{23}\Big]\\
&+\ \mathcal{G}_3^{\rm NE}(k_1^-,k_2^-,k_3^-;L^+)\Big[\Delta^{13}\Delta^{25}\Delta^{46}+\Delta^{16}\Delta^{24}\Delta^{35}\Big]\\
&+\mathcal{G}_3^{\rm NE}(k_2^-,k_1^-,k_3^-;L^+)\Big[\Delta^{13}\Delta^{26}\Delta^{45}+\Delta^{15}\Delta^{24}\Delta^{36}\Big]\\
&+\ \mathcal{G}_3^{\rm NE}(k_1^-,k_3^-,k_2^-;L^+)\Big[\Delta^{14}\Delta^{26}\Delta^{35}+\Delta^{15}\Delta^{23}\Delta^{46}\Big]\\
&+\mathcal{G}_4^{\rm NE}(k_1^-,k_2^-,k_3^-;L^+)\Big[\Delta^{14}\Delta^{25}\Delta^{36}+\Delta^{16}\Delta^{23}\Delta^{45}\Big]\ \Big\},
\end{aligned}
\tag{D.7}
$$

where the functions $\mathcal{G}_1^{\rm NE}(k_i^-;\lambda^+)$ and $\mathcal{G}_2^{\rm NE}(k_i^-,k_j^-;L^+)$ are the functions that account for non-eikonal effects and they are defined in Eq. (5.31) and Eq. (5.44), respectively. Moreover, for the triple inclusive gluon production the longitudinal coordinate integral produces two new functions $\mathcal{G}_3^{\rm NE}(k_i^-,k_j^-,k_k^-;L^+)$ and $\mathcal{G}_4^{\rm NE}(k_i^-,k_j^-,k_k^-;L^+)$ that also account for the non-eikonal effects and read

$$
\mathcal{G}_3^{\rm NE}(k_1^-,k_2^-,k_3^-;L^+)=2\,\frac{-\sin\left[(k_1^++k_2^+)L^+\right]+\sin\left[(k_1^--k_3^-)L^+\right]+\sin\left[(k_2^-+k_3^-)L^+\right]}{\left[(k_1^++k_2^+)L^+\right]\left[(k_1^--k_3^-)L^+\right]\left[(k_2^-+k_3^-)L^+\right]}
\tag{D.8}
$$

and

$$
\mathcal{G}_4^{\rm NE}(k_1^-,k_2^-,k_3^-;L^+)=\frac{\sin\left[\frac{(k_1^--k_2^-)}{2}L^+\right]\,\sin\left[\frac{(k_1^--k_3^-)}{2}L^+\right]\,\sin\left[\frac{(k_2^--k_3^-)}{2}L^+\right]}{\left[\frac{(k_1^--k_2^-)}{2}L^+\right]\left[\frac{(k_1^--k_3^-)}{2}L^+\right]\left[\frac{(k_2^--k_3^-)}{2}L^+\right]}\,.
\tag{D.9}
$$

Both functions go to 1 when we consider the shockwave (eikonal) limit $L^+\to 0$.

We can now substitute Eq. (D.7) into the dilute target limit of the non-eikonal triple inclusive gluon production cross section given in Eq. (D.3). By using the definition of Δ^{ij} given in Eq. (D.6) and integrating over the three transverse momenta, we get

$$
\begin{aligned}
&\frac{d\sigma}{d^2\mathbf{k}_1 d\eta_1\, d^2\mathbf{k}_2 d\eta_2\, d^2\mathbf{k}_3 d\eta_3}\bigg|^{\rm NE}_{\rm dilute}=\frac{g^{18}}{\pi^3(2\pi)^6}\int_{\mathbf{q}_1,\mathbf{q}_2,\mathbf{q}_3}\left|a(\mathbf{q}_1)\right|^2\left|a(\mathbf{q}_2)\right|^2\left|a(\mathbf{q}_3)\right|^2\\
&\times\mathcal{G}_1^{\rm NE}(k_1^-,\lambda^+)\mathcal{G}_1^{\rm NE}(k_2^-,\lambda^+)\mathcal{G}_1^{\rm NE}(k_3^-,\lambda^+)\\
&\times\Big\{C_A^3\Big\langle\rho^a_{\mathbf{k}_1-\mathbf{q}_1}\rho^b_{\mathbf{k}_2-\mathbf{q}_2}\rho^c_{\mathbf{k}_3-\mathbf{q}_3}\rho^a_{\mathbf{q}_1-\mathbf{k}_1}\rho^b_{\mathbf{q}_2-\mathbf{k}_2}\rho^c_{\mathbf{q}_3-\mathbf{k}_3}\Big\rangle_p L^i(\mathbf{k}_1,\mathbf{q}_1)L^i(\mathbf{k}_1,\mathbf{q}_1)L^j(\mathbf{k}_2,\mathbf{q}_2)L^j(\mathbf{k}_2,\mathbf{q}_2)\\
&\times L^k(\mathbf{k}_3,\mathbf{q}_3)L^k(\mathbf{k}_3,\mathbf{q}_3)\\
&+\Big(\Big[\mathcal{G}_2^{\rm NE}(k_1^-,k_2^-;L^+)\,C_A(T^aT^b)_{a_1b_1}(T^bT^a)_{a_2b_2}\delta_{a_3b_3}L^i(\mathbf{k}_1,\mathbf{q}_1)L^i(\mathbf{k}_1,\mathbf{q}_2)L^j(\mathbf{k}_2,\mathbf{q}_1)L^j(\mathbf{k}_2,\mathbf{q}_2)
\end{aligned}
$$

$$\times L^k(\mathbf{k}_3,\mathbf{q}_3)L^k(\mathbf{k}_3,\mathbf{q}_3),\Big\langle \rho^{a_1}_{\mathbf{k}_1-\mathbf{q}_1}\rho^{a_2}_{\mathbf{k}_2-\mathbf{q}_2}\rho^{a_3}_{\mathbf{k}_3-\mathbf{q}_3}\rho^{b_1}_{-\mathbf{k}_1+\mathbf{q}_2}\rho^{b_2}_{-\mathbf{k}_2+\mathbf{q}_1}\rho^{b_3}_{-\mathbf{k}_3+\mathbf{q}_3}\Big\rangle_p + (\underline{k}_2\to-\underline{k}_2)\Big]$$
$$+ (\underline{k}_1\leftrightarrow\underline{k}_3) + (\underline{k}_2\leftrightarrow\underline{k}_3)\Bigg)$$
$$+\Bigg(\Big[\mathcal{G}_3^{\mathrm{NE}}(k_1^-,k_2^-,k_3^-;L^+)(T^aT^b)_{a_1b_1}(T^aT^c)_{a_2b_2}(T^bT^c)_{a_3b_3}L^i(\mathbf{k}_1,\mathbf{q}_1)L^i(\mathbf{k}_1,\mathbf{q}_2)L^j(\mathbf{k}_2,-\mathbf{q}_1)L^j(\mathbf{k}_2,\mathbf{q}_3)$$
$$\times L^k(\mathbf{k}_3,\mathbf{q}_2)L^k(\mathbf{k}_3,-\mathbf{q}_3)\Big\langle \rho^{a_1}_{\mathbf{k}_1-\mathbf{q}_1}\rho^{a_2}_{\mathbf{k}_2+\mathbf{q}_1}\rho^{a_3}_{\mathbf{k}_3-\mathbf{q}_2}\rho^{b_1}_{-\mathbf{k}_1+\mathbf{q}_2}\rho^{b_2}_{-\mathbf{k}_2+\mathbf{q}_3}\rho^{b_3}_{-\mathbf{k}_3-\mathbf{q}_3}\Big\rangle_p + (\underline{k}_3\to-\underline{k}_3)\Big]$$
$$+ (\underline{k}_1\leftrightarrow\underline{k}_3) + (\underline{k}_2\leftrightarrow\underline{k}_3)\Bigg)$$
$$+\Bigg(\Big[\mathcal{G}_4^{\mathrm{NE}}(k_1^-,k_2^-,k_3^-;L^+)(T^aT^b)_{a_1b_1}(T^cT^a)_{a_2b_2}(T^bT^c)_{a_3b_3}L^i(\mathbf{k}_1,\mathbf{q}_1)L^i(\mathbf{k}_1,\mathbf{q}_2)L^j(\mathbf{k}_2,\mathbf{q}_1)L^j(\mathbf{k}_2,\mathbf{q}_3)$$
$$\times L^k(\mathbf{k}_3,\mathbf{q}_2)L^k(\mathbf{k}_3,\mathbf{q}_3)\Big\langle \rho^{a_1}_{\mathbf{k}_1-\mathbf{q}_1}\rho^{a_2}_{\mathbf{k}_2-\mathbf{q}_3}\rho^{a_3}_{\mathbf{k}_3-\mathbf{q}_2}\rho^{b_1}_{-\mathbf{k}_1+\mathbf{q}_2}\rho^{b_2}_{-\mathbf{k}_2+\mathbf{q}_1}\rho^{b_3}_{-\mathbf{k}_3+\mathbf{q}_3}\Big\rangle_p + (\underline{k}_2\leftrightarrow\underline{k}_3)\Big]\Bigg)\Bigg\}, \tag{D.10}$$

where we remind the notation $\underline{k}\equiv(k^-,\mathbf{k})$. Our next order of business is to perform the averaging over the projectile color charge densities. As in the previous sections, we adopt the generalized MV model for the average of two projectile color charge densities and write down all possible Wick contractions of their products. Then, the average of six generic projectile color charge densities can be written

$$\begin{aligned}\Big\langle \rho^{a_1}_{\mathbf{k}_1}\rho^{a_2}_{\mathbf{k}_2}\rho^{a_3}_{\mathbf{k}_3}\rho^{b_1}_{\mathbf{p}_1}\rho^{b_2}_{\mathbf{p}_2}\rho^{b_3}_{\mathbf{p}_3}\Big\rangle_p &= \big\langle \rho^{a_1}_{\mathbf{k}_1}\rho^{b_1}_{\mathbf{p}_1}\big\rangle\big\langle \rho^{a_2}_{\mathbf{k}_2}\rho^{b_2}_{\mathbf{p}_2}\big\rangle\big\langle \rho^{a_3}_{\mathbf{k}_3}\rho^{b_3}_{\mathbf{p}_3}\big\rangle\\
&+ \big\langle \rho^{a_1}_{\mathbf{k}_1}\rho^{b_1}_{\mathbf{p}_1}\big\rangle\Big[\big\langle \rho^{a_2}_{\mathbf{k}_2}\rho^{a_3}_{\mathbf{k}_3}\big\rangle\big\langle \rho^{b_2}_{\mathbf{p}_2}\rho^{b_3}_{\mathbf{p}_3}\big\rangle + \big\langle \rho^{a_2}_{\mathbf{k}_2}\rho^{b_3}_{\mathbf{p}_3}\big\rangle\big\langle \rho^{a_3}_{\mathbf{k}_3}\rho^{b_2}_{\mathbf{p}_2}\big\rangle\Big]\\
&+ \big\langle \rho^{a_2}_{\mathbf{k}_2}\rho^{b_2}_{\mathbf{p}_2}\big\rangle\Big[\big\langle \rho^{a_1}_{\mathbf{k}_1}\rho^{a_3}_{\mathbf{k}_3}\big\rangle\big\langle \rho^{b_1}_{\mathbf{p}_1}\rho^{b_3}_{\mathbf{p}_3}\big\rangle + \big\langle \rho^{a_1}_{\mathbf{k}_1}\rho^{b_3}_{\mathbf{p}_3}\big\rangle\big\langle \rho^{a_3}_{\mathbf{k}_3}\rho^{b_1}_{\mathbf{p}_1}\big\rangle\Big]\\
&+ \big\langle \rho^{a_3}_{\mathbf{k}_3}\rho^{b_3}_{\mathbf{p}_3}\big\rangle\Big[\big\langle \rho^{a_1}_{\mathbf{k}_1}\rho^{a_2}_{\mathbf{k}_2}\big\rangle\big\langle \rho^{b_1}_{\mathbf{p}_1}\rho^{b_2}_{\mathbf{p}_2}\big\rangle + \big\langle \rho^{a_1}_{\mathbf{k}_1}\rho^{b_2}_{\mathbf{p}_2}\big\rangle\big\langle \rho^{a_2}_{\mathbf{k}_2}\rho^{b_1}_{\mathbf{p}_1}\big\rangle\Big]\\
&+ \big\langle \rho^{a_1}_{\mathbf{k}_1}\rho^{a_2}_{\mathbf{k}_2}\big\rangle\Big[\big\langle \rho^{a_3}_{\mathbf{k}_3}\rho^{b_1}_{\mathbf{p}_1}\big\rangle\big\langle \rho^{b_2}_{\mathbf{p}_2}\rho^{b_3}_{\mathbf{p}_3}\big\rangle + \big\langle \rho^{a_3}_{\mathbf{k}_3}\rho^{b_2}_{\mathbf{p}_2}\big\rangle\big\langle \rho^{b_1}_{\mathbf{p}_1}\rho^{b_3}_{\mathbf{p}_3}\big\rangle\Big]\\
&+ \big\langle \rho^{a_2}_{\mathbf{k}_2}\rho^{a_3}_{\mathbf{k}_3}\big\rangle\Big[\big\langle \rho^{a_1}_{\mathbf{k}_1}\rho^{b_2}_{\mathbf{p}_2}\big\rangle\big\langle \rho^{b_1}_{\mathbf{p}_1}\rho^{b_3}_{\mathbf{p}_3}\big\rangle + \big\langle \rho^{a_1}_{\mathbf{k}_1}\rho^{b_3}_{\mathbf{p}_3}\big\rangle\big\langle \rho^{b_1}_{\mathbf{p}_1}\rho^{b_2}_{\mathbf{p}_2}\big\rangle\Big]\\
&+ \big\langle \rho^{a_2}_{\mathbf{k}_2}\rho^{b_1}_{\mathbf{p}_1}\big\rangle\Big[\big\langle \rho^{a_1}_{\mathbf{k}_1}\rho^{a_3}_{\mathbf{k}_3}\big\rangle\big\langle \rho^{b_2}_{\mathbf{p}_2}\rho^{b_3}_{\mathbf{p}_3}\big\rangle + \big\langle \rho^{a_1}_{\mathbf{k}_1}\rho^{b_3}_{\mathbf{p}_3}\big\rangle\big\langle \rho^{a_3}_{\mathbf{k}_3}\rho^{b_2}_{\mathbf{p}_2}\big\rangle\Big]\\
&+ \big\langle \rho^{a_2}_{\mathbf{k}_2}\rho^{b_3}_{\mathbf{p}_3}\big\rangle\Big[\big\langle \rho^{a_1}_{\mathbf{k}_1}\rho^{b_2}_{\mathbf{p}_2}\big\rangle\big\langle \rho^{a_3}_{\mathbf{k}_3}\rho^{b_1}_{\mathbf{p}_1}\big\rangle + \big\langle \rho^{a_1}_{\mathbf{k}_1}\rho^{a_3}_{\mathbf{k}_3}\big\rangle\big\langle \rho^{b_1}_{\mathbf{p}_1}\rho^{b_2}_{\mathbf{p}_2}\big\rangle\Big],\end{aligned} \tag{D.11}$$

where the two projectile color charge correlator is given by Eq. (5.24). One can use Eq. (D.11) in order to perform the projectile color charge density averaging in Eq. (D.10). The resulting expression consists of three distinct parts: a term with a single trace, a term with double trace and a term with three traces of the color generators (these terms are the analogue of three-dipole, dipole-quadrupole and sextuple contributions in [40] for the dilute-dense set up). Therefore, we write the dilute target limit of the non-eikonal triple inclusive gluon production cross section as sum of those three contributions:

$$\left.\frac{d\sigma}{d^2\mathbf{k}_1d\eta_1\,d^2\mathbf{k}_2d\eta_2\,d^2\mathbf{k}_3d\eta_3}\right|^{\mathrm{NE}}_{\mathrm{dilute}} = \left.\frac{d\sigma^{(3\mathrm{tr})}}{d^2\mathbf{k}_1d\eta_1\,d^2\mathbf{k}_2d\eta_2\,d^2\mathbf{k}_3d\eta_3}\right|^{\mathrm{NE}}_{\mathrm{dilute}}$$

$$+\left.\frac{d\sigma^{(2\mathrm{tr})}}{d^2\mathbf{k}_1 d\eta_1\, d^2\mathbf{k}_2 d\eta_2\, d^2\mathbf{k}_3 d\eta_3}\right|^{\mathrm{NE}}_{\mathrm{dilute}} + \left.\frac{d\sigma^{(1\mathrm{tr})}}{d^2\mathbf{k}_1 d\eta_1\, d^2\mathbf{k}_2 d\eta_2\, d^2\mathbf{k}_3 d\eta_3}\right|^{\mathrm{NE}}_{\mathrm{dilute}}. \quad \text{(D.12)}$$

Let us now write down the explicit expressions for each of these three contributions starting from the the three-trace one:

$$\left.\frac{d\sigma^{(3\mathrm{tr})}}{d^2\mathbf{k}_1 d\eta_1 d^2\mathbf{k}_2 d\eta_2 d^2\mathbf{k}_3 d\eta_3}\right|^{\mathrm{NE}}_{\mathrm{dilute}} = \frac{g^{18} N_c^3 (N_c^2-1)^3}{\pi^3 (2\pi)^6} \int_{\mathbf{q}_1,\mathbf{q}_2,\mathbf{q}_3} \left|a(\mathbf{q}_1)\right|^2 \left|a(\mathbf{q}_2)\right|^2 \left|a(\mathbf{q}_3)\right|^2$$
$$\times\ \mathcal{G}_1^{\mathrm{NE}}(k_1^-;\lambda^+)\,\mathcal{G}_1^{\mathrm{NE}}(k_2^-;\lambda^+)\,\mathcal{G}_1^{\mathrm{NE}}(k_3^-;\lambda^+)\left\{ I_{3\mathrm{tr}}^{(0)} + \frac{1}{(N_c^2-1)} I_{3\mathrm{tr}}^{(1)} + \frac{1}{(N_c^2-1)^2}\left[I_{3\mathrm{tr},1}^{(2)} + I_{3\mathrm{tr},2}^{(2)}\right]\right\}, \quad \text{(D.13)}$$

where

$$I_{3\mathrm{tr}}^{(0)} = \mu^2\big[\mathbf{k}_1-\mathbf{q}_1,\mathbf{q}_1-\mathbf{k}_1\big]\,\mu^2\big[\mathbf{k}_2-\mathbf{q}_2,\mathbf{q}_2-\mathbf{k}_2\big]\mu^2\big[\mathbf{k}_3-\mathbf{q}_3,\mathbf{q}_3-\mathbf{k}_3\big]$$
$$\times\, L^i(\mathbf{k}_1,\mathbf{q}_1)L^i(\mathbf{k}_1,\mathbf{q}_1)L^j(\mathbf{k}_2,\mathbf{q}_2)L^j(\mathbf{k}_2,\mathbf{q}_2)L^k(\mathbf{k}_3,\mathbf{q}_3)L^k(\mathbf{k}_3,\mathbf{q}_3). \quad \text{(D.14)}$$

For $\mathcal{O}\Big(1/(N_c^2-1)\Big)$ terms, we have introduced the following compact notation

$$I_{3\mathrm{tr}}^{(1)} = \Big[\tilde{I}_{3\mathrm{tr}}^{(1)} + \big(\underline{k}_2\to-\underline{k}_2\big)\Big] + \big(\underline{k}_1\leftrightarrow\underline{k}_3\big) + \big(\underline{k}_2\leftrightarrow\underline{k}_3\big) \quad \text{(D.15)}$$

with

$$\tilde{I}_{3\mathrm{tr}}^{(1)} = \mathcal{G}_2^{\mathrm{NE}}(k_1^-,k_2^-;L^+)\,\mu^2\big[\mathbf{k}_1-\mathbf{q}_1,\mathbf{q}_2-\mathbf{k}_1\big]\,\mu^2\big[\mathbf{k}_2-\mathbf{q}_2,\mathbf{q}_1-\mathbf{k}_2\big]\,\mu^2\big[\mathbf{k}_3-\mathbf{q}_3,\mathbf{q}_3-\mathbf{k}_3\big]$$
$$\times\ L^i(\mathbf{k}_1,\mathbf{q}_1)L^i(\mathbf{k}_1,\mathbf{q}_2)\,L^j(\mathbf{k}_2,\mathbf{q}_1)L^j(\mathbf{k}_2,\mathbf{q}_2)\,L^k(\mathbf{k}_3,\mathbf{q}_3)L^k(\mathbf{k}_3,\mathbf{q}_3). \quad \text{(D.16)}$$

A similar compact notation has been adopted for the $\mathcal{O}\Big(1/(N_c^2-1)^2\Big)$ terms in Eq. (D.13):

$$I_{3\mathrm{tr},1}^{(2)} = \Big[\tilde{I}_{3\mathrm{tr},1}^{(2)} + \big(\underline{k}_3\to-\underline{k}_3\big)\Big] + \big(\underline{k}_1\leftrightarrow\underline{k}_3\big) + \big(\underline{k}_2\leftrightarrow\underline{k}_3\big) \quad \text{(D.17)}$$

with

$$\tilde{I}_{3\mathrm{tr},1}^{(2)} = \mathcal{G}_3^{\mathrm{NE}}(k_1^-,k_2^-,k_3^-;L^+)\,\mu^2\big[\mathbf{k}_1-\mathbf{q}_1,\mathbf{q}_2-\mathbf{k}_1\big]\,\mu^2\big[\mathbf{k}_2+\mathbf{q}_1,\mathbf{q}_3-\mathbf{k}_2\big]\,\mu^2\big[\mathbf{k}_3-\mathbf{q}_2,-\mathbf{q}_3-\mathbf{k}_3\big]$$
$$\times\, L^i(\mathbf{k}_1,\mathbf{q}_1)L^i(\mathbf{k}_1,\mathbf{q}_2)\,L^j(\mathbf{k}_2,-\mathbf{q}_1)L^j(\mathbf{k}_2,\mathbf{q}_3)\,L^k(\mathbf{k}_3,\mathbf{q}_2)L^k(\mathbf{k}_3,-\mathbf{q}_3), \quad \text{(D.18)}$$

and

$$I_{3\mathrm{tr},2}^{(2)} = \tilde{I}_{3\mathrm{tr},2}^{(2)} + \big(\underline{k}_2\leftrightarrow\underline{k}_3\big) \quad \text{(D.19)}$$

with

$$\tilde{I}_{3\mathrm{tr},2}^{(2)} = \mathcal{G}_4^{\mathrm{NE}}(k_1^-,k_2^-,k_3^-;L^+)\,\mu^2\big[\mathbf{k}_1-\mathbf{q}_1,\mathbf{q}_2-\mathbf{k}_1\big]\,\mu^2\big[\mathbf{k}_2-\mathbf{q}_3,\mathbf{q}_1-\mathbf{k}_2\big]\,\mu^2\big[\mathbf{k}_3-\mathbf{q}_2,\mathbf{q}_3-\mathbf{k}_3\big]$$
$$\times\, L^i(\mathbf{k}_1,\mathbf{q}_1)L^i(\mathbf{k}_1,\mathbf{q}_2)\,L^j(\mathbf{k}_2,\mathbf{q}_1)L^j(\mathbf{k}_2,\mathbf{q}_3)\,L^k(\mathbf{k}_3,\mathbf{q}_2)L^k(\mathbf{k}_3,\mathbf{q}_3). \quad \text{(D.20)}$$

The double-trace contribution to the dilute target limit of the non-eikonal triple inclusive gluon production cross section can be organized in a similar way:

$$\left.\frac{d\sigma^{(2\mathrm{tr})}}{d^2\mathbf{k}_1 d\eta_1 d^2\mathbf{k}_2 d\eta_2 d^2\mathbf{k}_3 d\eta_3}\right|^{\mathrm{NE}}_{\mathrm{dilute}} = \frac{g^{18} N_c^3 (N_c^2-1)^3}{\pi^3 (2\pi)^6} \int_{\mathbf{q}_1,\mathbf{q}_2,\mathbf{q}_3} \left|a(\mathbf{q}_2)\right|^2 \left|a(\mathbf{q}_3)\right|^2$$

$$\times\ \mathcal{G}_1^{\mathrm{NE}}(k_1^-,\lambda^+)\,\mathcal{G}_1^{\mathrm{NE}}(k_2^-;\lambda^+)\,\mathcal{G}_1^{\mathrm{NE}}(k_3^-;\lambda^+)\left\{\left[I_{2\mathrm{tr},1}^{(1)}+I_{2\mathrm{tr},2}^{(1)}\right]+\frac{1}{(N_c^2-1)}\left[I_{2\mathrm{tr},1}^{(2)}+I_{2\mathrm{tr},2}^{(2)}+I_{2\mathrm{tr},3}^{(2)}\right]\right\}. \tag{D.21}$$

Similar compact notations can be adopted for each term in the double-trace contribution. Let us start with the $\mathcal{O}(1)$ terms:

$$I_{2\mathrm{tr},1}^{(1)}=\left[\tilde{I}_{2\mathrm{tr},1}^{(1)}+\left(\underline{k}_2\to-\underline{k}_2\right)\right]+\left(\underline{k}_1\leftrightarrow\underline{k}_2\right)+\left(\underline{k}_1\leftrightarrow\underline{k}_3\right), \tag{D.22}$$

with

$$\begin{aligned}\tilde{I}_{2\mathrm{tr},1}^{(1)}&=\mu^2\left[\mathbf{k}_1-\mathbf{q}_1,\mathbf{q}_1-\mathbf{k}_1\right]\mu^2\left[\mathbf{k}_2-\mathbf{q}_2,\mathbf{q}_3-\mathbf{k}_3\right]\mu^2\left[\mathbf{k}_3-\mathbf{q}_3,\mathbf{q}_2-\mathbf{k}_2\right]\\&\times\ L^i(\mathbf{k}_1,\mathbf{q}_1)L^i(\mathbf{k}_1,\mathbf{q}_1)\,L^j(\mathbf{k}_2,\mathbf{q}_2)L^j(\mathbf{k}_2,\mathbf{q}_2)\,L^k(\mathbf{k}_3,\mathbf{q}_3)L^k(\mathbf{k}_3,\mathbf{q}_3),\end{aligned} \tag{D.23}$$

and

$$I_{2\mathrm{tr},2}^{(1)}=\left[\tilde{I}_{2\mathrm{tr},2}^{(1)}+\left(\underline{k}_2\to-\underline{k}_2\right)\right]+\left(\underline{k}_1\leftrightarrow\underline{k}_3\right)+\left(\underline{k}_2\leftrightarrow\underline{k}_3\right) \tag{D.24}$$

with

$$\begin{aligned}\tilde{I}_{2\mathrm{tr},2}^{(1)}&=\mathcal{G}_2^{\mathrm{NE}}(k_1^-,k_2^-;L^+)\,\mu^2\left[\mathbf{k}_3-\mathbf{q}_3,\mathbf{q}_3-\mathbf{k}_3\right]L^i(\mathbf{k}_1,\mathbf{q}_1)L^i(\mathbf{k}_1,\mathbf{q}_2)\,L^j(\mathbf{k}_2,\mathbf{q}_1)L^j(\mathbf{k}_2,\mathbf{q}_2)\\&\times L^k(\mathbf{k}_3,\mathbf{q}_3)L^k(\mathbf{k}_3,\mathbf{q}_3)\Big\{\mu^2\left[\mathbf{k}_1-\mathbf{q}_1,\mathbf{q}_1-\mathbf{k}_2\right]\mu^2\left[\mathbf{k}_2-\mathbf{q}_2,\mathbf{q}_2-\mathbf{k}_1\right]\\&\qquad+\frac{1}{2}\mu^2\left[\mathbf{k}_1-\mathbf{q}_1,\mathbf{k}_2-\mathbf{q}_2\right]\mu^2\left[\mathbf{q}_2-\mathbf{k}_1,\mathbf{q}_1-\mathbf{k}_2\right]\Big\}.\end{aligned} \tag{D.25}$$

$\mathcal{O}\left(1/(N_c^2-1)\right)$ terms in the double-trace contribution can be written in a similar manner. The first term reads

$$I_{2\mathrm{tr},1}^{(2)}=\left[\tilde{I}_{2\mathrm{tr},1}^{(2)}+\left(\underline{k}_2\to-\underline{k}_2\right)\right]+\left(\underline{k}_1\leftrightarrow\underline{k}_3\right)+\left(\underline{k}_2\leftrightarrow\underline{k}_3\right), \tag{D.26}$$

with

$$\begin{aligned}\tilde{I}_{2\mathrm{tr},1}^{(2)}&=\mathcal{G}_2^{\mathrm{NE}}(k_1^-,k_2^-;L^+)\,\mu^2\left[\mathbf{k}_1-\mathbf{q}_1,\mathbf{q}_2-\mathbf{k}_1\right]L^i(\mathbf{k}_1,\mathbf{q}_1)L^i(\mathbf{k}_1,\mathbf{q}_2)\,L^j(\mathbf{k}_2,\mathbf{q}_1)L^j(\mathbf{k}_2,\mathbf{q}_2)\\&\times L^k(\mathbf{k}_3,\mathbf{q}_3)L^k(\mathbf{k}_3,\mathbf{q}_3)\Big\{\mu^2\left[\mathbf{k}_2-\mathbf{q}_2,\mathbf{q}_3-\mathbf{k}_3\right]\mu^2\left[\mathbf{k}_3-\mathbf{q}_2,\mathbf{q}_1-\mathbf{k}_2\right]\\&\qquad+\mu^2\left[\mathbf{k}_2-\mathbf{q}_2,\mathbf{k}_3-\mathbf{q}_3\right]\mu^2\left[\mathbf{q}_1-\mathbf{k}_2,\mathbf{q}_3-\mathbf{k}_3\right]\Big\}.\end{aligned} \tag{D.27}$$

The second term can be written as

$$I_{2\mathrm{tr},2}^{(2)}=\left[\tilde{I}_{2\mathrm{tr},2}^{(2)}+\left(\underline{k}_3\to-\underline{k}_3\right)\right]+\left(\underline{k}_1\leftrightarrow\underline{k}_3\right)+\left(\underline{k}_2\leftrightarrow\underline{k}_3\right), \tag{D.28}$$

with

$$\begin{aligned}&\tilde{I}_{2\mathrm{tr},2}^{(2)}=\mathcal{G}_3^{\mathrm{NE}}(k_1^-,k_2^-,k_3^-;L^+)\,L^i(\mathbf{k}_1,\mathbf{q}_1)L^i(\mathbf{k}_1,-\mathbf{q}_2)\,L^j(\mathbf{k}_2,-\mathbf{q}_1)L^j(\mathbf{k}_2,-\mathbf{q}_3)\\&\times L^k(\mathbf{k}_3,-\mathbf{q}_2)L^k(\mathbf{k}_3,\mathbf{q}_3)\mu^2\left[\mathbf{k}_1-\mathbf{q}_1,-\mathbf{q}_2-\mathbf{k}_1\right]\end{aligned}$$

$$\times \left(\frac{1}{2}\mu^2\big[\mathbf{k}_2+\mathbf{q}_1,\mathbf{q}_3-\mathbf{k}_3\big]\mu^2\big[\mathbf{k}_3+\mathbf{q}_2,-\mathbf{q}_3-\mathbf{k}_2\big] + \mu^2\big[\mathbf{k}_2+\mathbf{q}_1,\mathbf{k}_3+\mathbf{q}_2\big]\mu^2\big[-\mathbf{q}_3-\mathbf{k}_2,\mathbf{q}_3-\mathbf{k}_3\big] \right)$$
$$+ \mathcal{G}_3^{\mathrm{NE}}(k_1^-,k_2^-,k_3^-;L^+)\, L^i(\mathbf{k}_1,\mathbf{q}_1)L^i(\mathbf{k}_1,\mathbf{q}_3)\, L^j(\mathbf{k}_2,-\mathbf{q}_1)L^j(\mathbf{k}_2,\mathbf{q}_2)\, L^k(\mathbf{k}_3,\mathbf{q}_3)L^k(\mathbf{k}_3,-\mathbf{q}_2)$$
$$\times \mu^2\big[\mathbf{k}_2+\mathbf{q}_1,\mathbf{q}_2-\mathbf{k}_2\big]\left(\mu^2\big[\mathbf{k}_1-\mathbf{q}_1,-\mathbf{k}_3-\mathbf{q}_2\big]\mu^2\big[\mathbf{q}_3-\mathbf{k}_1,\mathbf{k}_3-\mathbf{q}_3\big] + \frac{1}{2}\mu^2\big[\mathbf{k}_1-\mathbf{q}_1,\mathbf{k}_3-\mathbf{q}_3\big]\mu^2\big[\mathbf{q}_3-\mathbf{k}_1,-\mathbf{k}_3-\mathbf{q}_2\big]\right)$$
$$+ \mathcal{G}_3^{\mathrm{NE}}(k_1^-,k_2^-,k_3^-;L^+)\, L^i(\mathbf{k}_1,\mathbf{q}_1)L^i(\mathbf{k}_1,-\mathbf{q}_2)\, L^j(\mathbf{k}_2,-\mathbf{q}_1)L^j(\mathbf{k}_2,\mathbf{q}_3)\, L^k(\mathbf{k}_3,-\mathbf{q}_2)L^k(\mathbf{k}_3,-\mathbf{q}_3)$$
$$\times \mu^2\big[\mathbf{k}_3+\mathbf{q}_2,-\mathbf{k}_3-\mathbf{q}_3\big]\left(\frac{1}{2}\mu^2\big[\mathbf{k}_1-\mathbf{q}_1,\mathbf{q}_3-\mathbf{k}_2\big]\mu^2\big[-\mathbf{q}_2-\mathbf{k}_1,\mathbf{k}_2+\mathbf{q}_1\big] + \mu^2\big[\mathbf{k}_1-\mathbf{q}_1,\mathbf{k}_2+\mathbf{q}_1\big]\mu^2\big[-\mathbf{q}_2-\mathbf{k}_1,\mathbf{q}_3-\mathbf{k}_2\big]\right). \tag{D.29}$$

Finally, the last term can be written as

$$I^{(2)}_{2\mathrm{tr},3} = \tilde{I}^{(2)}_{2\mathrm{tr},3} + \big(\underline{k}_2 \leftrightarrow \underline{k}_3\big) \tag{D.30}$$

with

$$\tilde{I}^{(2)}_{2\mathrm{tr},3} = \mathcal{G}_4^{\mathrm{NE}}(k_1^-,k_2^-,k_3^-;L^+)\, L^i(\mathbf{k}_1,\mathbf{q}_1)L^i(\mathbf{k}_1,\mathbf{q}_2)\, L^j(\mathbf{k}_2,\mathbf{q}_1)L^j(\mathbf{k}_2,\mathbf{q}_3)\, L^k(\mathbf{k}_3,\mathbf{q}_2)L^k(\mathbf{k}_3,\mathbf{q}_3)$$
$$\times \Big\{\mu^2\big[\mathbf{k}_1-\mathbf{q}_1,\mathbf{q}_2-\mathbf{k}_1\big]\left(\mu^2\big[\mathbf{k}_2-\mathbf{q}_3,\mathbf{q}_3-\mathbf{k}_3\big]\mu^2\big[\mathbf{k}_3-\mathbf{q}_2,\mathbf{q}_1-\mathbf{k}_2\big] + \frac{1}{2}\mu^2\big[\mathbf{k}_2-\mathbf{q}_3,\mathbf{k}_3-\mathbf{q}_2\big]\mu^2\big[\mathbf{q}_1-\mathbf{k}_2,\mathbf{q}_3-\mathbf{k}_3\big]\right)$$
$$+ \mu^2\big[\mathbf{k}_3-\mathbf{q}_2,\mathbf{q}_3-\mathbf{k}_3\big]\left(\mu^2\big[\mathbf{k}_1-\mathbf{q}_1,\mathbf{q}_1-\mathbf{k}_2\big]\mu^2\big[\mathbf{q}_2-\mathbf{k}_1,\mathbf{k}_2-\mathbf{q}_3\big] + \frac{1}{2}\mu^2\big[\mathbf{k}_1-\mathbf{q}_1,\mathbf{k}_2-\mathbf{q}_3\big]\mu^2\big[\mathbf{q}_2-\mathbf{k}_1,\mathbf{q}_1-\mathbf{k}_2\big]\right)\Big\}$$
$$+ \mathcal{G}_4^{\mathrm{NE}}(k_1^-,k_2^-,k_3^-;L^+)\, L^i(\mathbf{k}_1,\mathbf{q}_1)L^i(\mathbf{k}_1,\mathbf{q}_2)\, L^j(\mathbf{k}_2,\mathbf{q}_2)L^j(\mathbf{k}_2,\mathbf{q}_3)\, L^k(\mathbf{k}_3,\mathbf{q}_1)L^k(\mathbf{k}_3,\mathbf{q}_3)$$
$$\times \mu^2\big[\mathbf{k}_2-\mathbf{q}_3,\mathbf{q}_2-\mathbf{k}_2\big]\left(\mu^2\big[\mathbf{k}_1-\mathbf{q}_2,\mathbf{q}_3-\mathbf{k}_3\big]\mu^2\big[\mathbf{q}_1-\mathbf{k}_1,\mathbf{k}_3-\mathbf{q}_1\big] + \frac{1}{2}\mu^2\big[\mathbf{k}_1-\mathbf{q}_2,\mathbf{k}_3-\mathbf{q}_1\big]\mu^2\big[\mathbf{q}_1-\mathbf{k}_1,\mathbf{q}_3-\mathbf{k}_3\big]\right). \tag{D.31}$$

The last contribution to the dilute target limit of the non-eikonal triple inclusive gluon production cross section that we need to consider is the single-trace contribution which can be organized as follows:

$$\left.\frac{d\sigma^{(1\mathrm{tr})}}{d^2\mathbf{k}_1 d\eta_1 d^2\mathbf{k}_2 d\eta_2 d^2\mathbf{k}_3 d\eta_3}\right|^{\mathrm{NE}}_{\mathrm{dilute}} = \frac{g^{18}N_c^3(N_c^2-1)^3}{\pi^3(2\pi)^6}\int_{\mathbf{q}_1,\mathbf{q}_2,\mathbf{q}_3}\big|a(\mathbf{q}_1)\big|^2\big|a(\mathbf{q}_2)\big|^2\big|a(\mathbf{q}_3)\big|^2$$
$$\times\ \mathcal{G}_1^{\mathrm{NE}}(k_1^-;\lambda^+)\,\mathcal{G}_1^{\mathrm{NE}}(k_2^-;\lambda^+)\,\mathcal{G}_1^{\mathrm{NE}}(k_3^-;L^+)\left[I^{(2)}_{1\mathrm{tr},1}+I^{(2)}_{1\mathrm{tr},2}+I^{(2)}_{1\mathrm{tr},3}+I^{(2)}_{1\mathrm{tr},4}\right]. \tag{D.32}$$

The first term in the single-trace contribution can be written as

$$I^{(2)}_{1\mathrm{tr},1} = \left[\tilde{I}^{(2)}_{1\mathrm{tr},1} + \big(\underline{k}_2 \to -\underline{k}_2\big)\right] + \big(\underline{k}_2 \leftrightarrow \underline{k}_3\big) \tag{D.33}$$

with

$$\tilde{I}^{(2)}_{1\text{tr},1} = L^i(\mathbf{k}_1,\mathbf{q}_1)L^i(\mathbf{k}_1,\mathbf{q}_1)L^j(\mathbf{k}_2,\mathbf{q}_2)L^j(\mathbf{k}_2,\mathbf{q}_2)L^k(\mathbf{k}_3,\mathbf{q}_3)L^k(\mathbf{k}_3,\mathbf{q}_3)$$
$$\times \mu^2\big[\mathbf{k}_1-\mathbf{q}_1,\mathbf{k}_2-\mathbf{q}_2\big]\Big(\mu^2\big[\mathbf{k}_3-\mathbf{q}_3,\mathbf{q}_1-\mathbf{k}_1\big]\mu^2\big[\mathbf{q}_2-\mathbf{k}_2,\mathbf{q}_3-\mathbf{k}_3\big]$$
$$+\mu^2\big[\mathbf{k}_3-\mathbf{q}_3,\mathbf{q}_2-\mathbf{k}_2\big]\mu^2\big[\mathbf{q}_1-\mathbf{k}_1+\mathbf{q}_1,\mathbf{q}_3-\mathbf{k}_3\big]\Big). \quad \text{(D.34)}$$

In a similar manner, the second term in the single-trace contribution can be written as

$$I^{(2)}_{1\text{tr},2} = \Big[\tilde{I}^{(2)}_{1\text{tr},2} + \big(\underline{k}_2 \to -\underline{k}_2\big)\Big] + \big(\underline{k}_1 \leftrightarrow \underline{k}_3\big) + \big(\underline{k}_2 \leftrightarrow \underline{k}_3\big) \quad \text{(D.35)}$$

with

$$\tilde{I}^{(2)}_{1\text{tr},2} = \mathcal{G}_2^{\text{NE}}(k_1^-,k_2^-;L^+)\, L^i(\mathbf{k}_1,\mathbf{q}_1)L^i(\mathbf{k}_1,\mathbf{q}_2)\, L^j(\mathbf{k}_2,\mathbf{q}_1)L^j(\mathbf{k}_2,\mathbf{q}_2)\, L^k(\mathbf{k}_3,\mathbf{q}_3)L^k(\mathbf{k}_3,\mathbf{q}_3)$$
$$\times\Big\{\mu^2\big[\mathbf{k}_1-\mathbf{q}_2,\mathbf{k}_2-\mathbf{q}_1\big]\Big(\frac{1}{2}\mu^2\big[\mathbf{k}_3-\mathbf{q}_3,\mathbf{q}_1-\mathbf{k}_1\big]\mu^2\big[\mathbf{q}_2-\mathbf{k}_2,\mathbf{q}_3-\mathbf{k}_3\big]$$
$$+\frac{1}{2}\mu^2\big[\mathbf{k}_3-\mathbf{q}_3,\mathbf{q}_2-\mathbf{k}_2\big]\mu^2\big[\mathbf{q}_1-\mathbf{k}_1,\mathbf{q}_3-\mathbf{k}_3\big]\Big)$$
$$+\mu^2\big[\mathbf{k}_1-\mathbf{q}_1,\mathbf{k}_3-\mathbf{q}_3\big]\Big(\mu^2\big[\mathbf{k}_2-\mathbf{q}_2,\mathbf{q}_2-\mathbf{k}_1\big]\mu^2\big[\mathbf{q}_1-\mathbf{k}_2,\mathbf{q}_3-\mathbf{k}_3\big]$$
$$+\frac{1}{2}\mu^2\big[\mathbf{k}_2-\mathbf{q}_2,\mathbf{q}_3-\mathbf{k}_3\big]\mu^2\big[\mathbf{q}_2-\mathbf{k}_1,\mathbf{q}_1-\mathbf{k}_2\big]\Big)$$
$$+\mu^2\big[\mathbf{k}_1-\mathbf{q}_1,\mathbf{q}_1-\mathbf{k}_2\big]\Big(\mu^2\big[\mathbf{k}_2-\mathbf{q}_2,\mathbf{k}_3-\mathbf{q}_3\big]\mu^2\big[\mathbf{q}_2-\mathbf{k}_1,\mathbf{q}_3-\mathbf{k}_3\big]$$
$$+\mu^2\big[\mathbf{k}_2-\mathbf{q}_2,\mathbf{q}_3-\mathbf{k}_3\big]\mu^2\big[\mathbf{k}_3-\mathbf{q}_3,\mathbf{q}_2-\mathbf{k}_1\big]\Big)$$
$$+\mu^2\big[\mathbf{k}_1-\mathbf{q}_1,\mathbf{q}_3-\mathbf{k}_3\big]\Big(\frac{1}{2}\mu^2\big[\mathbf{k}_2-\mathbf{q}_2,\mathbf{k}_3-\mathbf{q}_3\big]\mu^2\big[\mathbf{q}_2-\mathbf{k}_1,\mathbf{q}_1-\mathbf{k}_2\big]$$
$$+\mu^2\big[\mathbf{k}_2-\mathbf{q}_2,\mathbf{q}_2-\mathbf{k}_1\big]\mu^2\big[\mathbf{k}_3-\mathbf{q}_3,\mathbf{q}_1-\mathbf{k}_2\big]\Big)\Big\}. \quad \text{(D.36)}$$

The third term in the single-trace contribution reads

$$I^{(2)}_{1\text{tr},3} = \Big[\tilde{I}^{(2)}_{1\text{tr},3} + \big(\underline{k}_3 \to -\underline{k}_3\big)\Big] + \big(\underline{k}_1 \leftrightarrow \underline{k}_3\big) + \big(\underline{k}_2 \leftrightarrow \underline{k}_3\big) \quad \text{(D.37)}$$

with

$$\tilde{I}^{(2)}_{1\text{tr},3} = \mathcal{G}_3(k_1^-,k_2^-,k_3^-;L^+)\, L^i(\mathbf{k}_1,\mathbf{q}_1)L^i(\mathbf{k}_1,-\mathbf{q}_2)\, L^j(\mathbf{k}_2,-\mathbf{q}_1)L^j(\mathbf{k}_2,-\mathbf{q}_3)\, L^k(\mathbf{k}_3,-\mathbf{q}_2)L^k(\mathbf{k}_3,\mathbf{q}_3)$$
$$\times\Big\{\mu^2\big[\mathbf{k}_1-\mathbf{q}_1,\mathbf{k}_2+\mathbf{q}_1\big]\Big(\mu^2\big[\mathbf{k}_3+\mathbf{q}_2,-\mathbf{q}_2-\mathbf{k}_1\big]\mu^2\big[-\mathbf{q}_3-\mathbf{k}_2,\mathbf{q}_3-\mathbf{k}_3\big]$$
$$+\frac{1}{2}\mu^2\big[\mathbf{k}_3+\mathbf{q}_2,-\mathbf{q}_3-\mathbf{k}_2\big]\mu^2\big[-\mathbf{q}_2-\mathbf{k}_1,\mathbf{q}_3-\mathbf{k}_3\big]\Big)$$
$$+\frac{1}{4}\mu^2\big[\mathbf{k}_1-\mathbf{q}_1,\mathbf{q}_3-\mathbf{k}_3\big]\mu^2\big[\mathbf{k}_2+\mathbf{q}_1,-\mathbf{q}_2-\mathbf{k}_1\big]\mu^2\big[\mathbf{k}_3+\mathbf{q}_2,-\mathbf{q}_3-\mathbf{k}_2\big]\Big\}$$

$$
\begin{aligned}
&+\mathcal{G}_3(k_1^-,k_2^-,k_3^-;L^+)\,L^i(\mathbf{k}_1,\mathbf{q}_1)L^i(\mathbf{k}_1,\mathbf{q}_3)\,L^j(\mathbf{k}_2,-\mathbf{q}_1)L^j(\mathbf{k}_2,\mathbf{q}_2)\,L^k(\mathbf{k}_3,\mathbf{q}_3)L^k(\mathbf{k}_3,-\mathbf{q}_2)\\
&\quad\times\frac{1}{2}\Big\{\mu^2\big[\mathbf{k}_1-\mathbf{q}_1,\mathbf{k}_3-\mathbf{q}_3\big]\,\mu^2\big[\mathbf{k}_2+\mathbf{q}_1,\mathbf{q}_3-\mathbf{k}_1\big]\,\mu^2\big[\mathbf{q}_2-\mathbf{k}_2,-\mathbf{k}_3-\mathbf{q}_2\big]\\
&\qquad+\mu^2\big[\mathbf{k}_1-\mathbf{q}_1,\mathbf{q}_2-\mathbf{k}_2\big]\,\mu^2\big[\mathbf{k}_2+\mathbf{q}_1,-\mathbf{k}_3-\mathbf{q}_2\big]\,\mu^2\big[\mathbf{k}_3-\mathbf{q}_3,\mathbf{q}_3-\mathbf{k}_1\big]\Big\}\\
&+\mathcal{G}_3(k_1^-,k_2^-,k_3^-;L^+)\,L^i(\mathbf{k}_1,\mathbf{q}_3)L^i(\mathbf{k}_1,\mathbf{q}_1)\,L^j(\mathbf{k}_2,-\mathbf{q}_3)L^j(\mathbf{k}_2,\mathbf{q}_2)\,L^k(\mathbf{k}_3,\mathbf{q}_1)L^k(\mathbf{k}_3,-\mathbf{q}_2)\\
&\quad\times\frac{1}{4}\,\mu^2\big[\mathbf{k}_1-\mathbf{q}_3,\mathbf{k}_3-\mathbf{q}_1\big]\,\mu^2\big[\mathbf{k}_2+\mathbf{q}_3,-\mathbf{k}_3-\mathbf{q}_2\big]\,\mu^2\big[\mathbf{q}_1-\mathbf{k}_1,\mathbf{q}_2-\mathbf{k}_2\big]\\
&+\mathcal{G}_3(k_1^-,k_2^-,k_3^-;L^+)\,L^i(\mathbf{k}_1,-\mathbf{q}_2)L^i(\mathbf{k}_1,\mathbf{q}_3)\,L^j(\mathbf{k}_2,\mathbf{q}_2)L^j(\mathbf{k}_2,-\mathbf{q}_1)\,L^k(\mathbf{k}_3,\mathbf{q}_3)L^k(\mathbf{k}_3,\mathbf{q}_1)\\
&\quad\times\frac{1}{4}\,\mu^2\big[\mathbf{k}_1+\mathbf{q}_2,-\mathbf{q}_1-\mathbf{k}_2\big]\,\mu^2\big[\mathbf{k}_2-\mathbf{q}_2,\mathbf{k}_3-\mathbf{q}_3\big]\,\mu^2\big[\mathbf{q}_3-\mathbf{k}_1,\mathbf{q}_1-\mathbf{k}_3\big].
\end{aligned}
\tag{D.38}
$$

Finally, the last term in the single-trace contribution can be written as

$$
I^{(2)}_{1\mathrm{tr},4}=\tilde{I}^{(2)}_{1\mathrm{tr},4}+\big(\underline{k}_2\leftrightarrow\underline{k}_3\big)
\tag{D.39}
$$

with

$$
\begin{aligned}
\tilde{I}^{(2)}_{1\mathrm{tr},4}&=\mathcal{G}_4^{\mathrm{NE}}(k_1^-,k_2^-,k_3^-;L^+)\,L^i(\mathbf{k}_1,\mathbf{q}_1)L^i(\mathbf{k}_1,\mathbf{q}_2)\,L^j(\mathbf{k}_2,\mathbf{q}_1)L^j(\mathbf{k}_2,\mathbf{q}_3)\,L^k(\mathbf{k}_3,\mathbf{q}_2)L^k(\mathbf{k}_3,\mathbf{q}_3)\\
&\quad\times\Big\{\mu^2\big[\mathbf{k}_1-\mathbf{q}_1,\mathbf{q}_1-\mathbf{k}_2\big]\,\Big(\frac{1}{2}\mu^2\big[\mathbf{k}_2-\mathbf{q}_3,\mathbf{k}_3-\mathbf{q}_2\big]\mu^2\big[\mathbf{q}_2-\mathbf{k}_1,\mathbf{q}_3-\mathbf{k}_3\big]\\
&\quad+\mu^2\big[\mathbf{k}_2-\mathbf{q}_3,\mathbf{q}_3-\mathbf{k}_3\big]\mu^2\big[\mathbf{k}_3-\mathbf{q}_2,\mathbf{q}_2-\mathbf{k}_1\big]\Big)\\
&\qquad+\frac{1}{4}\mu^2\big[\mathbf{k}_1-\mathbf{q}_1,\mathbf{q}_3-\mathbf{k}_3\big]\mu^2\big[\mathbf{k}_2-\mathbf{q}_3,\mathbf{k}_3-\mathbf{q}_2\big]\mu^2\big[\mathbf{q}_2-\mathbf{k}_1,\mathbf{q}_1-\mathbf{k}_2\big]\Big\}\\
&+\mathcal{G}_4^{\mathrm{NE}}(k_1^-,k_2^-,k_3^-;L^+)\,L^i(\mathbf{k}_1,\mathbf{q}_1)L^i(\mathbf{k}_1,\mathbf{q}_3)\,L^j(\mathbf{k}_2,\mathbf{q}_1)L^j(\mathbf{k}_2,\mathbf{q}_2)\,L^k(\mathbf{k}_3,\mathbf{q}_2)L^k(\mathbf{k}_3,\mathbf{q}_3)\\
&\quad\times\frac{1}{2}\Big\{\mu^2\big[\mathbf{k}_1-\mathbf{q}_1,\mathbf{k}_2-\mathbf{q}_2\big]\mu^2\big[\mathbf{k}_3-\mathbf{q}_3,\mathbf{q}_3-\mathbf{k}_1\big]\mu^2\big[\mathbf{q}_1-\mathbf{k}_2,\mathbf{q}_2-\mathbf{k}_3\big]\\
&\qquad+\mu^2\big[\mathbf{k}_1-\mathbf{q}_1,\mathbf{k}_3-\mathbf{q}_3\big]\mu^2\big[\mathbf{k}_2-\mathbf{q}_2,\mathbf{q}_2-\mathbf{k}_3\big]\mu^2\big[\mathbf{q}_3-\mathbf{k}_1,\mathbf{q}_1-\mathbf{k}_2\big]\Big\}\\
&+\mathcal{G}_4^{\mathrm{NE}}(k_1^-,k_2^-,k_3^-;L^+)\,L^i(\mathbf{k}_1,\mathbf{q}_2)L^i(\mathbf{k}_1,\mathbf{q}_3)\,L^j(\mathbf{k}_2,\mathbf{q}_1)L^j(\mathbf{k}_2,\mathbf{q}_2)\,L^k(\mathbf{k}_3,\mathbf{q}_1)L^k(\mathbf{k}_3,\mathbf{q}_3)\\
&\quad\times\frac{1}{4}\,\mu^2\big[\mathbf{k}_1-\mathbf{q}_2,\mathbf{k}_2-\mathbf{q}_1\big]\mu^2\big[\mathbf{k}_3-\mathbf{q}_3,\mathbf{q}_2-\mathbf{k}_2\big]\mu^2\big[\mathbf{q}_3-\mathbf{k}_1,\mathbf{q}_1-\mathbf{k}_3\big]\\
&+\mathcal{G}_4^{\mathrm{NE}}(k_1^-,k_2^-,k_3^-;L^+)\,L^i(\mathbf{k}_1,\mathbf{q}_1)L^i(\mathbf{k}_1,\mathbf{q}_3)\,L^j(\mathbf{k}_2,\mathbf{q}_2)L^j(\mathbf{k}_2,\mathbf{q}_3)\,L^k(\mathbf{k}_3,\mathbf{q}_2)L^k(\mathbf{k}_3,\mathbf{q}_1)\\
&\quad\times\frac{1}{4}\,\mu^2\big[\mathbf{k}_1-\mathbf{q}_3,\mathbf{k}_3-\mathbf{q}_1\big]\mu^2\big[\mathbf{k}_2-\mathbf{q}_2,\mathbf{q}_1-\mathbf{k}_1\big]\mu^2\big[\mathbf{q}_3-\mathbf{k}_2,\mathbf{q}_2-\mathbf{k}_3\big].
\end{aligned}
\tag{D.40}
$$

D.2 Quantum interpretation of each term

Let us now consider each term in Eq. (5.59) separately and identify their correlation features. For this analysis we follow the same strategy introduced in Section 5.3 and use the fact that

$$
\mu^2(\mathbf{k},\mathbf{p})\propto F\big[|\mathbf{k}+\mathbf{p}|R\big],
\tag{D.41}
$$

with R being the radius of the projectile and the form factor F peaked at zero.

- We start our analysis with the $\mathcal{O}(1)$ terms. The only $\mathcal{O}(1)$ term in the dilute target limit of the non-eikonal triple inclusive gluon production cross section is $I^{(0)}_{3\mathrm{tr}}$ term. It is equal to product of three single inclusive gluon production cross sections and it gives contribution to the totally uncorrelated production of three gluons.

- Next, we consider the $\mathcal{O}\big[1/(N_c^2-1)\big]$ terms. At this order, we have three different terms: one originating from three-trace contribution and two originating from double-trace contribution.

  (i) The explicit expression of the three-trace term, $I^{(1)}_{3\mathrm{tr}}$, is given in Eq. (D.16) and its symmetry partners in Eq. (D.15). This term is proportional to

  $$\mu^2\big[\mathbf{k}_1-\mathbf{q}_1,\mathbf{q}_2-\mathbf{k}_1\big]\,\mu^2\big[\mathbf{k}_2-\mathbf{q}_2,\mathbf{q}_1-\mathbf{k}_2\big]\,\mu^2\big[\mathbf{k}_3-\mathbf{q}_3,\mathbf{q}_3-\mathbf{k}_3\big] \propto F^2\big[|\mathbf{q}_2-\mathbf{q}_1|R\big]\mu^2\big[\mathbf{k}_3-\mathbf{q}_3,\mathbf{q}_3-\mathbf{k}_3\big] \quad \text{(D.42)}$$

  which is clearly a contribution to the forward Bose enhancement of the gluons $\mathbf{q}_1$ and $\mathbf{q}_2$ while the third gluon is emitted independently from the others. Its mirror image, given by $(\underline{k}_2 \to -\underline{k}_2)$, exhibits the same behaviour. The symmetry partners of this term which are obtained through $(\underline{k}_1 \leftrightarrow \underline{k}_3)$ and $(\underline{k}_2 \leftrightarrow \underline{k}_3)$ correspond to the two cases where the independently emitted gluon is the first and the second gluons, and the remaining two still give contribution to the forward Bose enhancement in the target wave function.

  (ii) The remaining two terms at this order, originate from the double-trace contribution. The explicit expression of the first of these terms is given in Eq. (D.23) and its symmetry partners are given in Eq. (D.22). This term is proportional to

  $$\mu^2\big[\mathbf{k}_1-\mathbf{q}_1,\mathbf{q}_1-\mathbf{k}_1\big]\,\mu^2\big[\mathbf{k}_2-\mathbf{q}_2,\mathbf{q}_3-\mathbf{k}_3\big]\,\mu^2\big[\mathbf{k}_3-\mathbf{q}_3,\mathbf{q}_2-\mathbf{k}_2\big] \propto F^2\big[|(\mathbf{k}_2-\mathbf{q}_2)-(\mathbf{k}_3-\mathbf{q}_3)|R\big]\,\mu^2\big[\mathbf{k}_1-\mathbf{q}_1,\mathbf{q}_1-\mathbf{k}_1\big] \quad \text{(D.43)}$$

  which can be easily identified as a contribution to the forward Bose enhancement of the gluons $\mathbf{k}_2-\mathbf{q}_2$ and $\mathbf{k}_3-\mathbf{q}_3$ in the projectile wave function while the first gluon is emitted independently of the remaining two. Clearly, the symmetry partners of this term corresponds to the independent emission of second and third gluons, while the remaining two gives contribution to the forward Bose enhancement in the projectile wave function.

  (iii) The explicit expression of the last term at this order, $I^{(1)}_{2\mathrm{tr},2}$, is given in Eq. (D.25) with its symmetry partners given in Eq. (D.24). This term is proportional to

  $$\mu^2\big[\mathbf{k}_3-\mathbf{q}_3,\mathbf{q}_3-\mathbf{k}_3\big]\Big\{\mu^2\big[\mathbf{k}_1-\mathbf{q}_1,\mathbf{q}_1-\mathbf{k}_2\big]\,\mu^2\big[\mathbf{k}_2-\mathbf{q}_2,\mathbf{q}_2-\mathbf{k}_1\big] + \frac{1}{2}\mu^2\big[\mathbf{k}_1-\mathbf{q}_1,\mathbf{k}_2-\mathbf{q}_2\big]\,\mu^2\big[\mathbf{q}_2-\mathbf{k}_1,\mathbf{q}_1-\mathbf{k}_2\big]\Big\} \propto \mu^2\big[\mathbf{k}_3-\mathbf{q}_3,\mathbf{q}_3-\mathbf{k}_3\big] \times\Big\{F^2\big[|\mathbf{k}_1-\mathbf{k}_2|R\big]+\frac{1}{2}F^2\big[|(\mathbf{k}_1-\mathbf{q}_1)+(\mathbf{k}_2-\mathbf{q}_2)|R\big]\Big\}. \quad \text{(D.44)}$$

The first term in the brackets corresponds to forward HBT of the gluons $\mathbf{k}_1$ and $\mathbf{k}_2$, and the second term corresponds to backward Bose enhancement of the gluons $\mathbf{k}_1-\mathbf{q}_1$ and $\mathbf{k}_2-\mathbf{q}_2$ in the projectile wave function while the third gluon is emitted independently from the other two. The mirror image of this term which obtained through ($\underline{k}_2 \to -\underline{k}_2$) corresponds to backward HBT of the gluons $\mathbf{k}_1$ and $\mathbf{k}_2$, and forward Bose enhancement of the gluons $\mathbf{k}_1-\mathbf{q}_1$ and $\mathbf{k}_2-\mathbf{q}_2$ in the projectile wave function while the third gluon is emitted independently. The symmetry partners of this term which are obtained via ($\underline{k}_1 \leftrightarrow \underline{k}_3$) and ($\underline{k}_2 \leftrightarrow \underline{k}_3$) correspond to the following two cases: emission of the first gluon (or the second gluon in the second symmetry partner) while the remaining two gluons exhibit the same behaviour and contribute to (forward/backward) HBT and (backward/forward) projectile Bose enhancement of the corresponding gluons.

- We can now proceed with the $\mathcal{O}\big[1/(N_c^2-1)^2\big]$ terms. At this order, we have terms originating from the three-trace, the double-trace and the single-trace contributions.

  (i) Let us start with the terms originating from the three-trace contribution:

  (a) The explicit expression for the first term in there, $I^{(2)}_{3\text{tr},1}$, is given in Eq. (D.18) and its symmetry partners are given in Eq. (D.17). This term is proportional to

$$\mu^2\big[\mathbf{k}_1-\mathbf{q}_1,\mathbf{q}_2-\mathbf{k}_1\big]\,\mu^2\big[\mathbf{k}_2+\mathbf{q}_1,\mathbf{q}_3-\mathbf{k}_2\big]\,\mu^2\big[\mathbf{k}_3-\mathbf{q}_2,-\mathbf{q}_3-\mathbf{k}_3\big] \propto F\big[|\mathbf{q}_2-\mathbf{q}_1|R\big]\,F\big[|\mathbf{q}_1+\mathbf{q}_3|R\big]F\big[|\mathbf{q}_2+\mathbf{q}_3|R\big]. \quad \text{(D.45)}$$

  This term gives contribution to the case where all three gluons are correlated. In particular, it contributes to forward target Bose enhancement of the gluons $\mathbf{q}_1$ and $\mathbf{q}_2$ with contributions to backward target Bose enhancement between the gluons $\mathbf{q}_1$ and $\mathbf{q}_3$ as well as $\mathbf{q}_2$ and $\mathbf{q}_3$. Since the form factors in this term are independent of the momenta of the produced gluons, the mirror image of this term and its symmetric partners exhibit exactly the same behaviour.

  (b) The second term in the three-trace contribution at $\mathcal{O}\big[1/(N_c^2-1)^2\big]$ is $I^{(2)}_{3\text{tr},2}$ which is defined in Eq. (D.20) and its symmetric partner is defined in Eq. (D.19). This term is proportional to

$$\mu^2\big[\mathbf{k}_1-\mathbf{q}_1,\mathbf{q}_2-\mathbf{k}_1\big]\,\mu^2\big[\mathbf{k}_2-\mathbf{q}_3,\mathbf{q}_1-\mathbf{k}_2\big]\,\mu^2\big[\mathbf{k}_3-\mathbf{q}_2,\mathbf{q}_3-\mathbf{k}_3\big] \propto F\big[|\mathbf{q}_1-\mathbf{q}_2|R\big]\,F\big[|\mathbf{q}_1-\mathbf{q}_3|R\big]\,F\big[|\mathbf{q}_2-\mathbf{q}_3|R\big]. \quad \text{(D.46)}$$

  Clearly, this term is a contribution to the forward Bose enhancement of the target gluons between the gluons $\mathbf{q}_1$ and $\mathbf{q}_2$, together with $\mathbf{q}_1$ and $\mathbf{q}_3$, as well as $\mathbf{q}_2$ and $\mathbf{q}_3$. Its symmetric partner defined in Eq. (D.19) exhibits the same behavior.

  Before we continue our analysis with the terms originating from the double-trace contributions at $\mathcal{O}\big[1/(N_c^2-1)^2\big]$, we would like to mention that the two terms $I^{(2)}_{3\text{tr},1}$ and $I^{(2)}_{3\text{tr},2}$ give contribution to the correlated production of all three gluons. However, the study performed in [40] has shown that the totally

correlated production of three gluons originate from the sextuple contribution which in our case corresponds to the single-trace contribution. This difference is due to the fact that the analogue of the terms $I^{(2)}_{3\mathrm{tr},1}$ and $I^{(2)}_{3\mathrm{tr},2}$ in the dense target limit are suppressed in powers of the number of colors and therefore discarded in [40]. In our study, we show that these terms are of the same order as the single-trace contribution and give contribution to the totally correlated production. The difference between the counting of the number of colors in the dilute and dense limits is addressed in detail in [41, 42].

(ii) Let us proceed with the terms that originate from double-trace contribution at order $\mathcal{O}\big[1/(N_c^2-1)^2\big]$:

(a) The first term is $I^{(2)}_{2\mathrm{tr},1}$ and it is defined in Eq. (D.27) with its symmetric partners defined in Eq. (D.26). This term is proportional to

$$\begin{aligned}
&\mu^2\big[\mathbf{k}_1-\mathbf{q}_1,\mathbf{q}_2-\mathbf{k}_1\big]\Big\{\mu^2\big[\mathbf{k}_2-\mathbf{q}_2,\mathbf{q}_3-\mathbf{k}_3\big]\,\mu^2\big[\mathbf{k}_3-\mathbf{q}_2,\mathbf{q}_1-\mathbf{k}_2\big]\\
&\qquad\qquad+\mu^2\big[\mathbf{k}_2-\mathbf{q}_2,\mathbf{k}_3-\mathbf{q}_3\big]\,\mu^2\big[\mathbf{q}_1-\mathbf{k}_2,\mathbf{q}_3-\mathbf{k}_3\big]\Big\}\\
&\propto F\big[|\mathbf{q}_1-\mathbf{q}_2|R\big]\Big\{F\big[|(\mathbf{k}_2-\mathbf{q}_2)-(\mathbf{k}_3-\mathbf{q}_3)|R\big]\,F\big[|\mathbf{k}_3-\mathbf{k}_2|R\big]\\
&\qquad\qquad+F^2\big[|(\mathbf{k}_2-\mathbf{q}_2)+(\mathbf{k}_3-\mathbf{q}_3)|R\big]\Big\}. \qquad \text{(D.47)}
\end{aligned}$$

The first term in Eq. (D.47) is a contribution to the forward target Bose enhancement of the gluons $\mathbf{q}_1$ and $\mathbf{q}_2$, together with the forward projectile Bose enhancement of the gluons $\mathbf{k}_2-\mathbf{q}_2$ and $\mathbf{k}_3-\mathbf{q}_3$ and forward HBT contribution to the gluons $\mathbf{k}_2$ and $\mathbf{k}_3$. However, due to the HBT contribution to the gluons $\mathbf{k}_2$ and $\mathbf{k}_3$, the second form factor in this term can be considered as peaking around $(\mathbf{q}_3-\mathbf{q}_2)$ and, in that case, it would contribute to the forward Bose enhancement of the gluons $\mathbf{q}_2$ and $\mathbf{q}_3$ in the gluon wave function. In [40] there were no such contributions, again due to the fact that this term is suppressed in powers of the number of colors in the dense target limit. We would like to mention that, in the translationally invariant limit, this term is suppressed by a phase space integration with respect to the other terms at $\mathcal{O}\big[1/(N_c^2-1)^2\big]$. The second term in Eq. (D.47) is a contribution to the forward Bose enhancement of the gluons $\mathbf{q}_1$ and $\mathbf{q}_2$ in the target wave function together with backward contribution the Bose enhancement of the gluons $\mathbf{k}_2-\mathbf{q}_2$ and $\mathbf{k}_3-\mathbf{q}_3$ in the projectile wave function.

(b) The second term that originates from the double-trace operator at $\mathcal{O}\big[1/(N_c^2-1)^2\big]$ is $I^{(2)}_{2\mathrm{tr},2}$. It is defined in Eq. (D.29) with its symmetry partners in Eq. (D.28). This terms has three different pieces. The first piece is proportional to

$$\begin{aligned}
&\mu^2\big[\mathbf{k}_1-\mathbf{q}_1,-\mathbf{q}_2-\mathbf{k}_1\big]\left(\frac{1}{2}\mu^2\big[\mathbf{k}_2+\mathbf{q}_1,\mathbf{q}_3-\mathbf{k}_3\big]\mu^2\big[\mathbf{k}_3+\mathbf{q}_2,-\mathbf{q}_3-\mathbf{k}_2\big]\right.\\
&\qquad\qquad\left.+\mu^2\big[\mathbf{k}_2+\mathbf{q}_1,\mathbf{k}_3+\mathbf{q}_2\big]\mu^2\big[-\mathbf{q}_3-\mathbf{k}_2,\mathbf{q}_3-\mathbf{k}_3\big]\right)
\end{aligned}$$

$$\propto F\big[|\mathbf{q}_1+\mathbf{q}_2|R\big]\left(\frac{1}{2}F^2\big[|(\mathbf{k}_2-\mathbf{q}_2)-(\mathbf{k}_3-\mathbf{q}_3)|R\big]\;+\;F^2\big[|\mathbf{k}_2+\mathbf{k}_3|R\big]\right). \tag{D.48}$$

Clearly, the first term is a contribution to the backward Bose enhancement of the gluons $\mathbf{q}_1$ and $\mathbf{q}_2$ in the target wave function with a contribution to the forward Bose enhancement of the gluons $\mathbf{k}_2-\mathbf{q}_2$ and $\mathbf{k}_3-\mathbf{q}_3$ in the projectile wave function. The second term is a contribution to the backward Bose enhancement of the gluons $\mathbf{q}_1$ and $\mathbf{q}_2$ in the target wave function with a backward HBT to contribution to the gluons $\mathbf{k}_2$ and $\mathbf{k}_3$. The second piece of $I^{(2)}_{2\mathrm{tr},2}$ is proportional to

$$\begin{aligned}&\mu^2\big[\mathbf{k}_2+\mathbf{q}_1,\mathbf{q}_2-\mathbf{k}_2\big]\left(\mu^2\big[\mathbf{k}_1-\mathbf{q}_1,-\mathbf{k}_3-\mathbf{q}_2\big]\mu^2\big[\mathbf{q}_3-\mathbf{k}_1,\mathbf{k}_3-\mathbf{q}_3\big]\right.\\&\qquad\left.+\frac{1}{2}\mu^2\big[\mathbf{k}_1-\mathbf{q}_1,\mathbf{k}_3-\mathbf{q}_3\big]\mu^2\big[\mathbf{q}_3-\mathbf{k}_1,-\mathbf{k}_3-\mathbf{q}_2\big]\right)\\&\propto F\big[|\mathbf{q}_1+\mathbf{q}_2|R\big]\left(F^2\big[|\mathbf{k}_1-\mathbf{k}_3|R\big]+\frac{1}{2}F^2\big[|(\mathbf{k}_1-\mathbf{q}_1)+(\mathbf{k}_3-\mathbf{q}_3)|R\big]\right).\end{aligned} \tag{D.49}$$

The first term in Eq. (D.49) is a contribution to the backward Bose enhancement of the gluons $\mathbf{q}_1$ and $\mathbf{q}_2$ in the target wave function with a forward contribution to the HBT of the gluons $\mathbf{k}_1$ and $\mathbf{k}_3$. The second term in Eq. (D.49) is a contribution to the backward Bose enhancement of the gluons $\mathbf{q}_1$ and $\mathbf{q}_2$ in the target wave function with a backward contribution to the Bose enhancement of the gluons $\mathbf{k}_1-\mathbf{q}_1$ and $\mathbf{k}_3-\mathbf{q}_3$ in the projectile wave function. The last piece of $I^{(2)}_{2\mathrm{tr},2}$ is proportional to

$$\begin{aligned}&\mu^2\big[\mathbf{k}_3+\mathbf{q}_2,-\mathbf{k}_3-\mathbf{q}_3\big]\left(\frac{1}{2}\mu^2\big[\mathbf{k}_1-\mathbf{q}_1,\mathbf{q}_3-\mathbf{k}_2\big]\mu^2\big[-\mathbf{q}_2-\mathbf{k}_1,\mathbf{k}_2+\mathbf{q}_1\big]\right.\\&\qquad\left.+\mu^2\big[\mathbf{k}_1-\mathbf{q}_1,\mathbf{k}_2+\mathbf{q}_1\big]\mu^2\big[-\mathbf{q}_2-\mathbf{k}_1,\mathbf{q}_3-\mathbf{k}_2\big]\right)\\&\propto F\big[|\mathbf{q}_2-\mathbf{q}_3|R\big]\left(\frac{1}{2}F\big[|(\mathbf{k}_1-\mathbf{q}_1)-(\mathbf{k}_3-\mathbf{q}_3)|R\big]F\big[|(\mathbf{k}_1-\mathbf{q}_1)-(\mathbf{k}_2-\mathbf{q}_2)|R\big]\right.\\&\qquad\left.+\;F^2\big[|\mathbf{k}_1-\mathbf{k}_2|R\big]\right).\end{aligned} \tag{D.50}$$

The first term in this equation is a contribution to forward Bose enhancement of the gluons $\mathbf{q}_2$ and $\mathbf{q}_3$ in the target wave function together with forward Bose enhancement of the gluons $\mathbf{k}_1-\mathbf{q}_1$ and $\mathbf{k}_3-\mathbf{q}_3$ as well as $\mathbf{k}_1-\mathbf{q}_1$ and $\mathbf{k}_2-\mathbf{q}_2$ in the projectile wave function. The second term is a contribution to forward Bose enhancement of the gluons $\mathbf{q}_2$ and $\mathbf{q}_3$ in the target wave function together with the forward HBT of the gluons $\mathbf{k}_1$ and $\mathbf{k}_2$. The symmetry partners of all three pieces in $I_{2\mathrm{tr},2}$ that are defined in Eq. (D.28) can be easily identified in the same way.

(c) The last term that originates from the double-trace contribution is $I^{(2)}_{2\mathrm{tr},3}$ which is defined in Eq. (D.31) together with its symmetry partner defined

in Eq. (D.30). The first piece in $I^{(2)}_{2\mathrm{tr},3}$ is proportional to

$$\begin{aligned}
&\mu^2\big[\mathbf{k}_1-\mathbf{q}_1,\mathbf{q}_2-\mathbf{k}_1\big]\left(\mu^2\big[\mathbf{k}_2-\mathbf{q}_3,\mathbf{q}_3-\mathbf{k}_3\big]\mu^2\big[\mathbf{k}_3-\mathbf{q}_2,\mathbf{q}_1-\mathbf{k}_2\big]\right.\\
&\qquad\left.+\frac{1}{2}\mu^2\big[\mathbf{k}_2-\mathbf{q}_3,\mathbf{k}_3-\mathbf{q}_2\big]\mu^2\big[\mathbf{q}_1-\mathbf{k}_2,\mathbf{q}_3-\mathbf{k}_3\big]\right)\\
&\propto F\big[|\mathbf{q}_1-\mathbf{q}_2|R\big]\left(F^2\big[|\mathbf{k}_2-\mathbf{k}_3|R\big]+\frac{1}{2}F^2\big[|(\mathbf{k}_2-\mathbf{q}_2)+(\mathbf{k}_3-\mathbf{q}_3)|R\big]\right).
\end{aligned}\tag{D.51}$$

The first term here is clearly a contribution to the forward Bose enhancement of the gluons $\mathbf{q}_1$ and $\mathbf{q}_2$ in the target wave function together with a contribution to forward HBT of gluons $\mathbf{k}_2$ and $\mathbf{k}_3$. The second term is a contribution to the forward Bose enhancement of the gluons $\mathbf{q}_1$ and $\mathbf{q}_2$ in the target wave function together with a contribution to the backward Bose enhancement of the gluons $\mathbf{k}_2-\mathbf{q}_2$ and $\mathbf{k}_3-\mathbf{q}_3$ in the projectile wave function. The second piece of $I^{(2)}_{2\mathrm{tr},3}$ is proportional to

$$\begin{aligned}
&\mu^2\big[\mathbf{k}_3-\mathbf{q}_2,\mathbf{q}_3-\mathbf{k}_3\big]\left(\mu^2\big[\mathbf{k}_1-\mathbf{q}_1,\mathbf{q}_1-\mathbf{k}_2\big]\mu^2\big[\mathbf{q}_2-\mathbf{k}_1,\mathbf{k}_2-\mathbf{q}_3\big]\right.\\
&\qquad\left.+\frac{1}{2}\mu^2\big[\mathbf{k}_1-\mathbf{q}_1,\mathbf{k}_2-\mathbf{q}_3\big]\mu^2\big[\mathbf{q}_2-\mathbf{k}_1,\mathbf{q}_1-\mathbf{k}_2\big]\right)\\
&\propto F\big[|\mathbf{q}_2-\mathbf{q}_3|R\big]\left(F^2\big[|\mathbf{k}_1-\mathbf{k}_2|R\big]+\frac{1}{2}F^2\big[|(\mathbf{k}_1-\mathbf{q}_1)+(\mathbf{k}_2-\mathbf{q}_2)|R\big]\right).
\end{aligned}\tag{D.52}$$

The first term in this equation is a contribution to the forward Bose enhancement of the gluons $\mathbf{q}_2$ and $\mathbf{q}_3$ in the target wave function with a forward contribution to HBT of gluons $\mathbf{k}_1$ and $\mathbf{k}_2$. The second term in Eq. (D.52) is a contribution to the forward Bose enhancement of the gluons $\mathbf{q}_2$ and $\mathbf{q}_3$ in the target wave function with a backward contribution to the Bose enhancement of the gluons $\mathbf{k}_1-\mathbf{q}_1$ and $\mathbf{k}_2-\mathbf{q}_2$ in the projectile wave function. Finally, the third piece of $I^{(2)}_{2\mathrm{tr},3}$ is proportional to

$$\begin{aligned}
&\mu^2\big[\mathbf{k}_2-\mathbf{q}_3,\mathbf{q}_2-\mathbf{k}_2\big]\left(\mu^2\big[\mathbf{k}_1-\mathbf{q}_2,\mathbf{q}_3-\mathbf{k}_3\big]\mu^2\big[\mathbf{q}_1-\mathbf{k}_1,\mathbf{k}_3-\mathbf{q}_1\big]\right.\\
&\qquad\left.+\frac{1}{2}\mu^2\big[\mathbf{k}_1-\mathbf{q}_2,\mathbf{k}_3-\mathbf{q}_1\big]\mu^2\big[\mathbf{q}_1-\mathbf{k}_1,\mathbf{q}_3-\mathbf{k}_3\big]\right)\\
&\propto F\big[|\mathbf{q}_2-\mathbf{q}_3|R\big]\left(F^2\big[|\mathbf{k}_1-\mathbf{k}_3|R\big]+\frac{1}{2}F^2\big[|(\mathbf{k}_1-\mathbf{q}_1)+(\mathbf{k}_3-\mathbf{q}_3)|R\big]\right).
\end{aligned}\tag{D.53}$$

The first term here is a contribution to the forward Bose enhancement of the gluons $\mathbf{q}_2$ and $\mathbf{q}_3$ in the target wave function together with a contribution to the forward HBT of the gluons $\mathbf{k}_1$ and $\mathbf{k}_3$. The second term in Eq. (D.53) is a contribution to the forward Bose enhancement of the

gluons $\mathbf{q}_2$ and $\mathbf{q}_3$ in the target wave function together with a contribution to backward Bose enhancement to the gluons $\mathbf{k}_1-\mathbf{q}_1$ and $\mathbf{k}_3-\mathbf{q}_3$ in the projectile wave function. The symmetry partner of the $I^{(2)}_{2\text{tr},3}$ that is defined in Eq. (D.30) can be identified easily in the same manner.

(iii) Finally, we can analyze the terms that are originate from the single-trace contribution. They are four of them:

(a) The first one, $I^{(2)}_{1\text{tr},1}$, is defined in Eq. (D.34) with its symmetry partners given in Eq. (D.33). The first term is proportional to

$$\begin{aligned}
&\mu^2\big[\mathbf{k}_1-\mathbf{q}_1,\mathbf{k}_2-\mathbf{q}_2\big]\Big(\mu^2\big[\mathbf{k}_3-\mathbf{q}_3,\mathbf{q}_1-\mathbf{k}_1\big]\mu^2\big[\mathbf{q}_2-\mathbf{k}_2,\mathbf{q}_3-\mathbf{k}_3\big]\\
&+\mu^2\big[\mathbf{k}_3-\mathbf{q}_3,\mathbf{q}_2-\mathbf{k}_2\big]\mu^2\big[\mathbf{q}_1-\mathbf{k}_1,\mathbf{q}_3-\mathbf{k}_3\big]\Big)\propto F\big[|(\mathbf{k}_1-\mathbf{q}_1)+(\mathbf{k}_2-\mathbf{q}_2)|R\big]\\
&\times\Big(F\big[|(\mathbf{k}_3-\mathbf{q}_3)-(\mathbf{k}_1-\mathbf{q}_1)|R\big]\,F\big[|(\mathbf{k}_2-\mathbf{q}_2)+(\mathbf{k}_3-\mathbf{q}_3)|R\big]\\
&\quad+F\big[|(\mathbf{k}_3-\mathbf{q}_3)-(\mathbf{k}_2-\mathbf{q}_2)|R\big]\,F\big[|(\mathbf{k}_1-\mathbf{q}_1)+(\mathbf{k}_3-\mathbf{q}_3)|R\big]\Big).
\end{aligned}\tag{D.54}$$

Clearly, the first term in this equation is a contribution to backward Bose enhancement of the gluons $\mathbf{k}_1-\mathbf{q}_1$ and $\mathbf{k}_2-\mathbf{q}_2$ together with contribution to forward Bose enhancement of the gluons $\mathbf{k}_1-\mathbf{q}_1$ and $\mathbf{k}_3-\mathbf{q}_3$ as well as a contribution to backward Bose enhancement of the gluons $\mathbf{k}_2-\mathbf{q}_2$ and $\mathbf{k}_3-\mathbf{q}_3$, all in the projectile wave function. The second term in Eq. (D.54) is a contribution to backward Bose enhancement of the gluons $\mathbf{k}_1-\mathbf{q}_1$ and $\mathbf{k}_2-\mathbf{q}_2$ together with a contribution to forward Bose enhancement of the gluons $\mathbf{k}_3-\mathbf{q}_3$ and $\mathbf{k}_2-\mathbf{q}_2$ as well as a contribution to backward Bose enhancement of the gluons $\mathbf{k}_1-\mathbf{q}_1$ and $\mathbf{k}_3-\mathbf{q}_3$, all in the projectile wave function. The symmetry partners of this term are given in Eq. (D.33) and, again, they can be easily identified by using the same procedure.

(b) The second term that originates from the single-trace contribution, $I^{(2)}_{1\text{tr},2}$, is defined in Eq. (D.36) with its symmetric partners given in Eq. (D.35). This term has four pieces and the first piece is proportional to

$$\begin{aligned}
&\mu^2\big[\mathbf{k}_1-\mathbf{q}_2,\mathbf{k}_2-\mathbf{q}_1\big]\Big(\frac{1}{2}\mu^2\big[\mathbf{k}_3-\mathbf{q}_3,\mathbf{q}_1-\mathbf{k}_1\big]\mu^2\big[\mathbf{q}_2-\mathbf{k}_2,\mathbf{q}_3-\mathbf{k}_3\big]\\
&+\frac{1}{2}\mu^2\big[\mathbf{k}_3-\mathbf{q}_3,\mathbf{q}_2-\mathbf{k}_2\big]\mu^2\big[\mathbf{q}_1-\mathbf{k}_1,\mathbf{q}_3-\mathbf{k}_3\big]\Big)\propto F\big[|(\mathbf{k}_1-\mathbf{q}_1)+(\mathbf{k}_2-\mathbf{q}_2)|R\big]\\
&\times\Big(\frac{1}{2}F\big[|(\mathbf{k}_3-\mathbf{q}_3)-(\mathbf{k}_1-\mathbf{q}_1)|R\big]\,F\big[|(\mathbf{k}_2-\mathbf{q}_2)+(\mathbf{k}_3-\mathbf{q}_3)|R\big]\\
&\quad+\frac{1}{2}F\big[|(\mathbf{k}_3-\mathbf{q}_3)-(\mathbf{k}_2-\mathbf{q}_2)|R\big]\,F\big[(\mathbf{k}_1-\mathbf{q}_1)+(\mathbf{k}_3-\mathbf{q}_3)\big]\Big).
\end{aligned}\tag{D.55}$$

The first term in this equation is a contribution to backward Bose enhancement of the gluons $\mathbf{k}_1-\mathbf{q}_1$ and $\mathbf{k}_2-\mathbf{q}_2$ as well as $\mathbf{k}_2-\mathbf{q}_2$ and $\mathbf{k}_3-\mathbf{q}_3$

in the projectile wave function together with a forward contribution to Bose enhancement of the gluons $\mathbf{k}_1-\mathbf{q}_1$ and $\mathbf{k}_3-\mathbf{q}_3$ in the projectile wave function. The second term in Eq. (D.55) is a contribution to backward Bose enhancement of the gluons $\mathbf{k}_1-\mathbf{q}_1$ and $\mathbf{k}_2-\mathbf{q}_2$ as well as $\mathbf{k}_1-\mathbf{q}_1$ and $\mathbf{k}_3-\mathbf{q}_3$ in the projectile wave function together with a forward contribution to Bose enhancement of the gluons $\mathbf{k}_2-\mathbf{q}_2$ and $\mathbf{k}_3-\mathbf{q}_3$ in the projectile wave function. The second piece of $I^{(2)}_{1\mathrm{tr},2}$ is proportional to

$$\begin{aligned}
&\mu^2\big[\mathbf{k}_1-\mathbf{q}_1,\mathbf{k}_3-\mathbf{q}_3\big]\left(\mu^2\big[\mathbf{k}_2-\mathbf{q}_2,\mathbf{q}_2-\mathbf{k}_1\big]\mu^2\big[\mathbf{q}_1-\mathbf{k}_2,\mathbf{q}_3-\mathbf{k}_3\big]\right.\\
&\left.+\frac{1}{2}\mu^2\big[\mathbf{k}_2-\mathbf{q}_2,\mathbf{q}_3-\mathbf{k}_3\big]\mu^2\big[\mathbf{q}_2-\mathbf{k}_1,\mathbf{q}_1-\mathbf{k}_2\big]\right)\propto F\big[|(\mathbf{k}_1-\mathbf{q}_1)+(\mathbf{k}_3-\mathbf{q}_3)|R\big]\\
&\times\left(F\big[|\mathbf{k}_1-\mathbf{k}_2|R\big]\,F\big[|(\mathbf{k}_1-\mathbf{q}_1)+(\mathbf{k}_3-\mathbf{q}_3)|R\big]\right.\\
&\left.+\,\frac{1}{2}\,F\big[|(\mathbf{k}_2-\mathbf{q}_2)-(\mathbf{k}_3-\mathbf{q}_3)|R\big]\,F\big[|(\mathbf{k}_1-\mathbf{q}_1)+(\mathbf{k}_2-\mathbf{q}_2)|R\big]\right).
\end{aligned}\tag{D.56}$$

The first term here is a contribution to backward Bose enhancement of the gluons $\mathbf{k}_1-\mathbf{q}_1$ and $\mathbf{k}_3-\mathbf{q}_3$ in the projectile wave function together with a contribution to forward HBT of the gluons $\mathbf{k}_1$ and $\mathbf{k}_2$. The second term in Eq. (D.56) is a contribution to backward Bose enhancement of the gluons $\mathbf{k}_1-\mathbf{q}_1$ and $\mathbf{k}_3-\mathbf{q}_3$ as well as the gluons $\mathbf{k}_1-\mathbf{q}_1$ and $\mathbf{k}_2-\mathbf{q}_2$ in the projectile wave function together with a contribution to forward Bose enhancement of the gluons $\mathbf{k}_2-\mathbf{q}_2$ and $\mathbf{k}_3-\mathbf{q}_3$ in the projectile wave function. The third piece of $I^{(2)}_{1\mathrm{tr},2}$ is proportional to

$$\begin{aligned}
&\mu^2\big[\mathbf{k}_1-\mathbf{q}_1,\mathbf{q}_1-\mathbf{k}_2\big]\left(\mu^2\big[\mathbf{k}_2-\mathbf{q}_2,\mathbf{k}_3-\mathbf{q}_3\big]\mu^2\big[\mathbf{q}_2-\mathbf{k}_1,\mathbf{q}_3-\mathbf{k}_3\big]\right.\\
&\left.+\,\mu^2\big[\mathbf{k}_2-\mathbf{q}_2,\mathbf{q}_3-\mathbf{k}_3\big]\mu^2\big[\mathbf{k}_3-\mathbf{q}_3,\mathbf{q}_2-\mathbf{k}_1\big]\right)\propto F\big[|\mathbf{k}_1-\mathbf{k}_2|R\big]\\
&\times\left(F^2\big[|(\mathbf{k}_2-\mathbf{q}_2)+(\mathbf{k}_3-\mathbf{q}_3)|R\big]\;+\;F^2\big[|(\mathbf{k}_2-\mathbf{q}_2)-(\mathbf{k}_3-\mathbf{q}_3)|R\big]\right).
\end{aligned}\tag{D.57}$$

Clearly, the first term this equation is a contribution to forward HBT of the gluons $\mathbf{k}_1$ and $\mathbf{k}_2$ together with a contribution to backward Bose enhancement of the gluons $\mathbf{k}_2-\mathbf{q}_2$ and $\mathbf{k}_3-\mathbf{q}_3$ in the projectile wave function, while the second term is a contribution to forward HBT of the gluons $\mathbf{k}_1$ and $\mathbf{k}_2$ together with a contribution to forward Bose enhancement of the gluons $\mathbf{k}_2-\mathbf{q}_2$ and $\mathbf{k}_3-\mathbf{q}_3$ in the projectile wave function. The last piece of the $I^{(2)}_{1\mathrm{tr},2}$ is proportional to

$$\begin{aligned}
&\mu^2\big[\mathbf{k}_1-\mathbf{q}_1,\mathbf{q}_3-\mathbf{k}_3\big]\left(\frac{1}{2}\mu^2\big[\mathbf{k}_2-\mathbf{q}_2,\mathbf{k}_3-\mathbf{q}_3\big]\mu^2\big[\mathbf{q}_2-\mathbf{k}_1,\mathbf{q}_1-\mathbf{k}_2\big]\right.\\
&\left.+\,\mu^2\big[\mathbf{k}_2-\mathbf{q}_2,\mathbf{q}_2-\mathbf{k}_1\big]\mu^2\big[\mathbf{k}_3-\mathbf{q}_3,\mathbf{q}_1-\mathbf{k}_2\big]\right)\propto F\big[|(\mathbf{k}_1-\mathbf{q}_1)-(\mathbf{k}_3-\mathbf{q}_3)|R\big]
\end{aligned}$$

$$\left(\frac{1}{2}\,F\big[|(\mathbf{k}_2-\mathbf{q}_2)+(\mathbf{k}_3-\mathbf{q}_3)|R\big]\,F\big[|(\mathbf{k}_1-\mathbf{q}_1)+(\mathbf{k}_2-\mathbf{q}_2)|R\big]\right.$$
$$\left.+\;F\big[|\mathbf{k}_1-\mathbf{k}_2|R\big]\,F\big[|(\mathbf{k}_1-\mathbf{q}_1)-(\mathbf{k}_3-\mathbf{q}_3)|R\big]\right). \tag{D.58}$$

The first term in this equation is a contribution to the forward Bose enhancement of the gluons $\mathbf{k}_1-\mathbf{q}_1$ and $\mathbf{k}_3-\mathbf{q}_3$ together with a contribution to the backward Bose enhancement of the gluons $\mathbf{k}_2-\mathbf{q}_2$ and $\mathbf{k}_3-\mathbf{q}_3$ as well as the gluons $\mathbf{k}_1-\mathbf{q}_1$ and $\mathbf{k}_2-\mathbf{q}_2$ in the projectile wave function. The second term in Eq. (D.58) is a contribution to forward Bose enhancement of the gluons $\mathbf{k}_1-\mathbf{q}_1$ and $\mathbf{k}_3-\mathbf{q}_3$ in the projectile wave function together with a contribution to forward HBT of the gluons $\mathbf{k}_1$ and $\mathbf{k}_2$. The identification of the symmetry partners of $I^{(2)}_{1\mathrm{tr},2}$ can be performed in a straight forward way by adopting the same procedure.

(c) The third term that originates from the single-trace contribution, $I^{(2)}_{1\mathrm{tr},3}$ is defined in Eq. (D.38) and its symmetry partners are given in Eq. (D.37). This term has also four pieces and the first one is proportional to

$$\left\{\mu^2\big[\mathbf{k}_1-\mathbf{q}_1,\mathbf{k}_2+\mathbf{q}_1\big]\left(\mu^2\big[\mathbf{k}_3+\mathbf{q}_2,-\mathbf{q}_2-\mathbf{k}_1\big]\mu^2\big[-\mathbf{q}_3-\mathbf{k}_2,\mathbf{q}_3-\mathbf{k}_3\big]\right.\right.$$
$$\left.+\frac{1}{2}\mu^2\big[\mathbf{k}_3+\mathbf{q}_2,-\mathbf{q}_3-\mathbf{k}_2\big]\mu^2\big[-\mathbf{q}_2-\mathbf{k}_1,\mathbf{q}_3-\mathbf{k}_3\big]\right)$$
$$\left.+\frac{1}{4}\mu^2\big[\mathbf{k}_1-\mathbf{q}_1,\mathbf{q}_3-\mathbf{k}_3\big]\mu^2\big[\mathbf{k}_2+\mathbf{q}_1,-\mathbf{q}_2-\mathbf{k}_1\big]\mu^2\big[\mathbf{k}_3+\mathbf{q}_2,-\mathbf{q}_3-\mathbf{k}_2\big]\right\}$$
$$\propto\left\{F\big[|\mathbf{k}_1+\mathbf{k}_2|R\big]\left(F\big[|\mathbf{k}_1-\mathbf{k}_3|R\big]\,F\big[|\mathbf{k}_2+\mathbf{k}_3|R\big]+\frac{1}{2}\,F^2\big[|(\mathbf{k}_3-\mathbf{q}_3)-(\mathbf{k}_2-\mathbf{q}_2)|R\big]\right)\right.$$
$$+\frac{1}{4}\,F\big[|(\mathbf{k}_1-\mathbf{q}_1)-(\mathbf{k}_3-\mathbf{q}_3)|R\big]\,F\big[|(\mathbf{k}_1-\mathbf{q}_1)-(\mathbf{k}_2-\mathbf{q}_2)|R\big]$$
$$\left.\times\,F\big[|(\mathbf{k}_2-\mathbf{q}_2)-(\mathbf{k}_3-\mathbf{q}_3)|R\big]\right\}. \tag{D.59}$$

The first term in this equation is a contribution to the backward HBT of the gluons $\mathbf{k}_1$ and $\mathbf{k}_2$ as well as the gluons $\mathbf{k}_2$ and $\mathbf{k}_3$ together with a contribution to forward HBT of the gluons $\mathbf{k}_1$ and $\mathbf{k}_3$. The second term in Eq. (D.59) is a contribution to backward HBT of the gluons $\mathbf{k}_1$ and $\mathbf{k}_2$ together with a contribution to forward Bose enhancement of the gluons $\mathbf{k}_2-\mathbf{q}_2$ and $\mathbf{k}_3-\mathbf{q}_3$ in the projectile wave function. The third term is a contribution to forward Bose enhancement of the all three gluons $\mathbf{k}_1-\mathbf{q}_1$, $\mathbf{k}_2-\mathbf{q}_2$ and $\mathbf{k}_3-\mathbf{q}_3$ in the projectile wave function. The second piece of $I^{(2)}_{1\mathrm{tr},3}$ is proportional to

$$\left(\mu^2\big[\mathbf{k}_1-\mathbf{q}_1,\mathbf{k}_3-\mathbf{q}_3\big]\,\mu^2\big[\mathbf{k}_2+\mathbf{q}_1,\mathbf{q}_3-\mathbf{k}_1\big]\,\mu^2\big[\mathbf{q}_2-\mathbf{k}_2,-\mathbf{k}_3-\mathbf{q}_2\big]\right.$$
$$\left.+\;\mu^2\big[\mathbf{k}_1-\mathbf{q}_1,\mathbf{q}_2-\mathbf{k}_2\big]\,\mu^2\big[\mathbf{k}_2+\mathbf{q}_1,-\mathbf{k}_3-\mathbf{q}_2\big]\,\mu^2\big[\mathbf{k}_3-\mathbf{q}_3,\mathbf{q}_3-\mathbf{k}_1\big]\right)$$

$$\propto \Big(F\big[|\mathbf{k}_2+\mathbf{k}_3|R\big]\, F^2\big[|(\mathbf{k}_1-\mathbf{q}_1)+(\mathbf{k}_3-\mathbf{q}_3)|R\big] + F\big[|\mathbf{k}_1-\mathbf{k}_3|R\big]\, F^2\big[|(\mathbf{k}_1-\mathbf{q}_1)-(\mathbf{k}_2-\mathbf{q}_2)|R\big] \Big). \tag{D.60}$$

The first term here is a contribution to backward HBT of the gluons $\mathbf{k}_2$ and $\mathbf{k}_3$ together with a contribution to backward Bose enhancement of the gluons $\mathbf{k}_1-\mathbf{q}_1$ and $\mathbf{k}_3-\mathbf{q}_3$ in the projectile wave function. The second term in this equation is a contribution to forward HBT of the gluons $\mathbf{k}_1$ and $\mathbf{k}_3$ together with a contribution to forward Bose enhancement of the gluons $\mathbf{k}_1-\mathbf{q}_1$ and $\mathbf{k}_2-\mathbf{q}_2$ in the projectile wave function. The third piece of $I^{(2)}_{1\mathrm{tr},3}$ is proportional to

$$\begin{aligned}&\mu^2\big[\mathbf{k}_1-\mathbf{q}_3,\mathbf{k}_3-\mathbf{q}_1\big]\,\mu^2\big[\mathbf{k}_2+\mathbf{q}_3,-\mathbf{k}_3-\mathbf{q}_2\big]\,\mu^2\big[\mathbf{q}_1-\mathbf{k}_1,\mathbf{q}_2-\mathbf{k}_2\big]\\ &\propto F\big[|(\mathbf{k}_1-\mathbf{q}_1)+(\mathbf{k}_3-\mathbf{q}_3)|R\big]\, F\big[|(\mathbf{k}_2-\mathbf{q}_2)-(\mathbf{k}_3-\mathbf{q}_3)|R\big]\\ &\qquad\times F\big[|(\mathbf{k}_1-\mathbf{q}_1)+(\mathbf{k}_2-\mathbf{q}_2)|R\big].\end{aligned} \tag{D.61}$$

This term is a contribution to backward Bose enhancement of the gluons $\mathbf{k}_1-\mathbf{q}_1$ and $\mathbf{k}_3-\mathbf{q}_3$ as well as the gluons $\mathbf{k}_1-\mathbf{q}_1$ and $\mathbf{k}_2-\mathbf{q}_2$ in the projectile wave function together with a contribution to forward Bose enhancement of the gluons $\mathbf{k}_2-\mathbf{q}_2$ and $\mathbf{k}_3-\mathbf{q}_3$ in the projectile wave function. The last piece of $I^{(2)}_{1\mathrm{tr},3}$ is proportional to

$$\begin{aligned}&\mu^2\big[\mathbf{k}_1+\mathbf{q}_2,-\mathbf{q}_1-\mathbf{k}_2\big]\,\mu^2\big[\mathbf{k}_2-\mathbf{q}_2,\mathbf{k}_3-\mathbf{q}_3\big]\,\mu^2\big[\mathbf{q}_3-\mathbf{k}_1,\mathbf{q}_1-\mathbf{k}_3\big]\\ &\propto F\big[|(\mathbf{k}_1-\mathbf{q}_1)-(\mathbf{k}_2-\mathbf{q}_2)|R\big]\, F\big[|(\mathbf{k}_2-\mathbf{q}_2)+(\mathbf{k}_3-\mathbf{q}_3)|R\big]\\ &\qquad\times F\big[|(\mathbf{k}_1-\mathbf{q}_1)+(\mathbf{k}_3-\mathbf{q}_3)|R\big].\end{aligned} \tag{D.62}$$

This term is a contribution to the backward Bose enhancement of the gluons $\mathbf{k}_1-\mathbf{q}_1$ and $\mathbf{k}_3-\mathbf{q}_3$ as well as the gluons $\mathbf{k}_2-\mathbf{q}_2$ and $\mathbf{k}_3-\mathbf{q}_3$ in the projectile wave function together with a contribution to the forward Bose enhancement of the gluons $\mathbf{k}_1-\mathbf{q}_1$ and $\mathbf{k}_2-\mathbf{q}_2$ in the projectile wave function. The symmetry partners of $I^{(2)}_{1\mathrm{tr},3}$ can be identified in a similar manner.

(d) The last term that originates from the single-trace contribution, $I^{(2)}_{1\mathrm{tr},4}$, is defined in Eq. (D.40) with its symmetry partners given in Eq. (D.39). This term has four pieces and the first one is proportional to

$$\begin{aligned}&\Big\{\mu^2\big[\mathbf{k}_1-\mathbf{q}_1,\mathbf{q}_1-\mathbf{k}_2\big]\Big(\frac{1}{2}\mu^2\big[\mathbf{k}_2-\mathbf{q}_3,\mathbf{k}_3-\mathbf{q}_2\big]\mu^2\big[\mathbf{q}_2-\mathbf{k}_1,\mathbf{q}_3-\mathbf{k}_3\big]\\ &\qquad+\mu^2\big[\mathbf{k}_2-\mathbf{q}_3,\mathbf{q}_3-\mathbf{k}_3\big]\mu^2\big[\mathbf{k}_3-\mathbf{q}_2,\mathbf{q}_2-\mathbf{k}_1\big]\Big)\\ &\quad+\frac{1}{4}\mu^2\big[\mathbf{k}_1-\mathbf{q}_1,\mathbf{q}_3-\mathbf{k}_3\big]\mu^2\big[\mathbf{k}_2-\mathbf{q}_3,\mathbf{k}_3-\mathbf{q}_2\big]\mu^2\big[\mathbf{q}_2-\mathbf{k}_1,\mathbf{q}_1-\mathbf{k}_2\big]\Big\}\\ &\propto\Big\{F\big[|\mathbf{k}_1-\mathbf{k}_2|R\big]\Big(\frac{1}{2}F^2\big[|(\mathbf{k}_2-\mathbf{q}_2)+(\mathbf{k}_3-\mathbf{q}_3)|R\big]+F\big[|\mathbf{k}_2-\mathbf{k}_3|R\big]\,F\big[|\mathbf{k}_1-\mathbf{k}_3|R\big]\Big)\\ &+\frac{1}{4}F\big[|(\mathbf{k}_1-\mathbf{q}_1)-(\mathbf{k}_3-\mathbf{q}_3)|R\big]\,F\big[|(\mathbf{k}_2-\mathbf{q}_2)+(\mathbf{k}_3-\mathbf{q}_3)|R\big]\end{aligned}$$

$$\times F\big[|(\mathbf{k}_1-\mathbf{q}_1)+(\mathbf{k}_2-\mathbf{q}_2)|R\big]\Big\}. \tag{D.63}$$

The first term in this equation is a contribution to the forward HBT of the gluons $\mathbf{k}_1$ and $\mathbf{k}_2$ together with a contribution to the backward Bose enhancement of the gluons $\mathbf{k}_2-\mathbf{q}_2$ and $\mathbf{k}_3-\mathbf{q}_3$ in the projectile wave function. The second term in Eq. (D.63) is a contribution to forward HBT of the three gluons $\mathbf{k}_1$, $\mathbf{k}_2$ and $\mathbf{k}_3$. The last term is a contribution the backward Bose enhancement of the gluons $\mathbf{k}_1-\mathbf{q}_1$ and $\mathbf{k}_2-\mathbf{q}_2$ as well as the gluons $\mathbf{k}_2-\mathbf{q}_2$ and $\mathbf{k}_3-\mathbf{q}_3$ together with a contribution to the forward Bose enhancement of the gluons $\mathbf{k}_1-\mathbf{q}_1$ and $\mathbf{k}_3-\mathbf{q}_3$ in the projectile wave function. The second piece of $I^{(2)}_{1\mathrm{tr},4}$ is proportional to

$$\begin{aligned}
&\Big(\mu^2\big[\mathbf{k}_1-\mathbf{q}_1,\mathbf{k}_2-\mathbf{q}_2\big]\mu^2\big[\mathbf{k}_3-\mathbf{q}_3,\mathbf{q}_3-\mathbf{k}_1\big]\mu^2\big[\mathbf{q}_1-\mathbf{k}_2,\mathbf{q}_2-\mathbf{k}_3\big]\\
&\quad+\mu^2\big[\mathbf{k}_1-\mathbf{q}_1,\mathbf{k}_3-\mathbf{q}_3\big]\mu^2\big[\mathbf{k}_2-\mathbf{q}_2,\mathbf{q}_2-\mathbf{k}_3\big]\mu^2\big[\mathbf{q}_3-\mathbf{k}_1,\mathbf{q}_1-\mathbf{k}_2\big]\Big)\\
&\propto\Big(F^2\big[|(\mathbf{k}_1-\mathbf{q}_1)+(\mathbf{k}_2-\mathbf{q}_2)|R\big]\,F\big[|\mathbf{k}_1-\mathbf{k}_3|R\big]\\
&\qquad+\;F^2\big[|(\mathbf{k}_1-\mathbf{q}_1)+(\mathbf{k}_3-\mathbf{q}_3)|R\big]\,F\big[|\mathbf{k}_2-\mathbf{k}_3|R\big]\Big).
\end{aligned} \tag{D.64}$$

The first term in this equation is a contribution to the forward HBT of the gluons $\mathbf{k}_1$ and $\mathbf{k}_3$ together with a contribution to the backward Bose enhancement of the gluons $\mathbf{k}_1-\mathbf{q}_1$ and $\mathbf{k}_2-\mathbf{q}_2$ in the projectile wave function. The second term in Eq. (D.64) is a contribution to the forward HBT of the gluons $\mathbf{k}_1$ and $\mathbf{k}_2$ together with a contribution to the backward Bose enhancement of the gluons $\mathbf{k}_1-\mathbf{q}_1$ and $\mathbf{k}_3-\mathbf{q}_3$ in the projectile wave function. The third piece of $I^{(2)}_{1\mathrm{tr},4}$ is proportional to

$$\begin{aligned}
&\mu^2\big[\mathbf{k}_1-\mathbf{q}_2,\mathbf{k}_2-\mathbf{q}_1\big]\mu^2\big[\mathbf{k}_3-\mathbf{q}_3,\mathbf{q}_2-\mathbf{k}_2\big]\mu^2\big[\mathbf{q}_3-\mathbf{k}_1,\mathbf{q}_1-\mathbf{k}_3\big]\\
&\propto F\big[|(\mathbf{k}_1-\mathbf{q}_1)+(\mathbf{k}_2-\mathbf{q}_2)|R\big]\,F\big[|(\mathbf{k}_3-\mathbf{q}_3)-(\mathbf{k}_2-\mathbf{q}_2)|R\big]\\
&\qquad\times F\big[|(\mathbf{k}_3-\mathbf{q}_3)+(\mathbf{k}_1-\mathbf{q}_1)|R\big].
\end{aligned} \tag{D.65}$$

This term is a contribution to the backward Bose enhancement of the gluons $\mathbf{k}_1-\mathbf{q}_1$ and $\mathbf{k}_2-\mathbf{q}_2$ as well as the gluons $\mathbf{k}_1-\mathbf{q}_1$ and $\mathbf{k}_3-\mathbf{q}_3$ together with a contribution to forward Bose enhancement of the gluons $\mathbf{k}_2-\mathbf{q}_2$ and $\mathbf{k}_3-\mathbf{q}_3$ in the projectile wave function. The last piece of $I^{(2)}_{1\mathrm{tr},4}$ is proportional to

$$\begin{aligned}
&\mu^2\big[\mathbf{k}_1-\mathbf{q}_3,\mathbf{k}_3-\mathbf{q}_1\big]\mu^2\big[\mathbf{k}_2-\mathbf{q}_2,\mathbf{q}_1-\mathbf{k}_1\big]\mu^2\big[\mathbf{q}_3-\mathbf{k}_2,\mathbf{q}_2-\mathbf{k}_3\big]\\
&\propto F\big[|(\mathbf{k}_1-\mathbf{q}_1)+(\mathbf{k}_3-\mathbf{q}_3)|R\big]\,F\big[|(\mathbf{k}_1-\mathbf{q}_1)-(\mathbf{k}_2-\mathbf{q}_2)|R\big]\\
&\qquad\times F\big[|(\mathbf{k}_2-\mathbf{q}_2)+(\mathbf{k}_3-\mathbf{q}_3)|R\big].
\end{aligned} \tag{D.66}$$

This term is a contribution to the backward Bose enhancement of the gluons $\mathbf{k}_1-\mathbf{q}_1$ and $\mathbf{k}_3-\mathbf{q}_3$ as well as the gluons $\mathbf{k}_2-\mathbf{q}_2$ and $\mathbf{k}_3-\mathbf{q}_3$ together with a contribution to the forward Bose enhancement of the gluons $\mathbf{k}_1-\mathbf{q}_1$ and $\mathbf{k}_2-\mathbf{q}_2$. The symmetry partners to $I^{(2)}_{1\mathrm{tr},4}$ can be identified in a similar way.

USC
UNIVERSIDADE
DE SANTIAGO
DE COMPOSTELA

Appendix E

Harmonic oscillator path integrals

In this section we will solve the path integrals that appear in Chapter 6. Before starting our discussion we define the following matrix:

$$[F_N(x)]_{ij} = \begin{cases} x & \text{if } i = j \\ -1 & \text{if } |i-j| = 1 \\ 0 & \text{otherwise} \end{cases}, \tag{E.1}$$

being x a positive real scalar and $i, j = 1, \cdots N$. Therefore F_N is a $N \times N$ tridiagonal matrix with x in the main diagonal and -1 in the neighbor diagonals. Since this matrix will be a key ingredient in the calculation of this section we will study some its properties.

By performing the Laplace expansion of this matrix it is easy to see that it follows the following recursive equation:

$$\det F_N(x) = x \det F_{N-1}(x) - \det F_{N-2}(x). \tag{E.2}$$

The solution of this equation is

$$\det F_N(x) = \frac{2^{-(N+1)}}{\sqrt{x^2-4}} \left(x_+^{N+1} - x_-^{N+1}\right), \tag{E.3}$$

where $x_\pm = x \pm \sqrt{x^2-4}$.

The inverse of $F_N(x)$ can be computed by using the expression of the inverse of a block matrix

$$\begin{aligned} \begin{pmatrix} \mathbf{A} & \mathbf{B} \\ \mathbf{C} & \mathbf{D} \end{pmatrix}^{-1} &= \begin{pmatrix} \left(\mathbf{A}-\mathbf{B}\mathbf{D}^{-1}\mathbf{C}\right)^{-1} & -\left(\mathbf{A}-\mathbf{B}\mathbf{D}^{-1}\mathbf{C}\right)^{-1}\mathbf{B}\mathbf{D}^{-1} \\ -\mathbf{D}^{-1}\mathbf{C}\left(\mathbf{A}-\mathbf{B}\mathbf{D}^{-1}\mathbf{C}\right)^{-1} & \mathbf{D}^{-1}+\mathbf{D}^{-1}\mathbf{C}\left(\mathbf{A}-\mathbf{B}\mathbf{D}^{-1}\mathbf{C}\right)^{-1}\mathbf{B}\mathbf{D}^{-1} \end{pmatrix} \\ &= \begin{pmatrix} \mathbf{A}^{-1}+\mathbf{A}^{-1}\mathbf{B}\left(\mathbf{D}-\mathbf{C}\mathbf{A}^{-1}\mathbf{B}\right)^{-1}\mathbf{C}\mathbf{A}^{-1} & -\mathbf{A}^{-1}\mathbf{B}\left(\mathbf{D}-\mathbf{C}\mathbf{A}^{-1}\mathbf{B}\right)^{-1} \\ -\left(\mathbf{D}-\mathbf{C}\mathbf{A}^{-1}\mathbf{B}\right)^{-1}\mathbf{C}\mathbf{A}^{-1} & \left(\mathbf{D}-\mathbf{C}\mathbf{A}^{-1}\mathbf{B}\right)^{-1} \end{pmatrix}. \end{aligned} \tag{E.4}$$

Noting that $F_N(x)$ can be written as a block matrix with $\mathbf{A} = x$, $\mathbf{D} = F_{N-1}(x)$, $\mathbf{C}_i = -\delta_{i,2}$ and $\mathbf{B}_j = -\delta_{j,2}$, we can compute the inverse of its component $(1,1)$ by using the first equality of Eq. (E.4)

$$[F_N^{-1}(x)]_{1,1} = \left(x - [F_{N-1}^{-1}(x)]_{1,1}\right)^{-1}. \tag{E.5}$$

Analogously, we could use the second equality of Eq. (E.4) with $\mathbf{A} = F_{N-1}(x)$, $\mathbf{D} = x$, $\mathbf{C}_j = -\delta_{j,N-1}$ and $\mathbf{B}_i = -\delta_{i,N-1}$ to obtain the same recursive equation for $[F_N(x)^{-1}]_{N,N}$. Solving Eq. (E.5) we obtain

$$[F_N^{-1}(x)]_{1,1} = [F_N^{-1}(x)]_{N,N} = \frac{2^{-N}}{\sqrt{x^2-4}\det F_N(x)}\left(x_+^N - x_-^N\right). \tag{E.6}$$

Inspecting Eq. (E.4), we realize that the rest of the components of $F_N^{-1}(x)$ can be computed just as a function of its $(1,1)$ and (N,N) components. In this manuscript we will only need the $(1,N)$ and $(N,1)$ components of this matrix that can be written as

$$[F_N^{-1}(x)]_{1,N} = [F_N^{-1}(x)]_{N,1} = \frac{1}{\det F_N(x)}. \tag{E.7}$$

We now proceed to solve the path integrals. The first path integral that we encounter in Chapter 6 is the one of a single harmonic oscillator of mass m and coupling κ

$$\int_{\mathbf{y}}^{\mathbf{x}} [\mathcal{D}\mathbf{z}] \exp\left\{\int_{y^+}^{x^+} dz^+ \left[m\dot{\mathbf{z}}^2 - \kappa \mathbf{z}^2\right]\right\}, \tag{E.8}$$

where in Eq. (6.17) $m = \frac{ik^+}{2}$ and $\kappa = \frac{Q_s^2}{4L^+}$. By discretizing the longitudinal axis into N slices we can write this equation as

$$\begin{aligned}
&\lim_{N\to\infty} \int \left(\prod_{n=1}^{N-1} d^2\mathbf{z}_n\right) \left(\frac{-mN}{\pi\Delta^+}\right)^N \exp\left\{\sum_{n=1}^{N}\left[\frac{mN}{\Delta^+}(\mathbf{z}_n - \mathbf{z}_{n-1})^2 - \frac{\kappa\Delta^+}{N}\mathbf{z}_n^2\right]\right\} \\
&= \lim_{N\to\infty} \int \left(\prod_{n=1}^{N-1} d^2\mathbf{z}_n\right) \left(\frac{a}{2\pi}\right)^N \exp\left\{\sum_{n=1}^{N}\left[-\frac{a}{2}(\mathbf{z}_n - \mathbf{z}_{n-1})^2 - b\mathbf{z}_n^2\right]\right\},
\end{aligned} \tag{E.9}$$

where we have defined $\Delta^+ = x^+ - y^+$ and

$$a = -\frac{2mN}{\Delta^+}, \qquad b = \frac{\kappa\Delta^+}{N}. \tag{E.10}$$

In order to solve this integral it is convenient to write it in a matrix form. In order to do so we define the vector $\vec{x} = (\mathbf{z}_1, \ldots, \mathbf{z}_{N-1})$ and we can make the following simplifications:

$$\sum_{n=1}^{N}(\mathbf{z}_n - \mathbf{z}_{n-1})^2 = \mathbf{z}_0^2 + \mathbf{z}_N^2 - 2\mathbf{z}_0\cdot\mathbf{z}_1 - 2\mathbf{z}_{N-1}\cdot\mathbf{z}_N + \vec{x}^T F_{N-1}(2)\vec{x}, \tag{E.11}$$

and

$$\sum_{n=1}^{N}\mathbf{z}_n^2 = \mathbf{z}_N^2 + \vec{x}^T\mathbb{I}\vec{x}, \tag{E.12}$$

where the matrix $F_N(x)$ is defined in Eq. (E.1).

Thus, by introducing the vector $\vec{x}$, we can write Eq. (E.9) as a multidimensional Gaussian integral

$$\lim_{N\to\infty}\int d^{2(N-1)}\vec{x}\left(\frac{a}{2\pi}\right)^N \exp\left\{-\frac{a}{2}(\mathbf{z}_0^2 + \mathbf{z}_N^2) - \frac{a}{2}\vec{x}^T F_{N-1}\left(2 + \frac{2b}{a}\right)\vec{x} + \vec{J}\cdot\vec{x}\right\} \tag{E.13}$$

where we have defined the "current" vector

$$J^i = a\mathbf{z}_0\delta^{1,i} + a\mathbf{z}_N\delta^{N-1,i}. \tag{E.14}$$

Since the solution of a multi-dimensional Gaussian integral is

$$\int d^D x \exp\left\{-\frac{a}{2}x^T M x + B\cdot x\right\} = \frac{(2\pi)^{D/2}}{\det M}\exp\left\{\frac{1}{2}B^T M^{-1}B\right\}, \tag{E.15}$$

where M is a constant matrix $D\times D$ and B is a constant D-dimensional vector., we can write Eq. (E.13) as

$$\lim_{N\to\infty}\left(\frac{a}{2\pi}\right)^N \frac{(2\pi)^{N-1}}{a^{N-1}\det F_{N-1}\left(2+\frac{2b}{a}\right)}\exp\left\{-\frac{a}{2}(\mathbf{z}_0^2+\mathbf{z}_N^2)+\frac{1}{2a}\vec{J}^T F_{N-1}^{-1}\left(2+\frac{2b}{a}\right)\vec{J}\right\}. \tag{E.16}$$

Using Eq. (E.3) and taking the $N\to\infty$ limit we obtain that

$$\lim_{N\to\infty}\left(\frac{a}{2\pi}\right)^N \frac{(2\pi)^{N-1}}{a^{N-1}\det F_{N-1}\left(2+\frac{2b}{a}\right)} = \frac{-m\omega}{\pi}\frac{1}{\sin\omega\Delta^+}, \tag{E.17}$$

where we define

$$\omega^2 = -\frac{2b}{a}\frac{N^2}{(\Delta^+)^2} = \frac{\kappa}{m} \tag{E.18}$$

and we have used the fact that

$$\lim_{N\to\infty}\frac{N}{\det F_{N-1}\left(2-\frac{x^2}{N^2}\right)} = \frac{x}{\sin x}. \tag{E.19}$$

On the other hand, using Eqs. (E.6) and (E.7) and taking the $N\to\infty$ limit we have that

$$\begin{aligned}
&\lim_{N\to\infty}\left[-\frac{a}{2}(\mathbf{z}_0^2+\mathbf{z}_N^2)+\frac{1}{2a}\vec{J}^T F_{N-1}^{-1}\left(2+\frac{2b}{a}\right)\vec{J}\right]\\
&=\lim_{N\to\infty}\left[-\frac{a}{2}(\mathbf{z}_0^2+\mathbf{z}_N^2)\left(1-\left[F_{N-1}^{-1}\left(2+\frac{2b}{a}\right)\right]_{1,1}\right)+a\mathbf{z}_0\mathbf{z}_N\left[F_{N-1}^{-1}\left(2+\frac{2b}{a}\right)\right]_{1,N-1}\right]\\
&=m\omega\left[\frac{\mathbf{z}_0^2+\mathbf{z}_N^2}{\tan\omega\Delta^+}-2\frac{\mathbf{z}_0\mathbf{z}_N}{\sin\omega\Delta^+}\right],
\end{aligned} \tag{E.20}$$

where we have used that

$$\lim_{N\to\infty} N\left(1-\left[F_{N-1}\left(2-\frac{x^2}{N^2}\right)\right]_{1,1}\right) = \frac{x}{\tan x}. \tag{E.21}$$

Therefore we obtain the well known solution of the harmonic oscillator path integral

$$\int_{\mathbf{y}}^{\mathbf{x}}[\mathcal{D}\mathbf{z}]\exp\left\{\int_{y^+}^{x^+}dz^+\left[m\dot{\mathbf{z}}^2-\kappa\mathbf{z}^2\right]\right\}$$

$$= \frac{-m\omega}{\pi}\frac{1}{\sin\omega\Delta^+}\exp\left\{m\omega\left[\frac{\mathbf{z}_0^2+\mathbf{z}_N^2}{\tan\omega\Delta^+}-2\frac{\mathbf{z}_0\mathbf{z}_N}{\sin\omega\Delta^+}\right]\right\}. \tag{E.22}$$

The second path integral that appears in Chapter 6 is the one analogous to the 2 coupled harmonic oscillators of masses m_1 and $-m_2$ and coupling κ:

$$\int_{\mathbf{y}}^{\mathbf{x}}[\mathcal{D}\mathbf{z}_1][\mathcal{D}\mathbf{z}_2]\exp\left\{\int_{y^+}^{x^+}dz^+\left[m_1\dot{\mathbf{z}}_1^2-m_2\dot{\mathbf{z}}_2^2-\kappa(\mathbf{z}_1-\mathbf{z}_2)^2\right]\right\}. \tag{E.23}$$

In order to solve this integral it is convenient to make the change of variables

$$\mathbf{B}=\frac{m_1\mathbf{z}_1+m_2\mathbf{z}_2}{m_1+m_2},\qquad \mathbf{R}=\mathbf{z}_1-\mathbf{z}_2, \tag{E.24}$$

in such a way that the integral can be rewritten as

$$\int_{\mathbf{y}}^{\mathbf{x}}[\mathcal{D}\mathbf{B}][\mathcal{D}\mathbf{R}]\exp\left\{\int_{y^+}^{x^+}dz^+\left[\Delta m\dot{\mathbf{B}}^2-\frac{\Delta m\mu}{M}\dot{\mathbf{R}}^2+4\mu\dot{\mathbf{B}}\cdot\dot{\mathbf{R}}-\kappa\mathbf{R}^2\right]\right\} \tag{E.25}$$

where we have introduced

$$\Delta m=m_1-m_2,\quad \mu=\frac{m_1m_2}{m_1+m_2}\quad\text{and}\quad M=m_1+m_2. \tag{E.26}$$

In the discrete limit we can write the path integral as

$$\lim_{N\to\infty}\int\left(\prod_{n=1}^{N-1}d^2\mathbf{r}_nd^2\mathbf{b}_n\right)\left(\frac{-m_1N}{\pi\Delta^+}\right)^N\left(\frac{m_2N}{\pi\Delta^+}\right)^N$$
$$\times\exp\left\{\sum_{n=1}^{N}\left[-\frac{a_1}{2}(\mathbf{r}_n-\mathbf{r}_{n-1})^2-\frac{a_2}{2}(\mathbf{b}_n-\mathbf{b}_{n-1})^2-\frac{a_3}{2}(\mathbf{r}_n-\mathbf{r}_{n-1})\cdot(\mathbf{b}_n-\mathbf{b}_{n-1})-b\mathbf{r}_n^2\right]\right\}, \tag{E.27}$$

with

$$a_1=\frac{2\Delta m\mu N}{M\Delta^+},\quad a_2=-\frac{2\Delta mN}{\Delta^+}\quad\text{and}\quad a_3=-\frac{8\mu N}{\Delta^+}. \tag{E.28}$$

The next step is to write, again, the path integral in a matrix form, i.e. as a multi-dimensional Gaussian integral. We therefore define $\vec{x}_{\mathbf{r}}=(\mathbf{r}_1,\ldots,\mathbf{r}_{N-1})$ and $\vec{x}_{\mathbf{b}}=(\mathbf{b}_1,\ldots,\mathbf{b}_{N-1})$ in order to make the following simplification:

$$\begin{aligned}
&\sum_{n=1}^{N}\left[-\frac{a_1}{2}(\mathbf{r}_n-\mathbf{r}_{n-1})^2-\frac{a_2}{2}(\mathbf{b}_n-\mathbf{b}_{n-1})^2-\frac{a_3}{2}(\mathbf{r}_n-\mathbf{r}_{n-1})(\mathbf{b}_n-\mathbf{b}_{n-1})-b\mathbf{r}_n^2\right]\\
&=-\frac{a_1}{2}\vec{x}_{\mathbf{r}}^T\left(F_{N-1}(2)+\frac{2b}{a_1}\mathbb{I}\right)\vec{x}_{\mathbf{r}}-\frac{a_2}{2}\mathbf{x}_b^TF_{N-1}(2)\vec{x}_{\mathbf{b}}\\
&\qquad\qquad-\frac{a_3}{2}\left(\frac{1}{2}\vec{x}_{\mathbf{r}}^TF_{N-1}(2)\vec{x}_{\mathbf{b}}+\frac{1}{2}\vec{x}_{\mathbf{b}}^TF_{N-1}(2)\vec{x}_{\mathbf{r}}\right)\\
&-\frac{a_1}{2}\left[\mathbf{r}_0^2+\mathbf{r}_N^2-2\mathbf{r}_0\mathbf{r}_1-2\mathbf{r}_{N-1}\mathbf{r}_N\right]-\frac{a_2}{2}\left[\mathbf{b}_0^2+\mathbf{b}_N^2-2\mathbf{b}_0\mathbf{b}_1-2\mathbf{b}_{N-1}\mathbf{b}_N\right]
\end{aligned}$$

$$-\frac{a_3}{2}\left[\mathbf{r}_0\mathbf{b}_0+\mathbf{r}_N\mathbf{b}_N-\mathbf{r}_0\mathbf{b}_1-\mathbf{r}_1\mathbf{b}_0-\mathbf{r}_{N-1}\mathbf{b}_N-\mathbf{b}_{N-1}\mathbf{r}_N\right]-b\mathbf{r}_N^2 \tag{E.29}$$

Therefore the path integral can be simplified further by defining the matrix

$$\mathcal{A}_{2(N-1)}=\begin{pmatrix} a_1F_{N-1}\left(2+\frac{2b}{a_1}\right) & \frac{a_3}{2}F_{N-1}(2) \\ \frac{a_3}{2}F_{N-1}(2) & a_2F_{N-1}(2)\end{pmatrix}, \tag{E.30}$$

the current

$$\begin{aligned} J^i=&\left(a_1\mathbf{r}_0+\frac{a_3}{2}\mathbf{b}_0\right)\delta^{i,1}+\left(a_1\mathbf{r}_N+\frac{a_3}{2}\mathbf{b}_N\right)\delta^{i,N-1}\\ &+\left(a_2\mathbf{b}_0+\frac{a_3}{2}\mathbf{r}_0\right)\delta^{i,N}+\left(a_2\mathbf{b}_N+\frac{a_3}{2}\mathbf{r}_N\right)\delta^{i,2(N-1)}, \end{aligned} \tag{E.31}$$

and $\vec{x}=(\mathbf{r}_1,\ldots,\mathbf{r}_N,\mathbf{b}_0,\ldots,\mathbf{b}_N)$. Thus we can write it as

$$\begin{aligned} &\lim_{N\to\infty}\int d^{4(N-1)}\vec{x}\left(\frac{-m_1N}{\pi\Delta^+}\right)^N\left(\frac{m_2N}{\pi\Delta^+}\right)^N\exp\left\{-\frac{1}{2}\vec{x}^T\mathcal{A}_{2(N-1)}\vec{x}+\vec{J}\cdot\vec{x}\right\}\\ &\qquad\times\exp\left\{-\frac{a_1}{2}[\mathbf{r}_0^2+\mathbf{r}_N^2]-\frac{a_2}{2}[\mathbf{b}_0^2+\mathbf{b}_N^2]-\frac{a_3}{2}[\mathbf{r}_0\mathbf{b}_0+\mathbf{r}_N\mathbf{b}_N]-b\mathbf{r}_N^2\right\}\\ &=\lim_{N\to\infty}\left(\frac{-m_1N}{\pi\Delta^+}\right)^N\left(\frac{m_2N}{\pi\Delta^+}\right)^N\frac{(2\pi)^{2(N-1)}}{\det\mathcal{A}_{2(N-1)}}\exp\left\{\frac{1}{2}\vec{J}^T\mathcal{A}^{-1}_{2(N-1)}\vec{J}\right\}\\ &\qquad\times\exp\left\{-\frac{a_1}{2}[\mathbf{r}_0^2+\mathbf{r}_N^2]-\frac{a_2}{2}[\mathbf{b}_0^2+\mathbf{b}_N^2]-\frac{a_3}{2}[\mathbf{r}_0\mathbf{b}_0+\mathbf{r}_N\mathbf{b}_N]-b\mathbf{r}_N^2\right\}, \end{aligned} \tag{E.32}$$

where we have used Eq. (E.15) in order to solve the integral over $\vec{x}$.

The determinant of the matrix $\mathcal{A}$ can be evaluated by using the following property of block matrices:

$$\det\begin{pmatrix}A & B\\ C & D\end{pmatrix}=\det(A-BD^{-1}C)\det D. \tag{E.33}$$

By using this property we can write

$$\det\mathcal{A}_{2(N-1)}=a_1^{N-1}a_2^{N-1}f^{N-1}\det F_{N-1}\left(2+\frac{2b}{fa_1}\right)\det F_{N-1}(2), \tag{E.34}$$

where we have used the fact that $F_N(x)+bF_N(y)=(1+b)F_N\left(\frac{x+by}{1+b}\right)$ and defined

$$f=1-\frac{a_3^2}{4a_1a_2}=\frac{M^2}{\Delta m^2}. \tag{E.35}$$

Therefore we can compute the limit $N\to\infty$ of the factor of Eq. (E.32) by using Eq. (E.19) as

$$\lim_{N\to\infty}\left(\frac{-m_1N}{\pi\Delta^+}\right)^N\left(\frac{m_2N}{\pi\Delta^+}\right)^N\frac{(2\pi)^{2(N-1)}}{\det\mathcal{A}_{2(N-1)}}$$

$$= -\frac{m_1 m_2}{\pi^2(\Delta^+)^2} \lim_{N\to\infty} \frac{N}{\det F_{N-1}\left(2+\frac{2b}{fa_1}\right)} \frac{N}{\det F_{N-1}(2)} = -\frac{-m_1 m_2}{\pi^2 \Delta^+} \frac{\omega_-}{\sin \omega_- \Delta^+}, \tag{E.36}$$

where

$$\omega_-^2 = \frac{\kappa}{m_1} - \frac{\kappa}{m_2} = \omega_1^2 - \omega_2^2. \tag{E.37}$$

On the other hand, the limit $N \to \infty$ of the argument of the exponential of Eq. (E.32) can be evaluated by using Eq. (E.4) and writing the inverse of the matrix $\mathcal{A}$ as

$$\mathcal{A}^{-1}_{2(N-1)} = \begin{pmatrix} \frac{1}{fa_1} F_{N-1}\left(2+\frac{2b}{fa_1}\right)^{-1} & \frac{-a_3}{2fa_1a_2} F_{N-1}\left(2+\frac{2b}{fa_1}\right)^{-1} \\ \frac{-a_3}{2fa_1a_2} F_{N-1}\left(2+\frac{2b}{fa_1}\right)^{-1} & \frac{1}{a_2} F_{N-1}(2)^{-1} + \frac{a_3^2}{4fa_1a_2^2} F_{N-1}\left(2+\frac{2b}{fa_1}\right)^{-1} \end{pmatrix}. \tag{E.38}$$

Therefore we can write

$$\begin{aligned} &\frac{1}{2}\vec{J}^T \mathcal{A}^{-1}_{2(N-1)} \vec{J} - \frac{a_1}{2}[\mathbf{r}_0^2 + \mathbf{r}_N^2] - \frac{a_2}{2}[\mathbf{b}_0^2 + \mathbf{b}_N^2] - \frac{a_3}{2}[\mathbf{r}_0\mathbf{b}_0 + \mathbf{r}_N\mathbf{b}_N] - b\mathbf{r}_N^2 \\ &= (\mathbf{r}_0^2 + \mathbf{r}_N^2)\left[-\frac{a_1}{2}(1-A_1) + \frac{a_3^2}{8a_2}[(1-A_1)-(1-A_2)]\right] \\ &- \frac{a_2}{2}(\mathbf{b}_0^2 + \mathbf{b}_N^2)(1-A_2) - \frac{a_3}{2}(\mathbf{r}_0\cdot\mathbf{b}_0 + \mathbf{r}_N\cdot\mathbf{b}_N)(1-A_2) \\ &+ \mathbf{r}_0\cdot\mathbf{r}_N\left[a_1B_1 + \frac{a_3^2}{4a_2}(B_2 - B_1)\right] + \frac{a_3}{2}B_2(\mathbf{r}_0\cdot\mathbf{b}_N + \mathbf{r}_N\cdot\mathbf{b}_0) + a_2B_2\mathbf{b}_0\cdot\mathbf{b}_N - b\mathbf{r}_N^2, \end{aligned} \tag{E.39}$$

where we have introduced for simplicity

$$A_1 \equiv \left[F_{N-1}\left(2+\frac{2b}{fa_1}\right)^{-1}\right]_{1,N-1}, \qquad A_2 \equiv \left[F_{N-1}(2)^{-1}\right]_{1,N-1}, \tag{E.40}$$

$$B_1 \equiv \left[F_{N-1}\left(2+\frac{2b}{fa_1}\right)^{-1}\right]_{1,1}, \qquad B_2 \equiv \left[F_{N-1}(2)^{-1}\right]_{1,1}. \tag{E.41}$$

Finally, by using Eqs. (E.19) and (E.21) and the definitions of the coefficients a_i it is straightforward to see that

$$\begin{aligned} &\lim_{N\to\infty}\left[\frac{1}{2}\mathbf{J}^T\mathcal{A}^{-1}_{2(N-1)}\mathbf{J} - \frac{a_1}{2}[\mathbf{r}_0^2+\mathbf{r}_N^2] - \frac{a_2}{2}[\mathbf{b}_0^2+\mathbf{b}_N^2] - \frac{a_3}{2}[\mathbf{r}_0\mathbf{b}_0+\mathbf{r}_N\mathbf{b}_N] - b\mathbf{r}_N^2\right] \\ &= (\mathbf{r}_0^2+\mathbf{r}_N^2)\frac{\mu}{\Delta^+}\left[\frac{4\mu}{\Delta m} - \frac{M\omega_-\Delta^+}{\Delta m}\frac{1}{\tan\omega_-\Delta^+}\right] - 2\mathbf{r}_0\mathbf{r}_N\frac{\mu}{\Delta^+}\left[\frac{4\mu}{\Delta m} - \frac{M\omega_-\Delta^+}{\Delta m}\frac{1}{\sin\omega_-\Delta^+}\right] \\ &+ \frac{\Delta m}{\Delta^+}(\mathbf{b}_0-\mathbf{b}_N)^2 + \frac{4\mu}{\Delta^+}(\mathbf{r}_0-\mathbf{r}_N)(\mathbf{b}_0-\mathbf{b}_N) \end{aligned} \tag{E.42}$$

Thus we can write the solution of the double harmonic oscillator as

$$\int_{\mathbf{y}}^{\mathbf{x}} \mathcal{D}\mathbf{z}_1\mathcal{D}\mathbf{z}_2 \exp\left\{\int_{y^+}^{x^+} dz^+\left[m_1\dot{\mathbf{z}}_1^2 - m_2\dot{\mathbf{z}}_2^2 - \kappa(\mathbf{z}_1-\mathbf{z}_2)^2\right]\right\}$$

$$= -\frac{-m_1 m_2 \omega_-}{\pi^2 \Delta^+} \frac{1}{\sin \omega_- \Delta^+} \exp\Bigg\{ (\mathbf{r}_0^2 + \mathbf{r}_N^2) \frac{\mu}{\Delta^+} \left[\frac{4\mu}{\Delta m} - \frac{M\omega_- \Delta^+}{\Delta m} \frac{1}{\tan \omega_- \Delta^+} \right]$$

$$- 2\mathbf{r}_0 \mathbf{r}_N \frac{\mu}{\Delta^+} \left[\frac{4\mu}{\Delta m} - \frac{M\omega_- \Delta^+}{\Delta m} \frac{1}{\sin \omega_- \Delta^+} \right] + \frac{\Delta m}{\Delta^+} (\mathbf{b}_0 - \mathbf{b}_N)^2 + \frac{4\mu}{\Delta^+} (\mathbf{r}_0 - \mathbf{r}_N)(\mathbf{b}_0 - \mathbf{b}_N) \Bigg\}, \tag{E.43}$$

or equivalently,

$$\int_{\mathbf{y}}^{\mathbf{x}} \mathcal{D}\mathbf{z}_1 \mathcal{D}\mathbf{z}_2 \exp\left\{ \int_{y^+}^{x^+} dz^+ \left[\frac{\kappa}{\omega_1^2} \dot{\mathbf{z}}_1^2 - \frac{\kappa}{\omega_2^2} \dot{\mathbf{z}}_2^2 - \kappa (\mathbf{z}_1 - \mathbf{z}_2)^2 \right] \right\}$$

$$= -\frac{\kappa^2}{\pi^2 \Delta^+ \omega_1^2 \omega_2^2} \frac{\omega_-}{\sin \omega_- \Delta^+} \exp\Bigg\{ \frac{\kappa}{\omega_-^2} \Bigg[(\mathbf{r}_0^2 + \mathbf{r}_N^2) \frac{\omega_-}{\tan \omega_- \Delta^+} - 2\mathbf{r}_0 \cdot \mathbf{r}_N \frac{\omega_-}{\sin \omega_- \Delta^+}$$

$$- \frac{1}{\Delta^+ \omega_1^2 \omega_2^2 \omega_+^4} \Big(2\omega_1^2 \omega_2^2 (\mathbf{r}_N - \mathbf{r}_0) + \omega_+^2 \omega_-^2 (\mathbf{b}_0 - \mathbf{b}_N) \Big)^2 \Bigg] \Bigg\}, \tag{E.44}$$

where $\omega_\pm^2 = \omega_1^2 \pm \omega_2^2$.

USC
UNIVERSIDADE
DE SANTIAGO
DE COMPOSTELA

Bibliography

[1] H. Fritzsch, M. Gell-Mann and H. Leutwyler, *Advantages of the Color Octet Gluon Picture*, *Phys. Lett. B* **47** (1973) 365.

[2] H. Fritzsch and M. Gell-Mann, *Current algebra: Quarks and what else?*, *eConf* **C720906V2** (1972) 135 [hep-ph/0208010].

[3] H.D. Politzer, *Reliable Perturbative Results for Strong Interactions?*, *Phys. Rev. Lett.* **30** (1973) 1346.

[4] M. Gell-Mann, *A Schematic Model of Baryons and Mesons*, *Phys. Lett.* **8** (1964) 214.

[5] G. Zweig, *An SU(3) model for strong interaction symmetry and its breaking*, in *Developments in the quark theory of hadrons. Vol.1 1964 - 1978*, D.B. Lichtenberg and S.P. Rosen, eds., pp. 22–101 (1964).

[6] Particle Data Group collaboration, *Review of particle physics*, *J. Phys. G* **37** (2010) 075021.

[7] M.Y. Han and Y. Nambu, *Three Triplet Model with Double SU(3) Symmetry*, *Phys. Rev.* **139** (1965) B1006.

[8] C.-N. Yang and R.L. Mills, *Conservation of Isotopic Spin and Isotopic Gauge Invariance*, *Phys. Rev.* **96** (1954) 191.

[9] E. Witten, *Current Algebra, Baryons, and Quark Confinement*, *Nucl. Phys. B* **223** (1983) 433.

[10] D.J. Gross and F. Wilczek, *Ultraviolet Behavior of Nonabelian Gauge Theories*, *Phys. Rev. Lett.* **30** (1973) 1343.

[11] J. Kuti and V.F. Weisskopf, *Inelastic lepton - nucleon scattering and lepton pair production in the relativistic quark parton model*, *Phys. Rev. D* **4** (1971) 3418.

[12] V.N. Gribov and L.N. Lipatov, *Deep inelastic electron scattering in perturbation theory*, *Phys. Lett. B* **37** (1971) 78.

[13] L.V. Gribov, E.M. Levin and M.G. Ryskin, *Semihard Processes in QCD*, *Phys. Rept.* **100** (1983) 1.

[14] Y.L. Dokshitzer, *Calculation of the Structure Functions for Deep Inelastic Scattering and e+ e- Annihilation by Perturbation Theory in Quantum Chromodynamics.*, *Sov. Phys. JETP* **46** (1977) 641.

[15] V.N. Gribov and L.N. Lipatov, *e+ e- pair annihilation and deep inelastic e p scattering in perturbation theory*, *Sov. J. Nucl. Phys.* **15** (1972) 675.

[16] L.N. Lipatov, *The parton model and perturbation theory*, *Yad. Fiz.* **20** (1974) 181.

[17] G. Altarelli and G. Parisi, *Asymptotic Freedom in Parton Language*, *Nucl. Phys. B* **126** (1977) 298.

[18] E.A. Kuraev, L.N. Lipatov and V.S. Fadin, *The Pomeranchuk Singularity in Nonabelian Gauge Theories*, *Sov. Phys. JETP* **45** (1977) 199.

[19] I.I. Balitsky and L.N. Lipatov, *The Pomeranchuk Singularity in Quantum Chromodynamics*, *Sov. J. Nucl. Phys.* **28** (1978) 822.

[20] M. Froissart, *Asymptotic behavior and subtractions in the Mandelstam representation*, *Phys. Rev.* **123** (1961) 1053.

[21] PHENIX collaboration, *Suppression of hadrons with large transverse momentum in central Au+Au collisions at $\sqrt{s_{NN}}$ = 130-GeV*, *Phys. Rev. Lett.* **88** (2002) 022301 [nucl-ex/0109003].

[22] S. Cao and X.-N. Wang, *Jet quenching and medium response in high-energy heavy-ion collisions: a review*, *Rept. Prog. Phys.* **84** (2021) 024301 [2002.04028].

[23] PHENIX collaboration, *Formation of dense partonic matter in relativistic nucleus-nucleus collisions at RHIC: Experimental evaluation by the PHENIX collaboration*, *Nucl. Phys. A* **757** (2005) 184 [nucl-ex/0410003].

[24] CMS collaboration, *Observation of Long-Range Near-Side Angular Correlations in Proton-Proton Collisions at the LHC*, *JHEP* **09** (2010) 091 [1009.4122].

[25] CMS collaboration, *Observation of long-range near-side angular correlations in proton-lead collisions at the LHC*, *Phys. Lett.* **B718** (2013) 795 [1210.5482].

[26] L.D. McLerran and R. Venugopalan, *Computing quark and gluon distribution functions for very large nuclei*, *Phys. Rev. D* **49** (1994) 2233 [hep-ph/9309289].

[27] L.D. McLerran and R. Venugopalan, *Gluon distribution functions for very large nuclei at small transverse momentum*, *Phys. Rev. D* **49** (1994) 3352 [hep-ph/9311205].

[28] J. Jalilian-Marian, A. Kovner, L. McLerran and H. Weigert, *Intrinsic glue distribution at very smallx*, *Physical Review D* **55** (1997) 5414.

[29] J. Jalilian-Marian, A. Kovner, A. Leonidov and H. Weigert, *Wilson renormalization group for lowxphysics: Towards the high density regime*, *Physical Review D* **59** (1998) .

[30] E. Iancu, A. Leonidov and L. McLerran, *Nonlinear gluon evolution in the color glass condensate: I*, *Nuclear Physics A* **692** (2001) 583.

[31] E. Iancu, A. Leonidov and L. McLerran, *The renormalization group equation for the color glass condensate*, *Physics Letters B* **510** (2001) 133.

[32] E. Ferreiro, E. Iancu, A. Leonidov and L. McLerran, *Nonlinear gluon evolution in the color glass condensate: Ii*, *Nuclear Physics A* **703** (2002) 489.

[33] E. Iancu and R. Venugopalan, *The color glass condensate and high energy scattering in qcd*, *Quark?Gluon Plasma 3* (2004) 249.

[34] F. Gelis, E. Iancu, J. Jalilian-Marian and R. Venugopalan, *The color glass condensate*, *Annual Review of Nuclear and Particle Science* **60** (2010) 463.

[35] T. LAPPI, *Small x physics and rhic data*, *International Journal of Modern Physics E* **20** (2011) 1.

[36] E. Iancu, A. Leonidov and L. McLerran, *The Color glass condensate: An Introduction*, in *Cargese Summer School on QCD Perspectives on Hot and Dense Matter*, pp. 73–145, 2, 2002 [hep-ph/0202270].

[37] L. McLerran, *The Color Glass Condensate and Glasma*, 0804.1736.

[38] P. Agostini, T. Altinoluk and N. Armesto, *Multi-particle production in proton–nucleus collisions in the color glass condensate*, *Eur. Phys. J. C* **81** (2021) 760 [2103.08485].

[39] T. Altinoluk and A. Dumitru, *Particle production in high-energy collisions beyond the shockwave limit*, *Phys. Rev. D* **94** (2016) 074032 [1512.00279].

[40] T. Altinoluk, N. Armesto, A. Kovner and M. Lublinsky, *Double and triple inclusive gluon production at mid rapidity: quantum interference in p-A scattering*, *Eur. Phys. J. C* **78** (2018) 702 [1805.07739].

[41] T. Altinoluk, A. Kovner, E. Levin and M. Lublinsky, *Reggeon Field Theory for Large Pomeron Loops*, *JHEP* **04** (2014) 075 [1401.7431].

[42] T. Altinoluk, N. Armesto, A. Kovner, E. Levin and M. Lublinsky, *KLWMIJ Reggeon field theory beyond the large N_c limit*, *JHEP* **08** (2014) 007 [1402.5936].

[43] T. Altinoluk, N. Armesto, G. Beuf, M. Martínez and C.A. Salgado, *Next-to-eikonal corrections in the CGC: gluon production and spin asymmetries in pA collisions*, *JHEP* **07** (2014) 068 [1404.2219].

[44] T. Altinoluk, N. Armesto, G. Beuf and A. Moscoso, *Next-to-next-to-eikonal corrections in the CGC*, *JHEP* **01** (2016) 114 [1505.01400].

[45] P. Agostini, T. Altinoluk and N. Armesto, *Effect of non-eikonal corrections on azimuthal asymmetries in the Color Glass Condensate*, *Eur. Phys. J. C* **79** (2019) 790 [1907.03668].

[46] P. Agostini, T. Altinoluk and N. Armesto, *Non-eikonal corrections to multi-particle production in the Color Glass Condensate*, *Eur. Phys. J. C* **79** (2019) 600 [1902.04483].

[47] Y.V. Kovchegov and E. Levin, *Quantum chromodynamics at high energy*, vol. 33, Cambridge University Press (8, 2012), 10.1017/CBO9781139022187.

[48] M.E. Peskin and D.V. Schroeder, *An Introduction to quantum field theory*, Addison-Wesley, Reading, USA (1995).

[49] D.J. Gross and F. Wilczek, *Ultraviolet behavior of non-abelian gauge theories*, *Phys. Rev. Lett.* **30** (1973) 1343.

[50] H.D. Politzer, *Reliable perturbative results for strong interactions?*, *Phys. Rev. Lett.* **30** (1973) 1346.

[51] Particle Data Group collaboration, *Review of Particle Physics*, *PTEP* **2020** (2020) 083C01.

[52] H.-W. Lin et al., *Parton distributions and lattice QCD calculations: a community white paper*, *Prog. Part. Nucl. Phys.* **100** (2018) 107 [1711.07916].

[53] J.D. Bjorken, *Asymptotic sum rules at infinite momentum*, *Phys. Rev.* **179** (1969) 1547.

[54] R.P. Feynman, *The behavior of hadron collisions at extreme energies*, *Conf. Proc. C* **690905** (1969) 237.

[55] C.G. Callan and D.J. Gross, *High-energy electroproduction and the constitution of the electric current*, *Phys. Rev. Lett.* **22** (1969) 156.

[56] NNPDF collaboration, *Parton distributions for the LHC Run II*, *JHEP* **04** (2015) 040 [1410.8849].

[57] M. Froissart, *Asymptotic behavior and subtractions in the mandelstam representation*, *Phys. Rev.* **123** (1961) 1053.

[58] A.H. Mueller and J.-w. Qiu, *Gluon Recombination and Shadowing at Small Values of x*, *Nucl. Phys. B* **268** (1986) 427.

[59] F. Gelis, R. Peschanski, G. Soyez and L. Schoeffel, *Systematics of geometric scaling*, *Physics Letters B* **647** (2007) 376.

[60] A.M. Sta?to, K. Golec-Biernat and J. Kwieci?ski, *Geometric scaling for the total?*pcross section in the lowxregion*, *Physical Review Letters* **86** (2001) 596.

[61] L. McLerran and R. Venugopalan, *Fock space distributions, structure functions, higher twists, and small x*, *Physical Review D* **59** (1999) .

[62] A. Dumitru and E. Petreska, *Initial conditions for dipole evolution beyond the McLerran-Venugopalan model*, *Nucl. Phys. A* **879** (2012) 59 [1112.4760].

[63] F. Cougoulic and Y.V. Kovchegov, *Helicity-dependent extension of the McLerran–Venugopalan model*, *Nucl. Phys. A* **1004** (2020) 122051 [2005.14688].

[64] A. Ayala, J. Jalilian-Marian, L. McLerran and R. Venugopalan, *Quantum corrections to the weizsacker-williams gluon distribution function at small x*, *Physical Review D* **53** (1996) 458.

[65] I. Balitsky, *Operator expansion for high-energy scattering*, *Nuclear Physics B* **463** (1996) 99.

[66] A. Kovner, J.G. Milhano and H. Weigert, *Relating different approaches to nonlinear QCD evolution at finite gluon density*, *Phys. Rev. D* **62** (2000) 114005 [hep-ph/0004014].

[67] Y.V. Kovchegov, *Small-xf2structure function of a nucleus including multiple pomeron exchanges*, *Physical Review D* **60** (1999) .

[68] Y.V. Kovchegov, *Unitarization of the bfkl pomeron on a nucleus*, *Physical Review D* **61** (2000) .

[69] F. Gelis and R. Venugopalan, *Particle production in field theories coupled to strong external sources, i: Formalism and main results*, *Nuclear Physics A* **776** (2006) 135.

[70] B. Muller and A. Trayanov, *Deterministic chaos in non Abelian lattice gauge theory*, *Phys. Rev. Lett.* **68** (1992) 3387.

[71] P. Romatschke and R. Venugopalan, *Collective non-abelian instabilities in a melting color glass condensate*, *Physical Review Letters* **96** (2006) .

[72] T. BIRÓ, C. GONG, B. MÜLLER and A. TRAYANOV, *Hamiltonian dynamics of yang-mills fields on a lattice*, *International Journal of Modern Physics C* **05** (1994) 113.

[73] T. Kunihiro, B. Müller, A. Ohnishi, A. Schäfer, T.T. Takahashi and A. Yamamoto, *Chaotic behavior in classical yang-mills dynamics*, *Physical Review D* **82** (2010) .

[74] F. Gelis, T. Lappi and R. Venugopalan, *High energy factorization in nucleus-nucleus collisions. II. Multigluon correlations*, *Phys. Rev. D* **78** (2008) 054020 [0807.1306].

[75] F. Gelis, T. Lappi and R. Venugopalan, *High energy factorization in nucleus-nucleus collisions*, *Phys. Rev. D* **78** (2008) 054019 [0804.2630].

[76] F. Gelis, T. Lappi and R. Venugopalan, *High energy factorization in nucleus-nucleus collisions. 3. Long range rapidity correlations*, *Phys. Rev. D* **79** (2009) 094017 [0810.4829].

[77] A. Krasnitz and R. Venugopalan, *The Initial energy density of gluons produced in very high-energy nuclear collisions*, *Phys. Rev. Lett.* **84** (2000) 4309 [hep-ph/9909203].

[78] A. Krasnitz and R. Venugopalan, *The Initial gluon multiplicity in heavy ion collisions*, *Phys. Rev. Lett.* **86** (2001) 1717 [hep-ph/0007108].

[79] A. Krasnitz, Y. Nara and R. Venugopalan, *Classical gluodynamics of high-energy nuclear collisions: An Erratumn and an update*, *Nucl. Phys. A* **727** (2003) 427 [hep-ph/0305112].

[80] A. Krasnitz, Y. Nara and R. Venugopalan, *Coherent gluon production in very high-energy heavy ion collisions*, *Phys. Rev. Lett.* **87** (2001) 192302 [hep-ph/0108092].

[81] T. Lappi, *Production of gluons in the classical field model for heavy ion collisions*, *Phys. Rev. C* **67** (2003) 054903 [hep-ph/0303076].

[82] Y.V. Kovchegov and A.H. Mueller, *Gluon production in current nucleus and nucleon - nucleus collisions in a quasiclassical approximation*, *Nucl. Phys. B* **529** (1998) 451 [hep-ph/9802440].

[83] Y.V. Kovchegov and K. Tuchin, *Inclusive gluon production in DIS at high parton density*, *Phys. Rev. D* **65** (2002) 074026 [hep-ph/0111362].

[84] A. Dumitru and L.D. McLerran, *How protons shatter colored glass*, *Nucl. Phys. A* **700** (2002) 492 [hep-ph/0105268].

[85] J.P. Blaizot, F. Gelis and R. Venugopalan, *High-energy pA collisions in the color glass condensate approach. 1. Gluon production and the Cronin effect*, *Nucl. Phys. A* **743** (2004) 13 [hep-ph/0402256].

[86] Y. Mehtar-Tani, *Relating the description of gluon production in pA collisions and parton energy loss in AA collisions*, *Phys. Rev. C* **75** (2007) 034908 [hep-ph/0606236].

[87] F. Gelis and Y. Mehtar-Tani, *Gluon propagation inside a high-energy nucleus*, *Phys. Rev. D* **73** (2006) 034019 [hep-ph/0512079].

[88] R.P. Feynman, *Space-time approach to non-relativistic quantum mechanics*, *Rev. Mod. Phys.* **20** (1948) 367.

[89] F. Gelis, T. Lappi and R. Venugopalan, *High energy scattering in Quantum Chromodynamics*, *Int. J. Mod. Phys. E* **16** (2007) 2595 [0708.0047].

[90] J.D. Bjorken, J.B. Kogut and D.E. Soper, *Quantum Electrodynamics at Infinite Momentum: Scattering from an External Field*, *Phys. Rev. D* **3** (1971) 1382.

[91] S.J. Brodsky, H.-C. Pauli and S.S. Pinsky, *Quantum chromodynamics and other field theories on the light cone*, *Phys. Rept.* **301** (1998) 299 [hep-ph/9705477].

[92] A. Dumitru, A. Hayashigaki and J. Jalilian-Marian, *The Color glass condensate and hadron production in the forward region*, *Nucl. Phys. A* **765** (2006) 464 [hep-ph/0506308].

[93] E. Iancu and Y. Mulian, *Forward trijet production in proton–nucleus collisions*, *Nucl. Phys. A* **985** (2019) 66 [1809.05526].

[94] A. Kovner and M. Lublinsky, *In pursuit of Pomeron loops: The JIMWLK equation and the Wess-Zumino term*, *Phys. Rev. D* **71** (2005) 085004 [hep-ph/0501198].

[95] C.F. von Weizsacker, *Radiation emitted in collisions of very fast electrons*, *Z. Phys.* **88** (1934) 612.

[96] E.J. Williams, *Correlation of certain collision problems with radiation theory*, *Kong. Dan. Vid. Sel. Mat. Fys. Med.* **13N4** (1935) 1.

[97] C. Lorce and B. Pasquini, *Quark Wigner Distributions and Orbital Angular Momentum*, *Phys. Rev. D* **84** (2011) 014015 [1106.0139].

[98] A. Kovner and M. Lublinsky, *Entanglement entropy and entropy production in the Color Glass Condensate framework*, *Phys. Rev. D* **92** (2015) 034016 [1506.05394].

[99] D.E. Kharzeev and E.M. Levin, *Deep inelastic scattering as a probe of entanglement*, *Phys. Rev. D* **95** (2017) 114008 [1702.03489].

[100] N. Armesto, F. Dominguez, A. Kovner, M. Lublinsky and V. Skokov, *The Color Glass Condensate density matrix: Lindblad evolution, entanglement entropy and Wigner functional*, *JHEP* **05** (2019) 025 [1901.08080].

[101] H. Duan, C. Akkaya, A. Kovner and V.V. Skokov, *Entanglement, partial set of measurements, and diagonality of the density matrix in the parton model*, *Phys. Rev. D* **101** (2020) 036017 [2001.01726].

[102] T. Lappi, *Azimuthal harmonics of color fields in a high energy nucleus*, *Phys. Lett. B* **744** (2015) 315 [1501.05505].

[103] T. Lappi, B. Schenke, S. Schlichting and R. Venugopalan, *Tracing the origin of azimuthal gluon correlations in the color glass condensate*, *JHEP* **01** (2016) 061 [1509.03499].

[104] K. Dusling, M. Mace and R. Venugopalan, *Multiparticle collectivity from initial state correlations in high energy proton-nucleus collisions*, *Phys. Rev. Lett.* **120** (2018) 042002 [1705.00745].

[105] K. Dusling, M. Mace and R. Venugopalan, *Parton model description of multiparticle azimuthal correlations in pA collisions*, *Phys. Rev. D* **97** (2018) 016014 [1706.06260].

[106] M.K. Davy, C. Marquet, Y. Shi, B.-W. Xiao and C. Zhang, *Two particle azimuthal harmonics in pA collisions*, *Nucl. Phys. A* **983** (2019) 293 [1808.09851].

[107] A. Dumitru, F. Gelis, L. McLerran and R. Venugopalan, *Glasma flux tubes and the near side ridge phenomenon at RHIC*, *Nucl. Phys.* **A810** (2008) 91 [0804.3858].

[108] K. Dusling, D. Fernandez-Fraile and R. Venugopalan, *Three-particle correlation from glasma flux tubes*, *Nucl. Phys. A* **828** (2009) 161 [0902.4435].

[109] M. Gyulassy and L.D. McLerran, *Yang-Mills radiation in ultrarelativistic nuclear collisions*, *Phys. Rev. C* **56** (1997) 2219 [nucl-th/9704034].

[110] Y.V. Kovchegov and D.H. Rischke, *Classical gluon radiation in ultrarelativistic nucleus-nucleus collisions*, *Phys. Rev. C* **56** (1997) 1084 [hep-ph/9704201].

[111] P. Tribedy and R. Venugopalan, *Saturation models of HERA DIS data and inclusive hadron distributions in p+p collisions at the LHC*, *Nucl. Phys. A* **850** (2011) 136 [1011.1895].

[112] J.L. ALbacete and A. Dumitru, *A model for gluon production in heavy-ion collisions at the LHC with rcBK unintegrated gluon densities*, 1011.5161.

[113] P. Tribedy and R. Venugopalan, *QCD saturation at the LHC: Comparisons of models to p + p and A + A data and predictions for p + Pb collisions*, *Phys. Lett. B* **710** (2012) 125 [1112.2445].

[114] J.L. Albacete, A. Dumitru, H. Fujii and Y. Nara, *CGC predictions for p + Pb collisions at the LHC*, *Nucl. Phys. A* **897** (2013) 1 [1209.2001].

[115] T. Lappi and L. McLerran, *Some features of the glasma*, *Nucl. Phys. A* **772** (2006) 200 [hep-ph/0602189].

[116] A. Kurkela, *Initial state of Heavy-Ion Collisions: Isotropization and thermalization*, *Nucl. Phys. A* **956** (2016) 136 [1601.03283].

[117] P. Romatschke and U. Romatschke, *Relativistic Fluid Dynamics In and Out of Equilibrium*, Cambridge Monographs on Mathematical Physics, Cambridge University Press (5, 2019), 10.1017/9781108651998, [1712.05815].

[118] Y. Mehtar-Tani, J.G. Milhano and K. Tywoniuk, *Jet physics in heavy-ion collisions*, *Int. J. Mod. Phys. A* **28** (2013) 1340013 [1302.2579].

[119] C. Gale, S. Jeon, B. Schenke, P. Tribedy and R. Venugopalan, *Event-by-event anisotropic flow in heavy-ion collisions from combined Yang-Mills and viscous fluid dynamics*, *Phys. Rev. Lett.* **110** (2013) 012302 [1209.6330].

[120] CMS collaboration, *Centrality dependence of dihadron correlations and azimuthal anisotropy harmonics in PbPb collisions at* $\sqrt{s_{NN}} = 2.76$ *TeV*, *Eur. Phys. J. C* **72** (2012) 2012 [1201.3158].

[121] ATLAS collaboration, *Measurement of long-range pseudorapidity correlations and azimuthal harmonics in* $\sqrt{s_{NN}} = 5.02$ *TeV proton-lead collisions with the ATLAS detector*, *Phys. Rev. C* **90** (2014) 044906 [1409.1792].

[122] S. Schlichting and P. Tribedy, *Collectivity in Small Collision Systems: An Initial-State Perspective*, *Adv. High Energy Phys.* **2016** (2016) 8460349 [1611.00329].

[123] C. Loizides, *Experimental overview on small collision systems at the LHC*, *Nucl. Phys. A* **956** (2016) 200 [1602.09138].

[124] B. Schenke, *Origins of collectivity in small systems*, *Nucl. Phys. A* **967** (2017) 105 [1704.03914].

[125] J.L. Nagle and W.A. Zajc, *Small System Collectivity in Relativistic Hadronic and Nuclear Collisions*, *Ann. Rev. Nucl. Part. Sci.* **68** (2018) 211 [1801.03477].

[126] CMS collaboration, *Multiplicity and Transverse Momentum Dependence of Two- and Four-Particle Correlations in pPb and PbPb Collisions*, *Phys. Lett. B* **724** (2013) 213 [1305.0609].

[127] CMS collaboration, *Evidence for collectivity in pp collisions at the LHC*, *Phys. Lett. B* **765** (2017) 193 [1606.06198].

[128] CMS collaboration, *Evidence for Collective Multiparticle Correlations in p-Pb Collisions*, *Phys. Rev. Lett.* **115** (2015) 012301 [1502.05382].

[129] ALICE collaboration, *Multiparticle azimuthal correlations in p -Pb and Pb-Pb collisions at the CERN Large Hadron Collider*, *Phys. Rev. C* **90** (2014) 054901 [1406.2474].

[130] ATLAS collaboration, *Measurement with the ATLAS detector of multi-particle azimuthal correlations in p+Pb collisions at* $\sqrt{s_{NN}}$ *=5.02 TeV*, *Phys. Lett. B* **725** (2013) 60 [1303.2084].

[131] ATLAS collaboration, *Correlated long-range mixed-harmonic fluctuations measured in pp, p+Pb and low-multiplicity Pb+Pb collisions with the ATLAS detector*, *Phys. Lett. B* **789** (2019) 444 [1807.02012].

[132] ATLAS collaboration, *Measurement of multi-particle azimuthal correlations in pp, p+Pb and low-multiplicity Pb+Pb collisions with the ATLAS detector*, *Eur. Phys. J. C* **77** (2017) 428 [1705.04176].

[133] ATLAS collaboration, *Measurement of long-range multiparticle azimuthal correlations with the subevent cumulant method in pp and p + Pb collisions with the ATLAS detector at the CERN Large Hadron Collider*, *Phys. Rev. C* **97** (2018) 024904 [1708.03559].

[134] B. Schenke and R. Venugopalan, *Eccentric protons? Sensitivity of flow to system size and shape in p+p, p+Pb and Pb+Pb collisions*, *Phys. Rev. Lett.* **113** (2014) 102301 [1405.3605].

[135] ATLAS collaboration, *Measurement of the distributions of event-by-event flow harmonics in lead-lead collisions at = 2.76 TeV with the ATLAS detector at the LHC*, *JHEP* **11** (2013) 183 [1305.2942].

[136] P. Bozek, *Collective flow in p-Pb and d-Pd collisions at TeV energies*, *Phys. Rev. C* **85** (2012) 014911 [1112.0915].

[137] ALICE collaboration, *Higher harmonic anisotropic flow measurements of charged particles in Pb-Pb collisions at* $\sqrt{s_{NN}}$*=2.76 TeV*, *Phys. Rev. Lett.* **107** (2011) 032301 [1105.3865].

[138] P. Bozek and W. Broniowski, *Collective dynamics in high-energy proton-nucleus collisions*, *Phys. Rev. C* **88** (2013) 014903 [1304.3044].

[139] P. Bozek and W. Broniowski, *Hydrodynamic modeling of* ^{3}*He–Au collisions at* $\sqrt{sNN}$*=200 GeV*, *Phys. Lett. B* **747** (2015) 135 [1503.00468].

[140] W. Zhao, Y. Zhou, H. Xu, W. Deng and H. Song, *Hydrodynamic collectivity in proton–proton collisions at 13 TeV*, *Phys. Lett. B* **780** (2018) 495 [1801.00271].

[141] H. Niemi and G.S. Denicol, *How large is the Knudsen number reached in fluid dynamical simulations of ultrarelativistic heavy ion collisions?*, 1404.7327.

[142] A. Kurkela, U.A. Wiedemann and B. Wu, *Flow in AA and pA as an interplay of fluid-like and non-fluid like excitations*, *Eur. Phys. J. C* **79** (2019) 965 [1905.05139].

[143] E. Iancu and D.N. Triantafyllopoulos, *JIMWLK evolution for multi-particle production in Langevin form*, *JHEP* **11** (2013) 067 [1307.1559].

[144] K. Dusling, F. Gelis, T. Lappi and R. Venugopalan, *Long range two-particle rapidity correlations in A+A collisions from high energy QCD evolution*, *Nucl. Phys. A* **836** (2010) 159 [0911.2720].

[145] T. Altinoluk, N. Armesto, G. Beuf, A. Kovner and M. Lublinsky, *Bose enhancement and the ridge*, *Phys. Lett. B* **751** (2015) 448 [1503.07126].

[146] Y.V. Kovchegov and D.E. Wertepny, *Long-Range Rapidity Correlations in Heavy-Light Ion Collisions*, *Nucl. Phys. A* **906** (2013) 50 [1212.1195].

[147] T. Altinoluk, N. Armesto, G. Beuf, A. Kovner and M. Lublinsky, *Hanbury?Brown?Twiss measurements at large rapidity separations, or can we measure the proton radius in p-A collisions?*, *Phys. Lett.* **B752** (2016) 113 [1509.03223].

[148] K. Dusling, W. Li and B. Schenke, *Novel collective phenomena in high-energy proton–proton and proton–nucleus collisions*, *Int. J. Mod. Phys. E* **25** (2016) 1630002 [1509.07939].

[149] K. Dusling and R. Venugopalan, *Comparison of the color glass condensate to dihadron correlations in proton-proton and proton-nucleus collisions*, *Phys. Rev. D* **87** (2013) 094034 [1302.7018].

[150] A. Dumitru, K. Dusling, F. Gelis, J. Jalilian-Marian, T. Lappi and R. Venugopalan, *The Ridge in proton-proton collisions at the LHC*, *Phys. Lett. B* **697** (2011) 21 [1009.5295].

[151] A. Kovner and M. Lublinsky, *Angular Correlations in Gluon Production at High Energy*, *Phys. Rev. D* **83** (2011) 034017 [1012.3398].

[152] A. Kovner and M. Lublinsky, *On Angular Correlations and High Energy Evolution*, *Phys. Rev. D* **84** (2011) 094011 [1109.0347].

[153] A. Kovner and M. Lublinsky, *Angular and long range rapidity correlations in particle production at high energy*, *Int. J. Mod. Phys. E* **22** (2013) 1330001 [1211.1928].

[154] J. Jalilian-Marian, A. Kovner, L.D. McLerran and H. Weigert, *The Intrinsic glue distribution at very small x*, *Phys. Rev. D* **55** (1997) 5414 [hep-ph/9606337].

[155] A. Dumitru and A.V. Giannini, *Initial state angular asymmetries in high energy p+A collisions: spontaneous breaking of rotational symmetry by a color electric field and C-odd fluctuations*, *Nucl. Phys. A* **933** (2015) 212 [1406.5781].

[156] A. Dumitru, L. McLerran and V. Skokov, *Azimuthal asymmetries and the emergence of "collectivity" from multi-particle correlations in high-energy pA collisions*, *Phys. Lett. B* **743** (2015) 134 [1410.4844].

[157] A. Dumitru and V. Skokov, *Anisotropy of the semiclassical gluon field of a large nucleus at high energy*, *Phys. Rev. D* **91** (2015) 074006 [1411.6630].

[158] N. Borghini, P.M. Dinh and J.-Y. Ollitrault, *A New method for measuring azimuthal distributions in nucleus-nucleus collisions*, *Phys. Rev. C* **63** (2001) 054906 [nucl-th/0007063].

[159] N. Borghini, P.M. Dinh and J.-Y. Ollitrault, *Flow analysis from multiparticle azimuthal correlations*, *Phys. Rev. C* **64** (2001) 054901 [nucl-th/0105040].

[160] N. Borghini, P.M. Dinh and J.-Y. Ollitrault, *Flow analysis from cumulants: A Practical guide*, in *International Workshop on the Physics of the Quark Gluon Plasma*, 10, 2001 [nucl-ex/0110016].

[161] A. Bilandzic, R. Snellings and S. Voloshin, *Flow analysis with cumulants: Direct calculations*, *Phys. Rev. C* **83** (2011) 044913 [1010.0233].

[162] CMS collaboration, *Multiplicity and Transverse Momentum Dependence of Two- and Four-Particle Correlations in pPb and PbPb Collisions*, *Phys. Lett. B* **724** (2013) 213 [1305.0609].

[163] ATLAS collaboration, *Measurement of flow harmonics correlations with mean transverse momentum in lead-lead and proton-lead collisions at* $\sqrt{s_{NN}} = 5.02$ *TeV with the ATLAS detector*, *Eur. Phys. J. C* **79** (2019) 985 [1907.05176].

[164] P. Bozek, *Transverse-momentum–flow correlations in relativistic heavy-ion collisions*, *Phys. Rev. C* **93** (2016) 044908 [1601.04513].

[165] G. Giacalone, B. Schenke and C. Shen, *Observable signatures of initial state momentum anisotropies in nuclear collisions*, *Phys. Rev. Lett.* **125** (2020) 192301 [2006.15721].

[166] S.H. Lim and J.L. Nagle, *Exploring Origins for Correlations between Flow Harmonics and Transverse Momentum in Small Collision Systems (Unambiguous Ambiguity)*, 2103.01348.

[167] T. Altinoluk, N. Armesto, A. Kovner, M. Lublinsky and V.V. Skokov, *Angular correlations in pA collisions from CGC: multiplicity and mean transverse momentum dependence of* v_2, 2012.01810.

[168] c. Özonder, *Triple-gluon and quadruple-gluon azimuthal correlations from glasma and higher-dimensional ridges*, *Phys. Rev. D* **91** (2015) 034005 [1409.6347].

[169] A. Kovner and A.H. Rezaeian, *Double parton scattering in the CGC: Double quark production and effects of quantum statistics*, *Phys. Rev.* **D96** (2017) 074018 [1707.06985].

[170] A. Kovner and A.H. Rezaeian, *Multiquark production in* $p + A$ *collisions: Quantum interference effects*, *Phys. Rev.* **D97** (2018) 074008 [1801.04875].

[171] A. Kovner, M. Lublinsky and V. Skokov, *Exploring correlations in the CGC wave function: odd azimuthal anisotropy*, *Phys. Rev. D* **96** (2017) 016010 [1612.07790].

[172] Y.V. Kovchegov and V.V. Skokov, *How classical gluon fields generate odd azimuthal harmonics for the two-gluon correlation function in high-energy collisions*, *Phys. Rev. D* **97** (2018) 094021 [1802.08166].

[173] R. Baier, A. Kovner, M. Nardi and U.A. Wiedemann, *Particle correlations in saturated QCD matter*, *Phys. Rev. D* **72** (2005) 094013 [hep-ph/0506126].

[174] A. Kovner and M. Lublinsky, *One gluon, two gluon: Multigluon production via high energy evolution*, *JHEP* **11** (2006) 083 [hep-ph/0609227].

[175] C.S. Lam and G. Mahlon, *Color neutrality and the gluon distribution in a very large nucleus*, *Phys. Rev. D* **61** (2000) 014005 [hep-ph/9907281].

[176] C. Marquet, *Forward inclusive dijet production and azimuthal correlations in p(A) collisions*, *Nucl. Phys. A* **796** (2007) 41 [0708.0231].

[177] F. Gelis and A. Peshier, *Probing colored glass via q anti-q photoproduction*, *Nucl. Phys. A* **697** (2002) 879 [hep-ph/0107142].

[178] A. Kovner and U.A. Wiedemann, *Eikonal evolution and gluon radiation*, *Phys. Rev. D* **64** (2001) 114002 [hep-ph/0106240].

[179] K.J. Golec-Biernat and M. Wusthoff, *Saturation effects in deep inelastic scattering at low Q**2 and its implications on diffraction*, *Phys. Rev. D* **59** (1998) 014017 [hep-ph/9807513].

[180] J.P. Blaizot, F. Gelis and R. Venugopalan, *High-energy pA collisions in the color glass condensate approach. 2. Quark production*, *Nucl. Phys. A* **743** (2004) 57 [hep-ph/0402257].

[181] F. Dominguez, C. Marquet and B. Wu, *On multiple scatterings of mesons in hot and cold QCD matter*, *Nucl. Phys. A* **823** (2009) 99 [0812.3878].

[182] F. Dominguez, C. Marquet, B.-W. Xiao and F. Yuan, *Universality of Unintegrated Gluon Distributions at small x*, *Phys. Rev. D* **83** (2011) 105005 [1101.0715].

[183] F. Dominguez, C. Marquet, A.M. Stasto and B.-W. Xiao, *Universality of multiparticle production in QCD at high energies*, *Phys. Rev. D* **87** (2013) 034007 [1210.1141].

[184] Y. Shi, C. Zhang and E. Wang, *Multipole scattering amplitudes in the Color Glass Condensate formalism*, *Phys. Rev. D* **95** (2017) 116014 [1704.00266].

[185] F. Gelis, T. Lappi and L. McLerran, *Glittering Glasmas*, *Nucl. Phys. A* **828** (2009) 149 [0905.3234].

[186] T. Altinoluk, N. Armesto and D.E. Wertepny, *Correlations and the ridge in the Color Glass Condensate beyond the glasma graph approximation*, *JHEP* **05** (2018) 207 [1804.02910].

[187] ALICE collaboration, *Multiparticle azimuthal correlations in p -Pb and Pb-Pb collisions at the CERN Large Hadron Collider*, *Phys. Rev. C* **90** (2014) 054901 [1406.2474].

[188] CMS collaboration, *Evidence for collectivity in pp collisions at the LHC*, *Phys. Lett.* **B765** (2017) 193 [1606.06198].

[189] K.J. Golec-Biernat and M. Wusthoff, *Saturation effects in deep inelastic scattering at low Q**2 and its implications on diffraction*, *Phys. Rev. D* **59** (1998) 014017 [hep-ph/9807513].

[190] K.J. Golec-Biernat and M. Wusthoff, *Saturation in diffractive deep inelastic scattering*, *Phys. Rev. D* **60** (1999) 114023 [hep-ph/9903358].

[191] A. Kovner and U.A. Wiedemann, *Gluon radiation and parton energy loss*, hep-ph/0304151.

[192] J. Casalderrey-Solana and C.A. Salgado, *Introductory lectures on jet quenching in heavy ion collisions*, *Acta Phys. Polon. B* **38** (2007) 3731 [0712.3443].

[193] I. Balitsky and A. Tarasov, *Rapidity evolution of gluon TMD from low to moderate x*, *JHEP* **10** (2015) 017 [1505.02151].

[194] I. Balitsky and A. Tarasov, *Gluon TMD in particle production from low to moderate x*, *JHEP* **06** (2016) 164 [1603.06548].

[195] Y.V. Kovchegov, D. Pitonyak and M.D. Sievert, *Helicity Evolution at Small-x*, *JHEP* **01** (2016) 072 [1511.06737].

[196] Y.V. Kovchegov, D. Pitonyak and M.D. Sievert, *Helicity Evolution at Small x: Flavor Singlet and Non-Singlet Observables*, *Phys. Rev. D* **95** (2017) 014033 [1610.06197].

[197] Y.V. Kovchegov, D. Pitonyak and M.D. Sievert, *Small-x Asymptotics of the Quark Helicity Distribution: Analytic Results*, *Phys. Lett. B* **772** (2017) 136 [1703.05809].

[198] Y.V. Kovchegov, D. Pitonyak and M.D. Sievert, *Small-x Asymptotics of the Gluon Helicity Distribution*, *JHEP* **10** (2017) 198 [1706.04236].

[199] G.A. Chirilli, *Sub-eikonal corrections to scattering amplitudes at high energy*, *JHEP* **01** (2019) 118 [1807.11435].

[200] E. Laenen, L. Magnea and G. Stavenga, *On next-to-eikonal corrections to threshold resummation for the Drell-Yan and DIS cross sections*, *Phys. Lett. B* **669** (2008) 173 [0807.4412].

[201] E. Laenen, G. Stavenga and C.D. White, *Path integral approach to eikonal and next-to-eikonal exponentiation*, *JHEP* **03** (2009) 054 [0811.2067].

[202] E. Laenen, L. Magnea, G. Stavenga and C.D. White, *Next-to-Eikonal Corrections to Soft Gluon Radiation: A Diagrammatic Approach*, *JHEP* **01** (2011) 141 [1010.1860].

[203] T. Altinoluk and G. Beuf, *Quark and scalar propagators at next-to-eikonal accuracy in the CGC through a dynamical background gluon field*, 2109.01620.

[204] T. Altinoluk, G. Beuf, A. Czajka and A. Tymowska, *Quarks at next-to-eikonal accuracy in the CGC: Forward quark-nucleus scattering*, *Phys. Rev. D* **104** (2021) 014019 [2012.03886].

[205] G.A. Chirilli, *High-energy operator product expansion at sub-eikonal level*, *JHEP* **06** (2021) 096 [2101.12744].

[206] M. Martinez, M.D. Sievert and D.E. Wertepny, *Multiparticle Production at Mid-Rapidity in the Color-Glass Condensate*, *JHEP* **02** (2019) 024 [1808.04896].

[207] L. McLerran and V. Skokov, *Odd Azimuthal Anisotropy of the Glasma for pA Scattering*, *Nucl. Phys. A* **959** (2017) 83 [1611.09870].

[208] A. Kovner, M. Lublinsky and V. Skokov, *Initial state qqg correlations as a background for the Chiral Magnetic Effect in collision of small systems*, *Phys. Rev. D* **96** (2017) 096003 [1706.02330].

[209] U.A. Wiedemann, *Gluon radiation off hard quarks in a nuclear environment: Opacity expansion*, *Nucl. Phys. B* **588** (2000) 303 [hep-ph/0005129].

[210] M. Gyulassy, P. Levai and I. Vitev, *Reaction operator approach to nonAbelian energy loss*, *Nucl. Phys. B* **594** (2001) 371 [nucl-th/0006010].

[211] U.A. Wiedemann, *Transverse dynamics of hard partons in nuclear media and the QCD dipole*, *Nucl. Phys. B* **582** (2000) 409 [hep-ph/0003021].

[212] c. Özönder, *Predictions on three-particle azimuthal correlations in proton-proton collisions*, *Turk. J. Phys.* **42** (2018) 78 [1712.05571].

[213] A. Accardi et al., *Electron Ion Collider: The Next QCD Frontier: Understanding the glue that binds us all*, *Eur. Phys. J. A* **52** (2016) 268 [1212.1701].

[214] Y.V. Kovchegov and M.D. Sievert, *Small-x Helicity Evolution: an Operator Treatment*, *Phys. Rev. D* **99** (2019) 054032 [1808.09010].

[215] F. Cougoulic and Y.V. Kovchegov, *Helicity-dependent generalization of the JIMWLK evolution*, *Phys. Rev. D* **100** (2019) 114020 [1910.04268].

[216] Y.V. Kovchegov and M.G. Santiago, *Quark Sivers Function at Small x: Spin-Dependent Odderon and the Sub-Eikonal Evolution*, 2108.03667.

[217] Jefferson Lab Angular Momentum collaboration, *First analysis of world polarized DIS data with small-x helicity evolution*, *Phys. Rev. D* **104** (2021) L031501 [2102.06159].

[218] B.G. Zakharov, *Light cone path integral approach to the Landau-Pomeranchuk-Migdal effect*, *Phys. Atom. Nucl.* **61** (1998) 838 [hep-ph/9807540].

[219] R. Baier, Y.L. Dokshitzer, A.H. Mueller, S. Peigne and D. Schiff, *Radiative energy loss and p(T) broadening of high-energy partons in nuclei*, *Nucl. Phys. B* **484** (1997) 265 [hep-ph/9608322].

[220] R. Baier, Y.L. Dokshitzer, A.H. Mueller, S. Peigne and D. Schiff, *Radiative energy loss of high-energy quarks and gluons in a finite volume quark - gluon plasma*, *Nucl. Phys. B* **483** (1997) 291 [hep-ph/9607355].

[221] B.G. Zakharov, *Radiative energy loss of high-energy quarks in finite size nuclear matter and quark - gluon plasma*, *JETP Lett.* **65** (1997) 615 [hep-ph/9704255].

USC
UNIVERSIDADE
DE SANTIAGO
DE COMPOSTELA

Publications used in the thesis

We collect in the following pages all the relevant information about the publications used in the thesis. We have reproduced part of their content in Chapters 4 and 5.

Non-eikonal corrections to multi-particle production in the Color Glass Condensate, *Eur. Phys. J. C* **79** (2019) 600

Authors

Pedro Agostini,[ab] Tolga Altinoluk,[c] Néstor Armesto,[ab]

[a] Departamento de Física de Partículas, Universidade de Santiago de Compostela, E-15782 Santiago de Compostela, Spain

[b] Instituto Galego de Física de Altas Enerxías (IGFAE), Universidade de Santiago de Compostela, E-15782 Santiago de Compostela, Spain

[c] National Centre for Nuclear Research, 00-681 Warsaw, Poland

PhD Student Contribution

Active participation in all the calculations presented in the paper, as well as in the discussions and meetings.

Chapter of the thesis in which it is used: 5

Journal and Article Information

Journal name: The European Physical Journal C

Publisher: Springer

ISSN: 1434-6052 (print)

Year of publication: 2019

DOI: https://doi.org/10.1140/epjc/s10052-019-7097-5

Impact factor in 2019: 4.847

Effect of non-eikonal corrections on azimuthal asymmetries in the Color Glass Condensate, *Eur. Phys. J. C* **79** (2019) 790

Authors

Pedro Agostini,[ab] Tolga Altinoluk,[c] Néstor Armesto,[ab]

[a] Departamento de Física de Partículas, Universidade de Santiago de Compostela, E-15782 Santiago de Compostela, Spain

[b] Instituto Galego de Física de Altas Enerxías (IGFAE), Universidade de Santiago de Compostela, E-15782 Santiago de Compostela, Spain

[c] National Centre for Nuclear Research, 00-681 Warsaw, Poland

PhD Student Contribution

Active participation in all the calculations presented in the paper, as well as in the discussions and meetings.

Chapter of the thesis in which it is used: 5

Journal and Article Information

Journal name: The European Physical Journal C

Publisher: Springer

ISSN: 1434-6052 (print)

Year of publication: 2019

DOI: https://doi.org/10.1140/epjc/s10052-019-7315-1

Impact factor in 2019: 4.847

Multi-particle production in proton–nucleus collisions in the color glass condensate, *Eur. Phys. J. C* **81** (2021) 760

Authors

Pedro Agostini,[ab] Tolga Altinoluk,[c] Néstor Armesto,[ab]

[a] Departamento de Física de Partículas, Universidade de Santiago de Compostela, E-15782 Santiago de Compostela, Spain

[b] Instituto Galego de Física de Altas Enerxías (IGFAE), Universidade de Santiago de Compostela, E-15782 Santiago de Compostela, Spain

[c] National Centre for Nuclear Research, 00-681 Warsaw, Poland

PhD Student Contribution

Active participation in all the calculations presented in the paper, as well as in the discussions and meetings.

Chapter of the thesis in which it is used: 4

Journal and Article Information

Journal name: The European Physical Journal C

Publisher: Springer

ISSN: 1434-6052 (print)

Year of publication: 2021

DOI: https://doi.org/10.1140/epjc/s10052-021-09475-0

Impact factor in 2021: 4.389